Innate Immune Recognition of *Salmonella* and *Francisella*: Two Model Intracellular Bacterial Pathogens.

Inauguraldissertation

zur
Erlangung der Würde eines Doktors der Philosophie
vorgelegt der
Philosophisch-Naturwissenschaftlichen Fakultät
der Universität Basel

von
Roland Felix Dreier
aus Trub BE

BASEL, 2017

Genehmigt von der Philosophisch-Naturwissenschaftlichen Fakultät

auf Antrag von:

Prof. Dr. Petr Brož
Dissertationsleiter
Prof. Dr. Dirk Bumann
Korreferent

Basel, den 21.03.2017

Prof. Dr. Martin Spiess
Dekan

Abstract

The innate immune system is the first line of host defense against invading pathogens. In multicellular organisms, specialized innate immune cells recognize conserved pathogen-associated molecular patters (PAMPs) with germline-encoded pattern recognition receptors (PRR). Thereby, the organism discriminates between self and non-self and engages mechanisms to eliminate the invader. Beside PAMPs, PRRs recognize mislocalized self-molecules, so called danger-associated molecular patterns (DAMPs), which are indicators of tissue or cellular damage.
Upon PAMP or DAMP recognition, PRRs induce innate immune signaling pathways leading to the activation of pro-inflammatory genes and interferon production, which are important mediators of inflammation. Therefore the recognition of invading pathogen and thereby activation of innate immune signaling pathways determines the success of the immune system to eliminate the potential threat.
Innate immune signaling pathways largely depend on phosphorylation cascades. Today, global phosphorylation changes are analyzed by mass spectrometry, however the number of detected phosphopeptides remains unchanged despite technical improvements. Therefore, we investigated the issue of phosphopeptide detection in mass spectrometry.
The analyses of phosphopeptide-enriched samples revealed lower signal intensities in MS1 spectra compared to total cell lysate samples, which resulted in poor phosphopeptide detection with mass spectrometry. Based on these observations, we hypothesized that the phosphate groups of phosphopeptides account for this poor detection. Indeed, we significantly increased the signal intensities in MS1 spectra after enzymatic removal of phosphate groups from phosphopeptides, and consequently we detected three-times more peptides in phosphatase-treated samples. Validation experiments elucidated that most of the newly detected peptides were initially phosphorylated. Moreover, the newly detected peptides enlarged the activated signaling network upon *Salmonella* infection. Importantly, we identified known innate immune signaling pathways, which were missing in the analyses of phospho-enriched samples.
Taken together, the phosphate groups of phosphopeptides globally suppress peptide ionization efficacy and therefore account for the low phosphopeptide detection rate by mass spectrometry. By removing the phosphate groups, we identify three times more peptides after phosphatase treatment. The newly detected peptides enlarge the network of activated innate immune signaling pathways upon *Salmonella*

infection and include signaling pathways that are important but have not been detected in phospho-enriched samples. Therefore our findings improve the analyses of innate immune signaling pathways by mass spectrometry and consequently the understanding of innate immunity.
One of the main mechanisms to eliminate invading microbes is by phagocytosis and degradation within phago-lysosomes. However, professional pathogens have developed various defense mechanisms to resist intracellular killing and can even use innate immune cells as replicative niches. For example, the bacterial pathogen *Francisella tularensis* causes a severe and life-threatening disease called tularemia in humans, because *Francisella* survives and replicates in macrophages and dendritic cells. Critical for *Francisella* pathogenicity is the ability of the phagocytosed bacteria to escape from the phagosome to the host cytosol. Even though we know that genes encoded on the *Francisella* pathogenicity island (FPI) are essential for escaping from the phagosome, the mechanism is unknown. Homology analyses have suggested that the FPI encodes a type 6 secretion system (T6SS). However experimental evidence is missing, which show that the FPI encodes a functional T6SS. Therefore, we investigated whether the FPI encodes a functional T6SS and what impact a functional T6SS has on *Francisella* virulence in vitro and in vivo.
We showed that the FPI of *Francisella novicida* (*F. novicida*) encodes a functional T6SS that assembles exclusively at bacterial poles. T6SS function depended on the unfoldase ClpB, which specifically recognizes contracted T6SS sheaths leading to their disassembly. Furthermore we characterized FPI genes that showed no homology with known T6SSs. We identified IglF, IglG, IglI and IglJ as structural components of the T6SS and PdpC, PdpD, PdpE and AnmK as potential T6SS effector proteins. Whereas PdpE and AnmK were dispensable for phagosomal escape, AIM2 inflammasome activation and virulence in mice, *pdpC*- and *pdpD*-deficient bacteria were impaired in all aforementioned analyses. This suggests that PdpC and PdpD are bacterial effector proteins involved in phagosomal escape and thereby in the establishment of a *F. novicida* infection.
Taken together, *F. novicida* uses its T6SS to deliver the effector proteins PdpC and PdpD into host cells. PdpC and PdpD are involved in phagosomal rupture and consequently in bacterial escape to the cytosol. These findings are a major breakthrough in the understanding of *Francisella* pathogenicity and could lead to new vaccination strategies to eradicate the life-threatening human disease tularemia.

Contents

I Introduction **9**

1 Innate Immunity 10

1.1 Cells of the innate immune system 12

1.2 Pattern recognition receptors 20

1.2.1 Toll-like receptor 4 26

1.3 Interferon 29

1.4 Inflammasomes 31

1.4.1 Inflammasome receptors 32

1.4.2 ASC 37

1.4.3 Caspase-1 38

1.4.4 Interleukin-1β / Interleukin-18 39

1.4.5 The non-canonical inflammasome 39

2 Intracellular bacterial pathogens 42

2.1 *Salmonella* 44

2.2 *Francisella* 48

2.2.1 The *Francisella* pathogenicity island 52

II Aim of Research **59**

III Results **61**

1 Research article I 62

2 Research article II 119

2.1 Additional results related to research article II 141

3 Research article III 145
4 The composition of the canonical inflammasome complex. 171
4.1 Introduction 171
4.2 Material and Methods 172
4.3 Results 176
4.4 Discussion and Outlook 186

IV Discussion and Outlook **193**
1 How can we improve the new phosphoproteomics approach? 193
2 The *Francisella* pathogenicity island encodes a functional T6SS . . 196
3 Why is the AIM2 inflammasome not activated during mitosis? . . . 201

References **205**

Acknowledgements **237**

V Appendix **239**
1 Research article IV 240
2 Research article V 260
3 Dharmacon siRNA library 282

Chapter I

Introduction

1 Innate Immunity

All living organisms face the challenge of fighting off invading pathogens and therefore need to discriminate between self and non-self. After detecting non-self, the organisms need to react to the potential threat and eliminate it, otherwise the organism may not survive the pathogen. The reaction of an organism to a potential threat is executed by the immune system and called immune response. Even in prokaryotes basic forms of immunity can be found, such as restriction enzymes and clustered regularly interspaced palindromic repeats (CRISPR) that recognize and restrict bacteriophages [1]. Furthermore, unicellular amoebae, like Dictyostelium, developed the ability to internalize foreign material for feeding [2].
The evolution of multicellular organisms allowed for a more sophisticated immune system with specialized immune cells. In invertebrates, such as sponges, snails, insects, worms or jellyfishes, the ability to internalize material was developed even further and received the name phagocytosis. During phagocytosis, specialized cells called phagocytes detect and internalize foreign material with their surface receptors, thereby discriminating between self and non-self [3]. The identification of the receptors that recognize specific patterns on foreign material led to the discovery of innate immunity; a concept first proposed by Charles Janeway in 1989 [4]. The receptors of the innate immune system, better known as pattern recognition patterns (PRRs) are germline-encoded, and thus invariable. Their specific ligands are called pathogen-associated molecular patterns (PAMPs) or danger-associated molecular patterns (DAMPs). [4, 5].
The immune system continued to develop in vertebrates, which have both an innate and adaptive immune system. The adaptive immune system consists of B and T cells that express immunoglobulins (antibodies) and T cell receptors (TCRs), respectively [6]. However, the fundamental concept of self/non-self discrimination holds true for antibodies and TCR, but the way of recognition is different. In innate immunity germline-encoded PRRs are limited to conserved patterns of foreign material. In contrast, TCRs and antibodies of the adaptive immune system are plastic and thereby adapt to newly arising patterns on foreign material (called antigen). This huge recognition range is generated through somatic instead of germline-encoded mechanisms. Antigen specificity is generated through receptor gene segment recombination events, which create any target specificity of the receptor [7,8]. As receptor recombination requires time, the adaptive immune system reaches maximal efficiency after days or weeks of first antigen exposure, whereas the innate immune system acts effectively immediate after first PAMP or DAMP exposure. However, PAMPs or DAMPs do not directly activate T and B cells. Cells of the innate immune system produce and present the antigen required for TCR or antibody development to the cells of the adaptive immune system. Thus, the innate and adaptive immune system act cooperatively to mount an efficient immune response and to eradicate a detected threat [6, 8, 9].
Around 1900, the discovery of antibodies and phagocytes initiated the research

field of the innate and adaptive immune system. However, more adequate techniques were available to purify antibodies and thereby enabling the research into the function of antibodies. This resulted in a attention shift from the discovery of phagocytes by Metchnikoff to the discovery of antibodies by Ehrlich [10, 11]. It took almost a century until Charles Janeway proposed the basic concepts of innate immunity in a lecture at the Cold Spring Harbor Symposium in 1989 [4], thereby re-starting research in innate immunity. However, the understanding of the innate immune system still lags behind the understanding of the adaptive immune system. Given that the innate immune system is the first line of defense against invading pathogens, it is crucial to understand how the innate immune system is activated. Moreover the innate immune system is required for an efficient adaptive immune response. However, the crosstalk between the innate and adaptive immune system remains elusive and therefore has to be studied in more depth.

1.1 Cells of the innate immune system

When pathogens enter an organism, they are immediately recognized by the innate immune system, which prevents them from spreading throughout the organism. The physical and chemical barrier of the innate immune system are the epithelial cells in the skin, lung or gastrointestinal tract, which prevent free access of pathogens into the body. However, pathogens have developed mechanisms, which allow them to penetrate through these physical and chemical barriers. In such cases, a second layer of innate immunity stands guard underneath the epithelial cell layer or in the blood stream to detect and kill invading pathogens. This layer includes humoral innate immune components and specialized innate immune cells [9, 12].
The humoral innate immune components are soluble molecules that bind to and kill invading pathogens or opsonize them for efficient innate immune cell recognition and phagocytosis. Two prominent components of humoral innate immunity are antimicrobial peptides (AMPs) and the complement system. AMPs, such as defensins and cathelicidins, are inserted into pathogen membranes and destabilize them, which kills the pathogen [13].
The complement system recognizes and binds pathogen surfaces. Deposition of complement components on the pathogen surface results in the formation and insertion of a pore into the pathogen membrane that kills the pathogen. Moreover, the decoration of the pathogen surface with complement components opsonize the pathogen and thereby favor pathogen phagocytosis by innate immune cells [14]. In addition to pathogen killing and opsonization, complement activation generates soluble cleavage products such as C3a and C5a, which attract innate immune cells to the site of infection and provide activation and survival signals for T cells [15–17].
The importance of the crosstalk between different components of the innate immune system as well as the crosstalk between the innate and adaptive immune system is highlighted by the role of the complement system. Complement-dependent pathogen detection results in pathogen opsonization that facilitates pathogen uptake by innate immune cells. In parallel, soluble cleavage products during the process of opsonization attract innate and adaptive immune cells to the site of infection and facilitate immune cell activation. Consequently, the local, complement-driven inflammation initiates a multilayered, complex immune response involving soluble and cellular components of the innate and adaptive immune system.
The recognition of invading pathogens through specialized innate immune cells is absolutely crucial for an efficient immune response. Innate immune cells largely originate from haematopoietic stem cells (HSCs) in the bone marrow (Figure I.1). The HSCs generate all mature blood cells and produce roughly 10^9 red blood cells and 10^8 immune cells per hour [18]. During the process of stem cell differentiation, the HSCs pass through various progenitor stages, each accompanied by a loss of trans-differentiation capability. Even though it is clear that HSCs follow a differentiation path with various progenitor stages, the hierarchy of differentiation from HSCs to fully differentiated cells is still debated. Various models of HSCs differentiation exist to date [19–22]. The common denominator of all these models is

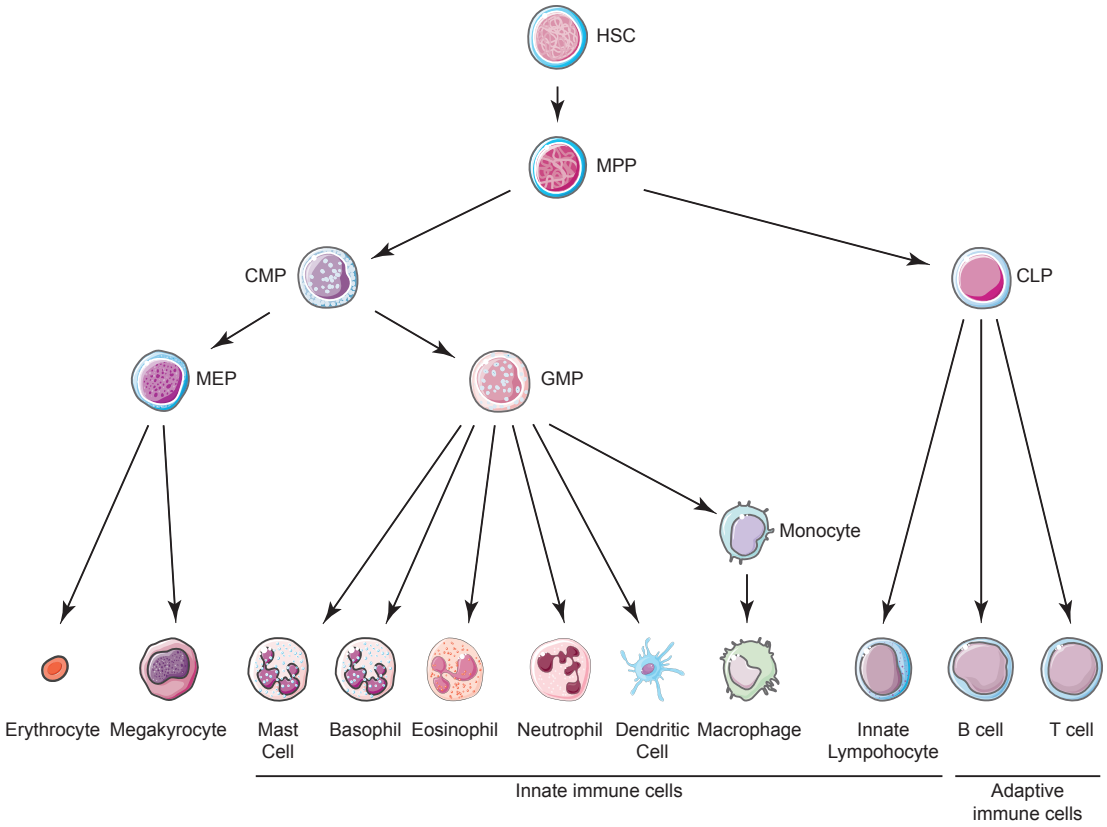

Figure I.1 Differentiation of haematopoietic stem cells. Haematopoietic stem cells (HSCs) in the bone marrow generate all mature blood cells. HSCs differentiate through various multipotent progenitors cells (MPPs). MPPs then split into two main directions following the common myeloid or common lymphoid progenitor route (CMPs or CLPs, respectively). CMPs differentiate into all red blood cells (erythrocytes and megakaryocytes) and the majority of innate immune cells, whereas CLPs differentiate into cells of the adaptive and innate immune system. MEP, Megakaryocyte-erythrocyte progenitor; GMP, Granulocyte-monocyte progenitor. *Adapted from Wang and Wagers* [18].

the existence of two distinct progenitor cells; the common lymphoid progenitors (CLPs) and the common myeloid progenitors (CMP). The CLPs differentiate to B and T cells and are therefore the source of the adaptive immune system. Moreover, CLPs differentiate into innate lymphocytes including natural killer (NK) cells and innate lymphoid cells (ILCs). Thus, CLPs contribute to the development of the innate immune system [23].
In contrast, CMPs develop into myeloid-erythroid progenitors (MEP) and granulocyte -monocyte progenitors (GMPs). MEPs give rise to red blood cells, including erythrocytes and megakaryocytes. GMPs differentiate into the majority of innate immune cells including monocytes/macrophages, dendritic cells, neutrophils, eosinophils, basophils and mast cells [18]. Therefore, GMPs contribute significantly to the development of innate immune cells. Innate immune cells are categorized

into eight different groups based on surface protein markers and immune function. These eight groups and their function in innate immunity are discussed in more detail in the next paragraphs.

Monocytes

Monocytes are phagocytes and are found in the blood stream, where they circulate with a short lifetime. To maintain monocyte numbers in the blood, the bone marrow has to produce new monocytes constantly. In the bone marrow, monocyte differentiation depends on macrophage colony-stimulating factor (M-CSF). In mice, two monocyte subgroups are found and distinguished by the differential expression of surface markers. The first subgroups are proinflammatory ($Ly6C^{hi}$) monocytes, which express high levels of lymphocyte antigen 6C (Ly6C) and C-C chemokine receptor 2 (CCR2) but low levels of CX3C chemokine receptor 1 (CX3CR1). The second subgroup are patrolling ($Ly6C^{low}$) monocytes, which express low levels of Ly6C and CCR2 but high levels of CXC3CR1 [24].

Proinflammatory monocytes are potent pathogen killers and accumulate at the site of infection or sterile injury in a CCR2-dependent manner. In addition, proinflammatory monocytes transport antigens from the site of infection to lymph nodes, where they present the antigen to adaptive immune cells and thereby activate them [25]. Moreover, proinflammatory monocytes can differentiate into macrophages or dendritic cells and replenish the pool of tissue-resident macrophages or dendritic cells under steady-state and tissue injury conditions [26, 27].

Patrolling monocytes survey the vasculature by constant crawling along the endothelial layer of blood vessels. Yona and colleagues suggest that patrolling monocytes originate from proinflammatory monocytes and have anti-inflammatory functions [28]. Given that patrolling monocytes can immediately migrate into the tissue after bacterial infections [29], they are involved in early inflammation responses as well as tissue repair after injury [30].

In humans, three monocyte subsets are described. The classical monocytes are similar to proinflammatory monocytes in mice and are characterized by $CD14^{++}$ and $CD16^{-}$ (FCγRIII immunoglobulin receptor). Nonclassical monocytes are defined by $CD14^{+}$ and $CD16^{++}$, representing murine patrolling monocytes. In contrast to mice, humans harbor a third subset of monocytes, namely intermediate monocytes, which are defined by $CD14^{+}$ and $CD16^{+}$. These intermediate monocytes are on the transition between classical and nonclassical monocytes harboring both phagocytic function and anti-inflammatory effects [31, 32].

Taken together, monocytes are important mediators of inflammation due to their high mobility, their aggressive pro-inflammatory state and their high plasticity. Their mobility enables them to migrate to the site of tissue injury or infection. Their pro-inflammatory state allows them to efficiently encounter and kill invading pathogens. Their plasticity allows them to differentiate into tissue-resident macrophages and dendritic cells, thereby contributing to cell homeostasis in the tissue.

Moreover, plasticity allows proinflammatory monocytes to trans-differentiate into patrolling monocytes. This monocyte trans-differentiation switches from pro- to anti-inflammatory immune responses, resulting in tissue repair. Thus monocytes are potent pathogen killing cells but also mediate the restitution of the infected or injured tissue.

Macrophages

Macrophages are the first phagocytes described by Metchnikoff in 1905 [10]. Macrophages populate many types of tissue and are therefore also called tissue-resident macrophages. Compared to monocytes, macrophages show reduced motility but elevated phagocytic activity [33]. Depending on the localization, each macrophage population shows a tissue-specific transcriptional profile [34]. The major macrophage populations are located in the liver (Kupffer cells), lung (alveolar macrophages), brain (microglia) and spleen (splenic macrophages), but macrophages are also found in the heart, dermis, pancreas and intestine [24, 28, 35, 36]. A dogma established by van Furth and colleagues claimed that tissue-resident macrophages are continuously replenished by monocytes from the bone marrow [37]. However, recent publications challenge this dogma. They suggest that the major macrophage populations are established at the embryonic state, despite the fact that monocytes partially contribute to the repopulation of tissue-resident macrophages of the heart, dermis, pancreas and intestine [26, 27, 38, 39]. Two observations strongly support this new hypothesis. Firstly, tissue-resident macrophages have the capacity to self-maintain their populations and secondly, they are present in embryos from day 10.5 on and therefore are developed before the generation of hematopoietic stem cells [36].

The main function of macrophages is the maintenance of tissue homeostasis. Macrophages remove cellular material, like apoptotic cells, from the tissue by phagocytosis [40]. Importantly, the removal of cellular material is silent, as the receptors involved in phagocytosis of dead self-material fail to induce an immune response. Therefore no inflammatory stimulators are produced during this process [41]. Besides maintaining tissue homeostasis, macrophages are activated by the detection of non-self material. Once they are activated, they have three functions in the tissue: host defense, wound healing and immune regulation. Historically, macrophages are categorized into classically activated (M1) and alternatively activated (M2) macrophages [42, 43]. M1 macrophages express high levels of IL-12, which stimulates cytotoxic T_h1 cells [44] and low levels of IL-10, a potent anti-inflammatory cytokine [45]. M1 macrophages are activated by tumor necrosis factor α (TNFα) and interferon (IFN)-γ. They enhance intracellular pathogen killing, cytokine secretion and expression of co-stimulatory molecules to activate other innate and adaptive immune cells. IFN-γ is produced by natural killer (NK) cells and the T cell subgroup T_h1. Even though both TNFα and IFN-γ induce the expression and secretion of pro-inflammatory cytokines, only IFN-γ induces the production of

oxygen and nitrogen radicals. Both radicals have potent bactericidal activities [46]. Besides being activated by other cells, macrophages produce their own activation signals by PRR-dependent danger recognition. For example, macrophage Toll-like receptor (TLR) signaling induces the expression of TNFα and IFN-β, a close relative of IFN-γ. TLR and IFN signaling is discussed in more details in chapter I, section 1.2.1 and 1.3.
In contrast to M1 macrophages, the M2 macrophage state is induced by interleukin-4 (IL-4) or IL-13. IL-4 is one of the earliest markers of tissue injury and is produced by basophils, mast cells or T_h2 cells [47]. Upon activation, M2 macrophages express arginase-1 and the mannose and IL-4α receptor [48]. In macrophages, Arginase expression is important for the production of extracellular matrix and therefore tissue repair [49]. In contrast to M1 macrophages, M2 macrophages are unable to present antigens to adaptive immune cells, they show decreased pathogen killing capacity and they produce minimal amounts of pro-inflammatory cytokines like IL-12 [50]. Instead, M2 macrophages express high levels of anti-inflammatory IL-10 which is required for tissue repair after pathogen invasion or injury.
Even though the M1 and M2 classification is widely accepted, additional macrophage activation states have been described and extend beyond the historical M1 and M2 macrophage classification [50, 51]. Based on experimental data, Mosser and colleagues have proposed an adapted activation state model to illustrate the different activation states with a color scheme. In this activation model, the three primary colors represent the three main macrophage functions; host defense, wound healing and immune regulation. The summary of signals that activate a macrophage is compared to the mixture of the three primary colors resulting in a unique color. In the color scheme, the primary colors gradually blend into each other with infinite numbers of intermediate colors. Thus the macrophage activation state is seen as continuum between the three major functions host defense, wound healing and immune regulation. Therefore, the state of macrophage activation is rather a mixture of different functions than a strict classification into the three main functions host defense, wound healing and immune regulation. As a consequence, an activated macrophage can for example show host defense and wound healing properties at the same time, depending on the activation signals the macrophage received.

Dendritic cells

Ralph Steinman discovered dendritic cells (DCs) in 1973 and received the Nobel Prize for his discovery in 2011 [52]. DCs are prototypic antigen presenting cells, which link the innate and adaptive immune system [53]. DCs constitutively express the surface markers CD45, major histocompatibility complex II (MHC-II) and CD11c. Plasmacytoid DCs (pDCs) and classical DCs (cDCs) constitute the two major groups in a very heterogeneous DC population. cDCs cover the majority of DC subpopulations and are further divided into lymphoid and nonlymphoid cDCs and Langerhans cells (LCs) [54]. Similar to tissue-resident macrophages, LCs

in the dermis have the potential of self-renewal and do not originate from the bone marrow [55, 56]. In contrast to LCs, cDCs and pDCs cannot self-renew and they are constantly replenished from the bone marrow. However under certain circumstances, cDCs proliferate locally in the tissue [57, 58].
Regardless of DC localization in the body, DCs constantly sample their environment for PAMPs and DAMPs as an indicator of tissue injury or infection. To detect PAMPs and DAMPs, DCs express a diverse arsenal of different PRRs [59]. After PAMP or DAMP recognition and internalization, the PAMP or DAMP is processed intracellular and the resulting antigen is loaded onto the surface receptor MHC-II. MHC-II-antigen-loaded DCs migrate to the lymph nodes, where they activate naïve T cells to launch an effective adaptive immune response [60,61].

Neutrophils
Neutrophils originate from myeloid precursors in the bone marrow. They are short-lived under steady state conditions and constantly undergo apoptosis [46]. Granulocyte colony-stimulating factor (G-CSF) and granulocyte-macrophage colony-stimulating factor (GM-CSF) are important for neutrophil progenitor proliferation in the bone marrow [62, 63]. Neutrophils circulate in the blood and are recruited to the site of infection or injury through cytokines produced by macrophages [64, 65]. Importantly, G-CSF and GM-CSF produced at the site of infection are anti-apoptotic and stimulate neutrophil survival and increase neutrophil responsiveness to the infection [66, 67]. As neutrophils circulate in the blood, cell adhesion at the side of infection or injury is very important to induce an immune response [68]. Once at the site of infection or injury, neutrophils produce cytokines that attract and activate innate and adaptive immune cells [69, 70].
Neutrophils are the most effective pathogen killers of the innate immune system [33]. They primarily kill complement- or antibody-opsonized extracellular pathogens by phagocytosis; or kill extracellular pathogens directly through neutrophil extracellular traps (NETs). After phagocytosis of extracellular pathogens, intracellular granules fuse with the pathogen-containing phagosome. Granules contain digestive and hydrolytic enzymes and their fusion with the phagosome expose pathogens to these strong microbicidal molecules [71–73]. In addition, neutrophils produce reactive oxygen species, which are their most important mediators of pathogen killing [33, 74, 75]. The production of reactive oxygen species is described in more detail in chapter I, section 2.
As a side effect of antimicrobials, they induce tissue damage when released by neutrophils. Therefore, the release of granular content requires tight control. Moreover, neutrophils induce tissue repair mechanisms in macrophages at the site of infection or injury to compensate for antimicrobial-induced tissue damage [76, 77].

Innate lymphocytes

Innate lymphocytes (ILCs) originate from the common lymphocyte precursor (CLP) in the bone marrow. In contrast to B or T cell maturation, ILC maturation happens independent of somatic recombination [78, 79]. ILCs are enriched at barrier tissues such as skin, lung and intestine. Mature ILCs serve as an early source of cytokines to activate innate and adaptive immune cells [80]. ILCs are divided into three classes.

Group 1 ILCs (ILC1s) are the best-studied class and include among others natural killer (NK) cells. NK cells are important for the defense against viral pathogens and tumor cells [81]. ILC1s produce IFN-γ and TNFα in response to the pro-inflammatory cytokine IL-12 produced by tissue-resident macrophages [82, 83]. IFN-γ and TNFα fully activate macrophages as described in the previous paragraph. Thus, ILC1s promote inflammation in response to infections or injuries [80].

Group 2 ILCs (ILC2s) are important in host defense against extracellular parasites. IL-25 and IL-33 are produced in response to parasite infections and induce tissue repair mechanisms in ILC2s [84, 85]. Moreover, ILC2s are an important source of IL-13 that acts on intestinal goblet cells. In goblet cells, IL-13 increases mucus production to hinder parasite entry and enhances muscle contractility to mechanically remove parasites from the intestine [85].

Group 3 ILCs (ILC3s) are important in the host defense mechanism against fungi or bacteria and produce the cytokines IL-17 and IL-22 in response to IL-1β, IL-6 and IL-23 [86–88]. IL-22 act on non-hematopoietic cells and stimulate the production of antimicrobial peptides [89], thereby limiting pathogen dissemination and tissue damage. In addition, ILC2s and ILC3s have distinct functions in the promotion or limitation of chronic inflammation depending on the stimuli and location [80].

Mast cells, basophils, eosinophils

Mast cells, basophils and eosinophils belong to the group of granulocytes, like neutrophils. They originate from precursors in the bone marrow.

Mast cells and basophils act in a similar way by inducing a type-2-immune response in tissue-resident immune cells, which is characterized by anti-inflammatory signaling and tissue repair [90]. Upon activation, mast cells and basophils release their granular content in a IgE-dependent manner, a process called degranulation [91]. Basophil degranulation contributes to the control of helminth infections [92]. As described for neutrophils, the granular content of basophils and mast cells is highly cytotoxic and immunogenic, leading to strong immune responses. Thus excessive and recurrent degranulation of basophils and mast cells play an important role in IgE-mediated chronic, allergic inflammation and asthma [93, 94].

On the other hand, eosinophils have a short lifetime. They accumulate in the intestinal tissue, where they control intestinal homeostasis and the survival of antibody-producing plasma cells [95–97]. Eosinophils are maintained in the intestinal tissue by IL-13-producing ILC2s [98]. Pathogen- or allergen-induced inflammation acti-

vates eosinophils, leading to their degranulation and the release of the granular, highly cytotoxic content [99]. In addition, eosinophils release mitochondrial DNA as extracellular traps to kill extracellular pathogens [100].

Taken together, innate immune cells are mostly integrated in barrier tissues of the skin, intestine, liver, spleen or lung. In these tissues, innate immune cells wait for invading pathogens or tissue injury to immediately induce inflammation and eliminate the potential threat. In addition to this host defense mechanism, innate immune cells are involved in tissue homeostasis guaranteeing that the physical barrier is kept intact. Moreover, innate immune cells either regulate their own activation state or cross-activate other innate and adaptive immune cells. Only when the adaptive immune system is activated in an innate immune-dependent manner, a maximal and efficient immune response can be reached.
Given that antimicrobials are cytotoxic, innate immune cell activation harms the own tissue or organs, thus their activation is tightly regulated and innate immune cells have the ability to repair tissue.
Deregulation of innate immune cells is either associated with autoimmune diseases, caused by uncontrolled immune cell activation, or associated with recurring infections and cancer, as a result of immune cell activation failure [46, 51, 80]. This highlights the importance of the regulation and adequate activation of the innate immune system to balance the benefits and disadvantages for the organism.

1.2 Pattern recognition receptors

As described in chapter I, section 1, the discrimination between self and non-self is the key mechanism in innate immunity. Innate immune cells use germline-encoded receptors, so-called pattern recognition receptors (PRRs), to recognize conserved microbial molecules known as pathogen-associated molecular patterns (PAMPs). However, also non-immune cells express PRRs and can thereby recognize PAMPs and thus contribute to local inflammation [4]. Importantly, PAMPs are subjected to low mutation rates because they have a detrimental role in pathogen biology. Therefore, PAMPs are an ideal ligand for germline-encoded PRRs, which themselves are invariable. The most prominent PAMP is the gram-negative bacterial outer membrane component lipopolysaccharide (LPS), though bacterial flagellin, lipoproteins of gram-positive bacteria or unmethylated DNA and viral RNA are also recognized by PRRs [101]. Over the years it has been discovered that PRRs also recognize host-derived signals, better known as danger-associated molecular patters (DAMPs), alarmins or endogenous adjuvants. DAMPs are normally hidden within cells or cellular compartments and they are released or secreted under conditions of cellular stress or tissue injury [102–104]. Prototypic DAMPs are Interleukin-1 (IL-1), IL-33, high-mobility group box 1 (HMGB1), amyloid β (Aβ), mitochondrial DNA, ATP, uric acid and double- and singlestranded RNA [40,105]. The PRRs are either membrane bound or cytosolic. The membrane bound PRRs are either anchored in the plasma membrane surveying the extracellular space or anchored in endosomal membranes surveying phagocytosed material for the presence of potential harm [106]. Historically, five different PRR classes have been identified, namely the Toll-like receptors (TLRs), the C-type lectin receptors (CLRs), the nucleotide-binding and oligomerization domain (NOD)-like receptors (NLRs), the retinoic acid inducible gene-I (RIG-I)-like receptors (RLRs) and the absent in melanoma 2 (AIM2)-like receptors (ALRs) [5]. Recently, many new cytosolic PRRs that recognize DNA or cyclic-di-nucleotides (CDNs) were discovered [107].
PRR activation results in the transcriptional activation of a ligand-specific set of pro-inflammatory cytokines and/or interferons (IFN) or to the activation of inflammasomes. Inflammasomes, cytokines and IFNs are essential mediators of an efficient innate and adaptive immune response [106,108]. Given that PRRs are the crucial receptors for recognizing non-self, the different classes and their ligands are described in the next paragraphs.

Toll-like receptors
Toll-like receptors (TLRs) are by far the best studied PRRs and include TLR1-10 in humans and TLR1-9 and TLR11-13 in mice [106]. TLRs are localized to the plasma membrane (TLR1,5,6,10), on intracellular endosomes (TLR3,7-9,11-13) or to both compartments (TLR2,4) and the localization is critical for signaling [109]. TLRs consist of three important domains for ligand recognition and signaling. The

horseshoe-like leucin-rich repeats (LRRs) recognize and bind the ligand, the transmembrane domain anchors the PRR in the membrane and the Toll/interleukin-1 receptor (TIR) homology domain is responsible for downstream signaling [8, 110]. Endosomal TLR7-9 are anchored in the membrane as preformed dimers and are important for the recognition of invading viruses [111]. Single stranded RNA (ssRNA) activates TLR7 and TLR8, whereas unmethylated DNA activates TLR9 [112].
All plasma membrane-localized TLRs and TLR3 are anchored in the membrane as monomers [111]. After ligand recognition, these TLRs form homo- or heterodimers. TLR3 and TLR5 form homodimers after double stranded RNA (dsRNA) and bacterial flagellin recognition, respectively [113, 114], whereas TLR4 forms homodimers after recognition of a wide range of PAMPs and DAMPs, however the most prominent one is bacterial LPS [106]. Recently, it has been speculated that many described TLR4-activating PAMPs and DAMPs has been contaminated with LPS and thus these results are misleading. TLR4 activation is described in more details in chapter I, section 1.2.1.
In contrast to TLR3, -4 and -5, heterodimers of TLR1 and TLR2 recognize triacylated lipoproteins [115], whereas heterodimers of TLR2 and TLR6 recognize di-acylated lipoproteins. Lipoproteins are important components of the bacterial, fungal and parasitic cell wall but are also present on viral particles [116].
In addition to humans, mice express TLR11, -12 and -13, which recognize bacterial flagellin, parasitic profilin and bacterial ribosomal RNA, respectively. Like TLR7-9, they exist as preformed dimers and are localized to endosomes [107].
Activated TLRs, with the exception of TLR3, recruit via their cytosolic TIR domains the two signal adaptors myeloid differentiation primary response protein 88 (MYD88) and MYD88 adaptor-like protein (MAL). MYD88/MAL recruitment results in the activation of nuclear factor kappa-light-chain-enhancer of activated B cells (NF-κB) and adaptor protein 1 (AP-1) (Figure I.2). NF-κB and AP-1 are transcription factors and induce the expression of pro-inflammatory genes [106, 111]. In contrast, TLR3 and TLR4 recruit via their TIR domains the signal adaptors TIR domain-containing adaptor protein-inducing IFN-β (TRIF) and TRIF-related adaptor molecule (TRAM). TRIF/TRAM recruitment to TLR3 and TLR4 activates the transcription factor IFN regulatory factor 3 (IRF3) to induce the expression of type-I-interferon [113].
Taken together, TLR signaling activates both immune and non-immune cells to effectively fight a pathogen infection. Moreover, TLR signaling induces inflammation to propagate the immune response. In chapter I, section 1.2.1 the activation mechanism of TLR4 and the underlying signaling cascade is described in more detail.

C-type lectin receptors

C-type lectin receptors (CLRs) are primarily found on the plasma membrane. Hundreds of CLRs have been identified and form a very heterogeneous group. CLRs

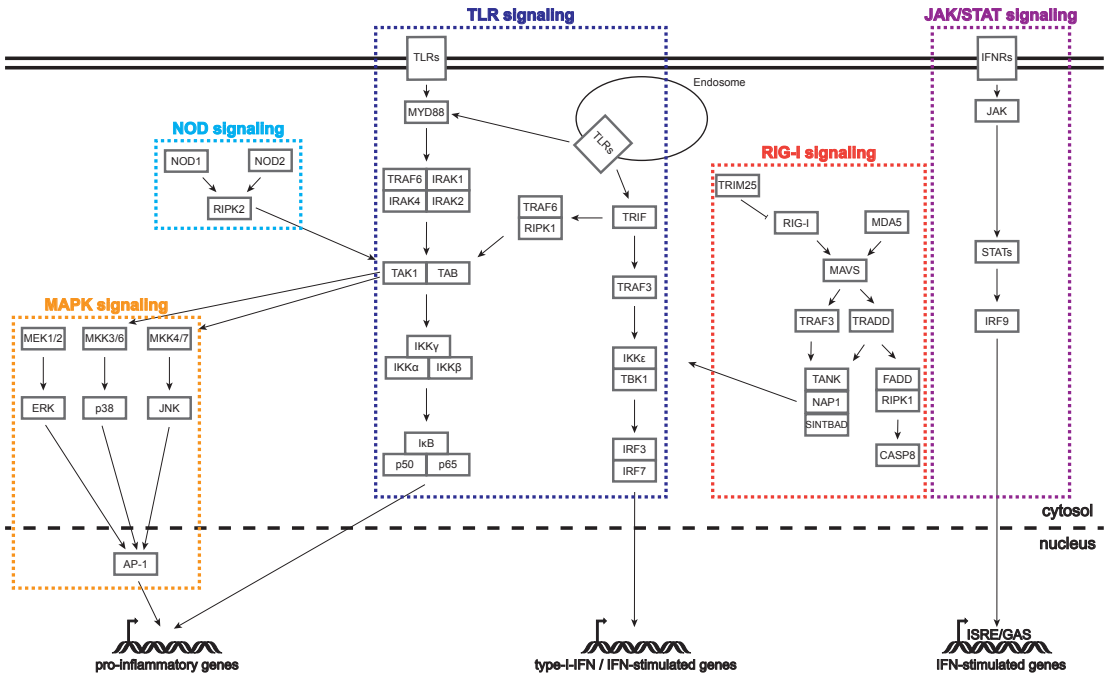

Figure I.2 Schematic overview of selected innate immune signaling pathways. Innate immune cells signal via different pathways from the plasma membrane, endosomes and the cytosol to induce the expression of pro-inflammatory genes, type-I-interferon (IFN) or IFN-stimulated genes. MEK, Mitogen-activated protein kinase (MAPK)/extracellular signal-regulated kinase (ERK) kinase; MKK, MAPK kinase; JNK, c-Jun N-terminal kinase; AP-1, Adaptor protein 1; NOD, Nucleotide-binding oligomerization domain-containing protein; RIPK2, Receptor-interacting serine/threonine-protein kinase; TLR, Toll-like receptor; MYD88, Myeloid differentiation primary response protein 88; TRAF, Tumor necrosis factor (TNF) receptor associated factor; IRAK, Interleukin-1 receptor associated kinase; TAK1, Transforming growth factor (TGF) beta-activated kinase 1; TAB, TAK1 binding protein; IkB, I kappa B; IKK, IkB kinase; TRIF, Toll-interleukin receptor (TIR) domain-containing adapter protein inducing IFNβ; TBK, TANK-binding kinase; IRF, Interferon regulatory factor; TRIM, Tripartite motif-containing protein; RIG, Retinoic acid inducible gene; MDA, Melanoma differentiation gene; MAVS, Mitochondrial antiviral signaling protein; TRADD, TNF receptor type 1-associated Death domain (DD) protein; TANK, TRAF family member-associated nuclear factor kappa-light chain enhancer of activated B cells (NF-κB) activator; NAP, NF-κB-activating kinase-associated protein; SINTBAD, TBK1-binding protein 1; FADD, FAS-associated death domain protein; CASP8, Caspase-8; IFNR, IFN receptor; JAK, Janus kinase; STAT, signal transducer and activator of transcription; ISRE, IFN-stimulated response element; GAS, Gamma-activated sequence. *Adapted from Dreier et al.* Chapter III, section 1.

are characterized by a C-type lectin-like domain (CTLD) and recognize different carbohydrates on the cell surface of viruses, bacteria and fungi [106]. Based on their structure, the CLRs are divided into 17 different groups [117,118]. The best characterized CLRs are Dectin-1 and Dectin-2. Dectin-1 is expressed by DCs, macrophages, neutrophils and monocytes and recognizes fungal β-1,3-glucans [119], as well as

bacteria-bound mucins and bacterial β-glucans [120]. Upon ligand recognition, activated Dectin-1 recruits and activates the kinase SYK through the cytosolic ITAM domain [121, 122]. Consequently, receptor-activated SYK activates the NF-κB and mitogen activated protein kinase (MAPK) signaling pathway through TRAF6 and TAK1, respectively, resulting in pro-inflammatory gene expression [123]. The NF-κB and MAPK signaling pathway is discussed in greater details in chapter I, section 1.2.1.
Dectin-2 is activated through fungal α-mannans [124] or the parasite Schistosoma [125]. Dectin-2 activation by IgE causes an allergic reaction [126]. In contrast to Dectin-1, Dectin-2 misses the intracellular ITAM domain. Therefore, Dectin-2 needs to bind to FcRγ, which contains the ITAM domain for downstream signaling. The downstream signaling of the FcRγ ITAM domain is analogues to the Dectin-1 signaling and both result in the expression of pro-inflammatory genes [106].

NOD-like receptors

NOD-like receptors (NLRs) are cytosolic receptors that consist of a N-terminal effector domain, a central nucleotide-binding and oligomerization domain called NACHT and C-terminal LRRs [127]. There are 23 NLR family members in humans and more than 34 in mice [128]. The NLRs are categorized into 4 subfamilies (NLRA,B,C,P) based on the N-terminal effector domains.
The NLRA subfamily includes only CIITA and contains an acidic transactivation effector domain. CIITA transcriptionally activates MHC class II genes, which enables cells to present antigens to adaptive immune cells [129].
The NLRB subfamily includes only NAIP in humans but includes NAIP1-7 in mice. NAIPs contain multiple baculoviral inhibitory repeat like effector domains (BIRs). The role of NAIP proteins is discussed in greater detail in chapter I, section 1.4.1.
The NLRC subfamily consists of NLRC1-5 and NLRX1. NLRC1, -2 and -4 contain a caspase activation and recruitment effector domain (CARD), whereas NLRC3, -5 and NLRX1 have an unidentified effector domain. NLRC1 (NOD1) and NLRC2 (NOD2) are the best studied NLRs and recognize peptidoglycan moieties of Gram-negative and/or Gram-positive bacteria [130, 131]. NOD1 and NOD2 oligomerize after peptidoglycan moiety recognition and activate NF-κB through the recruitment of receptor-interacting serine/threonine-protein kinase 2 (RIPK2) (Figure I.2) [132]. In parallel to NF-κB activation, NOD1 and NOD2 activate TAK1 to induce MAPK signaling [133]. NF-κB and MAPK signaling induce the expression of pro-inflammatory genes and is discussed in greater details in chapter I, section 1.2.1. In addition to NF-κB and MAPK activation, NOD1, NOD2 and NLRX1 activate autophagy through the recruitment of ATG16L1 [134, 135].
Moreover, NLRC3 negatively regulates NF-κB signaling [136], NLRC4 induces inflammasome activation [137] and NLRC5 acts as transcriptional activator of MHC class I genes [138]. NLRC4-dependent inflammasome activation is discussed in more details in chapter I, section 1.4.1.

The NLRP subfamily harbors a pyrin effector domain (PYD) and consists of NLRP1-14 in humans. In mice, three variants of NLRP1 (Nlrp1a-c), seven variants of NLRP4 (Nlrp4a-g) and three variants of NLRP9 (Nlrp9a-c) exist. In contrast to humans, mice lack homologs of NLRP7, -8, -11 and -13 [128]. NLRP1 was the first discovered inflammasome receptor [139]. However, the best studied inflammasome receptor is NLRP3 [140]. NLRP3-dependent inflammasome activation is discussed in more details in chapter I, section 1.4.1.
In addition to NLRP1 and NLRP3, NLRP2, -6, -7 and -12 have been proposed to induce an inflammasome [141–144]. However, it is debated whether these receptors resemble an inflammasome. Besides inflammasome activation, NLRP2 and NLRP6 regulate pro-inflammatory gene expression [145–147]. Moreover, NLRP4 is a negative regulator of autophagy and type-I-interferon signaling [148, 149]. The function of the remaining NLRPs is completely unknown and requires further investigation.

RIG-I-like receptors

The RIG-I-like receptors (RLRs) detect the presence of foreign cytosolic RNA through three DexH/D box helicases and possess a CARD domain for downstream signaling [150]. RLRs include three members: the retinoic acid-inducible gene-I (RIG-I), the melanoma differentiation gene 5 (MDA5) and the laboratory of genetics and physiology 2 (LGP2) [151]. LGP2 is a negative regulator of RIG-I and MDA5 [152]. RIG-I and MDA5 detect features, such as 5' triphosphate RNA, long double-stranded RNA or poly-uridine regions [153–155], that are only present on viral but not self RNA. Based on RNA length, RIG-I and MDA5 recognize each a diverse group of viruses [156]. After RNA-dependent RIG-I or MDA5 activation, they bind via their CARD domain to the adaptor molecule mitochondrial antiviral signaling protein (MAVS), which is anchored to mitochondrial membranes [157, 158]. After RIG-I or MDA5 binding, MAVS undergoes self-oligomerization [159] and the MAVS oligomer recruits and activates TNF receptor associated factor 2, 5 and 6 (TRAF2,-5 and-6) (Figure I.2). Consequently, TRAF2/5/6 activate TANK-binding kinase 1 (TBK1) and IκB kinase ϵ (IKK-ϵ). These two kinases activate the transcription factors IRF3 and IRF7, which enter the nucleus and induce the expression of type-I-IFNs. Moreover, TRAF2 and -6 activate NF-κB leading to the expression of pro-inflammatory cytokines [160].

AIM2-like receptors

The AIM2-like receptors (ALRs) recognize intracellular, cytosolic DNA and contain two domains: a pyrin (PYD) and a HIN200 domain. Similar to NLRPs, the effector PYD domain is responsible for downstream protein-protein interactions and signaling, whereas the HIN200 domain is responsible for DNA binding [106]. To date, two members of the ALR family have been identified, namely AIM2 and IFI16. AIM2 activate an inflammasome after the recognition of at least 80 bp long

dsDNA [161–165], which will be discussed in more detail in chapter I, section 1.4. On the other hand, IFI16 has been shown to express type-I-IFN [166, 167]. However, a study by Gray and colleagues have shown that none of the ALRs is involved in type-I-IFN induction [168]. Furthermore, IFI16 has also been reported to activate an inflammasome [107]. However, if IFI16 truly resembles an inflammasome requires further investigation.

Cytosolic DNA sensors

As described above, ALRs recognize cytosolic dsDNA. However, many more proteins exist with the ability to recognize cytosolic DNA or cyclic-di-nucleotides (CDNs). The most prominent members of this group of proteins are the cyclic-GMP-AMP (cGAMP) synthase (cGAS) [169, 170] and the stimulator of IFN genes protein (STING) [171].

cGAS binds to the backbone of cytosolic dsDNA, which induces a conformational change in the cGAS active site that enables the active site to catalyze cGAMP synthesis [172]. About 15 base pairs of dsDNA binds and activates cGAS in vitro. However, in vivo, longer pieces of dsDNA are required for cGAS activation [173].

STING is localized to the membrane of the endoplasmic reticulum (ER) [174] and recognizes the second messenger cGAMP produced by cGAS [175, 176]. In addition, STING directly recognizes ci-di-AMP, which is secreted by intracellular *Listeria* [177] or DNA from intracellular viruses, bacteria and parasites [171]. However, the recent discovery of cGAS-dependent DNA binding upstream of STING suggests that STING is not a direct but indirect sensor of DNA through cGAS.

After cGAMP-dependent STING activation, STING translocates from the ER to an ER-Golgi intermediate compartment [178]. Translocated STING recruits TBK1 and IRF3, resulting in TBK1-dependent STING and IRF3 phosphorylation at a conserved LxIS phospho-motif. Interestingly, the LxIS phospho-motif is also important for MAVS and TRIF signaling, the two other signaling pathways that result in type-I-IFN production [179, 180]. The phosphorylation of IRF3 results in its homodimerization and translocation into the nucleus, where IRF3 induces the expression of type-I-IFNs. In addition to IRF3 activation, STING phosphorylates the IKK complex leading to NF-κB-dependent pro-inflammatory gene expression.

Besides cGAS and STING, proteins containing a DExD/H box domain have been shown to bind cytosolic DNA, CDNs or RNA. For example, DDX41 and DDX3 are proteins of the group of cytosolic DNA sensors. The ATP-dependent RNA helicase DDX41 binds DNA and CDNs thereby inducing IFN expression through STING and TBK1 [181]. On the other hand, DDX3 interact with RIG-I, MDA5 and MAVS to induce IFNs in response to viral RNA [182]. Additional DDX and IFIT proteins are thought to be involved in cytosolic nucleotide sensing and their specific role in the cellular immune response requires clarification [107].

In summary, PRRs play an important role in the innate immune response against

invading pathogens. In order to activate an immune response, PRRs recognize conserved PAMPs and DAMPs, which indicate an ongoing infection or tissue injury. Upon PRR activation, PRR signaling cascades induce the expression of pro-inflammatory genes in immune and non-immune cells, which activate the cell itself as well as surrounding immune cells to effectively resolve the infection or tissue injury. Thus, PRR activation serves as the initial signaling event to activate the immune system. Given that different PRRs recognize specific ligands, the immune response can be tailored to various kinds of infections or tissue injuries to adequately respond to the threat. However, pathogens have developed mechanisms, which interfere with PRR signaling to dampen or redirect the immune response. How pathogens modulate the immune response is discussed in greater details in chapter I, section 2.1 and 2.2.

1.2.1 Toll-like receptor 4

Toll-like receptor 4 (TLR4) was the first functionally described TLR in mammals [183] and the discovery of this essential innate immune receptor and its Drosophila homologue TOLL was awarded with the Nobel prize in 2011 [184, 185]. As described in chapter I, section 1.2, the main PAMP recognized by TLR4 is the major Gram-negative bacterial outer membrane component LPS, which is composed of Lipid A, a core oligosaccharide and the O antigen [186]. The LPS component Lipid A anchors LPS in the bacterial membrane and is the TLR4-activating part of LPS. However, TLR4 cannot bind to Lipid A directly and therefore requires a multireceptor complex composed of CD14, LPS-binding protein (LBP) and myeloid differentiation factor 2 (MD-2) [106].
CD14 is localized to cholesterol rich regions in the plasma membrane, which are called lipid rafts. Lipid rafts are the signaling centers of the plasma membrane, clustering together many important cytosolic receptor signaling components [187]. In the plasma membrane each TLR4 monomer interacts with one MD-2 protein outside of lipid rafts [187–189].
LBP is a soluble protein that extracts LPS monomers from bacteria and presents it to the plasma membrane receptor CD14 [190]. LPS-loaded CD14 in lipid rafts induces TLR4/MD-2 heterodimer relocalization to lipid rafts, where LPS is transferred from CD14 to MD-2. The LPS transfer induces monomeric TLR4/MD-2 dimerizationm which is absolutely essential for signaling [191, 192]. Besides transferring LPS to MD-2, CD14 directly endocytoses LPS under certain conditions, thereby delivering LPS to the cytosol [193].
The cytosolic TIR domains of TLR4 are in close proximity to each other after TLR4 homodimerization and now able to bind to the downstream adaptor molecules MYD88 and MAL, which are both essential for signal transduction [194–196]. MYD88 and MAL binding to TLR4 is only possible in lipid rafts, as MAL is localized to the plasma membrane by phosphatidylinositol 4,5-bisphosphate (PIP2),

which is typically found in lipid rafts [197]. MYD88 binding to TLR4 induces its oligomerization to form a large signaling platform called the myddosome [198]. Once the oligomerization has taken place, the C-terminal death domain (DD) of MYD88 recruits IL-1 receptor-associated kinase (IRAK) family members (Figure I.2) [198, 199]. First, the serine/threonine kinase IRAK4 is recruited by the myddosome which subsequently recruits and phosphorylates IRAK1 and IRAK2 thereby activating them [200, 201]. Phosphorylated IRAK1 and IRAK2 then recruit the E3 ubiquitin ligase TNF receptor associated factor 6 (TRAF6), which ubiquitinates the IRAK proteins with special K63/M1-linked hybrid polyubiquitination (pUb) chains [202, 203]. The K63-linked pUb chains then recruit the TAK1/TAB1-3 complex, whereas the M1-linked pUb chains recruit the canonical IKK complex consisting of IKKα, IKKβ and IKKγ (NEMO) [203]. Forming hybrid pUb chains are an elegant way to bring the IKK and TAK1 complex together as TAK1 phosphorylates IKKβ for canonical NF-κB activation [204]. Once IKKβ is activated by TAK1, IKKβ phosphorylates the NF-κB inhibitor IκBα, which is then polyubiquitinated and consequently degraded by the proteasomal machinery [205,206]. Given that the NF-κB inhibitor IκBα is degraded, the p50/p65 NF-κB heterodimer translocates to the nucleus where it induces the expression of pro-inflammatory genes [207].
Aside from NF-κB activation, TAK1 activates the MAPKs p38 and JNK, which subsequently activate the transcription factor AP-1 [204]. AP-1 is a dimeric transcription factor composed of Jun, Fos or ATF protein heterodimers and regulates in conjunction with NF-κB the expression of pro-inflammatory genes [208].
Besides MYD88/MAL-dependent TLR4 signaling at the plasma membrane, TLR4 is endocytosed in a CD14-dependent manner. This process causes TLR4 to be relocated from the plasma to endosomal membranes [209, 210]. In endosomes, the TIR domains of TLR4 interact with the TIR domain-containing adaptor protein inducing IFNβ (TRIF)-related adaptor molecule (TRAM). It has been speculated that MAL that bound to TLR4 at the plasma membrane is replaced by TRAM at the endosomal membranes, though the exact mechanism by which this occurs is still unknown [106]. Once TRAM is bound to TLR4, it recruits TRIF. Consequently, TRIF induces type-I-IFN production through the subsequent recruitment and activation of TRAF3, TBK1 and IKKϵ [211, 212]. Next, TBK1 and IKKϵ phosphorylate IRF3 causing its translocation into the nucleus where it induces type-I-IFN expression [180, 213]. A more detailed description of TRIF signaling can be found in chapter I, section 1.2. In addition to type-I-IFN induction, TRIF activates NF-κB and IRF7 in a TRAF6-dependent and IRAK1/IKKϵ-dependent manner, respectively [212, 214, 215].

Taken together, TLR4 recognize a lot of different PAMPs and DAMPs and is therefore activated by multiple pathogenic infections. However, it is speculated that the TLR4-activating PAMPs and DAMPs have been contaminated with LPS, thereby resulting in misleading conclusions. TLR4 signaling at the plasma membrane induces the expression of pro-inflammatory genes through MYD88-dependent NF-κB and MAPK signaling, whereas endosomal TLR4 induces TRIF-dependent type-I-

IFN production. Thus, cellular localization dictates distinct TLR4 signaling pathways. Moreover, the ability to recruit multiple signaling branches to activated TLR4 in a temporal distinct fashion tightly regulates the signaling array, allowing for signal branching, incorporation of other signaling events and multilayered induction of pro-inflammatory genes. However as TLR4 induces a very broad array of pro-inflammatory genes, dysfunction or successful interference with TLR4 signaling can have a dramatic influence on the immune response, such as bacterial modifications of their Lipid A to render it undetectable for TLR4 [216, 217].

1.3 Interferon

As described in chapter I, sections 1.2 and 1.2.1, TLR3- and TLR4-dependent signaling induces the expression of type-I-interferons (type-I-IFNs).
IFNs were first described in 1957 as a substance produced by cells, which is involved in defeating influenza infections [218,219]. Based on their receptor activation, three IFN classes exist, namely type-I-, -II- and -III-IFNs [220, 221]. Each IFN class induces the expression of a unique set of interferon stimulated genes (ISGs) via their corresponding receptors and under specific conditions [222], thereby equipping cells with potent weapons to fight viral, parasitic and bacterial infections [223]. Even though IFNs induce potent killing mechanisms, IFNs also suppress the immune system and thereby allowing the spread of viral and bacterial infections [224]. The different IFN classes are described in more details in the following.
Type-I-IFNs are the largest class and they are produced by almost all cells [224]. Type-I-IFNs mainly include IFN-β and 13 partially homologous IFN-α subtypes in humans (14 subtypes in mice). Additional type-I-IFN members are the poorly described IFN-ϵ, IFN-κ, IFN-ω, IFN-θ and IFN-δ [225].
The set of ISGs induced by type-I-IFNs is defined by the receptor density in the plasma membrane and the binding affinity of the specific IFN to the receptor [226, 227]. Type-I-IFNs bind to IFN-α receptor 1 (IFNAR1)/IFNAR2 heterodimers at the plasma membrane [228], which induce IFNAR1/IFNAR2 ligation and thereby trigger the phosphorylation of receptor associated kinases Janus kinase 1 (JAK1) and tyrosine kinase 2 (TYK2). Activated JAK1 and TYK2 phosphorylate highly conserved tyrosine residues on the IFN receptor, which enables signal transducer and activator of transcription 1 (STAT1) and STAT2 binding [229,230]. STAT1/2 receptor binding leads to their auto-phosphorylation on conserved tyrosine residues (e.g. STAT1 on Y701) and subsequent STAT1/STAT2 heterodimerization. STAT1/STAT2 heterodimers expose their nuclear localization signal and interact with IFN regulatory factor 9 (IRF9) to form the ISG factor 3 (ISGF3) complex [231–234]. ISGF3 translocates into the nucleus, where it binds to IFN-stimulated response elements (ISREs) in the promoter region of ISGs and induces their transcription [235, 236].
Type-III-IFNs have been recently discovered, they include IFN-λ1,-2,-3 and -4 and show structural similarity with the IL-10 cytokine family [237, 238]. Type-III-IFNs bind to IL-10 receptor 2 (IL-10R2) and IFN-λ receptor 1 (INFLR1), which form the active receptor heterodimer [222, 239]. Importantly, type-III-IFNs activate exclusively epithelial cells because IFNLR1 is only expressed in these cells [239]. Apart from different receptor binding, type-III-IFNs induce the same signaling cascade and a similar set of ISGs compared to type-I-IFNs [240].
Type-II-IFNs only consist of IFN-γ, which is predominantly produced by T cells and innate lymphocytes [241,242]. In contrast to type-I- and -II-IFNs, IFN-γ forms homodimers and binds to a receptor heterotetramer, which is composed of two IFN-γ receptor 1 (IFNGR1) and two IFNGR2 [243]. Even though only T and NK cells express IFN-γ, the IFNGR subunits are widely spread and thus almost

all cells respond to IFN-γ [244]. Instead of receptor-associated JAK1 and TYK2 in type-I-IFN signaling, JAK1 and JAK2 are associated with and activated by IFNGR [245, 246]. In contrast to type-I-IFN signaling, JAK1 and JAK2 phosphorylate only STAT1. Phosphorylated STAT1 forms STAT1 homodimers, which are called the IFN-gamma activation factor (GAF). GAF translocates into the nucleus, where it binds to γ-activated sequences (GAS) in the promoter region of ISGs and induces their transcription [247]. Interestingly, many IFN-γ-induced ISGs themselves are transcription factors (e.g. IRF-1) and are therefore able to change the transcriptional profile of an IFN-γ-activated cell [248].
Taken together, IFNs are important mediators of inflammation in innate immune and non-immune cells through the induction of hundreds of ISGs. As a result of ISG expression, invading pathogens are encountered at the site of cellular entry, which limits pathogen spreading.

1.4 Inflammasomes

In 2002, Tschopp and co-workers were the first to coin the term inflammasome, to describe a cytosolic, multiprotein complex formed by an inflammasome receptor, the adaptor molecule apoptosis associated speck-like protein containing a CARD (ASC) and caspase-1 [139]. The inflammasome is an important component of the innate immune system and induces a strong immune response. As described for other PRRs, each inflammasome receptor recognizes specific ligands or signals, which induce receptor oligomerization (Figure I.3). The receptor oligomer serves as a recruitment and oligomerization platform for the adaptor molecule ASC. ASC forms long filaments, which aggregate into a one-micron large complex called the ASC speck. The ASC speck then serves as an activation platform for caspase-1 [249,250]. As described in chapter I, section 1.2, the four PRRs NLRP1, NLRP3, NLRC4 and AIM2 as well as the protein pyrin have been shown to induce an inflammasome [249]. The inflammasome receptors sense a variety of different PAMPs and DAMPs, for example bacterial flagellin, pore-forming toxins, cytosolic DNA, extracellular ATP, uric acid crystals or the presence of intracellular bacterial effector molecules [251]. Upon activation, autoproteolytic cleavage of caspase-1 in the inflammasome complex induces a lytic form of programmed cell death called pyroptosis [139, 252]. Pyroptosis is morphologically distinct from other forms of cell death, such as apoptosis or necroptosis, and is characterized by plasma membrane rupture and the release of cytosolic content, cell swelling, positive Annexin V staining, chromatin condensation and absence of DNA laddering and loss of mitochondrial membrane potential [253, 254]. Cell lysis has an important role in inflammasome-dependent immune activation as many DAMPs are released from cells, which causes the inflammation to propagate to the surrounding. In addition to inflammation, pyroptosis destroys the replicative niche of intracellular bacteria and thereby exposes them to the extracellular milieu where they are primarily killed by neutrophils [254, 255].
Another hallmark of pyroptosis is caspase-1-dependent cleavage and release of interleukin (IL)-1β and IL-18 [256]. IL-1β and IL-18 potently induce inflammation and recruit additional immune cells to the site of infection. Moreover, IL-18 leads to T and NK cell-dependent IFN-γ production [257].
Recently, Gasdermin-D has been discovered as the main driver of pyroptosis [258–260]. Caspase-1-dependent Gasdermin-D cleavage at aspartate D276 produces N-terminal Gasdermin-D fragments that form membrane pores, which result in cell lysis [261–264]. More importantly, Gasdermin-D is specific to pyroptosis given that only caspase-1, and not apoptotic caspases, efficiently cleaves Gasdermin-D. Moreover, a few N-terminal Gasdermin-D fragments already induce pyroptosis [258–260]. Interestingly, *Gsdmd*-deficient cells still induce pyroptosis at later time points after inflammasome activation suggesting that there is another mediator of inflammasome-dependent pyroptosis besides Gasdermin-D [259].
As inflammasome activation induces a strong immune response, ligand recognition and inflammasome assembly are tightly controlled. Importantly, deregulated

inflammasome signaling is associated with a variety of autoimmune and autoinflammatory diseases, as well as an increased susceptibility to pathogenic infections, making them a primary target for current research in innate immunity [249, 255]. In the next sections, the different inflammasome components and their regulation are discussed in more details.

1.4.1 Inflammasome receptors

NLRC4

With respect to receptor activation, NLRC4 is the best-studied inflammasome (Figure I.3). NLRC4 has been identified to respond to bacterial flagellin [137, 265, 266], however the needle and rod subunit of the bacterial type III secretions system (T3SS) also activate NLRC4 [267, 268]. Interestingly, NLRC4 does not directly bind its ligands via leucin rich repeats as described for TLRs, but uses upstream sensors, so-called NAIPs, that have the ability to directly bind NLRC4 activators [269]. In mice, NAIP1 recognizes the T3SS needle protein, NAIP2 the T3SS rod protein and NAIP5/6 flagellin [268, 270]. Humans only have one NAIP that recognizes the T3SS rod protein [271]. However, it has been reported that a second isoform called NAIP* exists in humans and this isoform recognizes bacterial flagellin instead of the T3SS rod protein [272].

Besides the characterization of the exact ligands, structural analyses of NLRC4 activation has resolved the receptor complex induced after ligand recognition. NLRC4 is structured in leucin rich repeats (LRRs), a central NOD oligomerization domain and a CARD domain. Under steady state conditions, the LRRs inhibit NLRC4 by masking the central NOD oligomerization domain [273]. NAIP ligand binding induces a conformational change in NAIP, which enables NAIP to serve as nucleation surface for NLRC4 activation. NLRC4 forms a wheel- or disk-like structure and its assembly works like the domino effect. The initially activated NAIP and every newly activated NLRC4 in the growing receptor protomer serves as new nucleation surface for the next NLRC4 molecule. Importantly, activated NAIPs cannot activate a second NAIP protein, therefore the resulting NAIP-NLRC4 protomer contains one single NAIP and 9-11 NLRC4 molecules [274–276]. On top of the NAIP-NLRC4 protomer, the NLRC4 CARD domains recruit ASC leading to ASC oligomerization. In contrast to NLRPs, NLRC4 can directly recruit caspase-1 through its CARD domain. However, as this caspase-1 recruitment is sufficient for cell death, IL-1β release is completely ASC-dependent [277].

NLRC4 activation is not only ligand-dependent but also relies on post-translational modifications. It has been shown that NLRC4 phosphorylation at S533 in the NOD domain by protein kinase C (PKC) is important for NLRC4 activation in response to *Salmonella* but not *Shigella* infections [278, 279]. How this phosphorylation influences the activation of NLRC4 and why this only works for *Salmonella* but not *Shigella* remains unclear.

Taken together, NAIPs bind bacterial ligands to induce an NLRC4 inflammasome to fight bacterial infections. The conformational switch from auto-inhibited to the active NLRC4 protomer is the major regulatory step in NLRC4 inflammasome activation. Thus, interfering with NLRC4 auto-inhibition might lead to a constitutive active NLRC4, resulting in sustained inflammation. Indeed, gain of function mutations resulting in a constitutive active NLRC4 cause a recurrent autoinflammatory disease called macrophage activation syndrome (MAS) [280–282].

NLRP3

NLRP3 is by far the most studied inflammasome receptor and consists of LRRs, a central NOD oligomerization domain and an effector pyrin (PYD) domain (Figure I.3). NLRP3 has been discovered as inflammasome receptor in the context of bacterial infections [140]. Today, more than 30 different PAMPs and DAMPs are known to activate NLRP3, including uric acid crystals, silica, asbestos, alum, extracellular ATP, pore-forming toxins, dysfunctional mitochondria, phagosomal damage, RNA-DNA hybrids as well as several viral, bacterial, fungal and protozoan pathogens [249,250]. As these triggers are very diverse, it is still unclear how NLRP3 recognizes all these different stimuli. However, it has been shown that almost all NLRP3 activators induce the release of intracellular potassium [283]. Therefore NLRP3 can be seen as a "guardian" of cell integrity. Nevertheless, whether NLRP3 directly senses low levels of intracellular potassium or whether another sensor is required for NLRP3, remains unknown. Over the years, several proteins including GBP5, PKR and SHP have been shown to directly bind to and influence NLRP3 inflammasome activation [284–286]. However, the involvement of GBP5 and PKR in NLRP3 activation could not be reproduced in other studies [287, 288]. Thus it is questionable at the moment whether these identified proteins influence NLRP3 activation or not.

Recently, three independent groups have reported a critical role for NIMA-related kinase 7 (NEK7) in NLRP3 oligomerization downstream of potassium efflux [289–291]. Moreover they have shown direct interaction between NEK7 and NLRP3. Whether NEK7 is the potassium efflux sensor and the initiator of NLRP3 oligomerization in a similar way to NAIP proteins in the NLRC4 inflammasome has not been adressed by these studies and could shed light on how NLRP3 is activated.

Besides NLRP3 regulation through direct interaction partners, NLRP3 activation is regulated by posttranslational modifications. TLR signaling upregulates the expression of NLRP3 and induces NLRP3 deubiquitination by the Lys63-specific deubiquitinase BRCC3, which is critical for NLRP3 activation [292].

A better understanding of the activation and regulation of NLRP3 is especially important as NLRP3 is associated with many autoinflammatory and autoimmune diseases [293]. NLRP3 mutations are found in cryopyrin-associated periodic syndroms (CAPS), where NLRP3 mutations lead to NLRP3 hyperactivation which results in recurrent fever and inflammation [294, 295]. Another autoinflammatory

disease where metabolic changes lead to the deposition of uric acid (MSU) crystals in the joints, is gout [296]. These MSU crystals activate the NLRP3 inflammasome, which causes severe joint inflammation and pain [297]. Moreover, type 2 diabetes is associated with NLRP3 activation, which leads to obesity-induced inflammation and cell death of pancreatic β-cells. As a consequence, these patients get glucose tolerant and insulin insensitive [298, 299].
Taken together, NLRP3 is activated by more than 30 different PAMPs and DAMPs, which are all related to the metabolic state of the cell. Even though a lot of research has been directed to the discovery of the NLRP3 activation mechanism, it is still unclear how NLRP3 senses all these different stimuli and what the structure of an activated NLRP3 receptor complex is. However, understanding the NLRP3 activation mechanism and the composition of the NLRP3 inflammasome complex is of particular importance as NLRP3 is involved in many autoinflammatory and autoimmune diseases.

AIM2

AIM2 recognizes cytosolic and microbial double stranded DNA (dsDNA) [162–164] and plays therefore an important role in the host defense against various viruses and intracellular bacteria such as *Listeria* or *Francisella* (Figure I.3) [300–303]. AIM2 has a N-terminal pyrin (PYD) and a C-terminal HIN200 domain but lacks a NOD domain for self-oligomerization [165]. Therefore AIM2 activation is fundamentally different compared to activation of NLRC4, and the receptor complex formed by AIM2 most likely differs from the wheel-like shape of the NAIP-NLRC4 complex. The HIN200 domain binds to four base pairs in the big DNA groove and several HIN200 domains form filaments around dsDNA [304]. The long linker between the HIN200 and PYD domain suggests that the PYD domains from several DNA-bound AIM2 molecules form a PYD complex that serves as starting point for ASC oligomerization [165, 304].
AIM2 is not only activated during pathogenic infections, but is also involved in cancer development. Reduced cellular AIM2 levels are associated with prostate or colorectal cancer development. Cancer cells are thought to have a discontinued nuclear envelope as a result of their high division rate. As a consequence of a discontinued nuclear envelope, cytosolic AIM2 has access to nuclear DNA and thereby would induce inflammasome-dependent cancer cell death [305–308]. In addition, increased AIM2 expression is associated with autoimmune diseases like psoriasis, abdominal aortic aneurysm and systemic lupus erythematosus [309–311]. As shown for psoriasis, it is very likely that the different autoimmune diseases are linked to the recognition of self-DNA in the cytosol [311].
Taken together, AIM2 recognizes cytosolic dsDNA in the context of viral and bacterial infections. Moreover, AIM2 is involved in cancer development and autoimmune diseases, most likely through the recognition of mislocalised self-DNA in the cytosol [312].

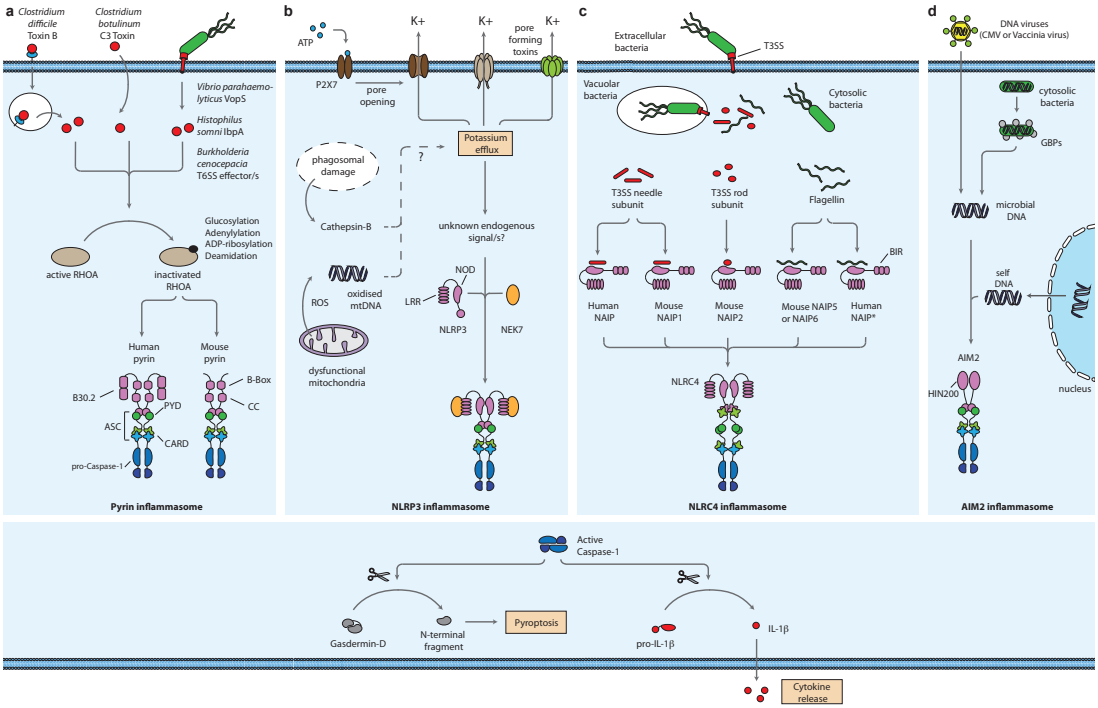

Figure I.3 Overview of canonical inflammasome activation. Activated canonical inflammasome receptors recruit the adaptor molecule ASC, which oligomerizes and forms a large multiprotein complex called the ASC speck. The ASC speck then recruits pro-caspase-1, which is activated by auto-proteolysis. Active caspase-1 cleaves Gasdermin-D and processes the cytokines pro-IL-1β and pro-IL-18 to their mature form. The N-terminal Gasdermin-D fragment induces pyroptosis, a lytic form of cell death, and thereby releases IL-1β and IL-18. (**a**) Pyrin is activated upon dephosphorylation, which result from bacteria-induced RHOA inactivation. (**b**) NLRP3 is activated by over 30 different stimuli, which results in a decrease in intracellular potassium. NLRP3 activation requires NEK7 binding. (**c**) NAIP proteins directly recognize flagellin, and the needle and rod subunit of the bacterial T3SS. The activated NAIP recruits and activates NLRC4 (**d**) AIM2 recognizes cytosolic host or microbial double stranded DNA (dsDNA). T6SS, Type 6 secretion system; PYD, pyrin domain; CARD, Caspase recruitment domain; CC, coiled coil; P2X7, P2X purinoceptor 7; ROS, reactive oxygen species; mtDNA, mitochondrial DNA; LRR, Leucin rich repeat; NOD, Nucleotide-binding oligomerization domain; NLRP3, NACHT, LRR and PYD (NLR)-containing protein 3; NEK7, NIMA-related kinase 7; T3SS, Type 3 secretion system; NAIP, NLR family, apoptosis inhibitory protein; BIR, Baculovirus inhibitor of apoptosis protein repeat; NLRC4, NACHT, LRR and CARD-containing protein 4; CMV, Cytomegalovirus; GBP, Guanylate binding proteins; AIM2, Absent in melanoma 2; IL, Interleukin. *Adapted from Broz and Dixit* [249].

Pyrin

Pyrin (also called TRIM20) is encoded by the *MEFV* gene [249] and is structured in a pyrin (PYD) domain, two B-boxes and one coiled coil domain in mice. In contrast

to mice, human pyrin contains a C-terminal B30.2 domain (Figure I.3). Mutations in this B30.2 domain are associated with the autoinflammatory disease Familial Mediterranean Fever (FMF) in humans. Two independent groups have reported that pyrin acts as a negative regulator of other inflammasomes, as FMF is induced by loss of function mutations in the B30.2 domain [313, 314]. Indeed supportive data for this hypothesis was published in 2015 showing direct interaction of pyrin with NLRP1 and NLRP3 via B30.2 domain. This interaction leads to autophagic degradation of the proteins, which inhibits the inflammasomes [315]. However, a second hypothesis to explain the FMF phenotype has been proposed on the observations that gain of function mutations in the B30.2 domain lead to excessive caspase-1 activation and IL-1β release [316]. Data supporting the second hypothesis was published in 2014 showing that pyrin itself forms an inflammasome [317]. Therefore, it is very likely that FMF results from a constantly activated pyrin inflammasome due to gain of function mutations in the B30.2 domain rather than loss of NLRP1 and NLRP3 inhibition [317].

Even though it was shown in 2014 that pyrin activates an inflammasome, its activation mechanism was under debate. It has been shown that pyrin recognizes the inactivation of RHOA, which is a member of the small GTPase family responsible for actin polymerization. RHOA inactivation occurs through RHOA modifications induced by bacterial Clostridium difficile toxin B or effector proteins of the bacterial T6- and T3SS [317, 318]. Interestingly, pyrin does not recognize inactivation of RAC or CDC42, two close homologs of RHOA. Moreover, it has been reported that pyrin and ASC are localized to actin rich regions. In addition, pyrin has been shown to detect aberrations in actin depolymerization as a result of RHOA inactivation [293, 319]. Given that pyrin gets activated irrespective of the type of RHOA modification and localizes to actin [317], it is likely that instead of direct RHOA modification sensing, pyrin detects downstream consequences of RHOA inactivation related to altered actin dynamics. As mouse and human pyrin detect RHOA inactivation and mice are lacking the B30.2 domain, it is unlikely that this domain is responsible for actin-dependent pyrin activation.

In 2016, Park and colleagues resolved the activation mechanism of pyrin [320]. Under steady state conditions, pyrin is phosphorylated by kinases downstream of RHOA, which enables 14-3-3 protein binding and thereby pyrin inhibition. Upon bacterial infections, their effectors or toxins inactivate RHOA, which consequently results in pyrin de-phosphorylation and thereby its activation. In line with these observations, S242A gain of function mutations are associated with another pyrin-related autoinflammatory disease called pyrin-associated autoinflammation with neutrophilic dermatosis [321].

Taken together, pyrin is inhibited through constant phosphorylation by downstream kinases of RHOA. Upon bacteria-induced RHOA inactivation, pyrin phosphorylation is blocked and therefore it can assemble an inflammasome. However, it remains unclear what role the B30.2 domain has in inflammasome activation and induction of autoinflammatory diseases like FMF and pyrin-associated autoinflammation with neutrophilic dermatosis.

1.4.2 ASC

The apoptosis associated speck-like protein containing a CARD (ASC) consists of two domains, namely CARD and pyrin (PYD) [322]. All activated inflammasome receptor protomers generate a nucleation site for ASC recruitment and oligomerization. ASC recruitment to the receptor oligomer happens through PYD-PYD homotypic interactions with the PYD domains of NLRP1, NLRP3, AIM2 and pyrin [323, 324]. Once ASC has been recruited by the receptor oligomer, the ASC PYD domains form long three start helical filaments, while the CARD domains on the surface of the PYD filaments serve as recruitment domains for caspase-1. In addition, the ASC CARD domains nucleate the different ASC PYD filaments into a single, macromolecular complex called the ASC speck [277, 325]. Mutations in the PYD domain that abrogate filament formation are completely deficient in cell death and IL-1β release, thereby highlighting the importance of ASC speck formation for inflammasome signaling [277, 325].
Regarding NLRC4, the situation is a bit different, as NLRC4 possesses a CARD instead of a PYD domain. Therefore, activated NLRC4 can directly recruit and activate caspase-1. Indeed cell death is not diminished in *Asc*-deficient compared to wild-type macrophages when treated with NLRC4-specific activators [252, 266], however IL-1β release is dramatically reduced. This shows that the ASC speck is essential for efficient caspase-1 activation and IL-1β release [252, 266]. Most likely, the first ASC bind to the CARD domain of NLRC4 thereby providing its PYD domain for ASC oligomerization. This is supported by a paper of Dick and colleagues, who have shown that caspase-1-dependent Gasdermin-D cleavage as a prerequisite for cell death is not affected in *Asc*-deficient macrophages, while IL-1β cleavage is dramatically reduced [277]. Thus, the ASC speck enables signal amplification from small and local ligand concentrations to the production of large amounts of active cytokines. In the case of NLRC4 activation, one ligand molecule bound to one NAIP protein induces a robust immune response [249].
As ASC oligomerization is such a potent inducer of inflammation, ASC activation is tightly regulated. For example, ASC is phosphorylated by SYK and JNK at multiple sites and this phosphorylation is required for caspase-1 activation [326, 327]. Moreover, IKKα acts as a negative regulator of ASC oligomerization by localizing ASC to the nucleus and thereby sequestering ASC away from the inflammasome receptors in the cytosol. IKKα-dependent ASC phosphorylation is required for IKKα binding to ASC [328]. Besides ASC phosphorylation, a recent report has shown critical ASC deubiquitination by USP50 for ASC speck formation [329]. In addition to mice, humans express pyrin only proteins (POPs) that bind to ASC and inhibit ASC speck formation [330–332].
Taken together, inflammasome receptor-dependent ASC oligomerization induces the formation of a cytosolic complex called ASC speck. The ASC speck efficiently

activates caspase-1 to produce large amounts of mature IL-1β and IL-18. To regulate ASC speck formation, various post-translation modifications have been described. However, it is still unclear what components are part of the ASC speck; except ASC, the inflammasome receptor and caspase-1. Thus the ASC speck serves as signal amplification step to transform a local, small amount of ligand into a global immune response.

1.4.3 Caspase-1

The term caspase was first introduced in 1996 where the "C" refers to cysteine protease and "aspase" to the ability to cleave proteins after an aspartate [333]. However, today caspase is better known for Cysteine-dependent aspartate-directed protease. Caspases are divided into two groups: apoptotic and inflammatory caspases. Apoptotic caspases are involved in the execution of a immunologically silent form of cell death called apoptosis. They include the initiator caspase-2, -8, -9 and -10 and the executioner caspase-3, -6 and -7. Inflammatory caspases include caspase-1, -4, -5, -11 and -12 in humans, where caspase-11 is expressed in mice and caspase-4 and -5 in humans only [334]. All inflammatory caspases except for caspase-12 are activated by known inflammasomes [139]. However, we cannot exclude that caspase-12 is activated by a yet to be discovered inflammasome.
In 1989, caspase-1 was first described to cleave IL-1β into its active form, therefore it was initially named IL-1β-converting enzyme (ICE) [335,336]. Caspase-1 is expressed as an inactive pro-form and contains a CARD domain. The ASC speck recruits pro-caspase-1 via CARD-CARD interactions, bringing two pro-caspase-1 molecules into close proximity. Consequently, pro-caspase-1 is auto-proteolytically cleaved into the CARD, p20 (including the catalytic cysteine) and p10 subunit. Active caspase-1 dissociate from the ASC speck and forms a heterodimeric cysteine protease that is composed of two p20 and two p10 subunits [252,256]. Caspase-1 has two main functions in cells. On one hand, caspase-1 induces pyroptosis through the cleavage of Gasdermin-D and on the other hand processes the cytokines pro-IL-1β and pro-IL-18 into their mature form. Interestingly, even though the active cysteine of caspase-1 is essential for both pyroptosis and cytokine processing, a caspase-1 uncleavable mutant still induces pyroptosis but not cytokine processing [252].
Taken together, inflammasomes activate caspase-1, which cleaves intracellular substrates including Gasdermin-D, IL-1β and IL-18. Thus, caspase-1 executes pyroptosis and activates IL-1β and IL-18, both leading to the propagation of the immune response.

1.4.4 Interleukin-1β / Interleukin-18

The interleukin (IL) family is composed of 11 soluble members: IL-1α, IL-1β, IL-1 receptor agonist (IL-1Ra), IL-18, IL-33 and IL-1F5, -6, -7, -8, -9 and -10 [337]. IL-1 family members have a huge impact on immune response progression and are the main drivers of inflammation.
The best characterized IL-1s are IL-1β and IL-18, which propagate inflammation by binding to and thereby activating the plasma membrane receptors IL-1 receptor 1 (IL-1R1)/IL-1 accessory protein (IL-1RAP) and IL-18R/IL-18RAP, respectively. IL-1R1/IL-18R signaling activates the NF-κB and MAPK pathway in a MYD88-dependent manner, which induces the expression of pro-inflammatory genes as described in chapter I, section 1.2.1. Interestingly, whereas IL-1α, IL-33 and IL-1Fs are expressed as active molecules, IL-1β and IL-18 are expressed as an inactive pro-form. To obtain the active cytokines, pro-IL-1β and pro-IL-18 are cleaved by caspase-1 upon inflammasome activation [139, 338].
All IL-1 family members, except for IL-1Ra, are expressed without a classical signal peptide for ER/Golgi-dependent secretion [339]. Therefore, it is unclear through which mechanism the IL-1 cytokines are released from cells. IL-1β and IL-18 are shown to be secreted in a caspase-1-Gasdermin-D-dependent manner as IL-1β secretion but not IL-1β processing is impaired in *GsdmD*-deficient cells [258, 260]. Thus it might be that the IL-1 cytokines are passively released upon inflammasome-dependent cell death.
Given that IL-1β and IL-18 are potent pro-inflammatory cytokines, they are regulated at many stages. First, they are expressed in an inactive pro-form and require inflammasome-dependent maturation. Second, IL-1Ra competes with IL-1β for IL-1R binding, whereas IL-R2 binds to IL-1RAP at the plasma membrane and thereby sequestering IL-1RAP from IL-1R1 [340, 341]. Third, IL-18 binding protein (IL-18BP) competes with IL-18 for IL-18R binding [342]. In all three cases, IL-1β and IL-18 receptor signaling is blocked and therefore prevents inflammation to propagate.
Many auto-inflammatory diseases, including different forms of arthritis, various inflammatory skin diseases, multiple sclerosis, systemic lupus erythematosus, asthma, Crohn's disease and ulcerative colitis, are associated with either elevated levels of active IL-1β and IL-18 in the circulation or excessive IL-1R signaling, [339]. Thus, there is an urgent need to better understand inflammasome activation, which could lead to the identification of mechanisms to block or decrease IL-1β and IL-18 maturation and thereby interfering with these severe and persistent diseases.

1.4.5 The non-canonical inflammasome

In contrast to the previously described canonical, caspase-1-activating inflammasomes, a non-canonical inflammasome was discovered in 2011 and was shown to ac-

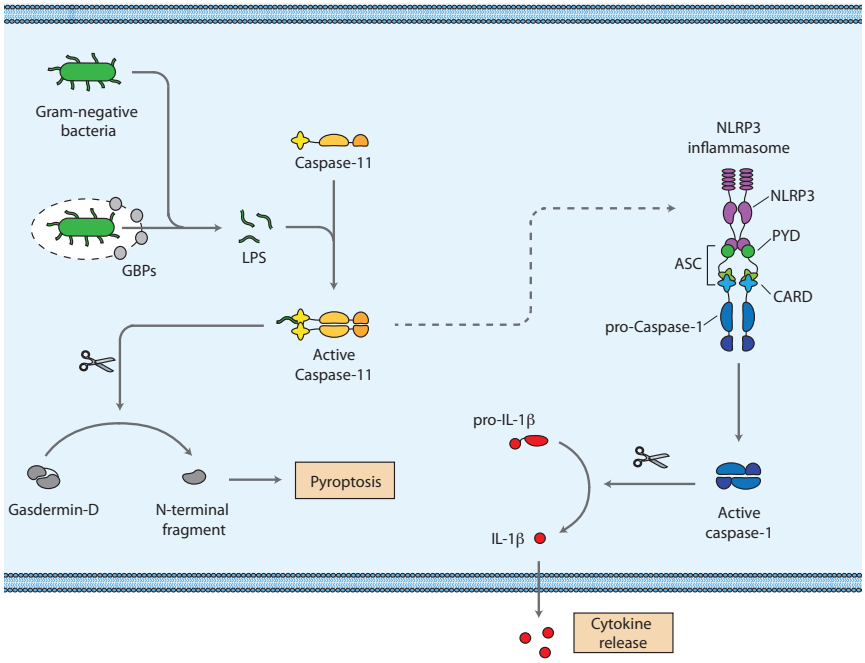

Figure I.4 Overview of the non-canonical inflammasome activation. Caspase-11 is activated by direct binding of bacterial LPS. Active caspase-11 cleaves Gasdermin-D. The N-terminal Gasdermin-D fragment induces pyroptosis, a lytic form of cell death. GBPs facilitate caspase-11-dependent LPS recognition from vacuolar bacteria such as *Salmonella*. Moreover, caspase-11 activates the canonical NLRP3 inflammasome, which lead to caspase-1 activation and consequently IL-1β and IL-18 maturation and release. LPS, Lipopolysaccharide; PYD, pyrin domain; CARD, Caspase recruitment domain; NLRP3, NACHT, LRR and PYD-containing protein 3; GBP, Guanylate binding protein; IL, Interleukin. *Adapted from Broz and Dixit* [249].

tivate caspase-11 in mice (or caspase-4/-5 in humans) (Figure I.4) [343]. Caspase-11 activation is the main driver of bacteria-induced septic shock and thus LPS-induced lethality, which is a major cause of death worldwide [258, 259, 344, 345]. In contrast to receptor-dependent caspase-1 activation, caspase-11 activation requires direct binding to intracellular LPS [346]. Active caspase-11 cleaves Gasdermin-D but not IL-1β or Il-18, thereby inducing cell death but not cytokine release. However, caspase-11 activates the canonical NLRP3 inflammasome, which then processes IL-1β and IL-18 through caspase-1 activation. Caspase-11-dependent NLRP3 activation requires potassium efflux, which is most likely induced by caspase-11-dependent cell death [343, 347–349]. Moreover, caspase-11 is transcriptionally activated by TLR signaling. In the context of a bacterial infection, expression of interferon-stimulated genes is required for caspase-11-dependent recognition of cytosolic LPS [350, 351]. As described in research article IV in chapter V, section 1, we show that IFN signaling induces the expression of guanylate binding proteins (GBPs), which in turn exposes bacterial LPS to caspase-11 in the cytosol [288]. However the exact mechanism of LPS presentation to caspase-11 is not fully understood.

Taken together, caspase-11 activation upon cytosolic LPS binding induces the non-canonical inflammasome, which is the main driver of septic shock, a major contributor to bacteria-induced lethality worldwide. However, it is still not fully understood how LPS activates caspase-11 in vivo. For a better understanding of septic shock, it is essential to study the mechanism of LPS presentation to caspase-11 in more details. Notably, mice are six orders of magnitude more resistant to septic shock than humans due to lower LPS sensitivity [352]. Thus, results from murine septic shock models require careful considerations when conclusions are drawn and translated to humans.

2 Intracellular bacterial pathogens

As described in chapter I, section 1.1, innate immune cells are one of the first detectors of invading pathogens and have the ability to efficiently kill them. As described in chapter I, section 1.2, innate immune cells are equipped with pattern recognition receptors (PRRs) to detect invading pathogens and to induce an immune response.
Monocytes, tissue-resident macrophages and neutrophils are professional phagocytes and efficiently kill bacterial pathogens. Upon surface receptor-dependent bacterial recognition, these three innate immune cell types take up bacteria, a process that is called phagocytosis [10]. Phagocytosis encloses the bacteria in a host-derived vacuolar compartment called the phagosome, which subsequently matures into a phagolysosome through lysosomal fusion events. Lysosomes contain bactericidal proteases like cathepsins, which are exposed to the bacteria after phagosomal fusion and thereby degrade the contents of phago-lysosomes, such as internalized pathogens [353]. Moreover, along the maturation process, the phagosome acidifies to a pH of around 5.5 by the V-ATPase, which pumps protons into the phagosome. Phagosomal acidification not only inhibits pathogen growth, but also enhances the killing capacity of lysosomal molecules and provides substrates for the generation of reactive oxygen species (ROS) [354].
The nicotinamine adenine dinucleotide phosphate oxidase (NADPH oxidase) complexes incorporate into the phagosomal membrane and produce short-lived reactive oxygen species (ROS), such as O_2^- [33]. In the phagosome, O_2^- is converted by superoxide dismutase and myeloperoxidase into hydrogen peroxide (H_2O_2) and hypochlorous acid (HOCl), respectively [353,355]. ROS are powerful oxidants that cause DNA, membrane lipid and protein damage thereby harming the bacteria [33]. Reactive nitrogen species (RNS) are another radical class that are produced in phagosomes. They are generated by the inducible nitric oxide (NO) synthase (iNOS), which produces NO. NO is further transformed into peroxynitrate ($ONOO^-$) upon reaction with ROS [356]. RNS interfere with DNA replication and inactivate zinc- and metalloproteins, thereby inhibiting bacterial duplication and respiration, respectively [356].
In addition to ROS and RNS production, phagosomes acquire bactericidal metals such as copper and zinc [357].
Additionally, in neutrophils, antimicrobial peptides (AMPs)-containing granules fuse with phagosomes. AMPs are a diverse group of molecules, which target bacterial membranes to induce bacteriolysis. They include defensins, cathelicidins, endo- and exopeptidases, lysozymes, cathepsins and matrix metalloproteases [353].
Even though the phagosome is very efficient in bacterial killing, intracellular bacteria such as *Salmonella* or *Mycobacterium* have developed diverse mechanisms to resist or avoid killing within phagosomes and they can even remodel the phagosome into a replicative niche. In these cases, phagocytes can sequester important bacterial nutrients like essential amino acids or iron away from the phagosome and

thereby inhibit or decrease intracellular bacterial replication [33,358].
Escape from the phagosome into the cytosol of phagocytes might seem an ideal solution to avoid phago-lysosomal degradation, yet only a minority of intracellular bacterial pathogens uses this strategy. The reason for this is most likely that the cytosol features many additional bacterial killing mechanisms as well as many pattern recognition receptors that alert cells of bacterial presence, and even might induce host cell death. For example it has been shown that phagocytes sequester nutrients in cellular compartments that are not accessible for the bacteria, thereby reducing bacterial replication [358]. Furthermore, bacterial replication is restricted by autophagy, an intracellular protein degradation process that can also engulf cytosolic bacteria in a process called xenophagy. Xenophagy is initiated by autophagy cargo receptors that recognize ubiquitin chains, which are added to the bacterial surface by cytosolic ubiquitin ligases [359]. Moreover, autophagy cargo receptors recognize galectin-8, which binds to β-galactosides that are exposed to the cytosol upon phagosomal damage. Xenophagy-dependent bacterial engulfment results in autophagosome formation, which then fuses with lysosomes to kill the engulfed bacteria.
Another cytosolic bacterial killing mechanism is mediated by GBP-dependent bacterial lysis and described in great details in research articles IV and V in chapter V, section 1. Moreover, inflammasome activation results in cell death and thereby destruction of the bacterial replicative niche and consequently the exposure of the bacteria to other innate immune cells [251,254].
Taken together, phagocytes are the most potent bacterial killers of the innate immune system. They are equipped with an arsenal of mechanisms to eradicate bacteria. However, bacteria have developed mechanisms to interfere with the cellular killing machineries by either resisting the applied stress, actively neutralizing the bactericidal molecules or blocking the induction of the cellular killing machinery to use phagocytes as replicative niche. In the next sections, two bacterial pathogens and their different approaches to use phagocytes as their replicative niche are described in more details.

2.1 *Salmonella*

Salmonellae are Gram-negative, intracellular bacteria with a wide host range. The species *Salmonella enterica* includes more than 2500 serovars distinguished by their LPS and flagellar antigens [360,361]. *Salmonella enterica* subsp. *enterica* serovars account for most of the *Salmonella*-associated health problems and induce three distinct diseases in humans: typhoid fever, gastroenteritis and bacteremia.
Salmonella enterica subsp. *enterica* serovar Typhi (hereafter *S.* Typhi) and Paratyphi are human-restricted pathogens and cause the systemic disease typhoid fever [360,361]. More than 20 Million cases of typhoid fever are counted annually resulting in more than 400'000 deaths per year [362].
In contrast to *S.* Typhi, non-typhoidal *Salmonella* (NTS) serovars Enteritidis and Typhimurium (hereafter *S.* Typhimurium) are the major causes of gastroenteritis in immunocompetent and bacteremia in immunocompromised humans. Around 90 Million humans suffer from NTS-induced gastroenteritis with around 150'000 deaths annually [363], whereas NTS-induced bacteremia is commonly observed in HIV-positive adults or African children already burdened by malaria or malnutrition. Out of 100'000 children in Sub-Saharan Africa, 300 develop NTS bacteremia with 200'000 child deaths annually [364,365]. Thus, the overall *Salmonella* burden combining typhoid fever, gastroenteritis and bacteremia leads globally to a Million deaths a year. This mortality rate is most likely an underestimate as exact numbers from the rural African areas are missing and all healthy 16 month old children in Malawi have detectable *Salmonella*-specific antibodies, indicating an universal exposure of new born children to *Salmonella* in Africa [363,366].
Salmonella infections are mostly associated with poor hygiene standards, as *Salmonella* infects humans orally by contaminated food or water. Once in the small intestine, NTS and typhoidal *Salmonella* differ in their dissemination. Importantly, NTS-induced gastroenteritis is restricted to acute intestinal inflammation without dissemination beyond the gastrointestinal tract, whereas NTS-induced bacteremia and *S.* Typhi-induced typhoid fever is a chronic infection associated with bacterial dissemination beyond the gastrointestinal tract.
In the case of NTS-induced gastroenteritis, a small proportion of luminal *S.* Typhimurium induces their uptake into epithelial cells of the small intestine by using the *Salmonella* pathogenicity island 1 (SPI-1) type 3 secretion system (T3SS-1) or they are taken up by M cells [367]. The T3SS-1 injects an arsenal of effector proteins into epithelial cells to induce actin rearrangement and membrane ruffling, leading to the engulfment and cellular uptake of *S.* Typhimurium [368,369]. Besides inducing bacterial uptake, T3SS-1 effectors actively promote intestinal inflammation by inducing the production of the cytokine IL-8 in epithelial cells [370,371]. As a consequence, IL-8 facilitates transepithelial migration of neutrophils from the lamina propria into the intestinal lumen, where they produce ROS. ROS converts microbiota-derived thiosulfate into tetrathionate, which is used by *Salmonella* but not the microbiota as electron acceptor during anaerobic or microaerophilic growth [372]. Moreover, intestinal inflammation results in the production and

luminal secretion of lipocalin 2. Lipocalin 2 sequesters the microbiota-derived siderophore enterochelin but not the *Salmonella*-derived siderophore salmochelin. Siderophores bind to iron and then are taken up by the bacteria to metabolite iron. Thus, *Salmonella* starve the microbiota from iron [373]. The consequence of *Salmonella*-induced inflammation is a growth advantage of *Salmonella* in the lumen of the small intestine relative to the microbiota, thereby subsequently outcompeting the microbiota.
Once *Salmonella* has penetrated into epithelial cells, it resides in the phagosome and secretes effector proteins of a second T3SS encoded on SPI-2 (T3SS-2) to modify the phagosome into a so called *Salmonella* containing vacuole (SCV) [374]. The SCV modifications include changes in its cholesterol, phospholipid and protein composition [375–378]. In addition, T3SS-2 effectors induce the coupling of the SCV to the microtubule network to enable intracellular movement of the SCV [379, 380]. Moreover, switching from T3SS-1 to T3SS-2 expression has an anti-inflammatory effect. The T3SS-2 reduce the delivery of NLRC4 activators into the cell and T3SS-2 effectors actively block cytosolic pro-inflammatory signaling cascades [381–384]. All these mechanisms help *Salmonella* to establish an intracellular, vacuolar replicative niche to survive in epithelial cells.
Whereas *S.* Typhimurium induces gastroenteritis in immunocompetent humans, *S.* Typhimurium induces severe bacteremia in mice. Therefore, *S.* Typhimurium is used as a mouse model for bacteremia in immunocompromised humans [385]. In NTS-induced bacteremia, *S.* Typhimurium infects the host orally, as seen for NTS-induced gastroenteritis, ending up in the small intestine, where *S.* Typhimurium crosses the epithelial layer and disseminates via the blood stream into multiple organs, such as the liver and spleen [386]. There, *S.* Typhimurium infects macrophages and establishes an SCV as described for epithelial cells.
However, once *S.* Typhimurium has crossed the epithelial layer, it is detectable by soluble components of the innate immune system. Indeed, reactive hydroxyl groups in the O-antigen repeat units of LPS activate the complement component C3 leading to the deposition of C3b on the bacterial surface, which favors bacterial phagocytosis by immune cells [387, 388]. As described in chapter I, section 1, the complement system induces bacteriolysis via insertion of a membrane attack complex into the bacterial membrane. However, *S.* Typhimurium avoids complement-dependent lysis by the expression of long O-antigen chains. The long O-antigens create a physical distance between the deposited membrane attack complex and the bacterial outer membrane, thereby avoiding its destruction [389,390]. Nevertheless, the soluble complement component C5a, which is produced during complement activation, attracts neutrophils to the site of infection and enhances LPS-dependent TLR4 signaling in monocytes, thereby favoring bacterial killing at the infection site [391,392].
Once *S.* Typhimurium has crossed the epithelial layer, it downregulates the expression of flagellin and the T3SS-1, thereby avoiding flagellin-mediated, TLR5-dependent immune activation. Indeed, TLR5 has a minor effect in immune detection of *S.* Typhimurium, whereas TLR2, TLR4 and TLR9 are the major inducers

of inflammation in NTS-induced bacteremia [393, 394]. Furthermore, downregulation of flagellin and the T3SS-1 components PrgJ and PrgI reduces the activation of the NLRC4 inflammasome by intracellular *S.* Typhimurium [267, 395], and thus might specifically serve to avoid detection during the systemic phase of the disease. However, intracellular *S.* Typhimurium LPS still activates the non-canonical inflammasome in a GBP-dependent manner, thus leading to cell death and cytokine maturation [288, 351]. Inflammasome-dependent cell death upon *S.* Typhimurium infection has a beneficial role for the host because cell death destroys the replicative niche of *Salmonella* and exposes the bacteria to neutrophils, which are the most potent bacterial killers [396]. The role of GBPs in non-canonical inflammasome activation is described in research article IV in chapter V, section 1.
In contrast to NTS-induced local, self-limiting gastroenteritis characterized by diarrhea and abdominal pain, *S.* Typhi induces a chronic and relapsing infection called typhoid fever in healthy humans [360, 361]. *S.* Typhi uses the same infection route as *S.* Typhimurium and crosses the epithelial layer in the small intestine to disseminate into the body. However, the first signs of typhoid fever occur around 2 weeks after the initial infection [397, 398]. During the first two weeks of infection, *S.* Typhi evades immune recognition in the small intestine and the blood stream due to several additional virulence mechanism that it has acquired and due to a loss of certain genes that are normally present in gastroenteritis-inducing *Salmonella.* The most important gene acquisition is the viaB locus located on SPI-7, which encodes 10 genes that are important for the regulation, biosynthesis and export of the virulence-associated (Vi) capsular polysaccharide [399, 400]. Vi capsular polysaccharides cover the bacterial surface and have no free hydroxyl groups, therefore the complement system cannot be activated [401]. In contrast to *S.* Typhimurium, *S.* Typhi expresses shorter LPS O-antigens that are entirely shielded by Vi capsular polysaccharides [402]. Moreover, the SPI-7-encoded protein TviA represses T3SS-1 and flagella expression in conditions of low osmolarity that is present in the intestinal mucosa. Therefore *S.* Typhi is becoming stealthy as soon as it transmigrates through the epithelial layer [403, 404]. Besides this major differences between *S.* Typhi and *S.* Typhimurium, effector proteins important in establishing gastroenteritis in *S.* Typhimurium infections are absent or present as pseudogenes in *S.* Typhi, which might contribute to the difference in disease outcome [405, 406].
In summary, *Salmonella enterica* induce gastroenteritis, bacteremia or typhoid fever depending on the serovar and humans health. *Salmonella* infections contribute heavily to the worldwide burden of gastrointestinal diseases and bacteria-caused death, especially in immunocompromised adults and children in the developing world. Thus, understanding the *Salmonella*-host interplay between immune recognition of the host and immune evasion by *Salmonella* might help to develop new approaches for reducing the global burden of *Salmonella* infections. *S.* Typhimurium is a model organism for intracellular, vacuolar bacterial pathogens, especially in the field of innate and cell-autonomous immunity. However, the mouse models established with *S.* Typhimurium do not completely resemble the in vivo situation in humans and besides, mice cannot be infected with *S.* Typhi [407, 408]. Thus the

interpretation of experimental findings done in mice and the resulting conclusions for a human infection require careful consideration.

2.2 *Francisella*

Francisella tularensis is a Gram-negative, intracellular bacterial pathogen; it is highly infectious and causes the zoonotic disease tularemia, which is characterized by fever, aches and signs of toxicity lasting for several days. In humans, the mortality rate of untreated pneumonic tularemia reaches up to 60 % [409]. *Francisella tularensis* is divided into 4 subspecies (subsp.), where subsp. *tularensis* (*F. tularensis*; also known as type A) and subsp. *holarctica* (*F. holarctica*; also known as type B) are the most virulent ones in humans. In contrast to *F. tularensis*, *Francisella tularensis* subsp. *novicida* (*F. novicida*) causes tularemia in immunocompromised humans, however, it is highly virulent in mice [410–412]. Thus *F. novicida* is used as a mouse model to study tularemia. The fourth subspecies is *Francisella mediasiatica* and causes an intermediate disease phenotype in humans [413].
Francisella tularensis transmits by terrestrial and aquatic mammals, amoebae or arthropods; or via inhalation of infectious aerosols. Arthropod transmission is thought to be the dominant route between animals but also between animals and humans [414, 415]. Due to its high virulence, high morbidity and ease of transmission, the US centers for Disease Control and Prevention classified *F. tularensis* as a Tier 1 select agent because of its potential to become a bioterrorist weapon [416]. Upon oral, subcutaneous or pneumonic transmission, *Francisella tularensis* mostly infects phagocytes, where they survive and replicate (Figure I.5) [417]. As *Francisella tularensis* cannot trigger its own uptake, opsonization of *Francisella tularensis* by the complement system helps the bacteria to be taken up by phagocytosis [418, 419]. Even though opsonization favors bacterial uptake, non-opsonized *Francisella tularensis* can be taken up by macrophages with the help of the mannose receptor. Thus, *Francisella tularensis* uses different internalization mechanisms and receptors to get into phagocytes [420]. Interestingly, the bacterial LPS and capsule protect *Francisella tularensis* from complement-induced bacterial lysis despite complement opsonization [421].
Within macrophages, the bacteria-containing phagosome acquires both early and late endosomal markers, such as EEA-1, LAMP-1 and RAB5. However before lysosomal fusion, *Francisella tularensis* escapes from the phagosome into the cytosol, which normally happens between 1-4 hours post entry [422–424]. Phagosomal escape is completely dependent on the *Francisella* pathogenicity island (FPI), as FPI-deficient strains are unable to escape from the phagosome [425–428]. Whereas it is clear that the FPI is crucial for phagosomal escape, there is conflicting data about the triggering signal for phagosomal escape. Two independent groups postulate that phagosomal acidification triggers *Francisella* escape into the cytosol because blocking phagosomal acidification reduces the presence of *Francisella* in the cytosol [429, 430]. However, a third group has shown that phagosomal acidification is not the trigger for bacterial escape [431]. Thus if phagosomal acidification is the trigger for *Francisella* to escape into the cytosol requires clarification. Moreover, it is not understood how the FPI induces phagosomal escape. However it is known that the FPI encodes genes with some homology to a type 6 secretion sys-

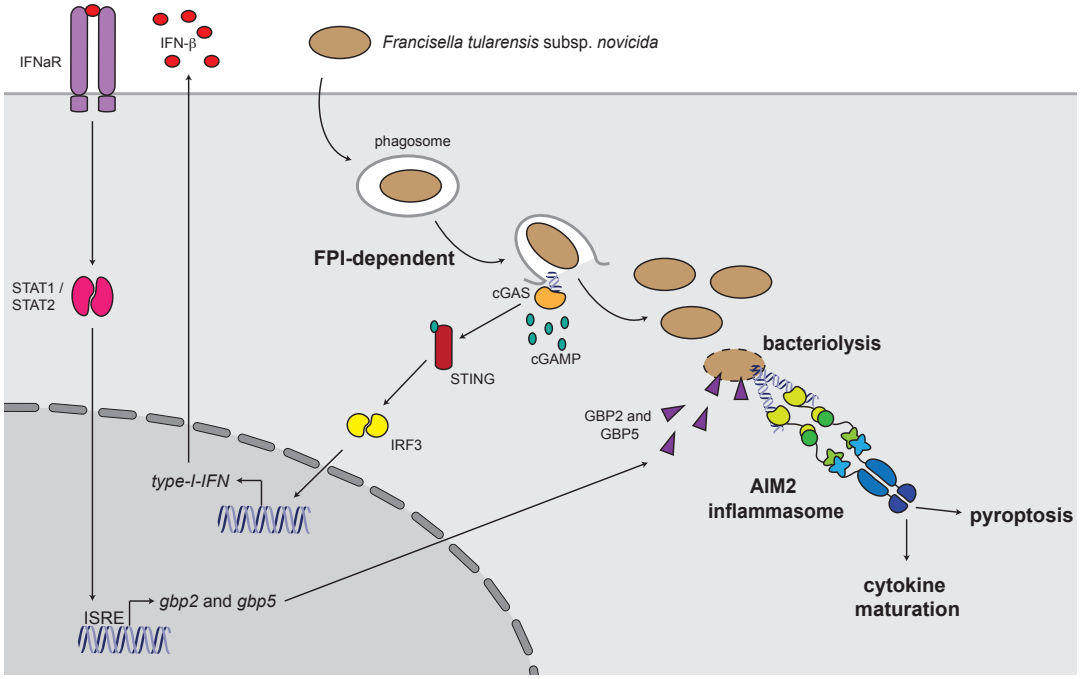

Figure I.5 The *Francisella* infection model. *Francisella tularensis* subspecies survive and replicate in the cytosol of phagocytes, primarily macrophages and dendritic cells. Upon bacterial phagocytosis, *Francisella tularensis* escapes from the phagosome to the cytosol in an FPI-dependent manner. In the cytosol, bacterial DNA is recognized by cGAS, which leads to the production of the cyclic di-nucleotide cGAMP. cGAMP is recognized by STING, leading to IRF3-dependent transcription of type-I-IFN, such as IFN-β. IFN-β then binds to and activates IFNaR, which induces via STAT1/STAT2 heterodimers the expression of ISG, among them GBP2 and GBP5. GBP2/GBP5-dependent bacterial lysis exposes bacterial DNA to the cytosol, where it activates the AIM2 inflammasome. IFN, interferon; IFNaR, IFN α receptor; STAT, signal transducer and activator of transcription; ISRE, IFN stimulated response elements; GBP, Guanylate binding protein; FPI, *Francisella* pathogenicity island; cGAMP, cyclic-GMP-AMP; cGAS, cGAMP synthase; STING, Stimulator of IFN genes protein; IRF, IFN regulatory factor; AIM2, absent in melanoma 2.

tem (T6SS). The potential role and mechanism of the FPI in *Francisella* virulence is described in the next paragraph and in chapter III, section 2.
Even though the FPI is important for *Francisella* intracellular survival despite the host type, certain FPI genes are differentially required for the survival in arthropods, amoebae or mammalian hosts [432, 433]. Besides differential requirement of FPI genes for virulence, the cytosolic site of bacterial replication is distinct in various hosts. Whereas *Francisella* escapes into the cytosol in arthropod and mammalian cells, *Francisella* replicates in intact vacuoles in amoebae [434, 435]. Thus, the FPI is differently used for the infection of various hosts, though the exact mechanisms that regulate host specificity are not fully understood.
In mammals, *Francisella tularensis* largely evades immune recognition through

different mechanisms. Especially while infection establishment during the first 72 hours, the most virulent strain *F. tularensis* suppresses all pro-inflammatory signals [436]. In general, virulence of different *Francisella tularensis* subspecies negatively correlates with the activation of the immune system. *Francisella tularensis* suppresses immune recognition by the expression of a capsule. Indeed, acapsular *Francisella* strains are more sensitive to antibody-mediated killing and attenuated in a guinea pig or mouse infection model [437–440]. The capsule size is between 100-250 kDa and the composition is similar to the repeating O-antigen subunits of *Francisella* LPS [441–443]. As expected from the structural similarity, many enzymes are shared between LPS and capsule biosynthesis, however the capsule is not anchored in the membrane by lipid A as seen for LPS [438, 444, 445].
Besides capsule expression, *Francisella* modifies its LPS to avoid immune recognition. The *Francisella* Lipid A is tetraacylated compared to hexaacylation in most Gram-negative bacteria. In addition, the acyl chains are 16-18 carbons long compared to 12-14 carbons in *E. coli* and the sugar backbone of Lipid A is either non-phosphorylated or mono-phosphorylated. When the sugar backbone is mono-phosphorylated, the phosphate groups are masked by the addition of galactosamines [216, 217, 443, 446–448]. All these LPS modifications diminish the recognition of *Francisella* LPS by TLR4 and thereby no TLR4-dependent induction of pro-inflammatory genes is observed in *Francisella* infections [186, 449]. The only TLR that is activated by *F. novicida* and *F. holarctica* is TLR2 through the recognition of bacterial lipoproteins [450–452].
Besides preventing TLR4 activation, the lack of phosphates on Lipid A changes the overall charge of *Francisella* LPS that gives raise to resistance to antimicrobial peptides (AMPs) [186, 453].
As a consequence of LPS modifications, *F. novicida* does not activate the non-canonical inflammasome because its Lipid A cannot be recognized by caspase-11 [344]. *Francisella* LPS is initially produced with pentaacylated Lipid A and afterwards, one acyl chain is removed by LpxF in the periplasm [446]. Interestingly, pentacylated Lipid A produced by LpxF mutants is recognized by caspase-11 but undetectable by TLR4 [344, 446].
In addition, type IV pili have been shown to be required for full virulence in *F. tularensis*. However, type IV pili phenotypically vary between *Francisella* culture conditions and therefore conflicting data exist about the importance of type IV pili in virulence [454–456].
As mentioned above, *Francisella tularensis* primarily uses the cytosol of phagocytes as replicative niche (Figure I.5). In phagocytes, cytosolic *F. novicida* induces type-I-IFN in a MYD88/TRIF-independent manner indicating that TLR2 signaling from the plasma membrane is not required for this process [457]. Indeed, type-I-IFN is induced by the synergistic recognition of cytosolic DNA by cGAS and IFI16 [167], which signal via STING to induce IRF1/IRF3 translocation into the nucleus and consequently induce type-I-IFNs [457–459]. However, the contribution of IFI16 in *Francisella*-induced type-I-IFN is questionable, as Gray and colleagues have shown that IFI16 is not involved in type-I-IFN production in mice [168]. While the path-

way leading to type-I-IFN is well understood in the context of *F. novicida* infection, it is less clear upon *F. holarctica* infections. *F. holarctica* induces type-I-IFN in a STING- and TLR2-dependent manner [459,460]. How TLR2 and STING signaling regulate type-I-IFN production is currently unknown.
Cytosolic *F. novicida* and *F. holarctica* activate the AIM2 inflammasome, the second immune signaling pathway activated in mice [137,300–302]. Indeed, it has been shown that *F. novicida* and *F. holarctica* neither induce the NLRP1, NLRP3, NLRC4 nor pyrin inflammasome in mice [302,461,462]. To activate the AIM2 inflammasome, type-I-IFN production is absolutely required. We and others have shown that type-I-IFN induces the expression of guanylate binding proteins (GBPs) that target cytosolic *F. novicida*, induce bacteriolysis and consequently the release of bacterial DNA into the cytosol [458,463]. Importantly, GBPs are not required for *Francisella* escape into the cytosol and not required for AIM2 inflammasome assembly [463]. GBP involvement in *F. novicida*-dependent AIM2 inflammasome activation is described in more details in research article IV in chapter III, section V.
Interestingly, another member of the small GTPase family, IRGB10, has been found to be recruited to cytosolic *F. novicida* in a GBP-dependent manner and has shown to be required for AIM2 inflammasome activation [464]. While this indicates that GBPs do not themselves possess membranolytic activity but rather serve as recruitment factors for other proteins (e.g. IRGB10), it is unclear if IRGB10 directly lyses *F. novicida* in the cytosol or itself recruits a yet uncharacterized cytosolic membrane attack complex similar as membrane-deposited C3 in the complement system.
As seen for murine cells, *Francisella* escapes from the phagosome is essential for virulence in human cells, as *F. holarctica* and *F. novicida* mutants deficient for phagosomal escape are completely avilurent [465]. However in contrast to murine cells, *F. novicida*, *F. holarctica* and *F. tularensis* activate NLRP3 in human macrophages and in a Hek293 reconstitution system [466]. Why murine NLRP3 fails to detect *Francisella tularensis* remains unknown.
In addition to the activation of NLRP3 in human macrophages, IL-1β release is decreased in *pyrin*-deficient primary human monocytes infected with *F. novicida* [467], indicating that *F. novicida* activates the pyrin inflammasome as well. Interestingly, pyrin is expressed at functional levels in murine macrophages nevertheless unable to be activated by *F. novicida* [317]. One big difference between human and mouse pyrin is the lack of the C-terminal B30.2 domain in murine pyrin [314]. If the B30.2 domain is responsible for *F. novicida* detection and how the B30.2 domain detects *F. novicida* is not known. Pyrin has been reported to sense bacteria-induced RHOA modifications [317,320]. However it is not reported so far that *Francisella tularensis* uses actin-based motility or expresses Rho GTPase modifiers. Another interesting aspect about pyrin is its cellular expression profile. Fresh human monocytes express pyrin at high levels, while the expression decreases during monocyte to macrophage differentiation. This reduction of pyrin expression correlates with the ability to release active IL-1β in response to *Fran-*

cisella infection [468,469]. Interestingly, macrophage differentiation in the presence of M-CSF maintains *pyrin* expression levels and the capacity to release IL-1β upon *Francisella* infection [467].
Taken together, *Francisella tularensis* activates a limited number of innate immune signaling pathways due to modifications of its LPS and to capsule expression. Moreover, there is a negative correlation between immune detection and virulence. Whereas *F. novicida* activates a robust immune response leading to bacterial clearance in immunocompetent humans, the highly virulent *F. tularensis* is almost not detected by the immune system leading to high mortality rates. One reason for this phenomenon might reside in the bacterial robustness to intracellular stress, as *F. novicida* is more sensitive to H_2O_2-mediated killing compared to *F. tularensis* [470], or in the bacterial sensitivity to GBP-induced lysis. Overall, the highly virulent strain *F. tularensis* does not provide the cytosolic signal to activate NLRP3, AIM2 or pyrin that is necessary for an efficient immune response.

2.2.1 The *Francisella* pathogenicity island

As described above, *Francisella tularensis* virulence relies on phagosomal escape and this is *Francisella* pathogenicity island (FPI)-dependent [422, 426, 428]. The FPI is encoded on a genome sequence of 33 kb, contains 16-18 open reading frames (ORFs) depending on the *Francisella tularensis* strain and represents a low G/C content compared to the rest of the genome, indicating the acquisition over horizontal gene transfer [426, 471]. 16 ORFs of the FPI (FTN_1309 - FTN_1324) are conserved in all sequenced *Francisella tularensis* strains and the FPI is duplicated in three out of four *Francisella tularensis* subspecies (Figure I.6 b) [471,472]. The two FPIs are functionally redundant and *F. tularensis* can tolerate the loss of one copy without substantial virulence defect [473–475]. *F. novicida* has only one identified FPI copy on the genome. However, there is a gene cluster called *Francisella* novicida island (FNI) in the *F. novicida* genome that shows some homology with the FPI, even though functional analysis of this second gene cluster is missing [471, 476].
Bioinformatical analysis of the FPI has identified weak homology of at least 7 FPI genes with type 6 secretion system (T6SS) gene clusters from other bacteria [477]. The bacterial T6SS is a protein secretion system and has been first functionally described in *Vibrio cholerae* in 2006 [478]. Based on homology analysis, the T6SS is thought to originate from bacteriophages [479,480]. T6SSs are present in almost 25 % of all Gram-negative bacteria including *Salmonella*, *Pseudomonas*, *Vibrio* and *Burkholderia* [481,482]. They have a role in virulence, host immunomodulation and interbacterial killing [483–487].
The T6SS composes of a baseplate complex in the bacterial membrane and a contractile injectisome (Figure I.6 a). The baseplate complex is anchored in the bacterial outer membrane by the lipoprotein TssJ, which interacts with TssM (also

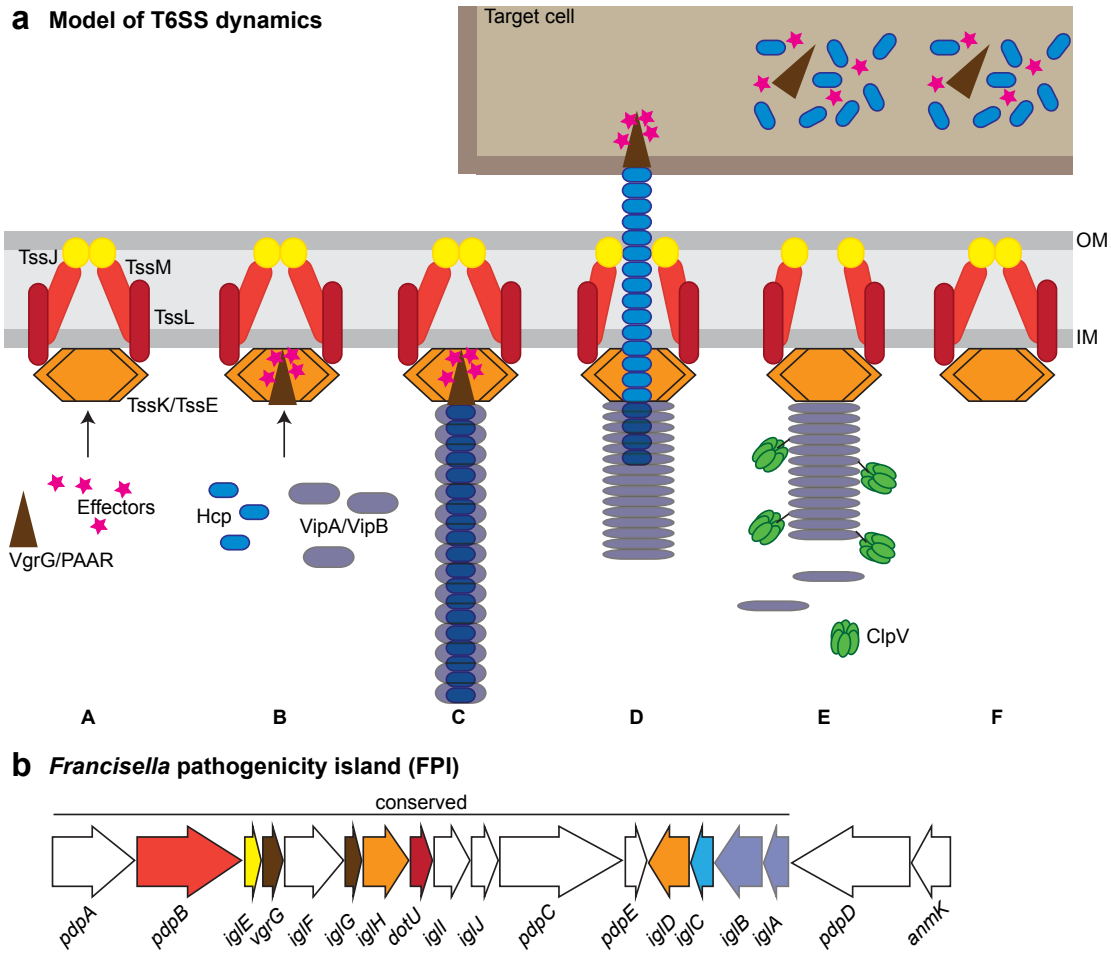

Figure I.6 The *Francisella* pathogenicity island. (**a**) Model of T6SS dynamics. T6SS assembly starts at the baseplate complex (A), which consists of TssJ, TssM TssL, TssK and TssE. The baseplate complex subsequently recruits the tip complex VgrG/PAAR and effector proteins (B), followed by Hcp that forms hexameric rings. Around the Hcp tube a sheath of VipA/VipB is formed (C). Upon a trigger, the T6SS sheath contracts and thereby propels the tip complex, the associated effector proteins and the Hcp tube into the target cell (D). The contracted sheath is then recognized by the unfoldase ClpV (E), which disassembles the sheath and therefore prepares the bacteria for another T6SS assembly (F). (**b**) Genome locus of the *Francisella* pathogenicity island (FPI) of *Francisella tularenis* subspecies *novicida*. The FPI consist of at least 16 genes, which are conserved among all four *Francisella tularensis* subspecies. The genes highlighted in colors show homology with T6SS components explained in (a) and are color-matched. OM, outer membrane; IM, Inner membrane; T6SS, Type 6 secretion system; Tss, Type 6 secretion; VgrG, Valine-glycine-rich repeat protein G; PAAR, Proline-alanine-alanine-arginine protein; Hcp, Haemolysin coregulated protein; ClpV, Caseionlytic protease virulence; Vip, ClpV-interacting protein; Pdp, Pathogenicity determinant protein; Igl, Intracellular growth locus; DotU, Defect in organelle trafficking U.

called IcmF) that is anchored in the inner membrane and spans the periplasm. TssL (also called DotU) is the second baseplate complex protein and is anchored

in the inner membrane, where it interacts with TssM [488–492]. TssM and TssL interact with TssK and TssE, which form the actual baseplate in the bacterial cytoplasm [493]. The T6SS assembly starts with the recruitment of the tip complex to the baseplate (Figure I.6 a). The tip complex is composed of a trimeric VgrG complex and PAAR proteins, which sit on top of the VgrG complex [494–496]. Together, the tip complex forms the arrowhead of the T6SS. At the baseplate, VgrG recruits the inner tube protein Hcp that forms stacking rings of Hcp hexamers with a diameter of 40 A. Therefore the Hcp tube is too small for the delivery of most folded effector proteins as described for type 3- or type 4 secretion systems [479, 480, 497]. Around the Hcp tube, a sheath composed of VipA and VipB is build. Together, Hcp, VipA and VipB form the shaft of the arrow of the T6SS. Interestingly, in vitro studies have shown sheath filament disintegration by ClpV, a Clp family AAA+ adenosine triphosphatase (ATPase) [498, 499]. Clp family members form hexameric rings and unfold proteins by pulling the proteins through their central ring [500].
Basler and colleagues have visualized T6SS dynamics in bacteria showing that a VipA-containing sheath structure extends, contracts, disassembles and reassembles again. T6SS contraction mechanically shortens the T6SS sheath thereby pushing out the inner tube together with the tip complex. Indeed, T6SS contraction is required for Hcp and tip secretion into the supernatant and delivery of tip complex proteins into target cells [501, 502].
Importantly, ClpV only recognizes and disassembles the contracted form of the T6SS sheath [499, 503].
Besides VgrG and PAAR, the T6SS tip complex can contain more proteins, which all show specific effector functions in the target cell. These proteins act as lysozymes, actin modifiers, nucleases, lipidases, muramidases or peptidases [482, 494, 504–506]. Interestingly, structural T6SS components such as VgrG and PAAR harbor domains with effector functions as well [494, 496].
The additional effector proteins bind to and decorate the tip complex or reside within the proximal part of the Hcp lumen, thereby being delivered to the target cell [496, 507]. As the effector proteins could also destroy the T6SS-positive bacteria, they are usually co-expressed together with immunity proteins that inactivate the effectors [504, 505].
T6SS activity is strongly regulated in bacteria, because T6SS expression and assembly is costly. T6SS expression is regulated by transcription factors that are activated for example by quorum sensing, biofilm formation, iron depletion or temperature [508–511]. In addition, bacteria can induce full T6SS activity upon surface sensing or cell-cell contact [499, 501, 512].
Taken together, the T6SS delivers effector proteins into prokaryotic and eukaryotic target cells. The delivery is dependent on T6SS sheath contraction. The contracted sheath is then recognized by ClpV that disassembles the sheath again thereby providing starting material for the assembly of a new T6SS.
As mentioned above, it is speculated that the *Francisella* pathogenicity island (FPI) expresses a T6SS. Over the years the function of many FPI-encoded genes

have been analyzed resulting in conflicting observations regarding their impact on virulence and their potential to express a T6SS. In the next section, the different FPI genes and their potential function in virulence are discussed in more details. As we are only working with *F. novicida* in our lab, the nomenclature of the FPI is based on *F. novicida* as defined by Ludu and colleagues in 2008 (Figure I.6 b) [427].

Pathogenicity determinant protein A (**PdpA**; FTN_1309) shows no homology with known T6SS gene. It is involved in virulence as *F. novicida pdpA* mutants (*F. novicida* Δ*pdpA*) show reduced growth in primary murine bone marrow-derived macrophages (BMDMs) and J774 macrophages compared to wild-type *F. novicida*. Moreover, *F. novicida* Δ*pdpA* is avirulent in a chicken embryo infection model [513, 514]. Interestingly, *F. novicida* Δ*pdpA* remains LAMP1-positive 12 hours post-infection indicating a defect in phagosomal escape [513].

PdpB (FTN_1310; also called icmF) shows homology with the membrane spanning T6SS baseplate complex component TssM. Indeed, PdpB is located to the inner bacterial membrane and spans the periplasm [477]. *F. novicida* Δ*pdpB* has a growth defect in J774 macrophages [515, 516].

Intracellular growth locus E (**IglE**; FTN_1311) shows homology with the baseplate complex component TssJ. Indeed, IglE is a lipoprotein and located to the bacterial outer membrane, where it interacts with PdpB in the periplasm, confirming the functional homology with TssJ [477, 517]. Moreover, *F. novicida* Δ*iglE* has a growth defect in J774 macrophages [515].

Valine-glycine-rich repeat protein G (**VgrG**; FTN_1312) shows homology with the tip complex component VgrG. However, the *Francisella* VgrG is much shorter than the one of *Vibrio* and encodes only the cell puncturing domain without additional N- or C-terminal effector domains [413]. *F. novicida* Δ*vgrG* shows a reduction in cytoplasmic bacteria, intracellular growth and IL-1β release in J774 macrophages comparable to a FPI mutant [515, 518]. These observations suggest that the FPI encodes a T6SS. However FPI-independent VgrG secretion has been also shown, which has been not observed in *Vibrio cholera* or *Pseudomonas aeruginosa* and thus argues against an FPI-encoded T6SS [494, 518].

IglF (FTN_1313) has no homology with known T6SS genes [477]. It is involved in intracellular growth as *F. novicida* Δ*iglF* shows a growth defect in J774 macrophages [515]. Moreover, a bacterial two hybrid screen has identified a specific interaction between IglF and IglG [476]. The authors of this paper propose IglF as a T6SS effector protein, however biological evidence for this suggestion is lacking in the paper.

IglG (FTN_1314) shows homology to the tip complex protein PAAR [476, 477]. However, the function of IglG is controversial. Four independent groups have shown no growth defect of *F. holarctica* Δ*iglG* in BMDMs and J774 macrophages [516, 519–521], whereas two independent groups have reported a growth defect for *F. novicida* Δ*iglG* and *F. holarctica* Δ*iglG* in the same cells [476, 515]. In line with the distinct observations in growth, there are conflicting results about the importance of IglG in vivo. In one publication, the bacterial burden of *F. hol-*

arctica Δ*iglG* in the skin, liver and spleen upon subcutaneous mice infection is reduced [516], whereas the bacterial burden in the spleen and liver is unchanged in another publication using the same bacteria and infection model [521]. In line with the first observation, mice infected with *F. novicida* Δ*iglG* and *F. tularensis* Δ*iglG* survive the infection, whereas all mice infected with wild-type *Francisella* die within the first seven days of infection [476]. Importantly, microinjected *F. holarctica* Δ*iglG* grows normally in J774 macrophages and BMDMs [520]. Thus, the role and function of IglG is still under debate, even though the recent work of Rigard and colleagues strongly suggests that IglG is an important virulence factor involved in phagosomal escape and might interact at the T6SS tip with potential effector proteins such as IglF [476].

IglH (FTN_1315) shows homology to the baseplate component TssE [476,477]. It is involved in intracellular growth as *F. novicida* Δ*iglH* shows a growth defect in J774 macrophages [515].

Defect in organelle trafficking U (**DotU**; FTN_1316) shares homology with the baseplate complex component TssL. Indeed, DotU is located to the inner membrane where it stabilizes PdpB [477, 515]. Furthermore, *F. novicida* Δ*dotU* shows a growth defect in J774 macrophages [515].

IglI (FTN_1317) has no homology with known T6SS genes [477]. The role of IglI in *Francisella* virulence is controversially discussed in the field. *F. novicida* IglI is secreted into J774 macrophages in a FPI-dependent manner and intracellular growth and IL-1β production is IglI-dependent [515, 518]. In line with these observations, *F. tularensis* Δ*iglI* is avirulant in a mouse infection model [522]. However, *F. holarctica* Δ*iglI* grows normally in J774 macrophages but fails to replicate in BMDMs [519, 520]. Importantly, microinjected *F. holarctica* Δ*iglI* grows normally in J774 macrophages and BMDMs [520]. Thus, IglI might have subspecies specific roles and further investigations are required to clarify the function of IglI.

IglJ (FTN_1318) has no homology with known T6SS genes [477]. It is required for intracellular survival as *F. novicida* Δ*iglJ* shows a growth defect in J774 macrophages [515] and *iglJ* deletion in *F. tularensis* attenuates virulence in mice [522].

PdpC (FTN_1319) has no homology with known T6SS genes [477]. It has no impact on intracellular survival as *F. novicida* Δ*pdpC* replicates normally in J774 macrophages [515]. However, *pdpC* deletion in *F. tularensis* and *F. holarctica* attenuates bacterial growth in J774 macrophages and BMDMs and reduces the amount of cytosolic bacteria in these cells [519–522]. In line with these observations, *F. tularensis* Δ*pdpC* is completely avirulent in an intranasal mouse infection model [522]. Interestingly despite bacterial clearance at the end of the infection, a subset of *F. tularensis* Δ*pdpC* specifically disseminates from the lung to the spleen but not the liver, where they replicate to a certain extend [522]. Thus, PdpC might have a subspecies- and tissue-specific function.

PdpE (FTN_1320) has no homology with known T6SS genes [477]. It does not affect intracellular growth of *F. novicida* and *F. holarctica* in J774 macrophages and BMDMs [515, 516, 520]. Moreover, PdpE is not involved in IL-1β release [516]. Thus, the role of PdpE in *Francisella* infection is not clear.

IglD (FTN_1321) has homology to the baseplate component TssK [476,477]. However, *F. novicida* Δ*iglD* replicates normally in J774 macrophages [515] arguing against the theory of a FPI-encoded T6SS.
IglC (FTN_1322) has homology to the inner tube protein Hcp [476, 477]. IglC is important for *F. novicida*, *F. holarctica* and *F. tularensis* virulence and is often used as avirulent control in many publications [515, 516, 519, 520, 523].
IglB (FTN_1323) and **IglA** (FTN_1324) show homology to the sheath proteins VipB and VipA, respectively [476, 477, 523]. They are required for intracellular growth of *F. novicida* and *F. holarctica* in J774 macrophages and BMDMs [425, 515, 516, 520]. Indeed, Clemens and colleagues have solved the atomic structure of a *F. novicida* IglA/IglB filament that shares structural homology with the sheath of the T6SS [523].
PdpD (FTN_1325) has no homology with known T6SS genes [477] and is not conserved in all *Francisella tularensis* subspecies. Whereas *F. novicida* has a 48 codon insertion compared to *F. tularensis*, *F. holarctica* only harbors a truncated version of *pdpD* that is most likely not functional [427]. Even though *F. novicida* Δ*pdpD* does not show any growth defect in J774 macrophages and BMDMs, infections of chicken embryos and mice show an enhanced survival when infected with *F. novicida* Δ*pdpD* [427]. Thus, the discrepancy between in vitro and in vivo infections requires further investigation.
Anhydro-N-acetylmuramic acid kinase (**AnmK**; FTN_1326) has no homology with known T6SS genes [477] and is also not conserved in all *Francisella tularensis* subspecies. Whereas *F. novicida* has a full length *anmK*, *F. holarctica* lacks *anmK* and *F. tularensis* has two prematured stop codons in the *anmK* sequence, which most likely render AnmK non-functional [427]. Moreover, *F. novicida* Δ*anmK* shows no growth defect in J774 macrophages and BMDMs and bacterial loads of infected chicken embryos and mice are comparable to wild-type *F. novicida* [427]. Thus, the role of AnmK in *F. novicida* virulence requires further investigation.

Taken together, the FPI is essential for *Francisella tularensis* virulence by mediating bacterial escape from the phagosome into the cytosol. Different research groups have examined the impact of FPI genes on bacterial escape into the cytosol, on activation of the cellular immune response, on intracellular growth and on virulence in vivo. However, the results of the different studies contradict each other, partially due to the use of different bacterial strains and cell lines.
Moreover, homology of FPI genes with components of T6SSs has resulted in the assumption that the FPI encodes a T6SS. Indeed, cryo-electron microscopy studies have solved the structure of an IglA/IglB filament that shows structural similarity with T6SS sheaths. However, the evidence is lacking that these IglA/IglB sheaths are part of an active and dynamic T6SS. Moreover, the impact of T6SS dynamics on *Francisella tularensis* virulence in vitro and in vivo is unclear. Especially puzzling for the understanding of the potential *Francisella* T6SS is the lack of an ATPase on the FPI to disassemble the contracted sheath again, as seen for other T6SS-expressing bacteria. Without the ATPase, the T6SS is not functional in bac-

teria. Thus, a comprehensive analysis of the FPI and the formation and activity of the potential T6SS would greatly increase our understanding about the key virulence factor of *Francisella tularensis* in establishing a life-threatening infection in humans.

Chapter II

Aim of Research

The aim of my PhD thesis is the investigation of innate immune cell activation upon bacterial infections and the bacterial mechanisms used to infect host cells and evade killing within phagolysosomes. Understanding the activation of innate immune cells is of particular interest as they result in the expression of pro-inflammatory genes and the production of interferons, which control bacterial infections. The investigation of innate immune cell activation upon bacterial infections is conducted in three different projects.

In the first project, we investigate phosphorylation changes in innate immune cells upon bacterial infections with mass spectrometry. Innate immune signaling pathways largely depend on phosphorylation cascades, therefore analyzing phosphorylation changes give information about the activated innate immune signaling pathways. However, current mass spectrometric techniques show limitations in the detection of phosphopeptides. Therefore, we will improve the detection of phosphopeptides to get a comprehensive picture of phosphorylation changes in innate immune cells. To achieve this aim, we will infect primary murine bone marrow-derived macrophages (BMDMs) with the intracellular model bacteria *S.* Typhimurium and analyze phosphorylation changes during the first 8 hours of infection with mass spectrometry.

In the second project, we investigate bacterial mechanisms to infect host cells and evade killing in phagolysosomes. As a model organism, we study the intracellular bacterium *Francisella novicida*, which escapes from the phagosome before it fuses with lysosomes by destroying the phagosomal membrane and entering the cytosol, a step essential for *Francisella* pathogenicity. It has been shown that *Francisella* pathogenicity island (FPI)-encoded genes are involved in phagosomal escape and it has been suggested that the FPI-encoded genes assemble a type 6 secretion system (T6SS). However, to date it is unclear whether or not the FPI encodes a functional T6SS and whether the functional T6SS is responsible for phagosomal escape. Thus, we will analyze if the FPI encodes a functional T6SS and determine its consequences on *Francisella novicida* virulence *in vitro* and *in vivo*.

In the third project, we investigate the composition and stoichiometry of canonical

inflammasome complexes. The inflammasome complex is a multiprotein signaling complex, which is an important mediator of inflammation. However, the composition of the inflammasome complex is not well defined. Therefore we will stimulate the formation of different canonical inflammasome complexes, pull down the inflammasome complex and determine the components and their stoichiometry by mass spectrometry.

Chapter III

Results

1 Research article I

Global ion suppression limits the potential of mass spectrometry based phosphoproteomics

R. F. Dreier*, E. Ahrné*, P. Broz and A. Schmidt.
* denotes equal contribution.

Manuscript submitted. *Nature Communications.*

Statement of contribution
I performed all *Salmonella* infections and sample preparations for mass spectrometry. In addition, I performed the phosphatase treatment and TMT labeling. Furthermore, I analyzed the obtained mass spectrometry data and identified significantly regulated peptides. Furthermore, I validated the significantly regulated peptides by GO term, KEGG, STRING and western blot analysis and defined the peptides for PRM validation. Finally, I wrote the manuscript together with Alex Schmidt, Erik Ahrné and Petr Broz.

Global ion suppression limits the potential of mass spectrometry based phosphoproteomics

Roland Felix Dreier*, Erik Ahrné*, Petr Broz, Alexander Schmidt

Biozentrum, University of Basel, Klingelbergstrasse 50/70, 4056 Basel, Switzerland

Corresponding authors: Alexander Schmidt (alex.schmidt@unibas.ch) and Petr Broz (petr.broz@unibas.ch)

* These authors contributed equally to this work

ABSTRACT (148 words)

Mass spectrometry-based proteomics has become the method of choice to pinpoint and monitor thousands of post-translational modifications, predominately phosphorylation sites, in cellular signaling studies. Critical for achieving this analytical depth is the enrichment for phosphorylated peptides prior to LC-MS analysis. Despite the high prevalence of this modification, the numbers of identified phosphopeptides lag behind those achieved for unmodified peptides, and the cause for this still remains controversial. Here we introduce an effective phosphatase protocol that considerably improves global ionization efficiency and therefore overall sensitivity and coverage of standard phosphoproteomics studies. We demonstrate the power of our method on the model system of *Salmonella*-infected macrophages by extending the current quantitative picture of immune signaling pathways involved in infection. In combination with a new sensitive, label-free targeted MS method for phosphorylation site validation, our novel approach thus opens new avenues to explore cellular phosphorylation based signaling networks in more detail.

Main text (~4200 words)

Alterations in cell signaling have been associated with almost all major diseases and are therefore in the center of biological research for the last decades. Mass spectrometry (LC-MS) based proteomics has become the method of choice to identify and quantitate key modifications, most frequently phosphorylation sites, involved in signaling pathways on a system-wide level. Recent advances in instrumentation, software and sample preparation allow for extensive phosphoproteome analysis covering tens of thousands phosphorylation sites in large-scale studies. To achieve this analytical depth, enrichment of phosphorylated peptides prior to LC-MS analysis is required. Albeit this workflow is now routinely used and well established, the number of phosphorylated peptides identified in one dimensional LC-MS analyses lags behind those achieved for unmodified peptides[1-4], despite a high number of phosphopeptide species being present in these samples as demonstrated in multidimensional and targeted LC-MS experiments[5,6]. The underlying reasons for reduced identification rates of phosphorylated peptides have been assessed and discussed, sometimes controversially, in previous studies. This includes suppressed ionization efficiency in positive ion mode due to the increase in negative changes[7,8], less efficient fragmentation that limit MS/MS-spectra assignment[9], reduced binding efficiency during reverse phase chromatography[10], and losses during purification and chromatography due to interactions with metal parts[11]. However, all studies to date addressing low identification rates of phosphorylated peptides are based on a few pre-selected peptides[12] or small-scale synthetic peptide libraries[13], and report contradictory results, ranging from either no impact[12] to reduced MS signals upon phosphorylation[7]. Besides, most of the results in these studies were obtained using MALDI ionization that has nowadays been almost completely replaced by ESI for the analysis of complex phosphopeptide samples. Here, we developed a highly efficient phosphatase-based protocol and investigated this issue on a phosphoproteome wide level. To this end we used phosphopeptide enriched samples obtained from HeLa S3 cells and *Salmonella*-infected macrophages to analyze innate immune signaling. This allowed us to assess the impact of phosphorylation on thousands of peptides with unprecedented detail and under real experimental conditions. We demonstrate that after enzymatic removal of all phosphate groups in phosphopeptide enriched samples, precursor ion intensities

and proteome coverage increased several folds. We further show that most of the additional peptides identified after phosphatase treatment were indeed phosphorylated and that phosphopeptide quantities were conserved. Finally, using western blots and targeted mass spectrometry, we could define the exact sites of phosphorylation and validate the observed abundance changes for most targets. Overall, using our simple approach, we largely extend the current quantitative picture of immune signaling pathways involved in *Salmonella* infection.

RESULT AND DISCUSSION

Ionization efficiency is globally reduced in phosphopeptide enriched samples

It is still under debate if phosphorylation has a negative impact on peptide identification by LC-MS. To address this issue on a phosphoproteome wide level, with currently employed LC-MS instrumentation and under real experimental conditions, we prepared phosphopeptide enriched samples and developed a highly efficient dephosphorylation protocol to directly compare identified phosphopeptides with their unmodified counterparts. In contrast to the synthetic peptides libraries used in previous studies[12,13], the samples deployed in this study reflect real phosphopeptides generated in large-scale phosphoproteomics studies including frequent missed cleavages, large abundance differences and common contaminations[5].

Crucial for this comparison is the efficient removal of all phosphate groups from phosphopeptide enriched samples. Therefore, we developed a novel quantitative workflow, outlined in Fig. 1, based on a mix of two potent phosphatases (lambda- and alkaline-phosphatase) and applied it to phosphopeptide enriched samples obtained from whole HeLa S3 cell lysates. As shown in Fig. 2a and Supplementary Tables 1-3, the phosphatase mix virtually removed all phosphorylations after only 1 hour of treatment (>99.7% complete). Interestingly, after removing phosphorylations, the number of unique peptide sequences identified by LC-MS increased almost 2-fold (Fig. 2b). When looking at the LC-MS chromatograms (Supplementary Figure 1) we noticed an approximate 10-fold increase in precursor ion intensities after phosphatase treatment (Fig. 2c), across the full MS abundance range (Supplementary Figure 2). Apparently, the MS signals are globally suppressed during

electrospray ionization for phosphopeptide enriched samples. Most likely, the high concentration of negatively charged phosphate groups present in these samples suppressed the formation of positively charged ions required for MS analysis (positive mode) and reduced the overall MS response. It is important to note that a similar global decrease in ESI-MS response has been found previously upon the presence of negatively charged anionic detergents, like SDS[10,14]. Here, MS signal losses were observed starting at 10 mM, a concentration range that is also reached by the phosphopeptides present in a typical phosphoproteomics LC-MS experiment (Supplementary Figure 2).

To further test the hypothesis of global ion suppression in phosphopeptide enriched samples, we looked at unmodified peptides coming from unspecific binders and commonly found contaminants (e.g. keratins, trypsin). Interestingly, the MS signals of these peptides were also strongly suppressed to almost the same level as phosphorylated peptides (Fig. 2d) confirming our hypothesis. The higher and more variable increase observed for phosphopeptides indicates that phosphorylation had an additional, albeit small, negative impact on ionization efficiency which is more phosphopeptide dependent. The slightly higher suppression of phosphopeptides also suggests that there is a higher proportion of phosphorylated than unmodified peptides amongst the additional peptides identified after phosphate removal. In summary, due to its much higher impact, sample matrix related ion suppression is the main driver of the reduced MS response/identification rates observed.

To analyze this background dependent general ion suppression in more detail, we spiked 20 unmodified reference peptides into two different complex peptide matrices consisting of either a whole human cell digest or a phosphopeptide enriched human sample. Subsequently, we monitored and compared the MS response of these 20 peptides for both peptide matrices at three different concentrations to determine differences in ion suppression. As shown in Fig. 2e, increasing amounts of background reduced the MS response of all 20 peptides, however, the suppression was significantly stronger for phosphopeptide enriched backgrounds. This was observed for two different LC-MS platforms with generally higher ion suppression being found for the Q Exactive LC-MS platform (Supplementary Figure 3a and Supplementary Table 4). Importantly, the difference in ion suppression between the

two backgrounds increased with amount. While for 0.2 µg of background the median target peptide intensity was 20% lower in the phosphopeptide enriched matrix compared to the whole cell digest background, the difference increased to 2.5-fold for the highest background amount applied (Supplementary Figure 3b). This increasing difference as a function of background concentration could be described by a logarithmic curve levelling off at around 2.5-fold (Supplementary Figure 3c). The increased ion suppression of phosphopeptide enriched over whole cell lysate samples confirms our previous findings of a profound and global ion suppression of all peptide ions, including unmodified species, in phosphopeptide enriched samples. Notably, the smaller impact on ion suppression observed here compared to the previous experiment (Fig. 2d, 8-fold) was most likely due to the use of a whole cell digest sample, which has different properties and a higher complexity compared to the dephosphorylated sample alone.

To conclude, we observed considerably increased identification rates after enzymatic phosphate removal that were predominantly based on enhanced precursor ion intensities. This led to MS sequencing of additional peptide precursor ions, which were almost completely suppressed in the original phosphopeptide enriched sample (Supplementary Figure 4a). Notably, favorable MS fragmentation behavior and associated higher ion scores after phosphatase treatment could be observed that explained a small part of around 7% of the coverage enhancement (Supplementary Figure 4b).

Application to immune signaling in response to *Salmonella* infection

After successfully establishing and testing the new protocol, we enlarged the experimental setup and analysed phosphorylation dynamics of macrophages upon bacterial infection. *Salmonella enterica* subsp. enterica serovar Typhimurium *(S.* Typhimurium*)* is a Gram-negative facultative intracellular bacterium and a major cause of food-borne enterocolitis. *Salmonella* is one of the best-studied intracellular pathogens and the innate immune signaling pathways that are engaged during *Salmonella* infection of macrophages have been well described[15,16]. We infected murine primary bone marrow derived macrophages (BMDMs) with *S.* Typhimurium Δ*orgA* for 0, 1, 2, 4 and 8 hours in biological triplicates and the samples were subjected to our in-depth label-free quantitative phosphoproteomics LC-MS analysis

described above. To increase phosphoproteome coverage, all samples were analyzed on two LC-MS platforms with different MS-sequencing characteristics and the results were combined (Supplementary Tables 5-7). Using the standard phosphoproteomics approach, we quantified 6607 phosphopeptides from the phosphopeptide enriched samples (Supplementary Figure 5a). When implementing the additional phosphatase treatment, precursor ion intensities were strongly enhanced (Supplementary Figure 5b-e) and the number of quantified peptides increased significantly by a factor of 2.3 to 15'494 peptides (Supplementary Figure 5a). Thus, we could confirm the initial observations shown above for human cell lysates. It is important to note that the large majority (87%) of all phosphopeptides quantified before phosphatase treatment were also covered after phosphatase treatment, indicating that this additional procedure had little impact on MS detectability. The small number (13%) of peptides exclusively quantified in their phosphorylated state mainly comprised very short and basic peptides, whose mass fell outside the analyzed mass range after phosphate group removal. Since any information about the phosphorylation is lost after phosphatase treatment, we next assessed (I) the proportion of phosphopeptides in the additional peptides quantified, (II) the conservation of peptide quantities and (III) finally validated a subset of the most interesting peptides using sensitive, high-resolution targeted MS and western blot analyses.

Phosphopeptide content of additional identified peptides

Having shown that we can considerably increase peptide coverage by phosphate group removal, we next evaluated how many of these additional peptides identified were actually phosphorylated. Therefore, we used a Random Forest classification algorithm and trained it using unmodified serine or threonine containing peptides identified in the phosphopeptide enriched samples before phosphatase treatment as negative and confidently identified phosphopeptides as positive controls. The list of investigated features included; the number of trypsin missed cleavages, peptide molecular weight, Intensity Based Absolute Quantification (iBAQ) value of the originating protein[17], peptide evidence in the PhosphoSitePlus database (PSite+ Evidence)[18] and peptide amino acid frequencies. We subsequently applied the Random Forest model to classify the candidate phosphopeptides; i.e. all phosphopeptides and all unmodified peptides (originating from unspecific binding

peptides or contaminants) extracted from our phosphoproteomics dataset. As illustrated in Supplementary Figure 6a, the selected features allowed a clear separation between unmodified and phosphorylated peptides for all datasets. Using the resulting distribution of Posterior Error Probabilities, we computed a conservative estimate of the phosphopeptide False Discovery Rate (FDR) of 0.175; i.e. approximately 82.5% of the additional peptides identified after phosphatase treatment were expected to have been phosphorylated (Supplementary Figure 6b). This value is similar to the TiO_2 enrichment efficiency achieved in this experiment (83%, Supplementary Figure 5f) and further indicates that we do have a similar and high content of phosphorylated peptides in the additionally identified peptides.

The most discriminating feature of the random forest algorithm included phosphorylation site evidence (Supplementary Figure 6c). More than 80% of all identified peptides, phosphorylation has already been reported to be phosphorylated in the PhosphoSitePlus database[18] (Supplementary Figure 6d). Further top features include protein abundance (iBAQ), the content of serine, proline and missed cleavages in the peptide sequence (Supplementary Figure 6c). Like in other affinity purification strategies[19], high abundant proteins are more likely to be unspecific binders and therefore contaminants than lower concentrated proteins (Supplementary Figure 6e). A high occurrence of serine in phosphopeptides is also expected, since it represents the preferred site of phosphorylation[5]. The high discriminating power of proline points to the presence of the sequence motif “SP” that is targeted by the very potent ERK kinases. As the “SP/TP” kinase motif is one of the most prominent[20], we determined its content in the peptides identified before and after phosphatase treatment (Supplementary Figure 7a). We obtained similar numbers of the “SP/TP” motif in the peptides identified before and after phosphatase treatment. Importantly, the occurrence was much higher than in a whole cell digest. The same was also true for other known kinase motifs (Supplementary Figure 7b-d, Supplementary Tables 8-9). Together, this supports the high content of phosphopeptides present in the additionally identified peptides.

To further prove the validity of the additional peptides for phosphoproteomics studies, we carried out a chemical approach that removes Ser-/Thr-linked phosphate groups from peptides by beta-elimination[21,22]. In contrast to the enzymatic phosphorylation

removal, the site of phosphorylation can still be determined by LC-MS, due to the formation of a dehydrated side chain (Supplementary Figure 8a). When applied to our sample, we could identify, even after several optimization steps, no more than around 2500 dehydration sites and therefore a much lower number of phosphorylations compared to our standard phosphoproteomics approach. Additionally, beta-elimination remained incomplete for many phosphopeptides (Supplementary Table 10). Thus, despite its advantage of preserving phosphorylation site information, the low coverage and yield did not make this chemical approach applicable as a general tool for large-scale quantitative phosphoproteomics workflows. Nonetheless, it was interesting to see that the 2500 phosphopeptides identified by this chemical approach overlapped much better with the phosphatase treated dataset than the phosphopeptide enriched dataset (Supplementary Figure 8b). This not only further proves the phosphopeptide content of the additional peptides identified after phosphatase treatment, but also indicates that some phosphorylated peptides escape detection by the standard phosphoproteomics workflow.

To check which phosphopeptides have a lower chance of LC-MS identification, we had a closer look on the peptides exclusively identified before and after phosphatase treatment. Interestingly, we found significant differences in the content of basic and acidic amino acids (Supplementary Figure 9a&b), in that peptides identified before phosphatase treatment contained more basic and less acidic residues. This can be explained by the fact that phosphate groups remain negatively charged during MS ionization and reduce the charge state of the corresponding peptide ions (Supplementary Figure 9c). Since a net charge of at least two is required for MS-sequencing in ESI positive mode, more basic amino acids are necessary to compensate the negative charges of the phosphate groups. This largely explains the increased coverage achieved after phosphate removal, because most of the identified peptides contained only few (1-2) basic amino acids (Supplementary Figure 9d). Notably, MS-sequencing of very basic peptides (>4 basic amino acids) is improved upon charge state reduction[23], which we also observed for the phosphopeptides identified in this study (Supplementary Figure 9e, Supplementary Table 11). However, since these peptides represent only a minor fraction of all identified peptides (<2%), the contribution to the overall coverage is negligible. It is

important to note that the low coverage of peptides with few basic amino acids might point to a general overrepresentation of peptides with basic kinase motifs (containing K, H or R; e.g. KxS or RRxS) in standard LC-MS based phosphoproteomics studies, since phosphorylations next to tryptic cleavage sites (K,R) induce missed cleavages and are often found in peptides with high basic amino acid levels[24]. On the other hand, the content of acidic amino acids had much less impact on peptide detectability in the present dataset (Supplementary Figure 9f).

To conclude, these experiments confirmed that most of the additional peptides identified after phosphatase treatment were originally phosphorylated and that the main increase in coverage followed from peptides with only few basic amino acids that are lowly charged upon phosphorylation and therefore not MS-sequenced by standard phosphoproteomics LC-MS analysis.

Quantitative information is conserved after phosphatase treatment

Having shown that most of the newly detected peptides were indeed phosphorylated, we next assessed their suitability for quantification. Therefore, we first compared the number of significantly regulated peptides identified before and after phosphatase treatment. Overall, we found twice as many significantly regulated peptides after phosphatase treatment (Fig. 3a). Peptides significant after phosphate removal covered about 90% of the significantly regulated peptides found in the phosphorylated sample (Fig. 3a). The corresponding proteins matched the same GO-terms and KEGG pathways[25,26] (Supplementary Tables 12-13), indicating that the phosphatase treatment has, if at all, only a minimal impact on phosphopeptide quantification and that the coverage of our study could thus also be extended to the quantitative level (Fig 3b, Supplementary Figure 10a). Indeed, when correlating the ratios of significantly regulated peptides obtained before and after phosphatase treatment we obtained a very high coefficient of determination (r2=0.914, Fig. 3c). Even when only considering the significantly regulated peptides obtained after phosphatase treatment and comparing them to the ratios of the corresponding phosphopeptide, the correlation and accuracy were high (r2=0.817, Supplementary Figure 10b), indicating that the regulation trend could be correctly determined for 96.2% of the phosphopeptides from their dephosphorylated counterparts.

It is important to note that the higher number of significantly regulated peptides obtained after phosphatase treatment is not only related to the overall increase in peptide coverage, but also a consequence of the improved MS response (Supplementary Figure 5b). In fact, signal-to-noise ratios were increased and coefficients of variation (CVs) were decreased across all sample triplicates after phosphatase treatment (Fig. 3d). As a consequence of this elevated precision, p-values were generally lower and more peptides passed the given significance threshold applied (Supplementary Figure 11).

To conclude, the phosphatase treatment could increase the number of significantly regulated peptides and this increase is due to an overall increase in peptide coverage as well as improved precision.

Innate immune signaling pathway dynamics upon *Salmonella* infection

As shown in Figure 3b, we were able to increase the number of phosphoproteins per innate immune signaling pathway after phosphatase treatment. As the activation of innate immunity is very important to fight a *Salmonella* infection, we further analyzed these innate immune signaling pathways by subjecting the identified proteins to a STRING based protein-protein interaction analysis[27]. To obtain a better network coverage, we included 25 additional proteins known to be important for signaling but not detected in our analysis. With the inclusion of these proteins, STRING could build an interaction network with 94 out of 102 proteins from our analysis. In agreement with the KEGG analysis, the phosphatase treatment doubled the amount of interacting proteins in the STRING network (Fig. 4a). Especially the TLR and JAK/STAT signaling pathways were represented in much greater detail after phosphatase treatment (Fig 4a). During *Salmonella* infection TLR4 responds to bacterial lipopolysaccharide (LPS) and signals through the MYD88 / NF-κB axis to induce the expression of pro-inflammatory proteins like, TNFα, IL-1β or caspase-11. Moreover, TLR4 signals through TRIF / IKKε to induce type I interferons, which then activate the JAK/STAT signaling pathway[28-30]. The TLR4 as well as JAK/STAT signaling pathway are very important for a successful innate immune response against invading bacteria like *Salmonella*[15].

As the JAK/STAT signaling pathway is activated upon TLR4-dependent type I interferon production[30], we wanted to confirm this hierarchy in the phosphatase treated samples. We first analyzed signaling downstream of TLR4 by looking at NF-κB and IKKε phosphorylation. The NF-κB complex is activated through phosphorylation of subunit p65 (Rela) at S536 and IKKε is activated by S172 phosphorylation[31,32]. Western blot analysis showed NF-κB activation as soon as 30 min post infection, which was consistent with an increase in phosphopeptide abundance of proteins upstream of NF-κB (e.g. IRAK2, 3, 4 or IKKβ (Ikbkb) (Fig. 4c). Similar to NF-κB activation, IKKε is phosphorylated as soon as 30 min post infection. In line with this, the upstream IKKε activator TRIF (Ticam1) showed a similar peptide abundance pattern in the phosphatase treated samples (Fig. 4c). Even more striking, STAT1 phosphorylation at Y701 and therefore activation of the Jak/STAT signaling pathway[33] happened after TLR signaling and the peptides detected after phosphatase treatment showed a very similar abundance pattern (e.g. STAT3, STAT6 or IRF9) (Fig. 4c). Especially the STAT6 peptide abundance pattern phenocopied STAT1 activation (Fig. 4c). Therefore, we were able to correlate the abundance profile of specific peptides identified after phosphatase treatment to signaling dynamics of the analyzed innate immune signaling pathways.

Interestingly, a cluster of significantly regulated proteins associated with the RIG-I signaling pathway (Fig. 4a). This pathway is linked to cytosolic dsRNA recognition upon viral infections and, so far, not linked to bacterial infections[34]. Thus, its role in mounting a proper immune response against bacterial pathogens needs to be examined.

Taken together, there is a clear correlation between the dynamics of the detected peptides after phosphatase treatment and the known phosphorylation pattern of proteins in the same pathway. Therefore, the new workflow provided extended insights into the activation profile of signaling pathways over time.

Validation of significant peptides

Validation of quantitative results by an orthologues approach is crucial in any large-scale study[35]. It is desirable that such a method not only confirms the change in abundance, but also to confirms and precisely localize the phosphorylation. One well

established method to validate phosphorylation sites is the usage of phosphorylation specific antibodies. Indeed, the phosphorylation dynamics of p38 T180 / Y182 before and after phosphatase treatment were identical and resembled the phosphorylation pattern observed by Western blot (Fig. 4d). However, for most hits identified after phosphatase treatment, the availability of specific antibodies was highly limited. Therefore, we focused on parallel reaction monitoring (PRM) LC-MS assays[36,37] to validate 24 phosphopeptide candidates that belong to proteins involved in innate immune signaling (Fig. 4a and Supplementary Table 14).

Here, we carried out two different workflows; the standard stable-isotope dilution (SID-) PRM approach that requires synthetic heavy peptide references (Fig. 5a) and a novel, high-selective label-free quantification (LFQ-) PRM workflow based on conventional database search identification that does not require any internal standards or reference MS spectra (Fig. 5b). This was only possible by applying a more selective precursor ion selection (0.7 Th, before 2 Th) and a higher resolution (>120k at 200m/z, before 30k) than previously reported[36,37]. This boosted the quality of MS/MS spectra and enabled unambiguous and sensitive quantification and identification of target phosphopeptides. The LFQ-PRM is particularly interesting for the validation of phosphorylation sites, since, due to their identical parent ion mass, all potential sites of a peptide are covered by a single PRM assay. Conversely, in the SID-PRM approach, every potential phosphorylation site requires a different assay and therefore a different heavy reference peptide[38].

When applied to our samples, we first performed LFQ-PRM analyses with different sensitivity settings (see method sections for details). Overall, using this simple approach, we could identify and quantify 18 unique phosphorylation sites located on 15 of the 24 selected phosphopeptide candidates (Table 1, Supplementary Tables 16-19). Notably, LFQ-PRM allowed the identification and quantification of different phosphorylation sites within peptides using a single assay as illustrated for the two sites monitored in the peptide “DA(*p)T*PPV*(p)S*PINMEDQER” (Fig. 5c-e, Supplementary Figure 12). This was possible due to the full chromatographic separation and the presents of specific transitions of the two variants (Fig. 5d). The same was true for the peptide “AASGSQPEPSPDQSATNSPESSSR” for which three different phosphorylations could be identified and quantified (Supplementary Figure

13). Interestingly, the LFQ-PRM workflow was particular effective in identifying long phosphopeptides (>20 amino acids), while many of the shorter peptides (<10 amino acids) were not covered (Table 1). This might point to the general favorable identification of longer peptides by database searching, due to their higher number of fragments and reduced search space, usually with higher significance than shorter peptides[39]. Because larger peptides are still difficult and expensive to synthesize, the LFQ-PRM approach seems to be an excellent complement to the standard SID-PRM workflow. Still, spiking in heavy reference peptides is the method of choice for sensitive and confident quantification in targeted MS. Therefore, we ordered synthetic mono-phosphorylated heavy reference peptides covering all known phosphorylation sites of the missing peptides and, if no site has been reported so far, all possible sites were included (Supplementary Table 15). After establishing SID-PRM assays, we applied them to quantitate phosphorylation sites of the selected peptides from phosphopeptide enriched samples using the same high selective MS parameters as for the LFQ-PRM workflow. This enabled the precise localization of 4 additional phosphorylation sites on 4, mostly shorter, peptide candidates (Supplementary Table 20). The remaining 5 phosphopeptide candidates could not be detected and validated by SID-PRM. In total, 19 (79%) of the 24 selected candidate phosphopeptides were validated, two were phosphorylated at multiple positions, and the abundance change was confirmed for 18 of them (Table 1, Supplementary Table 21). For instance, the ratios of the two sites obtained by LFQ- and SID-PRM for peptide “DA(*p)T*PPV*(p)S*PINMEDQER” matched very well the ratios obtained from the large-scale phosphatase samples and confirmed their significant upregulation after 4 hours of infection (Fig. 5e). In fact, a good correlation between LFQ- and SID-PRM and the large-scale phosphatase dataset was observed for all significantly regulated hits (Supplementary Figure 15), further confirming the validity of our peptide candidates for quantitative phosphoproteomics analysis.

To conclude, we localized the phosphorylation site(s) and verified their abundance change(s) for the large majority (>80%) of selected hits. In particular, the LFQ-PRM workflow performed very well validating most of the selected phosphopeptide candidates of interest and therefore represents an attractive addition to the standard SID-PRM target validation.

CONCLUSION

We present a straightforward and very effective workflow that considerably increased the analytical depth achieved in monitoring phosphoproteomics changes of immune signaling pathways involved in infection. This was achieved by a simple additional phosphatase treatment step after phosphopeptide enrichment that significantly increased MS-sensitivity by several folds. As a result, coverage and quantification were improved, which are of particular importance when working with limited sample amounts. Despite these advantages, the complete enzymatic dephosphorylation strategy is by no means perfect. Most obviously, modification localization information is lost, making it necessary to carry out additional validation experiments. Furthermore, quantification of single sites in multiply phosphorylated peptides can be challenging, since, after dephosphorylation, only the sum of all phosphorylation forms of a peptide are quantified. However, as shown in Supplementary Figure 10b, the ratios of doubly phosphorylated peptides before and after phosphatase treatment correlated very well. This was due to fact that the significantly regulated sites had a much higher stoichiometry and mainly contributed to the dephosphorylated peptide abundance.

Clearly, equally efficient and uniform dephosphorylation or negative charge neutralization strategies that preserve phosphorylation site information would be desirable. We thoroughly evaluated different dephosphorylation methods in this study, including chemical and enzymatic approaches, but found enzymatic phosphatase treatment to be by far the most efficient method providing most peptide identifications. An interesting approach would be enzymatic phosphoric acid removal, which would transform phosphorylations to MS-detectable dehydrated sites, but available enzymes are currently limited to specific peptides species[40] preventing its application to global studies. Finally, despite the good enrichment efficiency achieved in this study (>80%, Supplementary Figure 5f), the method will certainly benefit from recent, highly efficient phosphopeptide enrichment technologies[3,4,41]. Here, almost every additionally identified peptide after phosphate removal would originate from a phosphopeptide, which will speed up target validation.

Overall, albeit not perfect, the dephosphorylation strategy applied clearly demonstrates that ion suppression considerably limits the potential of large-scale LC-MS based phosphoproteomics studies, which are currently all based on phosphopeptide enriched samples. Furthermore, the observed biases against acidic and peptides with few basic amino acids might point, despite the impressive coverages achieved in recent studies, to a general underrepresentation of acidic phosphopeptides and kinase motifs and an overrepresentation of motifs containing basic amino acids that favor missed cleavages in present large-scale datasets. For this reason, overcoming ion suppression during LC-MS for samples enriched for phosphopeptides is an important step towards comprehensive and unbiased phosphoproteomics analyses.

METHODS

Cell culture and infection.

HeLa S3 cells were cultured in Dulbecco's modified Eagle's medium (DMEM, Invitrogen, Carlsbad, CA) supplemented with 10% heat-inactivated fetal calf serum (FCS) and penicillin-streptomycin (100 IU/ml and 100 µg/ml, respectively, GIBCO) at 37°C in a 5% CO2 atmosphere in a humidified incubator. Cells were collected by centrifugation, washed twice with PBS and stored in liquid nitrogen until further use. Primary murine bone marrow derived macrophages (BMDMs) were differentiated in DMEM (Sigma) with 20 % M-CSF (supernatants of L929 mouse fibroblasts), 10% v/v FCS, 10 mM HEPES, nonessential amino acids and penicillin (100 IU/ml) / streptomycin (100 µg/ml) (all BioConcept). 1 day before infection, BMDMs were seeded into 6- or 96-well plates (Greiner) at a density of 1.5 x 10^6 or 5 x 10^4 cells per well in DMEM (Sigma) with 10 % M-CSF (supernatants of L929 mouse fibroblasts), 10 % v/v FCS, 10 mM HEPES and nonessential amino acids (all BioConcept). *Salmonella enterica* subsp. enterica serovar Typhimurium strain SL1344 *ΔorgA* (hereafter *S.* Typhimurium *ΔorgA*) were grown over night at 37°C with aeration in lysogeny broth (LB) medium supplemented with 90 µg/ml streptomycin (Sigma) and 2 µg/ml tetracycline (ICN Biomedicals). The bacteria were added to the BMDMs at a multiplicity of infection of 100. The plates were centrifuged for 5 min at 500xg to ensure similar adhesion of the bacteria to the cells and were incubated at 37°C for the indicated length of time. After 60 min, the medium was replaced with fresh medium containing 100 µg/ml gentamicin (BioConcept) to kill extracellular bacteria

and after 120 min, the medium was replaced with fresh medium containing 10 µg/ml gentamicin (BioConcept) for the residual time of infection.

Sample preparation.

BMDMs were seeded in 6-well plates and infected with *S.* Typhimurium *ΔorgA* as indicated above. At the indicated time points, the plates were put on ice and the BMDMs washed twice with ice-cold 1x phosphate-buffered saline (PBS). 80 µl urea lysis buffer (8 M urea (AppliChem), 0.1 M Ammoniumbicarbonate (Sigma), 1x PhosSTOP (Roche)) was added to each well and incubated on ice for 10 min. For HeLa cell preparation, 10^7 cells were lysed in 200 µl urea lysis buffer. Samples were vortexed, sonicated at 4°C (Hielscher), shaked for 5 min on a thermomixer (Eppendorf) at room temperature and centrifuged for 20 min at 4°C full speed. Supernatants were collected and protein concentration was measured with BCA Protein Assay kit (Invitrogen). Per sample, 2 mg of protein mass were used, 1.9 mg were employed for phosphopeptide enrichment and 100 µg for protein quantification by TMT. At first, disulfide bonds were reduced with tris(2-carboxyethyl)phosphine (TCEP) at a final concentration of 10 mM at 37°C for 1 hour. Free thiols were alkylated with 20 mM iodoacetamide (IAM, Sigma) at room temperature for 30 minutes in the dark and access of IAM were quenched by adding excess of N-acetylcysteine. Samples were incubated for 4 h with Lys-C endopeptidase (1:200 w/w), diluted with 0.1 M ammoniumbicarbonate to a final urea concentration of 1.6 M and digested overnight at 37°C with sequencing-grade modified trypsin (Promega) at a protein-to-enzyme ratio of 50:1. Subsequently, peptides were desalted on a C18 Sep-Pak cartridge (VAC 3cc, 500 mg, Waters) according to the manufacturer's instructions, split in peptide aliquots of 1.9 and 0.1 mg, dried under vacuum and stored at -80°C until further use.

Phosphopeptide enrichment.

Phosphopeptides were isolated from 1.9 mg of total peptide mass with TiO_2 as described previously[42]. Briefly, dried peptides were dissolved in an 80% acetonitrile (ACN)–2.5% trifluoroacetic acid (TFA) solution saturated with phthalic acid. Peptides were added to the same amount of equilibrated TiO_2 (5-µm bead size, GL Science) in a blocked Mobicol spin column (MoBiTec) that was incubated for 30 minutes with end-over-end rotation. The column was washed twice with the saturated phthalic acid

solution, twice with 80% ACN and 0.1% TFA, and finally twice with 0.1% TFA. The peptides were eluted with a 0.3 M NH_4OH solution. The pH of the eluates was adjusted to be below 2.5 with 5% TFA solution and 2 M HCl. Phosphopeptides were again desalted with C18 reversed-phase spin columns according to the manufacturer's instructions (Microspin, Harvard Apparatus), dried under vacuum and stored at -80°C until further use.

Enzymatic peptide dephosphorylation using phosphatase

Dried phosphopeptides were dissolved in 50 µl reaction buffer (50 mM HEPES, 100 mM NaCl, 1 mM $MnCl_2$, 1 mM $MgCl_2$, pH 7.4), 2000 units of Lambda Protein Phosphatase (Lambda PP) and 20 units of Alkaline Phosphatase Calf Intestinal (CIP, both from New England BioLabs) were added and the sample was shaken at 600 rpm and 30°C for 1 h. After adding 10 µl of 5% TFA solution, peptide samples were desalted, dried under vacuum and stored at -80°C until further use.

Chemical peptide Ser-/Thr-dephosphorylation by beta-elimination

The beta-elimination was carried as previously described[21]. In brief, dried phosphopeptides were dissolved in 90 µl of 10% water in methanol and 3 µl of 0.15 M $Ba(OH)_2$ using ultra sonication. The reaction was allowed to proceed for 1 h at 45°C under continuous shaking at 600 rpm, mixtures were neutralized by addition of 3 µl of 0.3 M HCl, and dried under vacuum. Samples were dissolved in 100 µl of 0.1% TFA and desalted, dried under vacuum and stored at -80°C until further use.

TMT labeling

Sample aliquots containing 25 µg of dried peptides were subsequently labeled with isobaric tag (TMT 6-plex, Thermo Fisher Scientific) following a recently established protocol[43]. To control for ratio distortion during quantification, a peptide calibration mixture consisting of six digested standard proteins mixed in different amounts were added to each sample before TMT labeling. After pooling the TMT labeled peptide samples, peptides were again desalted on C18 reversed-phase spin columns according to the manufacturer's instructions (Macrospin, Harvard Apparatus) and dried under vacuum. We carried out two independent 6-plex TMT experiments covering all six time points with biological duplicates.

HpH fractionation of TMT labeled samples

TMT-labeled peptides were fractionated by high-pH reversed phase separation using a XBridge Peptide BEH C18 column (3,5 µm, 130 Å, 1 mm x 150 mm, Waters) on an Agilent 1260 Infinity HPLC system. Peptides were loaded on column in buffer A (ammonium formate (20 mM, pH 10) in water) and eluted using a two-step linear gradient starting from 2% to 10% in 5 minutes and then to 50% (v/v) buffer B (90% acetonitrile / 10% ammonium formate (20 mM, pH 10) over 55 minutes at a flow rate of 42 µl/min. Elution of peptides was monitored with a UV detector (215 nm, 254 nm). A total of 36 fractions were collected, pooled into 12 fractions using a post-concatenation strategy as previously described[44], dried under vacuum and subjected to LC-MS/MS analysis.

LC-MS/MS analysis

The setup of the µRPLC-MS system was as described previously[43]. Chromatographic separation of peptides was carried out using an EASY nano-LC 1000 system (Thermo Fisher Scientific), equipped with a heated RP-HPLC column (75 µm x 50 cm) packed in-house with 1.9 µm C18 resin (Reprosil-AQ Pur, Dr. Maisch). Aliquots of 1 µg total peptides were analyzed per LC-MS/MS run using a linear gradient ranging from 95% solvent A (0.15% formic acid, 2% acetonitrile) and 5% solvent B (98% acetonitrile, 2% water, 0.15% formic acid) to 30% solvent B over 180 minutes at a flow rate of 200 nl/min. Mass spectrometry analysis was performed on a dual pressure LTQ-Orbitrap Elite or Q-Exactive HF mass spectrometer equipped with a nanoelectrospray ion source (both Thermo Fisher Scientific) and a custom made column heater set to 60°C. For LFQ samples, each MS1 scan (acquired in the Orbitrap) was followed by collision-induced-dissociation (CID, acquired in the linear ion trap) of the 20 most abundant precursor ions with dynamic exclusion for 60 seconds. Total cycle time was approximately 2 s. For MS1, 1E6 ions were accumulated in the Orbitrap cell over a maximum time of 300 ms and scanned at a resolution of 240,000 FWHM (at 400 m/z). MS2 scans were acquired at a target setting of 10,000 ions, accumulation time of 25 ms and rapid scan rate using a normalized collision energy of 35%. The preview mode was activated and the mass selection window was set to 2 Da. LFQ-MS1 based experiment were also carried out on a QE-HF. Here, 3E6 ions were collected for MS1 scans for no more than 100 ms and analyzed at a resolution of 120,000 FWHM (at 200 m/z). MS2 scans were

acquired of the 20 most intense precursor ions at a target setting of 100,000 ions, accumulation time of 50 ms, isolation window of 1.4 Th and at resolution of 15,000 FWHM (at 200 m/z) using a normalized collision energy of 28%. All TMT samples were analyzed on the QE-HF using the same setting as above with a few adjustments as recently described[43]. MS2 scans of only the 10 most abundant precursor ions were performed and the collision energy was increased to 35%. The mass isolation window was set to 1.1 Th and the resolution of the MS2 scans was increased to 30,000 FWHM (at 200 m/z). Total cycle time was approximately 1-2 s.

Phosphopeptide analysis using label-free quantification

The acquired raw-files were imported into the Progenesis QI software (v2.0, Nonlinear Dynamics Limited), which was used to extract peptide precursor ion intensities across all samples applying the default parameters. The generated mgf-files were searched using MASCOT against a decoy database (consisting of forward and reverse protein sequences) of the predicted proteome from *mus musculus* (UniProt, download date: 2016/11/6, total 33984 entries) and *homo sapiens* (UniProt, download date: 2015/06/29, total 41158 entries) including known contaminants such as porcine trypsin, human keratins and high abundant bovine serum proteins (Uniprot). The search criteria were set as follows: full tryptic specificity was required (cleavage after lysine or arginine residues, unless followed by proline); 3 missed cleavages were allowed; carbamidomethylation (C) was set as fixed modification; oxidation (M) and phosphorylation (STY) were applied as variable modifications; mass tolerance of 10 ppm (precursor) and 0.6 (CID, ion trap) and 0.02 Da (HCD, orbitrap) (fragments). The database search results were filtered using the ion score to set the false discovery rate (FDR) to 1% on the peptide and protein level, respectively, based on the number of reverse protein sequence hits in the datasets. The relative quantitative data obtained were normalized and statistically analyzed using SafeQuant[43] (see statistical data analysis below for details). Localization confidence was determined using Ascore[45] as implemented in Scaffold-PTM (version 2.1.3, Proteome Software Inc., Portland, OR).

Protein quantification using TMT

The acquired raw-files were converted to the mascot generic file (mgf) format using the msconvert tool (part of ProteoWizard, version 3.0.4624 (2013-6-3)). The mgf files

were searched, using Mascot (Matrix Science, Version 2.4.0), against the *mus musculus* database mentioned above including the six Calibration-mix Proteins (uniprot accession numbers: P00489, P02789, P01012, P02666, P00722, B6V3I5, www.uniprot.org downloaded 22/10/2014)[43]. The Mascot search criteria were set as follows: 10 ppm precursor ion mass tolerance, 0.02 Da fragment ion mass tolerance, full tryptic specificity required (cleavage after lysine or arginine residues unless followed by proline), maximum 2 missed cleavages, fixed modifications: carbamidomethylation (C) and TMT6plex (K and peptide n-terminus), variable modification: oxidation (M). The database search results were post-processed using the Scaffold Q+ software (version 4.3.2, Proteome Software Inc., Portland, OR). Here, protein scores were calculated using the Protein Prophet algorithm[46]. Next, peptide and protein level identifications were filtered to achieve a maximum False Discovery Rate of 1%, on both levels. The FDR was determined using the Scaffold Local FDR algorithm. Proteins that contained similar peptides and could not be differentiated based on MS/MS analysis alone were grouped to satisfy the principles of parsimony. Proteins sharing significant peptide evidence were grouped into clusters.

TMT reporter ion intensities were extracted using Scaffold Q+. Protein relative quantification was performed using our in-house developed SafeQuant R package[43]. This analysis included multiple steps; adjustment of reporter ion intensities for isotopic impurities according to the manufacturer's instructions, global data normalization by equalizing the total reporter ion intensity across all channels, summation of reporter ion intensities per protein and channel, calculation of protein abundance ratios and testing for differential abundance using empirical Bayes moderated t-statistics where the resulting p-values, reflect the probability of detecting a given mean abundance difference across sample conditions by chance alone.

Statistical data analysis

SafeQuant Description

Quantitative analysis results from label-free and TMT quantification were further processed using the SafeQuant R package v.2.3.2. (https://github.com/eahrne/SafeQuant/) to obtain protein relative abundances. This analysis included global data normalization by equalizing the total peak/reporter

areas across all LC-MS runs, summation of peak areas per protein and LC-MS/MS run, followed by calculation of protein abundance ratios. The summarized protein expression values were used for statistical testing of between condition differentially abundant proteins. Here, empirical Bayes moderated t-Tests were applied, as implemented in the R/Bioconductor limma package (http://bioconductor.org/packages/release/bioc/html/limma.html). The resulting per protein and condition comparison p-values were adjusted for multiple testing using the Benjamini-Hochberg method.

Underlying Statistical Assumptions

All LC-MS analysis runs are acquired from independent biological samples. To meet additional assumptions (normality and homoscedasticity) underlying the use of linear regression models and Student t-Test MS-intensity signals are transformed from the linear to the log-scale.

Linear Regression

Unless stated otherwise linear regression was performed using the ordinary least square (OLS) method as implemented in *base* package of R v.3.1.2 (http://www.R-project.org/).

Power

The sample size of three biological replicates was chosen assuming a within-group MS-signal Coefficient of Variation of 10%. When applying a two-sample, two-sided Student t-test this gives adequate power (80%) to detect protein abundance fold changes higher than 1.65, per statistical test. Note that the statistical package used to assess protein abundance changes, SafeQuant, employs a moderated t-Test, which has been shown to provide higher power than the Student t-test[47]. We did not do any simulations to assess power, upon correction for multiple testing (Benjamini-Hochberg correction), as a function of different effect sizes and assumed proportions of differentially abundant proteins.

Validation of hits by targeted LC-MS

24 phosphopeptide candidates (Supplementary Table 14) were selected for validation using PRM analysis. First, a label-free quantification approach for all

peptides was carried out. Therefore, the precursor ion masses were calculated for all candidates in their mono-phosphorylated form and for charge states 2+, 3+ and 4+. After feeding the mass lists into the QE-HF, MS/MS scans were acquired in a targeted fashion for all masses. Importantly, the mass list was split to keep cycle times below 4 seconds. In a first round, MS2 scans were acquired at a target setting of 3e6 ions, max. accumulation time of 150 ms, isolation window of 0.7 Th and at resolution of 60,000 FWHM (at 200 m/z) using a normalized collision energy of 27%. The acquired MS2 spectra were database searched using Mascot (same parameters as described above) and MaxQuant[39] using the same settings as described recently[48]. In brief, MS raw files were imported to MaxQuant software (version 1.5.1.2) and peak lists were searched against the same database of the predicted proteome from *mus musculus* (UniProt, download date: 2016/11/6, total 33984 entries) and common contaminants as used for the Mascot search. The search criteria were set as follows: carbamidomethylation (C) was set as fixed modification; oxidation (M) and phosphorylation (STY) were applied as variable modifications; false discovery rate was set to 0.01 for proteins and peptides (minimum length of 7 amino acids) and was determined by searching a reverse database. Enzyme specificity was set as C-terminal to arginine and lysine, and a maximum of three missed cleavages were allowed in the database search. Peptide identification was performed with an allowed initial precursor mass deviation up to 7 p.p.m. and an allowed fragment mass deviation 20 p.p.m.

Confidently identified phosphopeptide candidates (identification by one search engine setting a FDR cut-off of 1% based on decoy hits was sufficient) were then excluded from analysis (Supplementary Table 16-17) and the samples were re-analyzed using a more sensitive targeted MS approach with higher cycle times. Therefore, max. ion accumulation time was set to 500 ms and the resolution was set to 240,000 FWHM (at 200 m/z). Using this LFQ-PRM approach, phosphorylation sites could be identified for 15 of the 24 selected candidates by Mascot/MaxQuant (Supplementary Table 18). Subsequently, PRM assays for LFQ quantification by Skyline were generated for all identified phosphopeptides using an in-house R-script that extracts the most intense and isoform specific transitions of each peptide from the annotated MS2 spectra. For the remaining candidates, heavy reference peptides were ordered covering all known and possible phosphorylation site (Supplementary

Table 15). In a first step of this stable isotope dilution (SID) based parallel reaction-monitoring (PRM) quantification[37], MS assays were generated from a shotgun LC-MS analysis of a mixture containing 500 fmol of each reference phosphopeptide. The mass spectrometric analysis and data analysis was similar to above with the following changes; a LC gradient of 60 minutes was used, 3e6 ions were accumulated for MS1 and scanned at a resolution of 120,000 FWHM (at 200 m/z). MS2 scans were acquired at a target setting of 100,000 ions, accumulation time of 50 ms and a normalized collision energy of 28%. For database searching by Mascot isotopically labeled arginine (+10 Da) and lysine (+8 Da) were added as variable modifications and the mass tolerance for MS2 fragments was set to 0.02 Da. The resulting dat-file was imported to skyline version 3.6.0 (https://brendanx-uw1.gs.washington.edu/labkey/project/home/software/Skyline/begin.view) to generate a spectral library and select the 5 to 10 best transitions for each peptide. For the quantitative SID-PRM experiment, the resolution of the orbitrap was set to 120,000 FWHM (at 200 m/z) and the fill time was set to 250 ms to reach a target value of 3e6 ions. Ion isolation window was set to 0.7 Th and the first mass was fixed to 100 Th. Each condition was analyzed in biological triplicates. All raw-files obtained from the SID-PRM and LFQ-PRM analysis were imported into Skyline for peptide quantification. For LFQ-PRM, only peaks/transitions that could be validated by confidently identified MS2 spectra using database searching were employed for quantification. To control for variation in injected sample amounts, precursor ion intensities obtained from an additional MS1 scan were used for normalization. Here, the intensity of all precursor ion with a charge of 2+ and more were extracted using Progenesis QI software (v2.0, Nonlinear Dynamics Limited) as described above, summed and used for normalization.

Immunoblot analysis.

BMDMs were seeded in 6-well plates and infected with *S.* Typhimurium *ΔorgA* and at the indicated time points, the samples were collected as describes above. 10 µg protein were subjected to SDS-polyacrylamid gels and electroporated onto PVDF membrane. Primary antibodies used were mouse anti-phospho-p65 (S536), rabbit anti-phospho-IKKε (S172), rabbit anti-IKKε, rabbit anti-phospho-STAT1 (Y701), rabbit anti-STAT1, rabbit anti-phospho-p38 (T180/Y182), rabbit anti-p38α (all Cell signalling; 1:1000 in 0.3% BSA/ 1x TBST), mouse anti-p65 (Santa Cruz; 1:1000 in

0.3% BSA/ 1x TBST) and mouse anti-actin (Millipore; 1:5000 in 0.3% BSA/ 1x TBST) and incubated overnight at 4°C. Secondary antibodies used were goat anti-mouse HRP and goat anti-rabbit HRP (both Southern Biotech, 1:3000 in 0.3% BSA/ 1x TBST) and incubated for 1 h at room temperature. Blots were analysed on a ImageQuant LAS4000 (GE Healthcare).

Data availability

All mass spectrometry raw data files have been deposited to the ProteomeXchange Consortium (accession code PXD007528, http://proteomecentral.proteomexchange.org, reviewer login: username: reviewer91090@ebi.ac.uk, password: AAGlAPa4) via the PRIDE partner repository[49].

ACKNOWLEDGEMENTS

This work was supported by an SNSF Professorship PP00P3_139120/1 to P.B. Further, the authors would like to thank Thomas Bock for critical reading of the manuscript.

AUTHOR CONTRIBUTIONS

P.B. and A.S. designed the study. R.D. and A.S. performed experiments. R.D., E.A. and A.S. analysed data. R.D., E.A., P.B. and A.S. wrote the manuscript.

COMPETING FINANCIAL INTERESTS

The authors declare no competing financial interests.

Table 1: Validation of selected phosphopeptide candidates by targeted LC-MS

Selected phosphopeptide candidate	Gene	Validated phosphorylation sites[1]	Phosphorylation position in protein	Phosphorylation site known[2]	Change (4h/0h), (+) PO4ase	Change confirmed by PRM-MS, (-) PO4ase
AASGSQPEPSPDQSATNSPESSSR	Bcl3	AASGS[+80]QPEPSPDQSATNSPESSSR	364	no	↑	Yes
AASGSQPEPSPDQSATNSPESSSR	Bcl3	AASGSQPEPS[+80]PDQSATNSPESSSR	369	yes	↑	Yes
AASGSQPEPSPDQSATNSPESSSR	Bcl3	AASGSQPEPSPDQSATNS[+80]PESSSR	377	no	↑	Yes
ASEQGAEVSPQPMAPHPGPDPK	Ikbke	ASEQGAEVS[+80]PQPMAPHPGPDPK	665	yes	↑	Yes
DAAFSSLSPPAVPASACPDLDLHYLALR	Tbkbp1	ND	ND	ND	↑	ND
DATPPVSPINMEDQER	Junb	DAT[+80]PPVSPINMEDQER	252	yes	↑	Yes
DATPPVSPINMEDQER	Junb	DATPPVS[+80]PINMEDQER	256	yes	↑	Yes
FHSFSFHELK	Irak4	FHS[+80]FSFHELK	166	no	↑	Yes
FRISHELESSSSEVN	Spp1	FRIS[+80]HELESSSSEVN	283	yes	↓	Yes
FSGISGCSDGASQEEGSASSTK	Rictor	FSGISGC[+57]S[+80]DGASQEEGSASSTK	1576	yes	↓	Yes
GYVSTTIK	Stat6	GY[+80]VSTTIK	641	yes	↑	Yes
KGSSSNEPSSDSLSSPTLLAL	Fos	KGS[+80]SSNEPSSDSLSSPTLLAL	362	yes	↑	Yes
KKPTPIQLNPAPDGSAVNGTSSAETNLEALQK	Map2k1	KKPTPIQLNPAPDGSAVNGTSS[+80]AETNLEALQK	25	yes	↑	Yes
NQHSLYTATTPPSSSPSR	Tab3	NQHSLYTATT[+80]PPSSSPSR	408	yes	↑	Yes
QPPSPASKPLPDDPNPA	Nfkbib	QPPS[+80]PASKPLPDDPNPA	346	yes	↓	Yes
QSSGASSSSFSSSR	Ddx3x	QSS[+80]GASSSSFSSSR	606	yes	↑	Yes
QSSGASSSSFSSSR	Ddx3x	QSSGASSSS[+80]FSSSR	612	yes	↑	Yes
RSPSPPEACR	Irf8	RS[+80]PSPPEACR	162	yes	↑	Yes
RSPSPPEACR	Irf8	RSPS[+80]PPEACR	164	yes	↑	Yes
RSISCVSPEREENMENGR	Irf9	RSISC[+57]VS[+80]PEREENMENGR	139	yes	↑	Yes
RVSPEPELQLR	Ifih1	RVS[+80]PEPELQLR	602	yes	↓	Yes
SLSAPQDK	Ripk2	SLS[+80]APQDK	364	yes	↑	Yes
SPLTSTTESVGK	Ticam1	ND	ND	ND	↓	ND
TLVHSSSDGHIDPQHTAGK	Tab3	TLVHS[+80]SSDGHIDPQHTAGK	101	yes (human)	↑	Yes
TLVHSSSDGHIDPQHTAGK	Tab3	TLVHSSS[+80]DGHIDPQHTAGK	103	yes	↑	Yes
TNGISDVQISPTLQR	Jak2	TNGISDVQIS[+80]PTLQR	523	yes	↑	Yes
TPVDDWTPPAR	Trim25	T[+80]PVDDWTPPAR	84	yes	↑	Yes
VCSIDLEIDSLSSLLDDMTK	Zyx	VCS[+80]IDLEIDSLSSLLDDMTK	144	yes	↓	ND
VSLESLK	Ticam1	ND	ND	ND	↓	ND
YTVGGSETFDSLTDLVEHFK	Ptpn6	ND	ND	ND	↓	ND

1) Phosphorylated amino acids are followed by [+80]
2) Phosphorylation sites reported in the phosphoSitePlus database (version: 2016/04/10, http://www.phosphosite.org)
ND = not detected

Figure legends

Figure 1: Extended phosphoproteomics approach overview. In a first step, cells were lysed, proteins extracted and digested to peptides. Then, phosphopeptides were enriched (we used TiO2 based enrichment, but the method is compatible with other enrichment strategies (e.g. IMAC)) followed by label-free quantification (LFQ) single dimension (1D) LC-MS analysis. Additionally, sample aliquots were subjected to protein quantification using tandem mass tags (TMT) to control for protein expression changes. All quantitative data were then statistically analyzed using our in-house software SafeQuant. To increase phosphoproteome coverage, we carried out a simple additional 1D-LC-MS experiment without the need for time and sample consuming fractionation steps. Specifically, remaining phosphopeptide sample aliquots were subjected to a phosphatase treatment that globally removed all serine, threonine and tyrosine phosphorylations followed by LFQ 1D-LC-MS and statistical analysis. In a final analysis, hits of interest were validated to determine the site of phosphorylation and confirm its quantification by either western blot or targeted LC-MS experiments.

Figure 2. LC-MS analysis of phosphopeptide enriched human cell digests before (-) and after (+) enzymatic phosphate removal. Number of identified unique phosphorylated (a) and all (b) peptides. Mean (line) as well as individual values for each replicate are shown. (c) Distribution of MS1 precursor intensities determined in both experiments. The median MS1 intensities are indicated. The change in MS1 intensities was significant (unpaired t-Test; two-tailed distribution assuming equal variance; homoscedastic, p-value <0.001). (d) Histogram showing the fold change of MS1 signals after phosphatase treatment for unmodified (green, n=5643) and phosphorylated peptides (blue, n=8694). The values indicate the median MS1 intensities. (e) Box plot showing the distribution of MS1 precursor intensities determined for 20 unmodified peptides spiked into different amounts of either a human cell digest (blue) or a phosphopeptide enriched sample thereof (black). Each box spans the interquartile range. The notches extend to the most extreme data point, which is no more than 1.5 times the interquartile range from the box. The thick horizontal line in each box indicates the median. Abbreviations: PO4ase=phosphatase. The calculated significance (t-Test; two-tailed distribution assuming equal variance; homoscedastic, p-value <0.001 (***)) are indicated.

Figure 3. Phosphatase treatment improved the quantification of significantly regulated peptides and proteins. (a) Representation of significantly regulated peptides (q-value < 0.01) in bone marrow-derived macrophages infected for 0.5, 1, 2, 4 and 8 h with *S*. Typhimurium *ΔorgA* before (blue) and after (red) phosphatase (PO4ase) treatment compared to uninfected cells. (b) Significantly enriched (p<0.01) immune signaling pathways (KEGG) of the corresponding proteins represented in (a). (c) Plot of ratios after 4 hours of infection of overlapping peptide sequences changing significantly in both datasets (q-value <0.01, MS-intensity >1E4). The linear regression (black dashed line) and the corresponding equation and R-square value are also shown. (d) Number of quantified hits with a CV <20 % between biological replicates after (red) and before (blue) phosphatase treatment.

Figure 4. Peptide phosphorylation dynamics before correlated with peptide abundances after phosphatase treatment. (a) STRING-based analysis of protein-protein interactions before (blue) and after (red) phosphatase treatment. Proteins highlighted in yellow were detected in phospho- and phosphatase-treated samples and in white proteins that were additional added to enlarge the network. Proteins validated by parallel reaction monitoring (PRM, see Figure 5) are indicated (*). Proteins analyzed by western blot (b and d) are shown with bigger font size. **(b)** Western blot analysis of protein phosphorylation in bone marrow-derived macrophages infected with *S*. Typhimurium *ΔorgA* representing the activation of MYD88 (p65), TRIF (IKKε) and JAK/STAT (STAT1) signaling pathways. **(c)** Peptide abundance of the signaling pathways represented in (b) after phosphatase treatment. **(d)** Comparison of western blot analysis of p38 MAPK phosphorylation in bone marrow-derived macrophages infected with *S*. Typhimurium *ΔorgA* with the respective peptide abundances before (blue) and after (red) phosphatase treatment. b,c Data are representatives of three independent experiments.

Figure 5. Validation of selected significantly regulated phosphopeptide candidates by targeted MS. Significantly changing dephosphorylated peptides were selected (Table 1) and subjected to validation by parallel reaction monitoring (PRM) to determine phosphorylation positons and validate abundance changes thereof. For this, we carried out two different strategies; (a) the classical stable isotope dilution

(SID)-PRM and a novel and (b) simple label-free quantification (LFQ)-PRM approach. For SID-PRM, heavy reference peptides carrying all possible phosphorylations were synthesized, analyzed by shotgun LC-MS and the 5-10 most intense fragments were selected for quantification. After spiking these heavy reference peptides in each phosphopeptide enriched sample, these and their light counterparts deriving from the endogenous phosphoprotein, were quantified using corresponding PRM assays. For LFQ-PRM (b), no heavy reference peptides are required and only the light peptide ions are subjected to PRM analysis. Here, an additional database search is carried out to identify the corresponding phosphopeptides and determine the most suited fragments for quantification. (c) For the peptide “DATPPVSPINMEDQER“ two different phosphorylation sites (pS7 and pT3) were identified (Supplementary Figure 13a&b). The location of shared (*, black) and discriminating (*, red) b- and y-fragments for the two peptides are indicated. (d) Quantification of both sites by PRM. Due to the presence of pS7 specific fragments (y13) and different elution times, both phosphorylation site could be accurately quantified. (e) Ratios determined for the two phosphorylation sites identified in peptide “DATPPVSPINMEDQER“ by the three different quantitative approaches performed (LFQ-/SID-PRM and LFQ-MS1 using untreated (-) PO4ase or dephosphorylated (+) PO4ase samples). The median value (line) as well as individual values for each replicate are shown.

Figure 1:

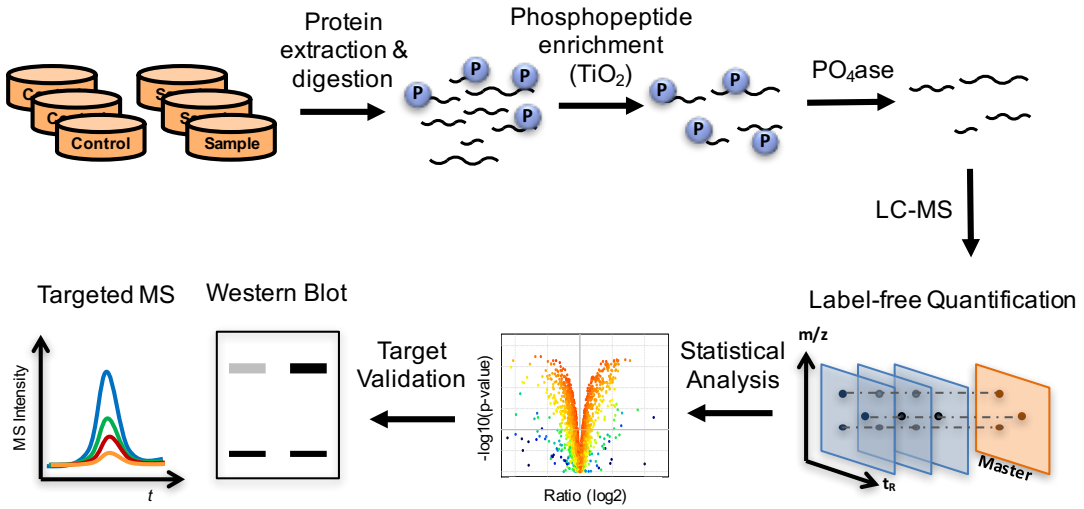
Control
Sample
Protein extraction & digestion
Phosphopeptide enrichment (TiO_2)
PO_4ase
LC-MS
Label-free Quantification
m/z
t_R
Master
Statistical Analysis
-log10(p-value)
Ratio (log2)
Target Validation
Western Blot
Targeted MS
MS Intensity
t

Figure 2:

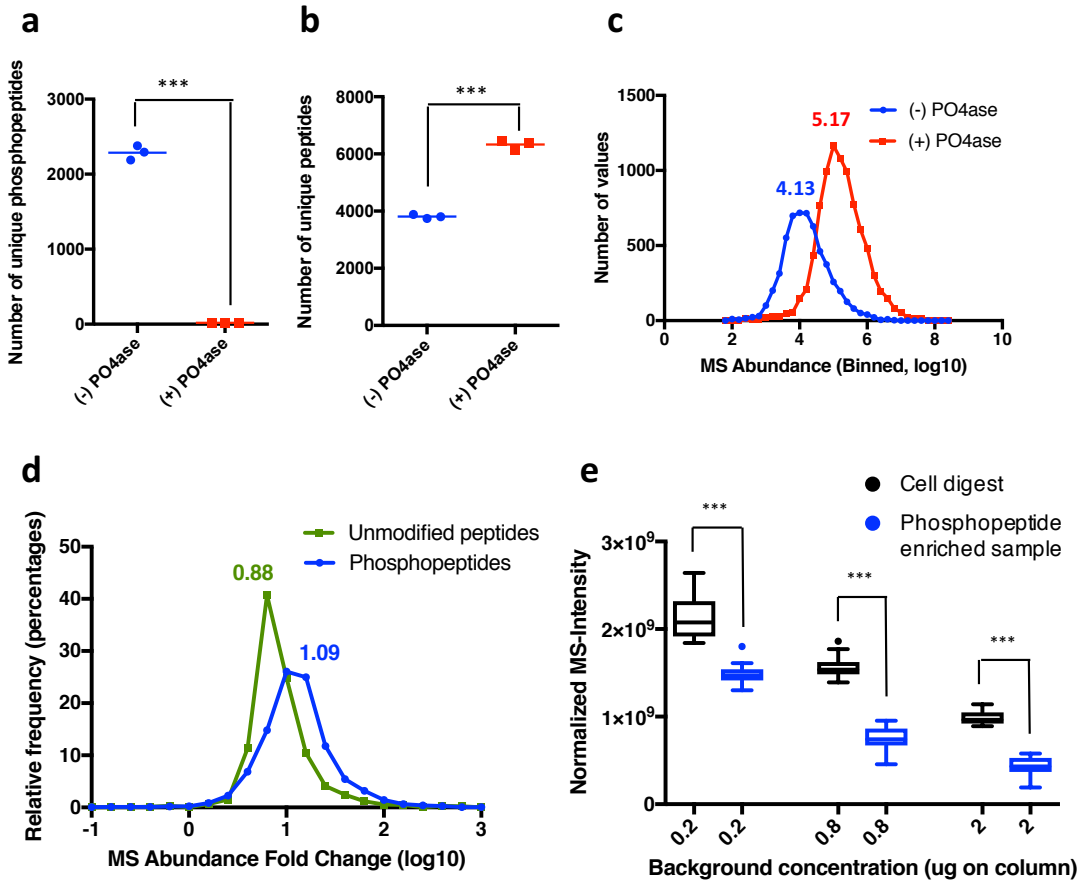
a
Number of unique phosphopeptides
3000
2000
1000
0
***
(-) PO4ase
(+) PO4ase
b
Number of unique peptides
8000
6000
4000
2000
0
***
(-) PO4ase
(+) PO4ase
c
Number of values
1500
1000
500
0
5.17
4.13
(-) PO4ase
(+) PO4ase
0
2
4
6
8
10
MS Abundance (Binned, log10)
d
Relative frequency (percentages)
50
40
30
20
10
0
0.88
1.09
Unmodified peptides
Phosphopeptides
-1
0
1
2
3
MS Abundance Fold Change (log10)
e
Normalized MS-Intensity
3×10⁹
2×10⁹
1×10⁹
0
***
***
***
Cell digest
Phosphopeptide enriched sample
0.2
0.2
0.8
0.8
2
2
Background concentration (ug on column)

Figure 3:

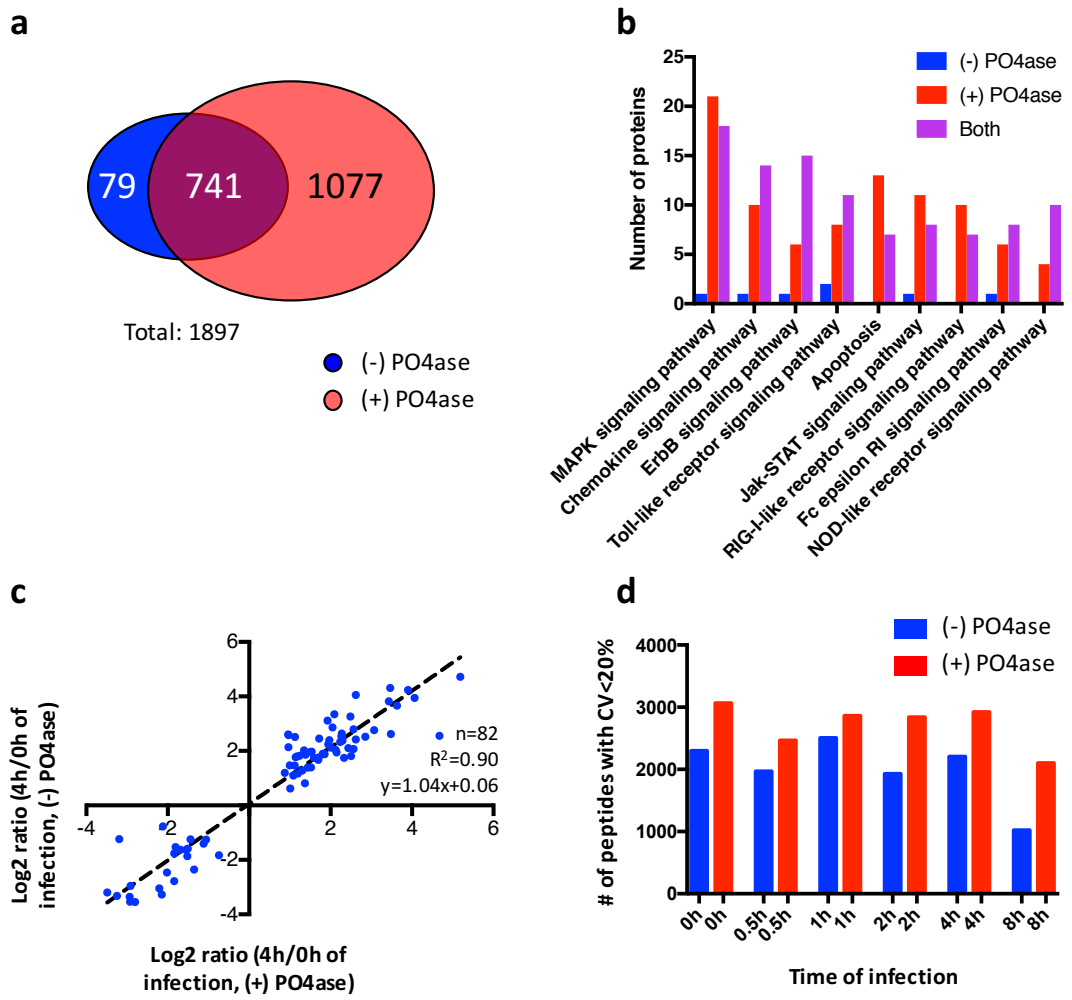
a
79
741
1077
Total: 1897
(-) PO4ase
(+) PO4ase
b
Number of proteins
(-) PO4ase
(+) PO4ase
Both
MAPK signaling pathway
Chemokine signaling pathway
ErbB signaling pathway
Toll-like receptor signaling pathway
Apoptosis
Jak-STAT signaling pathway
RIG-I-like receptor signaling pathway
Fc epsilon RI signaling pathway
NOD-like receptor signaling pathway
c
Log2 ratio (4h/0h of infection, (-) PO4ase)
n=82
R2=0.90
y=1.04x+0.06
Log2 ratio (4h/0h of infection, (+) PO4ase)
d
# of peptides with CV<20%
(-) PO4ase
(+) PO4ase
Time of infection

Figure 4:

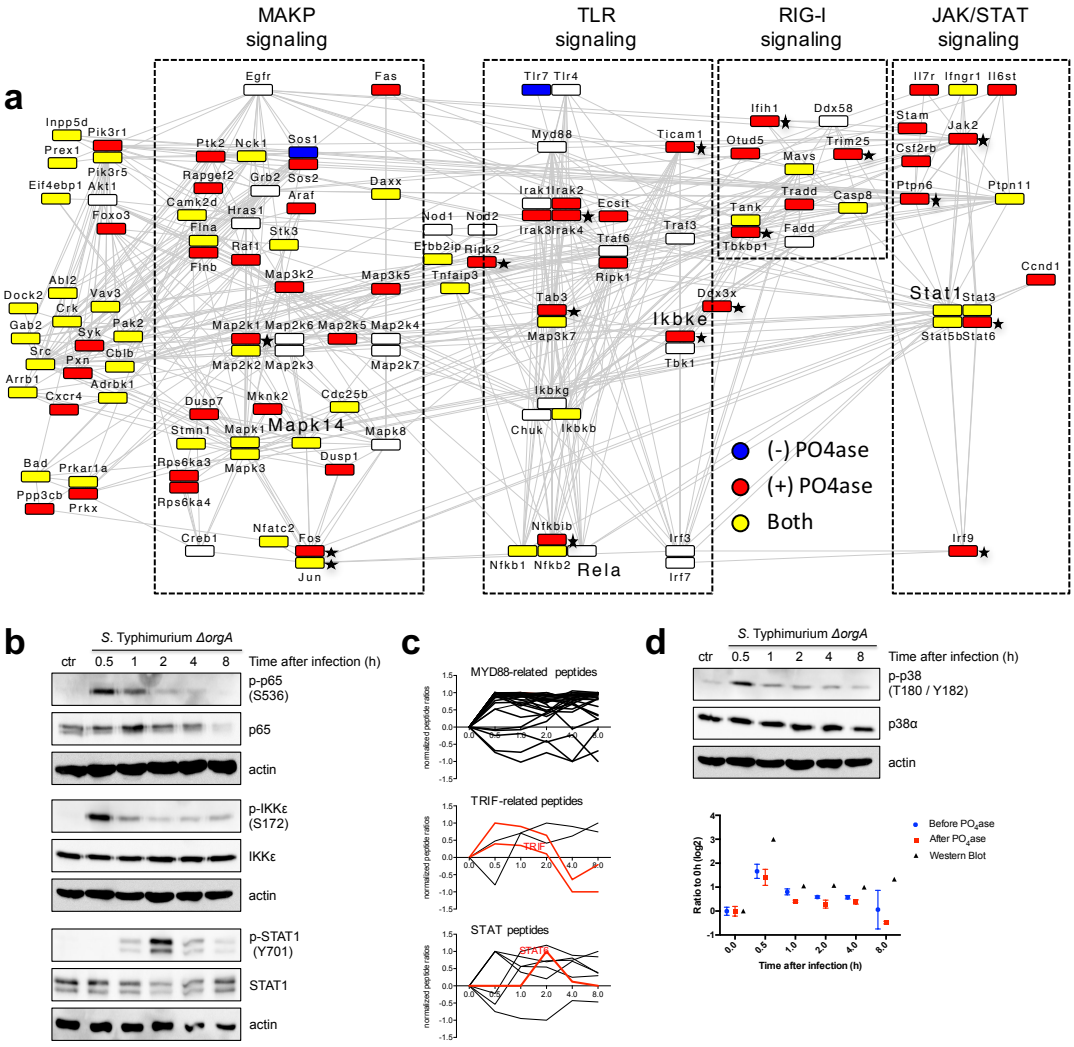
a
MAKP signaling
TLR signaling
RIG-I signaling
JAK/STAT signaling
Egfr
Fas
Tlr7 Tlr4
Ifih1
Ddx58
Il7r Ifngr1 Il6st
Inpp5d
Pik3r1
Prex1
Pik3r5
Eif4ebp1
Akt1
Foxo3
Ptk2 Nck1 Sos1
Rapgef2
Grb2 Sos2
Daxx
Camk2d
Hras1
Araf
Flna
Stk3
Raf1
Flnb
Map3k2
Map3k5
Nod1 Nod2
Erbb2ip
Ripk2
Tnfaip3
Myd88
Ticam1
Irak1 Irak2
Irak3 Irak4
Ecsit
Traf6
Traf3
Ripk1
Tab3
Map3k7
Ikbke
Tbk1
Ikbkg
Chuk Ikbkb
Ntkbib
Nfkb1 Nfkb2 Rela
Irf3
Irf7
Otud5
Mavs
Trim25
Tradd
Casp8
Tank
Fadd
Tbkbp1
Stam
Jak2
Csf2rb
Ptpn6
Ptpn11
Ccnd1
Stat1 Stat3
Stat5b Stat6
Irf9
Abl2
Dock2
Vav3
Crk
Gab2
Pak2
Syk
Src
Cblb
Pxn
Arrb1
Adrbk1
Cxcr4
Map2k1 Map2k6 Map2k5 Map2k4
Map2k2 Map2k3
Map2k7
Dusp7
Mknk2
Cdc25b
Stmn1
Mapk1
Mapk14
Mapk8
Rps6ka3
Mapk3
Dusp1
Rps6ka4
Bad
Prkar1a
Ppp3cb
Prkx
Creb1
Nfatc2
Fos
Jun
Ddx3x
(-) PO4ase
(+) PO4ase
Both
b
S. Typhimurium ΔorgA
ctr 0.5 1 2 4 8
Time after infection (h)
p-p65 (S536)
p65
actin
p-IKKε (S172)
IKKε
actin
p-STAT1 (Y701)
STAT1
actin
c
MYD88-related peptides
TRIF-related peptides
STAT peptides
normalized peptide ratios
d
S. Typhimurium ΔorgA
ctr 0.5 1 2 4 8
Time after infection (h)
p-p38 (T180 / Y182)
p38α
actin
Before PO4ase
After PO4ase
Western Blot
Ratio to 0h (log2)
Time after infection (h)

Figure 5:

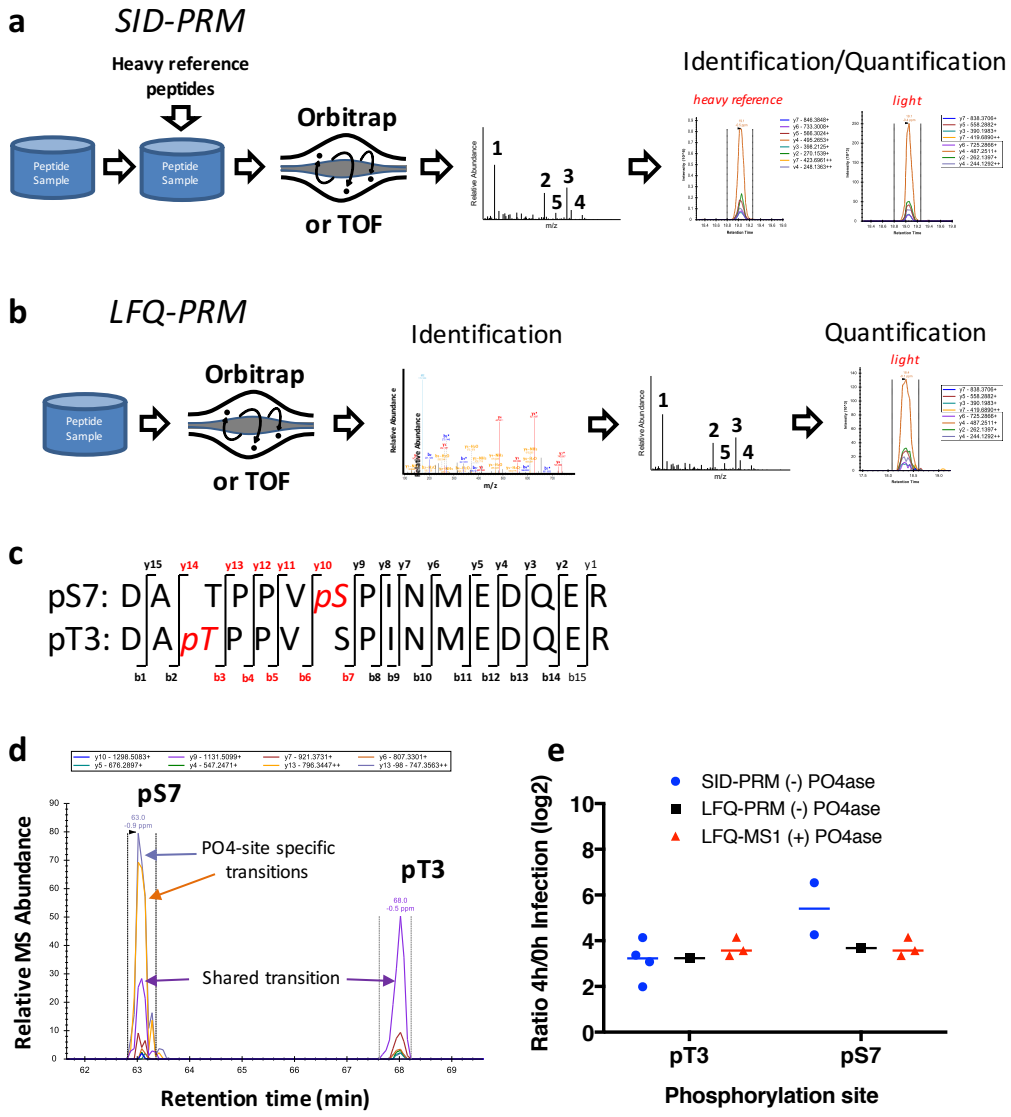
a
SID-PRM
Heavy reference peptides
Peptide Sample
Peptide Sample
Orbitrap
or TOF
Identification/Quantification
heavy reference
light
b
LFQ-PRM
Peptide Sample
Orbitrap
or TOF
Identification
Quantification
light
c
pS7: D A T P P V pS P I N M E D Q E R
pT3: D A pT P P V S P I N M E D Q E R
d
pS7
pT3
PO4-site specific transitions
Shared transition
Relative MS Abundance
Retention time (min)
e
SID-PRM (-) PO4ase
LFQ-PRM (-) PO4ase
LFQ-MS1 (+) PO4ase
Ratio 4h/0h Infection (log2)
pT3
pS7
Phosphorylation site

References:

1. Hebert, A. S. *et al.* The one hour yeast proteome. *Mol Cell Proteomics* **13,** 339–347 (2014).
2. Scheltema, R. A. *et al.* The Q Exactive HF, a Benchtop mass spectrometer with a pre-filter, high-performance quadrupole and an ultra-high-field Orbitrap analyzer. *Mol Cell Proteomics* **13,** 3698–3708 (2014).
3. Post, H. *et al.* Robust, Sensitive, and Automated Phosphopeptide Enrichment Optimized for Low Sample Amounts Applied to Primary Hippocampal Neurons. *J. Proteome Res.* **16,** 728–737 (2017).
4. Ruprecht, B. *et al.* Comprehensive and reproducible phosphopeptide enrichment using iron immobilized metal ion affinity chromatography (Fe-IMAC) columns. *Mol Cell Proteomics* **14,** 205–215 (2015).
5. Sharma, K. *et al.* Ultradeep human phosphoproteome reveals a distinct regulatory nature of Tyr and Ser/Thr-based signaling. *Cell Rep* **8,** 1583–1594 (2014).
6. Koch, H. *et al.* Phosphoproteome Profiling Reveals Molecular Mechanisms of Growth-Factor-Mediated Kinase Inhibitor Resistance in EGFR-Overexpressing Cancer Cells. *J. Proteome Res.* **15,** 4490–4504 (2016).
7. Gropengiesser, J., Varadarajan, B. T., Stephanowitz, H. & Krause, E. The relative influence of phosphorylation and methylation on responsiveness of peptides to MALDI and ESI mass spectrometry. *J Mass Spectrom* **44,** 821–831 (2009).
8. Annesley, T. M. Ion suppression in mass spectrometry. *Clin Chem* **49,** 1041–1044 (2003).
9. Ishihama, Y. *et al.* Enhancement of the efficiency of phosphoproteomic identification by removing phosphates after phosphopeptide enrichment. *J. Proteome Res.* **6,** 1139–1144 (2007).
10. Hommerson, P., Khan, A. M., de Jong, G. J. & Somsen, G. W. Comparison of electrospray ionization and atmospheric pressure photoionization for coupling of micellar electrokinetic chromatography with ion trap mass spectrometry. *J Chromatogr A* **1204,** 197–203 (2008).
11. Janek, K., Wenschuh, H., Bienert, M. & Krause, E. Phosphopeptide analysis by positive and negative ion matrix-assisted laser desorption/ionization mass spectrometry. *Rapid Commun Mass Spectrom* **15,** 1593–1599 (2001).
12. Steen, H., Jebanathirajah, J. A., Rush, J., Morrice, N. & Kirschner, M. W. Phosphorylation analysis by mass spectrometry: myths, facts, and the consequences for qualitative and quantitative measurements. *Mol Cell Proteomics* **5,** 172–181 (2006).
13. Marx, H. *et al.* A large synthetic peptide and phosphopeptide reference library for mass spectrometry-based proteomics. *Nat Biotechnol* **31,** 557–564 (2013).
14. Mandal, S. M., Dey, S., Mandal, M., Maria-Neto, S. & Franco, O. L. Comparative analyses of different surfactants on matrix-assisted laser desorption/ionization mass spectrometry peptide analysis. *Eur J Mass Spectrom (Chichester)* **16,** 567–575 (2010).
15. Keestra-Gounder, A. M., Tsolis, R. M. & Bäumler, A. J. Now you see me, now you don't: the interaction of Salmonella with innate immune receptors. *Nat Rev Micro* **13,** 206–216 (2015).
16. LaRock, D. L., Chaudhary, A. & Miller, S. I. Salmonellae interactions with host processes. *Nat Rev Micro* **13,** 191–205 (2015).
17. Sharma, K. *et al.* Cell type- and brain region-resolved mouse brain proteome.

Nat. Neurosci. **18,** 1819–1831 (2015).
18. Hornbeck, P. V. *et al.* PhosphoSitePlus, 2014: mutations, PTMs and recalibrations. *Nucleic Acids Res* **43,** D512–20 (2015).
19. Mellacheruvu, D. *et al.* The CRAPome: a contaminant repository for affinity purification-mass spectrometry data. *Nat Meth* **10,** 730–736 (2013).
20. Leney, A. C., Atmioui, El, D., Wu, W., Ovaa, H. & Heck, A. J. R. Elucidating crosstalk mechanisms between phosphorylation and O-GlcNAcylation. *Proceedings of the National Academy of Sciences* **114,** E7255–E7261 (2017).
21. Poot, A. J. *et al.* Selective enrichment of Ser-/Thr-phosphorylated peptides in the presence of Ser-/Thr-glycosylated peptides. *PROTEOMICS* **6,** 6394–6399 (2006).
22. Knight, Z. A. *et al.* Phosphospecific proteolysis for mapping sites of protein phosphorylation. *Nat Biotechnol* **21,** 1047–1054 (2003).
23. Bonaldi, T., Imhof, A. & Regula, J. T. A combination of different mass spectroscopic techniques for the analysis of dynamic changes of histone modifications. *PROTEOMICS* **4,** 1382–1396 (2004).
24. Dickhut, C., Feldmann, I., Lambert, J. & Zahedi, R. P. Impact of digestion conditions on phosphoproteomics. *J. Proteome Res.* **13,** 2761–2770 (2014).
25. Huang, D. W., Sherman, B. T. & Lempicki, R. A. Systematic and integrative analysis of large gene lists using DAVID bioinformatics resources. *Nat Protoc* **4,** 44–57 (2009).
26. Huang, D. W., Sherman, B. T. & Lempicki, R. A. Bioinformatics enrichment tools: paths toward the comprehensive functional analysis of large gene lists. *Nucleic Acids Res* **37,** 1–13 (2009).
27. Mering, von, C. *et al.* STRING: known and predicted protein-protein associations, integrated and transferred across organisms. *Nucleic Acids Res* **33,** D433–7 (2005).
28. Takeuchi, O. & Akira, S. Toll-like receptors; their physiological role and signal transduction system. *Int. Immunopharmacol.* **1,** 625–635 (2001).
29. Brubaker, S. W., Bonham, K. S., Zanoni, I. & Kagan, J. C. Innate immune pattern recognition: a cell biological perspective. *Annu. Rev. Immunol.* **33,** 257–290 (2015).
30. Schneider, W. M., Chevillotte, M. D. & Rice, C. M. Interferon-stimulated genes: a complex web of host defenses. *Annu. Rev. Immunol.* **32,** 513–545 (2014).
31. Peters, R. T., Liao, S. M. & Maniatis, T. IKKepsilon is part of a novel PMA-inducible IkappaB kinase complex. *Mol Cell* **5,** 513–522 (2000).
32. O'Mahony, A. M., Montano, M., Van Beneden, K., Chen, L.-F. & Greene, W. C. Human T-cell lymphotropic virus type 1 tax induction of biologically Active NF-kappaB requires IkappaB kinase-1-mediated phosphorylation of RelA/p65. *J Biol Chem* **279,** 18137–18145 (2004).
33. Ihle, J. N. *et al.* Signaling by the cytokine receptor superfamily: JAKs and STATs. *Trends Biochem. Sci.* **19,** 222–227 (1994).
34. Kato, H. *et al.* Differential roles of MDA5 and RIG-I helicases in the recognition of RNA viruses. *Nature* **441,** 101–105 (2006).
35. Gillette, M. A. & Carr, S. A. Quantitative analysis of peptides and proteins in biomedicine by targeted mass spectrometry. *Nat Meth* **10,** 28–34 (2013).
36. Gallien, S. *et al.* Targeted proteomic quantification on quadrupole-orbitrap mass spectrometer. *Mol Cell Proteomics* **11,** 1709–1723 (2012).
37. Peterson, A. C., Russell, J. D., Bailey, D. J., Westphall, M. S. & Coon, J. J. Parallel reaction monitoring for high resolution and high mass accuracy quantitative, targeted proteomics. *Mol Cell Proteomics* **11,** 1475–1488 (2012).

38. Picotti, P. & Aebersold, R. Selected reaction monitoring-based proteomics: workflows, potential, pitfalls and future directions. *Nat Meth* **9,** 555–566 (2012).
39. Cox, J. & Mann, M. MaxQuant enables high peptide identification rates, individualized p.p.b.-range mass accuracies and proteome-wide protein quantification. *Nat Biotechnol* **26,** 1367–1372 (2008).
40. Li, H. *et al.* The phosphothreonine lyase activity of a bacterial type III effector family. *Science* **315,** 1000–1003 (2007).
41. Humphrey, S. J., Azimifar, S. B. & Mann, M. High-throughput phosphoproteomics reveals in vivo insulin signaling dynamics. *Nat Biotechnol* **33,** 990–995 (2015).
42. Schmutz, C. *et al.* Systems-level overview of host protein phosphorylation during Shigella flexneri infection revealed by phosphoproteomics. *Mol Cell Proteomics* **12,** 2952–2968 (2013).
43. Ahrné, E. *et al.* Evaluation and Improvement of Quantification Accuracy in Isobaric Mass Tag-Based Protein Quantification Experiments. *J. Proteome Res.* **15,** 2537–2547 (2016).
44. Wang, Y. *et al.* Reversed-phase chromatography with multiple fraction concatenation strategy for proteome profiling of human MCF10A cells. *PROTEOMICS* **11,** 2019–2026 (2011).
45. Beausoleil, S. A., Villén, J., Gerber, S. A., Rush, J. & Gygi, S. P. A probability-based approach for high-throughput protein phosphorylation analysis and site localization. *Nat Biotechnol* **24,** 1285–1292 (2006).
46. Nesvizhskii, A. I., Keller, A., Kolker, E. & Aebersold, R. A statistical model for identifying proteins by tandem mass spectrometry. *Anal Chem* **75,** 4646–4658 (2003).
47. Yang, D., Parrish, R. S. & Brock, G. N. Empirical evaluation of consistency and accuracy of methods to detect differentially expressed genes based on microarray data. *Comput. Biol. Med.* **46,** 1–10 (2014).
48. Kulak, N. A., Pichler, G., Paron, I., Nagaraj, N. & Mann, M. Minimal, encapsulated proteomic-sample processing applied to copy-number estimation in eukaryotic cells. *Nat Meth* **11,** 319–324 (2014).
49. Vizcaíno, J. A. *et al.* The PRoteomics IDEntifications (PRIDE) database and associated tools: status in 2013. *Nucleic Acids Res* **41,** D1063–9 (2013).

Supplementary Materials for

Global ion suppression limits the potential of mass spectrometry based phosphoproteomics

Roland Felix Dreier*, Erik Ahrné*, Petr Broz, Alexander Schmidt

Biozentrum, University of Basel, Klingelbergstrasse 50/70, 4056 Basel, Switzerland

Corresponding authors: Alexander Schmidt (alex.schmidt@unibas.ch) and Petr Broz (petr.broz@unibas.ch)

* These authors contributed equally to this work

This PDF file includes:

Supplementary Figures:

Supplementary Figure 1: Base peak chromatograms displaying peptide elution patterns for phosphopeptide enriched samples before (blue) and after (red) phosphate removal using phosphatase treatment.

Supplementary Figure 2: Correlation of precursor ion intensities determined before (-) and after (+) phosphatase (PO4ase) treatment.

Supplementary Figure 3: Precursor ion intensities determined for 20 unmodified peptides spiked in different amounts to a whole human cell digest and a phosphopeptide enriched sample.

Supplementary Figure 4: Evaluation of tandem mass spectrometric analysis of phosphopeptides identified +/- phosphatase treatment.

Supplementary Figure 5: LC-MS analysis of phosphopeptide enriched murine macrophages after Salmonella infection for 6 different time points before (-) and after (+) enzymatic phosphate removal.

Supplementary Figure 6: Phosphopeptide content of additional identified peptides.

Supplementary Figure 7: Prevalence of a few selected frequent kinase motifs in the peptides identified before (blue) and after (red) phosphatase treatment.

Supplementary Figure 8: Beta-elimination of phosphopeptide enriched samples.

Supplementary Figure 9: Evaluation of physiochemical properties of peptide identified before (-) and after (+) phosphatase treatment.

Supplementary Figure 10: Functional and quantitative analysis of differentially abundant phosphorylated peptides.

Supplementary Figure 11: Impact of phosphatase treatment on determined quantification statistics.

Supplementary Figure 12: Identification and quantification of two different phosphorylation sites one peptide “DATPPVSPINMEDQER“ by LFQ-PRM.

Supplementary Figure 13: Identification and quantification of three different phosphorylation sites one peptide “AASGSQPEPSPDQSATNSPESSSR“ by LFQ-PRM.

Supplementary Figure 14: Correlation of ratios determined from successfully validated phosphopeptides candidates quantified in the large-scale experiment (after phosphatase treatment) and by follow up targeted parallel reaction monitoring (PRM) MS analysis (no phosphatase treatment).

Supplementary Figure 1:

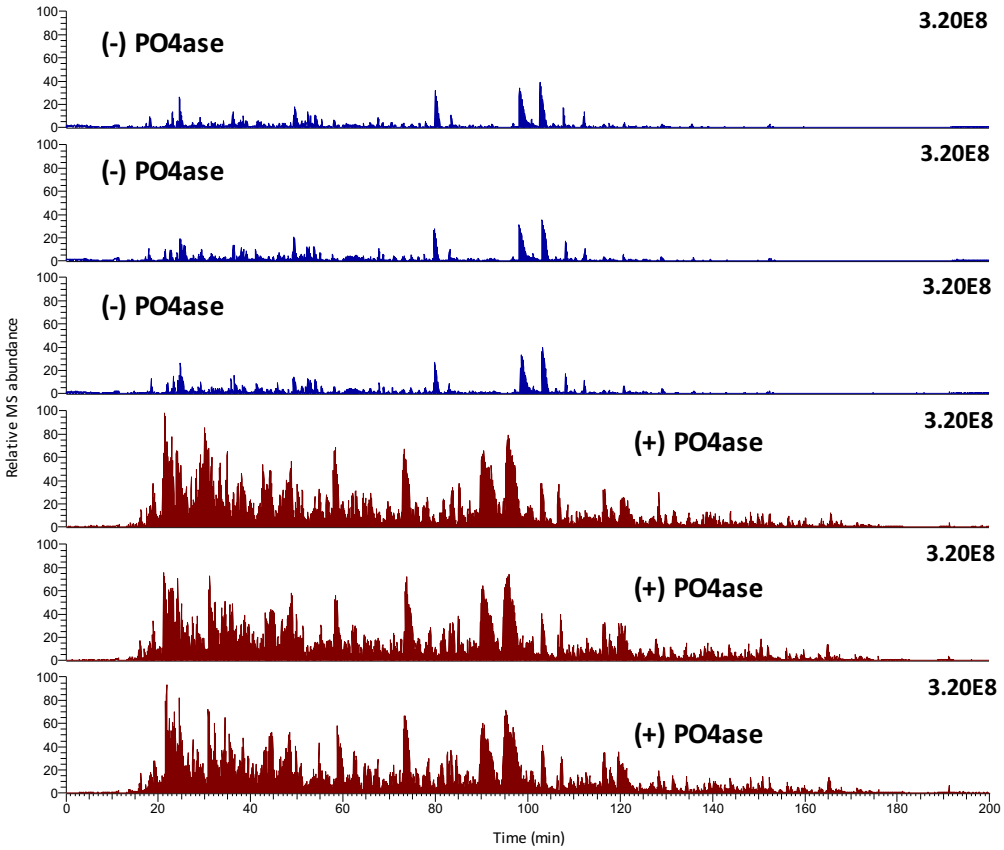

Supplementary Figure 1: Base peak chromatograms displaying peptide elution patterns for phosphopeptide enriched samples before (blue) and after (red) phosphate removal using phosphatase treatment. Triplicate analyses were carried out for each condition. The relative abundance scale was fixed for chromatograms to the number in the corner indicating the absolute ion current intensity of the most intense peak.

Supplementary Figure 2:

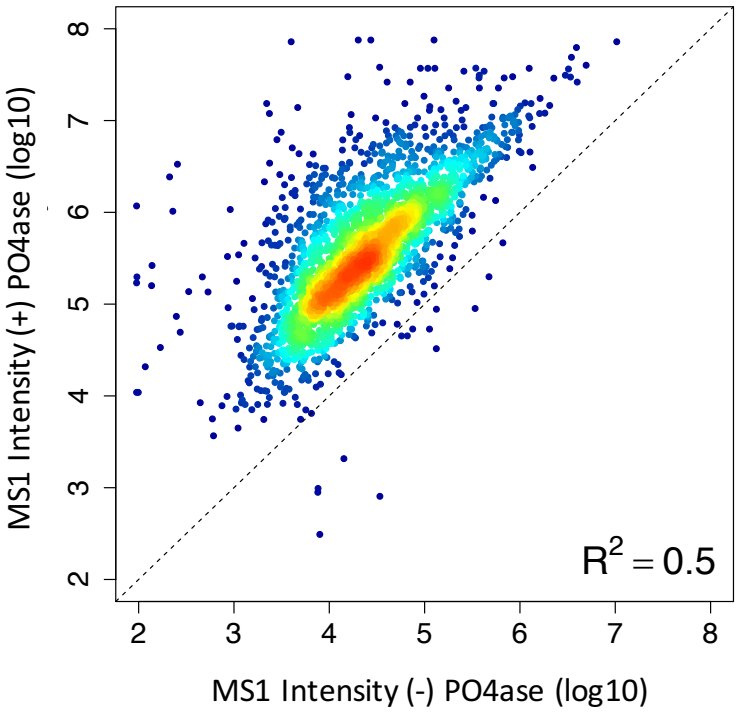

Supplementary Figure 2: Correlation of precursor ion intensities determined before (-) and after (+) phosphatase (PO4ase) treatment. Squared Pearson correlation coefficients (R^2) and a line showing perfect correlation (black, dashed) are indicated. (n=3471).

Calculation of phosphopeptide concentration during LC-MS analysis: Considering that a total of 1ug (around 1 nmol at an average peptide mass of 1000 Da) of phosphopeptides were analyzed over an LC gradient of 90 minutes at a flow rate of 200 nl/min (total volume 18 µl), the average phosphopeptide concentration can be estimated to be around 55 mM. This concentration is well in the range for which ionization suppression (starting at a concentration of 10 mM) was observed for other anionic molecules, like frequently used detergents, for instance SDS, that are also negatively charged in the mobile phase used here (0.1% formic acid)[1,2].

Supplementary Figure 3:

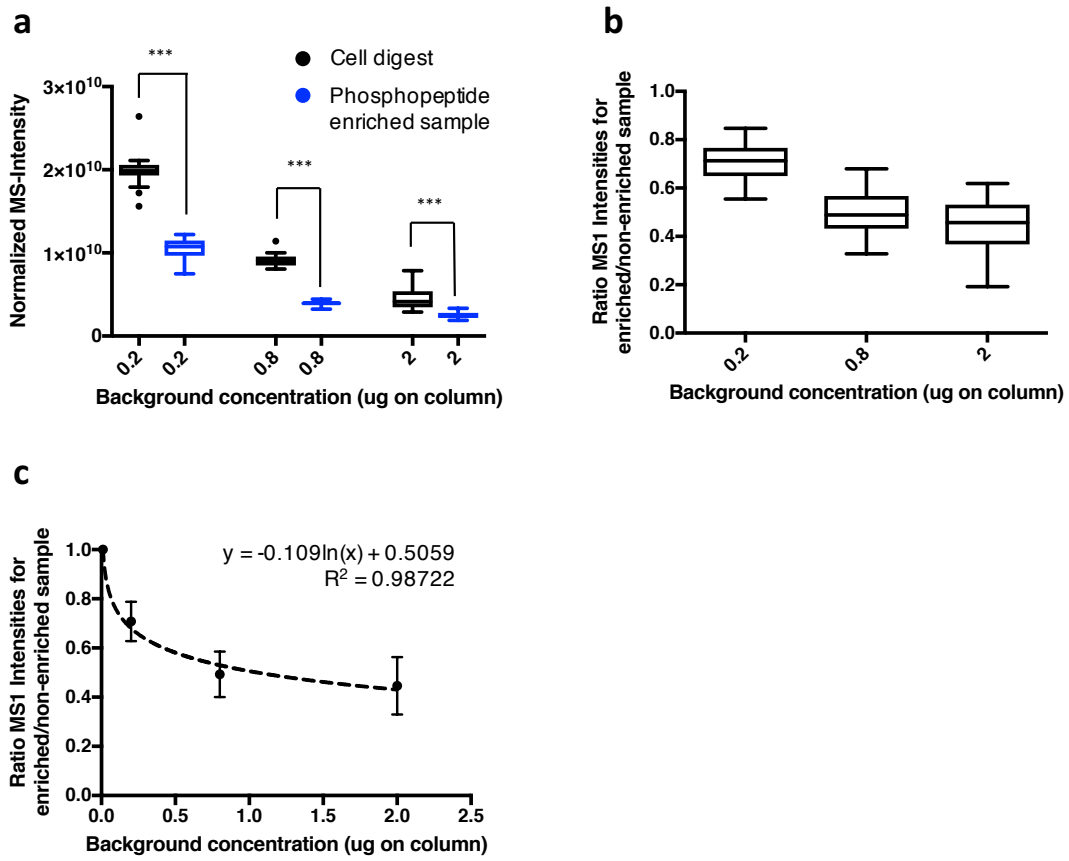

Supplementary Figure 3: Precursor ion intensities determined for 20 unmodified peptides spiked in different amounts to a whole human cell digest and a phosphopeptide enriched sample. (a) Box plots showing the distribution of MS1-intensites obtained for 20 reference peptides spiked in 3 different amounts of human cell digest (blue) or a phosphopeptide enriched human cell lysate (black). (b) Box plots showing the distribution of MS1-intensites ratio measured in phosphopeptide enriched versus non-enriched background. The notches extend to the most extreme data point, which is no more than 1.5 times the interquartile range from the box. The thick horizontal line in each box indicates the median. The calculated significance (t-Test; two-tailed distribution assuming equal variance; homoscedastic), p-values <0.001 (***)) are indicated. (c) Correlation of ratios determined in (b). Each box spans the interquartile range. Squared Pearson correlation coefficients (R^2) and the fitting equation are shown.

Supplementary Figure 4:

a

Number of phosphopeptide candidate ions (identified exclusively after PO4ase treatment) that were also MS-sequenced in their phosphorylated form before PO4ase treatment

Peptides	# of ions (z=2)	# of ions (z=3)	# of ions (z=4)	# of ions (z=2-4)	# of ions (z=2-4) in %
Unmodified	218	218	83	457	**9.4**
Phosphorylation	373	360	125	730	**15.0**
Acetylation (Neg. Ctrl.)	202	197	67	405	**8.3**

b

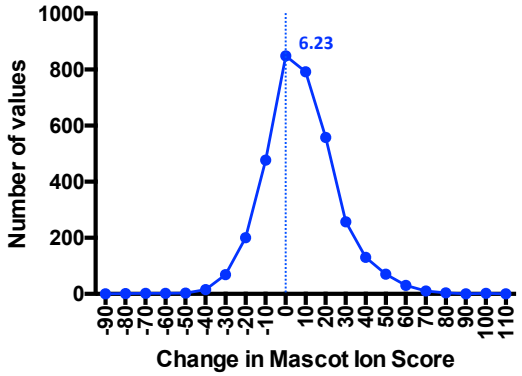

Supplementary Figure 4: Evaluation of tandem mass spectrometric analysis of phosphopeptides identified +/- phosphatase treatment. (a) To investigate in more detail the increased number of peptide sequences identified after phosphate removal (here referred to as phosphopeptide candidates), we determined how many precursors of the additional peptides were actually MS-sequenced in their phosphorylated form before phosphatase treatment according to their charge state (z). Surprisingly, we could find matching MS/MS spectra (using a precursor mass tolerance of 5 ppm and a retention time tolerance of 300 sec) for only 15% of the phosphopeptide candidates. This indicates that 85% of the phosphopeptide candidates were not identified in their phosphorylated state, because the precursor ion intensity was too low for triggering MS-sequencing. Therefore, the observed global ion suppression (Fig. 2c) is the main cause for the low number of identified peptides in phosphopeptide enriched samples. We additionally determined the numbers for matching acetylated peptides, which should not be present in the phosphopeptide enriched sample and presents a good negative control to determine random matching events. Here, we could match 8.3% of the hits, meaning that only around 7% of the phosphopeptide candidates were in fact MS-sequenced in their modified form. Finally, we also found a similar small number of matches for unmodified peptides. This shows that the phosphopeptide candidates were also not present in their unmodified but phosphorylated form in the original phosphopeptide enriched sample. (b) Difference in mascot ion score calculated for phosphorylated and unmodified peptides. Unchanged scores (blue dashed line) and the median value are indicated. This indicates that phosphorylation has a slight negative impact on peptide identification confidence and this improved after phosphorylation removal. This might also contribute to the increased identification rates achieved after phosphatase treatment, however, only to small degree. The large majority of additional hits arise from the overall increased MS-response and the resulting MS-sequencing of additional precursor ions.

Supplementary Figure 5:

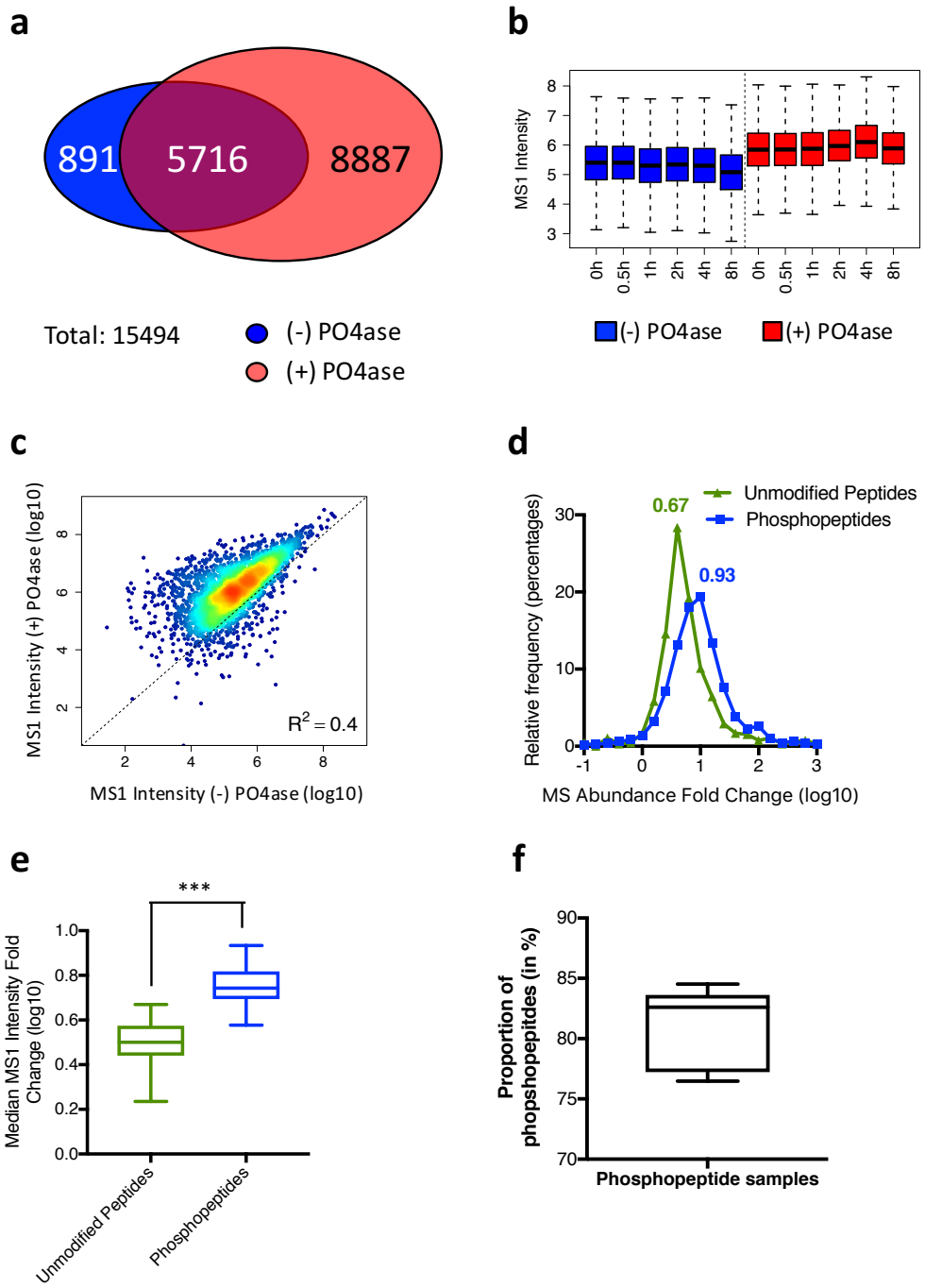

Supplementary Figure 5: LC-MS analysis of phosphopeptide enriched murine macrophages after Salmonella infection for 6 different time points before (-) and after (+) enzymatic phosphate removal. (a) Venn diagram showing the unique peptide sequences identified before (blue) and after (red) phosphatase treatment. (b) Box plot illustrating the distribution of MS1 precursor ion intensities determined for the different durations of infection before (blue) and after (red) enzymatic phosphate removal. Each box spans the interquartile range. The notches extend to the most

extreme data point, which is no more than 1.5 times the interquartile range from the box. The thick horizontal line in each box indicates the median. The increase of MS1 intensities determined after PO4ase treatment for the different time points (paired t-Test; two-tailed distribution assuming equal variance; homoscedastic) was significant (p-value <0.001) for all samples. (c) Correlation of precursor ion intensities determined before (-) and after (+) phosphatase treatment for one representative condition (8h). Squared Pearson correlation coefficients (R^2) and a line showing perfect correlation (black, dashed) are indicated. (d) Histogram showing the fold change of MS1 signals after phosphatase treatment for unmodified (green) and phosphorylated peptides (blue) for one representative sample (8h). The numbers indicate the median values. (e) Box plot illustrating the distribution of median MS1 precursor ion intensities fold changes determined for all 18 samples after enzymatic phosphate removal for unmodified (green) and phosphorylated (blue) peptides. Each box spans the interquartile range. The notches extend to the most extreme data point, which is no more than 1.5 times the interquartile range from the box. The thick horizontal line in each box indicates the median. The differences of ratios determined for unmodified and phosphorylated peptides was significant (paired t-Test; two-tailed distribution assuming equal variance; homoscedastic, p-value <0.001). (f) Box plot showing the proportions (in %) of phosphorylated over all peptides identified in the TiO2 enriched samples. Each box spans the interquartile range. The notches extend to the most extreme data point, which is no more than 1.5 times the interquartile range from the box. The thick horizontal line in each box indicates the median. (n=2799 for Figures b-f). Abbreviations: PO4ase=phosphatase.

Supplementary Figure 6:

a

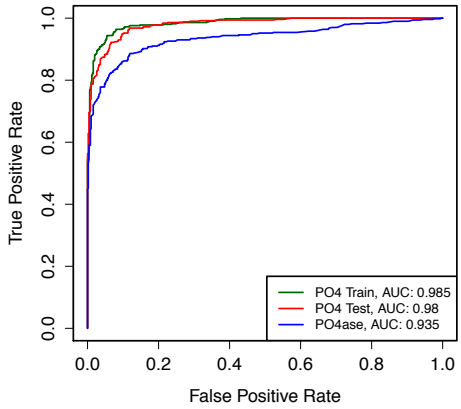

b

Table: (-) PO4ase Train, Classification Accuracy 0.94

	(Labelled) -	(Labelled) +
(Predicted) -	476	39
(Predicted) +	24	461

Table: (-) PO4ase Test, Classification Accuracy 0.92

	(Labelled) -	(Labelled) +
(Predicted) -	469	44
(Predicted) +	31	456

Table: (+) PO4ase, Classification Accuracy 0.88, FDR 0.175

	(Labelled) -	(Labelled) +
(Predicted) -	469	90
(Predicted) +	31	410

c

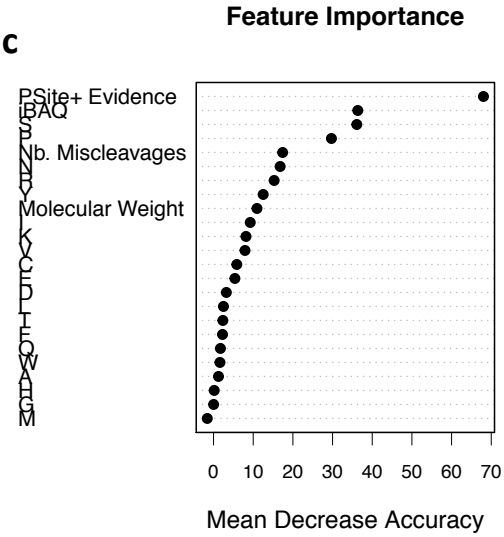

d

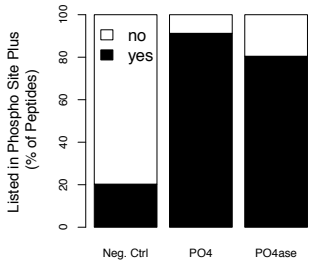

e

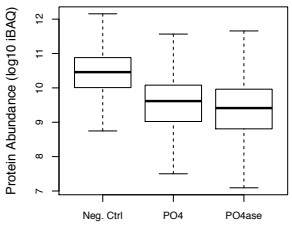

Supplementary Figure 6: Phosphopeptide content of additional identified peptides. We used a Random Forest classification algorithm[3] to show that the novel peptides identified in the PO4ase treated samples have phospho-specific features. The list of investigated features included; the number of trypsin missed cleavages (Nb. Miscleavages), peptide molecular weight (Molecular Weight), Intensity Based Absolute Quantification (iBAQ) value of the originating protein[4], the number of entries in the PhosphoSitePlus database per identified peptide(PSite+ Evidence)[5] and finally the prevalence of each amino acid per peptide; i.e. amino acid count divided by peptide length (amino acid one-letter code).

To train the classification algorithm, unmodified serine or threonine containing peptides identified in the phosphopeptide enriched samples before PO4ase treatment were used as negative controls and confidently identified phosphopeptides, found in the phosphopeptide (no PO4ase) and beta-elimination datasets, were used as positive controls.

In total, the training dataset (PO4 Train) included 500 negative control peptides (assigned a negative class label) and an equal number of positive control peptides (assigned a positive class label). Additionally, a separate test set (PO4 Test) with the same number of negative and positive control peptides as the training dataset was compiled. This test dataset was used to demonstrate that our confidently identified phosphopeptides could be distinguished from unmodified peptides found in our phospho-enriched samples, in the feature space described above. When classifying the test dataset peptides using the Random Forest algorithm a classification accuracy of 92% was achieved (b). A Receiver Operator characteristics curve is shown in (a) (The Area Under Curve was 0.98). Clearly, the phosphopeptides take on dramatically different values with respect to the selected features fed to the Random Forest algorithm. To better understand how the phosphopeptides differ from unmodified peptides, we ranked the importance of each feature by the Mean Decrease Accuracy; i.e. the decrease in classification accuracy as the values of a feature are randomly permutated (c). The top-ranking features were PSite+ Evidence, iBAQ and the prevalence of the amino acids serine and proline. It is intuitive that our identified phosphopeptides are listed more frequently in the PhosphoSitePlus database than the identified unmodified peptides. It is also expected that nonspecifically enriched peptides (i.e the identified unmodified peptides) map to highly abundant proteins. A likely explanation for the differences in serine and proline prevalence among positive and negative controls (serine and proline occur more frequently in the phosphopeptide set) is that the “SP” sequence is a frequently targeted motif by several kinases, like ERK.

Next, we created a second test datasets (PO4ase) by randomly sampling 500 peptides only identified in the PO4ase treated samples (i.e. a set of phosphopeptide candidates) and adding the 500 unmodified (negative control) peptides in PO4 Test.

When applying the Random Forest classification algorithm, the candidate phosphopeptides were separated from the unmodified negative control peptides with 88% accuracy (b). A Receiver Operator characteristics curve is shown in (a, The Area Under Curve was 0.94). As described in Choi et al.[6] the False Discovery Rate (FDR) can be computed from the distribution of Posterior Error Probabilities (PEP) assigned to the phosphopeptide candidate set (Eq. 1).

$$FDR = \frac{1}{n}\sum_{i=1}^{n} PEP_i$$

Equation S1)

Applying Eq. 1 to the *PO4ase* dataset gives us an estimated FDR of 0.175; i.e. approximately 82.5% of the 500 randomly sampled phosphopeptide candidates were expected to have been phosphorylated prior to PO4ase treatment. We regard this as a conservative estimate of the FDR as (I) the selected features do not allow for perfect classification on training data. The classification accuracy of the training data was 94% (b). (II) We ignore the possibility that a peptide could be present in the sample as both unmodified and phosphorylated. (III) As described below the phosphopeptides only identified after PO4ase treatment have slightly different sequence characteristics compares to the phosphopeptides identified before PO4ase treatment, which likely explains why they were not identified prior to removal of the phosphate group.

Supplementary Figure 7:

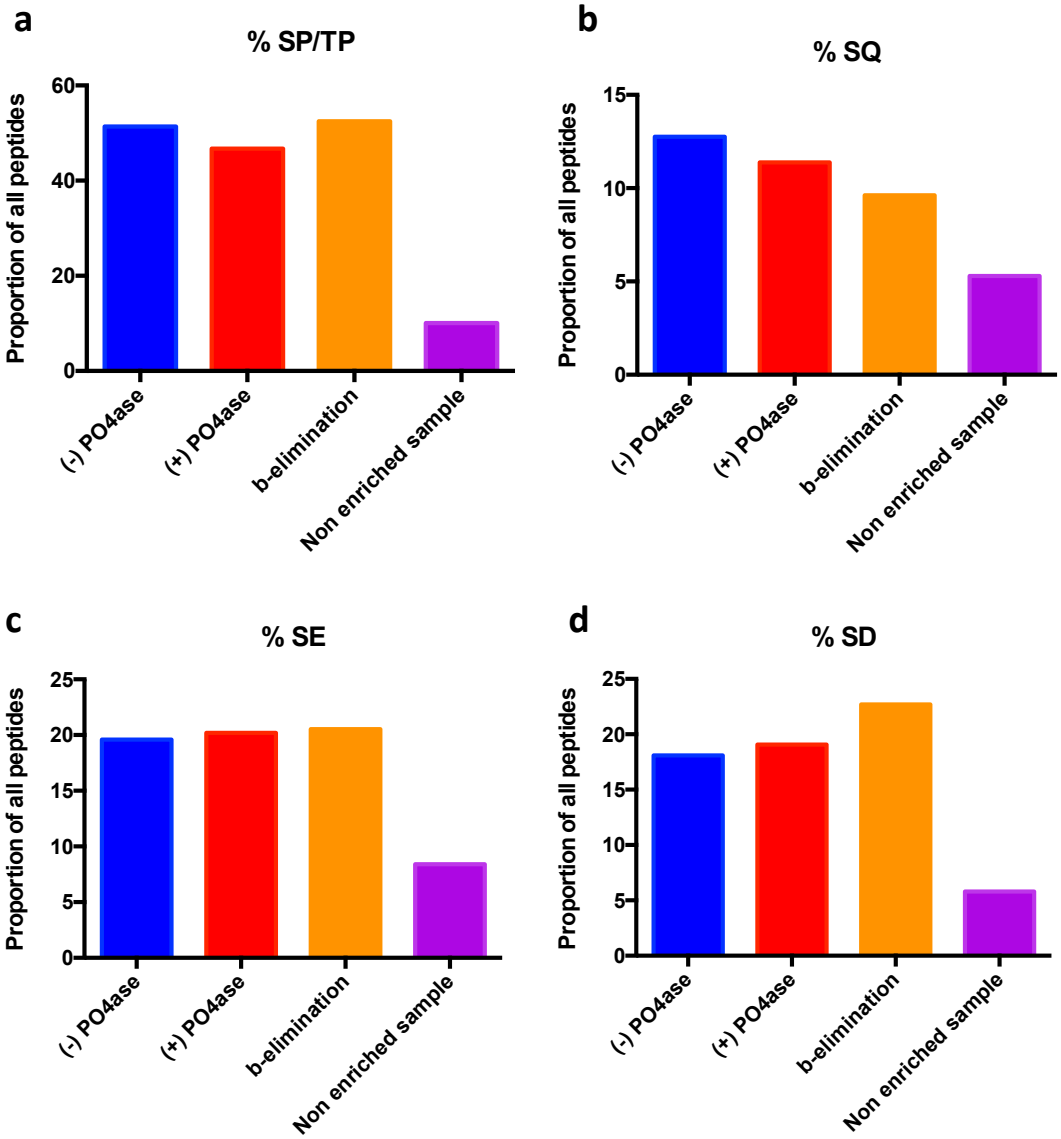

Supplementary Figure 7: Prevalence of a few selected frequent kinase motifs in the peptides identified before (blue) and after (red) phosphatase treatment. The proportions are also indicated for peptides identified after b-elimination (orange) and for a non-enriched total cell digest sample (purple). See Supplementary Tables 9&10 for details.

Supplementary Figure 8:

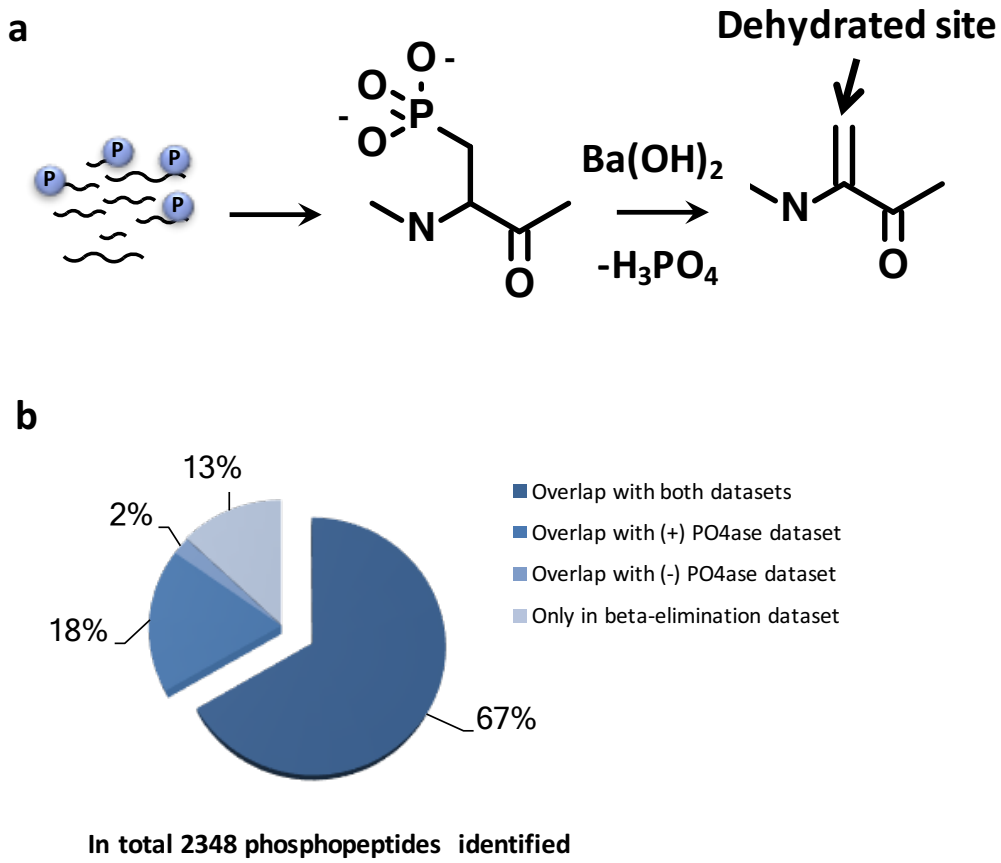

Supplementary Figure 8: Beta-elimination of phosphopeptide enriched samples according to Poot et. al.[7]. (a) Overview of the beta-elimination procedure. Phosphopeptide enriched samples were treated with barium hydroxide (0.15M) for 1 h at 37°C to remove phosphoric acid from phosphorylated serine and threonine residues by beta-elimination. The remaining dehydrated sites (red) on serine and threonine were then identified by LC-MS analysis. Notably, this approach is only applicable to serine and threonine phosphorylations and does not remove phosphoric acid from tyrosines. Chemical formulas were generated using PubChem Sketcher v2.4 (https://pubchem.ncbi.nlm.nih.gov/edit2/index.html) (b) Pie chart indicating the overlap (in %) of the phosphopeptides identified by beta-elimination with the datasets obtained before and after phosphatase (PO4ase) treatment.

Supplementary Figure 9:

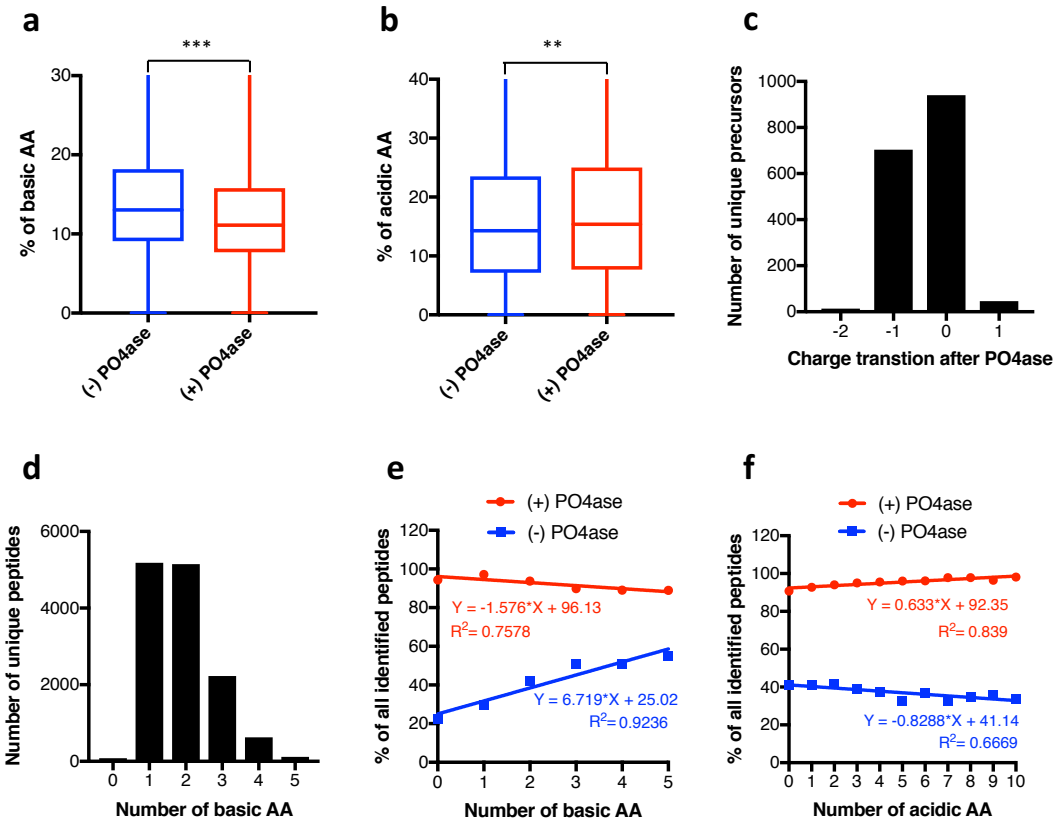

Supplementary Figure 9: Evaluation of physiochemical properties of peptide identified before (-) and after (+) phosphatase treatment. (a) Boxplot showing the distribution of the proportion of basic amino acids (histidine, lysine and arginine) to all amino acids of peptides identified before (blue, n=891) and after (red, n=8887) PO4ase treatment. The notches extend to the most extreme data point, which is no more than 1.5 times the interquartile range from the box. The thick horizontal line in each box indicates the median. The calculated significance (unpaired t-Test; two-tailed distribution assuming equal variance; homoscedastic), p-values <0.001 (***), <0.01 (**)) are indicated. (b) Like (a) for the proportion of acidic (glutamate and aspartate) amino acids. (c) Bar chart illustrating the change in precursor ion charge states of identified triple charged phosphorylated peptides after phosphate removal. (d) Bar chart showing the combined number of unique peptides identified in both datasets containing different numbers of basic amino acids. (e) Plot showing the percentage of all identified peptides covered by both datasets for peptides containing different numbers of basic amino acids. The lines indicate the linear regression determined for both datasets. The corresponding equations and R-square values are also shown. Both slopes were significant non-zero (p<0.025 (red), p<0.01 (blue)). (f) Like (e) for the proportion of acidic (glutamate and aspartate) amino acids. Both slopes were significant non-zero (p<0.01). Abbreviations: PO4ase=phosphatase, AA=amino acid.

Supplementary Figure 10:

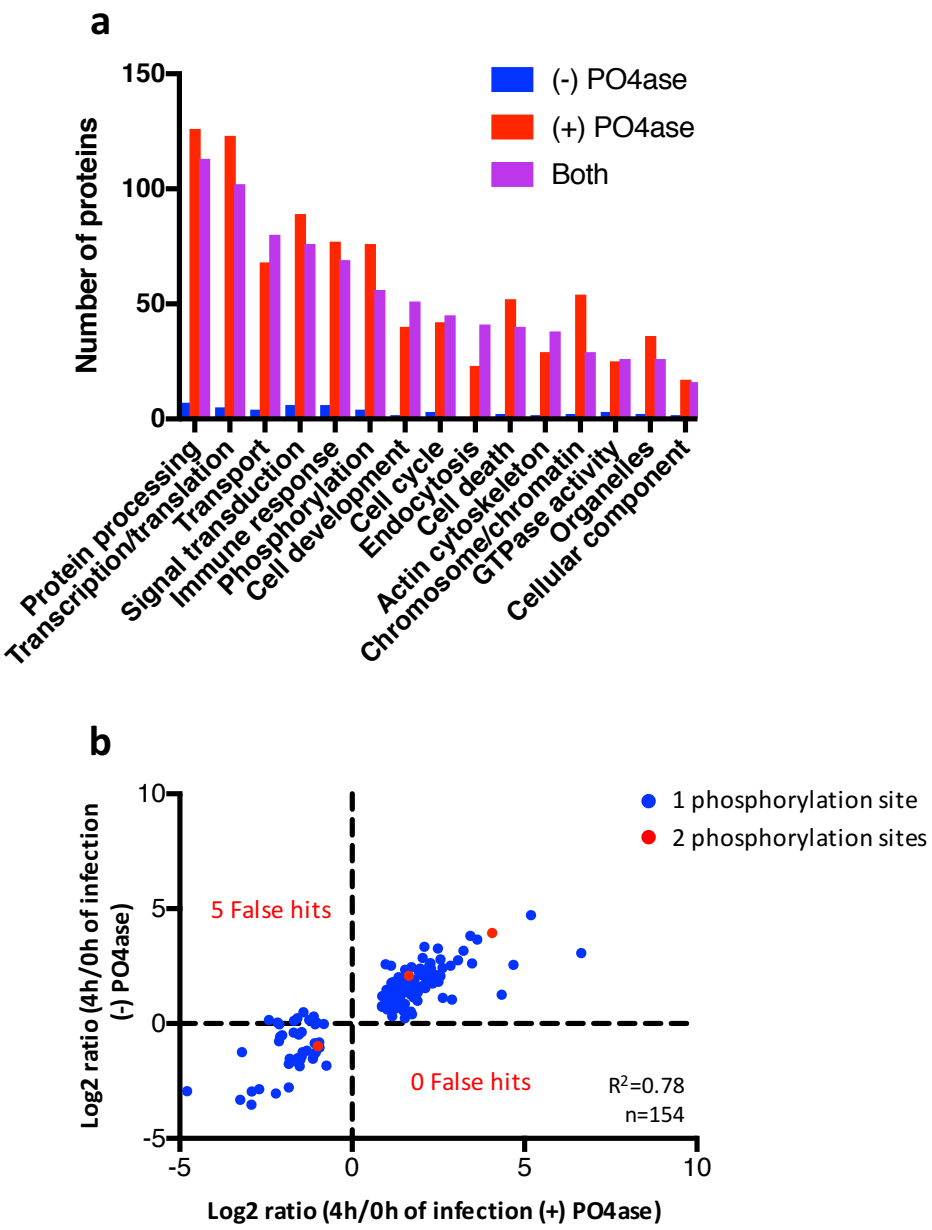

Supplementary Figure 10: Functional and quantitative analysis of differentially abundant phosphorylated peptides. (a) Significantly enriched (p<0.01) GO-terms of the corresponding proteins represented in Figure 3a. (b) Plot of ratios showing all peptides with overlapping sequences before and after PO4ase treatment quantified after 4 hours of infection applying the following filters: coefficient of variation (CV) below 20% (only before PO4ase), MS-Intensity >10,000, q-value <0.01 (only after PO4ase). Ratios determined from single (blue) and doubly (red) phosphorylated peptides (before phosphatase treatment) as well as the R-square value are shown. Besides, the number of false hits showing different ratio trends and the corresponding error rate are indicated.

Supplementary Figure 11:

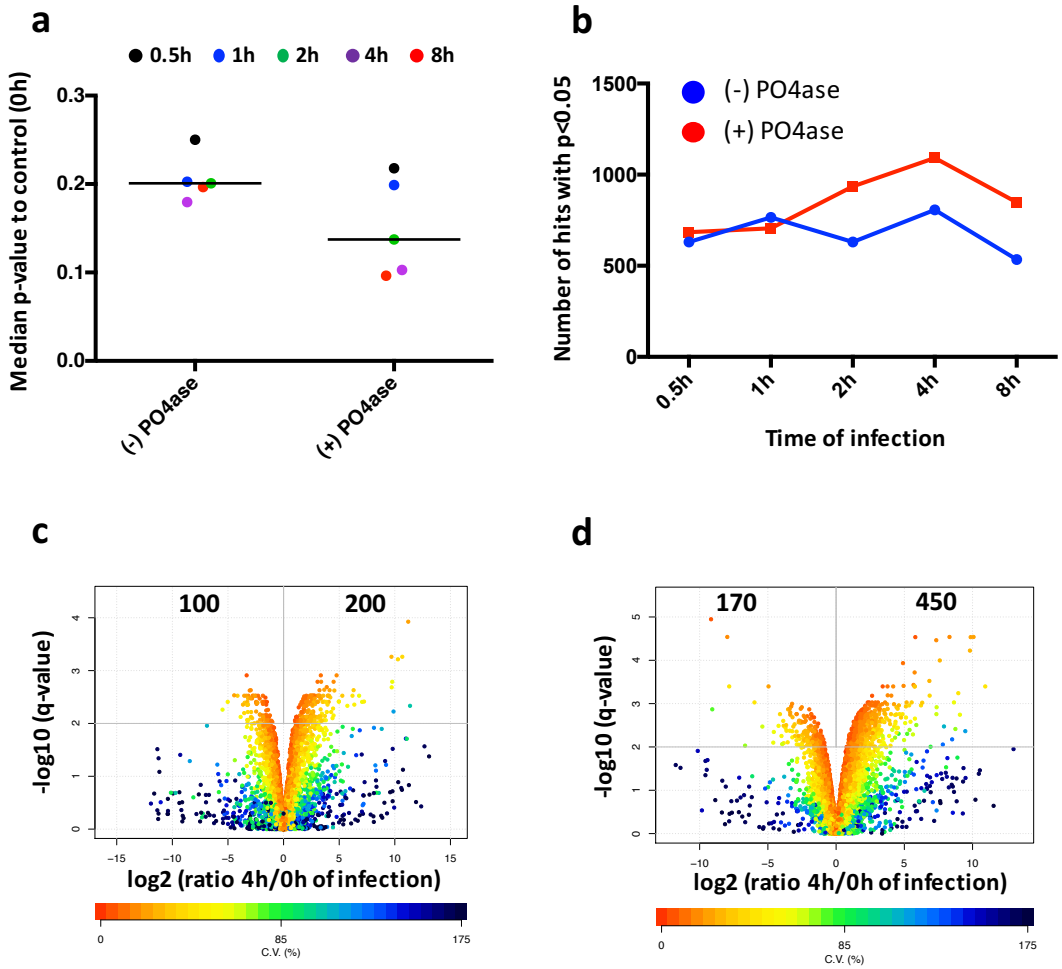

Supplementary Figure 11: Impact of phosphatase treatment on determined quantification statistics. (a) Median p-values (unpaired t-Test; two-tailed distribution assuming equal variance; homoscedastic, determined by SafeQuant[8] determined for all quantified peptides of the different infection time points to the control samples for datasets (-, n=6607) and (+, n=14,603) phosphatase (PO4ase). The time points (colors) as well as the median value (black line) are indicated. (b) Number of hits with p-value <0.05 for all different time points and both datasets. (c) Volcano plot of phosphopeptide quantified after 0 and 4 hours of infection generated by SafeQuant. The number of hits passing a q-value of 0.01 (grey line) are indicated (n=6607). (d) like (c) after phosphatase treatment (n=14,603).

Supplementary Figure 12:

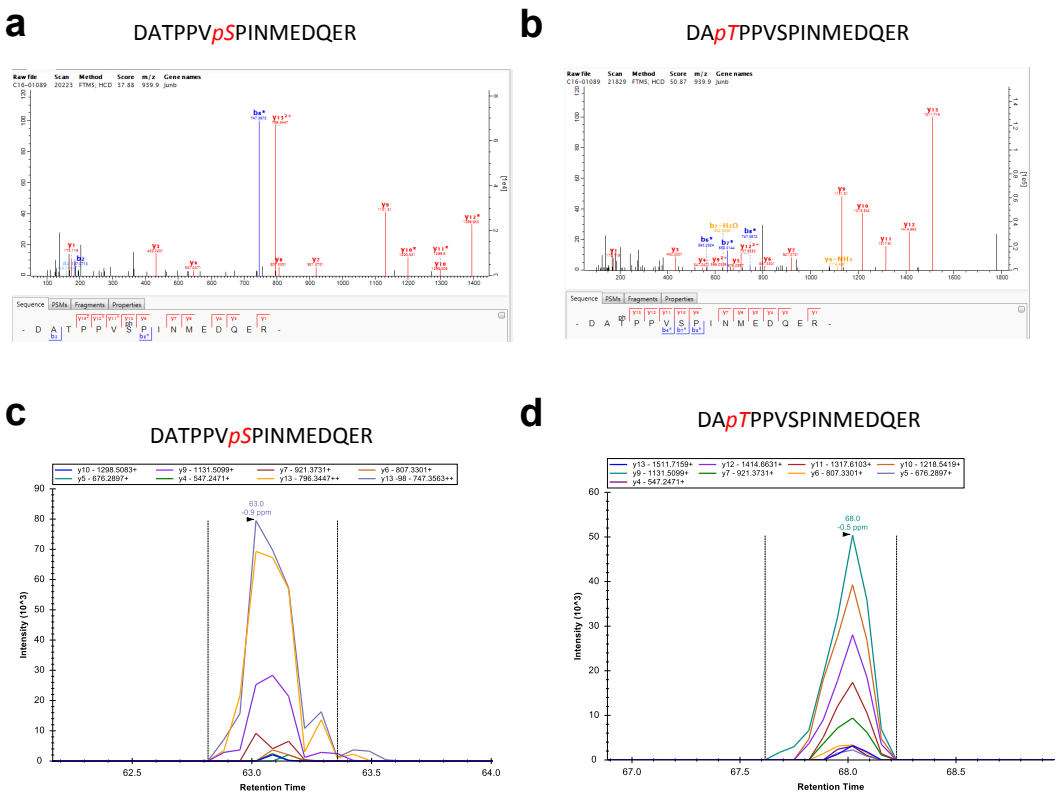

Supplementary Figure 12: Identification and quantification of two different phosphorylation sites one peptide "DATPPVSPINMEDQER" by LFQ-PRM (workflow see Fig. 5). (a) MS/MS spectrum showing the identification of phospho-serine at position 7 by LFQ-PRM and MaxQuant[9]. The assigned b- (blue) and y- (red) ions are indicated. (b) Like (a) for the identification of phospho-threonine at position 3. (c) Quantitative LFQ-PRM analysis of pS7 isoform using Skyline and an assay generated from (a). The different fragments employed for quantification are indicated. (d) Like (c) for the isoform pT3.

Supplementary Figure 13:

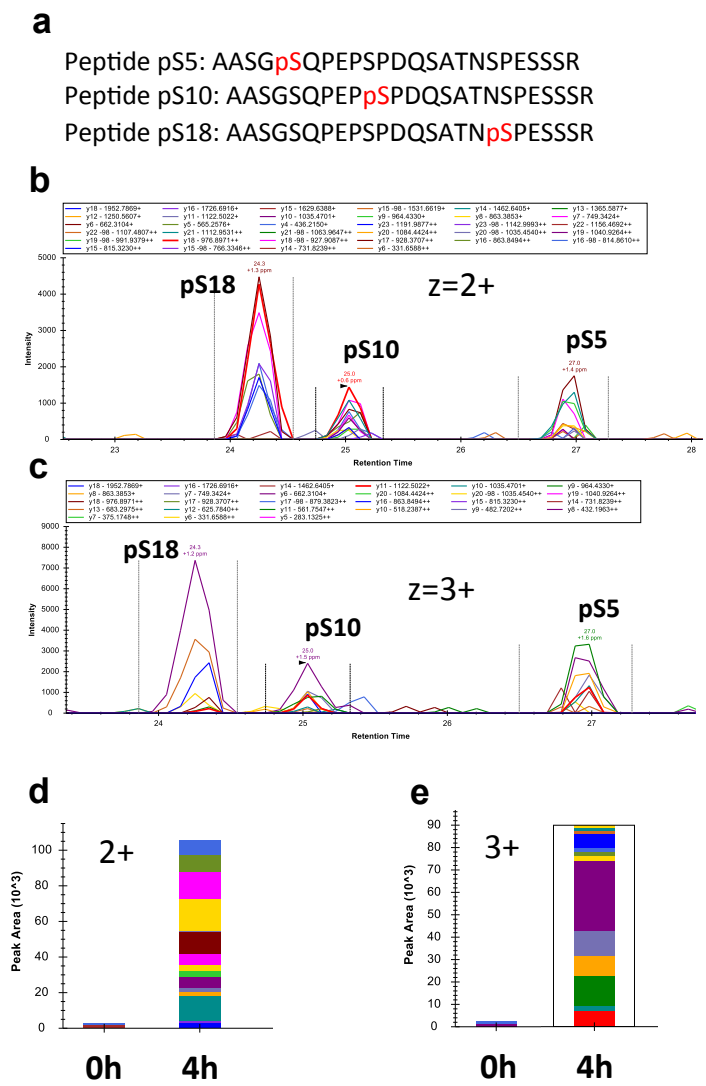

Supplementary Figure 13: Identification and quantification of three different phosphorylation sites one peptide "AASGSQPEPSPDQSATNSPESSSR" by LFQ-PRM (workflow see Fig. 5). (a) Sequences of three phospho-isoforms identified by LFQ-PRM on one peptide candidate selected for validation. The positions of the sites are indicated (red). (b) Transition based quantification by LFQ-PRM using Skyline[10] for all three phosphorylation isoforms found on the double charged precursor ion. Site specific transitions allowed the separate quantification of all three isoforms. (c) Like (b) for the triple charged precursor ion. (d) Bar chart showing the summed MS-intensities of all transitions employed for quantification of the pS18 isoform at 0 and 4 hours of infection for the double charged precursor. The contribution of each transition is shown with different colors (see (b)). (e) Like (d) for the triple charged precursor ion. See (c) for fragment colors. All corresponding values are shown in Table 1.

Supplementary Figure 14:

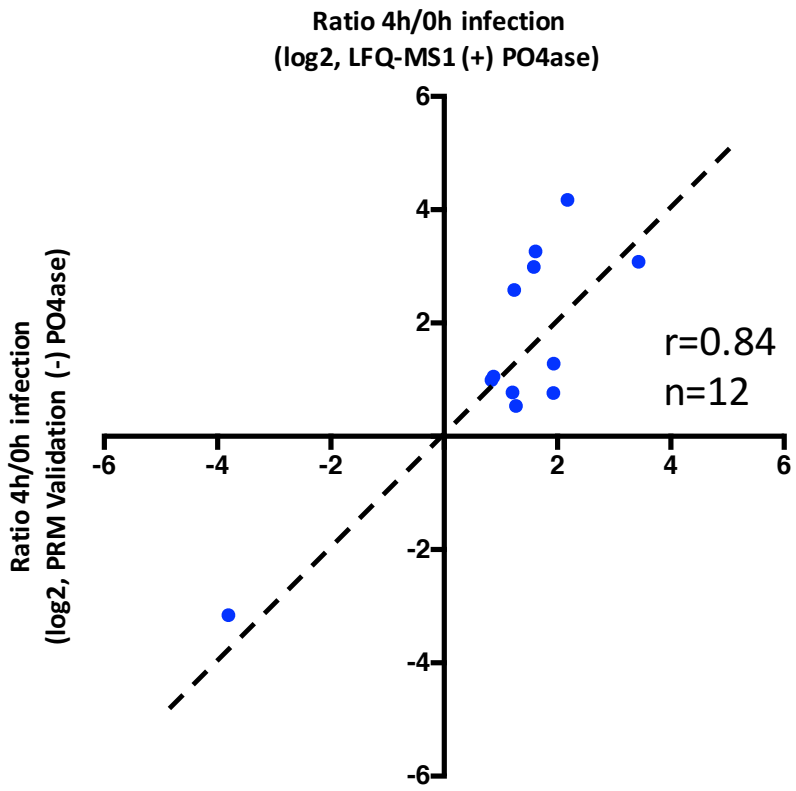

Supplementary Figure 14: Correlation of ratios determined from successfully validated phosphopeptides candidates quantified in the large-scale experiment (after phosphatase treatment) and by follow up targeted parallel reaction monitoring (PRM) MS analysis (no phosphatase treatment). All hits were validated using triplicate samples for no and 4 hours of infection. Pearson correlation coefficients (r) and a line showing perfect correlation (black, dashed) are indicated.

References:

1. Hommerson, P., Khan, A. M., de Jong, G. J. & Somsen, G. W. Comparison of electrospray ionization and atmospheric pressure photoionization for coupling of micellar electrokinetic chromatography with ion trap mass spectrometry. *J Chromatogr A* **1204,** 197–203 (2008).
2. Mandal, S. M., Dey, S., Mandal, M., Maria-Neto, S. & Franco, O. L. Comparative analyses of different surfactants on matrix-assisted laser desorption/ionization mass spectrometry peptide analysis. *Eur J Mass Spectrom (Chichester)* **16,** 567–575 (2010).
3. Liaw, A. & Wiener, M. Classification and regression by randomForest. *R news* (2002).
4. Sharma, K. *et al.* Cell type- and brain region-resolved mouse brain proteome. *Nat. Neurosci.* **18,** 1819–1831 (2015).
5. Hornbeck, P. V. *et al.* PhosphoSitePlus, 2014: mutations, PTMs and recalibrations. *Nucleic Acids Res* **43,** D512–20 (2015).
6. Choi, H., Ghosh, D. & Nesvizhskii, A. I. Statistical validation of peptide identifications in large-scale proteomics using the target-decoy database search strategy and flexible mixture modeling. *J. Proteome Res.* **7,** 286–292 (2008).
7. Poot, A. J. *et al.* Selective enrichment of Ser-/Thr-phosphorylated peptides in the presence of Ser-/Thr-glycosylated peptides. *PROTEOMICS* **6,** 6394–6399 (2006).
8. Ahrné, E. *et al.* Evaluation and Improvement of Quantification Accuracy in Isobaric Mass Tag-Based Protein Quantification Experiments. *J. Proteome Res.* **15,** 2537–2547 (2016).
9. Cox, J. & Mann, M. MaxQuant enables high peptide identification rates, individualized p.p.b.-range mass accuracies and proteome-wide protein quantification. *Nat Biotechnol* **26,** 1367–1372 (2008).
10. Maclean, B. *et al.* Skyline: an open source document editor for creating and analyzing targeted proteomics experiments. *Bioinformatics* **26,** 966–968 (2010).

2 Research article II

Francisella requires dynamic type VI secretion system and ClpB to deliver effectors for phagosomal escape.

R. F. Dreier*, M. Brodmann*, P. Broz and M. Basler.
* denotes equal contribution.

Nature Communications
2017 June 16; 8:15853. doi: 10.1038/ncomms15853. [524]

Statement of contribution
I performed all *Francisella* infections of primary murine bone marrow-derived macrophages and determined phagosomal escape, AIM2 inflammasome activation, intracellular replication and interferon induction of all *F. novicida* strains. In addition, I infected mice with *F. novicida* and determined bacterial burdens of spleen and liver as well as IL-18 levels in the serum. Furthermore, I generated the *F. novicida pdpC/pdpD/anmK* triple knockout. Finally, I wrote the manuscript together with Maj Brodmann, Marek Basler and Petr Broz.

nature COMMUNICATIONS

ARTICLE

Received 22 Dec 2016 | Accepted 8 May 2017 | Published 16 Jun 2017 DOI: 10.1038/ncomms15853 OPEN

Francisella requires dynamic type VI secretion system and ClpB to deliver effectors for phagosomal escape

Maj Brodmann[1,*], Roland F. Dreier[1,*], Petr Broz[1] & Marek Basler[1]

Francisella tularensis is an intracellular pathogen that causes the fatal zoonotic disease tularaemia. Critical for its pathogenesis is the ability of the phagocytosed bacteria to escape into the cell cytosol. For this, the bacteria use a non-canonical type VI secretion system (T6SS) encoded on the *Francisella* pathogenicity island (FPI). Here we show that in *F. novicida* T6SS assembly initiates at the bacterial poles both *in vitro* and within infected macrophages. T6SS dynamics and function depends on the general purpose ClpB unfoldase, which specifically colocalizes with contracted sheaths and is required for their disassembly. T6SS assembly depends on *iglF*, *iglG*, *iglI* and *iglJ*, whereas *pdpC*, *pdpD*, *pdpE* and *anmK* are dispensable. Importantly, strains lacking *pdpC* and *pdpD* are unable to escape from phagosome, activate AIM2 inflammasome or cause disease in mice. This suggests that PdpC and PdpD are T6SS effectors involved in phagosome rupture.

[1] Focal Area Infection Biology, Biozentrum, University of Basel, Klingelbergstrasse 50/70, CH-4056 Basel, Switzerland. * These authors contributed equally to this work. Correspondence and requests for materials should be addressed to P.B. (email: petr.broz@unibas.ch) or to M.Ba. (email: marek.basler@unibas.ch).

Francisella tularensis is a Gram-negative bacterium that causes the zoonotic disease tularaemia in human and animal host. The severity of tularaemia varies depending on the route of infection and the type of strain. The *Francisella tularensis* subsp. *tularensis* is the most virulent strain and aerosol transmission of a few bacteria can cause lethal pneumonia in humans[1]. Given the low infectious dose and the severity of the infection, subsp. *tularensis* has been classified as Tier 1 select agent. The related strain *Francisella tularensis* subsp. *novicida* (*F. novicida*) has in contrast low virulence in humans, but is highly virulent in mice and thus often used as a laboratory model for tularaemia[2]. The pathogenicity of both *Francisella* species is linked to their ability to replicate in the cytosol of phagocytes, such as macrophages or dendritic cells. After phagocytosis, the bacteria shortly reside within a membrane-bound phagosome, but subsequently disrupt the phagosomal membrane and escape into the host cell cytosol, where they replicate[3].

While phagosomal escape is essential for *Francisella* intracellular replication and virulence *in vivo*, it also allows the host to mount anti-microbial and innate immune defenses. Among these are the production of type I interferons (type I IFNs) via the cGAS-STING-IRF3 axis, the production of antimicrobial guanylate-binding proteins (GBPs) and the activation of the AIM2 (absent in melanoma 2) inflammasome, which controls the release of mature IL-1β and IL-18 as well as the induction of host cell death through pyroptosis[4–11]. Interferon production and inflammasome activation require the recognition of bacterial DNA in the cytosol, and have been linked to the lysis of cytosolic *Francisella*. Mice deficient in these responses fail to control bacterial replication, resulting in a fatal disease[4–6,8,9]. *Francisella* virulence and the escape from the phagosomal compartment requires a gene cluster referred to as the *Francisella* Pathogenicity Island (FPI)[12]. Two nearly identical copies of the FPI are found in subspecies *tularensis*, *holarctica* and *mediasiatica*. The *F. novicida* genome contains only a single FPI copy[13], but features a related island called '*Francisella novicida* Island (FNI)'[14,15]. The FPI has been suggested to encode a non-canonical type VI secretion system (T6SS)[16,17], which based on gene content and phylogeny is proposed to represent a unique T6SS subtype (T6SS^{ii})[18].

T6SS is a nanomachine capable of delivery of effector proteins across target cell membranes of both bacterial and eukaryotic cells and thus is often required for bacterial competition and pathogenesis[19–23]. One of the hallmarks of this system is its highly dynamic assembly that can be visualized by live-cell fluorescence microscopy[24,25]. Assembly of T6SS starts by formation of a membrane complex formed of TssJ, TssL and TssM[26]. This is followed by assembly of a baseplate complex from TssE, TssF, TssG, TssK and also VgrG, PAAR spike as well as TssA in some organisms[27–31]. Baseplate complex then initiates assembly of a long Hcp tube and TssB, TssC (or VipA, VipB) sheath wrapped around the tube[32]. Both spike and Hcp tube can associate with effectors and are delivered together into target cells upon rapid sheath contraction[33–39].

Even though the *F. novicida* sheath is structurally similar to the sheath of canonical T6SS of *V. cholerae*[40,41], it is unclear to what extent the canonical T6SS assembly mechanisms apply to *Francisella*. The reason is that *Francisella* T6SS is highly divergent and clear homologues of several core components are missing, such as TssE, TssF and TssG. In addition, many components such as TssK, VgrG, Hcp and PAAR have only low primary sequence homology to the canonical T6SS components. For example, IglG was recently shown to be structurally similar to PAAR proteins, which are required for T6SS function[15,29]. On the other hand, the FPI cluster contains many genes of unknown function, such as *iglF*, *iglI*, *iglJ*, *pdpA*, *pdpC*, *pdpE*, *pdpD* and *anmK*. PdpA, PdpC and PdpD were identified by mass-spectrometry as secreted by *Francisella* T6SS and PdpC/PdpD were proposed to be effectors required for phagosomal escape, intracellular growth and virulence[42–48]. Interestingly, the FPI cluster lacks a homologue of an unfoldase ClpV, which is present in all canonical T6SS clusters and recycles contracted sheaths[14,24,49,50]. Overall, the non-canonical gene composition suggests a unique mode of action of the *Francisella* T6SS.

Here we show that *F. novicida* T6SS sheath cycles between assembly, contraction and disassembly. Interestingly, the vast majority of T6SS sheath assemblies initiate close or at the cell pole. We show that ClpB colocalizes with contracted sheaths and is required for sheath disassembly, however, is dispensable for

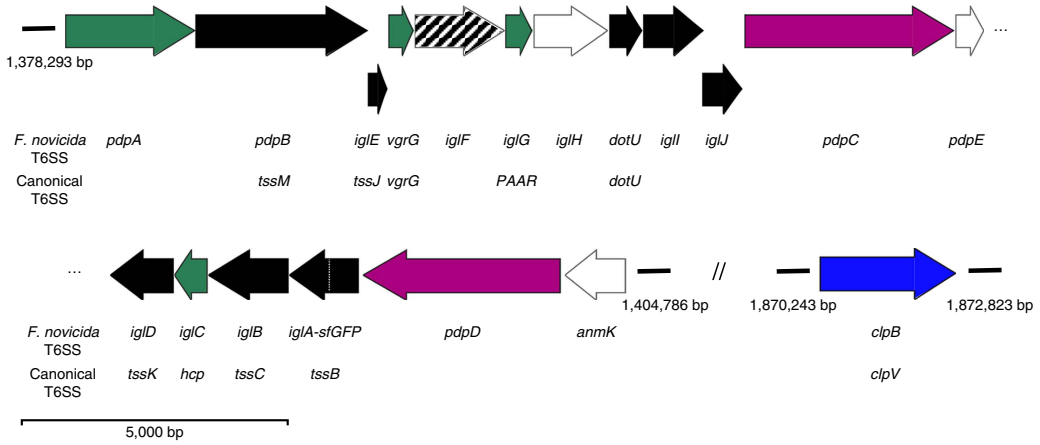

Figure 1 | A schematic overview of *Francisella* T6SS genes. Assignments for gene functions are based on previous studies cited in the main text and our observations: Black—structural components; Green—secreted structural components; Purple—secreted effectors; Blue—unfoldase; White—no clear evidence for function; Shaded—required for efficient assembly. The *Francisella* FPI (*pdpA–anmK*) nomenclature and the canonical T6SS nomenclature for the *F. novicida* genes is shown. Genes are drawn in scale.

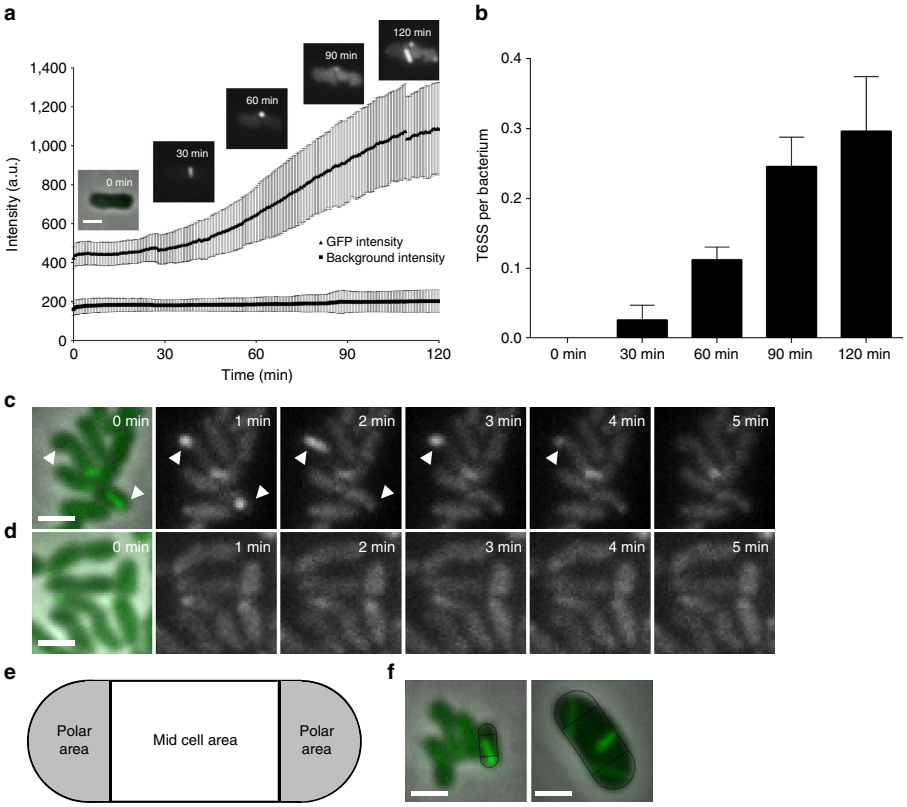

Figure 2 | Increase of GFP intensity correlates with increased number of dynamic T6SS per bacterium. (**a**) GFP signal intensities of *F. novicida* U112 *iglA-sfGFP* and fluorescence background were measured every minute for three regions of interest containing 1–30 bacteria. Two independent experiments were carried out. GFP intensity increase in a single *F. novicida* U112 *iglA-sfGFP* bacterium is shown at different time points. First image is a merge of phase contrast and GFP channels, following images represent GFP channel only. (**b**) Number of bacteria and T6SS structures were counted at time points between 0 and 120 min in three regions of interest containing 36–191 bacteria. Two independent experiments were carried out. Error bars represent s.d. (**c**,**d**) IglA-sfGFP localization in *F. novicida* U112 *iglA-sfGFP* wild type (**c**) and Δ*pdpB* (**d**). Arrowheads indicate T6SS sheath assembly and contraction. First image is a merge of phase contrast and GFP channels, following images represent GFP channel only. (**e**) Model for quantification of T6SS assembly position. Pole area was determined as 50% of total surface area equally distributed to both poles. (**f**) Model from **e** applied to *F. novicida* U112 *iglA-sfGFP* and *V. cholerae* 2740-80 *vipA-msfGFP*. Merge of phase contrast and GFP channels is shown. For **a**,**c**,**d** and **f** 3.3 × 3.3 μm fields of view are shown. Scale bar, 1 μm.

sheath assembly and contraction. T6SS dynamics and function depends on *iglF*, *iglG*, *iglI* and *iglJ*, while *pdpC* and *pdpD* are specifically required for phagosomal escape and virulence in a mouse model of tularaemia, but also for the engagement of the host innate immune response.

Results

***Francisella* T6SS is dynamic and assembles on the cell pole.** *Francisella* T6SS has a non-canonical gene composition and lacks ClpV suggesting unique mode of action (Fig. 1). To understand *Francisella* T6SS assembly and function, we searched for conditions that would allow us to image subcellular localization of TssB homologue IglA. We have serendipitously discovered that *F. novicida iglA-sfGFP* grown to an exponential phase in BHI media induced expression of IglA-sfGFP upon prolonged incubation on an agarose pad under a glass coverslip. Importantly, the increase in expression correlated with an increase in number of IglA-sfGFP structures detected in the bacteria (Fig. 2a,b). Time-lapse imaging at a rate of 20 frames per minute showed that IglA-sfGFP structures extended across the bacteria within 30 and 120 s with assembly speeds between 5 and 15 nm s^{-1}. After full assembly, the IglA-sfGFP structures immediately contracted to approximately half of their original length and became brighter (Fig. 2c; Supplementary Fig. 1a; Supplementary Movies 1 and 4). After contraction, the sheath structures were disassembled during the next ∼2–3 min (Fig. 2c; Supplementary Fig. 1a). The average fluorescence intensity of the bacteria before and after one cycle of assembly, contraction and disassembly was similar, suggesting that IglA-sfGFP remained stable and folded during this cycle (Supplementary Fig. 1b). Importantly, no IglA-sfGFP structures were detected in the bacteria lacking the TssM homologue encoded by *pdpB* (Fig. 1), suggesting that assembly of IglA-sfGFP structures is dependent

on the function of the whole T6SS (Fig. 2d; Supplementary Movie 2). The dynamics of IglA-sfGFP localization is similar to that of VipA-sfGFP in *V. cholerae* and is consistent with the fact that IglA and IglB form a structure closely resembling *V. cholerae* T6SS sheath[25,40,41].

Interestingly, we also noticed that IglA-sfGFP sheaths were preferentially assembled from the bacterial pole and thus often formed structures as long as the bacterial length. To quantify the preference for subcellular localization, we divided the bacterial perimeter equally to a polar region and a mid-cell region (Fig. 2e) and counted assemblies initiated in these two equally large regions. Out of 851 assemblies, 821 assemblies (96.5%) were initiated in the polar region. As a control, we performed the same analysis for *V. cholerae* and show that only 53.8% (425 from 790) assemblies were initiated in the polar region (Fig. 2f) as expected for assemblies without preferred localization[24,25,51]. Taken together, we show that *F. novicida* assembles a dynamic T6SS sheath on the cell poles and that the sheath cycles through assembly, contraction and disassembly similarly to what was previously described for other canonical T6SSs.

ClpB is required for disassembly of contracted sheaths. The fact that contracted sheaths were quickly disassembled without apparent degradation of IglA-sfGFP suggested that *F. novicida* recycles contracted sheaths using a mechanism similar to the canonical ClpV-mediated sheath disassembly. The closest homologue of *V. cholerae* ClpV in *F. novicida* genome is ClpB (FTN_1743) (36% sequence identity). Interestingly, *clpB* was previously shown to be required for survival of various stresses[52] but also essential for intracellular replication and virulence of *F. novicida*[53,54].

Here we show that *F. novicida* lacking *clpB* mainly contained bright IglA-sfGFP foci (Fig. 3a). Time-lapse imaging showed that the *F. novicida* Δ*clpB* occasionally assembled new sheaths with kinetics similar to that of the parental strain but after contraction, the sheaths were never disassembled and remained intact in the bacteria (Fig. 3a,b; Supplementary Movies 1 and 4). Such assembly was still dependent on functional T6SS, as no sheath extensions and contractions were detected in *F. novicida* Δ*clpB*/*pdpB*. However, some bright, non-dynamic IglA-sfGFP foci were detected in the absence of both *clpB* and *pdpB* (Supplementary Fig. 2a; Supplementary Movie 2). This indicates that activity of ClpB is required for recycling of contracted sheaths, however, in case of a defect in ClpB function, some non-dynamic IglA-sfGFP foci may form also in the absence of a fully functional T6SS.

To test directly the role of ClpB in disassembly of the contracted sheaths, we introduced *clpB-mCherry2* fusion to the native locus on the chromosome of the *iglA-sfGFP* or wild-type strain. Fusing mCherry2 to ClpB had no influence on the ability of *F. novicida* to survive heat shock indicating that such fusion is fully functional (Supplementary Fig. 2d). ClpB-mCherry2 subcellular localization cycled between uniform cytosolic and punctate localization and this dynamics was dependent on the presence of *pdpB* (Supplementary Fig. 2b,c, Supplementary Movie 3). When IglA-sfGFP and ClpB-mCherry2 were imaged simultaneously, ClpB spots colocalized specifically with the contracted sheaths (Fig. 3c; Supplementary Movies 3 and 5).

F. novicida uses the T6SS to escape from phagosome of cells like macrophages and consistently IglA-sfGFP spots could be detected in intracellular bacteria, implying the assembly of T6SS sheaths[40]. To test whether sheath assembly is dynamic under physiological conditions during infection, we infected primary murine bone marrow-derived macrophages (BMDMs) from wild-type C57BL/6 mice for 1 h with exponentially grown *F. novicida*. After washing away non-phagocytosed bacteria, the infected cells were fixed, stained with phalloidin and anti-*F. novicida* LPS antibody and analysed by super resolution structured illumination microscopy (SIM) to determine the relative localization of actin, bacteria and T6SS sheaths (Fig. 4a,b). This analysis confirmed that *F. novicida* reside inside the macrophage and assemble T6SS sheaths.

Next, we imaged IglA-sfGFP and ClpB-mCherry2 dynamics within *F. novicida* in live macrophages and observed that the sheaths cycled through assembly, contraction and disassembly. Importantly, ClpB-mCherry2 dynamically localized into spots that colocalized with the contracted sheaths, suggesting that ClpB is responsible for disassembly of the contracted sheaths also within phagosomes of infected macrophages (Fig. 4c; Supplementary Movie 6). In total, we analysed 30 sheath assembly, contraction and disassembly events inside live macrophages and all of the assemblies originated from the cell pole (Fig. 4c; Supplementary Movie 6). Together, these data suggest that sheath dynamics and subcellular localization observed during imaging of *F. novicida* on agarose pads is similar to that of the sheath in the bacteria residing inside of live macrophages.

To determine the importance of ClpB for *F. novicida* pathogenesis, we infected BMDMs with *F. novicida* wild-type, Δ*pdpB* and Δ*clpB* and determined the percentage of phagosomal and cytosolic bacteria using a phagosome-protection assay based on selective permeabilization of the plasma membrane with digitonin[9]. *F. novicida* Δ*clpB* had a significant defect in phagosomal escape at 4 h post infection, similarly to bacteria lacking the essential structural component PdpB (Fig. 3d; Supplementary Fig. 3a). Consistent with reduced cytosolic localization, we observed significantly reduced levels of pyroptosis induction and cytokine release in LPS-primed BMDMs infected for 10 h with *F. novicida* Δ*pdpB* and Δ*clpB*, while the wild-type strain elicited strong immune responses (Fig. 3e). Finally, we evaluated the role of ClpB *in vivo* in a mouse model of tularaemia. We infected age- and sex-matched wild-type C57BL/6 mice subcutaneously with 10^4 colony-forming units (CFUs) of *F. novicida* wild-type, Δ*pdpB* and Δ*clpB* and measured the bacterial burden at 2 days post infection. Mice infected with *F. novicida* Δ*clpB* displayed significantly reduced bacterial counts in the liver and spleen as compared to the mice infected with *F. novicida* wild type, and in many cases no bacteria could be recovered, similarly to what was observed with *F. novicida* Δ*pdpB* (Supplementary Fig. 3b). Overall these results indicate that ClpB acts as an unfoldase for the FPI-encoded T6SS sheath, and that its activity is essential for T6SS dynamics and consequently *F. novicida* virulence.

Differential requirement of FPI genes for sheath dynamics. Almost all FPI genes were shown to be required for intracellular replication probably due to a lack of phagosomal escape, however, many genes of the FPI cluster have no known homologues or were not characterized in detail[14]. Importantly, both structural components of T6SS as well as putative effectors secreted by T6SS are in principle essential for overall T6SS function, however, effectors may be to a certain degree dispensable for T6SS assembly. To provide an insight into which FPI genes are required for assembly of T6SS and which may potentially encode secreted effectors, we generated in-frame deletions of genes for which we were unable to predict function based on homology to known canonical T6SS components (Fig. 1). IglA-sfGFP subcellular localization was then imaged in those strains under the same conditions as used before for the parental strain.

In Δ*iglF* and Δ*iglG* strains, we detected on average 1 dynamic sheath assembly per 400 and 500 cells, respectively, in 5 min (Supplementary Movie 2). This suggests that IglF and IglG may

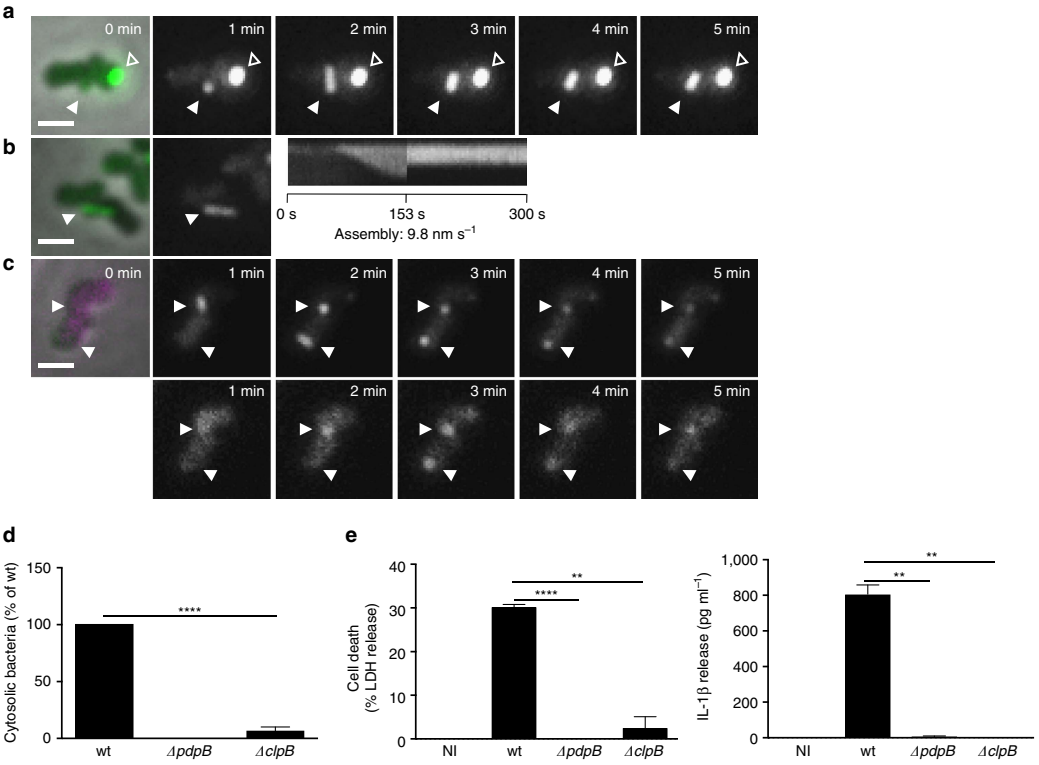

Figure 3 | Phagosomal rupture and AIM2 inflammasome activation is dependent on disassembly of T6SS sheaths by ClpB. (**a**) T6SS dynamics in *F. novicida* U112 *iglA-sfGFP ΔclpB*. Arrowheads indicate T6SS sheath assembly, contraction and location of sheath after contraction. Empty arrowheads indicate non-dynamic IglA-sfGFP foci. First image is a merge of phase contrast and GFP channels, following images represent GFP channel only. (**b**) Kymogram of *F. novicida* U112 *iglA-sfGFP ΔclpB* over 5 min (3 s per pixel). First image is a merge of phase contrast and GFP channels, following images represent GFP channel only. (**c**) Colocalization of ClpB-mCherry2 with IglA-sfGFP (arrows) in *F. novicida* U112 *iglA-sfGFP clpB-mCherry2*. First image is a merge of phase contrast, GFP and mCherry channels, following images represent GFP channel (upper panel) and mCherry channel (lower panel). (**d**) Quantification of cytosolic bacteria in unprimed wild-type BMDMs 4 h after infection with *F. novicida* U112 *iglA-sfGFP* wild type, *ΔpdpB* or *ΔclpB* (normalized to wild type). (**e**) Release of LDH and mature IL-1β from primed wild-type BMDMs 10 h after infection with *F. novicida* U112 *iglA-sfGFP* wild type, *ΔpdpB or ΔclpB* (NI—noninfected control). (**a**–**c**) 3.3 × 3.3 μm fields of view are shown. Scale bars, 1 μm. (**d**,**e**) Data are pooled from three independent experiments (**d**) (mean and s.d. are shown) or representatives of three independent experiments (**e**) (mean and s.d. of triplicate wells are shown). $^{**}P<0.01$ and $^{****}P<0.0001$ (two-tailed unpaired *t*-test with Welch's correction).

be required for efficient initiation of T6SS assembly. On the other hand, *iglI* and *iglJ* are essential for sheath assembly as no sheath assemblies were detected in more than 1,000 cells in 5 min even though IglA-sfGFP was expressed to the same level as in the parental strain (Fig. 5a; Supplementary Movie 2). Consistent with the defect in T6SS assembly, we found that Δ*iglF*, Δ*iglG*, Δ*iglI* and Δ*iglJ* strains were unable to escape into the cytosol of the infected macrophages, and consequently failed to activate cytosolic innate immune signalling (Fig. 5b,c). We cannot completely rule out the possibility that the observed phenotypes of mutants are due to polar effects on expression of other T6SS genes. However, defect in intracellular growth was previously successfully complemented for *iglF*, *iglG* and *iglI* genes[55].

Single deletion of *pdpE*, *pdpC*, *pdpD* and *anmK* or deletion of both *pdpD* and *anmK* (Δ*pdpD*/*anmK*) or *pdpC* and *pdpD* (Δ*pdpC*/*pdpD*) had no significant influence on sheath dynamics or localization (Fig. 6a; Supplementary Movie 1). Only deletion of all three genes *pdpC*, *pdpD* and *anmK* in the same strain decreased frequency of sheath assembly by 30% from an average of one structure per three cells to about one structure per five cells (Supplementary Fig. 4a). Nevertheless, sheath assemblies in Δ*pdpC*/*pdpD*/*anmK* still preferentially localized to the cell pole, assembled with a similar speed and cycled through extension, contraction and disassembly like in the parental strain (Supplementary Fig. 4b,c; Supplementary Movie 1). Importantly, Δ*pdpE* and Δ*pdpC*/*pdpD*/*anmK* assembled sheaths with dynamics undistinguishable from the parental strain within infected macrophages (Supplementary Fig. 5e,f). In conclusion, our analysis allowed us to identify FPI genes (*iglF*, *iglG*, *iglI* and *iglJ*) essential for T6SS assembly and a distinct set of FPI genes (*pdpE*, *pdpC*, *pdpD* and *anmK*) that are dispensable for T6SS assembly.

PdpC and PdpD are required for phagosomal escape. To test whether *pdpE*, *pdpC*, *pdpD* and *anmK* genes are required for the escape of *F. novicida* from phagosome, we infected BMDMs with

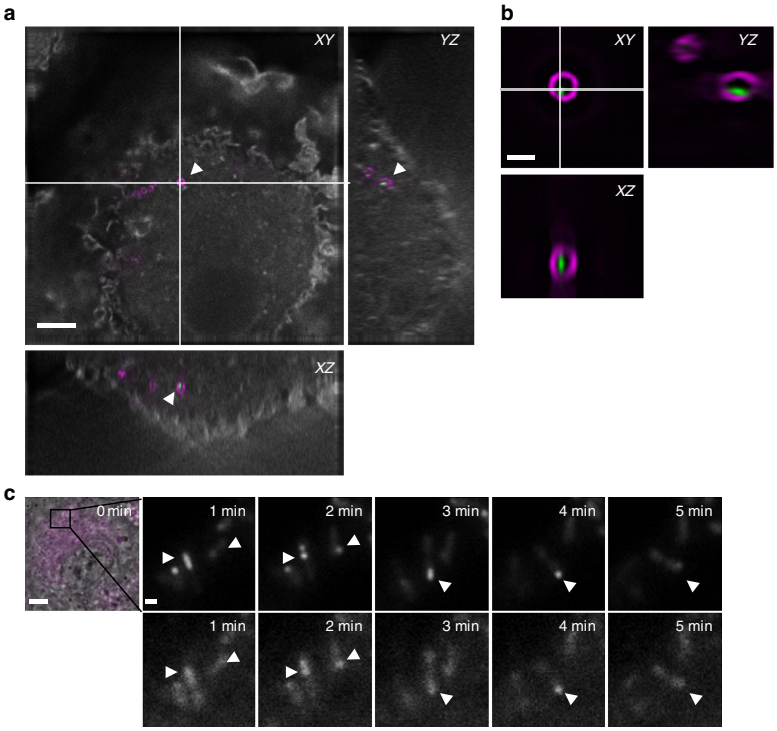

Figure 4 | T6SS dynamics in bone marrow-derived macrophages (BMDMs). (**a**) Merged wide field image and orthogonal view of BMDMs infected for 1 h with *F. novicida* U112 *iglA-sfGFP clpB-mCherry2*; in grey: actin staining, in magenta: LPS staining, in green: IglA-sfGFP. 41 × 41 µm field of view, scale bar, 5 µm. (**b**) Close up and orthogonal SIM view of bacterium highlighted with arrowheads in **a**; magenta: LPS staining, green: IglA-sfGFP. 5.1 × 5.1 µm field of view, scale bar, 1 µm. (**c**) Time-lapse images of unprimed wild-type BMDMs infected with *F. novicida* U112 *iglA-sfGFP clpB-mCherry2* for 1 h. First image consists of merged phase contrast, GFP and mCherry channels. 30 × 30 µm field of view is shown. Scale bar, 5 µm. Close ups consist of GFP channel (upper panel) and mCherry channel (lower panel). Close ups show 5 × 5 µm. Scale bar, 1 µm. Arrowheads indicate T6SS sheath assembly, contraction and location of sheath after contraction.

F. novicida Δ*pdpE*, Δ*anmK*, Δ*pdpC*, Δ*pdpD*, Δ*pdpD*/*anmK* or Δ*pdpC*/*pdpD*/*anmK* and determined the percentage of phagosomal and cytosolic bacteria compared to wild-type and Δ*pdpB* bacteria as outlined above (Supplementary Fig. 3a). Interestingly, we found that deletion of *pdpC* resulted in a very strong defect in phagosomal escape in comparison to wild-type bacteria, although the reduction was smaller than with bacteria lacking the structural component PdpB (Fig. 6b). *F. novicida* Δ*pdpD* and Δ*pdpD*/*anmK* also showed a defect in phagosomal escape, which was however less severe than the phenotype of a *pdpC* or *pdpB* deletion. No significant difference in phagosomal escape was observed between Δ*pdpD* and Δ*pdpD*/*anmK* strains, indicating that AnmK plays no role in phagosomal escape, consistent with the finding that phagosomal escape of the Δ*anmK* strain was indistinguishable from the wild-type strain (Fig. 6b). To determine whether the effect of a *pdpC* and *pdpD* deletion was additive, we generated a strain lacking *pdpC*, *pdpD* and also *anmK*. Interestingly, bacteria lacking *pdpC*/*pdpD*/*anmK* were unable to escape from the phagosomal compartment similarly to the Δ*pdpB* strain. In contrast, deletion of *pdpE* had no significant effect on phagosomal escape (Fig. 6b).

Next, we tested the role of *pdpE*, *pdpC*, *pdpD* and *anmK* in cytosolic innate immune detection of *F. novicida*. Consistent with the reduced level of cytosolic localization, we found that *F. novicida* Δ*pdpC* and Δ*pdpC*/*pdpD*/*anmK* induced significantly lower levels of type I IFN production in unprimed BMDMs infected for 10 h at an MOI of 100 (Supplementary Fig. 5c). The triple mutant Δ*pdpC*/*pdpD*/*anmK* had the most severe phenotype and only elicited IFN levels in the range of the Δ*pdpB* strain (Supplementary Fig. 5c).

Since type I IFNs control the activation of the AIM2 inflammasome during *F. novicida* infection[5], we examined the level of inflammasome activation in LPS-primed infected macrophages at different time points (Fig. 6c; Supplementary Fig. 5a). While infection with *F. novicida* lacking *pdpC* or *pdpD* resulted in significantly reduced levels of inflammasome activation, only the deletion of both *pdpC* and *pdpD* completely abrogated cell death induction and cytokine production in infected macrophages, which was consistent with the reduced levels of cytosolic localization and type I IFN induction in macrophages infected with mutants lacking both proteins (Fig. 6b; Supplementary Fig. 5c). Cell death induction and cytokine production in infected macrophages was unchanged between cells infected with wild-type and Δ*anmK* bacteria indicating that AnmK is not involved in modulating inflammasome activation (Fig. 6c). Consistently, cell death and cytokine production was comparable between cells infected with *F. novicida* Δ*pdpC*/*pdpD* and Δ*pdpC*/*pdpD*/*anmK* or *F. novicida* Δ*pdpD* and Δ*pdpD*/*anmK*. Importantly, the observed

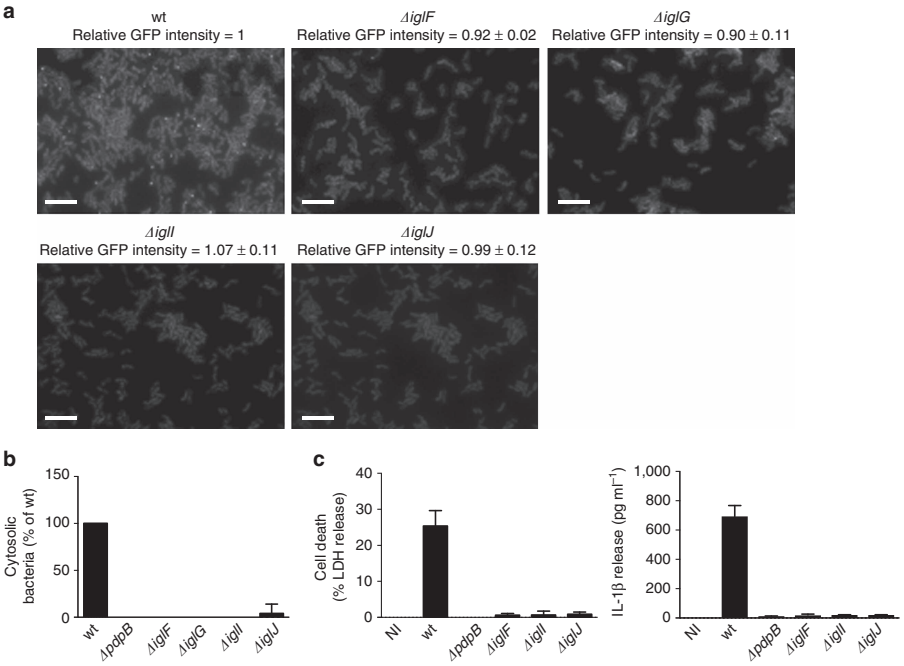

Figure 5 | Identification of genes required for assembly and function of *F. novicida* T6SS. (**a**) IglA-sfGFP localization in *F. novicida* U112 *iglA-sfGFP* wild type, *ΔiglF*, *ΔiglG*, *ΔiglI* and *ΔiglJ*. The GFP channel is shown. The numbers above the images represent the ratio of average GFP intensity of mutants compared to the parental strain with s.d. The average GFP intensities were quantified in three independent experiments. Thirty bacteria were analysed per experiment; 39 × 26 μm fields of view are shown. Scale bars, 5 μm. (**b**) Quantification of cytosolic bacteria in unprimed wild-type BMDMs 4 h after infection with *F. novicida* U112 *iglA-sfGFP* wild type, *ΔpdpB*, *ΔiglF*, *ΔiglG*, *ΔiglI* or *ΔiglJ* (normalized to wild type). (**c**) Release of LDH and IL-1β from primed wild-type BMDMs 10 h after infection with *F. novicida* U112 *iglA-sfGFP* wild type, *ΔpdpB*, *ΔiglF*, *ΔiglI* or *ΔiglJ* (NI—noninfected control). (**b**,**c**) Data are pooled from three independent experiments (**b**) (mean and s.d. are shown) or are representatives of three independent experiments (**c**) (mean and s.d. of triplicate wells are shown).

changes in inflammasome activation were independent of macrophage priming, since unprimed macrophages infected with wild-type or mutant *F. novicida* responded similarly (Supplementary Fig. 5b). Deletion of *pdpE* had no significant effect on the level of type I IFN induction, pyroptosis and cytokine release (Supplementary Fig. 5a–c).

Previous work has implicated the FPI in intracellular replication[55], therefore, we also examined intracellular replication of wild-type or mutant *F. novicida*. We monitored growth over 24 h of infection in BMDMs lacking the inflammasome adaptor protein ASC as they fail to trigger pyroptosis in response to bacterial infection[8]. *F. novicida* wild-type and Δ*pdpE* replicated over the course of the infection (Supplementary Fig. 5d), while bacteria that lacked a dynamic T6SS (Δ*pdpB* or Δ*clpB*) or bacteria that had a dynamic T6SS, but were deficient in phagosomal escape (Δ*pdpC* or Δ*pdpC*/*pdpD*/*anmK*), were cleared over the course of the infection. Consistent with reduced phagosomal escape, *pdpD*/*anmK*-deficient bacteria also displayed a reduced rate of replication compared to wild-type bacteria, however, the difference was not significant.

Finally, we examined the role of potential T6SS effectors *in vivo*. Age- and sex-matched wild-type C57BL/6 mice were infected subcutaneously with 10^4 CFUs of *F. novicida* wild-type or strains deficient for the putative effectors, and the bacterial burden in the liver and spleen as well as serum IL-18 levels were assessed at 2 days post infection (Fig. 6d,e). The bacterial burden closely correlated with phagosomal escape, in that a partial reduction in virulence could be observed in Δ*pdpC* and Δ*pdpD*/*anmK*-infected mice. Deletion of *pdpC* alone had a stronger effect than deletion of *pdpD*/*anmK* although this difference was only significant in the liver. Deleting all three potential effectors, Δ*pdpC*/*pdpD*/*anmK*, rendered the bacteria largely avirulent, similarly to the deletion of the T6SS structural component *pdpB*. Consistent with the reduced levels of inflammasome activation *in vitro* (Fig. 6c; Supplementary Fig. 5a), we found that deletion of *pdpB*, *pdpC*, *pdpD*/*anmK* or *pdpC*/*pdpD*/*anmK* resulted in significantly lower levels of serum IL-18. A deficiency in *pdpE* appeared to have no effect on virulence or host response, since infection with *F. novicida* Δ*pdpE* resulted in bacterial burden and cytokine levels that were comparable to infections with *F. novicida* wild type (Fig. 6d,e). In summary, these results confirm previous studies indicating that PdpC and PdpD are T6SS-secreted effectors. Moreover, we show that PdpC and PdpD are dispensable for T6SS dynamics and specifically facilitate the escape of *F. novicida* from the phagosome into the host cell cytosol and therefore are essential for *Francisella* virulence.

Discussion

We show here that *Francisella* T6SS sheath is under certain conditions highly dynamic and ClpB is necessary for sheath disassembly. Since ClpB-mCherry2 specifically colocalizes with

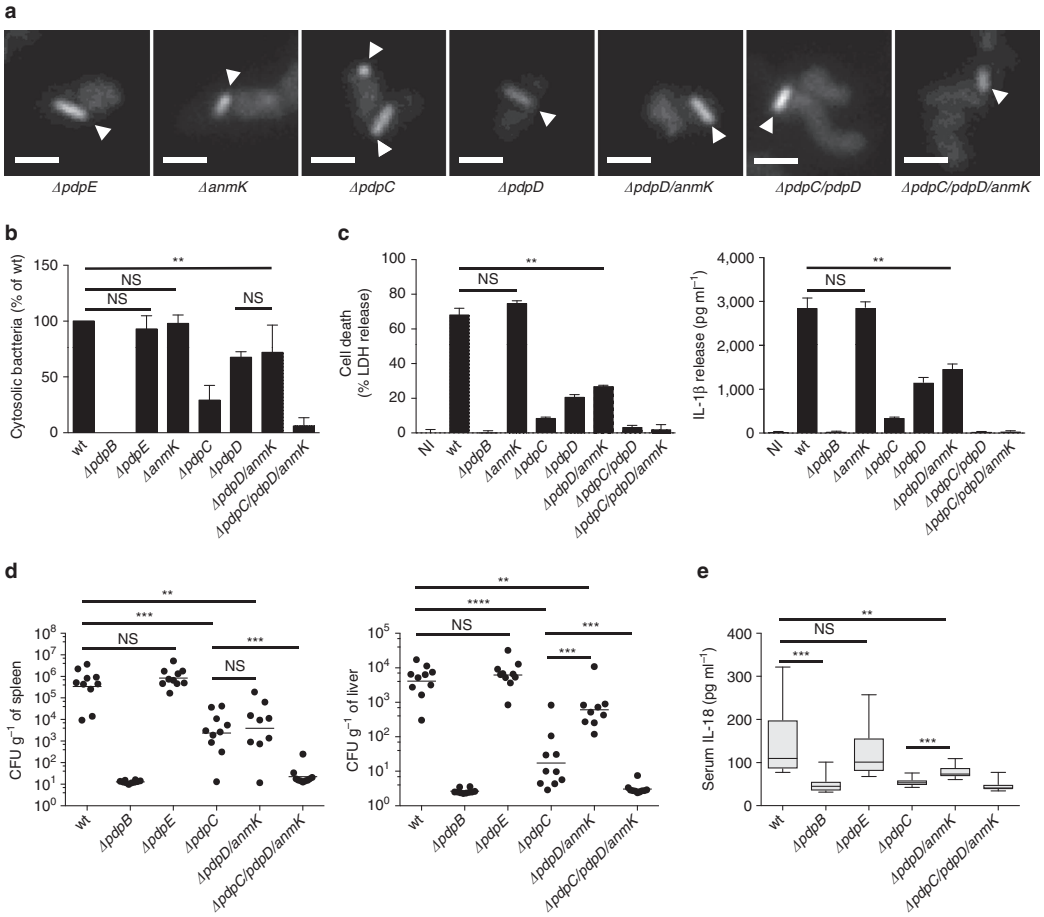

Figure 6 | Contribution of uncharacterized FPI genes to T6SS function. (**a**) T6SS sheath assembly (arrowheads) in *F. novicida* U112 *iglA-sfGFP ΔpdpE*, *ΔanmK*, *ΔpdpC*, *ΔpdpD*, *ΔpdpD/anmK*, *ΔpdpC/pdpD* and *ΔpdpC/pdpD/anmK*. GFP channel and 3.3 × 3.3 μm fields of view are shown. Scale bars, 1 μm. (**b**) Quantification of cytosolic bacteria in unprimed wild-type BMDMs 4 h after infection with *F. novicida* U112 *iglA-sfGFP* wild type, *ΔpdpB*, *ΔpdpE*, *ΔanmK*, *ΔpdpC*, *ΔpdpD*, *ΔpdpD/anmK* or *ΔpdpC/pdpD/anmK* (normalized to wild type). (**c**) Release of LDH and IL-1β from primed wild-type BMDMs 10 h after infection with *F. novicida* U112 *iglA-sfGFP* wild type, *ΔpdpB*, *ΔanmK*, *ΔpdpC*, *ΔpdpD*, *ΔpdpD/anmK*, *ΔpdpC/pdpD* or *ΔpdpC/pdpD/anmK* (NI—noninfected control). (**d**,**e**) Bacterial burden (as colony-forming units (CFUs) per gram tissue) in the spleen and liver (**d**) and serum IL-18 levels (**e**) of wild-type C57BL/6JRj mice infected subcutaneously for 2 days with 1×10^4 *F. novicida* U112 *iglA-sfGFP* wild type, *ΔpdpB*, *ΔpdpE*, *ΔpdpC*, *ΔpdpD/anmK* and *ΔpdpC/pdpD/anmK*. Small horizontal lines indicate the mean. Each symbol represents an individual mouse ($n = 5$ per experiment). Graphs show pooled data from two independent biological replicates with $n = 5$ per experiment ($n = 10$ total per group); small horizontal lines indicate the mean. (**b**–**e**) Data are pooled from three independent experiments (**b**) (mean and s.d. are shown) or two independent experiments (**d**,**e**) or are representatives of three independent experiments (**c**) (mean and s.d. of triplicate wells are shown). $^{**}P < 0.01$, $^{***}P < 0.001$ and $^{****}P < 0.0001$ (two-tailed unpaired *t*-test with Welch's correction (**b**,**c**) or Mann–Whitney test (**d**,**e**)).

the contracted sheaths, our data suggest that ClpB is directly involved in *Francisella* sheath disassembly similarly to ClpV in canonical T6SS (refs 24,49,50,56,57). Interestingly, *Francisella* ClpB was also shown to alter the immune response *in vivo*[58] and to be required for heat shock survival[52]. However, we show here that T6SS activity is dispensable for heat shock survival (Supplementary Fig. 2d). This suggests that, in contrast to canonical T6SS where ClpV is apparently solely dedicated to sheath disassembly, *Francisella* ClpB has a dual role. This raises the question how ClpB recognizes different substrates and whether a specific adaptor protein is required to recognize contracted sheaths similarly to adaptor proteins that recognize substrates for AAA+-mediated unfolding[59–62]. We show that ClpB is important for *F. novicida* virulence, which is consistent with what was shown previously[52–54,58]. Since all virulence related phenotypes of *clpB*-negative strain correlated with the phenotypes of the other strains with impaired T6SS dynamics (Fig. 3; Supplementary Figs 2 and 3), we propose that *in vivo* ClpB is mainly important for T6SS sheath disassembly. However, refolding of substrates unrelated to T6SS may be required to

survive certain stresses, which *Francisella* encounter during pathogenesis.

Detailed analysis of subcellular localization of dynamic T6SS sheath shows that *Francisella* T6SS assembles on the bacterial cell poles both *in vitro* as well as during infection of macrophages (Figs 2e,f and 3c; Supplementary Fig. 5e,f). Interestingly, similarly to what we show here for *Francisella*, ClpV-5 from T6SS-5 of *Burkholderia thailandensis* was found to preferentially localize to spots on bacterial poles[63]. Those spots were however less dynamic than ClpB spots in *Francisella* and thus it remains to be directly tested if assembly of T6SS-5 of *B. thailandensis* indeed initiates at the poles. Interestingly, both T6SS-5 of *B. thailandensis* and *Francisella* T6SS are required for manipulation of the eukaryotic cells after bacterial internalization. However, unlike in *Francisella*, T6SS-5 of *B. thailandensis* is only required for formation of multinucleated giant cells after bacteria escape from endosomes using T3SS[63–67]. Since T6SS sheaths almost always assemble as long as the bacteria, one possible advantage of the polar localization could be that the sheaths assembled from the pole in rod shaped bacteria would be generally longer than the sheaths assembled from the side of the cells. Given that the T6SS sheaths only contract to about half of their extended size[25], longer sheaths may increase the distance to which T6SS can deliver effectors. Interestingly, restricted subcellular localization was shown to decrease T6SS efficiency in inter-bacterial competitions despite increased overall activity[51]. However, since *F. novicida* is completely surrounded by phagosome membrane, restricted directionality of T6SS assembly should have no consequences for delivery of effectors to the host cell. In addition, polar localization of T6SS may increase chances of puncturing phagosomal membranes, as those may be physically closer to the bacterial poles when bacteria are in a tight membrane compartment. As it was shown previously for inter-bacterial interactions, proper aiming of the T6SS apparatus at the target bacteria increases efficiency of substrate translocation[37,51].

The primary function of the *Francisella* T6SS is to promote the escape of *Francisella* from the phagosome. We show that phagosome escape depends entirely on PdpC and PdpD, which are dispensable for T6SS assembly and dynamics (Fig. 6a,b; Supplementary Movie 1), suggesting that these proteins function as effectors necessary for phagosomal escape. It is also possible that PdpD and PdpC are required for activity or secretion of yet uncharacterized T6SS effectors to promote phagosomal escape, however previous work by Eshraghi *et al.*[42] has shown that *F. novicida* PdpC and PdpD are released by the T6SS in an *in vitro* secretion assay, supporting the hypothesis that these proteins function as secreted effectors in the target cell. Moreover, *F. tularensis* and *F. holarctica* lacking *pdpC* are unable to escape from the phagosome, induce cytotoxicity and replicate intracellularly, and they are avirulent in a mouse model of tularaemia[43,44,46–48]. These observations support our conclusions that PdpC contribute to *Francisella* virulence, independent of the *Francisella tularensis* subspecies. Whereas *pdpC* is conserved in all subspecies of *Francisella tularensis*, *pdpD* is differentially encoded[45]. Therefore, PdpD might have subspecies-specific virulence related functions.

PdpC and PdpD share no homology with known effectors or pore forming toxins, such as Listeriolysin O, type C phospholipases or phenol-soluble modulins, that allow other cytosolic bacteria (*Listeria monocytogenes*, *Shigella flexneri*, *Burkholderia thailandensis or Staphylococcus aureus*) to escape from the phagosome, and thus might represent a novel class of effectors with membranolytic function[68,69]. The exact mechanism of how these effectors destabilize the phagosomal membrane and if this results in the recruitment of galectin-8, a marker of ruptured vacuoles that recruits antimicrobial autophagy[70], remains to be analysed. The *Francisella* O-antigen allows the bacteria to avoid ubiquitination and uptake into LC3-positive compartments[71], but whether *Francisella* can actively inhibit or escape autophagy by injected effectors, as reported for *Listeria* and *Shigella* is unknown[72].

PdpE and AnmK, which are dispensable for T6SS assembly and phagosomal escape (Fig. 6a,b), might be effectors whose function is required once the bacteria enter the cytosol. However, their contribution to overall bacterial replication and virulence *in vivo* is minor (Fig. 6d,e; Supplementary Fig. 5d). In addition, OpiA and OpiB, encoded outside of the FPI cluster, were recently identified as T6SS secreted proteins, however, their contribution to intracellular replication is also minimal in comparison to the effects of a *pdpC* or *pdpD* deletion[42]. It is possible that these effectors have tissue-specific functions, or that they are required for *Francisella* replication in amoeba or within arthropod hosts[73,74].

Live-cell imaging of T6SS sheath dynamics suggests that IglF, IglG, IglI and IglJ are putative structural components required for T6SS assembly in *Francisella* (Fig. 5a; Supplementary Movie 2). These proteins could be homologues of components of canonical T6SS baseplate, which are difficult to identify using homology modelling[14,75] (Fig. 1). However, it is also conceivable that some of these proteins may be secreted effectors or be required for effector secretion, because deletion of certain effectors decreases T6SS function in *V. cholerae*[37,76]. Nonetheless, our finding that the dynamics of *Francisella* T6SS is possible to image *in vitro* will help to dissect the assembly of this non-canonical T6SS and to differentiate between structural components and translocated substrates. Further analysis of the structural components will reveal principles of T6SS evolution and defining the molecular mechanisms by which *Francisella* effectors modulate host cell signalling will significantly contribute to our understanding of *Francisella* virulence.

Methods

Bacterial strains and growth conditions. *Francisella tularensis* subsp. *novicida* strain U112 (hereafter *F. novicida*) and the derivative strains were grown at 37 °C with aeration in brain heart infusion (BHI) medium supplemented with 0.2% L-cysteine (Sigma) and appropriate antibiotics. Antibiotic concentrations used were 100 μg ml^{-1} ampicillin (AppliChem) or 15 μg ml^{-1} kanamycin (AppliChem). A detailed strain list can be found in Supplementary Table 1. For infection with *F. novicida*, BHI medium was inoculated with bacteria from BHI agar plate (supplemented with 0.2% L-cysteine (Sigma) and appropriate antibiotics) and were grown overnight at 37 °C with aeration.

Bacterial mutagenesis. All in-frame deletions were generated by homologous recombination using the suicide vector pDMK3 as previously described[77]. A list of plasmids, primers as well as remaining peptides encoded by deleted genes can be found in Supplementary Table 2. To obtain single colonies after recombination, bacteria were grown overnight at 37 °C on Mueller-Hinton agar (MHA) supplemented with 0.1% D-glucose (Millipore), 0.1% FCS (BioConcept), 100 μg ml^{-1} ampicillin (AppliChem) and 0.1% L-cysteine (Sigma) (hereafter MHA plate). Cloning product sequences were verified and chromosomal mutations were tested by PCR using primers located outside of the replaced region. Sites of homologous recombination of the chromosomal mutations were verified by sequencing.

Heat shock survival assay. Heat shock survival assay was adapted from ref. 52. In brief, bacteria were grown overnight as described above, diluted 1:40 in BHI medium and grown for 3 h at 37 °C with aeration. Then bacteria were diluted 1:10 in 250 μl BHI in a 1.5 ml tube and incubated in a water bath at 50 °C for 0, 15 or 30 min. At each time point the bacteria were transferred on ice and serial dilutions were plated on MHA plates. The next day, CFUs were counted and the concentration of surviving bacteria was calculated.

Fluorescence microscopy. Procedures and settings to detect a fluorescence signal in *F. novicida* were employed as previously described[37,41]. All imaging was carried out at 37 °C and humidity was regulated to 95% using a T-unit (Oko-lab). The exposure time was set to 150 ms for all channels. For bacterial imaging on agarose pads, *F. novicida* strains from BHI plate were washed once with BHI, diluted

1:40 in BHI medium and grown at 37 °C with aeration for 3–4 h. Bacteria from 1 ml culture were re-suspended in 50–100 µl phosphate-buffered saline (PBS), spotted on a pad of 1% agarose in PBS, covered with a cover glass (Roth) and either imaged directly or incubated at 37 °C for 1 h before imaging. Images were collected every 3 s for T6SS assembly speed quantification and every 30 s for assessment of T6SS dynamics. For imaging of infected macrophages, BMDMs were seeded onto cover glass (VWR) in 24-well plates at a density of 1.5×10^5 cells per well and infected with *F. novicida* at a multiplicity of infection of 100 in 1 ml OptiMEM (Life Technologies) as described below. Thirty minutes post infection, the BMDMs were washed three times with OptiMEM and the cover glass was mounted on a pad of 1% agarose in PBS BMDMs facing down. Images were collected every 30 s for assessment of T6SS dynamics.

Image analysis. Fiji[78] was used for all image analysis and manipulations as described previously[37,51]. The 'Time Series Analyzer V3.0' plugin was used for quantification of GFP signal intensity. For comparison of GFP signal intensities of mutants and wild type, only bacteria without assembled T6SS structures were considered. For quantification of T6SS activity in different mutants from 5 min time-lapse movies the 'temporal colour code' function was used. For kymograms and T6SS assembly speed quantification the 'reslice' function was used. For determination of subcellular localization of T6SS assembly the surface area of bacteria was divided into an equally sized polar and mid cell area. The surface area was calculated based on the model of a capsule using the manually measured length and width of the bacteria (see formulas below). T6SS assemblies initiating in one of the two pole areas were considered as T6SS assemblies at pole.

$$h_{\mathrm{m}} = \mathrm{Height}_{\mathrm{measured}}$$

$$l_{\mathrm{m}} = \mathrm{Length}_{\mathrm{measured}}$$

$$r = \frac{h_{\mathrm{m}}}{2}$$

$$l_{\mathrm{Cylinder}} = l_{\mathrm{m}} - h_{\mathrm{m}}$$

$$A_{\mathrm{total}} = A_{\mathrm{Sphere}} + A_{\mathrm{Cylinder}} = 4\pi r^2 + 2\pi r l_{\mathrm{Cylinder}}$$

$$A_{0.5} = 0.5 \times A_{\mathrm{total}}$$

For determination of subcellular localization of T6SS assembly, images of *V. cholerae* 2740-80 were reanalysed from ref. 37. Contrast on compared sets of images was adjusted equally. All imaging experiments were performed with at least two biological replicates.

Structured illumination microscopy. BMDMs were seeded onto cover glass (VWR) in 24-well plates at a density of 1.25×10^5 cells per well and infected with *F. novicida* at a multiplicity of infection of 100 for 1 h as described below. BMDMs were washed three times with PBS and fixed for 10 min at 37 °C with 4% paraformaldehyde (Electron Microscopy Science). Cover glass was incubated with chicken anti-*F. novicida* (1:2,000; a gift from D.M. Monack, Stanford University) for 1 h at room temperature, then was washed three times with PBS, incubated with goat anti-chicken coupled to Alexa 568 (1:500; Life Technologies) and DY-647-Phalloidin (1:500; Dyomics) for another 45 min at room temperature, washed three times with PBS and was mounted on glass slides with Vectashield (Vector labs). 3D-SM was performed on a microscope system DeltaVision OMX-Blaze version 4 (Applied Precision, Issaquah, WA). Images were acquired using a Plan Apo N 60 × 1.42 numerical aperture oil immersion objective lens (Olympus) and four liquid-cooled sCMOS cameras (pco Edge, full frame 2,560 × 2,160; Photometrics). Optical *z*-sections were separated by 0.125 µm. The laser lines 488 and 568 were used for 3D-SIM acquisition. Exposure times were typically between 10 and 140 ms, and the power of each laser was adjusted to achieve optimal intensities of between 5,000 and 8,000 counts in a raw image of 15-bit dynamic range at the lowest laser power possible to minimize photobleaching. Phalloidin Alexa-647 was acquired using the widefield mode of the system. Raw 3D-SIM images were processed and reconstructed using the DeltaVision OMX SoftWoRx software package (Applied Precision).

Cell culture and infection. Primary wild-type BMDMs from C57BL/6JRj mice (Janvier) were differentiated in DMEM (Sigma) with 20% M-CSF (supernatants of L929 mouse fibroblasts), 10% v/v FCS, 10 mM HEPES, nonessential amino acids and penicillin (100 IU ml^{-1})/streptomycin (100 µg ml^{-1}) (all BioConcept). One day before infection, BMDMs were seeded into 24- or 96-well plates (Eppendorf) at a density of 1.5×10^5 or 5×10^4 cells per well in DMEM (Sigma) with 10% M-CSF (supernatants of L929 mouse fibroblasts), 10% v/v FCS, 10 mM HEPES and nonessential amino acids (all BioConcept). Where required, BMDMs were pre-stimulated overnight with LPS (from *Escherichia coli* strain O111:B4 (InvivoGen; tlr-3pelps)). *F. novicida* were grown overnight at 37 °C with aeration as described above. The bacteria were added to the BMDMs at a multiplicity of infection of 100 or the indicated value. The plates were centrifuged for 5 min at 500*g* to ensure similar adhesion of the bacteria to the cells and were incubated for 120 min at 37 °C. Next, the medium was replaced with fresh medium containing 10 µg ml^{-1} gentamicin (BioConcept) to kill extracellular bacteria, then plates were incubated at 37 °C for the indicated length of time.

Cytokine and LDH release measurement. IL-1β and IL-18 were measured by enzyme-linked immunosorbent assay (eBioscience). Lactate dehydrogenase (LDH) was measured with an LDH Cytotoxicity Detection Kit (Takara). To correct for spontaneous cell lysis and to normalize the values, the percentage of LDH release was calculated as follows:

$$\frac{\mathrm{LDH\ value}_{\mathrm{infected}} - \mathrm{LDH\ value}_{\mathrm{uninfected}}}{\mathrm{LDH\ value}_{\mathrm{total\ lysis}} - \mathrm{LDH\ value}_{\mathrm{uninfected}}} \times 100$$

Phagosome protection assay. The amount of cytoplasmic and vacuolar bacteria was measured as previously described[79]. In brief, BMDMs were seeded into 24-well plates at a density of 1.5×10^5 cells per well and *F. novicida* were grown for 4 h at 37 °C with aeration as described above. BMDMs were infected with *F. novicida* at a multiplicity of infection of 100 for 4 h as outlined above. BMDMs were washed three times with KHM buffer (110 mM potassium acetate, 20 mM Hepes, 2 mM $MgCl_2$) and incubated for 1 min with 75 µg ml^{-1} digitonin (Sigma) followed by differential staining of cytoplasmic and total bacteria. Antibodies used for staining were chicken anti-*F. novicida* (1:2,000; a gift from D.M. Monack, Stanford University) and goat anti-chicken coupled to Alexa 647 (cytoplasmic bacteria) or Alexa 488 (total bacteria) (1:500; both from Life Technologies). Stained bacteria were analysed on a FACS-Canto-II. Percentage of cytosolic bacteria were normalized to wild-type *F. novicida* as follows:

$$\frac{\mathrm{FACS\ value} - \mathrm{FACS\ value}_{\Delta pdpB}}{\mathrm{FACS\ value}_{wt} - \mathrm{FACS\ value}_{\Delta pdpB}} \times 100$$

Intracellular bacterial growth assay. BMDMs were seeded into 24-well plates at a density of 1.5×10^5 cells per well and infected with *F. novicida* at a multiplicity of infection of 1 as described above. After 2 and 24 h of infection, the BMDMs were washed three times with PBS and lysed with 0.1% Triton-X 100 (Promega) for 10 min at 37 °C. The bacteria were stained for 10 min with chicken anti-*F. novicida* (1:2,000; a gift from D.M. Monack, Stanford University), washed once with PBS and stained for 10 min with goat anti-chicken coupled to Alexa 647 and Alexa 488 (1:500 each; both from Life Technologies). A volume of 20 µl 123count eBeads (eBioscience) was added to each sample. The samples were analysed on a FACS-Canto-II by counting the number of bacteria per 5,000 beads. The CFU ratio was calculated by dividing the number of bacteria at 24 h (output) with the number of bacteria at 2 h (input).

Type I interferon measurement. One day before infection, ISRE-L929 reporter cells (a gift from D.M. Monack, Stanford University) were seeded into black 96-well plates with micro-clear bottom (Greiner) at a density of 1×10^5 cells per well in DMEM (Sigma) with 10% v/v FCS and penicillin (100 IU ml^{-1})/streptomycin (100 µg ml^{-1}) (both BioConcept). BMDMs were seeded into 96-well plates at a density of 5×10^4 cells per well and infected with *F. novicida* at a multiplicity of infection of 100 as described above. After 10 h of infection, type I IFN production was measured with the Bright-Glo Luciferase Assay System (Promega) as previously described[80].

Animal infection. All animal experiments were approved (licence 2535-26742, Kantonales Veterinäramt Basel-Stadt) and were performed according to local guidelines (Tierschutz-Verordnung, Basel-Stadt) and the Swiss animal protection law (Tierschutz-Gesetz). Female 10 weeks old wt C57BL/6JRj mice (Janvier) were infected subcutaneously with 10^4 CFUs of indicated stationary-phase *F. novicida* strain in 50 µl PBS. Mice were killed 48 h post infection. Bacterial load of spleen and liver was analysed by plating the bacteria on MHA plates. The plates were incubated for 24 h at 37 °C. IL-18 levels in the blood were measured by enzyme-linked immunosorbent assay (eBioscience). No randomization or 'blinding' of researchers to sample identity was used.

Statistical analysis. Statistical data analysis was done using Prism 6.0h (GraphPad Software, Inc.). To evaluate the difference between two groups (T6SS per cell, T6SS assembly speed, subcellular localization of T6SS, bacterial survival, cell death, cytokine release, phagosomal escape, bacterial growth and IFN production) the unpaired two-tailed *t*-test with Welch's correction was used. Animal experiments were evaluated with a two-tailed Mann–Whitney test. *P* values are given in the figure legends.

Data availability. The authors declare that the data supporting the findings of this study are available within the paper and its Supplementary Information files.

References

1. Oyston, P. C. F., Sjostedt, A. & Titball, R. W. Tularaemia: bioterrorism defence renews interest in *Francisella tularensis*. *Nat. Rev. Microbiol.* **2,** 967–978 (2004).
2. Kingry, L. C. & Petersen, J. M. Comparative review of *Francisella tularensis* and *Francisella novicida*. *Front. Cell Infect. Microbiol.* **4,** 35 (2014).
3. Chong, A. & Celli, J. The Francisella intracellular life cycle: toward molecular mechanisms of intracellular survival and proliferation. *Front. Microbiol.* **1,** 138 (2010).
4. Fernandes-Alnemri, T. *et al.* The AIM2 inflammasome is critical for innate immunity to *Francisella tularensis*. *Nat. Immunol.* **11,** 385–393 (2010).
5. Henry, T., Brotcke, A., Weiss, D. S., Thompson, L. J. & Monack, D. M. Type I interferon signaling is required for activation of the inflammasome during Francisella infection. *J. Exp. Med.* **204,** 987–994 (2007).
6. Jones, J. W. *et al.* Absent in melanoma 2 is required for innate immune recognition of *Francisella tularensis*. *Proc. Natl Acad. Sci. USA* **107,** 9771–9776 (2010).
7. Man, S. M. *et al.* The transcription factor IRF1 and guanylate-binding proteins target activation of the AIM2 inflammasome by Francisella infection. *Nat. Immunol.* **16,** 467–475 (2015).
8. Mariathasan, S., Weiss, D. S., Dixit, V. M. & Monack, D. M. Innate immunity against *Francisella tularensis* is dependent on the ASC/caspase-1 axis. *J. Exp. Med.* **202,** 1043–1049 (2005).
9. Meunier, E. *et al.* Guanylate-binding proteins promote activation of the AIM2 inflammasome during infection with *Francisella novicida*. *Nat. Immunol.* **16,** 476–484 (2015).
10. Rathinam, V. A. K. *et al.* The AIM2 inflammasome is essential for host defense against cytosolic bacteria and DNA viruses. *Nat. Immunol.* **11,** 395–402 (2010).
11. Storek, K. M., Gertsvolf, N. A., Ohlson, M. B. & Monack, D. M. cGAS and Ifi204 cooperate to produce type I IFNs in response to Francisella infection. *J. Immunol.* **194,** 3236–3245 (2015).
12. Nano, F. E. *et al.* A *Francisella tularensis* pathogenicity island required for intramacrophage growth. *J. Bacteriol.* **186,** 6430–6436 (2004).
13. Nano, F. E. & Schmerk, C. The Francisella pathogenicity island. *Ann. NY Acad. Sci.* **1105,** 122–137 (2007).
14. Bröms, J. E., Sjöstedt, A. & Lavander, M. The role of the *Francisella Tularensis* pathogenicity island in type VI secretion, intracellular survival, and modulation of host cell signaling. *Front. Microbiol.* **1,** 136 (2010).
15. Rigard, M. *et al. Francisella tularensis* IglG belongs to a novel family of PAAR-like T6SS proteins and harbors a unique N-terminal extension required for virulence. *PLoS Pathog.* **12,** e1005821 (2016).
16. Bingle, L. E., Bailey, C. M. & Pallen, M. J. Type VI secretion: a beginner's guide. *Curr. Opin. Microbiol.* **11,** 3–8 (2008).
17. de Bruin, O. M., Ludu, J. S. & Nano, F. E. The Francisella pathogenicity island protein IglA localizes to the bacterial cytoplasm and is needed for intracellular growth. *BMC Microbiol.* **7,** 1 (2007).
18. Russell, A. B. *et al.* A type VI secretion-related pathway in Bacteroidetes mediates interbacterial antagonism. *Cell Host Microbe* **16,** 227–236 (2014).
19. Alcoforado Diniz, J., Liu, Y.-C. & Coulthurst, S. J. Molecular weaponry: diverse effectors delivered by the type VI secretion system. *Cell. Microbiol.* **17,** 1742–1751 (2015).
20. Durand, E., Cambillau, C., Cascales, E. & Journet, L. VgrG, Tae, Tle, and beyond: the versatile arsenal of type VI secretion effectors. *Trends Microbiol.* **22,** 498–507 (2014).
21. Hachani, A., Wood, T. E. & Filloux, A. Type VI secretion and anti-host effectors. *Curr. Opin. Microbiol.* **29,** 81–93 (2016).
22. Ho, B. T., Dong, T. G. & Mekalanos, J. J. A view to a kill: the bacterial type VI secretion system. *Cell Host Microbe* **15,** 9–21 (2014).
23. Russell, A. B., Peterson, S. B. & Mougous, J. D. Type VI secretion system effectors: poisons with a purpose. *Nat. Rev. Microbiol.* **12,** 137–148 (2014).
24. Basler, M. & Mekalanos, J. J. Type 6 secretion dynamics within and between bacterial cells. *Science* **337,** 815 (2012).
25. Basler, M., Pilhofer, M., Henderson, G. P., Jensen, G. J. & Mekalanos, J. J. Type VI secretion requires a dynamic contractile phage tail-like structure. *Nature* **483,** 182–186 (2012).
26. Durand, E. *et al.* Biogenesis and structure of a type VI secretion membrane core complex. *Nature* **523,** 555–560 (2015).
27. Brunet, Y. R., Zoued, A., Boyer, F., Douzi, B. & Cascales, E. The type VI secretion TssEFGK-VgrG phage-like baseplate is recruited to the TssJLM membrane complex via multiple contacts and serves as assembly platform for tail tube/sheath polymerization. *PLoS Genet.* **11,** e1005545 (2015).
28. Planamente, S. *et al.* TssA forms a gp6-like ring attached to the type VI secretion sheath. *EMBO J.* **35,** 1613–1627 (2016).
29. Shneider, M. M. *et al.* PAAR-repeat proteins sharpen and diversify the type VI secretion system spike. *Nature* **500,** 350–353 (2013).
30. Zoued, A. *et al.* TssK is a trimeric cytoplasmic protein interacting with components of both phage-like and membrane anchoring complexes of the type VI secretion system. *J. Biol. Chem.* **288,** 27031–27041 (2013).
31. Zoued, A. *et al.* Architecture and assembly of the type VI secretion system. *Biochim. Biophys. Acta* **1843,** 1664–1673 (2014).
32. Brunet, Y. R., Henin, J., Celia, H. & Cascales, E. Type VI secretion and bacteriophage tail tubes share a common assembly pathway. *EMBO Rep.* **15,** 315–321 (2014).
33. Flaugnatti, N. *et al.* A phospholipase A1 antibacterial type VI secretion effector interacts directly with the C-terminal domain of the VgrG spike protein for delivery. *Mol. Microbiol.* **99,** 1099–1118 (2016).
34. Hachani, A., Allsopp, L. P., Oduko, Y. & Filloux, A. The VgrG proteins are 'à la carte' delivery systems for bacterial type VI effectors. *J. Biol. Chem.* **289,** 17872–17884 (2014).
35. Liang, X. *et al.* Identification of divergent type VI secretion effectors using a conserved chaperone domain. *Proc. Natl Acad. Sci. USA* **112,** 9106–9111 (2015).
36. Silverman, J. M. *et al.* Haemolysin coregulated protein is an exported receptor and chaperone of type VI secretion substrates. *Mol. Cell* **51,** 584–593 (2013).
37. Vettiger, A. & Basler, M. Type VI secretion system substrates are transferred and reused among sister cells. *Cell* **167,** 99–110.e12 (2016).
38. Whitney, J. C. *et al.* Genetically distinct pathways guide effector export through the type VI secretion system. *Mol. Microbiol.* **92,** 529–542 (2014).
39. Whitney, J. C. *et al.* An interbacterial NAD(P)(+) glycohydrolase toxin requires elongation factor Tu for delivery to target cells. *Cell* **163,** 607–619 (2015).
40. Clemens, D. L., Ge, P., Lee, B.-Y., Horwitz, M. A. & Zhou, Z. H. Atomic structure of T6SS reveals interlaced array essential to function. *Cell* **160,** 940–951 (2015).
41. Kudryashev, M. *et al.* Structure of the type VI secretion system contractile sheath. *Cell* **160,** 952–962 (2015).
42. Eshraghi, A. *et al.* Secreted effectors encoded within and outside of the francisella pathogenicity island promote intramacrophage growth. *Cell Host Microbe* **20,** 573–583 (2016).
43. Lindgren, M., Eneslätt, K., Bröms, J. E. & Sjöstedt, A. Importance of PdpC, IglC, IglI, and IglG for modulation of a host cell death pathway induced by *Francisella tularensis*. *Infect. Immun.* **81,** 2076–2084 (2013).
44. Lindgren, M., Bröms, J. E., Meyer, L., Golovliov, V. & Sjöstedt, A. The *Francisella tularensis* LVS ΔpdpC mutant exhibits a unique phenotype during intracellular infection. *BMC Microbiol.* **13,** 20 (2013).
45. Ludu, J. S. *et al.* The Francisella pathogenicity island protein PdpD is required for full virulence and associates with homologues of the type VI secretion system. *J. Bacteriol.* **190,** 4584–4595 (2008).
46. Ozanic, M., Marecic, V., Lindgren, M., Sjöstedt, A. & Santic, M. Phenotypic characterization of the *Francisella tularensis* ΔpdpC and ΔiglG mutants. *Microbes Infect.* **18,** 768–776 (2016).
47. Uda, A. *et al.* Role of pathogenicity determinant protein C (PdpC) in determining the virulence of the *Francisella tularensis* subspecies tularensis SCHU. *PLoS ONE* **9,** e89075 (2014).
48. Long, M. E., Lindemann, S. R., Rasmussen, J. A., Jones, B. D. & Allen, L.-A. H. Disruption of *Francisella tularensis* Schu S4 iglI, iglJ, and pdpC genes results in attenuation for growth in human macrophages and *in vivo* virulence in mice and reveals a unique phenotype for pdpC. *Infect. Immun.* **81,** 850–861 (2013).
49. Bönemann, G., Pietrosiuk, A., Diemand, A., Zentgraf, H. & Mogk, A. Remodelling of VipA/VipB tubules by ClpV-mediated threading is crucial for type VI protein secretion. *EMBO J.* **28,** 315–325 (2009).
50. Förster, A. *et al.* Coevolution of the ATPase ClpV, the sheath proteins TssB and TssC, and the accessory protein TagJ/HsiE1 distinguishes type VI secretion classes. *J. Biol. Chem.* **289,** 33032–33043 (2014).
51. Basler, M., Ho, B. T. & Mekalanos, J. J. Tit-for-tat: type VI secretion system counterattack during bacterial cell-cell interactions. *Cell* **152,** 884–894 (2013).
52. Meibom, K. L. *et al.* The heat-shock protein ClpB of *Francisella tularensis* is involved in stress tolerance and is required for multiplication in target organs of infected mice. *Mol. Microbiol.* **67,** 1384–1401 (2008).
53. Ahlund, M. K., Rydén, P., Sjöstedt, A. & Stöven, S. Directed screen of *Francisella novicida* virulence determinants using Drosophila melanogaster. *Infect. Immun.* **78,** 3118–3128 (2010).
54. Gray, C. G., Cowley, S. C., Cheung, K. K. M. & Nano, F. E. The identification of five genetic loci of *Francisella novicida* associated with intracellular growth. *FEMS Microbiol. Lett.* **215,** 53–56 (2002).
55. de Bruin, O. M. *et al.* The biochemical properties of the Francisella pathogenicity island (FPI)-encoded proteins IglA, IglB, IglC, PdpB and DotU suggest roles in type VI secretion. *Microbiology* **157,** 3483–3491 (2011).
56. Gerc, A. J. *et al.* Visualization of the serratia type VI secretion system reveals unprovoked attacks and dynamic assembly. *Cell Rep.* **12,** 2131–2142 (2015).
57. Kapitein, N. *et al.* ClpV recycles VipA/VipB tubules and prevents non-productive tubule formation to ensure efficient type VI protein secretion. *Mol. Microbiol.* **87,** 1013–1028 (2013).
58. Barrigan, L. M. *et al.* Infection with *Francisella tularensis* LVS clpB leads to an altered yet protective immune response. *Infect. Immun.* **81,** 2028–2042 (2013).

59. Kirstein, J., Molière, N., Dougan, D. A. & Turgay, K. Adapting the machine: adaptor proteins for Hsp100/Clp and AAA+ proteases. *Nat. Rev. Microbiol.* **7,** 589–599 (2009).
60. Mogk, A. *et al.* Broad yet high substrate specificity: the challenge of AAA+ proteins. *J. Struct. Biol.* **146,** 90–98 (2004).
61. Sauer, R. T. & Baker, T. A. AAA+ proteases: ATP-fueled machines of protein destruction. *Annu. Rev. Biochem.* **80,** 587–612 (2011).
62. Sauer, R. T. *et al.* Sculpting the proteome with AAA(+) proteases and disassembly machines. *Cell* **119,** 9–18 (2004).
63. Schwarz, S. *et al.* VgrG-5 is a Burkholderia type VI secretion system-exported protein required for multinucleated giant cell formation and virulence. *Infect. Immun.* **82,** 1445–1452 (2014).
64. French, C. T. *et al.* Dissection of the Burkholderia intracellular life cycle using a photothermal nanoblade. *Proc. Natl Acad. Sci. USA* **108,** 12095–12100 (2011).
65. Galyov, E. E., Brett, P. J. & DeShazer, D. Molecular insights into Burkholderia pseudomallei and Burkholderia mallei pathogenesis. *Annu. Rev. Microbiol.* **64,** 495–517 (2010).
66. Schwarz, S. *et al.* Burkholderia type VI secretion systems have distinct roles in eukaryotic and bacterial cell interactions. *PLoS Pathog.* **6,** e1001068 (2010).
67. Toesca, I. J., French, C. T. & Miller, J. F. The type VI secretion system spike protein VgrG5 mediates membrane fusion during intercellular spread by pseudomallei group Burkholderia species. *Infect. Immun.* **82,** 1436–1444 (2014).
68. Grosz, M. *et al.* Cytoplasmic replication of *Staphylococcus aureus* upon phagosomal escape triggered by phenol-soluble modulin α. *Cell. Microbiol.* **16,** 451–465 (2014).
69. Hybiske, K. & Stephens, R. S. Exit strategies of intracellular pathogens. *Nat. Rev. Microbiol.* **6,** 99–110 (2008).
70. Thurston, T. L. M., Wandel, M. P., von Muhlinen, N., Foeglein, A. & Randow, F. Galectin 8 targets damaged vesicles for autophagy to defend cells against bacterial invasion. *Nature* **482,** 414–418 (2012).
71. Case, E. D. R. *et al.* The Francisella O-antigen mediates survival in the macrophage cytosol via autophagy avoidance. *Cell. Microbiol.* **16,** 862–877 (2014).
72. Deretic, V., Saitoh, T. & Akira, S. Autophagy in infection, inflammation and immunity. *Nat. Rev. Immunol.* **13,** 722–737 (2013).
73. Akimana, C. & Kwaik, Y. A. Francisella-arthropod vector interaction and its role in patho-adaptation to infect mammals. *Front. Microbiol.* **2,** 34 (2011).
74. Santic, M. *et al.* Intra-vacuolar proliferation of *F. novicida* within *H. vermiformis*. *Front. Microbiol.* **2,** 78 (2011).
75. Boyer, F., Fichant, G., Berthod, J., Vandenbrouck, Y. & Attree, I. Dissecting the bacterial type VI secretion system by a genome wide *in silico* analysis: what can be learned from available microbial genomic resources? *BMC Genomics* **10,** 104–104 (2009).
76. Dong, T. G., Ho, B. T., Yoder-Himes, D. R. & Mekalanos, J. J. Identification of T6SS-dependent effector and immunity proteins by Tn-seq in Vibrio cholerae. *Proc. Natl Acad. Sci. USA* **110,** 2623–2628 (2013).
77. Lindgren, H. *et al.* Resistance of *Francisella tularensis* strains against reactive nitrogen and oxygen species with special reference to the role of KatG. *Infect. Immun.* **75,** 1303–1309 (2007).
78. Schindelin, J. *et al.* Fiji: an open-source platform for biological-image analysis. *Nat. Methods* **9,** 676–682 (2012).
79. Meunier, E. *et al.* Caspase-11 activation requires lysis of pathogen-containing vacuoles by IFN-induced GTPases. *Nature* **509,** 366–370 (2014).
80. Peng, K., Broz, P., Jones, J., Joubert, L.-M. & Monack, D. Elevated AIM2-mediated pyroptosis triggered by hypercytotoxic Francisella mutant strains is attributed to increased intracellular bacteriolysis. *Cell. Microbiol.* **13,** 1586–1600 (2011).

Acknowledgements

We thank M.A. Horwitz (UCLA) for providing the strain *F. novicida* U112 *iglA-sfGFP*, D.M. Monack (Stanford University) for the conjugation plasmid, the anti-*Francisella* primary antibody and the ISRE-L929 cells, A. Harms and C. Dehio (Biozentrum, University of Basel) for the *E. coli* conjugation strain and the Imaging Core Facility and FACS Core Facility (Biozentrum, University of Basel) for technical support. We thank P.D. Ringel for his help with the analysis of subcellular localization of T6SS assembly. The work was supported by SNSF Starting Grant BSSGI0_155778 (to M.Ba.), SNSF grant 31003A_159525 (to M.Ba.), SNSF grant PP00P3_139120/1 (to P.B.) and the University of Basel. M.Br. was supported by the Biozentrum Basel International PhD Program 'Fellowships for Excellence'.

Author contributions

M.Br., R.F.D., P.B. and M.Ba. designed experiments, analysed and interpreted the results. M.Br. and R.F.D. generated strains and acquired all data. All authors wrote and approved the manuscript.

Additional information

Supplementary Information accompanies this paper at http://www.nature.com/naturecommunications

Competing interests: The authors declare no competing financial interests.

Reprints and permission information is available online at http://npg.nature.com/reprintsandpermissions/

How to cite this article: Brodmann, M. *et al. Francisella* requires dynamic type VI secretion system and ClpB to deliver effectors for phagosomal escape. *Nat. Commun.* **8,** 15853 doi: 10.1038/ncomms15853 (2017).

Publisher's note: Springer Nature remains neutral with regard to jurisdictional claims in published maps and institutional affiliations.

Supplementary Figures:

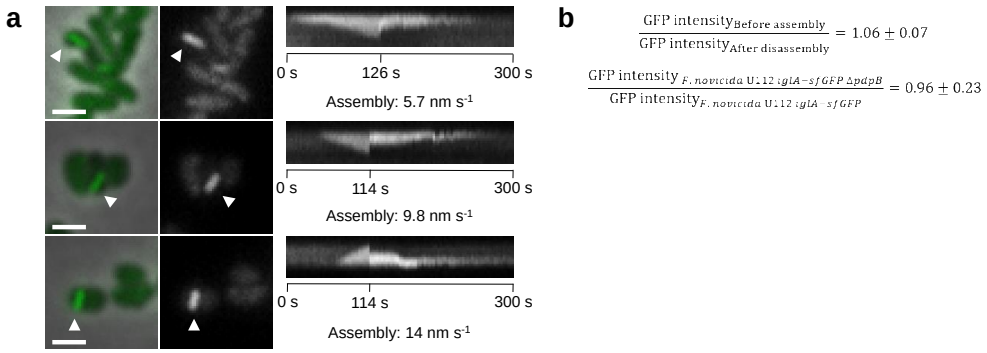

Supplementary Figure 1: Assembly speed varies between bacteria. (a) Kymograms of slow (~ 5 nm s^{-1}) to fast (~ 14 nm s^{-1}) T6SS assemblies (arrowheads) over 5 minutes (3 s per pixel) in *F. novicida* U112 *iglA-sfGFP*. First image is a merge of phase contrast and GFP channel, following images represent GFP channel only. 3.3 x 3.3 µm fields of view are shown. Scale bars represent 1 µm. **(b)** GFP intensities were measured a frame before and a frame after a complete assembly-disassembly cycle in two independent experiments. 30 bacteria were analyzed per experiment. GFP intensities measured in *F. novicida* U112 *iglA-sfGFP* wild-type *and ΔpdpB* were compared in four independent experiments. 30 bacteria were analyzed per experiment. Standard deviation was calculated.

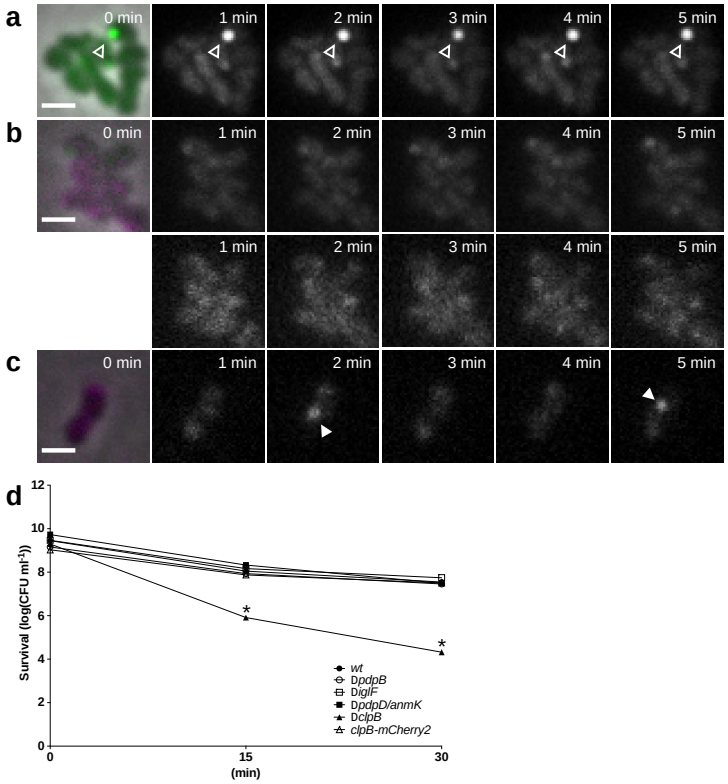

Supplementary Figure 2: T6SS activity is required for ClpB spot localization but dispensable for ClpB-dependent heat tolerance. (a) IglA-sfGFP localization and foci (empty arrowheads) in *F. novicida U112 iglA-sfGFP ΔclpB/pdpB*. First image is a merge of phase contrast and GFP channels, following images represent GFP channel only. 3.3 x 3.3 µm fields of view are shown. Scale bars represent 1 µm. **(b)** IglA-sfGFP and ClpB-mCherry2 localization in *F. novicida* U112 *iglA-sfGFP clpB-mCherry2 ΔpdpB*. First image is a merge of phase contrast, GFP and mCherry channels, following images represent GFP channel (upper panel) and mCherry channel (lower panel). **(c)** ClpB-mCherry2 localization dynamics in *F. novicida* U112 *clpB-mCherry2*. First image is a merge of phase contrast and mCherry channels, following images represent mCherry channel only. Arrowheads indicate ClpB recruitment. **(d)** Heat shock survival assay performed with *F. novicida U112 iglA-sfGFP* wild-type, *ΔpdpB*, *ΔiglF*, *ΔpdpD/anmK*, *ΔclpB* and *clpB-mCherry2* at 50 °C for 0, 15 and 30 min. Data are pooled from three independent experiments. *P < 0.05 (two-tailed unpaired *t*-test with Welch's correction). (a-c) 3.3 x 3.3 µm fields of view are shown. Scale bar represents 1 µm.

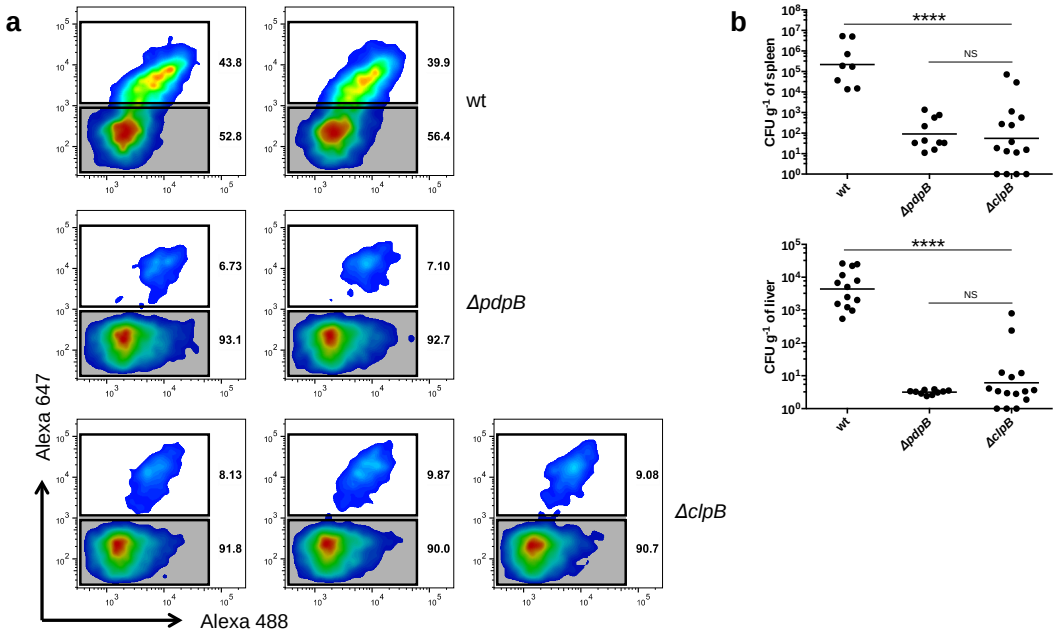

Supplementary Figure 3: *F. novicida* U112 *iglA-sfGFP ΔclpB* fails to escape into the cytosol and is avirulent *in vivo*. (a) Representative FACS blots from the quantification of cytosolic (white gates) and vacuolar bacteria (grey gates) by flow cytometry in unprimed wild-type BMDMs 4 h after infection with *F. novicida* U112 *iglA-sfGFP* wild-type, *ΔpdpB* or *ΔclpB.* Numbers next to the gates indicate the percentage of cytosolic and vacuolar bacteria. **(b)** Bacterial burden (as colony-forming units (CFU) per gram tissue) in the spleen and liver of wild-type C57BL/6JRj mice infected subcutaneously for 2 days with 1 x 10^4 *F. novicida* U112 *iglA-sfGFP* wild-type, *ΔpdpB* or *ΔclpB.* Each symbol represents an individual mouse (n = 8 (wild-type), 10 (*ΔpdpB)*, 15 (*ΔclpB*) (spleen), or n = 13 (wild-type), 10 (*ΔpdpB),* 15 (*ΔclpB*) (liver)); small horizontal lines indicate the mean. Data are pooled from two independent experiments. ****$P < 0.0001$; NS - not significant (Mann-Whitney test).

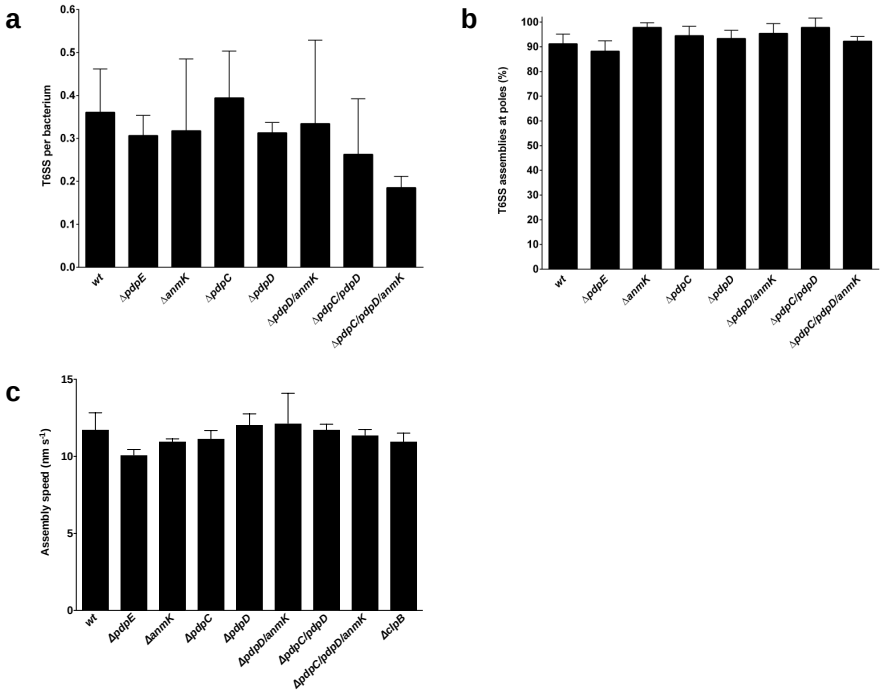

Supplementary Figure 4: *pdpE*, *anmK*, *pdpC* and *pdpD* and play no role in T6SS sheath localization and dynamics. (a) Quantification of number of T6SS sheath structures per bacterium within 5 min of imaging. **(b)** Quantification of T6SS sheath assembly at poles. **(c)** Quantification of T6SS assembly speed. Averages of three independent experiments. 30 bacteria per experiment were analyzed. Error bars represent standard deviation. No significant differences to wild-type (two-tailed unpaired *t*-test with Welch's correction).

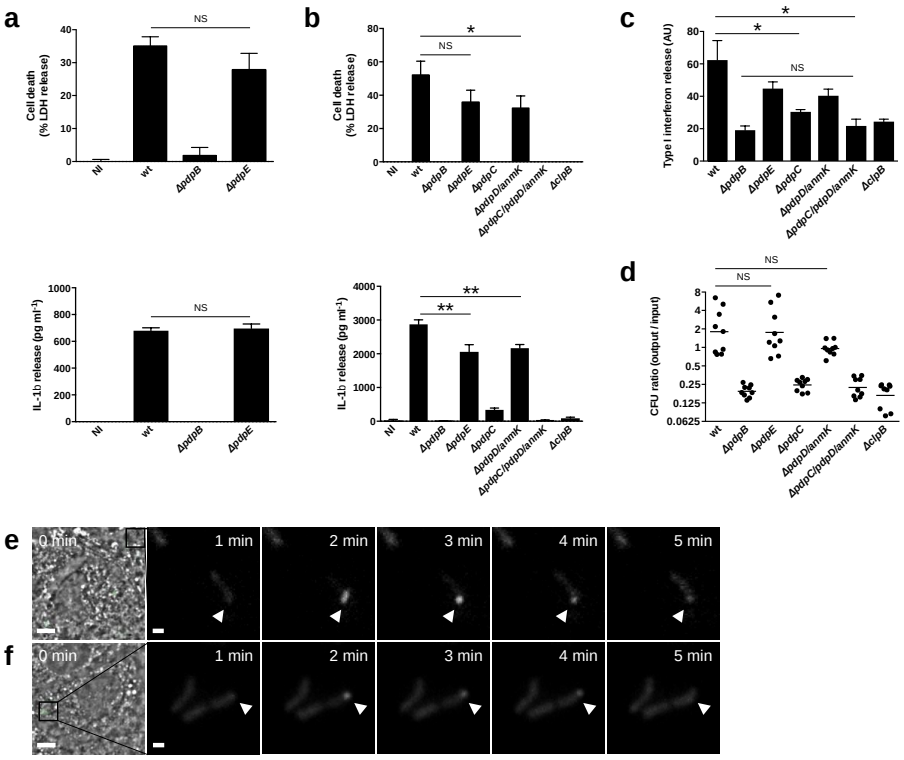

Supplementary Figure S5: Putative effector mutants show distinct innate immune activation and survival within macrophages. Release of LDH and IL-1β from **(a)** LPS-primed wild-type BMDMs 10 h or **(b)** unprimed wild-type BMDMs 24 h after infection with *F. novicida* U112 *iglA-sfGFP* wild-type, *ΔpdpB, ΔpdpE, ΔpdpC, ΔpdpD, ΔpdpD/anmK, ΔpdpC/pdpD/anmK* or *ΔclpB* (NI - noninfected control). **(c)** Quantification of type-I-interferon release in the supernatant of unprimed wild-type BMDMs infected for 10 h with *F. novicida* U112 *iglA-sfGFP* wild-type, *ΔpdpB, ΔpdpE, ΔpdpC, ΔpdpD, ΔpdpD/anmK, ΔpdpC/pdpD/anmK* or *ΔclpB.* **(d)** Intracellular growth within *Asc*$^{-/-}$ BMDMs during the first 24 h of infection with *F. novicida* U112 *iglA-sfGFP* wild-type, *ΔpdpB, ΔpdpE, ΔpdpC, ΔpdpD/anmK, ΔpdpC/pdpD/anmK* or *ΔclpB.* Growth was calculated as ratio of number of bacteria at 24 h (output) divided by the number of bacteria at 2 h (input). **(f, e**) Timelapse images from BMDMs infected for 1 h with *F. novicida* U112 *iglA-sfGFP ΔpdpE* **(e)** and *ΔpdpC/pdpD/anmK* **(f)**. 30 x 30 µm fields of view are shown. First image consists of merged phase contrast channel and GFP channel. Scale bar represents 5 µm. The close ups show 5 x 5 µm. Scale bar represents 1 µm. Close ups consist of GFP channel. (a-d) Data are representatives of three independent experiments (a-c) (mean and standard deviation of triplicate wells are shown) or pooled from three independent experiments (small horizontal lines indicate the mean) (d). *$P < 0.05$ and **$P < 0.01$; NS - not significant (two-tailed unpaired *t*-test with Welch's correction).

Table S1: Strains used in this study, related to Material and Methods

Organism	Genotype	Plasmid	Relevant features	Source
Francisella novicida U112	*iglA-sfGFP*		Parental strain, C-terminal chromosomal fusion of *sfGFP* to *iglA*	(Clemens et al., 2015)
	iglA-sfGFP ΔpdpB		Deletion of *pdpB*	This study
	iglA-sfGFP ΔclpB		Deletion of *clpB*	This study
	iglA-sfGFP ΔclpB/pdpB		Deletion of *clpB* and *pdpB*	This study
	iglA-sfGFP clpB-mCherry2		C-terminal chromosomal fusion of *mCherry2* to *clpB*	This study
	iglA-sfGFP clpB-mCherry2 ΔpdpB		C-terminal chromosomal fusion of *mCherry2* to *clpB,* deletion of *pdpB*	This study
	clpB-mCherry2		C-terminal chromosomal fusion of *mCherry2* to *clpB*	This study
	iglA-sfGFP ΔiglF		Deletion of *iglF*	This study
	iglA-sfGFP ΔiglG		Deletion of *iglG*	This study
	iglA-sfGFP ΔiglI		Deletion of *iglI*	This study
	iglA-sfGFP ΔiglJ		Deletion of *iglJ*	This study
	iglA-sfGFP ΔpdpE		Deletion of *pdpE*	This study
	iglA-sfGFP ΔanmK		Deletion of *anmK*	This study
	iglA-sfGFP ΔpdpC		Deletion of *pdpC*	This study
	iglA-sfGFP ΔpdpD		Deletion of *pdpD*	This study
	iglA-sfGFP ΔpdpD/anmK		Deletion of *pdpD* and *anmK*	This study
	iglA-sfGFP ΔpdpC/pdpD		Deletion of *pdpC* and *pdpD*	This study
	iglA-sfGFP ΔpdpC/pdpD/anmK		Deletion of *pdpC*, *pdpD* and *anmK*	This study

Table S2: Plasmids used to generate in-frame deletions in this study, related to Material and Methods.

Plasmid Name	Peptide scar left on the chromosome after allelic exchange	Primers used to generate in-frame deletion	
pDMK3-Δ*pdpB*	MNFIQKQGEVNVQ*	dFTN_1310_Del1_Xho1.FOR	TCAGTACTCGAGCAACTATATGAAAACTTACATAATT
		dFTN_1310_Del1.REV	CTCCTTGTTTTTGAATAAAATTCATACTTTTAATTT
		dFTN_1310_Del2_.FOR	ATGAATTTTATTCAAAAACAAGGAGAAGTTAATGT
		dFTN_1310_Del2.REV	ATAATAGCGGCCGCTTAGCAGAGCTTTTTATATT
		dFTN_1310_Det_FOR	ACATCAAGAAATACTCTGCCCTTC
		dFTN_1310_Det_REV	TATTATTATCCAACCATTGTTGCTG
pDMK3-Δ*clpB*	MNINKFTIKLANNNITFSK*	dFTN_1743_1_Spe1.FOR	TCAGTAACTAGTAGATAAATGCGACTATTGATG
		dFTN_1743_1.REV	TAATATTGTTATTAGCTAGTTTTATTGTAAATTTATTTATATTCATTATTT
		dFTN_1743_2.FOR	ATTTACAATAAAACTAGCTAATAACAATATTACATTCTCTAAA
		dFTN_1743_2_Sac1.REV	TCAGTAGAGCTCTCTTTTGTCATTGCAAAAGA
		dFTN_1743_Det.FOR	CAAGAATTCCATCAACCCAGA
		FTN_1743-mCherry_Det_REV	CCATCAAACTTAACAAAAGCTCCT
pDMK3-*clpB-mCherry2*		FTN_1743-mcherry1_Spe1.FOR	TCAGTAACTAGTGGTGTCGGTAAAACTGA
		FTN_1743-mcherry1.REV	CGGCCGCTTTAGAGAATGTAATATTGTTATTAGCG
		FTN_1743-mcherry2.FOR	CTCTAAAGCGGCCGCAGGA
		FTN_1743-mcherry2.REV	ATTAAACCGATTTTACTTGTACAGCTCGTC
		FTN_1743-mcherry3.FOR	CTGTACAAGTAAAATCGGTTTAATCAATATCTAAATTAT
		FTN_1743-mcherry3_Sac1.REV	TCAGTAGAGCTCGCTTTATAAGTTAGATTAATAGAGTTTG
		FTN_1743-mcherry_Det_FOR	GATGGAAGGCGAAAAAGACA
		FTN_1743-mcherry_Det_REV	CCATCAAACTTAACAAAAGCTCCT
pDMK3-Δ*iglF*	MNNDIDKWFESKQEAYWKI*	dFTN_1313_1_Spe1.FOR	TCAGTAACTAGTTTTCTCAAAGAATATATGATGATAATG
		dFTN_1313_1.REV	TTGCTTGCTTTCAAACCATTTATCAATATCATTATT
		dFTN_1313_2.FOR	TGGTTTGAAAGCAAGCAAGAAGC
		dFTN_1313_2_Sac1.REV	TCAGTAGAGCTCTATTTCTAATAAGCATGATTTA GGAA
		dFTN1313_Det.FOR	CTGGGTAATCAAGCACAAAGGT
		dFTN1313_Det.REV	GTGGCAAAGCTAGGATCTTCT
pDMK3-Δ*iglG*	MLNIINDSLKGGQINVKTS*	dFTN_1314_1_Xho1.FOR	TCAGTACTCGAGATAAAAAATCAACTCTACAAAAACC
		dFTN_1314_1.REV	TTTGTCCACCTTTTAAGGAGTCATTTATAATATTTAACATT
		dFTN_1314_2.FOR	CTCCTTAAAAGGTGGACAAATAAATGTAAA
		dFTN_1314_2_Not1.REV	TCAGTAGCGGCCGCTAATTTTTCGTCATTATAGTTTTCAG
		dFTN_1314_Det.FOR	TTTCGCTAACGTCACTACAAGC
		dFTN_1314_Det.REV	TCATCGAAGCAAATGAGGTG

pDMK3-Δ*iglI*	MSQIISTLNNDSVE KISNEIDEDYFEDL FDI*	dFTN_1317_1_Xho1.FOR	TCAGTACTCGAGAAATTTATAAATCAAAACACCTTTAGC
		dFTN_1317_1.REV	TTCTACCGAATCATTATTTAGTGTAGATATTATCTGACT
		dFTN_1317_2.FOR	ACACTAAATAATGATTCGGTAGAAAAAATTT
		dFTN_1317_2_NotI.REV	TCAGTAGCGGCCGCATTTCAAGTTCTATCTTAAATGGG
		dFTN_1317_Det.FOR	ATCGCAGCACACAATCTTTAAA
		dFTN_1317_Det.REV	TCAGATAGTGATTCGGATTTTTCA
pDMK3-Δ*iglJ*	MKTILKIFLTYKQQI YLGYFNL*	dFTN_1318_1_Xho1.FOR	TCAGTACTCGAGATAACATAGATTCTATTATAGAAATTGTACA
		dFTN_1318_1.REV	CCTAGATATATCTGTTGTTTATATGTCAAAAAGATCTTCAAA
		dFTN_1318_2.FOR	GATCTTTTTGACACAGATATATCTAGGTTATTTTAATTTATG
		dFTN_1318_2_NotI.REV	TCAGTAGCGGCCGCATCATTTGCGCTTATTTCAA
		dFTN_1318_Det.For	CGCAAATGCAGAATCAAGAA
		dFTN_1318_Det.Rev	CGACTAGCGCGTCTAAAAATG
pDMK3-Δ*pdpE*	MSKKVFQLLLHYE KKITII*	dFTN_1320_1_Xho1.FOR	TCAGTACTCGAGACCAACAGAAGAAAACTTTG
		dFTN_1320_1.REV	ATTTTCTTTTCATAATGTAATAATAATTGAAATACTTTTTTACTCATATT
		dFTN_1320_2.FOR	ATTTCAATTATTATTACATTATGAAAAGAAAATTACTATAATATAAC
		dFTN_1320_2_Not1.REV	TCAGTAGCGGCCGCGGTGATATTTTTGTAAAACTTAATAGG
		dFTN_1320_Det.FOR	GGGTTGGGCTATCACATCAA
		dFTN_1320_Det.REV	GTTGAAAGTTTGCAGACAGGTC
pDMK3-Δ*anmK*	LSEYKYCVGIIPSA TGAKSRVILGQINF F*	dFTN_1326_1_Xho1.FOR	TCAGTACTCGAGCTTAGGTATAATGGAATAAATGATTTAAC
		dFTN_1326_1.REV	GTGTAGGAATCATACCATCTGCAACCG
		dFTN_13125-26_2.FOR	CTATACTTTCTGATTCCTACACAATATTTATATTCAC
		dFTN_1325-26_2_Sac1.REV	TCAGTAGAGCTCGTGTATCTGCTAAAAAATTAGAGT
		dFTN_1326_Det.For	GCCGATGAAGCTTTACCACT
		dFTN_1325-26_Det.REV	TGCCTGCAGTAATATTCAAAGC
pDMK3-Δ*pdpC*	MNDKYELNIYSDF FKKISS*	dFTN_1319_1_Xho1.FOR	TCAGTACTCGAGCTAAATAACTTTGTGAGCCTTC
		dFTN_1319_1.REV	TTTAAAAAAGTCTGAATAGATATTTAGTTCATATTTGTCG
		dFTN_1319_2.FOR	GAACTAAATATCTATTCAGACTTTTTTAAAAAAATATCGTC
		dFTN_1319_2_Not1.REV	TCAGTAGCGGCCGCTGATAATATCGATGCAATATATGAAA
		dFTN_1319_Det.For	CCAGAATGATTCGGTAGAAAAA
		dFTN_1319_Det.Rev	AAAGGAAAGCAACAGCTCCA
pDMK3-Δ*pdpD*	MDQDINDLLYDTD DLKKEKVRKYRP MIWV*	dFTN_1325_1_Xho1.FOR	TCAGTACTCGAGCACTATCAACTTCTGTAGATCC
		dFTN_1325-26_1.REV	TGTGTAGGAATCAGAAAGTATAGACCAATGATC
		dFTN_13125.FOR	GTCTATACTTTCTTACTTTTTCTTTTTTGAGGTCA
		dFTN_1325_2_Not1.REV	TCAGTAGCGGCCGCCTAAAAATGCAAATATTGATGATATTTATG
		dFTN_1325-26_Det.FOR	GCACCTTTAGCCATTCTTGCT
		dFTN_1325_Det.Rev	AGGAGATATCGCTGCTGGAG

pDMK3-Δ*pdpD/anmK*	LSEYKYCVGIRKY RPMIWV*	dFTN_1325-26_1_Spe1.FOR	TCAGTAACTAGTCACTATCAACTTCTGTAGATCC
		dFTN_1325-26_1.REV	TGTGTAGGAATCAGAAAGTATAGACCAATGATC
		dFTN_13125-26_2.FOR	CTATACTTTCTGATTCCTACACAATATTTATATTCAC
		dFTN_1325-26_2_Sac1.REV	TCAGTAGAGCTCGTGTATCTGCTAAAAAATTAGAGT
		dFTN_1325-26_Det.FOR	GCACCTTTAGCCATTCTTGCT
		dFTN_1325-26_Det.REV	TGCCTGCAGTAATATTCAAAGC

2.1 Additional results related to research article II

Introduction

After macrophage phagocytosis, *Francisella* rapidly ruptures the phagosome to survive and replicate within the cytosol (chapter I, section 2.2). Although we showed that *Francisella* uses the FPI-encoded T6SS to rupture the phagosome (chapter III, section 2), it remains unclear what signal causes *Francisella* to activate the T6SS and thus induce phagosomal rupture. Two independent research groups reported that *Francisella* escape from the phagosome by sensing phagosomal acidification [429,430]. However in 2009, another research group found that phagosomal acidification has no impact on *Francisella* escape from the phagosome [431]. Given the conflicting reports in current literature, it remains unclear whether or not phagosomal acidification is the trigger to activate the T6SS, and therefore escape from the phagosome. This work sought to address the role of phagosomal acidification in the *Francisella* escape from the phagosome. *Francisella* escape from the phagosome is the critical point for *Francisella* in establishing a successful bacterial infection and therefore for its virulence. Furthermore, determining if phagosomal acidification triggers T6SS activity is important, since understanding the mechanism of T6SS activation could be a promising starting point for the development of a successful antibacterial drug.

Material and Methods

Cell culture and infection. Primary murine bone marrow derived macrophages (BMDMs) were seeded into 24- or 96-well plates at a density of 1.5 x 10^5 or 5 x 10^4 cells per well and infected with wild-type *Francisella novicida* U112 at a multiplicity of infection of 100 as previously described (chapter III, section 2) or transfected with 0.5 μg poly(dA:dT) (Invivogen) using our home-made PEI transfection reagent. Unless otherwise indicated, BMDMs were pre-treated 30 min prior to infection with 100 nM bafilomycin A1 (BafA1; Sigma). The concentration of BafA1 was kept constant over the entire course of infection.

Cytokine and LDH release measurement. IL-1β was measured by enzyme-linked immunosorbent assay (eBioscience). Lactate dehydrogenase (LDH) was measured with an LDH Cytotoxicity Detection Kit (Takara). To correct for spontaneous cell lysis and to normalize the values, the percentage of LDH release was calculated as follows:
(LDH infected - LDH uninfected) / (LDH total lysis - LDH uninfected) x 100.

Phagosome protection assay. BMDMs were seeded into 24-well plates at a density of 1.5 x 10^5 cells per well and infected with wild-type *Francisella novicida* U112 at a multiplicity of infection of 100, as previously described (chapter III, section 2). BMDMs were pretreated for 30 min with 100 nM BafA1 (Sigma) and

the concentration was kept constant over the entire course of infection.

Poly(dA:dT) electroporation. BMDMs were prestimulated for 4 h with lipopolysaccharide (from *Escherichia coli* strain O111:B4;InvivoGen) and 30 min with 100 nM BafA1. BMDMs were washed three times with warm 1x phosphate buffered saline (PBS) and 0.25 x 10^6 cells per reaction were electroporated with 0.25 μg poly(dA:dT) using the Neon transfection system (Invitrogen). 5 x 10^4 cells were seeded per well of a 96-well plate and LDH as well as IL-1β release assessed 3 h post electroporation as described above.

Results

To investigate the role of phagosomal acidification in *Francisella* escape from the phagosome, we analyzed the amount of cytosolic wild-type *Francisella novicida* U112 (hereafter *F. novicida*) in wild-type BMDMs left untreated or pretreated with 100 nM Bafilomycin A1 (BafA1), a vacuolar specific potassium ATPase inhibitor. After 4 h of infection, on average 50 % of *F. novicida* escaped into the cytosol (Figure III.1 a). Following Bafilomycin A1 treatment, a significant reduction in the number of cytosolic bacteria was observed, resulting in 30 % cytosolic bacteria. These data suggest that phagosomal acidification is partially required for *Francisella* to escape from the phagosome.

After escaping into the cytosol, *Francisella* activates two distinct innate immune pathways by releasing bacterial DNA into the cytosol. Bacterial DNA can be detected by cGAS leading to type-I-interferon production via STING-TBK1-IRF3 [169, 170] or by AIM2 leading to the formation of the AIM2 inflammasome [162–164]. AIM2 inflammasome activation is critical for the immune system for *Francisella* clearance. In cell culture experiments, inflammasome activation is analyzed by LDH and IL-1β release to the supernatant. When we assessed AIM2 inflammasome activation in BMDMs after *F. novicida* infection, BafA1 pretreatment completely abolished LDH as well as IL-1β release up to 12 hours post-infection; however, both measures increased over the course of infection in untreated BMDMs (Figure III.1 b). As we pretreated the BMDMs with BafA1 before infection, we could not determine if phagosomal acidification is critical to escape from the phagosome or to activate the AIM2 inflammasome. To analyze at which level of the infection BafA1 is influencing AIM2 inflammasome activation, we applied BafA1 at different time points after *Francisella* infection and analyzed cell death and IL-1β release at 10 hours post-infection. While applying BafA1 during the first 2 hours of infection abolished AIM2 inflammasome activation, applying BafA1 later than 2 hours post infection had no significant impact on AIM2 inflammasome activation (Figure III.1 c). We observed a similar phenomenon when we transfected BMDMs with the DNA analog poly(dA:dT) (Figure III.1 d) suggesting that BafA1 could directly impact AIM2 inflammasome activation or assembly. On the other hand, BafA1 might interfere with the delivery of DNA into

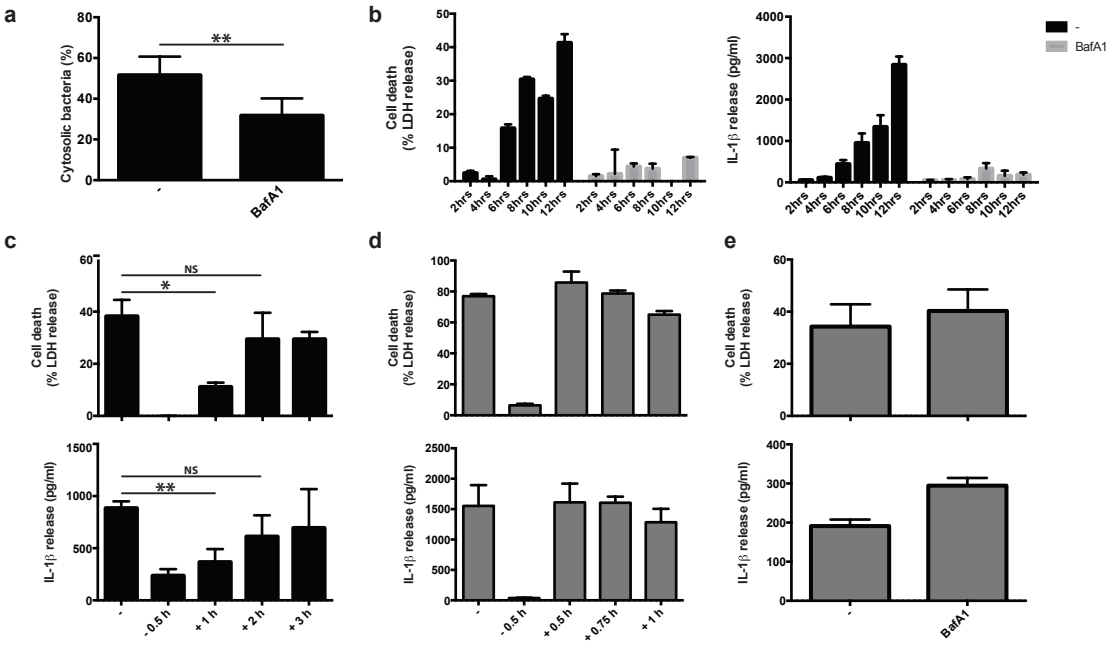

Figure III.1 BafA1 blocks AIM2 inflammasome activation in a type-I-interferon-dependent manner. (**a**) Quantification of cytosolic bacteria in unprimed wild-type primary murine bone marrow derived macrophages (BMDMs) 4 h after infection with wild-type *F. novicida* U112. (**b**) Release of LDH and IL-1β from primed wild-type BMDMs at indicated time points after wild-type *F. novicida* U112 infection pre-treated or not for 30 min with 100 nM Bafilomycin A1 (BafA1) (**c**) Release of LDH and IL-1β from primed wild-type BMDMs 10 h after infection with wild-type *F. novicida* U112 treated at indicated time points with 100 nM BafA1. (**d**) Release of LDH and IL-1β from primed wild-type BMDMs 3 h after transfection of 0.5 μg poly(dA:dT) treated at indicated time points with 100 nM BafA1. (**e**) Release of LDH and IL-1β from 30 min 100 nM BafA1 pre-treated, primed wild-type BMDMs 3 h after electroporation of 0.25 μg poly(dA:dT). Data are pooled from two experiments (a) or are representatives of two independent experiments (b-e) (mean and standard deviation of triplicate wells). $^*P < 0.05$ and $^{**}P < 0.01$; NS, not significant (two-tailed unpaired t-test with Welch's correction).

the cytosol, since the transfection reagents require endosomal acidification. We thus electroporated poly(dA:dT) into BMDMs and thereby directly activated the AIM2 inflammasome without need for transfection. Importantly, AIM2 activation by electroporated poly(dA:dT) was unaffected by BafA1 pretreatment (Figure III.1 e). These data suggest that phagosomal acidification is specifically required during *Francisella* infection and poly(dA:dT) transfection to activate the AIM2 inflammasome, but does not impact AIM2 inflammasome activation or assembly.

Discussion

This work established that phagosomal acidification partially blocks *Francisella* escape into the cytosol, but completely blocks *F. novicida*-dependent AIM2 inflammasome activation. The AIM2 inflammasome is only impaired if phagosomal acidification is blocked during the first 2 hours of *Francisella* infection and BafA1 treatment does not impair directly AIM2 inflammasome activation or assembly. Most likely, phagosomal acidification renders F. novicida competent to activate the AIM2 inflammasome while the bacteria still reside in the phagosome. If this relates however directly to AIM2 activation or rather is linked to the propensity to activate type-I-interferon signaling, has not been assessed in this study.

A prerequisite for efficient AIM2 inflammasome activation is the induction of type I interferon through cGAS/STING and the consequent expression of interferon regulated genes (IRGs) (chapter I, section 2.2). Among them are GBP2 and GBP5, which lyse *Francisella* and expose thereby bacterial DNA to AIM2 [458, 463]. Interestingly, cGAS also recognizes bacterial DNA to trigger type-I-interferon induction [169, 170]. One can speculate that phagosomal acidification specifically exposes bacterial DNA only recognized by cGAS but not AIM2 to the cytosol. If this DNA could also be detected by AIM2, inflammasome activation would start as soon as DNA is exposed to the cytosol, as the essential inflammasome components AIM2, ASC and caspase-1 are constitutively expressed in macrophages. However, this is not what we observe in *Francisella* infection [249]. In line with the hypothesis of acidification-dependent DNA exposure, Alnemri and colleagues observed no type-I-interferon induction in macrophages pretreated with BafA1 [302], suggesting that the initial exposure of *Francisella* to phagosomal acidification primes for cGAS-dependent type-I-interferon induction.

What explicit impact phagosomal acidification has on *Francisella* requires further investigation and could help to understand and discriminate the target specificity of cGAS and AIM2, two important receptors to detect foreign DNA in the cytosol.

3 Research article III

Detecting release of bacterial dsDNA into the host cytosol using fluorescence microscopy

R. F. Dreier, J. C. Santos and P. Broz.

Manuscript under revision. *Springer*.

Statement of contribution
I performed the *Francisella* infection of primary murine bone marrow-derived macrophages, the immunofluorescence staining and the confocal microscopy analysis. Finally, I wrote the manuscript together with José Carlos Santos and Petr Broz.

Detecting release of bacterial dsDNA into the host cytosol using fluorescence microscopy

Roland Felix Dreier[#], José Carlos Santos[#] and Petr Broz

Focal Area Infection Biology, Biozentrum, University of Basel, Basel, Switzerland

[#] equal contribution

Contact: petr.broz@unibas.ch

Running Head: Detection of bacterial DNA in the macrophage cytosol.

Abstract

Recognition of pathogens by the innate immune system relies on germline-encoded pattern recognition receptors (PRRs) that recognize unique microbial molecules, so-called pathogen-associated molecular patterns (PAMPs). Nucleic acids and their derivatives are one of the most important groups of PAMPs, and are recognized by a number of surface-associated as well as cytosolic PRRs. Cyclic GMP-AMP synthase (cGAS) recognizes the presence of pathogen- or host-derived dsDNA in the cytosol and initiates type-I-IFN production. Here, we describe a methodology that allows for evaluating the association of cGAS with released bacterial dsDNA during *Francisella novicida* infection of macrophages, by fluorescence confocal microscopy. This method can be adapted to the study of cGAS-dependent responses elicited by other intracellular bacterial pathogens and in other cell types.

Key words: cGAS; dsDNA; *F. novicida*; innate immunity; fluorescence confocal microscopy.

1. Introduction

Microbial pathogens, including viruses, parasites and bacteria, constantly challenge eukaryotic organisms, which have thus evolved mechanisms of defense, collectively called immunity. The first line of host defense against invading microbes is the innate immune system, which has diverse germline-encoded pattern recognition receptors (PRRs) that detect conserved pathogen-associated molecular patterns (PAMPs), allowing microbe

phagocytosis and induction of inflammation ***(1)***. In the cell, PRRs can have different subcellular locations, thus allowing a more precise and regulated detection of PAMPs. For example, PRRs located on the plasma membrane or on endosomal membranes, such as Toll-like receptors (TLRs), typically recognize extracellular PAMPs. On the other hand, cytosolic PRRs, including NOD-like receptors (NLRs), RIG-I-like receptors and a group of diverse DNA sensors, allow the detection of intracellular PAMPs ***(1-3)***, thus triggering different antimicrobial responses such as autophagy ***(4)***, production of type-I interferons (IFNs) ***(5)*** or assembly of cytosolic multiprotein complexes called inflammasomes ***(6)***.

Different host sensors can recognize DNA that is released by invading microbes into the host cytosol. This group of PRRs is crucial for mounting an innate immune response, but to date this response remains poorly characterized. Examples of cytosolic double stranded (ds) DNA sensors include IFNγ-inducible protein 16 (IFI16), absent in melanoma 2 (AIM2) and cyclic GMP-AMP synthase (cGAS) ***(7-9)***. Here, we focus on the mechanisms of cGAS detection of cytosolic dsDNA and the downstream events. cGAS is an enzyme that directly binds dsDNA and catalyzes the production of the second messenger cyclic GMP-AMP (cGAMP) from ATP and GTP ***(8, 10)***. cGAMP then binds to and activates the ER-resident adaptor protein STING, which in turn recruits and activates TBK1 and the transcription factor IRF3 by phosphorylation ***(8, 10, 11)***. IRF3 then dimerizes and translocates into the nucleus to induce the production of type-I IFNs, which signal in an autocrine and paracrine manner through the IFN-α/β receptor (IFNAR), inducing over

300 IFN-stimulated genes that are involved in modulating immune responses against microbial infections ***(12, 13)***.

Francisella tularensis subspecies (subsp.) *tularensis* is an intracellular gram-negative bacterial pathogen that causes tularemia, a life-threatening zoonotic disease that can affect humans leading to severe morbidity and mortality ***(14)***. Interestingly, the closely related *Francisella tularensis* subsp. *novicida* (*F. novicida*) is an exciting model organism to study host cytosolic immune responses triggered by DNA. In the mammalian host, *F. novicida's* main intracellular niche is the macrophage, which phagocytoses the bacteria into a phagosomal compartment, called the *Francisella*-containing phagosome (FCP). Rupture of the FCP membrane occurs rapidly, generally within 1-4 hours upon bacterial uptake, leading to bacterial escape into the host cytosol, where *F. novicida* undergoes extensive replication ***(15-18)***. The exact mechanism of FCP membrane rupture with consequent bacterial escape into the host cytosol is unknown, but it requires the expression of the *Francisella* pathogenicity island (FPI), a cluster of genes encoding a type VI secretion system (T6SS) ***(19, 20)***. Even though *F. novicida* escape from the FCP into the host cytosol is essential for bacterial pathogenesis, it also allows cytosolic innate immune recognition and initiation of host defense mechanisms. In parallel with FCP rupture, *F. novicida* lysis can occur, in a yet unknown mechanism, resulting in release of bacterial dsDNA into the macrophage cytosol, which functions as a danger signal that triggers innate immunity ***(21, 22)***. *F. novicida* dsDNA released into the host cytosol is recognized by cGAS, thus triggering STING-mediated production of type-I IFNs ***(22)***. Then, autocrine and paracrine type-I IFN signaling induce

production of AIM2, which contributes to the assembly and activation of the AIM2 inflammasome around released bacterial dsDNA ***(23)*** to activate caspase-1-mediated cell death and secretion of IL-1 family proinflammatory cytokines.

The cGAS-STING-dependent pathway also plays an important role in immune responses elicited by other intracellular bacterial pathogens. Escape of *Listeria monocytogenes* from its endocytic vacuole to the host cytosol leads to the detection of bacterial dsDNA by cGAS, triggering type-I IFN production in myeloid cells ***(24)***, which is thought to promote bacteria dissemination and proliferation ***(12)***. Moreover, recent studies have shown that *Mycobacterium tuberculosis* releases its genomic DNA into the cytosol of macrophages, which associates with cGAS, thus eliciting anti-mycobacterial immunity ***(25-27)***.

Collectively, these studies highlight the importance of cytosolic dsDNA recognition during bacterial infection, which is most likely initiated in a cGAS-dependent manner. Therefore, it is important to have methods to track when and where cGAS associates with bacterial dsDNA within the host cell, to better understand how this danger signal initiates an innate immune response. Here, we describe a methodology that allows evaluation of the association of cGAS with bacterial dsDNA released during *F. novicida* infection of macrophages, by fluorescence confocal microscopy. In addition, this method can be applied to the study of cGAS-dependent responses elicited by other intracellular bacterial pathogens and in other cell types.

2. Materials

2.1 Generation of murine bone marrow-derived macrophages (BMDMs).

1. Cell culture facility and equipment including water-jacketed CO_2 incubator and laminar flow hood.
2. Mice.
3. CO_2 tank including flow regulation.
4. Ice bucket.
5. Ice.
6. 70% ethanol.
7. Flushing medium: Dulbecco's Modified Eagle Medium (DMEM) high glucose, unsupplemented.
8. 20% Macrophage medium: DMEM high glucose with 20% Macrophage-Colony Stimulating Factor (M-CSF), 10% Fetal Calf Serum (FCS), 1x Non-Essential Amino Acids (NEAA), 1x Hepes and 100 units/mL Pen/Strep.
9. Sterile 50 mL tubes.
10. Sterile 2, 5, 10 and 25 mL pipettes.
11. 10 mL syringes.
12. 26 G 3/8 inch needles.
13. 1000 µL pipette.
14. Autoclaved scissors and forceps.
15. Paper towels.
16. Centrifuge with a rotor fitting 50 mL tubes.
17. Hemocytometer.
18. Inverted light microscope.

19. Sterile, non-tissue culture treated 10 cm petri dishes.
20. Ice-cold 1x phosphate-buffered saline (PBS), tissue culture grade.
21. Cell scrapers.
22. Ice-cold FCS.
23. Dimethyl sulfoxide (DMSO), tissue culture grade.
24. 2 mL cryotubes.
25. Isopropanol freezing chamber.

2.2 Thawing and propagation of murine bone marrow-derived macrophages (BMDMs).

1. Cell culture facility and equipment including water-jacketed CO_2 incubator and laminar flow hood.
2. Fridge.
3. Cryotube containing $1x10^7$ frozen murine BMDMs in 10 % DMSO / FCS.
4. 37°C water bath.
5. Sterile 50 mL tube.
6. 1000 µL pipette.
7. Sterile 2, 5, 10 and 25 mL pipettes.
8. Centrifuge with a rotor fitting 50 mL tubes.
9. Sterile, non-tissue culture treated 10 cm petri dishes.
10. Inverted light microscope.
11. Ice-cold 1x PBS, tissue culture grade.
12. Flushing medium: DMEM high glucose, unsupplemented.

13. 20% macrophage medium: DMEM high glucose with 20% M-CSF, 10% FCS, 1x NEAA, 1x Hepes and 100 units/mL Pen/Strep.

2.3 Harvesting and seeding BMDMs for *F. novicida* infection

1. Cell culture facility and equipment including water-jacketed CO_2 incubator and laminar flow hood.
2. Fridge.
3. Ice bucket.
4. Ice.
5. Sterile 50 mL tube.
6. Sterile 1.5 mL tubes.
7. Sterile 2, 5, 10 and 25 mL pipettes.
8. Centrifuge with a rotor fitting 50 mL tubes.
9. Hemocytometer.
10. Inverted light microscope.
11. Sterile tissue culture treated 24-well plates.
12. Sterile glass coverslips.
13. Ice-cold 1x PBS, tissue culture grade.
14. 10 % macrophage medium: DMEM high glucose with 10% M-CSF, 10% FCS, 1x NEAA and 1x Hepes.
15. Sterile, non-tissue culture treated 10 cm petri dishes.
16. Brain Heart Infusion (BHI) broth.
17. 10% L-cysteine stock solution in ddH_2O.
18. Ampicillin stock (100 mg/mL).
19. *F. novicida* frozen glycerol stocks.

20. BHI agar plates supplemented with 0.2% L-cysteine and 100 µg/mL Ampicillin.
21. Sterile bacterial culture tubes.
22. Bacterial incubator with rotor.

2.4 Infection of murine BMDMs with *F. novicida*

1. Cell culture facility and equipment including water-jacketed CO_2 incubator and laminar flow hood.
2. Spectrophotometer.
3. Plastic cuvettes.
4. 15 mL tubes.
5. BHI broth.
6. 10% macrophage medium: DMEM high glucose with 10% M-CSF, 10% FCS, 1x NEAA and 1x Hepes.
7. Gentamicin liquid stock (5000 µg/mL).
8. Centrifuge with swing-out buckets suitable for 24-well plates.

2.5 Fixation and staining of *F. novicida*-infected murine BMDMs

1. Cell culture facility and equipment including water-jacketed CO_2 incubator and laminar flow hood.
2. 4% Paraformaldehyde (PFA) diluted in 1x PBS.
3. 1x PBS, tissue culture grade.
4. Immunofluorescence (IF) buffer: 3% BSA, 0.1% azide, 0.2% Saponin in 1x PBS.
5. Forceps.

6. Paper towels.
7. Primary antibodies for cGAS [goat anti-cGAS (N-17), Santa Cruz sc-245858], *F. novicida* [chicken anti-*F. novicida*, Denise M. Monack laboratory]
8. Fluorophore-coupled secondary antibodies [donkey anti-goat Alexa-Fluor 488, goat anti-chicken Alexa-Fluor 568 (Molecular Probes)].
9. Hoechst.
10. Alexa-Fluor 647 Phalloidin (Molecular Probes).
11. Humidified chamber: non-tissue culture treated 15 cm petri dish, parafilm, paper towel, aluminium foil.
12. Mounting solution: Vecta Shield.
13. Microscopy glass slide.
14. 70% ethanol.
15. Transparent nail polish.
16. Confocal fluorescence microscope.

3. Methods

3.1 Generation of BMDMs

1. Fill one ice bucket with ice and place it next to the laminar flow hood.
2. Fill two 50 mL tubes with 70% Ethanol ethanol and place them under the laminar flow hood.
3. Put two forceps and one pair of scissors in each 50 mL tube and label one tube with “outer tools” and the other with “inner tools” (*see* **Note 1**). The separate use of exterior and interior surgical tools reduces potential contamination.
4. Fill one 50 mL tube with 5 mL, one with 25 mL and one with 50 mL flushing medium. Put the three 50 mL tubes on ice.
5. Place paper towel under the laminar flow hood to prepare the working space.
6. Euthanize the mice with CO_2 directly in their cage (*see* **Note 2**). Thereby minimizing stress applied to the mice as they stay in their known environment. Always observe the mice during euthanasia. Once the mice stop breathing, wait another 30 sec before you stop the CO_2 supply.
7. Take the mice out of the cage, place them under the laminar flow hood and spray them with 70% ethanol.
8. Make a small incision into the sternum above the pneumothorax. Thereby the pressure in the pneumothorax drops and the lungs collapse. This is one method to confirm euthanasia.
9. Transfer one mouse onto a new paper towel under the laminar flow hood.

10. **Start with the outer tools**. Hold one hind leg with one forceps and make a small incision underneath the ankle. Make sure to only cut the skin but not the flesh.
11. Starting form this incision, cut the skin from the ankle to the belly.
12. Still holding the foot with the forceps, extend the small incision fully around the ankle. Now, pull the skin upward over the foot and downward over the leg until the whole leg and the lower part of the body is exposed.
13. Spray the exposed leg with 70% ethanol to remove hair and disinfect the area.
14. Using scissors cut the anterior and posterior thigh muscles diagonal to the femur to gain clear access to the hipbone. Next, cut the hipbone to separate the leg from the body. Be careful not to cut the femur at this step.
15. Remove the entire leg, cut off the foot below the ankle, place the leg in a 50 mL tube filled with 25 mL flushing medium and put it back on ice.
16. Repeat the procedure for the other leg and if necessary for the other mice that are already euthanized.
17. Take out one of the legs from the 50 mL tube.
18. **Switch to inner tools**. Using scissors and forceps, remove the flesh around femur and tibia of each leg until the bones are exposed.
19. Separate femur and tibia by over bending the knee, and store them in a non-tissue culture treated 10 cm dish. Add a few drops of flushing medium on the bones to prevent them from drying out.
20. Repeat the procedure for the other legs.

21. To flush out the bone marrow, cut the femur/tibia on both ends. The bone marrow cavity with the bright red bone marrow should now be accessible.
22. Fill the 10 mL syringe with flushing medium, add the 26 G 3/8 inch needle and carefully insert the needle into the bone marrow cavity. Flush out the bone marrow from both sides of the bone into the 50 mL tube containing 5 mL flushing medium. The bone should now be white/transparent and no bone marrow should be visible anymore (The likelihood of contamination can be reduced by flushing each individual bone into a separate 50 mL tube and process each tube individually).
23. Repeat the procedure for the other bones.
24. Centrifuge the bone marrow for 5 min at 180 x g at 4°C, remove the supernatant and resuspend the bone marrow in 1 mL 20% macrophage medium using a 1000 µL pipette.
25. Add an additional 9 mL of 20% macrophage medium slowly and mix by swirling the tube (if only one mouse was processed, only add an additional 4 mL of 20% macrophage medium).
26. Count the progenitor cells under the microscope using a hemocytometer and determine the total number of progenitor cells in the suspension.
27. Plate 5 x 10^6 progenitor cells per non-treated 10 cm petri dish, add 10 mL of 20% macrophage medium and move all plates into the incubator set to 37°C / 5% CO_2.
28. After 3 days, add an additional 4 mL pre-warmed 20% macrophage medium to each non-cell culture treated 10 cm petri dish and move

them back to the incubator for another 3 days. This step ensures that the cells have enough MCSF to fully differentiate (*see* **Note 3**).

29. After 6 days, all progenitor cells should have been fully differentiated into BMDMs and are now adherent. Aspirate the medium from each petri dish before adding 5 mL of ice-cold 1x tissue-culture grade PBS to each dish and move the dishes into the fridge for 15 min.
30. With a cell scraper, gently scrape off the BMDMs and transfer them into a 50 mL tube. Scrape up to 5 petri dishes and combine them into the same 50 mL tube.
31. Centrifuge the cells for 5 min at 180 x g at 4°C, remove the supernatant and resuspend the cell pellet in 1 mL flushing medium using a 1000 µL pipette. Gently pipette up and down five times to disrupt cell clumps and obtain a single cell suspension.
32. Add an additional 9 mL flushing medium while constantly swirling the tube, and count the cells again with a hemocytometer under the microscope.
33. Centrifuge the cells for 5 min at 180 x g at 4°C, remove the supernatant and resuspend the cell pellet in 1 mL ice-cold FCS using a 1000 µL pipette. Prepare a 10% DMSO solution in ice-cold FCS to reach a final cell concentration of 10^7 cells/mL.
34. Aliquot 1 mL of the final cell suspension into cryotubes and freeze the cells in a -80°C freezer using isopropanol freezing chambers.
35. After 3-4 days, transfer the cryotubes to liquid nitrogen for long-term storage.

3.2 Thawing and propagation of murine BMDMs

1. Obtain the required amount of tubes containing frozen BMDMs from liquid nitrogen storage. From one vial containing 1 x 10^7 BMDMs, it is possible to expand the cell number up to 3 x 10^7 BMDMs (the following protocol describes how to thaw one tube).
2. Quickly place the cryotube in a 37°C water bath just until the frozen liquid is entirely thawed. Move the tube to the laminar flow hood.
3. Transfer the BMDMs into a 50 mL tube using a 1 or 2 mL pipette.
4. Slowly add 9 mL of cold flushing medium drop-wise while swirling.
5. Centrifuge the BMDMs for 5 min at 180 x g at 4°C, remove the supernatant and resuspend the cell pellet in 1 mL cold 20% macrophage medium using a 1000 µL pipette. Gently pipette up and down five times to disrupt cell clumps and obtain a single cell suspension.
6. Slowly add 9 mL of cold 20% macrophage medium drop-wise while swirling.
7. Transfer the BMDMs to one non-tissue culture treated 10 cm petri dish and incubate them overnight in the incubator at 37°C / 5% CO_2.
8. Check the macrophages under the microscope. Most of the BMDMs should be adherent the next day.
9. Remove the medium and add 5 mL cold tissue-culture grade PBS. Incubate the BMDMs at 4°C for 15 min in the fridge.
10. Gently scrape off the BMDMs and transfer them to a 50 mL tube. Rinse the petri dish with an additional 5 mL of cold tissue-culture grade PBS and add it to the same 50 mL tube.

11. Repeat step 5 and 6 of section 3.2.
12. Prepare five non-tissue culture treated 10 cm petri dishes with 8 mL of cold 20% macrophage medium in each. Add 2 mL of BMDM suspension per petri dish, distribute the BMDMs equally by rotating the petri dish and incubate them for 4 days in the incubator at 37°C / 5% CO_2. The BMDMs are now ready to be seeded for an experiment as outlined in section 3.3.

3.3 Harvesting and seeding BMDMs for an infection with *F. novicida*

1. Transfer the all non-tissue culture treated 10 cm petri dishes containing BMDMs to the laminar flow hood.
2. Remove the medium and add 5 mL cold tissue-culture grade PBS to each petri dish. Incubate the BMDMs at 4°C for 15 min.
3. Gently scrape off the BMDMs and transfer them to a 50 mL tube. Rinse the petri dishes with an additional 5 mL cold tissue-culture grade PBS and add it to the same 50 mL tube.
4. Centrifuge the BMDMs for 5 min at 180 x g at 4°C, remove the supernatant and resuspend the cell pellet in 1 mL cold 10% macrophage medium using a 1000 µL pipette. Gently pipette up and down five times to disrupt cell clumps and obtain a single cell suspension.
5. Slowly add 9 mL cold 10% macrophage medium drop-wise while swirling.
6. Count the BMDMs under the microscope using a hemocytometer and determine the concentration of BMDMs per mL in the suspension.

7. Add one sterile glass coverslip to each well of a sterile tissue culture treated 24-well plate.
8. Seed 1.5 x 10^5 BMDMs per well in 1 mL 10% macrophage medium on top of each glass coverslip.
9. Leave the seeded 24-well plate for 10 min in the laminar flow hood. This allows the BMDMs to adhere and distribute more equally throughout the well.
10. Incubate the BMDMs overnight in the incubator at 37°C / 5% CO_2.
11. Start an overnight culture of *F. novicida:* Inoculate the bacteria from a BHI agar plate supplemented with 0.2% L-cysteine and 100 µg/mL Ampicillin into 2 mL BHI broth supplemented with 0.2% L-cysteine / 100 µg/mL Ampicillin. (*see* **Note 4**).
12. Incubate *F. novicida* containing culture overnight at 37°C with agitation.

3.4 Infection of murine BMDMs with *F. novicida*

1. Transfer the *F. novicida* overnight culture to the laminar flow hood.
2. Measure the OD_{600} of the *F. novicida* overnight culture with a spectrophotometer. As an approximation, an OD_{600} of 1 converts to 10^9 bacteria per mL.
3. Prepare a *F. novicida* dilution in warm 10% macrophage medium to reach a multiplicity of infection (MOI) of 100 bacteria per cell (MOI 100).
4. Transfer the seeded 24-well plate to the laminar flow hood, remove the medium and seed 1 mL of *F. novicida* suspension at MOI 100 per well.

5. Centrifuge the 24-well plate for 5 min at 200 x g at 37°C to synchronize the infection.
6. Incubate the 24-well plate at 37°C / 5% CO_2 for 2 h.
7. Transfer the 24-well plate to the laminar flow hood and remove the cell medium (which contains extracellular *F. novicida*), gently wash the cells once with 1 mL warm 10% macrophage medium and add 1 mL warm 10% macrophage medium containing 10 µg/mL gentamicin to kill extracellular bacteria.
8. Transfer the 24-well plate back to the incubator at 37°C / 5% CO_2 for another 2 h.

3.5 Fixation and staining of *F. novicida*-infected murine BMDMs

1. After a total of 4 h of *F. novicida* infection, move the 24-well plate to the laminar flow hood, wash the cells three times with 0.5 mL warm 1x PBS per well and add 0.3 mL warm 4% PFA per well (the PFA can be diluted in 1x PBS).
2. Transfer the 24-well plate back to the incubator at 37°C / 5% CO_2 for 10 min to fix the BMDMs.
3. Remove the PFA and wash the fixed BMDMs three times with 0.5 mL 1x PBS per well.
4. With the help of forceps and a needle, gently transfer the coverslip cells onto the parafilm of the humidified chamber. Immediately cover the glass coverslip with 100 µL 1x PBS so the BMDMs do not dry out (*see* **Note 5**). The next steps are carried out in the humidified chamber.

5. Replace the 1x PBS with 100 µL immunofluorescence (IF) buffer and incubate the glass coverslips for 30 min at room temperature to block non-specific antibody binding.
6. Replace the IF buffer with 100 µL IF buffer containing 1:100 goat anti-cGAS primary antibody per glass coverslip and incubate for 1 h at room temperature.
7. Wash the glass coverslips three times with 1x PBS.
8. Add 100 µL IF buffer containing 1:200 donkey anti-goat Alexa-Fluor 488 secondary antibody and incubate for 45 min at room temperature.
9. Wash the glass coverslips three times with 1x PBS.
10. Add 100 µL IF buffer containing 1:4000 chicken anti-*F. novicida* primary antibody and incubate for 1 h at room temperature (*see* **Note 6**).
11. Wash the glass coverslips three times with 1x PBS.
12. Add 100 µL IF buffer containing 1:500 goat anti-chicken Alexa-Fluor 568 secondary antibody, 1:5000 Hoechst and 1:500 Alexa-Fluor 647 Phalloidin (*see* **Note 7**); and incubate for 45 min at room temperature.
13. Wash the glass coverslips three times with 1x PBS.
14. Clean a microscopy glass slide with 70% ethanol and add 2 µL of Vecta Shield per glass coverslip.
15. Using forceps, gently lift the glass coverslips and remove residual 1x PBS by blotting the edge and the side not containing the cells on paper towel.

16. Dip the glass coverslip 3-5 times into ddH_2O to wash away any residual salt contaminations. This is important as salt crystals can negatively influence the subsequent imaging quality.
17. Dry the coverslip again on paper towel by blotting the edge and the side not containing the cells on paper towel.
18. Mount the glass coverslip with BMDMs facing down on the microscopy glass slide containing Vecta Shield.
19. Seal the glass coverslip on the microscopy glass slide using transparent nail polish.
20. Visualise the cells using a confocal fluorescence microscope (Figure 1.). Fluorescence microscopy was performed in a PerkinElmer UltraView spinning disk confocal microscope, and Z-stacks of 200 nm step size were acquired using a 100 x/1.45 NA oil objective. The following excitation lasers were used: 405, 488, 561 and 640 nm. Fluorescence emission was detected with 445 (W60), 525 (W50), 615 (W70) and 705 (W90) nm filters, respectively. Data were analyzed and processed using FiJi software and all derived images shown correspond to maximum 3D projections.
21. The mounted glass coverslips can be stored at 4°C in the dark for later examination.

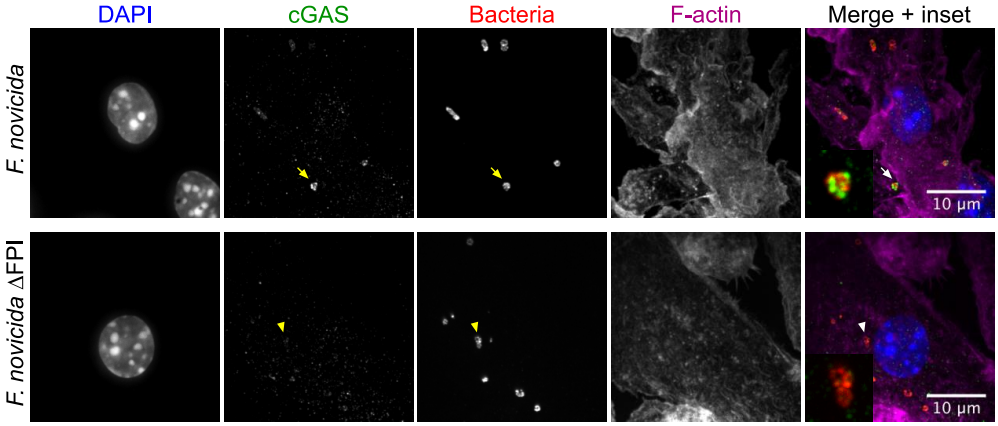

Figure 1 – cGAS associates with wild-type *F. novicida* but not with *F. novicida* ΔFPI (*see* **Note 8**). BMDMs were infected with *F. novicida* U112 (upper panel) or with the isogenic ΔFPI mutant (lower panel) for 4 hours, fixed and immunostained for cGAS and bacterial LPS. DNA was stained with Hoechst and F-actin with Phalloidin. Examples of cGAS-positive (arrow) or cGAS-negative bacteria (arrowhead) are depicted. Scale bar corresponds to 10 µm.

Notes

1. The "outer tools" are used to manipulate the exterior of the mouse, whereas the "inner tools" are only used once the fur has been removed. The separate use of surgical tools reduces potential contamination.
2. Euthanizing the mice directly in their cage minimizes stress applied to the animals, given that they are kept in their known environment. Always observe the mice during euthanasia and once the mice stop breathing, wait another 1 min before stopping the CO_2 supply.
3. Bone marrow progenitor cells can differentiate into various cell types depending on the differentiation conditions. The macrophage colony-

stimulating factor (M-CSF), also known as colony-stimulating factor-1 (CSF-1) is a hematopoietic growth factor differentiating bone marrow progenitor cells into non-dividing mature macrophages, so called bone-marrow derived macrophages (BMDMs) ***(28)***. M-CSF is produced in-house from 3T3 cells constitutively expressing M-CSF (3T3-MCSF). As M-CSF is secreted from these cells, the cell supernatant is collected into 50 mL aliquots and stored in an -80°C freezer. The M-CSF can be stored for 3-4 months in an -80°C freezer.

4. Infectivity of *F. novicida* depends a lot on the chosen growth condition and can drop dramatically when the growth conditions are not set up properly. For best growth, bacterial overnight cultures should be inoculated from plates instead of frozen stock. For this, *F. novicida* is streaked on a BHI plate supplemented with 0.2% L-cysteine and 100 µg/mL Ampicillin and incubated overnight in a 37°C bacterial incubator. Plates should not be kept longer than one week as this also negatively affects infectivity.
5. As an alternative, the coverslips can each be placed “cells-side down” on a drop of antibody solution on some parafilm, within a humidified chamber. A humidified chamber can be prepared by placing wet paper towel in the bottom of a petri dish covered with aluminum foil, preventing drying of the preparation and allowing incubation in the dark, which is crucial when handling fluorophores and fluorescent proteins. It is essential that the coverslips do not dry out at any step during the procedure, thus the antibody solutions must cover the whole coverslip.
6. In this protocol, both sets of primary and secondary antibodies are added sequentially (first primary followed by first fluorophore-conjugated

secondary antibody; followed by second primary followed by second fluorophore-conjugated secondary antibody). This is done because the donkey anti-goat secondary antibody used to stain cGAS would also recognize the goat anti-chicken secondary antibody used to stain the bacteria. By performing the staining sequentially, it is possible to avoid cross-reactivity between different antibodies, which is crucial in all immunofluorescence studies.

7. Phalloidin is a toxin isolated from the deadly *Amanita phalloides* “death cap" mushroom. It selectively binds filamentous actin (F-actin) and is used to reveal the distribution of these filaments in eukaryotic cells.
8. To activate a type-I IFN response, *F. novicida* needs to escape from the *Francisella* containing vacuole (FCP) into the cytosol. In the cytosol, cGAS is recruited to *F. novicida* and induces type-I IFNs via the STING/TBK1/IRF3 pathway ***(8)***. The *Francisella* pathogenicity island (FPI) is absolutely required for the escape into the cytosol ***(19)***. Therefore, a *F. novicida* mutant lacking the FPI (ΔFPI) serves as an ideal negative control for unspecific co-localization of cGAS and *F. novicida* antibody.

Acknowledgments

This work was supported by a Career Development Award (CDA00032/2015) from the Human Frontiers Science Program.

References

1. P. Broz and D.M. Monack (2013) Newly described pattern recognition receptors team up against intracellular pathogens, Nature reviews. Immunology. 13, 551–565.
2. O. Takeuchi and S. Akira (2010) Pattern Recognition Receptors and

Inflammation, Cell. 140, 805–820.
3. S.R. Paludan and A.G. Bowie (2013) Immune Sensing of DNA, Immunity. 38, 870–880.
4. V. Deretic, T. Saitoh, and S. Akira (2013) Autophagy in infection, inflammation and immunity, Nature reviews. Immunology. 13, 722–737.
5. K.M. Monroe, S.M. McWhirter, and R.E. Vance (2010) Induction of type I interferons by bacteria, Cellular microbiology. 12, 881–890.
6. P. Broz and V.M. Dixit (2016) Inflammasomes: mechanism of assembly, regulation and signalling, Nature reviews. Immunology.
7. V. Hornung, A. Ablasser, M. Charrel-Dennis, et al. (2009) AIM2 recognizes cytosolic dsDNA and forms a caspase-1-activating inflammasome with ASC, Nature. 458, 514–518.
8. L. Sun, J. Wu, F. Du, et al. (2013) Cyclic GMP-AMP Synthase Is a Cytosolic DNA Sensor That Activates the Type I Interferon Pathway, Science (New York, NY). 339, 786–791.
9. L. Unterholzner, S.E. Keating, M. Baran, et al. (2010) IFI16 is an innate immune sensor for intracellular DNA, Nature immunology. 11, 997–1004.
10. J. Wu, L. Sun, X. Chen, et al. (2013) Cyclic GMP-AMP is an endogenous second messenger in innate immune signaling by cytosolic DNA, Science (New York, NY). 339, 826–830.
11. Y. Tanaka and Z.J. Chen (2012) STING specifies IRF3 phosphorylation by TBK1 in the cytosolic DNA signaling pathway, Science signaling. 5, ra20.
12. G.M. Boxx and G. Cheng (2016) The Roles of Type I Interferon in Bacterial Infection, Cell host & microbe. 19, 760–769.
13. X. Cai, Y.-H. Chiu, and Z.J. Chen (2014) The cGAS-cGAMP-STING pathway of cytosolic DNA sensing and signaling, Molecular cell. 54, 289–296.
14. P.C.F. Oyston, A. Sjostedt, and R.W. Titball (2004) Tularaemia: bioterrorism defence renews interest in Francisella tularensis, Nature reviews Microbiology. 2, 967–978.
15. J.W. Jones, P. Broz, and D.M. Monack (2011) Innate immune recognition of francisella tularensis: activation of type-I interferons and the inflammasome, Frontiers in microbiology. 2, 16.
16. C.L. Jones, B.A. Napier, T.R. Sampson, et al. (2012) Subversion of host recognition and defense systems by Francisella spp, Microbiology and molecular biology reviews : MMBR. 76, 383–404.
17. A. Chong, T.D. Wehrly, V. Nair, et al. (2008) The early phagosomal stage of Francisella tularensis determines optimal phagosomal escape and Francisella pathogenicity island protein expression, Infection and immunity. 76, 5488–5499.
18. H. Geier and J. Celli (2011) Phagocytic receptors dictate phagosomal escape and intracellular proliferation of Francisella tularensis, Infection and immunity. 79, 2204–2214.
19. J.R. Barker, A. Chong, T.D. Wehrly, et al. (2009) The Francisella tularensis pathogenicity island encodes a secretion system that is required for phagosome escape and virulence, Molecular microbiology. 74, 1459–1470.
20. D.L. Clemens, P. Ge, B.-Y. Lee, et al. (2015) Atomic structure of T6SS

reveals interlaced array essential to function, Cell. 160, 940–951.
21. E. Meunier, P. Wallet, R.F. Dreier, et al. (2015) Guanylate-binding proteins promote activation of the AIM2 inflammasome during infection with Francisella novicida, Nature immunology. 16, 476–484.
22. K.M. Storek, N.A. Gertsvolf, M.B. Ohlson, et al. (2015) cGAS and Ifi204 cooperate to produce type I IFNs in response to Francisella infection, Journal of immunology (Baltimore, Md : 1950). 194, 3236–3245.
23. J.W. Jones, N. Kayagaki, P. Broz, et al. (2010) Absent in melanoma 2 is required for innate immune recognition of Francisella tularensis, Proceedings of the National Academy of Sciences of the United States of America. 107, 9771–9776.
24. K. Hansen, T. Prabakaran, A. Laustsen, et al. (2014) Listeria monocytogenes induces IFNβ expression through an IFI16-, cGAS- and STING-dependent pathway, The EMBO journal. 33, 1654–1666.
25. A.C. Collins, H. Cai, T. Li, et al. (2015) Cyclic GMP-AMP Synthase Is an Innate Immune DNA Sensor for Mycobacterium tuberculosis, Cell host & microbe. 17, 820–828.
26. R. Wassermann, M.F. Gulen, C. Sala, et al. (2015) Mycobacterium tuberculosis Differentially Activates cGAS- and Inflammasome-Dependent Intracellular Immune Responses through ESX-1, Cell host & microbe. 17, 799–810.
27. R.O. Watson, S.L. Bell, D.A. MacDuff, et al. (2015) The Cytosolic Sensor cGAS Detects Mycobacterium tuberculosis DNA to Induce Type I Interferons and Activate Autophagy, Cell host & microbe. 17, 811–819.
28. E.R. Stanley, K.L. Berg, D.B. Einstein, et al. (1997) Biology and action of colony--stimulating factor-1, Molecular reproduction and development. 46, 4–10.

4 The composition of the canonical inflammasome complex.

4.1 Introduction

Canonical inflammasomes are cytosolic immune signaling complexes that are activated by various PAMPs and DAMPs (for more details see chapter I, section 1.4). The canonical inflammasome complex consists minimally of three components: a pattern recognition receptor (PRR), the adaptor molecule ASC and caspase-1. After receptor activation by specific PAMPs and DAMPs, ASC molecules are recruited to the receptor and oligomerize into a large structure called the ASC speck. The ASC speck then recruits and activates caspase-1 leading to the induction of cell death and the release of IL-1β. Our group has demonstrated that oligomerization of ASC and thereby formation of the ASC speck is crucial for inflammasome signaling and responsible for efficient caspase-1 cleavage and IL-1β release [277].
Over the years, much evidence has suggested that phosphorylation, ubiquitination, and interaction with regulatory proteins can influence inflammasome activation and ASC speck formation, and are thus critical for inflammasome function and regulation [290, 292, 327, 328, 525, 526]. Tight regulation of inflammasome activation is crucial, as misregulation of the inflammasome is frequently associated with severe and persistent autoimmune and autoinflammatory diseases [527]. While several posttranslational modifications were discovered over the last few years, the composition and stoichiometry of the inflammasome complex and its interaction partners is poorly characterized.
Characterization of canonical inflammasome activation is important to better understand the function and mode of action of innate immunity, and could reveal novel targets for the treatment of autoimmune and autoinflammatory diseases. Much progress was achieved in the activation mechanisms of different inflammasomes and many inflammasome activation stimuli were identified. However, detailed information about the canonical inflammasome complexes is missing. Thus, we sought to characterize the composition of canonical inflammasome complexes by identifying novel components of the ASC speck. Moreover, we characterized the stoichiometry of the inflammasome components within ASC specks and determined interaction partners of caspase-1.

4.2 Material and Methods

Cell culture and infection.
Immortalized primary murine bone marrow-derived macrophages (iMACs) were grown in DMEM (Sigma) with 10 % M-CSF (supernatants of L929 mouse fibroblasts), 10 % v/v FCS, 10 mM HEPES, and penicillin (100 IU/ml)/streptomycin (100 μg/ml) (all BioConcept). 1 day before infection or treatment, iMACs were seeded into 6- or 96-well plates (all Greiner) at a density of 1.5 x 10^6 or 4 x 10^4 cells per well or in 10 cm petri dishes (Falcon) at a density of 15 x 10^6 per petri dish in DMEM with 10 % M-CSF, 10 % v/v FCS, 10 mM HEPES. iMACs were pre-stimulated for 4 h with lipopolysaccharide (LPS) (from *Escherichia coli* strain O111:B5 (InvivoGen)). To analyze NLRC4 activation, wild-type *S.* Typhimurium strain SL1344 was grown overnight at 37 °C with aeration in LB containing 90 μg/ml streptomycin (Sigma). *Salmonella* were subcultured for 4 h and were added to the iMACs at a multiplicity of infection of 20. The plates were centrifuged for 5 min at 500xg to ensure similar adhesion of the bacteria to the iMACs and were incubated for 90 min at 37 °C. To analyze NLRP3 activation, iMACs were treated with 5 mM ATP (Merck) for 90 min at 37 °C. Where indicated, 25 nM pan-caspase-inhibitor Z-Val-Ala-DL-Asp fluoromethylketone (zVAD) (Bachem) was added to the iMACs together with the treatment/infection.

Retroviral transduction.
iMACs were obtained from wild-type or *asc*-deficient primary murine bone marrow-derived macrophages (BMDMs) and complemented with the indicated GFP, ASC or caspase-1 constructs as previously described [252]. Immortalized *caspase-1*/ *caspase-11*-deficient BMDMs transiently expressing caspase-11 are used to complement with the indicated caspase-1 constructs.
In brief, per transduced iMAC well, supernatant of 3 wells of a 6-well plate are needed. In these 3 wells, GP2 cells were seeded at a density of 5 x 10^5 cells per well in DMEM with 10 % v/v FCS, 10 mM HEPES, and penicillin (100 IU/ml)/streptomycin (100 μg/ml) at day 1. At day 2, 9 μg of construct of interest was mixed with 6 μg VSVg construct and filled up to 0.75 ml with DMEM. 37.5 ul Lipofectamine 2000 (Invitrogen) was gently mixed with 0.75 ml DMEM and incubated for 5 min at room temperature. After 5 min incubation, the Lipofectamine 2000 was gently mixed with DNA and incubated for 20 min at room temperature. Add 0.5 ml Lipofectamine 2000/DNA complex solution per GP2 well drop-wise and incubate overnight at 37 °C. At day 3, the medium was removed from the GP2 cells and replaced with warm DMEM with 10 % M-CSF, 10 % v/v FCS, 10 mM HEPES, and penicillin (100 IU/ml)/streptomycin (100 ug/ml) and the GP2 cells moved to 32 °C. Per construct, iMACs were seeded in 1 well of a 6-well plate at density of 5 x 10^5 cells per well in DMEM with 10 % M-CSF, 10 % v/v FCS, 10 mM HEPES, and penicillin (100 IU/ml)/streptomycin (100 μg/ml) and

incubated at 37 °C. At day 4, the combined supernatant of the 3 transfected GP2 cell wells was filtered with a 0.45 μm filter (Sarstedt) and 12.5 μg/ml polybrene (Millipore) was added to favor cellular virus attachment. Then 1 ml of iMACs supernatant was removed, the GP2 supernatant was added drop-wise to the iMACs, the iMACs centrifuged for 2 h at 2900 rpm and incubated overnight at 32 °C. At day 5, the transduced iMACs were moved to 37 °C, expanded and sorted into 96-well plates using a FACSAria III (BD Biosciences).

Pull down protocol for mass spectrometry.
iMACs were seeded in 10 cm petri dishes and treated with 5 mM ATP or infected with *S.* Typhimurium as described above. Where indicated, 25 nM zVAD was added to the iMACs. After 90 min, the iMACs were collected into a 15 ml tube and centrifuged at 4 °C, 88xg for 5 min. The cell pellets were resuspended in 1 ml lysis buffer (20 mM Hepes pH 7.4, 10 mM KCl, 1 mM EDTA, 0.1 mM phenylmethylsulfonyl fluoride, 1 mM Na3VO4, 5 mM NaF, 0.5 % NP-40 (all Sigma), 1x protease inhibitor cocktail (Roche)), transferred into 2 ml Eppendorf tubes, vortexed for 10 s and lysed for 10 min on ice. The lysates were sonicated 5 times for 7 s (Hielscher) to break the ASC specks and centrifuged for 15 min at 10.000xg at 4 °C. 10 μl anti-HA magnetic beads (Thermo) were added to the supernatant and incubated for 1 h at 4 °C on a rotor. The magnetic beads were washed four times with 500 μl 0.1 M ammoniumbicarbonate (ABC) (Sigma) and the proteins were eluted by on bead digest. For this, beads were incubated with buffer 1 (5 μg/ml trypsine (Promega) in 1.6 M urea (AppliChem)/0.1 M ABC) for 30 min at 27 °C 800 rpm on Thermomixer (Eppendorf), the supernatant transferred to a new 1.5 ml Eppendorf tube, the beads washed two times with 40 μl buffer 2 (1 mM TCEP (Sigma) in 1.6 M urea/0.1 M ABC) and the supernatants combined into the same 1.5 ml tube. Protein digest was continued overnight on the bench.
The samples were acidified with 5 % trifluoroacetic acid (TFA) (Thermo) to reach a pH below 3. C18-columns (Harvard Apparatus) were conditioned twice with 150 ul acetonitrile (VWR) (1600 rpm, 30 s on table top centrifuge (Eppendorf)) and equilibrated three times with 150 μl buffer A (0.1 % TFA) (2400 rpm, 30 s on table top centrifuge). Samples were loaded on C18-columns and centrifuged into a new 2 ml Eppendorf tube (1800 rpm, 2 min on table top centrifuge). The flow through was reloaded on the same C18-columns and centrifuged again into the same tubes. The C18-columns were washed three times with 100 μl buffer C (5 % acetonitrile, 0.1 % TFA, 95 % HPLC water (v/v) (Fisher)) (2400 rpm, 30 s on table top centrifuge), the peptides eluted into new 2 ml Eppendorf tubes three times with 100 μl buffer B (50 % acetonitrile, 0.1 % TFA, 50 % HPLC water (v/v)) (1600 rpm, 30 s on table top centrifuge) and the peptides concentrated under vacuum to dryness. Peptides were either stored at -80 °C or resolved in 50 μl buffer A by ultrasonication for 10 s and incubation for 5 min at room temperature on Thermomixer and applied for mass spectrometry analysis. Mass spectrometry analysis and peptide analysis

using label-free quantification was done as described in chapter III, section 1.

ASC speck purification.
iMACs were seeded in 10 cm petri dishes and treated with ATP or infected with *S.* Typhimurium as described above. Sample preparation for mass spectrometry analysis was done as described above.
For ASC speck purification, the cell lysates were centrifuged at 400xg for 10 min at 4 °C and then the supernatants were centrifuged again at 2500xg at 4 °C for 30 min to spin down ASC specks before sonication. Then the pull down protocol was followed as described above continuing with sonication.

Immunoblot analysis.
iMACs were seeded in 6-well plates and treated with 5 mM ATP or infected with *S.* Typhimurium as described above. At different steps of the pull down protocol, protein samples were subjected to SDS-polyacrylamid gels and electroporated onto PVDF membranes. Primary antibodies used were mouse anti-HA.11 (EnzoLifeScience; 1:1000), rat anti-Casp1p20 (Genentech; 1:1000) and rabbit anti-ASC (AdipoGen; 1:1000) and the membranes incubated overnight at 4 °C with the primary antibodies. Secondary antibodies used were anti-mouse HRP, anti-rabbit HRP (both Southern Biotech; 1:3000) and anti-rat HRP (GE Healthcare; 1:3000), the membranes incubated with the appropriate secondary antibody for 1 h at room temperature and the membrane analyzed on an ImageQuant LAS 4000 (GE Healthcare).

Cytokine and LDH release measurement.
IL-1β was measured by enzyme-linked immunosorbent assay (eBioscience). Lactate dehydrogenase (LDH) was measured with an LDH Cytotoxicity Detection Kit (Takara). To correct for spontaneous cell lysis and to normalize the obtained values, the percentage of LDH release was calculated as follows:
(LDH infected - LDH uninfected) / (LDH total lysis - LDH uninfected) x 100.

ASC speck quantification with immunofluorescence.
iMACs were seeded onto cover glass (VWR) in 24-well plates at a density of 1.25 x 10^5 cells per well and infected with 5 mM ATP as described below. iMACs were washed three times with PBS and fixed for 10 min at 37 °C with 4 % Paraformaldehyde (Electron Microscopy Science). Cover glass was incubated with rabbit anti-ASC (AdipoGen; 1:500; $iWT^{GFPNter}$) or mouse anti-HA.11 (EnzoLifeScience; 1:500;

iASC$^{N/Cter}$) for 1 h at room temperature, then was washed three times with PBS, was incubated with Hoechst (1:5000); and donkey anti-rabbit coupled to Alexa 568 (1:500) or goat anti-mouse coupled to Alexa 568 (1:500) (all Life technologies) for another 45 min at room temperature, was washed three times with PBS and was mounted on glass slides with Vectashield (Vector labs). Glass slides were analyzed with a point scanning confocal microscope (Leica).

siRNA transfection.
Wild-type BMDMs were grown in DMEM with 20 % M-CSF, 10 % v/v FCS, 10 mM HEPES, and penicillin (100 IU/ml)/streptomycin (100 ug/ml) (BioConcept). 1 day before siRNA treatment, BMDMs were seeded into 96-well plates (Greiner) at a density of 3 x 10^4 or cells per well in DMEM (Sigma) with 10 % M-CSF (supernatants of L929 mouse fibroblasts), 10 % v/v FCS, 10 mM HEPES and nonessential aminoacids (BioConcept). 100 μl 1x GenMute Buffer, 2.5 μl GenMute reagent (SignaGen) and 2 μl 10 μM siRNA (Dharmacon; for details see chapter V, section 3) were mixed and incubated for 10 min at room temperature. 1 ml prewarmed 10 % macrophages medium was added, mixed, the supernatant from the macrophages removed and 105 μl of the siRNA/GenMute complexes added per well to be transfected. 48 h posttransfection, the BMDMs were prestimulated for 4 h with LPS (from *Escherichia coli* strain O111:B5) and treated with 5 mM ATP or 20 μM nigericin (Adipogen) for 90 min at 37 °C.

4.3 Results

The canonical inflammasome complex.
To study the composition of canonical inflammasome complexes, we first developed a mass spectrometry-based pull down approach. The approach was based on the analyses of inflammasome activation in immortalized primary murine bone marrow-derived macrophages (iMACs) complemented with HA-tagged versions of inflammasome components. iMACs are the closest murine macrophage-like cell line that are suitable for stable gene expression. In addition, iMACs deficient for inflammasomes components were readily available. Complementation of these deficient iMACs with the HA-tagged gene of interest avoided competition between untagged endogenous and tagged ectopically expressed protein.
First, we analyzed the composition of canonical inflammasomes. Canonical inflam-

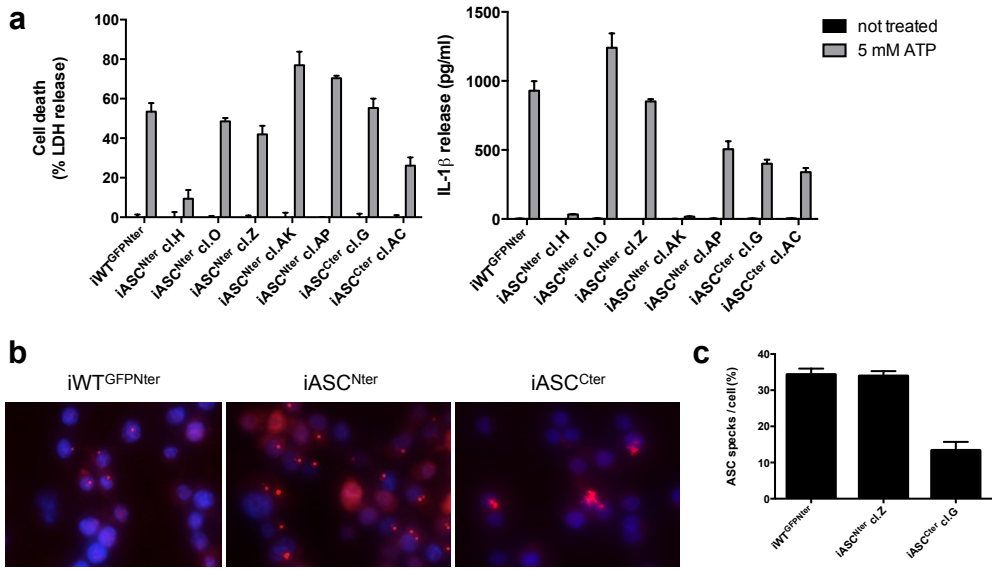

Figure III.2 Functional analyses of iASC$^{\mathbf{Nter}}$ and iASC$^{\mathbf{Cter}}$. Monoclonal cell lines of iWT^{GFPNter}, iASC^{Nter} or iASC^{Cter} were treated with 5 mM ATP for 90 min.(**a**) LDH and IL-1β release and (**b**) immunofluorescence pictures of ASC specks. Blue, nucleus; red, ASC. (**c**) ASC speck quantification of (b). cl., clone; Nter, N-terminal HA tag; Cter, C-terminal HA tag. (a) Data are representatives of two independent experiments (mean and standard deviation of triplicate wells).

masomes form ASC specks, which are multiprotein complexes of about a micron in diameter and mostly build of crosslinked ASC filaments [277]. To efficiently pull down the inflammasome complex, we cloned the major canonical inflammasome component ASC to a HA-tag and expressed the constructs in *Asc*-deficient iMACs. We tagged ASC at the N- or C-terminus (named iASC^{Nter} and iASC^{Cter}, respectively). Wild-type iMACs expressing GFP-HA (iWT^{GFPNter}) served as negative control for nonspecific binding in the pull down approach. After cloning all constructs, we produced monoclonal cell lines of the ASC-HA and GFP-HA con-

structs. Based on functional analyses, we selected clone C of iWT^{GFPNter}, clone Z of iASC^{Nter} and clone G of iASC^{Cter} for pull down experiments (Figure III.2).
The NLRP3 inflammasome is activated by over 30 different stimuli, among them extracellular ATP [528]. To induce NLRP3 inflammasome activation, we treated iWT^{GFPNter}, iASC^{Nter} and iASC^{Cter} with 5 mM ATP for 90 min and performed pull down experiments on cell lysate samples and identified the bound proteins by mass spectrometry (Figure III.3).
We identified a total of 2773 proteins in NLRP3-activated cells with a false discov-

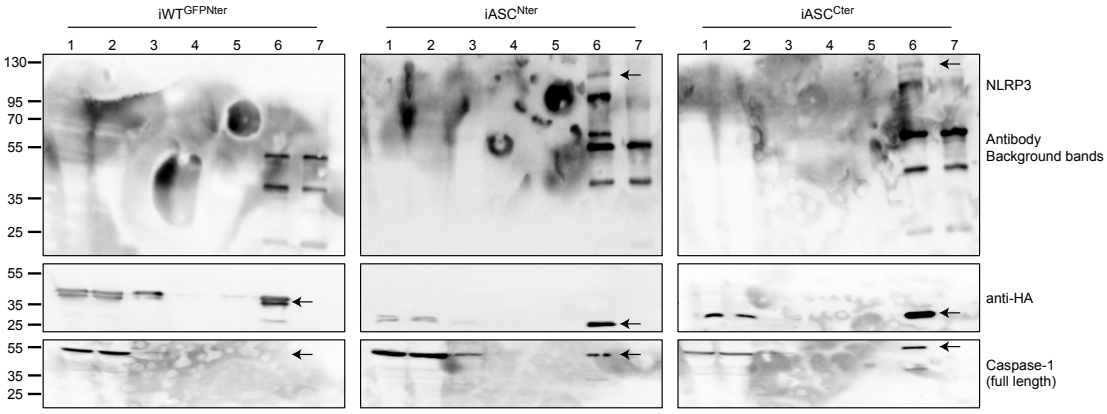

Figure III.3 Pull down of iWT^{GFPNter}, iASC^{Nter} and iASC^{Cter}. iWT^{GFPNter}, iASC^{Nter} and iASC^{Cter} were treated with 5 mM ATP for 90 min and samples from different steps of the pull down protocol were analyzed with western blot. 1, input; 2, supernatant beads; 3, first wash, 4, second wash; 5, fourth wash; 6, eluate; 7, beads only. Nter, N-terminal HA tag; Cter, C-terminal HA tag.

ery rate of 1 % (data available upon request). We enriched ASC from iASC^{Nter} and iASC^{Cter} but not iWT^{GFPNter} samples, demonstrating specific ASC enrichment and therefore validity of the pull down experiment (Table III.1). In addition to ASC, we detected caspase-1 in the iASC^{Nter} and iASC^{Cter} but not iWT^{GFPNter} samples, with roughly 20 % of ASC molecules binding caspase-1 (Table III.1). Interestingly, we only detected inflammasome-bound caspase-1 in iMACs treated with the pan-caspase inhibitor zVAD (Table III.1). Since zVAD blocks autoprocessing and autoactivation of pro-caspase-1, this finding indicates that active caspase-1 rapidly dissociates from the ASC speck, and that blocking activation prevents this dissociation, effectively trapping pro-caspase-1 within the structure, as suggested by Broz and colleagues [252]. Moreover, we detected a specific enrichment of NLRP3 in iASC^{Nter} and iASC^{Cter} samples (Table III.1), showing roughly 10 % of ASC molecules binding NLRP3. Interestingly, the inflammasome receptors AIM2 and NLRC4 were detected in iASC^{Nter} and iASC^{Cter}, but not iWT^{GFPNter} samples. As ATP specifically activates the NLRP3 inflammasome [528], it is possible that NLRC4 and AIM2 bound to ASC after the ASC specks have been formed, most likely during the prolonged incubation of the lysates with anti-HA beads. How-

Table III.1 Selected proteins identified in pull downs of NLRP3-activated cells. iWT^{GFPNter}, iASC^{Nter} and iASC^{Cter} were treated with 5 mM ATP for 90 min and HA beads-enriched samples were analyzed with mass spectrometry. Numbers represent the quantitative total spectra identified with mass spectrometry from total cell lysates, purified inflammasome samples (*) or total cell lysates without zVAD treatment (#). Nter, N-terminal HA tag; Cter, C-terminal HA tag.

Protein	iWT^{GFPNter}	iASC^{Nter}	iASC^{Cter}
GFP	21.5	0	0
GFP*	50.1	0	0
GFP#	21.5	0	0
ASC	0	71.1	46.5
ASC*	0	89.5	56.5
ASC#	1.3	82.3	32.7
Caspase-1	0	13.8	19.5
Caspase-1*	0	2.4	5.6
Caspase-1#	0	0	0
NLRP3	1.7	6.4	7.4
NLRP3*	0	7.3	0
NLRP3#	0	0	0
NLRC4	0	1.1	2.8
NLRC4*	0	0	0
NLRC4#	0	0	0
AIM2	0	4.2	0
AIM2*	0	0	0
AIM2#	0	0	0
CASP8	0	5.3	0
CASP8*	0	0	0
CASP8#	0	0	0
NEK7	0	0	0
NEK7*	0	0	0
NEK7#	0	0	0

ever, if inflammasome receptors bind to ASC specks after ASC oligomerization is currently unknown, as it is thought that the HIN200 and LRR domains of AIM2 and NLRC4, respectively, keep the PYD and CARD domain of the receptors in an inactive state before ligand recognition [249].

To test the possibility whether inflammasome receptors associate unspecifically with the ASC speck during beads incubation, we activated NLRP3 with 5 mM ATP and isolated the inflammasome complex from cell lysates by centrifugation before subjecting them to anti-HA beads. Mass spectrometry analyses of isolated inflammasome complexes showed NLRP3 but not AIM2 or NLRC4 binding to ASC (Table III.1), indicating that indeed NLRC4 and AIM2 are recruited to ASC specks after inflammasome activation (Table III.1). However, how AIM2 and NLRC4 are activated upon specific NLRP3 activation and their biological relevance in this experimental setting is currently unknown.

In 2014, Martin and colleagues showed interaction of ASC with IKKα and IKKα-dependent phosphorylation of ASC [328]. Moreover, three independent groups

demonstrated additional critical ASC phosphorylation events for ASC speck formation [326,327,529]. However, we neither detected an interaction between IKKα and ASC nor ASC phosphorylation in our experimental setting (data available upon request).

After analyzing the NLRP3 inflammasome complex, we investigated the NLRC4

Table III.2 Selected proteins identified in pull downs of NLRC4-activated cells. Selected proteins from NLRC4 (STm) or NLRP3 (ATP)-activated iMACs. Numbers represent the quantitative total spectra identified with mass spectrometry from total cell lysates or purified inflammasome samples (*). The purified inflammasome samples originate only from *S.* Typhimurium-infected cells. STm, *S.* Typhimurium; Nter, N-terminal HA tag; Cter, C-terminal HA tag.

Protein	**iWT^{GFPNter}**		**iASC^{Nter}**		**iASC^{Cter}**	
	ATP	STm	ATP	Stm	ATP	STm
GFP	14.8	21.1	0	0	0	0
GFP*	-	12.8	-	0	-	0
ASC	0	0	48.6	52.1	32.2	24.2
ASC*	-	0	-	5.3	-	25.0
Caspase-1	0	0	6.6	4.8	20.5	9.7
Caspase-1*	-	0	-	1.5	-	8.9
NLRP3	1.5	2.1	4.2	6.4	4.2	6.4
NLRP3*	-	2.6	-	3.8	-	14.3
NLRC4	0	0	0	0	2.2	0
NLRC4*	-	0	-	0	-	0.9
AIM2	0	0	2.4	4.3	0	0
AIM2*	-	0	-	0	-	3.6
Casp8	0	0	1.8	3.2	0.7	0
Casp8*	0	0	0.9			
NEK7	0	0	0.6	0.5	0	1.2
NEK7*	0	0	0			

inflammasome complex. NLRC4 is activated by bacterial ligands such as flagellin or components of type 3 secretion systems. To activate NLRC4, we infected iWT^{GFPNter}, iASC^{Nter} and iASC^{Cter} with exponentially growing *S.* Typhimurium, pulled down the NLRC4 inflammasome complexes and analyzed them by mass spectrometry. We identified a total of 3304 proteins in NLRC4-activated cells with a false discovery rate of 1 % (data available upon request). Compared to NLRP3-activated samples (Table III.1 and Table III.2), we detected comparable amounts of ASC and caspase-1 in lysate samples of iASC^{Nter} and iASC^{Cter} (Table III.2). Interestingly, we were unable to detect NLRC4 bound to ASC in NLRC4-activated cells (Table III.2). In contrast, we detected AIM2 and NLRP3 in lysate samples of iASC^{Nter} and iASC^{Cter} (Table III.2). These observations suggest that unspecific inflammasome receptor binding is true for the NLRC4 inflammasome as well. To test this hypothesis, we performed pulldown experiments on purified inflammasome samples to examine receptor binding after ASC speck formation. In purified inflammasome samples, we detected NLRC4 in NLRC4-activated cells (Table III.2). Moreover, the amount of detected AIM2 decreased in purified inflammasome sam-

ples indicating that AIM2 bound to ASC after inflammasome activation (Table III.2). In contrast, the amount of NLRP3 between cell lysate and purified inflammasome samples was unchanged indicating that NLRP3 is recruited to the ASC speck in NLRC4-activated cells (Table III.2). Our observations are consistent with a publication by Qu and colleagues where they showed NLRC4-dependent NLRP3 recruitment into the NLRC4 inflammasome complex after *S.* Typhimurium infection [530].
In 2013, Man and colleagues reported apoptotic caspase-8 recruitment to and caspase-8 activation at canonical inflammasome complexes [531]. In line with these observations, we identified ASC-bound caspase-8 in NLRP3- and NLRC4-activated samples (Table III.1 and III.2).
Taken together, iASC^{Nter} and iASC^{Cter} pull down experiments successfully enriched the NLRP3 and NLRC4 inflammasome complex and confirmed ASC as the major component of the canonical inflammasome complex. Irrespective of the activated inflammasome receptor, around 20 % of ASC bind caspase-1 in the canonical inflammasome complex. Pull down experiments comparing zVAD-treated and untreated cells showed that ASC interacts only with inactive caspase-1 and that the interaction with active, processed caspase-1 is transient, most likely since processed caspase-1 dissociates from the inflammasome complex after activation. Our analyses showed that ASC and caspase-1 are the major components of the inflammasome complex. Besides ASC and caspase-1, we observed the recruitment of multiple inflammasome receptors in NLRC4- and NLRP3-activated iMACs. Whereas a recent paper could explain NLRP3 recruitment to the NLRC4 inflammasome [530], the biological function of NLRC4 and AIM2 recruitment by the NLRP3 inflammasome remains elusive and requires further examination.

Caspase-1 interaction partners.
Caspase-1 is recruited to and proteolytically activated at the canonical inflammasome complex and is the common executioner of all known canonical inflammasomes. Active caspase-1 cleaves intracellular substrates to induce pyroptosis, a lytic, pro-inflammatory form of cell death associated with cytokine production. Caspase-1 function and therefore induction of cell death and cytokine release fully depends on its catalytic activity and ability to be cleaved in the ASC speck [252]. Nevertheless, the recruitment to the ASC speck does not require catalytic activity and thus happens before caspase-1 cleavage.
The three best studied cleavage substrates of caspase-1 are Gasdermin-D and the two cytokines IL-1beta and IL-18 [249]. Gasdermin-D forms holes in the plasma membrane resulting in cell lysis, whereas IL-1β and IL-18 attract immune cells and induce inflammation in the surrounding tissue [249, 261–264]. However, Agard and colleagues reported more potential caspase-1 cleavage substrates, though their function in pyroptosis is not well understood [532]. To address this, we used our pull down approach to identify caspase-1 interaction partners and assessed their

contribution to the phenotype of pyroptosis.

We tagged caspase-1 at the N- or C-terminus with a HA-tag and expressed the

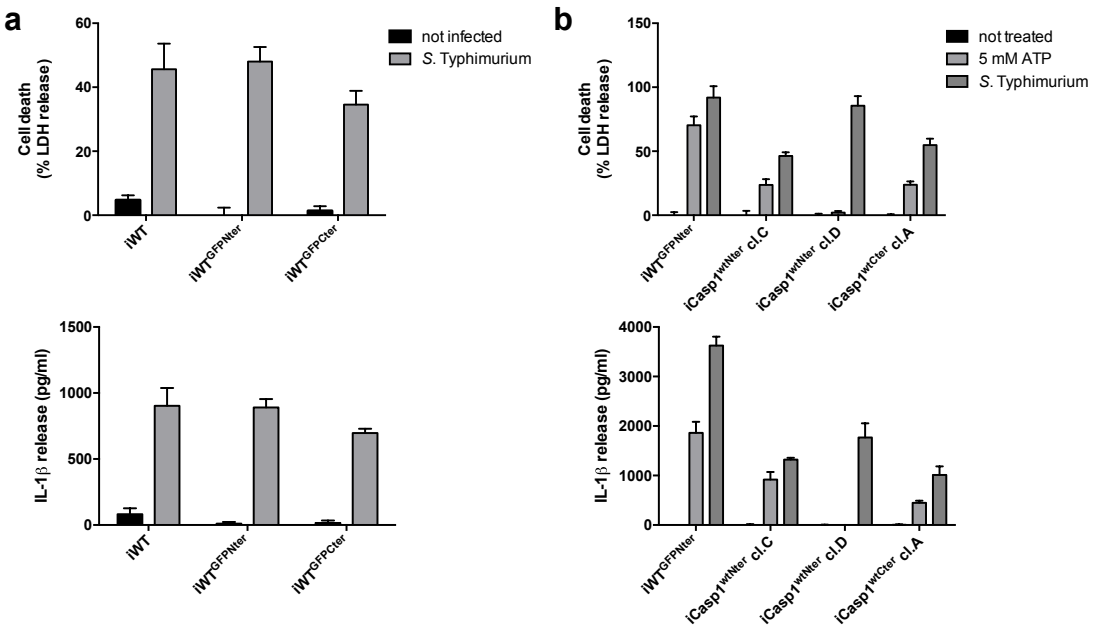

Figure III.4 Functional analyses of monoclonal iWT^{GFP}, iCasp1^{wtNter} and iCasp1^{wtCter}. (**a**) Cell death and IL-1β release of monoclonal iWT^{GFPNter} and iWT^{GFPCter} infected with *S.* Typhimurium for 90 min. (**b**) LDH and IL-1β release of monoclonal iWT^{GFPNter}, iCasp1^{wtNter} and iCasp1^{wtNter} 90 min after 5 mM ATP treatment or *S.* Typhimurium infection. cl., clone; wt, wild-type; Casp1, Caspase-1; Nter, N-terminal HA tag; Cter, C-terminal HA tag. (a,b) Data are representatives of two independent experiments (mean and standard deviation of triplicate wells).

constructs in *caspase-1*-deficient iMACs (named iCasp1^{wtNter} and iCasp1^{wtCter}, respectively). The previously constructed iWT^{GFPNter} served as negative control for unspecific binding in the pull down approach. After stable construct expression, we produced monoclonal cell lines of the caspase-1-HA constructs. Based on functional analyses, we selected clone C of iCasp1^{wtNter} and clone A of iCasp1^{wtCter} for pull down experiments (Figure III.4).

To specifically identify caspase-1 interaction partners before and after inflammasome recruitment, we slightly adapted the pull down protocol and skipped the sonication step. Without sonication, the inflammasome complex is not efficiently pulled down, whereas caspase-1 and GFP are efficiently recovered after beads elution (Figure III.5).

Using mass spectrometry, we identified a total of 1239 proteins in the iWT^{GFPNter} and iCasp1^{wtNter} samples with a false discovery rate of 1 % in NLRP3-activated cells (data available upon request). Out of these 1239 proteins, 273 proteins were exclusively found and 122 proteins enriched in the iCasp1^{wtNter} samples compared

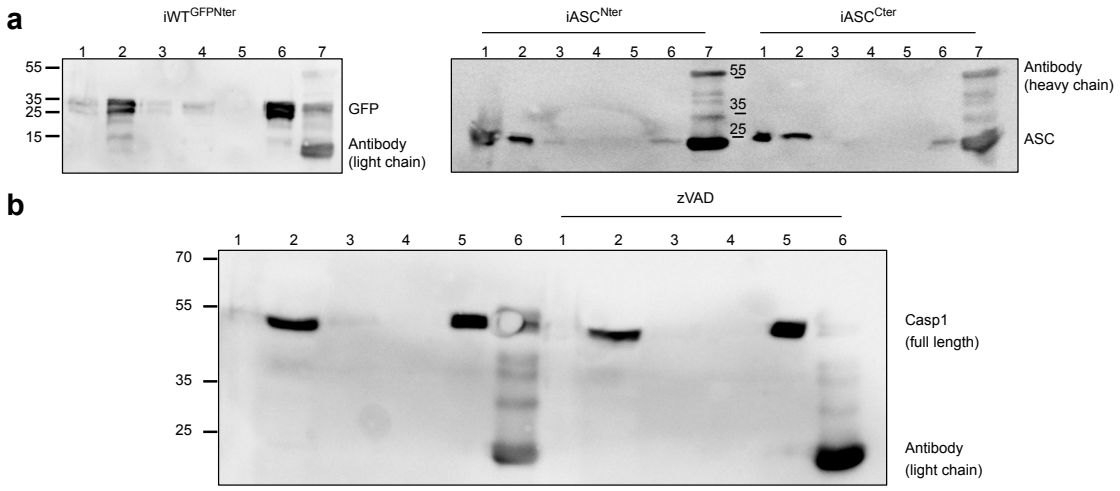

Figure III.5 iCasp1$^{\mathbf{wtNter}}$ pull down. (**a**) iWT^{GFPNter}, iASC^{Nter} and iASC^{Cter} were treated with 5 mM ATP for 90 min and samples from different steps of the pull down protocol without sonication were analyzed with western blot. 1, nuclear pellet; 2, input; 3, supernatant beads; 4, first wash; 5, fourth wash; 6, eluate; 7, cooked beads. (**b**) iWT^{GFPNter} and iCasp1^{Nter} were treated with 5 mM ATP for 90 min and samples from different steps of the pull down protocol without sonication were analyzed with western blot. 1, nuclear pellet; 2, input; 3, supernatant beads; 4, first wash; 5, eluate; 6, cooked beads. Where indicated, cells were treated with 25 nM zVAD. Casp1, Caspase-1; Nter, N-terminal HA tag; Cter, C-terminal HA tag.

to iWT^{GFPNter} samples (data available upon request). Among the proteins exclusively found in iCasp1^{wtNter} samples were IL-1β, Gasdermin-D, Zyxin, MCM4 and Wdr1 (Table III.3), which based on previous publications are directly cleaved by caspase-1 or secreted in a caspase-1-dependent manner [532, 533]. These results demonstrated the validity of our pull down approach and its ability to detect caspase-1 interaction partners and cleavage substrates.

We validated 20 potential caspase-1 interaction partners for their impact on cell death and IL-1β release by siRNA knock down experiments in primary murine bone marrow-derived macrophages (BMDMs) (Table III.3) . We transfected BMDMs with a pooled siRNA library and treated them with the pore-forming bacterial toxin nigericin to induce NLRP3 inflammasome activation. We used nigericin instead of ATP as we observed IL-1β but not cell death in ATP-treated BMDMs in this experimental setup (Figure III.6 a). Knock down of the positive control NLRP3 reproducibly reduced cell death and IL-1β release by 50 %, whereas none of the 20 potential caspase-1 interaction partners showed an impairment in cell death and IL-1β release (Figure III.6 b). Thus we could not observe an involvement of the 20 proteins in NLRP3-dependent cell death and IL-1β release. However, we cannot exclude that they account for other phenotypic characteristics of pyroptosis.

Another interesting protein found in our pull down experiment was Zyxin. Zyxin has a reported dual function in apoptosis, another form of programmed cell death [534, 535]. Zyxin promotes apoptosis through CARP-1 binding [534], but can also

Table III.3 Selected proteins identified in the caspase-1 pull down. Selected proteins from NLRP3-activated iMACs treated with (*) or without the pan-caspase inhibitor zVAD. Numbers indicate the total spectrum counts identified with mass spectrometry in total lysates. #, validated proteins with siRNA. Casp1, Caspase-1; Nter, N-terminal HA tag; Cter, C-terminal HA tag.

Protein	$iWT^{GFPNter}$	$iWT^{GFPNter}$(*)	$iCasp1^{wtNter}$	$iCasp1^{wtNter}$(*)
GFP	96	89	3	1
Caspase-1	0	0	41	43
IL-1β	0	0	2	2
Gasdermin-D	0	0	3	2
Zyxin	0	0	0	2
MCM4	0	0	9	12
Tgm2#	0	0	21	19
Gart#	0	0	20	12
Wdr1#	0	0	14	18
Samhd1#	0	0	13	13
Cmpk2#	0	0	11	11
Drg2#	0	0	10	10
Hspa14#	0	0	10	6
Rnf213#	0	0	3	14
Lrrfip1#	1	0	15	28
Hcls1#	5	3	25	27
Snx5#	8	3	17	20
Ptpn6#	3	3	21	19
Coro1c#	1	0	17	19
Ifit3#	2	2	13	17
Arpc1b#	4	1	17	16
Swap70#	1	0	8	15
Sec23b#	1	1	15	13
Rnh1#	1	0	11	12
Adsl#	2	0	11	12
Fyb#	1	0	7	12

block chromatin condensation, a hallmark of apoptosis [535]. To block chromatin condensation, Zyxin binds Acinus in the nucleus and thereby prevents Acinus from apoptotic caspase-dependent cleavage. Intriguingly, nuclear condensation is also observed in caspase-1-dependent cell death [249]. Moreover, Zyxin was validated as caspase-1 cleavage substrate by Agard and colleagues [532]. Thus we wondered what impact Zyxin had on canonical inflammasome activation. We tested *zyxin*-deficient BMDMs for their ability to induce various canonical inflammasomes, but could not observe a reduction of cell death and IL-1β release in *zyxin*-deficient compared to wild-type BMDMs (Figure III.7). Nevertheless, the effect of Zyxin on caspase-1-induced nuclear condensation remains unclear and further investigations could uncover the role of Zyxin cleavage in caspase-1-induced nuclear condensation. Taken together, caspase-1 pull down experiments identified known and potential caspase-1 interaction partners. However, the validation of 20 potential interaction partners did not show a defect in cell death and IL-1β release. Moreover, we confirmed that Zyxin directly interacts with caspase-1. However, Zyxin had

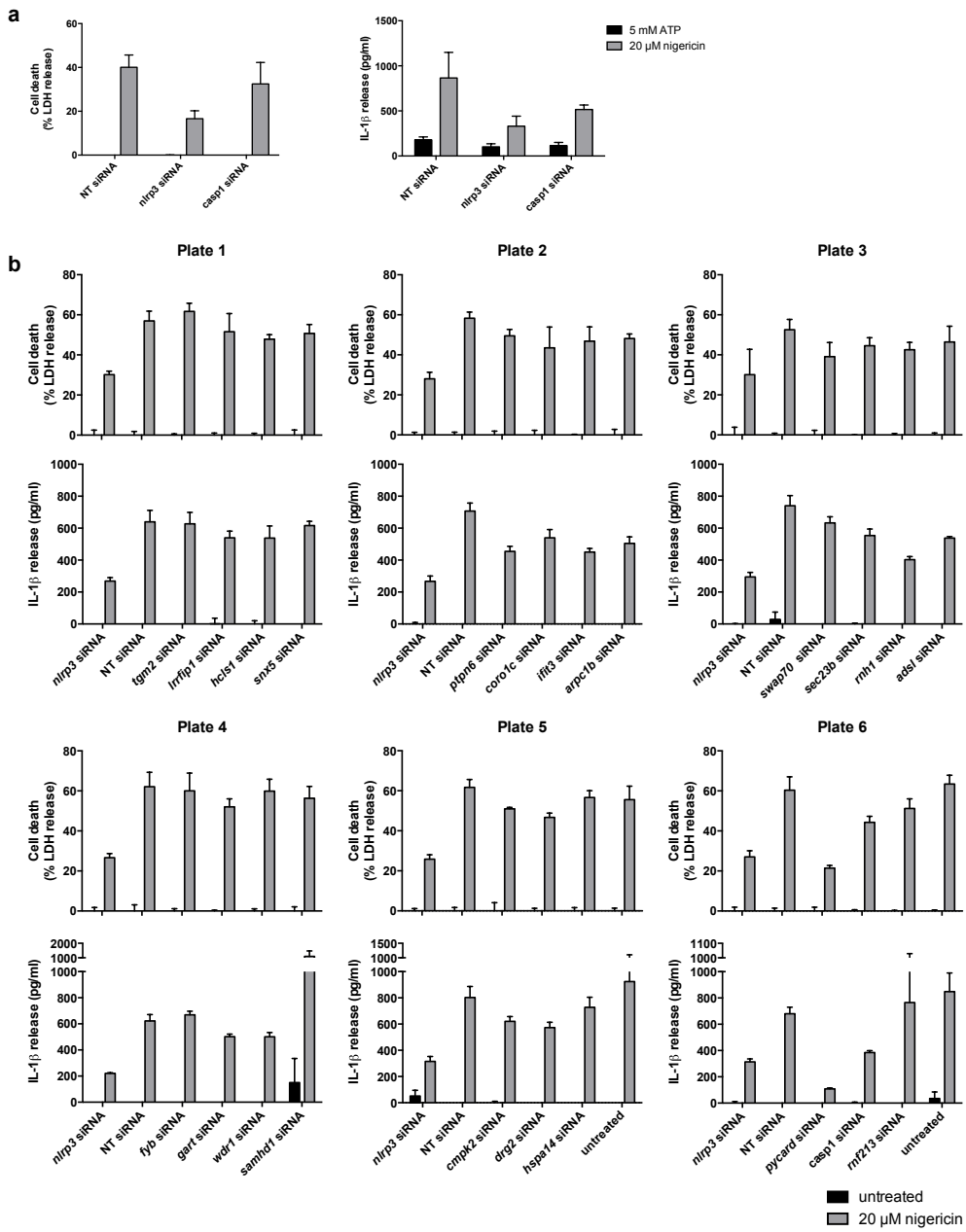

Figure III.6 Impact of potential caspase-1 interaction partners on cell death and IL-1β release. (**a**) LDH and IL-1β release from indicated siRNA-treated, 5mM ATP or 20 μM stimulated primary murine bone marrow derived macrophages (BMDMs). (**b**) LDH and IL-1β release from indicated siRNA-treated and 20 μM nigericin-stimulated wild-type BMDMs for 90 min. *nlrp3* siRNA was used as positive control. NT, nontargeting. Data are representatives of two independent experiments (mean and standard deviation of triplicate wells).

no impact on cell death and Il-1β release. Nevertheless, we cannot exclude that the 20 validated proteins and zyxin play a role in other characteristics of pyroptosis, such as chromosome condensation. Identifying proteins contributing to the

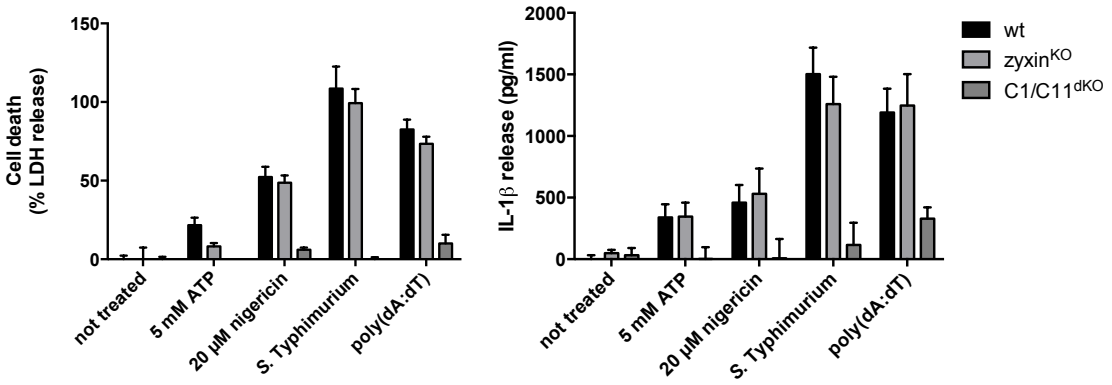

Figure III.7 Canonical inflammasome activation in *zyxin*$^{\mathbf{KO}}$. LDH and IL-1β release in wild-type (wt), *zyxin*^{KO} or *caspase-1 / caspase-11*^{dKO} (C1C11^{dKO}) primary murine bone marrow derived macrophages 90 min after treatment with 5 mM ATP or 20 μM nigericin to induce NLRP3, transfection of poly(dA:dT) to induce AIM2 or infection with *S.* Typhimurium to induce NLRC4 activation. Data are representatives of two independent experiments (mean and standard deviation of triplicate wells).

pyroptotic phenotype would greatly enhance our understanding about caspase-1 cleavage substrates and their function in inflammasome-induced inflammation. As the contribution to inflammation of other pyroptotic phenotypes besides cell death and cytokine release is unclear, identifying the responsible proteins would help to understand their contribution to inflammation.

4.4 Discussion and Outlook

The canonical inflammasome complex is an important mediator of inflammation and its misregulation is associated with autoinflammatory and autoimmune diseases [249, 536]. Whereas many activation signals of canonical inflammasomes were described so far, the composition and stoichiometry of canonical inflammasomes is not well understood. Canonical inflammasomes activate caspase-1, which then executes cell death and cytokine release to induce inflammation by cleaving cellular substrates. However, only a few cleavage substrates of caspase-1 are described so far. In the work presented here, we established a pull down protocol to identify the composition and stoichiometry of canonical inflammasome complexes and to identify interaction partners of caspase-1.

The analyses of the NLRP3 and NLRC4 inflammasome complex confirmed ASC as the major component of the inflammasome complex irrespective of the type of canonical inflammasome. We discovered that 20 % of ASC molecules bind caspase-1 indicating that caspase-1 is the second most abundant protein in the canonical inflammasome complex. It is important to mention that we only detected ASC-caspase-1 interaction when we used zVAD to block caspase-1 activation. These observations suggest that the interaction between caspase-1 and the inflammasome is transient, where inactive caspase-1 is recruited and active caspase-1 immediately dissociates from the complex again. Moreover, we identified multiple inflammasome receptors associated to the inflammasome complex upon NLRP3- and NLRC4-specific stimuli. However, it is unclear if the recruitment of multiple inflammasome receptors to the same inflammasome complex is of biological relevance.

The analyses of caspase-1 pull downs identified known and unknown caspase-1 interaction partners. Interestingly, the number of interactions between caspase-1 and known cleavage substrates was low, indicating that the substrates only bind caspase-1 at the moment of cleavage. The validation of identified unknown caspase-1 interaction partners could not reveal an important role for these proteins in inflammasome-dependent cell death and IL-1β release. However, we cannot exclude that these proteins result in different phenotypic characteristics of pyroptosis, besides membrane permeabilization and cytokine release, such as nuclear condensation.

Taken together, we demonstrated for the first time an in depth analysis of the composition and stoichiometry of the canonical inflammasome complex. Besides ASC and caspase-1, we could not identify any other highly abundant protein, indication that ASC specks are composed only of ASC and caspase-1. Moreover, several interesting questions and potential follow up projects arose from these analyses. Some of these questions and potential projects are discussed in the next paragraphs.

Why are multiple receptors recruited to the canonical inflammasome?
We identified multiple inflammasome receptors bound to one canonical inflammasome complex. AIM2 and NLRC4 were detected in NLRP3-activated samples and AIM2 and NLRP3 in NLRC4-activated samples, therefore the specificity of receptor binding in respect to the applied stimuli was not given.
An explanation for stimuli-independent receptor binding could be of technical reasons during sample preparation. The pull down protocol included a sonication step to break up the large ASC speck. This sonication step was absolutely required for efficient inflammasome complex pull down. Sonication could create blunted ASC filament ends, which serve as new interaction and recruitment sites for inflammasome receptors. During beads incubation with cell lysates after sonication, receptors would bind to these free ASC oligomers and are thereby detected in our analyses. Therefore, separating the cytosolic content from inflammasome complexes would reduce this phenomenon. Indeed, when we purified the inflammasome complex before sonication and beads incubation, we detected no AIM2 and NLRC4 in NLRP3-activated samples, indicating that free ASC binding sites might be occupied by inflammasome receptors. However, we still detected NLRP3 in NLRC4-activated samples. Moreover, it is unclear how multiple inflammasome receptors get activated upon receptor-specific stimuli.
Inflammasome receptors only bind ASC upon global conformational changes induced by direct or indirect ligand recognition. In the case of NLRC4, receptor activation is initiated through NAIP proteins that recognize the different bacterial ligands. The activated NAIPs then serve as initiators of NLRC4 oligomerization in a domino-like reaction associated with global structural domain rearrangements in NLRC4 [276]. These rearrangements make NLRC4 competent for ASC recruitment. As we detected NLRC4 in NLRP3-activated cells, it is possible that bacterial contaminants introduced during sample preparation activated NLRC4. However, there is also the possibility that ASC oligomers can induce NLRC4 activation. Therefore, the activation of NLRC4 in NLRP3-activated cells requires further investigation.
In contrast to NLRC4, AIM2 is activated by double stranded DNA (dsDNA) in the cytosol; forming a similar ASC recruitment platform as seen for NLRC4 [304]. As nuclear dsDNA is present in cell lysates, AIM2 could be activated during beads incubation after cell lysis and thereby detected in our pull down analyses.
In contrast, the activation mechanism and oligomerization of NLRP3 is not understood. NLRP3 is activated in the cytosol by over 30 different stimuli, which are all indicators of cellular metabolic issues [249]. As the pull down approach included cell lysis, the loss of cell integrity could have been the trigger of NLRP3 activation and binding to ASC in NLRC4-activated cells.
Therefore, we could hypothesize that caspase-1-dependent Gasdermin-D pore formation in NLRC4-activated cells results in potassium efflux and therefore NLRP3 activation. Indeed, our analyses of caspase-11-dependent NLRP3 activation has shown that caspase-11, Gasdermin-D-dependent cell lysis activates NLRP3 and consequently the release of mature IL-1β [263,348]. Moreover, it has been reported that the induction of another form of lytic cell death called necroptosis, which is

mediated by MLKL pore formation in the plasma membrane, triggers NLRP3 activation [537, 538]. Therefore, it might be that NLRP3 activation occurs in every form of lytic cell death and thus every activated ASC speck recruits NLRP3.
Alternatively, Qu and colleagues postulated that NLRC4 recruits NLRP3 to the inflammasome complex upon *Salmonella* infection [530]. However, we did not detect any ASC-bound NLRC4 in the same samples. In general, we detected less NLRC4 than NLRP3 associated with ASC. Thus, it is possible that NLRC4 initially bound to ASC and recruited NLRP3, but the NLRC4-ASC interaction was lost during sample preparation due to differential receptor binding affinities to ASC. It might be that the ASC-NLRC4 binding over CARD domains is not as stable as ASC-NLRP3 binding over PYD domains. Measuring the binding affinity of purified, activated inflammasome receptors to oligomerized ASC could clarify the possibility of differential receptor ASC binding affinities.
In 2016, Shi and colleagues discovered NEK7 as an important protein for NLRP3 inflammasome activation and ASC speck formation [539]. Intriguingly, we detected NEK7 bound to ASC in some conditions in our pull down experiments. The exact function of NEK7 is unknown, but it could be speculated that NEK7 serves as sensor protein for NLRP3 as NAIPs do for NLRC4. With our established pull down protocol on hand, we could identify NLRP3 interaction partners and potentially the activator of NLRP3, be it a sensor protein as in the case of NLRC4 or a ligand molecule like dsDNA as seen for AIM2. To perform the pull down experiment, I would express HA-tagged NLRP3 in *Asc*-deficient cells because of three reasons. First, NLRP3 can be activated in *Asc*-deficient cells and oligomerizes without ASC recruitment, leading to a small receptor complex instead of the large ASC speck. This could lead to better NLRP3 enrichment. Second, *Asc*-deficient cells do not induce NLRP3-dependent cell death and therefore cellular content is not lost in the supernatant during NLRP3 activation. Third, ASC speck formation and subsequent caspase-1 activation could induce negative feedback loops that block additional NLRP3 activation. As *Asc*-deficient cells do not induce NLRP3-dependent caspase-1 activation, cells could activate more NLRP3 oligomers and consequently accumulate potential NLRP3 interaction partners. This is of special importance as mass spectrometry analyses detect only highly abundant proteins in complex samples. As NLRC4 oligomers only contain one initiating NAIP protein and this activation mechanism could hold true for NLRP3 oligomers as well, the NLRP3 initiator would be above the detection threshold of mass spectrometry.
In addition to the identification of NLRP3 interaction partners and the potential NLRP3 initiator, electron microscopy studies of the activated, purified NLRP3 oligomer could solve its three dimensional architecture and give insights into NLRP3 oligomerization.
Taken together, understanding the activation mechanism of NLRP3 is of huge interest as misregulated NLRP3 is associated with autoimmune and autoinflammatory diseases in humans [527]. Studying the activation mechanism of NLRP3 could reveal new potential interventions to block or interfere NLRP3 activation and therefore mitigate NLRP3-associated autoinflammatory and autoimmune diseases.

Can we distinguish Caspase-1 interaction partners responsible for cell death and IL-1β release?

To detect caspase-1 in the canonical inflammasome complex we added the pan-caspase inhibitor zVAD, because wild-type caspase-1 dissociates from the inflammasome complex after activation. Full caspase-1 activation depends on its catalytic activity and ability to be cleaved in the ASC speck [252]. Nevertheless, the recruitment of caspase-1 to the ASC speck does not require catalytic activity or caspase-1 cleavage. Therefore, uncleavable and catalytic dead caspase-1 mutants could accumulate in the inflammasome complex and there trap caspase-1 interaction partners. By performing pull down experiments with caspase-1 mutants, we could analyze the composition of the inflammasome complex and caspase-1 interaction partners in the same experiment.

We already expressed HA-tagged catalytic dead and uncleavable caspase-1 mu-

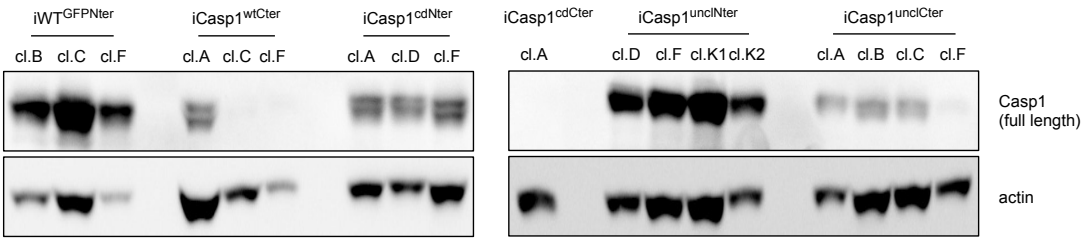

Figure III.8 Protein expression of monoclonal iWT^{GFPNter}, iCasp1^{cd} and iCasp1^{uncl}. Westernblot analysis of Caspase-1 in various untreated monoclonal cell lines. Actin served as loading control. cl., clone; cd, catalytic dead; uncl., uncleavable; Casp1, Caspase-1; Nter, N-terminal HA tag; Cter, C-terminal HA tag.

tants in *caspase-1*-deficient iMACs and produced monoclonal cell lines (Figure III.8). Moreover, we obtained promising data from a first pull down experiment comparing wild-type and uncleavable caspase-1 constructs, where we detected similar levels of caspase-1 and ASC (Table III.4). Moreover, we could reduce unspecific binding of inflammasome receptors to ASC and detected higher levels of specific NLRP3 and NLRC4 binding with the uncleavable caspase-1 construct. Therefore, we might obtain even better results using uncleavable or catalytic dead caspase-1 instead of ASC constructs to analyze the composition of canonical inflammasome complexes.

Besides potential improvements in the analyses of the inflammasome complex, the usage of caspase-1 mutant constructs could differentiate caspase-1 interaction partners depending on its activation state. Wild-type caspase-1 is fully active and induces cell death and IL-1β release, whereas uncleavable caspase-1 only induces cell death but not IL-1β release and catalytic dead caspase-1 is deficient for both [252].

Table III.4 Caspase-1 pull down of NLRC4- and NLRP3-activated cells. Selected proteins from NLRC4 (STm) and NLRP3 (ATP) activated iMACs. Numbers indicate the total spectrum counts identified with mass spectrometry from purified inflammasome samples. STm, *S.* Typhimurium; Casp1, Caspase-1; Nter, N-terminal HA tag; Cter, C-terminal HA tag.

Protein	**iWT^{GFPNter}**		**iCasp1^{wtNter}**		**iCasp1^{unclNter}**	
	ATP	STm	ATP	Stm	ATP	STm
GFP	2	6	0	0	0	0
Caspase-1	1	1	15	17	11	31
ASC	0	0	4	11	1	14
NLRP3	0	5	0	1	3	6
NLRC4	0	0	0	1	0	4
AIM2	0	0	5	6	0	1

Therefore, comparing pull down experiments from the three different caspase-1 constructs could determine proteins responsible for cell death, IL-1β release or both. Proteins interacting with all three caspase-1 constructs are components of the canonical inflammasome as they are all recruited by the inflammasome complex. In addition, proteins interacting with all three caspase-1 constructs could be interaction partners of inactive caspase-1 in the cytosol. Cytosolic and inflammasome complex interaction partners of caspase-1 could be discriminated by comparing pull downs of cell lysates with inflammasome-purified samples. Proteins associated with caspase-1 in the inflammasome complex would be enriched in the purified inflammasome samples, whereas cytosolic caspase-1 interaction partners are absent or reduced in these samples compared to cell lysate samples.
The comparison of wild-type and uncleavable caspase-1 could discriminate between caspase-1 interaction partners critical for cell death and IL-1β release. Proteins only interacting with wild-type and uncleavable caspase-1 are involved in cell death, whereas proteins only interacting with wild-type caspase-1 but not uncleavable caspase-1 are involved in IL-1β release. In addition, these proteins should not interact with the catalytic dead caspase-1, as this construct does not induce cell death and IL-1β release.
Taken together, the analyses of uncleavable and catalytic dead caspase-1 constructs could improve the analyses of canonical inflammasome components and their stoichiometry, as these caspase-1 mutants are recruited to the inflammasome complex but are not released anymore. Moreover, comparing pull down results of wild-type, uncleavable and catalytic dead caspase-1 constructs could discriminate caspase-1 interaction partners responsible for cell death from those responsible for IL-1β release. This could discover the cellular mechanism that releases IL-1β independent of cell death. Indeed, under certain conditions and stimuli, innate immune cells like monocytes, neutrophils or dendritic cells only release IL-1β without the induction of cell death [540–542]. Only releasing IL-1β but not the entire cellular content could be an important immune regulatory step of the organism to activate the immune system but at the same time reducing inflammation and thereby tissue damage.

Does Caspase-8 induce inflammasome-dependent, Gasdermin-D-independent cell death?

Recently, three individual groups identified Gasdermin-D as the most important downstream target of caspase-1 to induce pyroptosis [258–260]. Nevertheless, canonical inflammasome activation induces at late time points lytic cell death and IL-1β release in *GsdmD*-deficient macrophages. Under these conditions, He and colleagues detected caspase-3 cleavage; indicating caspase-8 activation [260]. Our results support these observations as we found caspase-8 being recruited by the NLRP3 and NLRC4 inflammasome. While caspase-8 has already been shown to cleave IL-1β [531], it should not induce a lytic form of cell death, but apoptosis, a immunologically silent form of death.

However a recent report by Rogers and colleagues has shown that lytic cell death can occur after stimulation of cells with apoptotic triggers, and that this involves caspase-3-dependent cleavage of a protein called DFNA5 [543]. Intriguingly, DFNA5 and Gasdermin-D both belong to the gasdermin protein family, and both share the ability to form membrane pores. Furthermore, caspase-3 is a cleavage substrate of caspase-8, thus potentially directing caspase-8 activation to lytic cell death. Therefore, I speculate that the inflammasome has a dual mode to induce cell death: If Gasdermin-D is present, caspase-1 induces rapid cell death and IL-1β release through Gasdermin-D cleavage. If Gasdermin-D is not present, the inflammasome induces at late time points a lytic form of cell death through caspase-8- and caspase-3-dependent DFNA5 cleavage and thereby IL-1β release. It needs to be investigated how similar Gasdermin-D-dependent pyroptosis and DFNA5-dependent lytic cell death is, but data published by Feng Shao's group indicate that they induce a similar type of lytic cell death [258]. Given that caspase-1 is still activated in *GsdmD*-deficient macrophages, all cleavage substrates except Gasdermin-D are present and thus it is likely that the other characteristics of pyroptosis are present as well. However, if inflammasomes induce cell death in a Gasdermin-D-independent, but DFNA5-dependent manner requires the generation of *Gsdmd/DFNA5* double knockout mice. The characterization of inflammasome-dependent, Gasdermin-D-independent cell death would describe an alternative inflammasome-dependent cell death mechanism if caspase-1 fails to induce cell death and IL-1β release. This would inform our understanding how the immune response is transferred from a cellular immune reaction induced by inflammasomes into a multifunctional and global immune response.

Chapter IV

Discussion and Outlook

During my PhD, I investigated innate immune cell activation upon *Salmonella* and *Francisella* infections. The activation of innate immune cells is particularly important, because it determines how efficient an infection is cleared. During my PhD, I contributed to five different publications, which are listed in chapter III, section 1, 2 and 3; and chapter V, section 1 and 2.
In the following sections, I discuss the findings of research article I (chapter III, section 1) and research article II (chapter III, section 2). Moreover, working with *Francisella* directed my attention to the recognition of cytosolic double stranded DNA by AIM2, and consequently the activation of the AIM2 inflammasome. Therefore, one important aspect of cytosolic AIM2 inflammasome activation is discussed in the last section of this chapter.

1 How can we improve the new phosphoproteomics approach?

Phosphorylation is one of the most frequent post-translational modifications to regulate intracellular signaling pathways. Upon pathogen infections, immune signaling pathways are activated, which involve phosphorylation cascades and result in a change of the cellular gene expression pattern [109, 180]. In the context of *Salmonella* infections, host immune signaling pathways, such as TLR4 signaling, activate pro-inflammatory genes and type-I-interferon production, which cooperatively fight the bacterial infection [544].
Presently, mass spectrometry is the method of choice to analyze phosphorylation changes in signaling pathways. However, we noticed that despite the recent technical improvements in mass spectrometry, the number of detected phosphopeptides was significantly lower than the expected number of cellular phosphopeptides (see research article I in chapter III, section 1). Moreover, phosphorylation changes in

immune signaling pathways were underrepresented in a mass spectrometric analysis of phospho-enriched samples from *Salmonella*-infected primary murine bone marrow derived macrophages (BMDMs). For example, TRIF signaling which causes type-I-interferon production, was not detected in phospho-enriched samples, although it is a signature response of cells to *Salmonella* infection [350,351].
It is currently under debate why fewer phosphopeptides are detected. In research article I in chapter III, section 1, we addressed the issue of low phosphopeptide detection in mass spectrometry. We demonstrated that the presence of negatively charged phosphate groups globally suppressed peptide signal intensities in MS1 spectra and therefore decreased the number of detected phosphopeptides. In mass spectrometry, the formation of positively charged peptide ions is required for peptide identification. Given that the phosphate group added a negative charge of 2 to phosphorylated peptides, the compensation of the additional negative charge of the phosphate group during peptide ionization was more difficult. Consequently, enzymatic removal of the phosphate group by phosphatases increased the signal intensities. Therefore, we detected three-times more peptides after phosphatase treatment in *Salmonella*-infected BMDMs, compared to phospho-enriched samples.
Even though phosphatase treatment increased the number of detected peptides, it had the disadvantage that the localization information of phosphate groups was lost during the process. Therefore, we validated the newly identified peptides with western blot, bioinformatical methodologies and targeted mass spectrometry. These analyses revealed that the newly identified peptides after phosphatase treatment enlarged the picture of activated immune signaling pathways upon *Salmonella* infection and revealed the important TRIF signaling pathway.
Even though phosphatase treatment is an excellent method to increase the number of detected phosphopeptides, a method that eliminates phosphate group-dependent peptide ionization suppression while preserving its localization would advance our method. Here, two different concepts are described which could lead to an improvement of the method.
The first concept removes the phosphate group from the phosphopeptides without losing the phosphosite information. This can be achieved by chemical β-elimination where the chemical removal of the phosphate group leaves a double bond scar [545,546]. We tested this approach to validate our phosphatase approach, but were unable to detect the same amount of peptides as detected in phosphatase-treated samples. A possible explanation for this is that a large amount of newly detected peptides after phosphatase treatment were not initially phosphorylated and we detected a lot of false positives in our analyses. However this explanation seems unlikely because different validation experiments showed that most of the newly detected peptides are initially phosphorylated. Therefore, the low detection rate of phosphopeptides after β-elimination must have been caused by something else.
Chemical beta-elimination only removes phosphate groups from serine and threonine, but not tyrosine residues [547]. Even though serine and threonine make up about 98 % of all phosphorylation events, the residual phosphate groups on tyrosine

residues cannot be removed by chemical β-elimination and might therefore account for efficient ionization suppression in β-eliminated samples [548]. Additionally, we showed that β-elimination only removes 80 % of all phosphate groups, compared to over 99 % in phosphatase-treated samples. Therefore, inefficient phosphate group removal in β-eliminated samples was most likely responsible for ionization suppression.

Besides chemical β-elimination, enzymatic β-elimination exists in nature, particularly in bacteria. The *Shigella* protein OspF and *Salmonella* protein SpvC are phosphothreonine lyases, which specifically dephosphorylate threonine residues by β-elimination [383, 549–551]. Given that OspF and SpvC are very target specific, it is unclear if they can be engineered to dephosphorylate serine, threonine and tyrosine residues irrespective of the peptide sequence.

In contrast to phosphate group removal, the second concept is based on the modification of phosphate groups to compensate for their negative charge.

In a chemical reaction, the two critical oxygen atoms of the phosphate group can be esterified. This chemical reaction requires an ester donor, such as methanol and the resulting product is called dimethylphosphate [552]. However, such chemical reactions are normally performed under harsh conditions and the impact of such reactions on the global peptide behavior in mass spectrometry analysis is not known.

Instead of a chemical reaction, phosphate groups can be enzymatically modified. *Francisella* expresses multiple enzymes, which facilitate the addition of galactosamine to the phosphate group of LipidA, thereby reducing its negative charge [553, 554]. Moreover, enzymes of *Neisseria* and *Acenitobacter* modify phosphate groups of LipidA with ethanolamine, thereby compensating for its negative charge [555, 556]. However, the chemical environment of the phosphate group of LipidA is very different from the one of phosphopeptides. Therefore it remains unclear whether or not enzymes can be engineered that compensate the negative charge of phosphate groups on phosphopeptides.

In summary, we discovered that the negative charged phosphate group adversely influences the detection of phosphorylated peptides with mass spectrometry by global suppression of peptide ionization efficacy. Therefore, this negative charge needs to be removed or compensated before mass spectrometry analyses. We propose the removal of phosphate groups by phosphatases, because it is a very effective and timesaving method. Using this method, we increased the number of detected peptides threefold compared to phospho-enriched samples, but lost the localization of the phosphate group. Thus, our method improved the identification and understanding of cellular signaling pathways, but requires careful validation to elucidate if and where a peptide was initially phosphorylated.

To preserve the phosphorylation site information, two concepts are plausible. The first approach removes the phosphate groups while leaving a scar to mark the initial phosphorylation site. The second approach compensates for the negative charge by adding residues to the problematic oxygen atoms of the phosphate group. Irrespective of the approach, it is important that the phosphate manipulation is very efficient as residual or unmodified phosphate groups suppress ionization efficiency.

2 The *Francisella* pathogenicity island encodes a functional T6SS

Almost ten years ago the *Francisella* pathogenicity island (FPI) was discovered as key factor for *Francisella tularensis* virulence in vitro and in vivo [557]. Since then, it has been speculated that the FPI encodes a type 6 secretion system (T6SS) due to homology analyses with known T6SS-encoding bacteria [477]. However, only a limited number of FPI genes show homology with known T6SSs, which makes it difficult to verify if the FPI encodes a functional T6SS. In 2015, Clemens and colleagues demonstrated that the FPI-encoded proteins IglA and IglB of *F. novicida* form filaments that display structural characteristics of T6SS sheaths [523, 558]. Even though the formation of IglA/IglB sheaths has been shown by Clemens and colleagues [523], it remains unclear whether or not the *Francisella* T6SS is functional and dynamic. Therefore, we asked if the FPI of *F. novicida* encodes a dynamic and functional T6SS and assigned functions as effectors or parts of the machinery to individual FPI genes (research article II in chapter III, section 2).
We showed for the first time that *F. novicida* assembles a dynamic and functional T6SS. Moreover, we demonstrated that a dynamic T6SS is required for *F. novicida* escape from the phagosome to the cytosol. In addition, we identified the unfoldase ClpB, which disassembles the contracted T6SS sheath and subsequently enables the bacteria for another round of T6SS assembly.
Moreover, we identified the FPI-encoded genes iglG, iglF, iglI and iglJ as structural components of the *Francisella* T6SS, whereas pdpE, pdpD, pdpC and anmK were not involved in T6SS assembly and therefore encode potential T6SS effector proteins. Indeed, PdpC and PdpD showed reduced virulence in vitro and in vivo. Thus, our analyses identified PdpC and PdpD as potential T6SS effector proteins, which orchestrate directly or indirectly *Francisella* escape from the phagosome.
We based our studies on *F. novicida*, which is the common lab strain to analyze *Francisella tularensis*. However, *F. tularensis* is the major cause of tularemia, a fatal disease in humans. Even though the infection process of *F. novicida* and *F. tularensis* is similar and phagosomal escape is the essential virulence step in *F. tularensis* as well, it would be important to confirm our results in *F. tularensis*.
Moreover, *Francisella tularensis* does not only infect humans, but also infects insects and amoebae. As described in chapter I, section 2.2, the expression of FPI-encoded genes results in a different life style in various hosts. Therefore, it would be important to verify whether effector proteins with no impact in mice, such as PdpE or AnmK, are important for virulence in other hosts.
Besides our observations, a recent publication by Eshraghi and colleagues propose PdpC and PdpD as potential T6SS effector proteins [559]. However, it remains unclear how PdpC and PdpC induce phagosomal rupture. Therefore, the next two

paragraphs discuss similarities and differences between our findings and observations by Eshraghi and colleagues, as well as potential mechanisms of PdpC and PdpD-induced phagosomal rupture.

Are PdpC and PdpD the only T6SS effector proteins responsible for phagosomal escape?

We demonstrated that PdpC and PdpD are not involved in T6SS dynamics but are the two *Francisella* T6SS effectors necessary for phagosomal escape. Our observations were partially confirmed by a recent publication of Eshraghi and colleagues [559], in which they identified that VgrG, IglC, OpiA, OpiB-1, OpiB-3, PdpD and PdpC are secreted to the bacterial supernatant in a T6SS-dependent manner, using a mass spectrometry-based approach.

VgrG has been identified as the main component of the T6SS tip complex in *Vibrio* and IglC shows homology to the T6SS inner tube protein Hcp [482,494]. Given that Eshraghi and colleagues identified the tip complex protein VgrG and the inner tube protein IglC in the *Francisella* supernatant, as seen for functional T6SSs of *Vibrio* and *Pseudomonas* [482], their detection in the *Francisella* supernatant confirms our observations of a dynamic *Francisella* T6SS.

In contrast to the other secreted proteins, *opiA*, *opiB-1* and *opiB-3* are not encoded on the FPI. However, their expression is regulated by the transcription factor MglA, which also induces the expression of FPI genes [413, 559]. *OpiB-1* and *opiB-3* are encoded on one operon consisting of *opiB-1*, *opiB-2* and *opiB-3* in *F. novicida* and therefore most likely originate from gene duplication. In line with this assumption, *F. tularensis* and *F. holarctica* only harbor one *opiB* gene. Importantly, Eshraghi and colleagues generated a triple knockout of *opiB-1*, *opiB-2* and *opiB-3* (named *opiB* mutant) and used this mutant for all functional experiments.

First they assessed phagosomal escape of *F. novicida*. They showed that the *pdpC/pdpD/opiA/opiB* quadruple knockout is unable to escape to the cytosol anymore. However, they showed no data on phagosomal escape of single mutants. In contrast, we analyzed phagosomal escape of *pdpC* and *pdpD* single mutants and the *pdpC/pdpD* double mutant. Our results showed that both the *pdpC* and *pdpD* single mutant is impaired in phagosomal escape, with a stronger reduction in cytosolic bacteria observed for the *pdpC* mutant. Moreover, we showed that the number of cytosolic *pdpC/pdpD* double mutants is comparable to FPI mutants. Thus, their results of the *pdpC/pdpD/opiA/opiB* quadruple mutant phenocopied our results of the *pdpC/pdpD* double mutant, suggesting that *opiA* and *opiB* have a minor impact on phagosomal escape. However, based on our analyses we cannot exclude that PdpC and PdpD facilitate the delivery of OpiA and OpiB or a yet to be identified T6SS effector protein that is responsible for phagosomal rupture.

Besides phagosomal escape, Eshraghi and colleagues analyzed intracellular growth of different bacterial mutants. They showed a significant reduction in intracellular growth of the *pdpC* single mutant and the *pdpD/opiA/opiB* triple mutant, how-

ever the *pdpD*, *opiA* and *opiB* single mutants grew like wild-type bacteria in the human macrophage-like cell line THP-1. Additional knockout of *pdpC* in the triple mutant background or the *pdpC/pdpD* double mutant showed intracellular growth rates comparable to FPI-mutants. Interestingly, intracellular growth was minimally restored in a quadruple knockout complemented with *opiA*.
Alternatively, we analyzed the number of intracellular bacteria of *pdpC* and *pdpD* single and *pdpD/pdpC* double mutants 24 hours post-infection in BMDMs. We observed a significant reduction in intracellular *pdpC*- and *pdpC/pdpD*-deficient *F. novicida*, whereas pdpD-deficient *F. novicida* showed a reduced but not significant drop in intracellular bacteria compared to wild-type *F. novicida*. Thus, the observations in intracellular bacterial growth are similar between the two studies with respect to *pdpD* and *pdpC* single mutants and *pdpD/pdpC* double mutant.
However, in contrast to Eshraghi and colleagues, we also analyzed the different bacterial mutants with respect to AIM2 inflammasome activation and virulence in a mouse infection model. *PdpC*-, *pdpD*- and *pdpC/pdpD*-deficient *F. novicida* showed significantly reduced AIM2 inflammasome activation. In line with these observations, mice infected with *pdpC*-, *pdpD*- or *pdpC/pdpD*-deficient *F. novicida* showed significantly reduced bacterial burden in the spleen and liver two days post-infections compared to wild-type *F. novicida*-infected mice. Importantly the bacterial burden of *pdpC/pdpD*-deficient *F. novicida* in the spleen and liver was comparable to an FPI mutant.
Based on our profound analyses including phagosomal escape, AIM2 inflammasome activation, intracellular growth and virulence in vivo, we propose a different conclusion than Eshraghi and colleagues. They concluded that PdpC, PdpD, OpiA and OpiB are cooperatively required for phagosomal escape and therefore virulence, whereas our data suggests that only PdpC and PdpD are required to escape from the phagosome. However, we cannot exclude that *opiA* and *opiB* contribute to phagosomal escape in a different experimental setting or in a specific cell type, or that *opiA* and *opiB* facilitate intracellular growth but not phagosomal escape. Thus, further analyses of these newly identified T6SS effectors are required. Additionally, given that *pdpD* is not conserved in *Francisella tularensis* strains, it is important to determine the function of PdpD in the highly virulent *F. tularensis* and *F. holarctica* strains.
Based on our analyses, we cannot exclude that effector proteins have different functions in specific cell types. Supporting this possibility, Long and colleagues infected mice intranasal with wild-type and *pdpC*-deficient *F. tularensis* [522]. In mice, wild-type *F. tularensis* disseminated from the lung to the spleen and liver, thereby establishing a detrimental infection. In contrast, all mice survived the infection of *pdpC*-deficient *F. tularensis*. However, *pdpC*-deficient *F. tularensis* disseminated from the lung to the spleen but not the liver during the early phase of infection. In line with their observations, we recovered more *pdpC*-deficient *F. novicida* from the spleen than the liver, suggesting that PdpC is more important in the infection of the liver than the spleen. These results suggest that *Francisella* effectors have tissue- and cell type-specific functions, at least to some degree. Thus, the involve-

ment of PdpC in liver and spleen infections and the characterization of the infected cell types in these two organs require further investigation.
In addition to the publication of Eshraghi and colleagues; T6SS analyses in *Vibrio* and *Pseudomonas* showed that the tip complex of T6SSs contains a limited number of effector proteins. As a consequence, only a small amount of effector proteins are delivered per T6SS contraction [482]. Therefore, we propose that *F. novicida* utilizes its T6SS several times to deliver a critical amount of PdpC and PdpD into host cells to escape from the phagosome. In agreement with our assumption, we observed that *clpB*-deficient *F. novicida* could not escape into the cytosol anymore. Interestingly, *clpB*-deficient *F. novicida* assembled and contracted one T6SS per bacteria, but could not disassemble the contracted T6SS sheath and was therefore unable to assemble another T6SS (see research article II in chapter III, section 2). Thus, it is important to determine the critical number of T6SS assemblies that allow *Francisella* to escape to the cytosol.

How do the *Francisella* effectors PdpC and PdpD induce phagosomal escape?

We demonstrated that PdpC and PdpD mediate bacterial escape from the phagosome to the cytosol, thereby preventing phagosomal killing. However, it is unclear how PdpC and PdpD induce phagosomal rupture to enable *F. novicida* escape into the cytosol.
First, it is possible that PdpC and PdpD facilitate the secretion of a yet unknown effector protein that induces phagosomal rupture directly or indirectly. However, no other secreted protein was detected by Eshraghi and colleague, suggesting that PdpC and PdpC facilitate phagosomal rupture [559].
Second, it is unknown whether the *Francisella* T6SS delivers PdpC and PdpD to the phagosome or to the host cytosol. If PdpC and PdpD are delivered to the phagosome, they induce phagosomal rupture from the inside, whereas PdpC and PdpD delivered to the cytosol induce phagosomal rupture from the outside. As T6SSs are shown to deliver effector proteins into eukaryotic target cells, it is technically feasible that the *Francisella* T6SS delivers PdpC and PdpD into the host cytosol [482]. However, whether PdpC and PdpD are delivered to the phagosome or to the cytosol remains to be elucidated.
Cellular localization of PdpC and PdpD can be analyzed with PdpC and PdpD overexpression experiments in eukaryotic cells, which have been used in the functional analyses of T3SS effector proteins [560]. In a preliminary experiment, we transiently expressed Hek293 cells with HA-tagged versions of PdpC and PdpD under a doxycycline-inducible promoter. Even though up to 80 % of Hek293 cells were successfully transfected with the expression vector, we were unable to detect PdpC and PdpD after doxycycline induction by western blot (data not shown). This observation suggests that PdpC and PdpD cannot be expressed in eukaryotic cells. However, the used nucleotide sequences of pdpC and pdpD were not codon

optimized for eukaryotic expression systems and therefore could pose a problem for PdpC and PdpD expression in eukaryotic cells.
Another method for analyzing PdpC and PdpD localization is to follow the secretion of endogenous bacterial PdpC and PdpD into host cells. Upon PdpC and PdpD delivery into the host cell, intracellular localization of PdpC and PdpD can be visualized by immunofluorescence. An advantage of this method is the usage of endogenous PdpC and PdpD, which removes any overexpression artifacts. However, due to the unavailability of antibodies for PdpC and PdpD, we endogenously attached a HA-tag to PdpC and PdpD. Even though we detected HA-tagged PdpC in the bacterial supernatant after T6SS induction using western blot, we were unable to detect HA-tagged PdpC in infected primary murine bone marrow derived macrophages (BMDMs) using immunofluorescence confocal microscopy, suggesting that there is not enough delivered PdpC-HA for a robust signal in confocal microscopy. Given that there is only a small amount of delivered PdpC-HA, one could try to analyze PdpC-HA localization by super resolution or structured illumination microscopy as these techniques are more sensitive and can increase the signal to noise ratio.
As an alternative to the HA-tag, PdpC and PdpD localization might be examined with the split GFP system. The split GFP system was described by Cabantous and colleagues [561]. The principle of the split GFP system is the differential expression of two non-fluorescent GFP fragments. One GFP fragment only represents GFP β-strand 11 (GFP_{11}), whereas the second fragment composes of GFP β-strands 1-10 ($GFP_{1\text{-}10}$). Given that GFP_{11} is around 10 amino acids long and therefore in the size range of the HA tag, PdpC and PdpD can be tagged with GFP_{11} possibly without disturbing its T6SS-dependent delivery. In contrast to the GFP_{11}-tagged bacterial effectors, $GFP_{1\text{-}10}$ is expressed in the host cytosol. Upon T6SS-dependent effector secretion, GFP_{11}-PdpC interacts with $GFP_{1\text{-}10}$ at the site of PdpC localization and induces a GFP signal.
Third, it is unclear how PdpC and PdpD mechanistically induce phagosomal rupture. Structural prediction analyses of PdpC and PdpD did not revealed any domains that facilitate PdpC and PdpD insertion into membranes. Thus, PdpC and PdpD probably represent a new group of membrane destabilizing/rupturing proteins or recruit and activate host proteins, which then rupture the phagosome.
Artificial liposomes could reveal mechanistic insights into PpdC- and PdpD- dependent phagosomal rupture. The principle of liposomal leakage assays is to mix liposomes with purified proteins, in our case PdpC and/or PdpD [263]. Liposomes are generated from purified lipids, which allows for customization of their lipid composition. In a first step, purified PdpC and PdpD recruitment by liposomes can be assessed by western blot or analytical ultracentrifugation, therefore determining the required lipid composition for their recruitment. This information can then be used for liposomal leakage assays [263], in which liposomes are preloaded with a fluorescent dye. Given that the dye is auto-quenched within liposomes, light emission is only detectable if PdpC and/or PdpD are able to rupture liposomes. If purified PdpC and/or PdpD alone cannot bind to and rupture liposomes, I would

add cell lysates to the reaction mixture and repeat the experiment.
Given that PdpC and PdpD were cloned with a HIS-tag for protein purification, PdpC and PdpD pull down experiments could identify their interaction partners in the host cell by mass spectrometry. Additionally, mass spectrometry analysis of purified liposomes might determine the interaction complex of PdpC and/or PdpD at the liposomes.
As a first step to perform liposomal leakage assays, we cloned PdpC and PdpD into a bacterial expression vector already containing in frame a 6x His tag for protein purification. Even though we could express smaller proteins, such as IglC with this method, we were unable to express PdpC and PdpD. Very long *Francisella* genes are probably not suitable for expression in a common *E. coli* expression strain. *E. coli* codon optimization or purification of 6x His-PdpC/-PdpD from *F. novicida* could perhaps solve this issue. However, it could be possible that PdpC and/or PdpD lyse *E. coli* and therefore cannot be expressed in bacteria. Indeed, it has been shown that other T6SS-positive bacteria express immunity proteins to neutralize the toxic effect of their T6SS effectors. However, we mutated all genes encoded on the FPI and did not observed the presence of immunity proteins on the FPI. Nevertheless, it is possible that *Francisella* expresses immunity proteins outside the FPI. Thus, in the case of effector-induced bacterial toxicity, an insect-based expression system might be suitable.

Taken together, we showed that *F. novicida* expresses a functional T6SS and ClpB disassembles the contracted sheath again. PdpC and PdpD are the two T6SS effectors that mediate bacterial escape from the phagosome to the cytosol. Escaping the phagosome is the essential virulence step in *Francisella* infections as *Francisella* lacking a functional T6SS is completely avirulent in vitro and in vivo. Thus, our findings contribute greatly to the understanding of the *Francisella* T6SS and *Francisella* virulence.

3 Why is the AIM2 inflammasome not activated during mitosis?

AIM2 is a cytosolic DNA sensor that recognizes foreign double stranded DNA (dsDNA) originating from bacteria or viruses, and mislocalized self-dsDNA. Upon dsDNA recognition, AIM2 oligomerizes and forms a canonical inflammasome to activate caspase-1. Active caspase-1 induces a pro-inflammatory, lytic form of cell death called pyroptosis. A hallmark of pyroptosis is caspase-1-dependent cleavage and therefore activation of IL-1β and IL-18, two important pro-inflammatory cytokines [249]. Beside its importance in pathogenic infections, prostate and colorectal cancer cells reduce cellular AIM2 levels. Thereby, the cancer cells avoid AIM2 activation, mostly likely because nuclear DNA is accessible for AIM2 due to a dis-

continued nuclear envelope in these cells [305–308]. In line with this assumption, it has been demonstrated that pharmacological disruption of the nuclear envelope leads to the exposure of nuclear DNA to the cytosol, resulting in AIM2 inflammasome activation [312]. In contrast, an increase in AIM2 inflammasome activation is linked to psoriasis, abdominal aortic aneurysm and systemic lupus erythematosus, three severe autoimmune diseases [309–311].

Cell division is not only a essential step in the development of an organism, but is also important for the homeostasis of tissue integrity and the replenishment of circulating immune cells. During the prometaphase of mitosis, the nuclear envelope breaks down and the duplicated chromosomes segregate equally into the daughter cells [562]. However, when the nuclear envelope is broken down, the DNA is theoretically accessible for AIM2 recognition. Yet no AIM2 inflammasome activation is observed during mitosis, raising the question how mitotic cells avoid AIM2-inflammasome-dependent cell death. Several possible mechanisms could enable mitosis without the induction of AIM2 inflammasome-dependent cell death.

One possibility is the transcriptional downregulation of important inflammasome components during cell division. The expression of AIM2 inflammasome components might oscillate in parallel with the cell cycle. Before nuclear envelope break down, the expression of AIM2 inflammasome components is temporarily downregulated and the DNA is not recognized by AIM2. Instead of transcriptional downregulation of AIM2 inflammasome components, an AIM2 inflammasome inhibitor could be specifically expressed during mitosis.

Alternatively, the expression of AIM2 inflammasome components is absent in proliferative cells and only expressed in fully differentiated cells, as these cells do not divide anymore. However, this is less likely, given that primary murine bone marrow derived macrophages (BMDMs) undergo a few cell divisions in cell culture without activating an AIM2 inflammasome. Nevertheless, we cannot ensure that cell culture observations fully resemble the in vivo conditions.

Transcriptional regulation of AIM2 inflammasome activation can be analyzed by first arresting cells at a specific point in their cell cycle. Afterwards the synchronized cells are released from cell cycle arrest and the cellular transcript and protein abundances are analyzed at different time points after release [563]. With this method, transcriptional and translational regulation of known AIM2 inflammasome components can be followed during cell cycle. However, it is difficult to identify new AIM2 inflammasome regulators during mitosis, as transcript and protein abundances globally change over the cellular life cycle. Consequently, hundreds of potential AIM2 inflammasome regulators are detected in these analyses and therefore the discrimination between true- and false positives is difficult.

Therefore, the experimental set up to identify new regulators of AIM2 activation during mitosis is a bit more complicated. I would perform a CRISPR screen in *Aim2*-deficient cells, which express AIM2 under an inducible promoter, but express ASC-mCherry constitutively. *Aim2*-deficiency during the production of the CRISPR knockout cells ensures that cells do not die during this process as cells are dividing and the screen is looking for inhibitors of AIM2-dependent cell death

during mitosis. Following the generation of the CRISPR knock out cells, they are synchronized in respect to their cell cycle and AIM2 expression is induced before cells are released from cell cycle arrest. During mitosis, cells with a mutation in an AIM2 regulatory gene activate AIM2 and form an ASC speck. As we express ASC-mCherry in all cells, the appearance of a red ASC speck is used as a readout. The ASC-positive cells are sorted by FACS and their genome is sequenced to identify the gene that inhibits AIM2 activation during mitosis.
Another possibility for AIM2 inhibition during mitosis might originate from the nuclear DNA itself. AIM2 recognizes 4 base pairs in the big DNA groove [165]. It is known that the DNA bases cytosine and adenine are methylated in eukaryotes and prokaryotes [564]. During DNA replication, the newly synthesized DNA strand is not methylated and the DNA is present in a hemimethylated state. Therefore, the time window between DNA replication and DNA methylation could serve as limiting step for AIM2 activation. However, several research groups have shown that DNA replication and methylation are not temporally distinguishable [565, 566]. Thus, it could be more likely that DNA condensation during mitosis switches DNA into a conformation that cannot be recognized by AIM2. Indeed it was shown that the condensation state of DNA negatively correlates with transcription efficiency [567].
To test the hypothesis of DNA modification, one could use surface plasmon resonance (SPR) [568], which measures binding capacities of a surface-immobilized protein to a soluble interaction partner. To measure AIM2-DNA binding, I would immobilize the HIN200 domain of AIM2 on the surface of the SPR and analyze DNA from different time points during cell cycle for their AIM2 binding ability. With SPR, not only the interaction but also the strength of the interaction between AIM2 and DNA is measured. The comparison of binding-competent and binding in-competent DNA should determine the specific DNA modifications or conformations that enable or inhibit AIM2 binding.
A third possibility for AIM2 inhibition during mitosis could be the segregation or compartmentalization of important AIM2 inflammasome components. Three recent publications have shown that NEK7 is essential for NLRP3 oligomerization and thereby NLRP3 inflammasome activation [289, 290, 539]. In addition, NEK7 is involved in mitotic spindle formation [569]. Moreover, NLRP3 is activated by perturbations of cell integrity, thus NLRP3 can be activated during mitosis. Given that NEK7 is involved in mitosis, the authors propose that NEK7 is not available for NLRP3-dependent inflammasome activation during mitosis. A similar mechanism could hold true in AIM2-dependent inflammasome activation where a protein, that is normally required for AIM2 inflammasome activation, has a specific mitotic function and is therefore not able to assist AIM2 inflammasome activation.
Taken together, AIM2 is activated by cytosol-accessible dsDNA. During mitosis, the nuclear envelope breaks down and nuclear DNA has access to the cytosol, where AIM2 recognizes the DNA and induces AIM2 inflammasome-dependent cell death. To prevent this, dividing cells have mechanisms to inhibit AIM2 activation, however these mechanisms are completely unknown. In this paragraph, three dif-

ferent mechanisms to prevent AIM2 activation during mitosis have been described. However, these are not exclusive and many more mechanisms could result in AIM2 inflammasome inhibition during mitosis.
Moreover, AIM2 belongs to the family of PYHIN proteins, which all possess a PYD and one or several HIN200 domains. Some of them are localized to the nucleus (such as IFI16) and reported to bind dsDNA [570]. However, a recent publication shows that only the HIN200 domain of AIM2 and IFI16 binds to dsDNA [168]. Therefore it would be important to determine under which circumstances the AIM2 and IFI16 HIN200 domain binds dsDNA and why the HIN200 domains of other PYHIN proteins do not bind dsDNA.
Moreover, as described in chapter I, section 1.2, there are other cytosolic DNA sensors which result in the induction of pro-inflammatory genes. In principle, these DNA sensors need to be silenced during mitosis, otherwise the organism induces an inflammatory response with every cell division. Constant inflammation is definitely not in favor of an organism and thus tight regulation of nuclear DNA recognition in the cytosol during mitosis is a very important but poorly understood mechanism.

References

[1] Horvath P. and Barrangou R. CRISPR/Cas, the Immune System of Bacteria and Archaea. *Science*, 327(5962):167–170, 2010.

[2] Desjardins M., Houde M. and Gagnon E. Phagocytosis: the convoluted way from nutrition to adaptive immunity. *Immunological Reviews*, 207(1):158–165, 2005.

[3] Dzik J. M. The ancestry and cumulative evolution of immune reactions. *Acta Biochimica Polonica*, 57(4):443–466, 2010.

[4] Janeway C. Approaching the Asymptote? Evolution and Revolution in Immunology. *Cold Spring Harbor Symposia on Quantitative Biology*, 54:1–13, 1989.

[5] Kumar H., Kawai T. and Akira S. Pathogen Recognition by the Innate Immune System. *International Reviews of Immunology*, 30(1):16–34, 2011.

[6] Litman G. W., Rast J. P. and Fugmann S. D. The origins of vertebrate adaptive immunity. *Nat Rev Immunol*, 10(8):543–553, 2010.

[7] Tonegawa S. Somatic generation of antibody diversity. *Nature*, 302(5909):575–581, 1983.

[8] Medzhitov R. and Jr. C. A. J. Innate Immunity: The Virtues of a Nonclonal System of Recognition. *Cell*, 91(3):295 – 298, 1997.

[9] Kimbrell D. A. and Beutler B. The evolution and genetics of innate immunity. *Nat Rev Genet*, 2(4):256–267, 2001.

[10] Metchnikoff E. *Immunity in Infective Diseases*. 1905.

[11] Ehrlich P. *On Immunity with Special Reference to Cell Life*. 1899.

[12] Buchmann K. Evolution of Innate Immunity: Clues from Invertebrates via Fish to Mammals. *Frontiers in Immunology*, 5:459–, 2014.

[13] Ganz T. Defensins: antimicrobial peptides of innate immunity. *Nat Rev Immunol*, 3(9):710–720, 2003.

[14] Freeley S., Kemper C. and Le Friec G. The ins and outs of complement-driven immune responses. *Immunological Reviews*, 274(1):16–32, 2016.

[15] Strainic M. G., Liu J., Huang D., An F., Lalli P. N., Muqim N., Shapiro V. S., Dubyak G., Heeger P. S. and Medof M. E. Locally Produced Complement Fragments C5a and C3a Provide Both Costimulatory and Survival Signals to Naive CD4+ T Cells. *Immunity*, 28(3):425 – 435, 2008.

[16] Lett-Brown M. A. and Leonard E. J. Histamine-Induced Inhibition of Normal Human Basophil Chemotaxis to C5a. *The Journal of Immunology*, 118(3):815–818, 1977.

[17] Ehrengruber T. D. D.,MU; Geiser. Activation of human neutrophils by C3a and C5A Comparison of the effects on shape changes, chemotaxis, secretion, and respiratory burst. *FEBS Letters*, 346(2-3):181–184, 1994.

[18] Wang L. D. and Wagers A. J. Dynamic niches in the origination and differentiation of haematopoietic stem cells. *Nat Rev Mol Cell Biol*, 12(10):643–655, 2011.

[19] Lai A. Y. and Kondo M. Asymmetrical lymphoid and myeloid lineage commitment in multipotent hematopoietic progenitors. *Journal of Experimental Medicine*, 203(8):1867–1873, 2006.

[20] Katsura Y. Redefinition of lymphoid progenitors. *Nat Rev Immunol*, 2(2):127–132, 2002.

[21] Ye M. and Graf T. Early decisions in lymphoid development. *Current Opinion in Immunology*, 19(2):123 – 128, 2007.

[22] Ceredig R., Rolink A. G. and Brown G. Models of haematopoiesis: seeing the wood for the trees. *Nat Rev Immunol*, 9(4):293–300, 2009.

[23] Gasteiger G. and Rudensky A. Y. Interactions between innate and adaptive lymphocytes. *Nat Rev Immunol*, 14(9):631–639, 2014.

[24] Jakubzick C., Gautier E., Gibbings S., Sojka D., Schlitzer A., Johnson T., Ivanov S., Duan Q., Bala S., Condon T., vanRooijen N., Grainger J., Belkaid Y., Maayan A., Riches D., Yokoyama W., Ginhoux F., Henson P. and Randolph G. Minimal Differentiation of Classical Monocytes as They Survey Steady-State Tissues and Transport Antigen to Lymph Nodes. *Immunity*, 39(3):599 – 610, 2013.

[25] Tsou C.-L., Peters W., Si Y., Slaymaker S., Aslanian A. M., Weisberg S. P., Mack M. and Charo I. F. Critical roles for CCR2 and MCP-3 in monocyte mobilization from bone marrow and recruitment to inflammatory sites. *The Journal of Clinical Investigation*, 117(4):902–909, 2007.

[26] Tamoutounour S., Guilliams M., Montanana-Sanchis F., Liu H., Terhorst D., Malosse C., Pollet E., Ardouin L., Luche H., Sanchez C., Dalod M., Malissen B. and Henri S. Origins and Functional Specialization of Macrophages and of Conventional and Monocyte-Derived Dendritic Cells in Mouse Skin. *Immunity*, 39(5):925 – 938, 2013.

[27] Epelman S., Lavine K., Beaudin A., Sojka D., Carrero J., Calderon B., Brija T., Gautier E., Ivanov S., Satpathy A., Schilling J., Schwendener R., Sergin I., Razani B., Forsberg E., Yokoyama W., Unanue E., Colonna M., Randolph G. and Mann D. Embryonic and Adult-Derived Resident Cardiac Macrophages Are Maintained through Distinct Mechanisms at Steady State and during Inflammation. *Immunity*, 40(1):91 – 104, 2014.

[28] Yona S., Kim K.-W., Wolf Y., Mildner A., Varol D., Breker M., Strauss-Ayali D., Viukov S., Guilliams M., Misharin A., Hume D., Perlman H., Malissen B., Zelzer E. and Jung S. Fate Mapping Reveals Origins and Dynamics of Monocytes and Tissue Macrophages under Homeostasis. *Immunity*, 38(1):79 – 91, 2013.

[29] Auffray C., Fogg D., Garfa M., Elain G., Join-Lambert O., Kayal S., Sarnacki S., Cumano A., Lauvau G. and Geissmann F. Monitoring of Blood Vessels and Tissues by a Population of Monocytes with Patrolling Behavior. *Science*, 317(5838):666–670, 2007.

[30] Kratofil R. M., Kubes P. and Deniset J. F. Monocyte Conversion During Inflammation and InjuryHighlights. *Arteriosclerosis, Thrombosis, and Vascular Biology*, 37(1):35–42, 2016.

[31] Wong K. L., Tai J. J.-Y., Wong W.-C., Han H., Sem X., Yeap W.-H., Kourilsky P. and Wong S.-C. Gene expression profiling reveals the defining features of the classical, intermediate, and nonclassical human monocyte subsets. *Blood*, 118(5):e16–e31, 2011.

[32] Shi C. and Pamer E. G. Monocyte recruitment during infection and inflammation. *Nat Rev Immunol*, 11(11):762–774, 2011.

[33] Kaufmann S. and Dorhoi A. Molecular Determinants in Phagocyte-Bacteria Interactions. *Immunity*, 44(3):476 – 491, 2016.

[34] Lavin Y., Winter D., Blecher-Gonen R., David E., Keren-Shaul H., Merad M., Jung S. and Amit I. Tissue-Resident Macrophage Enhancer Landscapes Are Shaped by the Local Microenvironment. *Cell*, 159(6):1312 – 1326, 2014.

[35] Ajami B., Bennett J. L., Krieger C., Tetzlaff W. and Rossi F. M. V. Local self-renewal can sustain CNS microglia maintenance and function throughout adult life. *Nat Neurosci*, 10(12):1538–1543, 2007.

[36] Ginhoux F. and Guilliams M. Tissue-Resident Macrophage Ontogeny and Homeostasis. *Immunity*, 44(3):439 – 449, 2016.

[37] van Furth R., Cohn Z. A., Hirsch J. G., Humphrey J. H., Spector W. G. and Langevoort H. L. The mononuclear phagocyte system: a new classification of macrophages, monocytes, and their precursor cells. *Bulletin of the World Health Organization*, 46(6):845–852, 1972.

[38] Bain C. C., Bravo-Blas A., Scott C. L., Gomez Perdiguero E., Geissmann F., Henri S., Malissen B., Osborne L. C., Artis D. and Mowat A. M. Constant replenishment from circulating monocytes maintains the macrophage pool in the intestine of adult mice. *Nat Immunol*, 15(10):929–937, 2014.

[39] Calderon B., Carrero J. A., Ferris S. T., Sojka D. K., Moore L., Epelman S., Murphy K. M., Yokoyama W. M., Randolph G. J. and Unanue E. R. The pancreas anatomy conditions the origin and properties of resident macrophages. *Journal of Experimental Medicine*, 212(10):1497–1512, 2015.

[40] Kono H. and Rock K. L. How dying cells alert the immune system to danger. *Nat Rev Immunol*, 8(4):279–289, 2008.

[41] Erwig L.-P. and Henson P. M. Immunological Consequences of Apoptotic Cell Phagocytosis. *The American Journal of Pathology*, 171(1):2 – 8, 2007.

[42] Mackaness G. B. CELLULAR RESISTANCE TO INFECTION. *Journal of Experimental Medicine*, 116(3):381–406, 1962.

[43] Gordon S. Alternative activation of macrophages. *Nat Rev Immunol*, 3(1):23–35, 2003.

[44] Trinchieri G. Interleukin-12 and the regulation of innate resistance and adaptive immunity. *Nat Rev Immunol*, 3(2):133–146, 2003.

[45] Gerber J. S. and Mosser D. M. Reversing Lipopolysaccharide Toxicity by Ligating the Macrophage FcÎş Receptors. *The Journal of Immunology*, 166(11):6861–6868, 2001.

[46] Dale D. C., Boxer L. and Liles W. C. The phagocytes: neutrophils and monocytes. *Blood*, 112(4):935–945, 2008.

[47] Loke P., Gallagher I., Nair M. G., Zang X., Brombacher F., Mohrs M., Allison J. P. and Allen J. E. Alternative Activation Is an Innate Response to Injury That Requires CD4+ T Cells to be Sustained during Chronic Infection. *The Journal of Immunology*, 179(6):3926–3936, 2007.

[48] O'Shea J. J. and Murray P. J. Cytokine Signaling Modules in Inflammatory Responses. *Immunity*, 28(4):477 – 487, 2008.

[49] Kreider T., Anthony R. M., Jr. J. F. U. and Gause W. C. Alternatively activated macrophages in helminth infections. *Current Opinion in Immunology*, 19(4):448 – 453, 2007.

[50] Edwards J. P., Zhang X., Frauwirth K. A. and Mosser D. M. Biochemical and functional characterization of three activated macrophage populations. *Journal of Leukocyte Biology*, 80(6):1298–1307, 2006.

[51] Mosser D. M. and Edwards J. P. Exploring the full spectrum of macrophage activation. *Nat Rev Immunol*, 8(12):958–969, 2008.

[52] Steinman R. M. and Cohn Z. A. IDENTIFICATION OF A NOVEL CELL TYPE IN PERIPHERAL LYMPHOID ORGANS OF MICE. *Journal of Experimental Medicine*, 137(5):1142–1162, 1973.

[53] Steinman R. M. Decisions About Dendritic Cells: Past, Present, and Future. *Annual Review of Immunology*, 30(1):1–22, 2012.

[54] Merad M., Sathe P., Helft J., Miller J. and Mortha A. The Dendritic Cell Lineage: Ontogeny and Function of Dendritic Cells and Their Subsets in the Steady State and the Inflamed Setting. *Annual Review of Immunology*, 31(1):563–604, 2013.

[55] Merad M., Manz M. G., Karsunky H., Wagers A., Peters W., Charo I., Weissman I. L., Cyster J. G. and Engleman E. G. Langerhans cells renew in the skin throughout life under steady-state conditions. *Nat Immunol*, 3(12):1135–1141, 2002.

[56] Chang-Rodriguez S., Hoetzenecker W., Schwaerzler C., Biedermann T., Saeland S. and Elbe-Buerger A. Fetal and neonatal murine skin harbors Langerhans cell precursors. *Journal of Leukocyte Biology*, 77(3):352–360, 2005.

[57] Ginhoux F., Liu K., Helft J., Bogunovic M., Greter M., Hashimoto D., Price J., Yin N., Bromberg J., Lira S. A., Stanley E. R., Nussenzweig M. and Merad M. The origin and development of nonlymphoid tissue CD103+ DCs. *Journal of Experimental Medicine*, 206(13):3115–3130, 2009.

[58] Liu K., Waskow C., Liu X., Yao K., Hoh J. and Nussenzweig M. Origin of dendritic cells in peripheral lymphoid organs of mice. *Nat Immunol*, 8(6):578–583, 2007.

[59] Banchereau J. and Steinman R. M. Dendritic cells and the control of immunity. *Nature*, 392(6673):245–252, 1998.

[60] FÃűrster R., Braun A. and Worbs T. Lymph node homing of T cells and dendritic cells via afferent lymphatics. *Trends in Immunology*, 33(6):271 – 280, 2012.

[61] Segura E. and Villadangos J. A. Antigen presentation by dendritic cells in vivo. *Current Opinion in Immunology*, 21(1):105 – 110, 2009.

[62] Lieschke G., Grail D., Hodgson G., Metcalf D., Stanley E., Cheers C., Fowler K., Basu S., Zhan Y. and Dunn A. Mice lacking granulocyte colony-stimulating factor have chronic neutropenia, granulocyte and macrophage progenitor cell deficiency, and impaired neutrophil mobilization. *Blood*, 84(6):1737–1746, 1994.

[63] Dale D. C., Liles W. C., Llewellyn C. and Price T. H. Effects of granulocyte-macrophage colony-stimulating factor (GM-CSF) on neutrophil kinetics and function in normal human volunteers. *American Journal of Hematology*, 57(1):7–15, 1998.

[64] Huber A., Kunkel S., Todd R. and Weiss S. Regulation of transendothelial neutrophil migration by endogenous interleukin-8. *Science*, 254(5028):99–102, 1991.

[65] Zimmerman G. A., Prescott S. M. and McIntyre T. M. Endothelial cell interactions with granulocytes: tethering and signaling molecules. *Immunology Today*, 13(3):93 – 100, 1992.

[66] Allen R. C., Stevens P. R., Price T. H., Chatta G. S. and Dale D. C. In Vivo Effects of Recombinant Human Granulocyte Colony-Stimulating Factor on Neutrophil Oxidative Functions in Normal Human Volunteers. *Journal of Infectious Diseases*, 175(5):1184–1192, 1997.

[67] Simon H.-U. Neutrophil apoptosis pathways and their modifications in inflammation. *Immunological Reviews*, 193(1):101–110, 2003.

[68] Crowley C. A., Curnutte J. T., Rosin R. E., Andre-Schwartz J., Gallin J. I., Klempner M., Snyderman R., Southwick F. S., Stossel T. P. and Babior B. M. An Inherited Abnormality of Neutrophil Adhesion. *New England Journal of Medicine*, 302(21):1163–1168, 1980.

[69] Novais F. O., Santiago R. C., Bafica A., Khouri R., Afonso L., Borges V. M., Brodskyn C., Barral-Netto M., Barral A. and de Oliveira C. I. Neutrophils and Macrophages Cooperate in Host Resistance against Leishmania braziliensis Infection. *The Journal of Immunology*, 183(12):8088–8098, 2009.

[70] Mantovani A., Cassatella M. A., Costantini C. and Jaillon S. Neutrophils in the activation and regulation of innate and adaptive immunity. *Nat Rev Immunol*, 11(8):519–531, 2011.

[71] Ganz T., Selsted M. E., Szklarek D., Harwig S. S., Daher K., Bainton D. F. and Lehrer R. I. Defensins. Natural peptide antibiotics of human neutrophils. *The Journal of Clinical Investigation*, 76(4):1427–1435, 1985.

[72] Elsbach P. and Weiss J. Role of the bactericidal/permeability-increasing protein in host defence. *Current Opinion in Immunology*, 10(1):45 – 49, 1998.

[73] Spitznagel J. K. Antibiotic proteins of human neutrophils. *The Journal of Clinical Investigation*, 86(5):1381–1386, 1990.

[74] Babior B. M., Curnutte J. T. and McMurrich B. J. The particulate superoxide-forming system from human neutrophils. Properties of the system and further evidence supporting its participation in the respiratory burst. *The Journal of Clinical Investigation*, 58(4):989–996, 1976.

[75] Klebanoff S. J. Myeloperoxidase-Halide-Hydrogen Peroxide Antibacterial System. *Journal of Bacteriology*, 95(6):2131–2138, 1968.

[76] Jaillon S., Galdiero M. R., Del Prete D., Cassatella M. A., Garlanda C. and Mantovani A. Neutrophils in innate and adaptive immunity. *Seminars in Immunopathology*, 35(4):377–394, 2013.

[77] Klebanoff S. J. Myeloperoxidase: friend and foe. *Journal of Leukocyte Biology*, 77(5):598–625, 2005.

[78] Diefenbach A., Colonna M. and Koyasu S. Development, Differentiation, and Diversity of Innate Lymphoid Cells. *Immunity*, 41(3):354 – 365, 2014.

[79] Artis D. and Spits H. The biology of innate lymphoid cells. *Nature*, 517(7534):293–301, 2015.

[80] Sonnenberg G. F. and Artis D. Innate lymphoid cells in the initiation, regulation and resolution of inflammation. *Nat Med*, 21(7):698–708, 2015.

[81] Erick T. K. and Brossay L. Phenotype and functions of conventional and non-conventional {NK} cells. *Current Opinion in Immunology*, 38:67 – 74, 2016.

[82] Fuchs A., Vermi W., Lee J., Lonardi S., Gilfillan S., Newberry R., Cella M. and Colonna M. Intraepithelial Type 1 Innate Lymphoid Cells Are a Unique Subset of IL-12- and IL-15-Responsive IFN-gamma-Producing Cells. *Immunity*, 38(4):769 – 781, 2013.

[83] Bernink J. H., Peters C. P., Munneke M., te Velde A. A., Meijer S. L., Weijer K., Hreggvidsdottir H. S., Heinsbroek S. E., Legrand N., Buskens C. J., Bemelman W. A., Mjosberg J. M. and Spits H. Human type 1 innate lymphoid cells accumulate in inflamed mucosal tissues. *Nat Immunol*, 14(3):221–229, 2013.

[84] Neill D. R., Wong S. H., Bellosi A., Flynn R. J., Daly M., Langford T. K. A., Bucks C., Kane C. M., Fallon P. G., Pannell R., Jolin H. E. and McKenzie A. N. J. Nuocytes represent a new innate effector leukocyte that mediates type-2 immunity. *Nature*, 464(7293):1367–1370, 2010.

[85] Price A. E., Liang H.-E., Sullivan B. M., Reinhardt R. L., Eisley C. J., Erle D. J. and Locksley R. M. Systemically dispersed innate IL13 expressing cells in type 2 immunity. *Proceedings of the National Academy of Sciences*, 107(25):11489–11494, 2010.

[86] Satoh-Takayama N., Vosshenrich C. A., Lesjean-Pottier S., Sawa S., Lochner M., Rattis F., Mention J.-J., Thiam K., Cerf-Bensussan N., Mandelboim O., Eberl G. and Santo J. P. D. Microbial Flora Drives Interleukin 22 Production in Intestinal NKp46+ Cells that Provide Innate Mucosal Immune Defense. *Immunity*, 29(6):958 – 970, 2008.

[87] Buonocore S., Ahern P. P., Uhlig H. H., Ivanov I. I., Littman D. R., Maloy K. J. and Powrie F. Innate lymphoid cells drive interleukin-23-dependent innate intestinal pathology. *Nature*, 464(7293):1371–1375, 2010.

[88] Zheng Y., Valdez P. A., Danilenko D. M., Hu Y., Sa S. M., Gong Q., Abbas A. R., Modrusan Z., Ghilardi N., de Sauvage F. J. and Ouyang W. Interleukin-22 mediates early host defense against attaching and effacing bacterial pathogens. *Nat Med*, 14(3):282–289, 2008.

[89] Sonnenberg G. F., Fouser L. A. and Artis D. Border patrol: regulation of immunity, inflammation and tissue homeostasis at barrier surfaces by IL-22. *Nat Immunol*, 12(5):383–390, 2011.

[90] Voehringer D. Protective and pathological roles of mast cells and basophils. *Nat Rev Immunol*, 13(5):362–375, 2013.

[91] Migalovich-Sheikhet H., Friedman S., Mankuta D. and Levi-Schaffer F. Novel Identified Receptors on Mast Cells. *Frontiers in Immunology*, 3:238–, 2012.

[92] Karasuyama H., Mukai K., Obata K., Tsujimura Y. and Wada T. Nonredundant Roles of Basophils in Immunity. *Annual Review of Immunology*, 29(1):45–69, 2011.

[93] LICHTENSTEIN L. M. and BOCHNER B. S. The Role of Basophils in Asthmaa. *Annals of the New York Academy of Sciences*, 629(1):48–61, 1991.

[94] da Silva E. Z. M., Jamur M. C. and Oliver C. Mast Cell Function. *Journal of Histochemistry & Cytochemistry*, 62(10):698–738, 2014.

[95] Rothenberg M. E., Mishra A., Brandt E. B. and Hogan S. P. Gastrointestinal eosinophils. *Immunological Reviews*, 179(1):139–155, 2001.

[96] Chu V. T., Frohlich A., Steinhauser G., Scheel T., Roch T., Fillatreau S., Lee J. J., Lohning M. and Berek C. Eosinophils are required for the maintenance of plasma cells in the bone marrow. *Nat Immunol*, 12(2):151–159, 2011.

[97] Chu V., Beller A., Rausch S., Strandmark J., Zaenker M., Arbach O., Kruglov A. and Berek C. Eosinophils Promote Generation and Maintenance of Immunoglobulin-A-Expressing Plasma Cells and Contribute to Gut Immune Homeostasis. *Immunity*, 40(4):582 – 593, 2014.

[98] Jung Y. and Rothenberg M. E. Roles and Regulation of Gastrointestinal Eosinophils in Immunity and Disease. *The Journal of Immunology*, 193(3):999–1005, 2014.

[99] Gleich G. J. Mechanisms of eosinophil-associated inflammation. *Journal of Allergy and Clinical Immunology*, 105(4):651 – 663, 2000.

[100] Yousefi S., Gold J. A., Andina N., Lee J. J., Kelly A. M., Kozlowski E., Schmid I., Straumann A., Reichenbach J., Gleich G. J. and Simon H.-U. Catapult-like release of mitochondrial DNA by eosinophils contributes to antibacterial defense. *Nat Med*, 14(9):949–953, 2008.

[101] Vance R. E., Isberg R. R. and Portnoy D. A. Patterns of Pathogenesis: Discrimination of Pathogenic and Nonpathogenic Microbes by the Innate Immune System. *Cell Host & Microbe*, 6(1):10 – 21, 2009.

[102] Venegas C. and Heneka M. T. Danger-associated molecular patterns in Alzheimers disease. *Journal of Leukocyte Biology*, 101(1):87–98, 2017.

[103] Matzinger P. Tolerance, Danger, and the Extended Family. *Annual Review of Immunology*, 12(1):991–1045, 1994.

[104] Gallo P. M. and Gallucci S. The Dendritic Cell Response to Classic, Emerging, and Homeostatic Danger Signals. Implications for Autoimmunity. *Frontiers in Immunology*, 4:138–, 2013.

[105] Gasser S., Orsulic S., Brown E. J. and Raulet D. H. The DNA damage pathway regulates innate immune system ligands of the NKG2D receptor. *Nature*, 436(7054):1186–1190, 2005.

[106] Brubaker S. W., Bonham K. S., Zanoni I. and Kagan J. C. Innate Immune Pattern Recognition: A Cell Biological Perspective. *Annual Review of Immunology*, 33(1):257–290, 2015.

[107] Broz P. and Monack D. M. Newly described pattern recognition receptors team up against intracellular pathogens. *Nat Rev Immunol*, 13(8):551–565, 2013.

[108] Palm N. W. and Medzhitov R. Pattern recognition receptors and control of adaptive immunity. *Immunological Reviews*, 227(1):221–233, 2009.

[109] Leifer C. A. and Medvedev A. E. Molecular mechanisms of regulation of Toll-like receptor signaling. *Journal of Leukocyte Biology*, 100(5):927–941, 2016.

[110] Kobe B. and Kajava A. V. The leucine-rich repeat as a protein recognition motif. *Current Opinion in Structural Biology*, 11(6):725 – 732, 2001.

[111] Gay N. J., Symmons M. F., Gangloff M. and Bryant C. E. Assembly and localization of Toll-like receptor signalling complexes. *Nat Rev Immunol*, 14(8):546–558, 2014.

[112] Hemmi H., Kaisho T., Takeuchi O., Sato S., Sanjo H., Hoshino K., Horiuchi T., Tomizawa H., Takeda K. and Akira S. Small anti-viral compounds activate immune cells via the TLR7 MyD88-dependent signaling pathway. *Nat Immunol*, 3(2):196–200, 2002.

[113] Alexopoulou L., Holt A. C., Medzhitov R. and Flavell R. A. Recognition of double-stranded RNA and activation of NF-kB by Toll-like receptor 3. *Nature*, 413(6857):732–738, 2001.

[114] Hayashi F., Smith K. D., Ozinsky A., Hawn T. R., Yi E. C., Goodlett D. R., Eng J. K., Akira S., Underhill D. M. and Aderem A. The innate immune response to bacterial flagellin is mediated by Toll-like receptor 5. *Nature*, 410(6832):1099–1103, 2001.

[115] Jin M. S., Kim S. E., Heo J. Y., Lee M. E., Kim H. M., Paik S.-G., Lee H. and Lee J.-O. Crystal Structure of the TLR1-TLR2 Heterodimer Induced by Binding of a Tri-Acylated Lipopeptide. *Cell*, 130(6):1071 – 1082, 2007.

[116] O'Neill L. A. J. and Bowie A. G. The family of five: TIR-domain-containing adaptors in Toll-like receptor signalling. *Nat Rev Immunol*, 7(5):353–364, 2007.

[117] Geijtenbeek T. B. H. and Gringhuis S. I. Signalling through C-type lectin receptors: shaping immune responses. *Nat Rev Immunol*, 9(7):465–479, 2009.

[118] Zelensky A. N. and Gready J. E. The C-type lectin-like domain superfamily. *FEBS Journal*, 272(24):6179–6217, 2005.

[119] Taylor P. R., Tsoni S. V., Willment J. A., Dennehy K. M., Rosas M., Findon H., Haynes K., Steele C., Botto M., Gordon S. and Brown G. D. Dectin-1 is required for beta-glucan recognition and control of fungal infection. *Nat Immunol*, 8(1):31–38, 2007.

[120] Hoving J. C., Wilson G. J. and Brown G. D. Signalling C-Type lectin receptors, microbial recognition and immunity. *Cellular Microbiology*, 16(2):185–194, 2014.

[121] Fuller G. L. J., Williams J. A. E., Tomlinson M. G., Eble J. A., Hanna S. L., Poehlmann S., Suzuki-Inoue K., Ozaki Y., Watson S. P. and Pearce A. C. The C-type Lectin Receptors CLEC-2 and Dectin-1, but Not DC-SIGN, Signal via a Novel YXXL-dependent Signaling Cascade. *Journal of Biological Chemistry*, 282(17):12397–12409, 2007.

[122] Kerrigan A. M. and Brown G. D. Syk-coupled C-type lectin receptors that mediate cellular activation via single tyrosine based activation motifs. *Immunological Reviews*, 234(1):335–352, 2010.

[123] Gorjestani S., Darnay B. G. and Lin X. Tumor Necrosis Factor Receptor-associated Factor 6 (TRAF6) and TGFbeta-activated Kinase 1 (TAK1) Play Essential Roles in the C-type Lectin Receptor Signaling in Response to Candida albicans Infection. *Journal of Biological Chemistry*, 287(53):44143–44150, 2012.

[124] Saijo S., Ikeda S., Yamabe K., Kakuta S., Ishigame H., Akitsu A., Fujikado N., Kusaka T., Kubo S., hyun Chung S., Komatsu R., Miura N., Adachi Y., Ohno N., Shibuya K., Yamamoto N., Kawakami K., Yamasaki S., Saito T., Akira S. and Iwakura Y. Dectin-2 Recognition of alpha-Mannans and Induction of Th17 Cell Differentiation Is Essential for Host Defense against Candida albicans. *Immunity*, 32(5):681 – 691, 2010.

[125] Ritter M., Gross O., Kays S., Ruland J., Nimmerjahn F., Saijo S., Tschopp J., Layland L. E. and Prazeres da Costa C. Schistosoma mansoni triggers Dectin-2, which activates the Nlrp3 inflammasome and alters adaptive immune responses. *Proceedings of the National Academy of Sciences*, 107(47):20459–20464, 2010.

[126] Salazar F., Sewell H. F., Shakib F. and Ghaemmaghami A. M. The role of lectins in allergic sensitization and allergic disease. *Journal of Allergy and Clinical Immunology*, 132(1):27 – 36, 2013.

[127] Ting J. P.-Y., Lovering R. C., Alnemri E. S., Bertin J., Boss J. M., Davis B. K., Flavell R. A., Girardin S. E., Godzik A., Harton J. A., Hoffman H. M., Hugot J.-P., Inohara N., MacKenzie A., Maltais L. J., Nunez G., Ogura Y., Otten L. A., Philpott D., Reed J. C., Reith W., Schreiber S., Steimle V. and Ward P. A. The NLR Gene Family: A Standard Nomenclature. *Immunity*, 28(3):285 – 287, 2008.

[128] Franchi L., Warner N., Viani K. and Nunez G. Function of Nod-like Receptors in Microbial Recognition and Host Defense. *Immunological reviews*, 227(1):106–128, 2009.

[129] Harton J. A. and Ting J. P.-Y. Class II Transactivator: Mastering the Art of Major Histocompatibility Complex Expression. *Molecular and Cellular Biology*, 20(17):6185–6194, 2000.

[130] Girardin S. E., Boneca I. G., Viala J., Chamaillard M., Labigne A., Thomas G., Philpott D. J. and Sansonetti P. J. Nod2 Is a General Sensor of Peptidoglycan through Muramyl Dipeptide (MDP) Detection. *Journal of Biological Chemistry*, 278(11):8869–8872, 2003.

[131] Girardin S. E., Boneca I. G., Carneiro L. A. M., Antignac A., Jéhanno M., Viala J., Tedin K., Taha M.-K., Labigne A., Zäthringer U., Coyle A. J., DiStefano P. S., Bertin J., Sansonetti P. J. and Philpott D. J. Nod1 Detects a Unique Muropeptide from Gram-Negative Bacterial Peptidoglycan. *Science*, 300(5625):1584–1587, 2003.

[132] Girardin S. E., Tournebize R., Mavris M., Page A.-L., Li X., Stark G. R., Bertin J., DiStefano P. S., Yaniv M., Sansonetti P. J. and Philpott D. J. CARD4/Nod1 mediates NF-kB and JNK activation by invasive Shigella flexneri. *EMBO reports*, 2(8):736–742, 2001.

[133] Kobayashi K., Inohara N., Hernandez L. D., Galan J. E., Nunez G., Janeway C. A., Medzhitov R. and Flavell R. A. RICK/Rip2/CARDIAK mediates signalling for receptors of the innate and adaptive immune systems. *Nature*, 416(6877):194–199, 2002.

[134] Travassos L. H., Carneiro L. A. M., Ramjeet M., Hussey S., Kim Y.-G., Magalhaes J. G., Yuan L., Soares F., Chea E., Le Bourhis L., Boneca I. G., Allaoui A., Jones N. L., Nunez G., Girardin S. E. and Philpott D. J. Nod1 and Nod2 direct autophagy by recruiting ATG16L1 to the plasma membrane at the site of bacterial entry. *Nat Immunol*, 11(1):55–62, 2010.

[135] Lei Y., Wen H., Yu Y., Taxman D., Zhang L., Widman D., Swanson K., Wen K.-W., Damania B., Moore C., Giguere P., Siderovski D., Hiscott J., Razani B., Semenkovich C., Chen X. and Ting J.-Y. The Mitochondrial Proteins NLRX1 and TUFM Form a Complex that Regulates Type I Interferon and Autophagy. *Immunity*, 36(6):933 – 946, 2012.

[136] Schneider M., Zimmermann A. G., Roberts R. A., Zhang L., Swanson K. V., Wen H., Davis B. K., Allen I. C., Holl E. K., Ye Z., Rahman A. H., Conti B. J., Eitas T. K., Koller B. H. and Ting J. P.-Y. The innate immune sensor NLRC3 attenuates Toll-like receptor signaling via modification of the signaling adaptor TRAF6 and transcription factor NF-kB. *Nat Immunol*, 13(9):823–831, 2012.

[137] Mariathasan S., Newton K., Monack D. M., Vucic D., French D. M., Lee W. P., Roose-Girma M., Erickson S. and Dixit V. M. Differential activation of the inflammasome by caspase-1 adaptors ASC and Ipaf. *Nature*, 430(6996):213–218, 2004.

[138] Meissner T. B., Li A., Biswas A., Lee K.-H., Liu Y.-J., Bayir E., Iliopoulos D., van den Elsen P. J. and Kobayashi K. S. NLR family member NLRC5 is a transcriptional regulator of MHC class I genes. *Proceedings of the National Academy of Sciences*, 107(31):13794–13799, 2010.

[139] Martinon F., Burns K. and Tschopp J. The Inflammasome: A Molecular Platform Triggering Activation of Inflammatory Caspases and Processing of proIL-1beta. *Molecular Cell*, 10(2):417 – 426, 2002.

[140] Martinon F., Agostini L., Meylan E. and Tschopp J. Identification of Bacterial Muramyl Dipeptide as Activator of the NALP3/Cryopyrin Inflammasome. *Current Biology*, 14(21):1929 – 1934, 2004.

[141] Vladimer G., Weng D., Paquette S., Vanaja S., Rathinam V., Aune M., Conlon J., Burbage J., Proulx M., Liu Q., Reed G., Mecsas J., Iwakura Y., Bertin J., Goguen J., Fitzgerald K. and Lien E. The {NLRP12} Inflammasome Recognizes Yersinia pestis. *Immunity*, 37(1):96 – 107, 2012.

[142] Khare S., Dorfleutner A., Bryan N., Yun C., Radian A., deAlmeida L., Rojanasakul Y. and Stehlik C. An NLRP7-Containing Inflammasome Mediates Recognition of Microbial Lipopeptides in Human Macrophages. *Immunity*, 36(3):464 – 476, 2012.

[143] Elinav E., Strowig T., Kau A., Henao-Mejia J., Thaiss C., Booth C., Peaper D., Bertin J., Eisenbarth S., Gordon J. and Flavell R. {NLRP6} Inflammasome Regulates Colonic Microbial Ecology and Risk for Colitis. *Cell*, 145(5):745 – 757, 2011.

[144] Minkiewicz J., de Rivero Vaccari J. P. and Keane R. W. Human astrocytes express a novel NLRP2 inflammasome. *Glia*, 61(7):1113–1121, 2013.

[145] Wang P., Zhu S., Yang L., Cui S., Pan W., Jackson R., Zheng Y., Rongvaux A., Sun Q., Yang G., Gao S., Lin R., You F., Flavell R. and Fikrig E. Nlrp6 regulates intestinal antiviral innate immunity. *Science*, 350(6262):826–830, 2015.

[146] Anand P. K., Malireddi R. K. S., Lukens J. R., Vogel P., Bertin J., Lamkanfi M. and Kanneganti T.-D. NLRP6 negatively regulates innate immunity and host defence against bacterial pathogens. *Nature*, 488(7411):389–393, 2012.

[147] Bruey J. M., Bruey-Sedano N., Newman R., Chandler S., Stehlik C. and Reed J. C. PAN1/NALP2/PYPAF2, an Inducible Inflammatory Mediator That Regulates NF-kB and Caspase-1 Activation in Macrophages. *Journal of Biological Chemistry*, 279(50):51897–51907, 2004.

[148] Jounai N., Kobiyama K., Shiina M., Ogata K., Ishii K. J. and Takeshita F. NLRP4 Negatively Regulates Autophagic Processes through an Association with Beclin1. *The Journal of Immunology*, 186(3):1646–1655, 2011.

[149] Cui J., Li Y., Zhu L., Liu D., Songyang Z., Wang H. Y. and Wang R.-F. NLRP4 negatively regulates type I interferon signaling by targeting the kinase TBK1 for degradation via the ubiquitin ligase DTX4. *Nat Immunol*, 13(4):387–395, 2012.

[150] Yoneyama M., Kikuchi M., Matsumoto K., Imaizumi T., Miyagishi M., Taira K., Foy E., Loo Y.-M., Gale M., Akira S., Yonehara S., Kato A. and Fujita T. Shared and Unique Functions of the DExD/H-Box Helicases RIG-I, MDA5, and LGP2 in Antiviral Innate Immunity. *The Journal of Immunology*, 175(5):2851–2858, 2005.

[151] Yoneyama M., Kikuchi M., Natsukawa T., Shinobu N., Imaizumi T., Miyagishi M., Taira K., Akira S. and Fujita T. The RNA helicase RIG-I has an essential function in double-stranded RNA-induced innate antiviral responses. *Nat Immunol*, 5(7):730–737, 2004.

[152] Rothenfusser S., Goutagny N., DiPerna G., Gong M., Monks B. G., Schoenemeyer A., Yamamoto M., Akira S. and Fitzgerald K. A. The RNA Helicase Lgp2 Inhibits TLR-Independent Sensing of Viral Replication by Retinoic Acid-Inducible Gene-I. *The Journal of Immunology*, 175(8):5260–5268, 2005.

[153] Hornung V., Ellegast J., Kim S., Brzózka K., Jung A., Kato H., Poeck H., Akira S., Conzelmann K.-K., Schlee M., Endres S. and Hartmann G. 5'-Triphosphate RNA Is the Ligand for RIG-I. *Science*, 314(5801):994–997, 2006.

[154] Uzri D. and Gehrke L. Nucleotide Sequences and Modifications That Determine RIG-I/RNA Binding and Signaling Activities. *Journal of Virology*, 83(9):4174–4184, 2009.

[155] Pichlmair A., Schulz O., Tan C.-P., Rehwinkel J., Kato H., Takeuchi O., Akira S., Way M., Schiavo G. and Reis e Sousa C. Activation of MDA5 Requires Higher-Order RNA Structures Generated during Virus Infection. *Journal of Virology*, 83(20):10761–10769, 2009.

[156] Kato H., Takeuchi O., Mikamo-Satoh E., Hirai R., Kawai T., Matsushita K., Hiiragi A., Dermody T. S., Fujita T. and Akira S. Length-dependent recognition of double-stranded ribonucleic acids by retinoic acid-inducible gene-I and melanoma differentiation-associated gene 5. *The Journal of Experimental Medicine*, 205(7):1601–1610, 2008.

[157] Kawai T., Takahashi K., Sato S., Coban C., Kumar H., Kato H., Ishii K. J., Takeuchi O. and Akira S. IPS-1, an adaptor triggering RIG-I- and Mda5-mediated type I interferon induction. *Nat Immunol*, 6(10):981–988, 2005.

[158] Liu H., Loo Y.-M., Horner S., Zornetzer G., Katze M. and Jr. M. G. The Mitochondrial Targeting Chaperone 14-3-3epsilon Regulates a RIG-I Translocon that Mediates Membrane Association and Innate Antiviral Immunity. *Cell Host & Microbe*, 11(5):528 – 537, 2012.

[159] Hou F., Sun L., Zheng H., Skaug B., Jiang Q.-X. and Chen Z. MAVS Forms Functional Prion-like Aggregates to Activate and Propagate Antiviral Innate Immune Response. *Cell*, 146(3):448 – 461, 2011.

[160] Liu S., Chen J., Cai X., Wu J., Chen X., Wu Y.-T., Sun L. and Chen Z. J. MAVS recruits multiple ubiquitin E3 ligases to activate antiviral signaling cascades. *eLife*, 2:e00785–, 2013.

[161] Burckstummer T., Baumann C., Bluml S., Dixit E., Durnberger G., Jahn H., Planyavsky M., Bilban M., Colinge J., Bennett K. L. and Superti-Furga G. An orthogonal proteomic-genomic screen identifies AIM2 as a cytoplasmic DNA sensor for the inflammasome. *Nat Immunol*, 10(3):266–272, 2009.

[162] Hornung V., Ablasser A., Charrel-Dennis M., Bauernfeind F., Horvath G., Caffrey D. R., Latz E. and Fitzgerald K. A. AIM2 recognizes cytosolic dsDNA and forms a caspase-1-activating inflammasome with ASC. *Nature*, 458(7237):514–518, 2009.

[163] Fernandes-Alnemri T., Yu J.-W., Datta P., Wu J. and Alnemri E. S. AIM2 activates the inflammasome and cell death in response to cytoplasmic DNA. *Nature*, 458(7237):509–513, 2009.

[164] Roberts T. L., Idris A., Dunn J. A., Kelly G. M., Burnton C. M., Hodgson S., Hardy L. L., Garceau V., Sweet M. J., Ross I. L., Hume D. A. and Stacey K. J. HIN-200 Proteins Regulate Caspase Activation in Response to Foreign Cytoplasmic DNA. *Science*, 323(5917):1057–1060, 2009.

[165] Jin T., Perry A., Jiang J., Smith P., Curry J., Unterholzner L., Jiang Z., Horvath G., Rathinam V., Johnstone R., Hornung V., Latz E., Bowie A., Fitzgerald K. and Xiao T. Structures of the HIN Domain:DNA Complexes Reveal Ligand Binding and Activation Mechanisms of the AIM2 Inflammasome and IFI16 Receptor. *Immunity*, 36(4):561 – 571, 2012.

[166] Unterholzner L., Keating S. E., Baran M., Horan K. A., Jensen S. B., Sharma S., Sirois C. M., Jin T., Latz E., Xiao T. S., Fitzgerald K. A., Paludan S. R. and Bowie A. G. IFI16 is an innate immune sensor for intracellular DNA. *Nat Immunol*, 11(11):997–1004, 2010.

[167] Storek K. M., Gertsvolf N. A., Ohlson M. B. and Monack D. M. cGAS and Ifi204 Cooperate To Produce Type I IFNs in Response to Francisella Infection. *The Journal of Immunology*, 2015.

[168] Gray E., Winship D., Snyder J., Child S., Geballe A. and Stetson D. The AIM2-like Receptors Are Dispensable for the Interferon Response to Intracellular DNA. *Immunity*, pages –, 2016.

[169] Sun L., Wu J., Du F., Chen X. and Chen Z. J. Cyclic GMP-AMP Synthase Is a Cytosolic DNA Sensor That Activates the Type I Interferon Pathway. *Science*, 339(6121):786–791, 2013.

[170] Diner E., Burdette D., Wilson S., Monroe K., Kellenberger C., Hyodo M., Hayakawa Y., Hammond M. and Vance R. The Innate Immune DNA Sensor cGAS Produces a Noncanonical Cyclic Dinucleotide that Activates Human STING. *Cell Reports*, 3(5):1355 – 1361, 2013.

[171] Ishikawa H., Ma Z. and Barber G. N. STING regulates intracellular DNA-mediated, type I interferon-dependent innate immunity. *Nature*, 461(7265):788–792, 2009.

[172] Zhang X., Wu J., Du F., Xu H., Sun L., Chen Z., Brautigam C., Zhang X. and Chen Z. The Cytosolic DNA Sensor cGAS Forms an Oligomeric Complex with DNA and Undergoes Switch-like Conformational Changes in the Activation Loop. *Cell Reports*, 6(3):421 – 430, 2014.

[173] Chen Q., Sun L. and Chen Z. J. Regulation and function of the cGAS-STING pathway of cytosolic DNA sensing. *Nat Immunol*, 17(10):1142–1149, 2016.

[174] Ishikawa H. and Barber G. N. STING is an endoplasmic reticulum adaptor that facilitates innate immune signalling. *Nature*, 455(7213):674–678, 2008.

[175] Burdette D. L., Monroe K. M., Sotelo-Troha K., Iwig J. S., Eckert B., Hyodo M., Hayakawa Y. and Vance R. E. STING is a direct innate immune sensor of cyclic di-GMP. *Nature*, 478(7370):515–518, 2011.

[176] Wu J., Sun L., Chen X., Du F., Shi H., Chen C. and Chen Z. J. Cyclic GMP-AMP Is an Endogenous Second Messenger in Innate Immune Signaling by Cytosolic DNA. *Science*, 339(6121):826–830, 2013.

[177] Woodward J. J., Iavarone A. T. and Portnoy D. A. c-di-AMP Secreted by Intracellular Listeria monocytogenes Activates a Host Type I Interferon Response. *Science*, 328(5986):1703–1705, 2010.

[178] Dobbs N., Burnaevskiy N., Chen D., Gonugunta V., Alto N. and Yan N. STING Activation by Translocation from the ER Is Associated with Infection and Autoinflammatory Disease. *Cell Host & Microbe*, 18(2):157 – 168, 2015.

[179] Zhong B., Yang Y., Li S., Wang Y.-Y., Li Y., Diao F., Lei C., He X., Zhang L., Tien P. and Shu H.-B. The Adaptor Protein MITA Links Virus-Sensing Receptors to IRF3 Transcription Factor Activation. *Immunity*, 29(4):538 – 550, 2008.

[180] Liu S., Cai X., Wu J., Cong Q., Chen X., Li T., Du F., Ren J., Wu Y.-T., Grishin N. V. and Chen Z. J. Phosphorylation of innate immune adaptor proteins MAVS, STING, and TRIF induces IRF3 activation. *Science*, 347(6227), 2015.

[181] Parvatiyar K., Zhang Z., Teles R. M., Ouyang S., Jiang Y., Iyer S. S., Zaver S. A., Schenk M., Zeng S., Zhong W., Liu Z.-J., Modlin R. L., Liu Y.-j. and Cheng G. The helicase DDX41 recognizes the bacterial secondary messengers cyclic di-GMP and cyclic di-AMP to activate a type I interferon immune response. *Nat Immunol*, 13(12):1155–1161, 2012.

[182] Oshiumi H., Sakai K., Matsumoto M. and Seya T. DEAD/H BOX 3 (DDX3) helicase binds the RIG-I adaptor IPS-1 to up-regulate IFN-beta-inducing potential. *European Journal of Immunology*, 40(4):940–948, 2010.

[183] Medzhitov R., Preston-Hurlburt P. and Janeway C. A. A human homologue of the Drosophila Toll protein signals activation of adaptive immunity. *Nature*, 388(6640):394–397, 1997.

[184] Poltorak A., He X., Smirnova I., Liu M.-Y., Huffel C. V., Du X., Birdwell D., Alejos E., Silva M., Galanos C., Freudenberg M., Ricciardi-Castagnoli P., Layton B. and Beutler B. Defective LPS Signaling in C3H/HeJ and C57BL/10ScCr Mice: Mutations in Tlr4 Gene. *Science*, 282(5396):2085–2088, 1998.

[185] Lemaitre B., Nicolas E., Michaut L., Reichhart J.-M. and Hoffmann J. A. The Dorsoventral Regulatory Gene Cassette spaetzle/Toll/cactus Controls the Potent Antifungal Response in Drosophila Adults. *Cell*, 86(6):973 – 983, 1996.

[186] Gunn J. S. and Ernst R. K. The Structure and Function of Francisella Lipopolysaccharide. *Annals of the New York Academy of Sciences*, 1105:202–218, 2007.

[187] Simons K. and Toomre D. Lipid rafts and signal transduction. *Nat Rev Mol Cell Biol*, 1(1):31–39, 2000.

[188] Kawasaki K., Akashi S., Shimazu R., Yoshida T., Miyake K. and Nishijima M. Mouse Toll-like Receptor 4 MD-2 Complex Mediates Lipopolysaccharide-mimetic Signal Transduction by Taxol. *Journal of Biological Chemistry*, 275(4):2251–2254, 2000.

[189] Meng J., Gong M., Björkbacka H. and Golenbock D. T. Genome-Wide Expression Profiling and Mutagenesis Studies Reveal that Lipopolysaccharide Responsiveness Appears To Be Absolutely Dependent on TLR4 and MD-2 Expression and Is Dependent upon Intermolecular Ionic Interactions. *The Journal of Immunology*, 187(7):3683–3693, 2011.

[190] Schumann R., Leong, Flaggs G., Gray P., Wright S., Mathison J., Tobias P. and Ulevitch R. Structure and function of lipopolysaccharide binding protein. *Science*, 249(4975):1429–1431, 1990.

[191] da Silva Correia J., Soldau K., Christen U., Tobias P. S. and Ulevitch R. J. Lipopolysaccharide Is in Close Proximity to Each of the Proteins in Its Membrane Receptor Complex: TRANSFER FROM CD14 TO TLR4 AND MD-2. *Journal of Biological Chemistry*, 276(24):21129–21135, 2001.

[192] Nagai Y., Akashi S., Nagafuku M., Ogata M., Iwakura Y., Akira S., Kitamura T., Kosugi A., Kimoto M. and Miyake K. Essential role of MD-2 in LPS responsiveness and TLR4 distribution. *Nat Immunol*, 3(7):667–672, 2002.

[193] Kitchens R. L., Wang P.-y. and Munford R. S. Bacterial Lipopolysaccharide Can Enter Monocytes Via Two CD14-Dependent Pathways. *The Journal of Immunology*, 161(10):5534–5545, 1998.

[194] Yamamoto M., Sato S., Hemmi H., Sanjo H., Uematsu S., Kaisho T., Hoshino K., Takeuchi O., Kobayashi M., Fujita T., Takeda K. and Akira S. Essential role for TIRAP in activation of the signalling cascade shared by TLR2 and TLR4. *Nature*, 420(6913):324–329, 2002.

[195] Horng T., Barton G. M., Flavell R. A. and Medzhitov R. The adaptor molecule TIRAP provides signalling specificity for Toll-like receptors. *Nature*, 420(6913):329–333, 2002.

[196] Fitzgerald K. A., Palsson-McDermott E. M., Bowie A. G., Jefferies C. A., Mansell A. S., Brady G., Brint E., Dunne A., Gray P., Harte M. T., McMurray D., Smith D. E., Sims J. E., Bird T. A. and O'Neill L. A. J. Mal (MyD88-adapter-like) is required for Toll-like receptor-4 signal transduction. *Nature*, 413(6851):78–83, 2001.

[197] Bonham K., Orzalli M., Hayashi K., Wolf A., Glanemann C., Weninger W., Iwasaki A., Knipe D. and Kagan J. A Promiscuous Lipid-Binding Protein Diversifies the Subcellular Sites of Toll-like Receptor Signal Transduction. *Cell*, 156(4):705 – 716, 2014.

[198] Lin S.-C., Lo Y.-C. and Wu H. Helical assembly in the MyD88-IRAK4-IRAK2 complex in TLR/IL-1R signalling. *Nature*, 465(7300):885–890, 2010.

[199] Motshwene P. G., Moncrieffe M. C., Grossmann J. G., Kao C., Ayaluru M., Sandercock A. M., Robinson C. V., Latz E. and Gay N. J. An Oligomeric Signaling Platform Formed by the Toll-like Receptor Signal Transducers MyD88 and IRAK-4. *Journal of Biological Chemistry*, 284(37):25404–25411, 2009.

[200] Suzuki N., Suzuki S., Duncan G. S., Millar D. G., Wada T., Mirtsos C., Takada H., Wakeham A., Itie A., Li S., Penninger J. M., Wesche H., Ohashi P. S., Mak T. W. and Yeh W.-C. Severe impairment of interleukin-1 and Toll-like receptor signalling in mice lacking IRAK-4. *Nature*, 416(6882):750–756, 2002.

[201] Kawagoe T., Sato S., Matsushita K., Kato H., Matsui K., Kumagai Y., Saitoh T., Kawai T., Takeuchi O. and Akira S. Sequential control of Toll-like receptor-dependent responses by IRAK1 and IRAK2. *Nat Immunol*, 9(6):684–691, 2008.

[202] Deng L., Wang C., Spencer E., Yang L., Braun A., You J., Slaughter C., Pickart C. and Chen Z. J. Activation of the IkB Kinase Complex by TRAF6 Requires a Dimeric Ubiquitin-Conjugating Enzyme Complex and a Unique Polyubiquitin Chain. *Cell*, 103(2):351 – 361, 2000.

[203] Emmerich C. H., Ordureau A., Strickson S., Arthur J. S. C., Pedrioli P. G. A., Komander D. and Cohen P. Activation of the canonical IKK complex by K63/M1-linked hybrid ubiquitin chains. *Proceedings of the National Academy of Sciences*, 110(38):15247–15252, 2013.

[204] Wang C., Deng L., Hong M., Akkaraju G. R., Inoue J.-i. and Chen Z. J. TAK1 is a ubiquitin-dependent kinase of MKK and IKK. *Nature*, 412(6844):346–351, 2001.

[205] Yaron A., Gonen H., Alkalay I., Hatzubai A., Jung S., Beyth S., Mercurio F., Manning A. M., Ciechanover A. and Ben-Neriah Y. Inhibition of NF-kappa-B cellular function via specific targeting of the I-kappa-B-ubiquitin ligase. *The EMBO Journal*, 16(21):6486–6494, 1997.

[206] Karin M. and Ben-Neriah Y. Phosphorylation Meets Ubiquitination: The Control of NF-kB Activity. *Annual Review of Immunology*, 18(1):621–663, 2000.

[207] Hayden M. S. and Ghosh S. Signaling to NF-kB. *Genes & Development*, 18(18):2195–2224, 2004.

[208] Hess J., Angel P. and Schorpp-Kistner M. AP-1 subunits: quarrel and harmony among siblings. *Journal of Cell Science*, 117(25):5965–5973, 2004.

[209] Roy S., Karmakar M. and Pearlman E. CD14 Mediates Toll-like Receptor 4 (TLR4) Endocytosis and Spleen Tyrosine Kinase (Syk) and Interferon Regulatory Transcription Factor 3 (IRF3) Activation in Epithelial Cells and Impairs Neutrophil Infiltration and Pseudomonas aeruginosa Killing in Vivo. *Journal of Biological Chemistry*, 289(2):1174–1182, 2014.

[210] Zanoni I., Ostuni R., Marek L., Barresi S., Barbalat R., Barton G., Granucci F. and Kagan J. CD14 Controls the LPS-Induced Endocytosis of Toll-like Receptor 4. *Cell*, 147(4):868 – 880, 2011.

[211] Enokizono Y., Kumeta H., Funami K., Horiuchi M., Sarmiento J., Yamashita K., Standley D. M., Matsumoto M., Seya T. and Inagaki F. Structures and interface mapping of the TIR domain-containing adaptor molecules involved in interferon signaling. *Proceedings of the National Academy of Sciences*, 110(49):19908–19913, 2013.

[212] Hacker H., Redecke V., Blagoev B., Kratchmarova I., Hsu L.-C., Wang G. G., Kamps M. P., Raz E., Wagner H., Hacker G., Mann M. and Karin M. Specificity in Toll-like receptor signalling through distinct effector functions of TRAF3 and TRAF6. *Nature*, 439(7073):204–207, 2006.

[213] Fitzgerald K. A., McWhirter S. M., Faia K. L., Rowe D. C., Latz E., Golenbock D. T., Coyle A. J., Liao S.-M. and Maniatis T. IKK[epsi] and TBK1 are essential components of the IRF3 signaling pathway. *Nat Immunol*, 4(5):491–496, 2003.

[214] Yamamoto M., Sato S., Hemmi H., Hoshino K., Kaisho T., Sanjo H., Takeuchi O., Sugiyama M., Okabe M., Takeda K. and Akira S. Role of Adaptor TRIF in the MyD88-Independent Toll-Like Receptor Signaling Pathway. *Science*, 301(5633):640–643, 2003.

[215] Yamamoto M., Sato S., Hemmi H., Uematsu S., Hoshino K., Kaisho T., Takeuchi O., Takeda K. and Akira S. TRAM is specifically involved in the Toll-like receptor 4-mediated MyD88-independent signaling pathway. *Nat Immunol*, 4(11):1144–1150, 2003.

[216] Kanistanon D., Powell D. A., Hajjar A. M., Pelletier M. R., Cohen I. E., Way S. S., Skerrett S. J., Wang X., Raetz C. R. H. and Ernst R. K. Role of Francisella Lipid A Phosphate Modification in Virulence and Long-Term Protective Immune Responses. *Infection and Immunity*, 80(3):943–951, 2011.

[217] Li Y., Powell D. A., Shaffer S. A., Rasko D. A., Pelletier M. R., Leszyk J. D., Scott A. J., Masoudi A., Goodlett D. R., Wang X., Raetz C. R. H. and Ernst R. K. LPS remodeling is an evolved survival strategy for bacteria. *Proceedings of the National Academy of Sciences of the United States of America*, 109(22):8716–8721, 2012.

[218] Isaacs A. and Lindenmann J. Virus Interference. I. The Interferon. *Proceedings of the Royal Society of London B: Biological Sciences*, 147(927):258–267, 1957.

[219] Isaacs A., Lindenmann J. and Valentine R. C. Virus Interference. II. Some Properties of Interferon. *Proceedings of the Royal Society of London B: Biological Sciences*, 147(927):268–273, 1957.

[220] de Weerd N. A., Samarajiwa S. A. and Hertzog P. J. Type I Interferon Receptors: Biochemistry and Biological Functions. *Journal of Biological Chemistry*, 282(28):20053–20057, 2007.

[221] Rubinstein M., Levy W. P., Moschera J. A., Lai C.-Y., Hershberg R. D., Bartlett R. T. and Pestka S. Human leukocyte interferon: Isolation and characterization of several molecular forms. *Archives of Biochemistry and Biophysics*, 210(1):307 – 318, 1981.

[222] Schneider W. M., Chevillotte M. D. and Rice C. M. Interferon-Stimulated Genes: A Complex Web of Host Defenses. *Annual Review of Immunology*, 32(1):513–545, 2014.

[223] MacMicking J. D. Interferon-inducible effector mechanisms in cell-autonomous immunity. *Nat Rev Immunol*, 12(5):367–382, 2012.

[224] McNab F., Mayer-Barber K., Sher A., Wack A. and O'Garra A. Type I interferons in infectious disease. *Nat Rev Immunol*, 15(2):87–103, 2015.

[225] Pestka S., Krause C. D. and Walter M. R. Interferons, interferon-like cytokines, and their receptors. *Immunological Reviews*, 202(1):8–32, 2004.

[226] Kalie E., Jaitin D. A., Podoplelova Y., Piehler J. and Schreiber G. The Stability of the Ternary Interferon-Receptor Complex Rather than the Affinity to the Individual Subunits Dictates Differential Biological Activities. *Journal of Biological Chemistry*, 283(47):32925–32936, 2008.

[227] Moraga I., Harari D., Schreiber G., Uze G. and Pellegrini S. Receptor Density Is Key to the Alpha2/Beta Interferon Differential Activities. *Molecular and Cellular Biology*, 29(17):4778–4787, 2009.

[228] Uzé G., Schreiber G., Piehler J. and Pellegrini S. *The Receptor of the Type I Interferon Family*, pages 71–95. Springer Berlin Heidelberg, Berlin, Heidelberg, 2007.

[229] Heim M., Kerr I., Stark G. and Darnell J. Contribution of STAT SH2 groups to specific interferon signaling by the Jak-STAT pathway. *Science*, 267(5202):1347–1349, 1995.

[230] Schindler C., Shuai K., Prezioso V. and Darnell J. Interferon-dependent tyrosine phosphorylation of a latent cytoplasmic transcription factor. *Science*, 257(5071):809–813, 1992.

[231] Shuai K., Stark G., Kerr I. and Darnell J. A single phosphotyrosine residue of Stat91 required for gene activation by interferon-gamma. *Science*, 261(5129):1744–1746, 1993.

[232] Fagerlund R., Melen K., Kinnunen L. and Julkunen I. Arginine/Lysine-rich Nuclear Localization Signals Mediate Interactions between Dimeric STATs and Importin alpha5. *Journal of Biological Chemistry*, 277(33):30072–30078, 2002.

[233] Fu X. Y., Kessler D. S., Veals S. A., Levy D. E. and Darnell J. E. ISGF3, the transcriptional activator induced by interferon alpha, consists of multiple interacting polypeptide chains. *Proceedings of the National Academy of Sciences*, 87(21):8555–8559, 1990.

[234] Levy D. E., Kessler D. S., Pine R. and Darnell J. E. Cytoplasmic activation of ISGF3, the positive regulator of interferon-alpha-stimulated transcription, reconstituted in vitro. *Genes & Development*, 3(9):1362–1371, 1989.

[235] Levy D. E., Kessler D. S., Pine R., Reich N. and Darnell J. E. Interferon-induced nuclear factors that bind a shared promoter element correlate with positive and negative transcriptional control. *Genes & Development*, 2(4):383–393, 1988.

[236] Levy D., Larner A., Chaudhuri A., Babiss L. E. and Darnell J. E. Interferon-stimulated transcription: isolation of an inducible gene and identification of its regulatory region. *Proceedings of the National Academy of Sciences*, 83(23):8929–8933, 1986.

[237] Sheppard P., Kindsvogel W., Xu W., Henderson K., Schlutsmeyer S., Whitmore T. E., Kuestner R., Garrigues U., Birks C., Roraback J., Ostrander C., Dong D., Shin J., Presnell S., Fox B., Haldeman B., Cooper E., Taft D., Gilbert T., Grant F. J., Tackett M., Krivan W., McKnight G., Clegg C., Foster D. and Klucher K. M. IL-28, IL-29 and their class II cytokine receptor IL-28R. *Nat Immunol*, 4(1):63–68, 2003.

[238] Prokunina-Olsson L., Muchmore B., Tang W., Pfeiffer R. M., Park H., Dickensheets H., Hergott D., Porter-Gill P., Mumy A., Kohaar I., Chen S., Brand N., Tarway M., Liu L., Sheikh F., Astemborski J., Bonkovsky H. L., Edlin B. R., Howell C. D., Morgan T. R., Thomas D. L., Rehermann B., Donnelly R. P. and O'Brien T. R. A variant upstream of IFNL3 (IL28B) creating a new interferon gene IFNL4 is associated with impaired clearance of hepatitis C virus. *Nat Genet*, 45(2):164–171, 2013.

[239] Sommereyns C., Paul S., Staeheli P. and Michiels T. IFN-Lambda Is Expressed in a Tissue-Dependent Fashion and Primarily Acts on Epithelial Cells In Vivo. *PLOS Pathogens*, 4(3):1–12, 2008.

[240] Bolen C. R., Ding S., Robek M. D. and Kleinstein S. H. Dynamic expression profiling of type I and type III interferon-stimulated hepatocytes reveals a stable hierarchy of gene expression. *Hepatology*, 59(4):1262–1272, 2014.

[241] Schoenborn J. R. and Wilson C. B. Regulation of Interferon gamma During Innate and Adaptive Immune Responses. volume 96 of *Advances in Immunology*, pages 41 – 101. Academic Press, 2007.

[242] Schroder K., Hertzog P. J., Ravasi T. and Hume D. A. Interferon-gamma: an overview of signals, mechanisms and functions. *Journal of Leukocyte Biology*, 75(2):163–189, 2004.

[243] Walter M. R., Windsor W. T., Nagabhushan T. L., Lundell D. J., Lunn C. A., Zauodny P. J. and Narula S. K. Crystal structure of a complex between interferon-gamma and its soluble high-affinity receptor. *Nature*, 376(6537):230–235, 1995.

[244] Valente G., Ozmen L., Novelli F., Geuna M., Palestro G., Forni G. and Garotta G. Distribution of interferon-Îş receptor in human tissues. *European Journal of Immunology*, 22(9):2403–2412, 1992.

[245] Greenlund A. C., Morales M. O., Viviano B. L., Yan H., Krolewski J. and Schreiber R. D. Stat recruitment by tyrosine-phosphorylated cytokine receptors: An ordered reversible affinity-driven process. *Immunity*, 2(6):677 – 687, 1995.

[246] Igarashi K., Garotta G., Ozmen L., Ziemiecki A., Wilks A. F., Harpur A. G., Larner A. C. and Finbloom D. S. Interferon-gamma induces tyrosine phosphorylation of interferon-gamma receptor and regulated association of protein tyrosine kinases, Jak1 and Jak2, with its receptor. *Journal of Biological Chemistry*, 269(20):14333–14336, 1994.

[247] DECKER T., KOVARIK P. and MEINKE A. GAS Elements: A Few Nucleotides with a Major Impact on Cytokine-Induced Gene Expression. *Journal of Interferon & Cytokine Research*, 17(3):121–134, 1997.

[248] Kerr I. M. and Stark G. R. The control of interferon-inducible gene expression. *FEBS Letters*, 285(2):194–198, 1991.

[249] Broz P. and Dixit V. M. Inflammasomes: mechanism of assembly, regulation and signalling. *Nat Rev Immunol*, advance online publication:–, 2016.

[250] Latz E., Xiao T. S. and Stutz A. Activation and regulation of the inflammasomes. *Nat Rev Immunol*, 13(6):397–411, 2013.

[251] von Moltke J., Ayres J. S., Kofoed E. M., Chavarria-Smith J. and Vance R. E. Recognition of Bacteria by Inflammasomes. *Annual Review of Immunology*, 31(1):73–106, 2013.

[252] Broz P., von Moltke J., Jones J. W., Vance R. E. and Monack D. M. Differential Requirement for Caspase-1 Autoproteolysis in Pathogen-Induced Cell Death and Cytokine Processing. *Cell Host & Microbe*, 8(6):471 – 483, 2010.

[253] Fink S. L. and Cookson B. T. Apoptosis, Pyroptosis, and Necrosis: Mechanistic Description of Dead and Dying Eukaryotic Cells. *Infection and Immunity*, 73(4):1907–1916, 2005.

[254] Jorgensen I. and Miao E. A. Pyroptotic cell death defends against intracellular pathogens. *Immunological Reviews*, 265(1):130–142, 2015.

[255] Broz P. and Monack D. M. Molecular mechanisms of inflammasome activation during microbial infections. *Immunological Reviews*, 243(1):174–190, 2011.

[256] Thornberry N. A., Bull H. G., Calaycay J. R., Chapman K. T., Howard A. D., Kostura M. J., Miller D. K., Molineaux S. M., Weidner J. R., Aunins J., Elliston K. O., Ayala J. M., Casano F. J., Chin J., Ding G. J.-F., Egger L. A., Gaffney E. P., Limjuco G., Palyha O. C., Raju S. M., Rolando A. M., Salley J. P., Yamin T.-T., Lee T. D., Shively J. E., MacCross M., Mumford R. A., Schmidt J. A. and Tocci M. J. A novel heterodimeric cysteine protease is required for interleukin-1beta processing in monocytes. *Nature*, 356(6372):768–774, 1992.

[257] Dinarello C. A. Immunological and Inflammatory Functions of the Interleukin-1 Family. *Annual Review of Immunology*, 27(1):519–550, 2009.

[258] Shi J., Zhao Y., Wang K., Shi X., Wang Y., Huang H., Zhuang Y., Cai T., Wang F. and Shao F. Cleavage of GSDMD by inflammatory caspases determines pyroptotic cell death. *Nature*, 526(7575):660–665, 2015.

[259] Kayagaki N., Stowe I. B., Lee B. L., O'Rourke K., Anderson K., Warming S., Cuellar T., Haley B., Roose-Girma M., Phung Q. T., Liu P. S., Lill J. R., Li H., Wu J., Kummerfeld S., Zhang J., Lee W. P., Snipas S. J., Salvesen G. S., Morris L. X., Fitzgerald L., Zhang Y., Bertram E. M., Goodnow C. C. and Dixit V. M. Caspase-11 cleaves gasdermin D for non-canonical inflammasome signalling. *Nature*, 526(7575):666–671, 2015.

[260] He W.-t., Wan H., Hu L., Chen P., Wang X., Huang Z., Yang Z.-H., Zhong C.-Q. and Han J. Gasdermin D is an executor of pyroptosis and required for interleukin-1[beta] secretion. *Cell Res*, 25(12):1285–1298, 2015.

[261] Aglietti R. A., Estevez A., Gupta A., Ramirez M. G., Liu P. S., Kayagaki N., Ciferri C., Dixit V. M. and Dueber E. C. GsdmD p30 elicited by caspase-11 during pyroptosis forms pores in membranes. *Proceedings of the National Academy of Sciences*, 113(28):7858–7863, 2016.

[262] Ding J., Wang K., Liu W., She Y., Sun Q., Shi J., Sun H., Wang D.-C. and Shao F. Pore-forming activity and structural autoinhibition of the gasdermin family. *Nature*, advance online publication:–, 2016.

[263] Sborgi L., Rühl S., Mulvihill E., Pipercevic J., Heilig R., Stahlberg H., Farady C. J., Müller D. J., Broz P. and Hiller S. GSDMD membrane pore formation constitutes the mechanism of pyroptotic cell death. *The EMBO Journal*, 2016.

[264] Liu X., Zhang Z., Ruan J., Pan Y., Magupalli V. G., Wu H. and Lieberman J. Inflammasome-activated gasdermin D causes pyroptosis by forming membrane pores. *Nature*, 535(7610):153–158, 2016.

[265] Miao E. A., Alpuche-Aranda C. M., Dors M., Clark A. E., Bader M. W., Miller S. I. and Aderem A. Cytoplasmic flagellin activates caspase-1 and secretion of interleukin 1[beta] via Ipaf. *Nat Immunol*, 7(6):569–575, 2006.

[266] Franchi L., Amer A., Body-Malapel M., Kanneganti T.-D., Ozoren N., Jagirdar R., Inohara N., Vandenabeele P., Bertin J., Coyle A., Grant E. P. and Nunez G. Cytosolic flagellin requires Ipaf for activation of caspase-1 and interleukin 1[beta] in salmonella-infected macrophages. *Nat Immunol*, 7(6):576–582, 2006.

[267] Miao E. A., Mao D. P., Yudkovsky N., Bonneau R., Lorang C. G., Warren S. E., Leaf I. A. and Aderem A. Innate immune detection of the type III secretion apparatus through the NLRC4 inflammasome. *Proceedings of the National Academy of Sciences*, 107(7):3076–3080, 2010.

[268] Zhao Y., Yang J., Shi J., Gong Y.-N., Lu Q., Xu H., Liu L. and Shao F. The NLRC4 inflammasome receptors for bacterial flagellin and type III secretion apparatus. *Nature*, 477(7366):596–600, 2011.

[269] Tenthorey J., Kofoed E., Daugherty M., Malik H. and Vance R. Molecular Basis for Specific Recognition of Bacterial Ligands by NAIP/NLRC4 Inflammasomes, 2014.

[270] Kofoed E. M. and Vance R. E. Innate immune recognition of bacterial ligands by NAIPs determines inflammasome specificity. *Nature*, 477(7366):592–595, 2011.

[271] Kofoed E. M. and Vance R. E. NAIPs: Building an innate immune barrier against bacterial pathogens. *BioEssays*, 34(7):589–598, 2012.

[272] Kortmann J., Brubaker S. W. and Monack D. M. Cutting Edge: Inflammasome Activation in Primary Human Macrophages Is Dependent on Flagellin. *The Journal of Immunology*, 195(3):815–819, 2015.

[273] Hu Z., Yan C., Liu P., Huang Z., Ma R., Zhang C., Wang R., Zhang Y., Martinon F., Miao D., Deng H., Wang J., Chang J. and Chai J. Crystal Structure of NLRC4 Reveals Its Autoinhibition Mechanism. *Science*, 341(6142):172–175, 2013.

[274] Halff E. F., Diebolder C. A., Versteeg M., Schouten A., Brondijk T. H. C. and Huizinga E. G. Formation and Structure of a NAIP5-NLRC4 Inflammasome Induced by Direct Interactions with Conserved N- and C-terminal Regions of Flagellin. *Journal of Biological Chemistry*, 287(46):38460–38472, 2012.

[275] Hu Z., Zhou Q., Zhang C., Fan S., Cheng W., Zhao Y., Shao F., Wang H.-W., Sui S.-F. and Chai J. Structural and biochemical basis for induced self-propagation of NLRC4. *Science*, 350(6259):399–404, 2015.

[276] Zhang L., Chen S., Ruan J., Wu J., Tong A. B., Yin Q., Li Y., David L., Lu A., Wang W. L., Marks C., Ouyang Q., Zhang X., Mao Y. and Wu H. Cryo-EM structure of the activated NAIP2-NLRC4 inflammasome reveals nucleated polymerization. *Science*, 2015.

[277] Dick M. S., Sborgi L., Ruehl S., Hiller S. and Broz P. ASC filament formation serves as a signal amplification mechanism for inflammasomes. *Nature Communications*, 7:11929–, 2016.

[278] Qu Y., Misaghi S., Izrael-Tomasevic A., Newton K., Gilmour L. L., Lamkanfi M., Louie S., Kayagaki N., Liu J., Komuves L., Cupp J. E., Arnott D., Monack D. and Dixit V. M. Phosphorylation of NLRC4 is critical for inflammasome activation. *Nature*, 490(7421):539–542, 2012.

[279] Suzuki S., Franchi L., He Y., Munoz-Planillo R., Mimuro H., Suzuki T., Sasakawa C. and Nunez G. Shigella Type III Secretion Protein MxiI Is Recognized by Naip2 to Induce Nlrc4 Inflammasome Activation Independently of Pkc-delta. *PLOS Pathogens*, 10(2):1–12, 2014.

[280] Romberg N., Al Moussawi K., Nelson-Williams C., Stiegler A. L., Loring E., Choi M., Overton J., Meffre E., Khokha M. K., Huttner A. J., West B., Podoltsev N. A., Boggon T. J., Kazmierczak B. I. and Lifton R. P. Mutation of NLRC4 causes a syndrome of enterocolitis and autoinflammation. *Nat Genet*, 46(10):1135–1139, 2014.

[281] Kitamura A., Sasaki Y., Abe T., Kano H. and Yasutomo K. An inherited mutation in NLRC4 causes autoinflammation in human and mice. *Journal of Experimental Medicine*, 211(12):2385–2396, 2014.

[282] Canna S. W., de Jesus A. A., Gouni S., Brooks S. R., Marrero B., Liu Y., DiMattia M. A., Zaal K. J. M., Sanchez G. A. M., Kim H., Chapelle D., Plass N., Huang Y., Villarino A. V., Biancotto A., Fleisher T. A., Duncan J. A., O'Shea J. J., Benseler S., Grom A., Deng Z., Laxer R. M. and Goldbach-Mansky R. An activating NLRC4 inflammasome mutation causes autoinflammation with recurrent macrophage activation syndrome. *Nat Genet*, 46(10):1140–1146, 2014.

[283] Munoz-Planillo R., Kuffa P., Martinez-Colon G., Smith B., Rajendiran T. and Nunez G. K+ Efflux Is the Common Trigger of {NLRP3} Inflammasome Activation by Bacterial Toxins and Particulate Matter. *Immunity*, 38(6):1142 – 1153, 2013.

[284] Yang C.-S., Kim J.-J., Kim T. S., Lee P. Y., Kim S. Y., Lee H.-M., Shin D.-M., Nguyen L. T., Lee M.-S., Jin H. S., Kim K.-K., Lee C.-H., Kim M. H., Park S. G., Kim J.-M., Choi H.-S. and Jo E.-K. Small heterodimer partner interacts with NLRP3 and negatively regulates activation of the NLRP3 inflammasome. *Nat Commun*, 6:–, 2015.

[285] Lu B., Nakamura T., Inouye K., Li J., Tang Y., Lundback P., Valdes-Ferrer S. I., Olofsson P. S., Kalb T., Roth J., Zou Y., Erlandsson-Harris H., Yang H., Ting J. P.-Y., Wang H., Andersson U., Antoine D. J., Chavan S. S., Hotamisligil G. S. and Tracey K. J. Novel role of PKR in inflammasome activation and HMGB1 release. *Nature*, 488(7413):670–674, 2012.

[286] Shenoy A. R., Wellington D. A., Kumar P., Kassa H., Booth C. J., Cresswell P. and MacMicking J. D. GBP5 Promotes NLRP3 Inflammasome Assembly and Immunity in Mammals. *Science*, 336(6080):481–485, 2012.

[287] He Y., Franchi L. and Nunez G. The protein kinase PKR is critical for LPS-induced iNOS production but dispensable for inflammasome activation in macrophages. *European Journal of Immunology*, 43(5):1147–1152, 2013.

[288] Meunier E., Dick M. S., Dreier R. F., Schurmann N., Broz D. K., Warming S., Roose-Girma M., Bumann D., Kayagaki N., Takeda K., Yamamoto M. and Broz P. Caspase-11 activation requires lysis of pathogen-containing vacuoles by IFN-induced GTPases. *Nature*, 509(7500):366–370, 2014.

[289] Schmid-Burgk J. L., Chauhan D., Schmidt T., Ebert T. S., Reinhardt J., Endl E. and Hornung V. A Genome-wide CRISPR (Clustered Regularly Interspaced Short Palindromic Repeats) Screen Identifies NEK7 as an Essential Component of NLRP3 Inflammasome Activation. *Journal of Biological Chemistry*, 291(1):103–109, 2016.

[290] He Y., Zeng M. Y., Yang D., Motro B. and Nunez G. NEK7 is an essential mediator of NLRP3 activation downstream of potassium efflux. *Nature*, 530(7590):354–357, 2016.

[291] Shi J., Gao W. and Shao F. Pyroptosis: Gasdermin-Mediated Programmed Necrotic Cell Death. *Trends in Biochemical Sciences*, pages –, 2016.

[292] Py B., Kim M.-S., Vakifahmetoglu-Norberg H. and Yuan J. Deubiquitination of NLRP3 by BRCC3 Critically Regulates Inflammasome Activity. *Molecular Cell*, 49(2):331 – 338, 2013.

[293] Kim M. L., Chae J. J., Park Y. H., De Nardo D., Stirzaker R. A., Ko H.-J., Tye H., Cengia L., DiRago L., Metcalf D., Roberts A. W., Kastner D. L., Lew A. M., Lyras D., Kile B. T., Croker B. A. and Masters S. L. Aberrant actin depolymerization triggers the pyrin inflammasome and autoinflammatory disease that is dependent on IL-18, not IL-1beta. *Journal of Experimental Medicine*, 212(6):927–938, 2015.

[294] Brydges S. D., Mueller J. L., McGeough M. D., Pena C. A., Misaghi A., Gandhi C., Putnam C. D., Boyle D. L., Firestein G. S., Horner A. A., Soroosh P., Watford W. T., O'Shea J. J., Kastner D. L. and Hoffman H. M. Inflammasome-Mediated Disease Animal Models Reveal Roles for Innate but Not Adaptive Immunity. *Immunity*, 30(6):875 – 887, 2009.

[295] Meng G., Zhang F., Fuss I., Kitani A. and Strober W. A Mutation in the Nlrp3 Gene Causing Inflammasome Hyperactivation Potentiates Th17 Cell-Dominant Immune Responses. *Immunity*, 30(6):860 – 874, 2009.

[296] Talbott J. H. SERUM URATE IN RELATIVES OF GOUTY PATIENTS 12. *The Journal of Clinical Investigation*, 19(4):645–648, 1940.

[297] Martinon F., Petrilli V., Mayor A., Tardivel A. and Tschopp J. Gout-associated uric acid crystals activate the NALP3 inflammasome. *Nature*, 440(7081):237–241, 2006.

[298] Vandanmagsar B., Youm Y.-H., Ravussin A., Galgani J. E., Stadler K., Mynatt R. L., Ravussin E., Stephens J. M. and Dixit V. D. The NLRP3 inflammasome instigates obesity-induced inflammation and insulin resistance. *Nat Med*, 17(2):179–188, 2011.

[299] Youm Y.-H., Adijiang A., Vandanmagsar B., Burk D., Ravussin A. and Dixit V. D. Elimination of the NLRP3-ASC Inflammasome Protects against Chronic Obesity-Induced Pancreatic Damage. *Endocrinology*, 152(11):4039–4045, 2011.

[300] Rathinam V. A. K., Jiang Z., Waggoner S. N., Sharma S., Cole L. E., Waggoner L., Vanaja S. K., Monks B. G., Ganesan S., Latz E., Hornung V., Vogel S. N., Szomolanyi-Tsuda E. and Fitzgerald K. A. The AIM2 inflammasome is essential for host defense against cytosolic bacteria and DNA viruses. *Nat Immunol*, 11(5):395–402, 2010.

[301] Jones J. W., Kayagaki N., Broz P., Henry T., Newton K., O'Rourke K., Chan S., Dong J., Qu Y., Roose-Girma M., Dixit V. M. and Monack D. M. Absent in melanoma 2 is required for innate immune recognition of Francisella tularensis. *Proceedings of the National Academy of Sciences*, 107(21):9771–9776, 2010.

[302] Fernandes-Alnemri T., Yu J.-W., Juliana C., Solorzano L., Kang S., Wu J., Datta P., McCormick M., Huang L., McDermott E., Eisenlohr L., Landel C. P. and Alnemri E. S. The AIM2 inflammasome is critical for innate immunity to Francisella tularensis. *Nat Immunol*, 11(5):385–393, 2010.

[303] Sauer J.-D., Witte C. E., Zemansky J., Hanson B., Lauer P. and Portnoy D. A. Listeria monocytogenes Triggers AIM2-Mediated Pyroptosis upon Infrequent Bacteriolysis in the Macrophage Cytosol. *Cell Host & Microbe*, 7(5):412 – 419, 2010.

[304] Lu A., Li Y., Yin Q., Ruan J., Yu X., Egelman E. and Wu H. Plasticity in PYD assembly revealed by cryo-EM structure of the PYD filament of AIM2. *Cell Discovery*, 1:15013–, 2015.

[305] Dihlmann S., Tao S., Echterdiek F., Herpel E., Jansen L., Chang-Claude J., Brenner H., Hoffmeister M. and Kloor M. Lack of Absent in Melanoma 2 (AIM2) expression in tumor cells is closely associated with poor survival in colorectal cancer patients. *International Journal of Cancer*, 135(10):2387–2396, 2014.

[306] Ponomareva L., Liu H., Duan X., Dickerson E., Shen H., Panchanathan R. and Choubey D. AIM2, an IFN-Inducible Cytosolic DNA Sensor, in the Development of Benign Prostate Hyperplasia and Prostate Cancer. *Molecular Cancer Research*, 11(10):1193–1202, 2013.

[307] Man S., Zhu Q., Zhu L., Liu Z., Karki R., Malik A., Sharma D., Li L., Malireddi R., Gurung P., Neale G., Olsen S., Carter R., McGoldrick D., Wu G., Finkelstein D., Vogel P., Gilbertson R. and Kanneganti T.-D. Critical Role for the DNA Sensor AIM2 in Stem Cell Proliferation and Cancer. *Cell*, 162(1):45 – 58, 2015.

[308] Wilson J. E., Petrucelli A. S., Chen L., Koblansky A. A., Truax A. D., Oyama Y., Rogers A. B., Brickey W. J., Wang Y., Schneider M., Muhlbauer M., Chou W.-C., Barker B. R., Jobin C., Allbritton N. L., Ramsden D. A., Davis B. K. and Ting J. P. Y. Inflammasome-independent role of AIM2 in suppressing colon tumorigenesis via DNA-PK and Akt. *Nat Med*, 21(8):906–913, 2015.

[309] Dihlmann S., Erhart P., Mehrabi A., Nickkholgh A., Lasitschka F., Boeckler D. and Hakimi M. Increased Expression and Activation of Absent in Melanoma 2 Inflammasome Components in Lymphocytic Infiltrates of Abdominal Aortic Aneurysms. *Molecular Medicine*, 20(1):230–237, 2014.

[310] Javierre B. M., Fernandez A. F., Richter J., Al-Shahrour F., Martin-Subero J. I., Rodriguez-Ubreva J., Berdasco M., Fraga M. F., O'Hanlon T. P., Rider L. G., Jacinto F. V., Lopez-Longo F. J., Dopazo J., Forn M., Peinado M. A., Carreno L., Sawalha A. H., Harley J. B., Siebert R., Esteller M., Miller F. W. and Ballestar E. Changes in the pattern of DNA methylation associate with twin discordance in systemic lupus erythematosus. *Genome Research*, 20(2):170–179, 2010.

[311] Dombrowski Y., Peric M., Koglin S., Kammerbauer C., Göß C., Anz D., Simanski M., Gläser R., Harder J., Hornung V., Gallo R. L., Ruzicka T., Besch R. and Schauber J. Cytosolic DNA Triggers Inflammasome Activation in Keratinocytes in Psoriatic Lesions. *Science Translational Medicine*, 3(82):82ra38–82ra38, 2011.

[312] Di Micco A., Frera G., Lugrin J., Jamilloux Y., Hsu E.-T., Tardivel A., De Gassart A., Zaffalon L., Bujisic B., Siegert S., Quadroni M., Broz P., Henry T., Hrycyna C. A. and Martinon F. AIM2 inflammasome is activated by pharmacological disruption of nuclear envelope integrity. *Proceedings of the National Academy of Sciences*, 113(32):E4671–E4680, 2016.

[313] Hesker P. R., Nguyen M., Kovarova M., Ting J. P.-Y. and Koller B. H. Genetic Loss of Murine Pyrin, the Familial Mediterranean Fever Protein, Increases Interleukin-1beta Levels. *PLOS ONE*, 7(11):1–9, 2012.

[314] Chae J. J., Wood G., Masters S. L., Richard K., Park G., Smith B. J. and Kastner D. L. The B30.2 domain of pyrin, the familial Mediterranean fever protein, interacts directly with caspase-1 to modulate IL-1beta production. *Proceedings of the National Academy of Sciences*, 103(26):9982–9987, 2006.

[315] Kimura T., Jain A., Choi S. W., Mandell M. A., Schroder K., Johansen T. and Deretic V. TRIM-mediated precision autophagy targets cytoplasmic regulators of innate immunity. *The Journal of Cell Biology*, 2015.

[316] Chae J., Cho Y.-H., Lee G.-S., Cheng J., Liu P., Feigenbaum L., Katz S. and Kastner D. Gain-of-Function Pyrin Mutations Induce NLRP3 Protein-Independent Interleukin-1beta Activation and Severe Autoinflammation in Mice. *Immunity*, 34(5):755 – 768, 2011.

[317] Xu H., Yang J., Gao W., Li L., Li P., Zhang L., Gong Y.-N., Peng X., Xi J. J., Chen S., Wang F. and Shao F. Innate immune sensing of bacterial modifications of Rho GTPases by the Pyrin inflammasome. *Nature*, 513(7517):237–241, 2014.

[318] Aubert D., Xu H., Yang J., Shi X., Gao W., Li L., Bisaro F., Chen S., Valvano M. and Shao F. A Burkholderia Type VI Effector Deamidates Rho GTPases to Activate the Pyrin Inflammasome and Trigger Inflammation. *Cell Host & Microbe*, 19(5):664 – 674, 2016.

[319] Waite A. L., Schaner P., Hu C., Richards N., Balci-Peynircioglu B., Hong A., Fox M. and Gumucio D. L. Pyrin and ASC Co-Localize to Cellular Sites that Are Rich in Polymerizing Actin. *Experimental Biology and Medicine*, 234(1):40–52, 2009.

[320] Park Y. H., Wood G., Kastner D. L. and Chae J. J. Pyrin inflammasome activation and RhoA signaling in the autoinflammatory diseases FMF and HIDS. *Nat Immunol*, 17(8):914–921, 2016.

[321] Masters S. L., Lagou V., Jéru I., Baker P. J., Van Eyck L., Parry D. A., Lawless D., De Nardo D., Garcia-Perez J. E., Dagley L. F., Holley C. L., Dooley J., Moghaddas F., Pasciuto E., Jeandel P.-Y., Sciot R., Lyras D., Webb A. I., Nicholson S. E., De Somer L., van Nieuwenhove E., Ruuth-Praz J., Copin B., Cochet E., Medlej-Hashim M., Megarbane A., Schroder K., Savic S., Goris A., Amselem S., Wouters C. and Liston A. Familial autoinflammation with neutrophilic dermatosis reveals a regulatory mechanism of pyrin activation. *Science Translational Medicine*, 8(332):332ra45–332ra45, 2016.

[322] Franklin B. S., Bossaller L., De Nardo D., Ratter J. M., Stutz A., Engels G., Brenker C., Nordhoff M., Mirandola S. R., Al-Amoudi A., Mangan M. S., Zimmer S., Monks B. G., Fricke M., Schmidt R. E., Espevik T., Jones B., Jarnicki A. G., Hansbro P. M., Busto P., Marshak-Rothstein A., Hornemann S., Aguzzi A., Kastenmuller W. and Latz E. The adaptor ASC has extracellular and 'prionoid' activities that propagate inflammation. *Nat Immunol*, advance online publication:–, 2014.

[323] Sborgi L., Ravotti F., Dandey V. P., Dick M. S., Mazur A., Reckel S., Chami M., Scherer S., Huber M., Boeckmann A., Egelman E. H., Stahlberg H., Broz P., Meier B. H. and Hiller S. Structure and assembly of the mouse ASC inflammasome by combined NMR spectroscopy and cryo-electron microscopy. *Proceedings of the National Academy of Sciences*, 112(43):13237–13242, 2015.

[324] Lu A., Magupalli V., Ruan J., Yin Q., Atianand M., Vos M. R., Schroeder G., Fitzgerald K., Wu H. and Egelman E. Unified Polymerization Mechanism for the Assembly of ASC-Dependent Inflammasomes. *Cell*, 156(6):1193 – 1206, 2014.

[325] Schmidt F. I., Lu A., Chen J. W., Ruan J., Tang C., Wu H. and Ploegh H. L. A single domain antibody fragment that recognizes the adaptor ASC defines the role of ASC domains in inflammasome assembly. *The Journal of Experimental Medicine*, 2016.

[326] Lin Y.-C., Huang D.-Y., Wang J.-S., Lin Y.-L., Hsieh S.-L., Huang K.-C. and Lin W.-W. Syk is involved in NLRP3 inflammasome-mediated caspase-1 activation through adaptor ASC phosphorylation and enhanced oligomerization. *Journal of Leukocyte Biology*, 97(5):825–835, 2015.

[327] Hara H., Tsuchiya K., Kawamura I., Fang R., Hernandez-Cuellar E., Shen Y., Mizuguchi J., Schweighoffer E., Tybulewicz V. and Mitsuyama M. Phosphorylation of the adaptor ASC acts as a molecular switch that controls the formation of speck-like aggregates and inflammasome activity. *Nat Immunol*, 14(12):1247–1255, 2013.

[328] Martin B. N., Wang C., Willette-Brown J., Herjan T., Gulen M. F., Zhou H., Bulek K., Franchi L., Sato T., Alnemri E. S., Narla G., Zhong X.-P., Thomas J., Klinman D., Fitzgerald K. A., Karin M., Nunez G., Dubyak G., Hu Y. and Li X. IKKalpha negatively regulates ASC-dependent inflammasome activation. *Nat Commun*, 5:–, 2014.

[329] Lee J. Y., Seo D., You J., Chung S., Park J. S., Lee J.-H., Jung S. M., Lee Y. S. and Park S. H. The deubiquitinating enzyme USP50 regulates inflammasome activation through targeting the ASC adaptor protein. *FEBS Letters*, pages n/a–n/a, 2017.

[330] Dorfleutner A., Bryan N. B., Talbott S. J., Funya K. N., Rellick S. L., Reed J. C., Shi X., Rojanasakul Y., Flynn D. C. and Stehlik C. Cellular Pyrin Domain-Only Protein 2 Is a Candidate Regulator of Inflammasome Activation. *Infection and Immunity*, 75(3):1484–1492, 2007.

[331] deAlmeida L., Khare S., Misharin A., Patel R., Ratsimandresy R., Wallin M., Perlman H., Greaves D., Hoffman H., Dorfleutner A. and Stehlik C. The PYRIN Domain-only Protein POP1 Inhibits Inflammasome Assembly and Ameliorates Inflammatory Disease. *Immunity*, 43(2):264 – 276, 2015.

[332] Bedoya F., Sandler L. L. and Harton J. A. Pyrin-Only Protein 2 Modulates NF-kB and Disrupts ASC:CLR Interactions. *The Journal of Immunology*, 178(6):3837–3845, 2007.

[333] Alnemri E. S., Livingston D. J., Nicholson D. W., Salvesen G., Thornberry N. A., Wong W. W. and Yuan J. Human ICE/CED-3 Protease Nomenclature. *Cell*, 87(2):171 –, 1996.

[334] Man S. M. and Kanneganti T.-D. Converging roles of caspases in inflammasome activation, cell death and innate immunity. *Nat Rev Immunol*, 16(1):7–21, 2016.

[335] Kostura M. J., Tocci M. J., Limjuco G., Chin J., Cameron P., Hillman A. G., Chartrain N. A. and Schmidt J. A. Identification of a monocyte specific pre-interleukin 1 beta convertase activity. *Proceedings of the National Academy of Sciences*, 86(14):5227–5231, 1989.

[336] Black R. A., Kronheim S. R. and Sleath P. R. Activation of interleukin- 1beta by a co-induced protease. *FEBS Letters*, 247(2):386–390, 1989.

[337] Sims J. E., Pan Y., Smith D. E., Nicklin M. J., Barton J. L., Bazan J., Kastelein R. A., Busfield S. J., Ford J. E., Lin H., Mulero J. J., Kumar S., Pan J. G. and Young P. R. A new nomenclature for IL-1-family genes. *Trends in Immunology*, 22(10):536 – 537, 2001.

[338] Talabot-Ayer D., Lamacchia C., Gabay C. and Palmer G. Interleukin-33 Is Biologically Active Independently of Caspase-1 Cleavage. *Journal of Biological Chemistry*, 284(29):19420–19426, 2009.

[339] Sims J. E. and Smith D. E. The IL-1 family: regulators of immunity. *Nat Rev Immunol*, 10(2):89–102, 2010.

[340] William P. Arend C. J. G.,Mark Malyak and Gabay C. INTERLEUKIN-1 RECEPTOR ANTAGONIST: Role in Biology. *Annual Review of Immunology*, 16(1):27–55, 1998.

[341] Colotta F., Re F., Muzio M., Bertini R., Polentarutti N., Sironi M., Giri J., Dower S., Sims J. and Mantovani A. Interleukin-1 type II receptor: a decoy target for IL-1 that is regulated by IL-4. *Science*, 261(5120):472–475, 1993.

[342] Shan N.-n., Zhu X.-j., Peng J., Qin P., Zhuang X.-w., Wang H.-c. and Hou M. Interleukin 18 and interleukin 18 binding protein in patients with idiopathic thrombocytopenic purpura. *British Journal of Haematology*, 144(5):755–761, 2009.

[343] Kayagaki N., Warming S., Lamkanfi M., Walle L. V., Louie S., Dong J., Newton K., Qu Y., Liu J., Heldens S., Zhang J., Lee W. P., Roose-Girma M. and Dixit V. M. Non-canonical inflammasome activation targets caspase-11. *Nature*, 479(7371):117–121, 2011.

[344] Hagar J. A., Powell D. A., Aachoui Y., Ernst R. K. and Miao E. A. Cytoplasmic LPS Activates Caspase-11: Implications in TLR4-Independent Endotoxic Shock. *Science*, 341(6151):1250–1253, 2013.

[345] Kayagaki N., Wong M. T., Stowe I. B., Ramani S. R., Gonzalez L. C., Akashi-Takamura S., Miyake K., Zhang J., Lee W. P., Muszy?ski A., Forsberg L. S., Carlson R. W. and Dixit V. M. Noncanonical Inflammasome Activation by Intracellular LPS Independent of TLR4. *Science*, 341(6151):1246–1249, 2013.

[346] Shi J., Zhao Y., Wang Y., Gao W., Ding J., Li P., Hu L. and Shao F. Inflammatory caspases are innate immune receptors for intracellular LPS. *Nature*, 514(7521):187–192, 2014.

[347] Baker P. J., Boucher D., Bierschenk D., Tebartz C., Whitney P. G., D'Silva D. B., Tanzer M. C., Monteleone M., Robertson A. A. B., Cooper M. A., Alvarez-Diaz S., Herold M. J., Bedoui S., Schroder K. and Masters S. L. NLRP3 inflammasome activation downstream of cytoplasmic LPS recognition by both caspase-4 and caspase-5. *European Journal of Immunology*, 45(10):2918–2926, 2015.

[348] Ruehl S. and Broz P. Caspase-11 activates a canonical NLRP3 inflammasome by promoting K+ efflux. *European Journal of Immunology*, 45(10):2927–2936, 2015.

[349] Schmid-Burgk J. L., Gaidt M. M., Schmidt T., Ebert T. S., Bartok E. and Hornung V. Caspase-4 mediates non-canonical activation of the NLRP3 inflammasome in human myeloid cells. *European Journal of Immunology*, 45(10):2911–2917, 2015.

[350] Rathinam V., Vanaja S., Waggoner L., Sokolovska A., Becker C., Stuart L., Leong J. and Fitzgerald K. TRIF Licenses Caspase-11-Dependent NLRP3 Inflammasome Activation by Gram-Negative Bacteria. *Cell*, 150(3):606 – 619, 2012.

[351] Broz P., Ruby T., Belhocine K., Bouley D. M., Kayagaki N., Dixit V. M. and Monack D. M. Caspase-11 increases susceptibility to Salmonella infection in the absence of caspase-1. *Nature*, 490(7419):288–291, 2012.

[352] Seok J., Warren H. S., Cuenca A. G., Mindrinos M. N., Baker H. V., Xu W., Richards D. R., McDonald-Smith G. P., Gao H., Hennessy L., Finnerty C. C., Lopez C. M., Honari S., Moore E. E., Minei J. P., Cuschieri J., Bankey P. E., Johnson J. L., Sperry J., Nathens A. B., Billiar T. R., West M. A., Jeschke M. G., Klein M. B., Gamelli R. L., Gibran N. S., Brownstein B. H., Miller-Graziano C., Calvano S. E., Mason P. H., Cobb J. P., Rahme L. G., Lowry S. F., Maier R. V., Moldawer L. L., Herndon D. N., Davis R. W., Xiao W., Tompkins R. G., the Inflammation and Host Response to Injury L. S. C. R. P. Genomic responses in mouse models poorly mimic human inflammatory diseases. *Proceedings of the National Academy of Sciences*, 110(9):3507–3512, 2013.

[353] Levin R., Grinstein S. and Canton J. The life cycle of phagosomes: formation, maturation, and resolution. *Immunological Reviews*, 273(1):156–179, 2016.

[354] Steinberg B., Huynh K. and Grinstein S. Phagosomal acidification: measurement, manipulation and functional consequences. *Biochemical Society Transactions*, 35(5):1083–1087, 2007.

[355] Burton N., Schuermann N., Casse O., Steeb A., Claudi B., Zankl J., Schmidt A. and Bumann D. Disparate Impact of Oxidative Host Defenses Determines the Fate of Salmonella during Systemic Infection in Mice. *Cell Host & Microbe*, 15(1):72 – 83, 2014.

[356] Fang F. C. Antimicrobial reactive oxygen and nitrogen species: concepts and controversies. *Nat Rev Micro*, 2(10):820–832, 2004.

[357] Neyrolles O., Wolschendorf F., Mitra A. and Niederweis M. Mycobacteria, metals, and the macrophage. *Immunological Reviews*, 264(1):249–263, 2015.

[358] Schaible U. E. and Kaufmann S. H. E. Iron and microbial infection. *Nat Rev Micro*, 2(12):946–953, 2004.

[359] Miller C. and Celli J. Avoidance and Subversion of Eukaryotic Homeostatic Autophagy Mechanisms by Bacterial Pathogens. *Journal of Molecular Biology*, 428(17):3387 – 3398, 2016.

[360] Keestra-Gounder A. M., Tsolis R. M. and Baumler A. J. Now you see me, now you don't: the interaction of Salmonella with innate immune receptors. *Nat Rev Micro*, 13(4):206–216, 2015.

[361] LaRock D. L., Chaudhary A. and Miller S. I. Salmonellae interactions with host processes. *Nat Rev Micro*, 13(4):191–205, 2015.

[362] Crump J. A., Luby S. P. and Mintz E. D. The global burden of typhoid fever. *Bulletin of the World Health Organization*, 82(5):346–353, 2004.

[363] Majowicz S. E., Musto J., Scallan E., Angulo F. J., Kirk M., O'Brien S. J., Jones T. F., Fazil A., Hoekstra R. M. and for the International Collaboration on Enteric Disease Burden of Illness Studies. The Global Burden of Nontyphoidal Salmonella Gastroenteritis. *Clinical Infectious Diseases*, 50(6):882–889, 2010.

[364] Gordon M. A. Salmonella infections in immunocompromised adults. *Journal of Infection*, 56(6):413 – 422, 2008.

[365] Berkley J. A., Lowe B. S., Mwangi I., Williams T., Bauni E., Mwarumba S., Ngetsa C., Slack M. P., Njenga S., Hart C. A., Maitland K., English M., Marsh K. and Scott J. A. G. Bacteremia among Children Admitted to a Rural Hospital in Kenya. *New England Journal of Medicine*, 352(1):39–47, 2005.

[366] MacLennan C. A., Gondwe E. N., Msefula C. L., Kingsley R. A., Thomson N. R., White S. A., Goodall M., Pickard D. J., Graham S. M., Dougan G., Hart C. A., Molyneux M. E. and Drayson M. T. The neglected role of antibody in protection against bacteremia caused by nontyphoidal strains of Salmonella in African children. *The Journal of Clinical Investigation*, 118(4):1553–1562, 2008.

[367] Haraga A., Ohlson M. B. and Miller S. I. Salmonellae interplay with host cells. *Nat Rev Micro*, 6(1):53–66, 2008.

[368] Mirold S., Ehrbar K., Weissmueller A., Prager R., Tschaepe H., Ruessmann H. and Hardt W.-D. Salmonella Host Cell Invasion Emerged by Acquisition of a Mosaic of Separate Genetic Elements, Including Salmonella Pathogenicity Island 1 (SPI1), SPI5, and sopE2. *Journal of Bacteriology*, 183(7):2348–2358, 2001.

[369] Alpuche-Aranda C. M., Racoosin E. L., Swanson J. A. and Miller S. I. Salmonella stimulate macrophage macropinocytosis and persist within spacious phagosomes. *Journal of Experimental Medicine*, 179(2):601–608, 1994.

[370] Hapfelmeier S., Ehrbar K., Stecher B., Barthel M., Kremer M. and Hardt W.-D. Role of the Salmonella Pathogenicity Island 1 Effector Proteins SipA, SopB, SopE, and SopE2 in Salmonella enterica Subspecies 1 Serovar Typhimurium Colitis in Streptomycin-Pretreated Mice. *Infection and Immunity*, 72(2):795–809, 2004.

[371] Zhang S., Santos R. L., Tsolis R. M., Stender S., Hardt W.-D., Baeumler A. J. and Adams L. G. The Salmonella enterica Serotype Typhimurium Effector Proteins SipA, SopA, SopB, SopD, and SopE2 Act in Concert To Induce Diarrhea in Calves. *Infection and Immunity*, 70(7):3843–3855, 2002.

[372] Winter S. E., Thiennimitr P., Winter M. G., Butler B. P., Huseby D. L., Crawford R. W., Russell J. M., Bevins C. L., Adams L. G., Tsolis R. M., Roth J. R. and Baumler A. J. Gut inflammation provides a respiratory electron acceptor for Salmonella. *Nature*, 467(7314):426–429, 2010.

[373] Raffatellu M., George M. D., Akiyama Y., Hornsby M. J., Nuccio S.-P., Paixao T. A., Butler B. P., Chu H., Santos R. L., Berger T., Mak T. W., Tsolis R. M., Bevins C. L., Solnick J. V., Dandekar S. and Baeumler A. J. Lipocalin-2 Resistance Confers an Advantage to Salmonella enterica Serotype Typhimurium for Growth and Survival in the Inflamed Intestine. *Cell Host & Microbe*, 5(5):476 – 486, 2009.

[374] Brawn L. C., Hayward R. D. and Koronakis V. Salmonella SPI1 Effector SipA Persists after Entry and Cooperates with a SPI2 Effector to Regulate Phagosome Maturation and Intracellular Replication. *Cell Host & Microbe*, 1(1):63 – 75, 2007.

[375] LaRock D. L., Brzovic P. S., Levin I., Blanc M.-P. and Miller S. I. A Salmonella typhimurium-translocated Glycerophospholipid:Cholesterol Acyltransferase Promotes Virulence by Binding to the RhoA Protein Switch Regions. *Journal of Biological Chemistry*, 287(35):29654–29663, 2012.

[376] Nawabi P., Catron D. M. and Haldar K. Esterification of cholesterol by a type III secretion effector during intracellular Salmonella infection. *Molecular Microbiology*, 68(1):173–185, 2008.

[377] Christen M., Coye L. H., Hontz J. S., LaRock D. L., Pfuetzner R. A., Megha and Miller S. I. Activation of a Bacterial Virulence Protein by the GTPase RhoA. *Science Signaling*, 2(95):ra71–ra71, 2009.

[378] Boucrot E., Henry T., Borg J.-P., Gorvel J.-P. and Méresse S. The Intracellular Fate of Salmonella Depends on the Recruitment of Kinesin. *Science*, 308(5725):1174–1178, 2005.

[379] Guignot J., Caron E., Beuzón C., Bucci C., Kagan J., Roy C. and Holden D. W. Microtubule motors control membrane dynamics of Salmonella-containing vacuoles. *Journal of Cell Science*, 117(7):1033–1045, 2004.

[380] Henry T., Couillault C., Rockenfeller P., Boucrot E., Dumont A., Schroeder N., Hermant A., Knodler L. A., Lecine P., Steele-Mortimer O., Borg J.-P., Gorvel J.-P. and Meresse S. The Salmonella effector protein PipB2 is a linker for kinesin-1. *Proceedings of the National Academy of Sciences*, 103(36):13497–13502, 2006.

[381] Haraga A. and Miller S. I. A Salmonella enterica Serovar Typhimurium Translocated Leucine-Rich Repeat Effector Protein Inhibits NF-ÎžB-Dependent Gene Expression. *Infection and Immunity*, 71(7):4052–4058, 2003.

[382] Jones R. M., Wu H., Wentworth C., Luo L., Collier-Hyams L. and Neish A. S. Salmonella AvrA Coordinates Suppression of Host Immune and Apoptotic Defenses via JNK Pathway Blockade. *Cell Host & Microbe*, 3(4):233 – 244, 2008.

[383] Haneda T., Ishii Y., Shimizu H., Ohshima K., Iida N., Danbara H. and Okada N. Salmonella type III effector SpvC, a phosphothreonine lyase, contributes to reduction in inflammatory response during intestinal phase of infection. *Cellular Microbiology*, 14(4):485–499, 2012.

[384] Mazurkiewicz P., Thomas J., Thompson J. A., Liu M., Arbibe L., Sansonetti P. and Holden D. W. SpvC is a Salmonella effector with phosphothreonine lyase activity on host mitogen-activated protein kinases. *Molecular Microbiology*, 67(6):1371–1383, 2008.

[385] Tsolis R. M., Xavier M. N., Santos R. L. and BÃďumler A. J. How To Become a Top Model: Impact of Animal Experimentation on Human Salmonella Disease Research. *Infection and Immunity*, 79(5):1806–1814, 2011.

[386] Rabsch W., Tschaepe H. and Baeumler A. J. Non-typhoidal salmonellosis: emerging problems. *Microbes and Infection*, 3(3):237 – 247, 2001.

[387] Law S. K. and Levine R. P. Interaction between the third complement protein and cell surface macromolecules. *Proceedings of the National Academy of Sciences*, 74(7):2701–2705, 1977.

[388] Tack B. F., Harrison R. A., Janatova J., Thomas M. L. and Prahl J. W. Evidence for presence of an internal thiolester bond in third component of human complement. *Proceedings of the National Academy of Sciences of the United States of America*, 77(10):5764–5768, 1980.

[389] Joiner K., Hammer C., Brown E. and Frank M. Studies on the mechanism of bacterial resistance to complement-mediated killing. II. C8 and C9 release C5b67 from the surface of salmonella minnesota S218 because the terminal complex does not insert into the bacterial outer membrane. *Journal of Experimental Medicine*, 155(3):809–919, 1982.

[390] Murray G. L., Attridge S. R. and Morona R. Regulation of Salmonella typhimurium lipopolysaccharide O antigen chain length is required for virulence; identification of FepE as a second Wzz. *Molecular Microbiology*, 47(5):1395–1406, 2003.

[391] Wangdi T., Lee C.-Y., Spees A. M., Yu C., Kingsbury D. D., Winter S. E., Hastey C. J., Wilson R. P., Heinrich V. and Baeumler A. J. The Vi Capsular Polysaccharide Enables Salmonella enterica Serovar Typhi to Evade Microbe-Guided Neutrophil Chemotaxis. *PLOS Pathogens*, 10(8):1–9, 2014.

[392] Montz H., Koch K. C., Zierz R. and Goetze O. The role of C5a in interleukin-6 production induced by lipopolysaccharide or interleukin-1. *Immunology*, 74(3):373–379, 1991.

[393] Bernheiden M., Heinrich J.-M., Minigo G., Schuett C., Stelter F., Freeman M., Golenbock D. and Jack R. S. LBP, CD14, TLR4 and the murine innate immune response to a peritoneal Salmonella infection. *Journal of Endotoxin Research*, 7(6):447–450, 2001.

[394] Weiss D. S., Raupach B., Takeda K., Akira S. and Zychlinsky A. Toll-Like Receptors Are Temporally Involved in Host Defense. *The Journal of Immunology*, 172(7):4463–4469, 2004.

[395] Broz P., Newton K., Lamkanfi M., Mariathasan S., Dixit V. M. and Monack D. M. Redundant roles for inflammasome receptors NLRP3 and NLRC4 in host defense against Salmonella. *The Journal of Experimental Medicine*, 207(8):1745–1755, 2010.

[396] Miao E. A., Leaf I. A., Treuting P. M., Mao D. P., Dors M., Sarkar A., Warren S. E., Wewers M. D. and Aderem A. Caspase-1-induced pyroptosis is an innate immune effector mechanism against intracellular bacteria. *Nat Immunol*, 11(12):1136–1142, 2010.

[397] Glynn J. R. and Palmer S. R. Incubation Period, Severity of Disease, and Infecting Dose: Evidence from a Salmonella Outbreak. *American Journal of Epidemiology*, 136(11):1369, 1992.

[398] Olsen S. J., Bleasdale S. C., Magnano A. R., Landrigan C., Holland B. H., Tauxe R. V., Mintz E. D. and Luby S. Outbreaks of typhoid fever in the United States, 1960-99. *Epidemiology and Infection*, 130(1):13–21, 2003.

[399] Virlogeux I., Waxin H., Ecobichon C. and Popoff M. Y. Role of the viaB locus in synthesis, transport and expression of Salmonella typhi Vi antigen. *Microbiology*, 141(12):3039–3047, 1995.

[400] Wetter M., Goulding D., Pickard D., Kowarik M., Waechter C. J., Dougan G. and Wacker M. Molecular Characterization of the viaB Locus Encoding the Biosynthetic Machinery for Vi Capsule Formation in Salmonella Typhi. *PLOS ONE*, 7(9):1–11, 2012.

[401] Wilson R. P., Winter S. E., Spees A. M., Winter M. G., Nishimori J. H., Sanchez J. F., Nuccio S.-P., Crawford R. W., Tuekel a. and Baeumler A. J. The Vi Capsular Polysaccharide Prevents Complement Receptor 3-Mediated Clearance of Salmonella enterica Serotype Typhi. *Infection and Immunity*, 79(2):830–837, 2011.

[402] Bravo D., Silva C., Carter J. A., Hoare A., Alvarez S. A., Blondel C. J., Zaldivar M., Valvano M. A. and Contreras I. Growth-phase regulation of lipopolysaccharide O-antigen chain length influences serum resistance in serovars of Salmonella. *Journal of Medical Microbiology*, 57(8):938–946, 2008.

[403] Winter S. E., Winter M. G., Thiennimitr P., Gerriets V. A., Nuccio S.-P., Ruessmann H. and Baeumler A. J. The TviA auxiliary protein renders the Salmonella enterica serotype Typhi RcsB regulon responsive to changes in osmolarity. *Molecular Microbiology*, 74(1):175–193, 2009.

[404] Winter S. E., Winter M. G., Godinez I., Yang H.-J., Ruessmann H., Andrews-Polymenis H. L. and Baeumler A. J. A Rapid Change in Virulence Gene Expression during the Transition from the Intestinal Lumen into Tissue Promotes Systemic Dissemination of Salmonella. *PLOS Pathogens*, 6(8):1–13, 2010.

[405] Trombert A. N., Berrocal L., Fuentes J. A. and Mora G. C. S. Typhimurium sseJ gene decreases the S. Typhi cytotoxicity toward cultured epithelial cells. *BMC Microbiology*, 10(1):312, 2010.

[406] McClelland M., Sanderson K. E., Clifton S. W., Latreille P., Porwollik S., Sabo A., Meyer R., Bieri T., Ozersky P., McLellan M., Harkins C. R., Wang C., Nguyen C., Berghoff A., Elliott G., Kohlberg S., Strong C., Du F., Carter J., Kremizki C., Layman D., Leonard S., Sun H., Fulton L., Nash W., Miner T., Minx P., Delehaunty K., Fronick C., Magrini V., Nhan M., Warren W., Florea L., Spieth J. and Wilson R. K. Comparison of genome degradation in Paratyphi A and Typhi, human-restricted serovars of Salmonella enterica that cause typhoid. *Nat Genet*, 36(12):1268–1274, 2004.

[407] Song J., Willinger T., Rongvaux A., Eynon E. E., Stevens S., Manz M. G., Flavell R. A. and Galan J. E. A Mouse Model for the Human Pathogen Salmonella Typhi. *Cell Host & Microbe*, 8(4):369 – 376, 2010.

[408] Mathur R., Oh H., Zhang D., Park S.-G., Seo J., Koblansky A., Hayden M. and Ghosh S. A Mouse Model of Salmonella Typhi Infection. *Cell*, 151(3):590 – 602, 2012.

[409] Parmely M. J., Fischer J. L. and Pinson D. M. Programmed Cell Death and the Pathogenesis of Tissue Injury Induced by Type A Francisella tularensis. *FEMS microbiology letters*, 301(1):1–11, 2009.

[410] Sjodin A., Svensson K., Ohrman C., Ahlinder J., Lindgren P., Duodu S., Johansson A., Colquhoun D. J., Larsson P. and Forsman M. Genome characterisation of the genus Francisella reveals insight into similar evolutionary paths in pathogens of mammals and fish. *BMC Genomics*, 13(1):268, 2012.

[411] Kingry L. and Petersen J. Comparative review of Francisella tularensis and Francisella novicida. *Frontiers in Cellular and Infection Microbiology*, 4:35, 2014.

[412] Oyston P. C. F. Francisella tularensis: unravelling the secrets of an intracellular pathogen. *Journal of Medical Microbiology*, 57(8):921–930, 2008.

[413] Broms J. E., Sjostedt A. and Lavander M. The Role of the Francisella Tularensis Pathogenicity Island in Type VI Secretion, Intracellular Survival, and Modulation of Host Cell Signaling. *Frontiers in Microbiology*, 1:136–, 2010.

[414] Ellis J., Oyston P. C. F., Green M. and Titball R. W. Tularemia. *Clinical Microbiology Reviews*, 15(4):631–646, 2002.

[415] KEIM P., JOHANSSON A. and WAGNER D. M. Molecular Epidemiology, Evolution, and Ecology of Francisella. *Annals of the New York Academy of Sciences*, 1105(1):30–66, 2007.

[416] DT D., TV I., DA H. and et al. Tularemia as a biological weapon: Medical and public health management. *JAMA*, 285(21):2763–2773, 2001.

[417] Jones B. D., Faron M., Rasmussen J. A. and Fletcher J. R. Uncovering the components of the Francisella tularensis virulence stealth strategy. *Frontiers in Cellular and Infection Microbiology*, 4:32–, 2014.

[418] Ben Nasr A., Haithcoat J., Masterson J. E., Gunn J. S., Eaves-Pyles T. and Klimpel G. R. Critical role for serum opsonins and complement receptors CR3 (CD11b/CD18) and CR4 (CD11c/CD18) in phagocytosis of Francisella tularensis by human dendritic cells (DC): uptake of Francisella leads to activation of immature DC and intracellular survival of the bacteria. *Journal of Leukocyte Biology*, 80(4):774–786, 2006.

[419] Pierini L. M. Uptake of serum-opsonized Francisella tularensis by macrophages can be mediated by class A scavenger receptors. *Cellular Microbiology*, 8(8):1361–1370, 2006.

[420] Geier H. and Celli J. Phagocytic Receptors Dictate Phagosomal Escape and Intracellular Proliferation of Francisella tularensis. *Infection and Immunity*, 79(6):2204–2214, 2011.

[421] Clay C. D., Soni S., Gunn J. S. and Schlesinger L. S. Evasion of Complement-Mediated Lysis and Complement C3 Deposition Are Regulated by Francisella tularensis Lipopolysaccharide O Antigen. *Journal of immunology (Baltimore, Md. : 1950)*, 181(8):5568–5578, 2008.

[422] Golovliov I., Baranov V., Krocova Z., Kovarova H. and Sjostedt A. An Attenuated Strain of the Facultative Intracellular Bacterium Francisella tularensis Can Escape the Phagosome of Monocytic Cells. *Infection and Immunity*, 71(10):5940–5950, 2003.

[423] Clemens D. L., Lee B.-Y. and Horwitz M. A. Virulent and Avirulent Strains of Francisella tularensis Prevent Acidification and Maturation of Their Phagosomes and Escape into the Cytoplasm in Human Macrophages. *Infection and Immunity*, 72(6):3204–3217, 2004.

[424] Santic M., Molmeret M., Klose K. E. and Kwaik Y. A. Francisella tularensis travels a novel, twisted road within macrophages. *Trends in Microbiology*, 14(1):37 – 44, 2006.

[425] de Bruin O. M., Ludu J. S. and Nano F. E. The Francisella pathogenicity island protein IglA localizes to the bacterial cytoplasm and is needed for intracellular growth. *BMC Microbiology*, 7:1–1, 2007.

[426] Nano F. E., Zhang N., Cowley S. C., Klose K. E., Cheung K. K. M., Roberts M. J., Ludu J. S., Letendre G. W., Meierovics A. I., Stephens G. and Elkins K. L. A Francisella tularensis Pathogenicity Island Required for Intramacrophage Growth. *Journal of Bacteriology*, 186(19):6430–6436, 2004.

[427] Ludu J. S., de Bruin O. M., Duplantis B. N., Schmerk C. L., Chou A. Y., Elkins K. L. and Nano F. E. The Francisella Pathogenicity Island Protein PdpD Is Required for Full Virulence and Associates with Homologues of the Type VI Secretion System. *Journal of Bacteriology*, 190(13):4584–4595, 2008.

[428] Weiss D. S., Brotcke A., Henry T., Margolis J. J., Chan K. and Monack D. M. In vivo negative selection screen identifies genes required for Francisella virulence. *Proceedings of the National Academy of Sciences of the United States of America*, 104(14):6037–6042, 2006.

[429] Chong A., Wehrly T. D., Nair V., Fischer E. R., Barker J. R., Klose K. E. and Celli J. The Early Phagosomal Stage of Francisella tularensis Determines Optimal Phagosomal Escape and Francisella Pathogenicity Island Protein Expression. *Infection and Immunity*, 76(12):5488–5499, 2008.

[430] Santic M., Asare R., Skrobonja I., Jones S. and Abu Kwaik Y. Acquisition of the Vacuolar ATPase Proton Pump and Phagosome Acidification Are Essential for Escape of Francisella tularensis into the Macrophage Cytosol. *Infection and Immunity*, 76(6):2671–2677, 2008.

[431] Clemens D. L., Lee B.-Y. and Horwitz M. A. Francisella tularensis Phagosomal Escape Does Not Require Acidification of the Phagosome. *Infection and Immunity*, 77(5):1757–1773, 2009.

[432] Ahlund M. K., Ryden P., Sjostedt A. and Stoven S. Directed Screen of Francisella novicida Virulence Determinants Using Drosophila melanogaster. *Infection and Immunity*, 78(7):3118–3128, 2010.

[433] Asare R., Akimana C., Jones S. and Abu Kwaik Y. Molecular bases of proliferation of Francisella tularensis in arthropod vectors. *Environmental Microbiology*, 12(9):2587–2612, 2010.

[434] Lauriano C. M., Barker J. R., Yoon S.-S., Nano F. E., Arulanandam B. P., Hassett D. J. and Klose K. E. MglA regulates transcription of virulence factors necessary for Francisella tularensis intraamoebae and intramacrophage survival. *Proceedings of the National Academy of Sciences*, 101(12):4246–4249, 2004.

[435] Santic M., Ozanic M., Semic V., Pavokovic G., Mrvcic V. and Abu Kwaik Y. Intra-Vacuolar Proliferation of F. Novicida within H. Vermiformis. *Frontiers in Microbiology*, 2:78, 2011.

[436] Kirimanjeswara G. S., Olmos S., Bakshi C. S. and Metzger D. W. Humoral and Cell-Mediated Immunity to the Intracellular Pathogen Francisella tularensis. *Immunological reviews*, 225:244–255, 2008.

[437] Lindemann S. R., Peng K., Long M. E., Hunt J. R., Apicella M. A., Monack D. M., Allen L.-A. H. and Jones B. D. Francisella tularensis Schu S4 O-Antigen and Capsule Biosynthesis Gene Mutants Induce Early Cell Death in Human Macrophages. *Infection and Immunity*, 79(2):581–594, 2010.

[438] Apicella M. A., Post D. M. B., Fowler A. C., Jones B. D., Rasmussen J. A., Hunt J. R., Imagawa S., Choudhury B., Inzana T. J., Maier T. M., Frank D. W., Zahrt T. C., Chaloner K., Jennings M. P., McLendon M. K. and Gibson B. W. Identification, Characterization and Immunogenicity of an O-Antigen Capsular Polysaccharide of Francisella tularensis. *PLoS ONE*, 5(7):e11060–, 2010.

[439] Cherwonogrodzky J. W., Knodel M. H. and Spence M. R. Increased encapsulation and virulence of Francisella tularensis live vaccine strain (LVS) by subculturing on synthetic medium. *Vaccine*, 12(9):773 – 775, 1994.

[440] Sandstrom G., Lofgren S. and Tarnvik A. A capsule-deficient mutant of Francisella tularensis LVS exhibits enhanced sensitivity to killing by serum but diminished sensitivity to killing by polymorphonuclear leukocytes. *Infection and Immunity*, 56(5):1194–1202, 1988.

[441] Thomas R. M., Titball R. W., Oyston P. C. F., Griffin K., Waters E., Hitchen P. G., Michell S. L., Grice I. D., Wilson J. C. and Prior J. L. The Immunologically Distinct O Antigens from Francisella tularensis Subspecies tularensis and Francisella novicida Are both Virulence Determinants and Protective Antigens. *Infection and Immunity*, 75(1):371–378, 2006.

[442] Wang Q., Shi X., Leymarie N., Madico G., Sharon J., Costello C. E. and Zaia J. Typical Preparation of Francisella tularensis O-antigen Yields a Mixture of Three Types of Saccharides(). *Biochemistry*, 50(50):10941–10950, 2011.

[443] Vinogradov E., Perry M. B. and Conlan J. W. Structural analysis of Francisella tularensis lipopolysaccharide. *European Journal of Biochemistry*, 269(24):6112–6118, 2002.

[444] Bandara A. B., Champion A. E., Wang X., Berg G., Apicella M. A., McLendon M., Azadi P., Snyder D. S. and Inzana T. J. Isolation and Mutagenesis of a Capsule-Like Complex (CLC) from Francisella tularensis, and Contribution of the CLC to F. tularensis Virulence in Mice. *PLoS ONE*, 6(4):e19003–, 2011.

[445] Rasmussen J. A., Post D. M. B., Gibson B. W., Lindemann S. R., Apicella M. A., Meyerholz D. K. and Jones B. D. Francisella tularensis Schu S4 Lipopolysaccharide Core Sugar and O-Antigen Mutants Are Attenuated in a Mouse Model of Tularemia. *Infection and Immunity*, 82(4):1523–1539, 2014.

[446] Wang X., Ribeiro A. A., Guan Z., Abraham S. N. and Raetz C. R. H. Attenuated virulence of a Francisella mutant lacking the lipid A 4 phosphatase. *Proceedings of the National Academy of Sciences of the United States of America*, 104(10):4136–4141, 2006.

[447] Wang X., Karbarz M. J., McGrath S. C., Cotter R. J. and Raetz C. R. H. MsbA Transporter-dependent Lipid A 1-Dephosphorylation on the Periplasmic Surface of the Inner Membrane: TOPOGRAPHY OF FRANCISELLA NOVICIDA LpxE EXPRESSED IN ESCHERICHIA COLI. *The Journal of biological chemistry*, 279(47):49470–49478, 2004.

[448] Phillips N. J., Schilling B., McLendon M. K., Apicella M. A. and Gibson B. W. Novel Modification of Lipid A of Francisella tularensis. *Infection and Immunity*, 72(9):5340–5348, 2004.

[449] Hajjar A. M., Harvey M. D., Shaffer S. A., Goodlett D. R., Sjostedt A., Edebro H., Forsman M., Bystrom M., Pelletier M., Wilson C. B., Miller S. I., Skerrett S. J. and Ernst R. K. Lack of In Vitro and In Vivo Recognition of Francisella tularensis Subspecies Lipopolysaccharide by Toll-Like Receptors. *Infection and Immunity*, 74(12):6730–6738, 2006.

[450] Thakran S., Li H., Lavine C. L., Miller M. A., Bina J. E., Bina X. R. and Re F. Identification of Francisella tularensis Lipoproteins That Stimulate the Toll-like Receptor (TLR) 2/TLR1 Heterodimer. *Journal of Biological Chemistry*, 283(7):3751–3760, 2008.

[451] Cole L. E., Shirey K. A., Barry E., Santiago A., Rallabhandi P., Elkins K. L., Puche A. C., Michalek S. M. and Vogel S. N. Toll-Like Receptor 2-Mediated Signaling Requirements for Francisella tularensis Live Vaccine Strain Infection of Murine Macrophages. *Infection and Immunity*, 75(8):4127–4137, 2007.

[452] Jones C. L. and Weiss D. S. TLR2 Signaling Contributes to Rapid Inflammasome Activation during F. novicida Infection. *PLOS ONE*, 6(6):1–11, 2011.

[453] Okan N. A. and Kasper D. L. The atypical lipopolysaccharide of Francisella. *Carbohydrate research*, 378:79–83, 2013.

[454] Gil H., Benach J. L. and Thanassi D. G. Presence of Pili on the Surface of Francisella tularensis. *Infection and Immunity*, 72(5):3042–3047, 2004.

[455] Forslund A.-L., Kuoppa K., Svensson K., Salomonsson E., Johansson A., Bystrom M., Oyston P. C. F., Michell S. L., Titball R. W., Noppa L., Frithz-Lindsten E., Forsman M. and Forsberg k. Direct repeat-mediated deletion of a type IV pilin gene results in major virulence attenuation of Francisella tularensis. *Molecular Microbiology*, 59(6):1818–1830, 2006.

[456] Forslund A.-L., Salomonsson E. N., Golovliov I., Kuoppa K., Michell S., Titball R., Oyston P., Noppa L., Sjostedt A. and Forsberg k. The type IV pilin, PilA, is required for full virulence of Francisella tularensis subspecies tularensis. *BMC Microbiology*, 10:227–227, 2010.

[457] Henry T., Brotcke A., Weiss D. S., Thompson L. J. and Monack D. M. Type I interferon signaling is required for activation of the inflammasome during Francisella infection. *The Journal of Experimental Medicine*, 204(5):987–994, 2007.

[458] Man S. M., Karki R., Malireddi R. K. S., Neale G., Vogel P., Yamamoto M., Lamkanfi M. and Kanneganti T.-D. The transcription factor IRF1 and guanylate-binding proteins target activation of the AIM2 inflammasome by Francisella infection. *Nat Immunol*, 16(5):467–475, 2015.

[459] Jin L., Hill K. K., Filak H., Mogan J., Knowles H., Zhang B., Perraud A.-L., Cambier J. C. and Lenz L. L. MPYS is required for IRF3 activation and type I IFN production in the response of cultured phagocytes to bacterial second messengers c-di-AMP and c-di-GMP(). *Journal of immunology (Baltimore, Md. : 1950)*, 187(5):2595–2601, 2011.

[460] Cole L. E., Santiago A., Barry E., Kang T. J., Shirey K. A., Roberts Z. J., Elkins K. L., Cross A. S. and Vogel S. N. The Macrophage Proinflammatory Response to Francisella tularensis LVS Requires Coordination of Multiple Signaling Pathways. *Journal of immunology (Baltimore, Md. : 1950)*, 180(10):6885–6891, 2008.

[461] Huang M. T.-H., Mortensen B. L., Taxman D. J., Craven R. R., Taft-Benz S., Kijek T. M., Fuller J. R., Davis B. K., Allen I. C., Brickey W. J., Gris D., Wen H., Kawula T. H. and Ting J. P.-Y. Deletion of ripA Alleviates Suppression of the Inflammasome and MAPK by Francisella tularensis. *Journal of immunology (Baltimore, Md. : 1950)*, 185(9):5476–5485, 2010.

[462] WEISS D. S., HENRY T. and MONACK D. M. Francisella Tularensis: Activation of the Inflammasome. *Annals of the New York Academy of Sciences*, 1105(1):219–237, 2007.

[463] Meunier E., Wallet P., Dreier R. F., Costanzo S., Anton L., Ruhl S., Dussurgey S., Dick M. S., Kistner A., Rigard M., Degrandi D., Pfeffer K., Yamamoto M., Henry T. and Broz P. Guanylate-binding proteins promote activation of the AIM2 inflammasome during infection with Francisella novicida. *Nat Immunol*, 16(5):476–484, 2015.

[464] Man S., Karki R., Sasai M., Place D., Kesavardhana S., Temirov J., Frase S., Zhu Q., Malireddi R., Kuriakose T., Peters J., Neale G., Brown S., Yamamoto M. and Kanneganti T.-D. IRGB10 Liberates Bacterial Ligands for Sensing by the AIM2 and Caspase-11-NLRP3 Inflammasomes. *Cell*, pages –, 2016.

[465] Gavrilin M. A., Bouakl I. J., Knatz N. L., Duncan M. D., Hall M. W., Gunn J. S. and Wewers M. D. Internalization and phagosome escape required for Francisella to induce human monocyte IL-1beta processing and release. *Proceedings of the National Academy of Sciences of the United States of America*, 103(1):141–146, 2006.

[466] Atianand M. K., Duffy E. B., Shah A., Kar S., Malik M. and Harton J. A. Francisella tularensis Reveals a Disparity between Human and Mouse NLRP3 Inflammasome Activation. *Journal of Biological Chemistry*, 286(45):39033–39042, 2011.

[467] Gavrilin M. A., Mitra S., Seshadri S., Nateri J., Berhe F., Hall M. W. and Wewers M. D. Pyrin Critical to Macrophage IL-1beta Response to Francisella Challenge. *The Journal of Immunology*, 182(12):7982–7989, 2009.

[468] Wewers M. D. and Herzyk D. J. Alveolar macrophages differ from blood monocytes in human IL-1 beta release. Quantitation by enzyme-linked immunoassay. *The Journal of Immunology*, 143(5):1635–1641, 1989.

[469] Seshadri S., Duncan M. D., Hart J. M., Gavrilin M. A. and Wewers M. D. Pyrin Levels in Human Monocytes and Monocyte-Derived Macrophages Regulate IL-1beta Processing and Release. *The Journal of Immunology*, 179(2):1274–1281, 2007.

[470] Crane D. D., Bauler T. J., Wehrly T. D. and Bosio C. M. Mitochondrial ROS potentiates indirect activation of the AIM2 inflammasome. *Frontiers in Microbiology*, 5:438–, 2014.

[471] Larsson P., Elfsmark D., Svensson K., Wikstrom P., Forsman M., Brettin T., Keim P. and Johansson A. Molecular Evolutionary Consequences of Niche Restriction in Francisella tularensis, a Facultative Intracellular Pathogen. *PLoS Pathogens*, 5(6):e1000472–, 2009.

[472] NANO F. E. and SCHMERK C. The Francisella Pathogenicity Island. *Annals of the New York Academy of Sciences*, 1105(1):122–137, 2007.

[473] Golovliov I., Sjostedt A., Mokrievich A. and Pavlov V. A method for allelic replacement in Francisella tularensis. *FEMS Microbiology Letters*, 222(2):273, 2006.

[474] Kawula T. H., Hall J. D., Fuller J. R. and Craven R. R. Use of Transposon-Transposase Complexes To Create Stable Insertion Mutant Strains of Francisella tularensis LVS. *Applied and Environmental Microbiology*, 70(11):6901–6904, 2004.

[475] Qin A. and Mann B. J. Identification of transposon insertion mutants of Francisella tularensis tularensis strain Schu S4 deficient in intracellular replication in the hepatic cell line HepG2. *BMC Microbiology*, 6:69–69, 2006.

[476] Rigard M., Broms J. E., Mosnier A., Hologne M., Martin A., Lindgren L., Punginelli C., Lays C., Walker O., Charbit A., Telouk P., Conlan W., Terradot L., Sjostedt A. and Henry T. Francisella tularensis IglG Belongs to a Novel Family of PAAR-Like T6SS Proteins and Harbors a Unique N-terminal Extension Required for Virulence. *PLoS Pathog*, 12(9):1–33, 2016.

[477] Bingle L. E., Bailey C. M. and Pallen M. J. Type VI secretion: a beginner's guide. *Current Opinion in Microbiology*, 11(1):3 – 8, 2008.

[478] Pukatzki S., Ma A. T., Sturtevant D., Krastins B., Sarracino D., Nelson W. C., Heidelberg J. F. and Mekalanos J. J. Identification of a conserved bacterial protein secretion system in Vibrio cholerae using the Dictyostelium host model system. *Proceedings of the National Academy of Sciences*, 103(5):1528–1533, 2006.

[479] Leiman P. G., Basler M., Ramagopal U. A., Bonanno J. B., Sauder J. M., Pukatzki S., Burley S. K., Almo S. C. and Mekalanos J. J. Type VI secretion apparatus and phage tail-associated protein complexes share a common evolutionary origin. *Proceedings of the National Academy of Sciences*, 106(11):4154–4159, 2009.

[480] Pell L., Kanelis V. d., Donaldson L., Howell P. and Davidson A. b. The phage lambda major tail protein structure reveals a common evolution for long-tailed phages and the type VI bacterial secretion system. *Proceedings of the National Academy of Sciences of the United States of America*, 106(11):4160–4165, 2009.

[481] Das S. and Chaudhuri K. Identification of a unique IAHP (IcmF associated homologous proteins) cluster in Vibrio cholerae and other proteobacteria through In Silico analysis. *In Silico Biology*, 3(3):287–300, 2003.

[482] Ho B., Dong T. and Mekalanos J. A View to a Kill: The Bacterial Type VI Secretion System. *Cell Host & Microbe*, 15(1):9 – 21, 2014.

[483] Hood R. D., Singh P., Hsu F., GÃijvener T., Carl M. A., Trinidad R. R., Silverman J. M., Ohlson B. B., Hicks K. G., Plemel R. L., Li M., Schwarz S., Wang W. Y., Merz A. J., Goodlett D. R. and Mougous J. D. A Type VI Secretion System of Pseudomonas aeruginosa Targets a Toxin to Bacteria. *Cell Host & Microbe*, 7(1):25 – 37, 2010.

[484] Schwarz S., West T. E., Boyer F., Chiang W.-C., Carl M. A., Hood R. D., Rohmer L., Tolker-Nielsen T., Skerrett S. J. and Mougous J. D. Burkholderia Type VI Secretion Systems Have Distinct Roles in Eukaryotic and Bacterial Cell Interactions. *PLOS Pathogens*, 6(8):1–14, 2010.

[485] Alteri C. J., Himpsl S. D., Pickens S. R., Lindner J. R., Zora J. S., Miller J. E., Arno P. D., Straight S. W. and Mobley H. L. T. Multicellular Bacteria Deploy the Type VI Secretion System to Preemptively Strike Neighboring Cells. *PLOS Pathogens*, 9(9):1–18, 2013.

[486] Ma A. T., McAuley S., Pukatzki S. and Mekalanos J. J. Translocation of a Vibrio cholerae Type VI Secretion Effector Requires Bacterial Endocytosis by Host Cells. *Cell Host & Microbe*, 5(3):234 – 243, 2009.

[487] Chow J. and Mazmanian S. K. A Pathobiont of the Microbiota Balances Host Colonization and Intestinal Inflammation. *Cell Host & Microbe*, 7(4):265 – 276, 2010.

[488] Felisberto-Rodrigues C., Durand E., Aschtgen M.-S., Blangy S., Ortiz-Lombardia M., Douzi B., Cambillau C. and Cascales E. Towards a Structural Comprehension of Bacterial Type VI Secretion Systems: Characterization of the TssJ-TssM Complex of an Escherichia coli Pathovar. *PLOS Pathogens*, 7(11):1–11, 2011.

[489] Ma L.-S., Lin J.-S. and Lai E.-M. An IcmF Family Protein, ImpLM, Is an Integral Inner Membrane Protein Interacting with ImpKL, and Its Walker A Motif Is Required for Type VI Secretion System-Mediated Hcp Secretion in Agrobacterium tumefaciens. *Journal of Bacteriology*, 191(13):4316–4329, 2009.

[490] VanRheenen S. M., Dumenil G. and Isberg R. R. IcmF and DotU Are Required for Optimal Effector Translocation and Trafficking of the Legionella pneumophila Vacuole. *Infection and Immunity*, 72(10):5972–5982, 2004.

[491] Durand E., Zoued A., Spinelli S., Watson P. J. H., Aschtgen M.-S., Journet L., Cambillau C. and Cascales E. Structural Characterization and Oligomerization of the TssL Protein, a Component Shared by Bacterial Type VI and Type IVb Secretion Systems. *Journal of Biological Chemistry*, 287(17):14157–14168, 2012.

[492] Lossi N. S., Dajani R., Freemont P. and Filloux A. Structure function analysis of HsiF, a gp25-like component of the type VI secretion system, in Pseudomonas aeruginosa. *Microbiology*, 157(12):3292–3305, 2011.

[493] Zoued A., Durand E., Bebeacua C., Brunet Y. R., Douzi B., Cambillau C., Cascales E. and Journet L. TssK Is a Trimeric Cytoplasmic Protein Interacting with Components of Both Phage-like and Membrane Anchoring Complexes of the Type VI Secretion System. *Journal of Biological Chemistry*, 288(38):27031–27041, 2013.

[494] Pukatzki S., Ma A. T., Revel A. T., Sturtevant D. and Mekalanos J. J. Type VI secretion system translocates a phage tail spike-like protein into target cells where it cross-links actin. *Proceedings of the National Academy of Sciences*, 104(39):15508–15513, 2007.

[495] Hachani A., Lossi N. S., Hamilton A., Jones C., Bleves S., Albesa-JovÃľ D. and Filloux A. Type VI Secretion System in Pseudomonas aeruginosa: SECRETION AND MULTIMERIZATION OF VgrG PROTEINS. *Journal of Biological Chemistry*, 286(14):12317–12327, 2011.

[496] Shneider M. M., Buth S. A., Ho B. T., Basler M., Mekalanos J. J. and Leiman P. G. PAAR-repeat proteins sharpen and diversify the type VI secretion system spike. *Nature*, 500(7462):350–353, 2013.

[497] Mougous J. D., Cuff M. E., Raunser S., Shen A., Zhou M., Gifford C. A., Goodman A. L., Joachimiak G., Ordoñez C. L., Lory S., Walz T., Joachimiak A. and Mekalanos J. J. A Virulence Locus of Pseudomonas aeruginosa Encodes a Protein Secretion Apparatus. *Science*, 312(5779):1526–1530, 2006.

[498] Boenemann G., Pietrosiuk A., Diemand A., Zentgraf H. and Mogk A. Remodelling of VipA/VipB tubules by ClpV mediated threading is crucial for type VI protein secretion. *EMBO J*, 28(4):315–, 2009.

[499] Basler M. and Mekalanos J. J. Type 6 Secretion Dynamics Within and Between Bacterial Cells. *Science*, 337(6096):815–815, 2012.

[500] Mogk A., Haslberger T., Tessarz P. and Bukau B. Common and specific mechanisms of AAA+ proteins involved in protein quality control. *Biochemical Society Transactions*, 36(1):120–125, 2008.

[501] Basler M., Ho B. and Mekalanos J. Tit-for-Tat: Type VI Secretion System Counterattack during Bacterial Cell-Cell Interactions. *Cell*, 152(4):884 – 894, 2013.

[502] Ho B. T., Basler M. and Mekalanos J. J. Type 6 Secretion System–Mediated Immunity to Type 4 Secretion System–Mediated Gene Transfer. *Science*, 342(6155):250–253, 2013.

[503] Basler M., Pilhofer M., Henderson G. P., Jensen G. J. and Mekalanos J. J. Type VI secretion requires a dynamic contractile phage tail-like structure. *Nature*, 483(7388):182–186, 2012.

[504] Brooks T. M., Unterweger D., Bachmann V., Kostiuk B. and Pukatzki S. Lytic Activity of the Vibrio cholerae Type VI Secretion Toxin VgrG-3 Is Inhibited by the Antitoxin TsaB. *Journal of Biological Chemistry*, 288(11):7618–7625, 2013.

[505] Dong T. G., Ho B. T., Yoder-Himes D. R. and Mekalanos J. J. Identification of T6SS-dependent effector and immunity proteins by Tn-seq in Vibrio cholerae. *Proceedings of the National Academy of Sciences*, 110(7):2623–2628, 2013.

[506] Koskiniemi S., Lamoureux J. G., Nikolakakis K. C., t'Kint de Roodenbeke C., Kaplan M. D., Low D. A. and Hayes C. S. Rhs proteins from diverse bacteria mediate intercellular competition. *Proceedings of the National Academy of Sciences*, 110(17):7032–7037, 2013.

[507] Zheng J. and Leung K. Y. Dissection of a type VI secretion system in Edwardsiella tarda. *Molecular Microbiology*, 66(5):1192–1206, 2007.

[508] Zheng J., Shin O. S., Cameron D. E. and Mekalanos J. J. Quorum sensing and a global regulator TsrA control expression of type VI secretion and virulence in Vibrio cholerae. *Proceedings of the National Academy of Sciences*, 107(49):21128–21133, 2010.

[509] Aubert D. F., Flannagan R. S. and Valvano M. A. A Novel Sensor Kinase-Response Regulator Hybrid Controls Biofilm Formation and Type VI Secretion System Activity in Burkholderia cenocepacia. *Infection and Immunity*, 76(5):1979–1991, 2008.

[510] Brunet Y. R., Bernard C. S., Gavioli M., LloubÃÍs R. and Cascales E. An Epigenetic Switch Involving Overlapping Fur and DNA Methylation Optimizes Expression of a Type VI Secretion Gene Cluster. *PLOS Genetics*, 7(7):1–11, 2011.

[511] Pieper R., Huang S.-T., Robinson J. M., Clark D. J., Alami H., Parmar P. P., Perry R. D., Fleischmann R. D. and Peterson S. N. Temperature and growth phase influence the outer-membrane proteome and the expression of a type VI secretion system in Yersinia pestis. *Microbiology*, 155(2):498–512, 2009.

[512] Silverman J. M., Austin L. S., Hsu F., Hicks K. G., Hood R. D. and Mougous J. D. Separate inputs modulate phosphorylation-dependent and -independent type VI secretion activation. *Molecular microbiology*, 82(5):1277–1290, 2011.

[513] Schmerk C. L., Duplantis B. N., Howard P. L. and Nano F. E. A Francisella novicida pdpA mutant exhibits limited intracellular replication and remains associated with the lysosomal marker LAMP-1. *Microbiology*, 155(Pt 5):1498–1504, 2009.

[514] Schmerk C. L., Duplantis B. N., Wang D., Burke R. D., Chou A. Y., Elkins K. L., Ludu J. S. and Nano F. E. Characterization of the pathogenicity island protein PdpA and its role in the virulence of Francisella novicida. *Microbiology*, 155(Pt 5):1489–1497, 2009.

[515] de Bruin O. M., Duplantis B. N., Ludu J. S., Hare R. F., Nix E. B., Schmerk C. L., Robb C. S., Boraston A. B., Hueffer K. and Nano F. E. The biochemical properties of the Francisella pathogenicity island (FPI)-encoded proteins IglA, IglB, IglC, PdpB and DotU suggest roles in type VI secretion. *Microbiology*, 157(12):3483–3491, 2011.

[516] Broms J. E., Lavander M., Meyer L. and Sjostedt A. IglG and IglI of the Francisella Pathogenicity Island Are Important Virulence Determinants of Francisella tularensis LVS. *Infection and Immunity*, 79(9):3683–3696, 2011.

[517] Nguyen J. Q., Gilley R. P., Zogaj X., Rodriguez S. A. and Klose K. E. Lipidation of the FPI protein IglE contributes to Francisella tularensis ssp. novicida intramacrophage replication and virulence. *Pathogens and disease*, 72(1):10–18, 2014.

[518] Barker J. R., Chong A., Wehrly T. D., Yu J.-J., Rodriguez S. A., Liu J., Celli J., Arulanandam B. P. and Klose K. E. The Francisella tularensis Pathogenicity Island Encodes a Secretion System that is required for Phagosome Escape and Virulence. *Molecular microbiology*, 74(6):1459–1470, 2009.

[519] Lindgren M., Eneslatt K., Broms J. E. and Sjostedt A. Importance of PdpC, IglC, IglI, and IglG for Modulation of a Host Cell Death Pathway Induced by Francisella tularensis. *Infection and Immunity*, 81(6):2076–2084, 2013.

[520] Meyer L., Broms J. E., Liu X., Rottenberg M. E. and Sjostedt A. Microinjection of Francisella tularensis and Listeria monocytogenes Reveals the Importance of Bacterial and Host Factors for Successful Replication. *Infection and Immunity*, 83(8):3233–3242, 2015.

[521] Ozanic M., Marecic V., Lindgren M., Sjostedt A. and Santic M. Phenotypic characterization of the Francisella tularensis deltapdpC and deltaiglG mutants. *Microbes and Infection*, pages –, 2016.

[522] Long M. E., Lindemann S. R., Rasmussen J. A., Jones B. D. and Allen L.-A. H. Disruption of Francisella tularensis Schu S4 iglI, iglJ, and pdpC Genes Results in Attenuation for Growth in Human Macrophages and In Vivo Virulence in Mice and Reveals a Unique Phenotype for pdpC. *Infection and Immunity*, 81(3):850–861, 2012.

[523] Clemens D., Ge P., Lee B.-Y., Horwitz M. and Zhou Z. Atomic Structure of T6SS Reveals Interlaced Array Essential to Function. *Cell*, 160(5):940 – 951, 2015.

[524] Brodmann M., Dreier R. F., Broz P. and Basler M. Francisella requires dynamic type VI secretion system and ClpB to deliver effectors for phagosomal escape. *Nature Communications*, 8:15853–, 2017.

[525] Ghonime M. G., Shamaa O. R., Eldomany R. A., Gavrilin M. A. and Wewers M. D. Tyrosine phosphatase inhibition induces an ASC-dependent pyroptosis. *Biochemical and Biophysical Research Communications*, 425(2):384 – 389, 2012.

[526] Le H. T. and Harton J. A. Pyrin- and CARD-only proteins as regulators of NLR functions. *Frontiers in Immunology*, 4(275), 2013.

[527] Kim Y. K., Shin J.-S. and Nahm M. H. NOD-Like Receptors in Infection, Immunity, and Diseases. *Yonsei Med J*, 57(1):5–14, 2016.

[528] Mariathasan S., Weiss D. S., Newton K., McBride J., O'Rourke K., Roose-Girma M., Lee W. P., Weinrauch Y., Monack D. M. and Dixit V. M. Cryopyrin activates the inflammasome in response to toxins and ATP. *Nature*, 440(7081):228–232, 2006.

[529] Chung I.-C., OuYang C.-N., Yuan S.-N., Li H.-P., Chen J.-T., Shieh H.-R., Chen Y.-J., Ojcius D. M., Chu C.-L., Yu J.-S., Chang Y.-S. and Chen L.-C. Pyk2 activates the NLRP3 inflammasome by directly phosphorylating ASC and contributes to inflammasome-dependent peritonitis. *Scientific Reports*, 6:36214–, 2016.

[530] Qu Y., Misaghi S., Newton K., Maltzman A., Izrael-Tomasevic A., Arnott D. and Dixit V. M. NLRP3 recruitment by NLRC4 during Salmonella infection. *Journal of Experimental Medicine*, 213(6):877–885, 2016.

[531] Man S. M., Tourlomousis P., Hopkins L., Monie T. P., Fitzgerald K. A. and Bryant C. E. Salmonella Infection Induces Recruitment of Caspase-8 to the Inflammasome To Modulate IL-1? Production. *The Journal of Immunology*, 191(10):5239–5246, 2013.

[532] Agard N. J., Maltby D. and Wells J. A. Inflammatory Stimuli Regulate Caspase Substrate Profiles. *Molecular & Cellular Proteomics : MCP*, 9(5):880–893, 2010.

[533] Keller M., Ruegg A., Werner S. and Beer H.-D. Active Caspase-1 Is a Regulator of Unconventional Protein Secretion. *Cell*, 132(5):818 – 831, 2008.

[534] Hervy M., Hoffman L. M., Jensen C. C., Smith M. and Beckerle M. C. The LIM Protein Zyxin Binds CARP-1 and Promotes Apoptosis. *Genes & Cancer*, 1(5):506–515, 2010.

[535] Chan C.-B., Liu X., Tang X., Fu H. and Ye K. Akt phosphorylation of zyxin mediates its interaction with acinus-S and prevents acinus-triggered chromatin condensation. *Cell Death Differ*, 14(9):1688–1699, 2007.

[536] Man S. M., Place D. E., Kuriakose T. and Kanneganti T.-D. Interferon-inducible guanylate-binding proteins at the interface of cell-autonomous immunity and inflammasome activation. *Journal of Leukocyte Biology*, 2016.

[537] Conos S. A., Chen K. W., De Nardo D., Hara H., Whitehead L., Nunez G., Masters S. L., Murphy J. M., Schroder K., Vaux D. L., Lawlor K. E., Lindqvist L. M. and Vince J. E. Active MLKL triggers the NLRP3 inflammasome in a cell-intrinsic manner. *Proceedings of the National Academy of Sciences*, 114(6):E961–E969, 2017.

[538] Gutierrez K. D., Davis M. A., Daniels B. P., Olsen T. M., Ralli-Jain P., Tait S. W. G., Gale M. and Oberst A. MLKL Activation Triggers NLRP3-Mediated Processing and Release of IL-1beta Independently of Gasdermin-D. *The Journal of Immunology*, 198(5):2156–2164, 2017.

[539] Shi H., Wang Y., Li X., Zhan X., Tang M., Fina M., Su L., Pratt D., Bu C. H., Hildebrand S., Lyon S., Scott L., Quan J., Sun Q., Russell J., Arnett S., Jurek P., Chen D., Kravchenko V. V., Mathison J. C., Moresco E. M. Y., Monson N. L., Ulevitch R. J. and Beutler B. NLRP3 activation and mitosis are mutually exclusive events coordinated by NEK7, a new inflammasome component. *Nat Immunol*, 17(3):250–258, 2016.

[540] Zanoni I., Tan Y., Di Gioia M., Broggi A., Ruan J., Shi J., Donado C. A., Shao F., Wu H., Springstead J. R. and Kagan J. C. An endogenous caspase-11 ligand elicits interleukin-1 release from living dendritic cells. *Science*, 2016.

[541] Gaidt M., Ebert T., Chauhan D., Schmidt T., Schmid-Burgk J., Rapino F., Robertson A., Cooper M., Graf T. and Hornung V. Human Monocytes Engage an Alternative Inflammasome Pathway. *Immunity*, 44(4):833 – 846, 2016.

[542] Chen K., Gross C., Sotomayor F., Stacey K., Tschopp J., Sweet M. and Schroder K. The Neutrophil NLRC4 Inflammasome Selectively Promotes IL-1beta Maturation without Pyroptosis during Acute Salmonella Challenge. *Cell Reports*, 8(2):570 – 582, 2014.

[543] Rogers C., Fernandes-Alnemri T., Mayes L., Alnemri D., Cingolani G. and Alnemri E. S. Cleavage of DFNA5 by caspase-3 during apoptosis mediates progression to secondary necrotic/pyroptotic cell death. *Nature Communications*, 8:14128–, 2017.

[544] Arpaia N., Godec J., Lau L., Sivick K. E., McLaughlin L. M., Jones M. B., Dracheva T., Peterson S. N., Monack D. M. and Barton G. M. TLR Signaling Is Required for Salmonella typhimurium Virulence. *Cell*, 144(5):675 – 688, 2011.

[545] Conrads T. P., Issaq H. J. and Veenstra T. D. New Tools for Quantitative Phosphoproteome Analysis. *Biochemical and Biophysical Research Communications*, 290(3):885 – 890, 2002.

[546] Amoresano A., Marino G., Cirulli C. and Quemeneur E. Mapping Phosphorylation Sites: A New Strategy Based on the Use of Isotopically-Labelled Dithiothreitol and Mass Spectrometry. *European Journal of Mass Spectrometry*, 10(3):401–412, 2004.

[547] Poot A. J., Ruijter E., Nuijens T., Dirksen E. H. C., Heck A. J. R., Slijper M., Rijkers D. T. S. and Liskamp R. M. J. Selective enrichment of Ser-/Thr-phosphorylated peptides in the presence of Ser-/Thr-glycosylated peptides. *PROTEOMICS*, 6(24):6394–6399, 2006.

[548] Olsen J. V., Blagoev B., Gnad F., Macek B., Kumar C., Mortensen P. and Mann M. Global, In Vivo, and Site-Specific Phosphorylation Dynamics in Signaling Networks. *Cell*, 127(3):635 – 648, 2006.

[549] Zhu Y., Li H., Long C., Hu L., Xu H., Liu L., Chen S., Wang D.-C. and Shao F. Structural Insights into the Enzymatic Mechanism of the Pathogenic {MAPK} Phosphothreonine Lyase. *Molecular Cell*, 28(5):899 – 913, 2007.

[550] Li H., Xu H., Zhou Y., Zhang J., Long C., Li S., Chen S., Zhou J.-M. and Shao F. The Phosphothreonine Lyase Activity of a Bacterial Type III Effector Family. *Science*, 315(5814):1000–1003, 2007.

[551] Zurawski D. V., Mitsuhata C., Mumy K. L., McCormick B. A. and Maurelli A. T. OspF and OspC1 Are Shigella flexneri Type III Secretion System Effectors That Are Required for Postinvasion Aspects of Virulence. *Infection and Immunity*, 74(10):5964–5976, 2006.

[552] Ficarro S. B., McCleland M. L., Stukenberg P. T., Burke D. J., Ross M. M., Shabanowitz J., Hunt D. F. and White F. M. Phosphoproteome analysis by mass spectrometry and its application to Saccharomyces cerevisiae. *Nat Biotech*, 20(3):301–305, 2002.

[553] Llewellyn A. C., Zhao J., Song F., Parvathareddy J., Xu Q., Napier B. A., Laroui H., Merlin D., Bina J. E., Cotter P. A., Miller M. A., Raetz C. R. H. and Weiss D. S. NaxD is a deacetylase required for lipid A modification and Francisella pathogenesis. *Molecular Microbiology*, 86(3):611–627, 2012.

[554] Song F., Guan Z. and Raetz C. R. H. Biosynthesis of Undecaprenyl Phosphate-Galactosamine and Undecaprenyl Phosphate-Glucose in Francisella novicida. *Biochemistry*, 48(6):1173–1182, 2009.

[555] Lewis L. A., Choudhury B., Balthazar J. T., Martin L. E., Ram S., Rice P. A., Stephens D. S., Carlson R. and Shafer W. M. Phosphoethanolamine Substitution of Lipid A and Resistance of Neisseria gonorrhoeae to Cationic Antimicrobial Peptides and Complement-Mediated Killing by Normal Human Serum. *Infection and Immunity*, 77(3):1112–1120, 2008.

[556] Arroyo L. A., Herrera C. M., Fernandez L., Hankins J. V., Trent M. S. and Hancock R. E. W. The pmrCAB Operon Mediates Polymyxin Resistance in Acinetobacter baumannii ATCC 17978 and Clinical Isolates through Phosphoethanolamine Modification of Lipid A. *Antimicrobial Agents and Chemotherapy*, 55(8):3743–3751, 2011.

[557] Wallet P., Lagrange B. and Henry T. *Francisella Inflammasomes: Integrated Responses to a Cytosolic Stealth Bacterium*, pages 229–256. Springer International Publishing, Cham, 2016.

[558] Kudryashev M., Wang R.-R., Brackmann M., Scherer S., Maier T., Baker D., DiMaio F., Stahlberg H., Egelman E. and Basler M. Structure of the Type VI Secretion System Contractile Sheath. *Cell*, 160(5):952 – 962, 2015.

[559] Eshraghi A., Kim J., Walls A., Ledvina H., Miller C., Ramsey K., Whitney J., Radey M., Peterson S., Ruhland B., Tran B., Goo Y., Goodlett D., Dove S., Celli J., Veesler D. and Mougous J. Secreted Effectors Encoded within and outside of the Francisella Pathogenicity Island Promote Intramacrophage Growth. *Cell Host & Microbe*, 20(5):573 – 583, 2016.

[560] Guenster R. A., Matthews S. A., Holden D. W. and Thurston T. L. M. SseK1 and SseK3 T3SS effectors inhibit NF-kB signalling and necroptotic cell death in Salmonella-infected macrophages. *Infection and Immunity*, 2017.

[561] Cabantous S., Terwilliger T. C. and Waldo G. S. Protein tagging and detection with engineered self-assembling fragments of green fluorescent protein. *Nat Biotech*, 23(1):102–107, 2005.

[562] Ungricht R. and Kutay U. Mechanisms and functions of nuclear envelope remodelling. *Nat Rev Mol Cell Biol*, advance online publication:–, 2017.

[563] Banfalvi G. *Overview of Cell Synchronization*, pages 1–23. Humana Press, Totowa, NJ, 2011.

[564] Ahmadi M., Gharibi T., Dolati S., Rostamzadeh D., Aslani S., Baradaran B., Younesi V. and Yousefi M. Epigenetic modifications and epigenetic based medication implementations of autoimmune diseases. *Biomedicine & Pharmacotherapy*, 87:596 – 608, 2017.

[565] Araujo F. D., Knox J. D., Szyf M., Price G. B. and Zannis-Hadjopoulos M. Concurrent Replication and Methylation at Mammalian Origins of Replication. *Molecular and Cellular Biology*, 18(6):3475–3482, 1998.

[566] Leonhardt H., Page A. W., Weier H.-U. and Bestor T. H. A targeting sequence directs DNA methyltransferase to sites of DNA replication in mammalian nuclei. *Cell*, 71(5):865 – 873, 1992.

[567] Vankova Hausnerova V. and Lanctot C. Chromatin decondensation is accompanied by a transient increase in transcriptional output. *Biology of the Cell*, 109(1):65–79, 2017.

[568] Szabo A., Stolz L. and Granzow R. Surface plasmon resonance and its use in biomolecular interaction analysis (BIA). *Current Opinion in Structural Biology*, 5(5):699 – 705, 1995.

[569] Fry A. M., O'Regan L., Sabir S. R. and Bayliss R. Cell cycle regulation by the NEK family of protein kinases. *Journal of Cell Science*, 125(19):4423–4433, 2012.

[570] Schattgen S. A. and Fitzgerald K. A. The PYHIN protein family as mediators of host defenses. *Immunological Reviews*, 243(1):109–118, 2011.

Acknowledgments

I would like to express my gratitude to...

- ... Prof. Dr. Petr Broz for giving me the opportunity to do my PhD thesis in his lab, for an excellent introduction into the exciting field of innate immunity and for the constructive discussions about my projects.
- ... my committee members Prof. Dr. Dirk Bumann and Prof. Dr. Martin Spiess for their interest in my projects and helpful inputs during committee meetings.
- ... the group members Dr. Etienne Meunier, Dr. José Viera dos Santos, Dr. Saori Yoshii, Dr. Mathias Dick, Sebastian Rühl, Leonie Anton, Rosalie Heilig and Kateryna Shkarina for a stimulating working atmosphere, countless laughs and enriching discussions about but not only science. You are an amazing crowd and because of you, I enjoyed every day in the lab.
- ... Michaela Hanisch, who supported me in all administrative issues.
- ... especially Prof. Dr. Marek Basler and Maj Brodmann for a wonderful and very fruitful collaboration. Without them, the *Francisella*-T6SS project would not have been possible.
- ... the in-house Proteomics Core Facility (PCF), Imaging Core Facility (IMCF) and FACS Core Facility (FCF) for their support in mass spectrometric analysis and data management, for confocal and SIM microscopy and for single cell sorting and FACS analysis.
- ... especially Dr. Alex Schmidt and Erik Ahrné for the introduction into mass spectrometry and the collaboration in these projects. Without them, the phosphoproteomics project would not have been possible.
- ... the floor managers Leo Faletti and Marina Kuhn and their teams for making sure that we can truly focus on science.
- ... the PhD reps and all people of the 4th and 6th floor for all the support in scientific issues but also for spending time outside of lab.
- ... all the people for helpful inputs and critical reading of the thesis manuscript.
- ... my family, especially my mother, my father and my sister for their interest in my work and the continuous support and confidence along my way.
- ... my friends for sharing good times besides science. You gave me the opportunity to see the world from a non-scientific perspective.

I dedicate the PhD thesis to my grandmother who passed away eight weeks ago. She always believed in me and my success, was proud about my career path and supported me during my PhD. Grossmami, your example of hard working but staying positive no matter what you were facing was an inspiration and motivation during my entire PhD.

Chapter V

Appendix

1 Research article IV

Caspase-11 activation requires lysis of pathogen-containing vacuoles by IFN-induced GTPases

E. Meunier, M. S. Dick*, **R. F. Dreier***, N. Schürmann, D. Kenzelmann Broz, S. Warming, M. Roose-Girma, D. Bumann, N. Kayagaki, K. Takeda, M. Yamamoto and P. Broz.
* denotes equal contribution.

Nature
2014 May 15; 509(7500):366-790. doi: 10.1038/nature13157. [288]

Statement of contribution

I performed the mass spectrometry analysis that identified GBPs as the most induced proteins upon *Salmonella* infections. Furthermore, I produced bone marrow-derived macrophages and performed multiple control experiments that were not included in the final manuscript. I was involved in the discussion of the results and writing of the manuscript.

LETTER

doi:10.1038/nature13157

Caspase-11 activation requires lysis of pathogen-containing vacuoles by IFN-induced GTPases

Etienne Meunier[1], Mathias S. Dick[1]*, Roland F. Dreier[1]*, Nura Schürmann[1], Daniela Kenzelmann Broz[2], Søren Warming[3], Merone Roose-Girma[3], Dirk Bumann[1], Nobuhiko Kayagaki[3], Kiyoshi Takeda[4], Masahiro Yamamoto[4] & Petr Broz[1]

Lipopolysaccharide from Gram-negative bacteria is sensed in the host cell cytoplasm by a non-canonical inflammasome pathway that ultimately results in caspase-11 activation and cell death[1–3]. In mouse macrophages, activation of this pathway requires the production of type-I interferons[4,5], indicating that interferon-induced genes have a critical role in initiating this pathway. Here we report that a cluster of small interferon-inducible GTPases, the so-called guanylate-binding proteins, is required for the full activity of the non-canonical caspase-11 inflammasome during infections with vacuolar Gram-negative bacteria. We show that guanylate-binding proteins are recruited to intracellular bacterial pathogens and are necessary to induce the lysis of the pathogen-containing vacuole. Lysis of the vacuole releases bacteria into the cytosol, thus allowing the detection of their lipopolysaccharide by a yet unknown lipopolysaccharide sensor. Moreover, recognition of the lysed vacuole by the danger sensor galectin-8 initiates the uptake of bacteria into autophagosomes, which results in a reduction of caspase-11 activation. These results indicate that host-mediated lysis of pathogen-containing vacuoles is an essential immune function and is necessary for efficient recognition of pathogens by inflammasome complexes in the cytosol.

Previous studies have reported that induction of caspase-11-dependent cell death by Gram-negative bacteria requires Trif-dependent production of type-I interferons (type-I-IFNs)[4,5] (Extended Data Fig. 1a). Type-I-IFN production is however not required for pro-caspase-11 induction[4,6,7] and is dispensable for caspase-11 activation by transfected lipopolysaccharide (LPS; Extended Data Fig. 1b)[2]. This indicates that interferon-stimulated genes (ISGs) play a major role in activating caspase-11 in response to intracellular bacteria. To investigate which ISGs were involved in activating caspase-11, we used proteomics-based expression analysis to identify proteins that were highly induced following *Salmonella* infection. Among the most strongly upregulated proteins were interferon-induced GTPases, such as the large 65–67 kDa guanylate-binding proteins (GBPs) and small 47 kDa immunity-related GTPases (IRGs) (data not shown). These proteins function in cell-autonomous immunity, that is, mechanisms that allow host cells to kill pathogens or restrict their replication, and have even been associated with the activation of inflammasomes[8–10].

Mice have 11 GBPs, which are highly homologous and are clustered in two genomic loci on chromosomes 3 and 5, respectively[8,11]. Recently, GBPs on chromosome 3 have been shown to restrict the replication of *Toxoplasma gondii* in peritoneal macrophages and mice[11]. We therefore infected bone-marrow-derived macrophages (BMDMs) from Gbp^{chr3} KO mice, which lack GBP1, 2, 3, 5 and 7 (Extended Data Fig. 2a–e), and wild-type littermates with a number of Gram-negative vacuolar pathogens that trigger caspase-11 activation (data not shown)[1,4,5] and determined the activity of the non-canonical inflammasome pathway at 16 h post-infection (Fig. 1a, b). Macrophages from Gbp^{chr3} KO mice showed a significant reduction of cell death (as measured by lactate dehydrogenase (LDH) release) and IL-1β secretion when infected with wild-type *Salmonella typhimurium*, a type three secretion system (T3SS)-deficient mutant of *S. typhimurium* (ΔSPI-2), *Vibrio cholerae*, *Enterobacter cloacae* or *Citrobacter koseri* (Fig. 1a), and this was independent of LPS or polyinosinic:polycytidylic acid (poly(I:C)) priming (Extended Data Fig. 2f, g). Gbp^{chr3}-deficiency also reduced secretion of caspase-1 p20 subunit, caspase-11 and mature IL-1β, IL-18 and IL-1α (Fig. 1b). Because interferons induce GBP expression (Extended Data Fig. 2b, c)[8], we investigated whether IFN-γ treatment would accelerate LDH release in response to *Salmonella* infection. IFN-γ-treated wild-type BMDMs released LDH as soon as 4 h after infection, whereas Gbp^{chr3} KO BMDMs failed to release LDH at early time points even after IFN-γ priming (Fig. 1c), indicating that GBP induction was required for activity of the non-canonical inflammasome pathway.

We next explored whether GBPs play a role in the activation of canonical inflammasomes. LPS-primed wild-type and Gbp^{chr3}-deficient macrophages released comparable levels of LDH and mature IL-1β when infected with logarithmic phase *S. typhimurium*, which exclusively engage the NLRC4 inflammasome via the SPI-1 T3SS (Fig. 1d)[12]. Similarly, Gbp^{chr3}-deficiency did not affect AIM2 inflammasome activation upon poly (deoxyadenylic-deoxythymidylic) acid (poly(dA:dT)) transfection (Fig. 1d). Although GBP5 had been previously linked to NLRP3 activation[9], we did not observe a defect in NLRP3 activation in Gbp^{chr3} KOs (Fig. 1d), possibly owing to different modes of pre-stimulation. These data indicate that GBPs are dispensable for canonical inflammasome activity, but are required for the activation of the non-canonical inflammasome pathway.

To investigate whether GBPs directly mediated the detection of intracellular LPS, we engaged the non-canonical inflammasome by transfecting macrophages with different types of ultra-pure LPS (Fig. 1e). Cytoplasmic LPS triggered LDH release and IL-1β secretion to a similar extent in both wild-type and Gbp^{chr3}-deficient BMDMs, indicating that GBPs were required upstream of LPS sensing and only during bacterial infection. We next investigated if GBPs were required for immune detection of vacuolar or cytosolic bacteria by infecting BMDMs with Δ*sifA S. typhimurium* and *Burkholderia thailandensis*, which rapidly enter the cytosol and activate caspase-11 (ref. 13). Unprimed Gbp^{chr3} KO and wild-type BMDMs responded comparably to these bacteria (Extended Data Fig. 3a–c). Because GBPs might affect this response when pre-induced, we also infected IFN-γ-primed BMDMs with Δ*sifA S. typhimurium* (Extended Data Fig. 3d). IFN-γ-priming indeed resulted in a small difference between wild-type and Gbp^{chr3} KO BMDMs after infection with Δ*sifA Salmonella*, yet not to the extent seen with wild-type *Salmonella* (Fig. 1c), indicating that GBPs mainly participate in the activation of the non-canonical inflammasome by vacuolar bacteria.

Finally, to investigate which GBP controls caspase-11 activation, all 11 murine *Gbp*s were individually knocked down in BMDMs and the cells were infected with flagellin-deficient *Salmonella*, which activate the non-canonical inflammasome but not NLRC4 (Extended Data Fig. 4a and Supplementary Information)[4]. Only knockdown of *Gbp2* resulted in reduced LDH release and IL-1β secretion (Extended Data Fig. 4b–d).

[1]Focal Area Infection Biology, Biozentrum, University of Basel, CH-4056 Basel, Switzerland. [2]Department Biomedicine, University of Basel, CH-4056 Basel, Switzerland. [3]Genentech Inc., South San Francisco, California 94080, USA. [4]Department of Microbiology and Immunology, Osaka University, Yamadaoka, Suita, Osaka 565-0871, Japan.
*These authors contributed equally to this work.

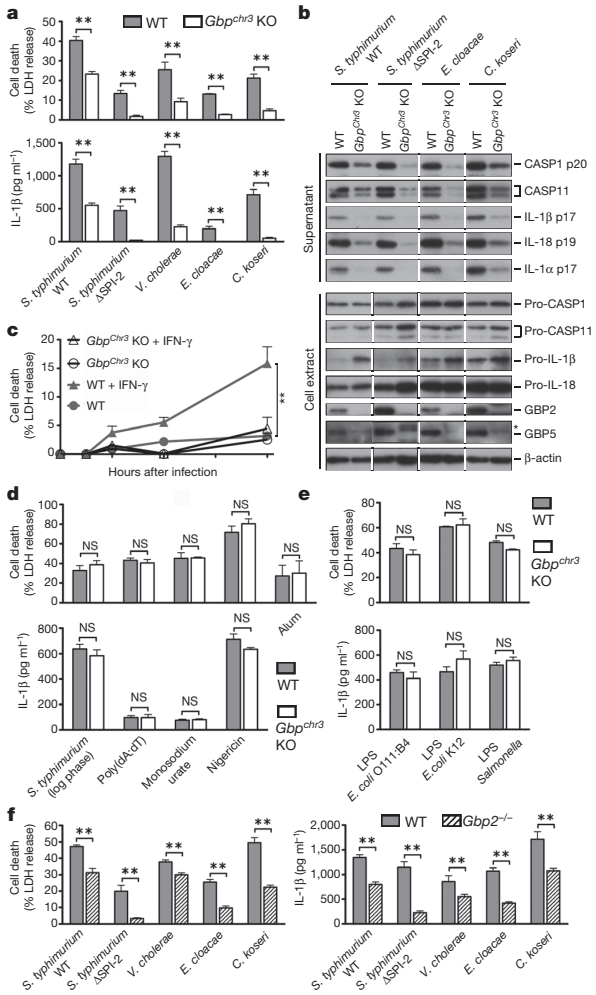

Figure 1 | Caspase-11 activation by intracellular bacterial pathogens requires GBPs. **a**, **b**, LDH release, IL-1β secretion (**a**) and immunoblots for caspase-1, caspase-11, IL-1β, IL-18 and IL-1α (**b**) from unprimed BMDMs infected for 16 h with the indicated bacteria (grown to stationary phase). **c**, Time course measuring LDH release from unprimed or IFN-γ-primed BMDMs infected with *S. typhimurium*. **d**, **e**, LDH release and IL-1β secretion from primed BMDMs infected with SPI-1-expressing logarithmic phase *S. typhimurium*, treated with monosodium urate, alum and nigericin or transfected with poly(dA:dT) and LPS. **f**, LDH release and IL-1β secretion from unprimed wild-type and $Gbp2^{-/-}$ BMDMs infected for 16 h with the indicated bacteria (grown to stationary phase). Graphs show mean and s.d. of quadruplicate wells and data are representative of two (**b**) and three (**a**, **c**–**f**) independent experiments. *Crossreactive band; **$P < 0.01$; NS, not significant (two-tailed *t*-test).

To validate these data we obtained BMDMs from $Gbp2^{-/-}$ mice and wild-type littermates[14] and infected them with vacuolar Gram-negative bacteria. As expected, we observed reduced levels of cell death, cytokine secretion and caspase release in $Gbp2^{-/-}$ BMDMs, indicating attenuated activation of the non-canonical inflammasome (Fig. 1f and Extended Data Fig. 4e), whereas direct LPS sensing or the activation of canonical inflammasomes was not affected (Extended Data Fig. 4f, g). In contrast, *Gbp5*-deficiency did not have any effect on canonical and non-canonical inflammasome activation (Extended Data Fig. 5). Nevertheless, *Gbp2*-deficiency did not reduce caspase-11 activation as markedly as Gbp^{chr3}-deficiency, indicating that whereas caspase-11 activation mainly requires GBP2, other GBPs might also be partially involved.

Reduced numbers of intracellular bacteria could account for low levels of caspase-11 activation in Gbp^{chr3}- and *Gbp2*-deficient macrophages. However, a comparison of wild-type and Gbp^{chr3} KO BMDMs showed that Gbp^{chr3}-deficiency resulted in significantly higher numbers of total and live *Salmonella* per cell (Fig. 2a), consistent with higher colony forming units numbers in Gbp^{chr3} KO BMDMs (Extended Data Fig. 6). In addition, fluorescence-activated cell sorting (FACS)-based analysis of dead (mCherry-negative, $FITC^+$) and live (mCherry-positive, $FITC^+$) *Salmonella* at 16 h post-infection found significantly fewer dead bacteria (~20%) in GBP^{chr3} KO and $Gbp2^{-/-}$ BMDMs when compared to wild-type BMDMs (>30%) (Fig. 2b). Importantly, bacterial killing in $Casp11^{-/-}$ BMDMs was comparable to wild-type BMDMs, indicating that the control of bacterial replication was directly linked to GBP function and not to the activation of the non-canonical inflammasome (Fig. 2b). In conclusion, we show that GBPs control bacterial replication on a cell-autonomous level, which is consistent with a previous report that GBP1 partially restricts *Mycobacterium bovis* and *Listeria monocytogenes* replication[10].

Restricting bacterial replication has been proposed to require the association of GBPs with pathogen-containing vacuoles and the recruitment of antimicrobial factors[8]. We therefore investigated whether GBPs targeted intracellular Gram-negative bacteria. Indeed, GBP2 could be detected on intracellular bacteria within hours after infection (Fig. 2c). Very little GBP-positive bacteria were detected in $Stat1^{-/-}$ BMDMs, which do not respond to type-I- and type-II-IFNs and largely failed to induce GBP expression (data not shown). Remarkably, GBP-positive *Salmonella* seemed to have lost mCherry expression (Fig. 2c), indicating that these bacteria were dead. To determine whether GBPs are recruited to dead bacteria we infected BMDMs with *Salmonella* killed by heat, paraformaldehyde or 70% ethanol treatment, yet only live *Salmonella* acquired GBP staining and activated the inflammasome (Fig. 2d). To examine this mechanism *in vivo*, we immunostained spleen tissue sections of mice infected with *Salmonella* for GBPs. Indeed, GBPs could also be found associated with approximately 20% of bacteria *in vivo*, and a significantly higher proportion of these bacteria were dead, based on the loss of mCherry expression (Fig. 2e–g). Furthermore, treatment with IFN-γ-neutralizing antibodies reduced the percentage of GBP-positive bacteria (Fig. 2f), consistent with reports that IFN-γ controls *Salmonella* replication *in vivo*[15,16]. Taken together, these results indicated that GBPs either kill bacteria directly or control an antimicrobial effector pathway, and raised the interesting possibility that GBP-mediated killing of bacteria might result in the release of LPS and caspase-11 activation[2,3].

To identify the antimicrobial effector pathway that is controlled by GBPs we first examined the role of free radicals[8]. Although GBP7 was reported to be required for reactive oxygen species (ROS) production and to interact with the phagosome oxidase complex[10], we did not find any role for ROS or NO production in caspase-11 activation (Extended Data Fig. 7). Furthermore, GBPs were also proposed to recruit components of the autophagy machinery to pathogen-containing vacuoles (PCVs), possibly resulting in bacterial killing within autophagosomes[8,10]. Indeed, many GBP-positive *S. typhimurium*, *E. cloacae* and *C. koseri* co-stained for the commonly used autophagy marker LC3 (Fig. 3a and Extended Data Fig. 8a). Recruitment of LC3 to intracellular *Salmonella* was partially GBP-dependent, because we found significantly lower numbers of LC3-positive *Salmonella* in Gbp^{chr3} KO compared to wild-type macrophages (Fig. 3b, c). Therefore, we speculated that autophagy-mediated killing might result in the release of LPS from bacteria and caspase-11 activation. Unexpectedly, however, pharmacological inhibition of autophagy with 3-methyladenine (3-MA) resulted in significantly higher levels of LDH release, IL-1β secretion and caspase-1/caspase-11 activation in macrophages infected with *S. typhimurium*, *E. cloacae* or *C. koseri* (Fig. 3d, e), indicating increased activation of the non-canonical inflammasome. Consistently, cell death was still caspase-11-dependent because $Casp11^{-/-}$ BMDMs did not release LDH when treated with 3-MA and infected with Gram-negative bacteria (Fig. 3f). Direct activation of caspase-11 by LPS transfection was independent of

RESEARCH LETTER

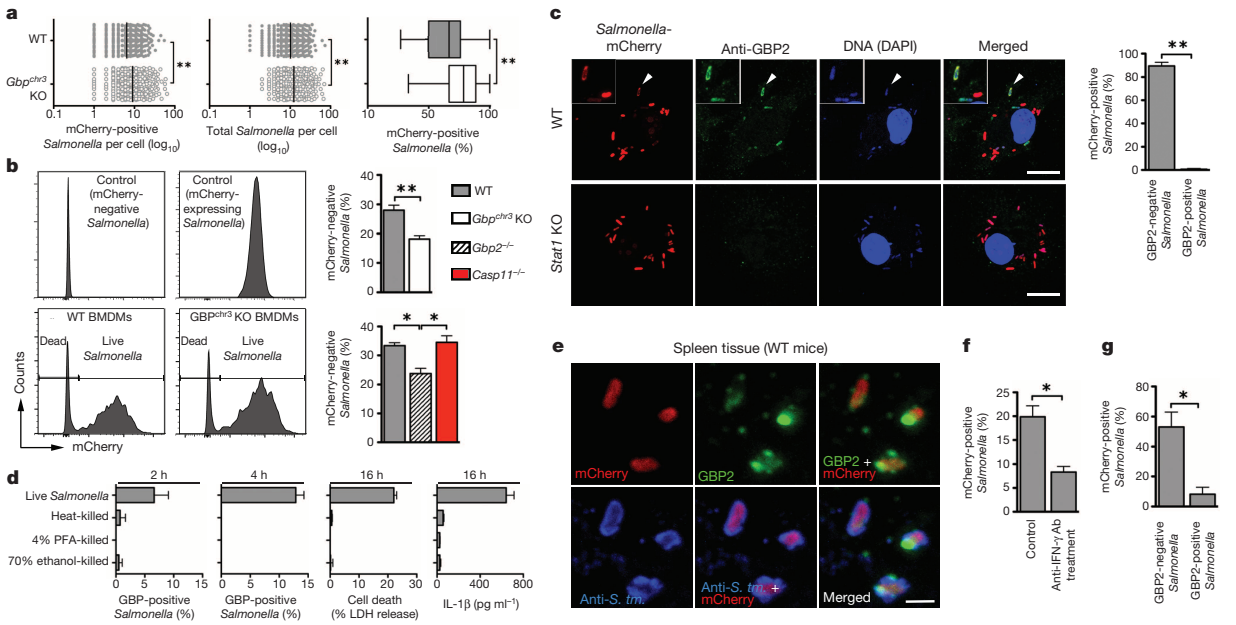

Figure 2 | GBPs control bacterial replication. **a**, **b**, Quantification of live (mCherry-positive) and dead (mCherry-negative) *S. typhimurium* per cell by immunofluorescence (**a**) or as percent of total by flow-cytometry (**b**) in unprimed BMDMs at 16 h post-infection. **c**, Immunostaining for GBP2 and quantification of live and dead *Salmonella* at 4 h post-infection. Arrowheads, bacteria shown in insets. **d**, Quantification of GBP-positive bacteria, LDH release and IL-1β secretion at indicated time points from BMDMs infected with *Salmonella*, live or killed by different means. **e**, Immunohistochemistry for GBP2 and *Salmonella* on spleen tissue from *Salmonella* (mCherry-positive)-infected mice (representative of $n = 3$ per group). *S. tm.*, *S. typhimurium*. **f**, **g**, Quantification of GBP-positive *Salmonella* in anti-IFN-γ-treated or control animals (**f**) and live and dead bacteria among GBP2-negative/-positive *Salmonella* (**g**) ($n = 3$ per group). Scale bars, 10 μm (**c**), 1 μm (**e**). Graphs show mean and 5–95 percentile (box plots) or s.d. of technical triplicates, and data are representative of three independent experiments. $^{*}P < 0.05$, $^{**}P < 0.01$ (two-tailed *t*-test).

autophagy (Fig. 3g), indicating that autophagy only counteracts non-canonical inflammasome activation during bacterial infections. To further confirm our data, we infected *Atg5*$^{-/-}$ BMDMs with *S. typhimurium* and we also observed significantly higher levels of non-canonical inflammasome activation compared to wild-type BMDMs (Fig. 3h, i). Taken together, these results indicated that, although GBPs promoted the uptake of bacteria into autophagosomes, autophagy actually counteracted caspase-11 activation. Thus, GBP-dependent LPS detection occurs before bacteria are targeted to autophagosomes.

A possible explanation could be that autophagy sequesters bacteria that had escaped from the vacuole, and thus prevents further LPS release into the cytosol. Recently, the cytosolic danger receptor galectin-8 was reported to function as a marker for lysed vacuoles. Galectin-8 binds β-galactosides, which are normally found on the inner leaflet of the vacuolar membrane and get exposed to the cytosol upon vacuolar lysis[17]. Indeed, quantification of galectin-8-positive *Salmonella* showed that significantly fewer bacteria were targeted by galectin-8 in *Gbp*^{chr3} KO BMDMs than in wild-type macrophages (Fig. 4a). Because galectin-8 colocalized with GBP- and LC3-positive *Salmonella* (Fig. 4b, c), we speculated that GBPs promote LC3 recruitment through galectin-8. Consistently, we found lower levels of galectin-8-positive *Salmonella* among LC3-positive *Salmonella* in *Gbp*^{chr3} KO compared to wild-type BMDMs (Fig. 4d). Galectin-8 interacts with the autophagy adaptor protein NDP52, which in humans contains binding sites for galectin-8, ubiquitin and LC3[18]. In line with a role for NDP52 in linking galectin-8 to LC3, murine NDP52 colocalized with galectin-8 on intracellular *Salmonella* (Extended Data Fig. 8b). Targeting of *Salmonella* to autophagosomes might also involve other autophagy cargo adaptors, because p62 was associated with the majority of LC3-positive bacteria, yet this was independent of GBPs (Extended Data Fig. 8c, d). Altogether, these results suggested that GBPs might promote the lysis of vacuoles or help to recruit galectin-8 to lysed vacuoles.

To confirm a direct role of GBPs in vacuolar lysis, we adapted a phagosome integrity assay based on differential permeabilization with digitonin (Extended Data Fig. 9). Comparing wild-type and *GBP*^{chr3} KO BMDMs, we found significantly lower numbers of cytosolic (FITC^{+}) *S. typhimurium* in *Gbp*^{chr3}-deficient cells (Fig. 4e, f). Similarly, *Gbp2*$^{-/-}$ BMDMs also harboured fewer cytosolic *S. typhimurium* compared to BMDMs from wild-type littermates (Fig. 4g). In contrast, we did not find a defect in cytosolic localization between wild-type and *Gbp*^{chr3} KO BMDMs infected with the specialized cytosolic pathogen *Shigella flexneri*, which uses its T3SS to destabilize the phagosome and escape into the cytoplasm (Fig. 4h)[19]. Although we cannot exclude that GBPs might also be involved in the recruitment or assembly of the non-canonical inflammasome, these results indicate that GBPs, in particular GBP2, directly promote the destruction of vacuoles.

In conclusion, our data demonstrate that host-induced destruction of PCVs or phagosomes is an essential immune function and assures recognition of vacuolar bacteria by cytosolic innate immune sensors (Extended Data Fig. 10). Additional studies are required to determine how GBPs distinguish 'self' and 'non-self' membranes and by which mechanism phagosomes are lysed. In mice, this might involve the IRGM proteins that can act as GDI (guanine nucleotide dissociation inhibitor) and inhibit IRG and GBP activity. Absence of IRGMs results in mislocalization of both IRGs and GBPs and even in degradation of lipid droplets[20–22], supporting a model in which IRGM proteins would protect 'self'-vacuoles from being targeted by host IRGs and GBPs[23]. Because both commensals and pathogens activate caspase-11 (ref. 1), it can be assumed that GBPs are not specific towards pathogens but are a general innate immune response against bacteria trapped in the phagosomes of macrophages. Finally, given the important role of LPS-induced caspase-11 activation in septic shock[1–3], pharmaceutical targeting of the above-described pathways might be used to modulate inflammation during bacterial sepsis.

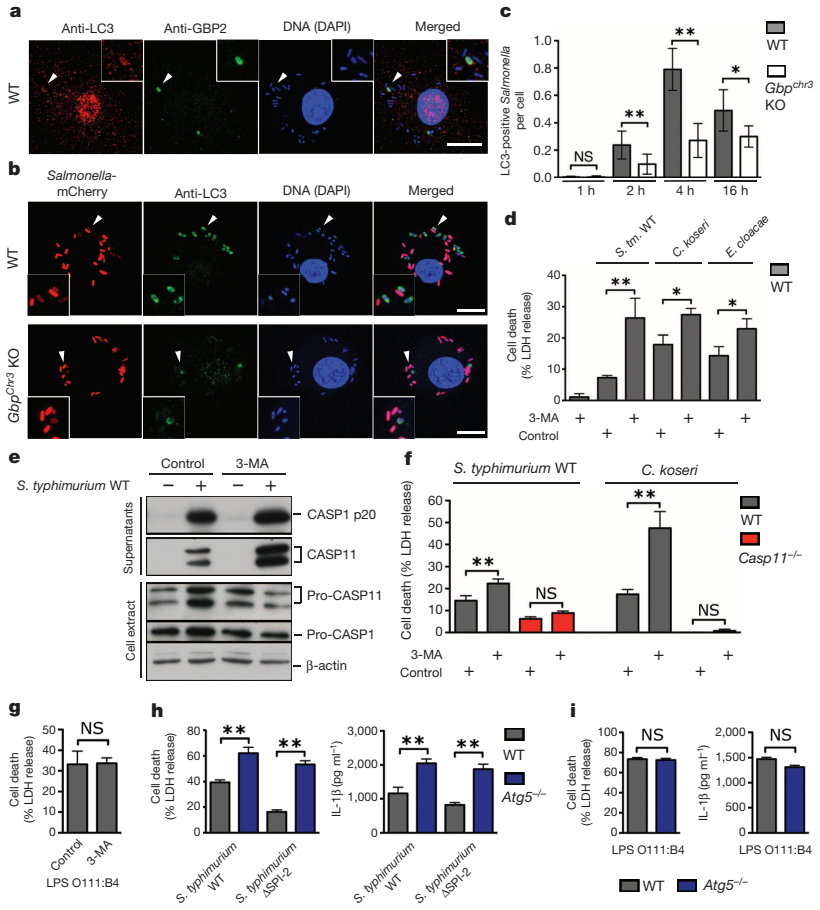

Figure 3 | Autophagy reduces caspase-11 activation. **a**, **b**, Unprimed BMDMs infected with *S. typhimurium* for 4 h and immunostained for LC3 and GBP2. Arrowheads, bacteria shown in insets. Scale bars, 10 μm. **c**, Quantification of results from **b**. **d**–**g**, LDH release and immunoblots for caspase-1 and caspase-11 from BMDMs infected for 16 h or transfected with LPS in presence or absence of 3-methyladenine (3-MA). **h**, **i**, LDH release and IL-1β secretion from BMDMs infected for 16 h or transfected with LPS. Graphs show mean and s.d. of quadruplicate wells and data are representative of two (**e**, **i**) and three (**a**–**d**, **f**–**h**) independent experiments. $^{*}P < 0.05$, $^{**}P < 0.01$; NS, not significant (two-tailed *t*-test).

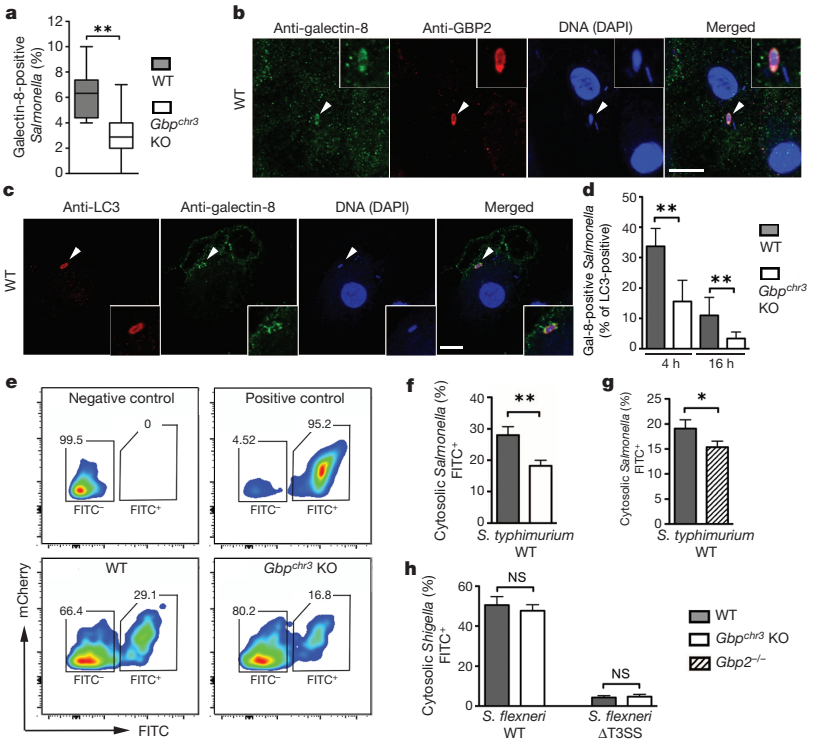

Figure 4 | GBP-mediated lysis of the PCV releases *Salmonella* into the cytosol. **a**, Quantification of galectin-8-positive *Salmonella* in unprimed BMDMs at 4 h post-infection. **b**, **c**, Unprimed BMDMs infected with *S. typhimurium* for 4 h and immunostained for galectin-8, GBP2 and LC3. Arrowheads, bacteria shown in insets. Scale bars, 10 μm. **d**, Quantification of galectin-8/LC3-double-positive *Salmonella* at indicated time points post-infection. **e**–**h**, Quantification of cytosolic and vacuolar bacteria by flow cytometry in BMDMs infected with mCherry-positive *S. typhimurium* (**e**–**g**) or *S. flexneri* (**h**, wild-type or ΔT3SS) for 4 h. Graphs show mean and s.d. or 5–95 percentile (Box plots) of technical triplicates. Data are representative of 2 (**g**, **h**), 3 (**a**–**d**) and 4 (**e**, **f**) independent experiments. $^{*}P < 0.05$, $^{**}P < 0.01$ (two-tailed *t*-test).

RESEARCH LETTER

METHODS SUMMARY

BMDMs were cultured and seeded for infections as described previously[4]. Priming was done overnight with PAM3CSK4 (1 μg ml^{-1}), LPS O111:B4 (0.1 μg ml^{-1}), murine IFN-β or murine IFN-γ (1 unit per μl). *S. typhimurium*, *S. flexneri*, *V. cholerae*, *E. cloacae*, *C. koseri* and *B. thailandensis* were grown overnight in LB or TSB medium at 37 °C with aeration. Bacteria were diluted in fresh pre-warmed macrophage medium and added to the macrophages at a multiplicity of infection (m.o.i.) of 100:1 for measurements of caspase-11 and caspase-1 activity or 10:1 for all other assays. For assaying NLRC4 activation, *Salmonella* were subcultured for 4 h to induce SPI-1 T3SS expression before infection (m.o.i. 20:1). *S. flexneri* were subcultured for 3 h to induce T3SS expression before infection (m.o.i. 30:1). When required, apocynin, L-NG-nitroarginine methyl ester (L-NAME), 3-methyladenine or vehicle controls were added 30 min before infection. Plates were centrifuged for 15 min at 500*g* to synchronize the infection and placed at 37 °C for 1 h. Next, 100 μg ml^{-1} gentamycin was added to kill extracellular bacteria. After 1 h incubation, the cells were washed once with DMEM and given fresh macrophage medium containing 10 μg ml^{-1} gentamicin for the remainder of the infection. Transfection with poly(dA:dT) or MSU, alum or nigericin treatment was done as described previously[2] or as indicated. All animal experiments were approved and performed according to local guidelines. Female BALB/c mice (10–14 weeks old) were infected intravenously with *Salmonella* (1,000 c.f.u.) and euthanized 4–5 days later. For antibody injections, mice received on day 3 two intraperitoneal injections of 200 μl PBS containing 0.2 mg anti-IFN-γ monoclonal or 0.2 mg rat IgG1, κ isotype control antibody.

Online Content Any additional Methods, Extended Data display items and Source Data are available in the online version of the paper; references unique to these sections appear only in the online paper.

Received 31 October 2013; accepted 14 February 2014.
Published online 16 April 2014.

1. Kayagaki, N. *et al.* Non-canonical inflammasome activation targets caspase-11. *Nature* **479,** 117–121 (2011).
2. Kayagaki, N. *et al.* Noncanonical inflammasome activation by intracellular LPS independent of TLR4. *Science* **341,** 1246–1249 (2013).
3. Hagar, J. A., Powell, D. A., Aachoui, Y., Ernst, R. K. & Miao, E. A. Cytoplasmic LPS activates caspase-11: implications in TLR4-independent endotoxic shock. *Science* **341,** 1250–1253 (2013).
4. Broz, P. *et al.* Caspase-11 increases susceptibility to *Salmonella* infection in the absence of caspase-1. *Nature* **490,** 288–291 (2012).
5. Rathinam, V. A. *et al.* TRIF licenses caspase-11-dependent NLRP3 inflammasome activation by Gram-negative bacteria. *Cell* **150,** 606–619 (2012).
6. Case, C. L. *et al.* Caspase-11 stimulates rapid flagellin-independent pyroptosis in response to *Legionella pneumophila*. *Proc. Natl Acad. Sci. USA* **110,** 1851–1856 (2013).
7. Casson, C. N. *et al.* Caspase-11 activation in response to bacterial secretion systems that access the host cytosol. *PLoS Pathog.* **9,** e1003400 (2013).
8. MacMicking, J. D. Interferon-inducible effector mechanisms in cell-autonomous immunity. *Nature Rev. Immunol.* **12,** 367–382 (2012).
9. Shenoy, A. R. *et al.* GBP5 promotes NLRP3 inflammasome assembly and immunity in mammals. *Science* **336,** 481–485 (2012).
10. Kim, B. H. *et al.* A family of IFN-gamma-inducible 65-kD GTPases protects against bacterial infection. *Science* **332,** 717–721 (2011).
11. Yamamoto, M. *et al.* A cluster of interferon-gamma-inducible p65 GTPases plays a critical role in host defense against *Toxoplasma gondii*. *Immunity* **37,** 302–313 (2012).
12. Broz, P. *et al.* Redundant roles for inflammasome receptors NLRP3 and NLRC4 in host defense against *Salmonella*. *J. Exp. Med.* **207,** 1745–1755 (2010).
13. Aachoui, Y. *et al.* Caspase-11 protects against bacteria that escape the vacuole. *Science* **339,** 975–978 (2013).
14. Degrandi, D. *et al.* Murine guanylate binding protein 2 (mGBP2) controls *Toxoplasma gondii* replication. *Proc. Natl Acad. Sci. USA* **110,** 294–299 (2013).
15. VanCott, J. L. *et al.* Regulation of host immune responses by modification of *Salmonella* virulence genes. *Nature Med.* **4,** 1247–1252 (1998).
16. Burton, N. A. *et al.* Disparate impact of oxidative host defenses determines the fate of *Salmonella* during systemic infection in mice. *Cell Host Microbe* **15,** 72–83 (2014).
17. Thurston, T. L., Wandel, M. P., von Muhlinen, N., Foeglein, A. & Randow, F. Galectin 8 targets damaged vesicles for autophagy to defend cells against bacterial invasion. *Nature* **482,** 414–418 (2012).
18. Deretic, V., Saitoh, T. & Akira, S. Autophagy in infection, inflammation and immunity. *Nature Rev. Immunol.* **13,** 722–737 (2013).
19. Paetzold, S., Lourido, S., Raupach, B. & Zychlinsky, A. *Shigella flexneri* phagosomal escape is independent of invasion. *Infect. Immun.* **75,** 4826–4830 (2007).
20. Hunn, J. P. *et al.* Regulatory interactions between IRG resistance GTPases in the cellular response to *Toxoplasma gondii*. *EMBO J.* **27,** 2495–2509 (2008).
21. Traver, M. K. *et al.* Immunity-related GTPase M (IRGM) proteins influence the localization of guanylate-binding protein 2 (GBP2) by modulating macroautophagy. *J. Biol. Chem.* **286,** 30471–30480 (2011).
22. Haldar, A. K. *et al.* IRG and GBP host resistance factors target aberrant, "non-self" vacuoles characterized by the missing of "self" IRGM proteins. *PLoS Pathog.* **9,** e1003414 (2013).
23. Coers, J. Self and non-self discrimination of intracellular membranes by the innate immune system. *PLoS Pathog.* **9,** e1003538 (2013).

Supplementary Information is available in the online version of the paper.

Acknowledgements We thank N. Mizushima and S. Virgin for *Atg5*-deficient BMDMs, K. Pfeffer for *Gbp2*-deficient BMDMs, J. Frey for *B. thailandensis*, the Biozentrum Proteomics and Imaging Core Facilities for technical assistance, K. Anderson, T. Soukup, R. Schwingendorf, J. C. Cox, V. M. Dixit for reagents and N. Personnic for discussions. This work was supported by an SNSF Professorship PP00P3_139120/1, University of Basel project grant ID2153162 to P.B. and a Marie Heim-Voegtlin Fellowship 145516 to D.K.B.

Author Contributions E.M. and P.B. designed the study and wrote the manuscript. E.M., R.F.D., M.S.D., N.S. and P.B. performed the experiments and analysed data; D.K.B., D.B., S.W., M.R.-G., N.K., M.Y. and K.T. contributed reagents.

Author Information Reprints and permissions information is available at www.nature.com/reprints. The authors declare no competing financial interests. Readers are welcome to comment on the online version of the paper. Correspondence and requests for materials should be addressed to P.B. (petr.broz@unibas.ch).

METHODS

Bacterial strains and plasmids. *Salmonella enterica* serovar Typhimurium (*S. typhimurium*) SL1344 and congenic mutants were published before[12]. Other bacterial strains used were *Shigella flexneri*, *Vibrio cholerae*, *Enterobacter cloacae*, *Citrobacter koseri* and *Burkholderia thailandensis* ATCC700388.

Mice. *Gbp*^{chr3} KO, *Gbp2*$^{-/-}$, *Atg5*$^{fl/fl}$-Lyz-Cre, *Cybb*$^{-/-}$ (gp91^{phox}), *Casp1*$^{-/-}$/*Casp11*$^{-/-}$ (a.k.a caspase-1 knockout), *Casp11*$^{-/-}$ and *Casp1*$^{-/-}$ (*Casp1*$^{-/-}$/*Casp11*^{tg}) mice have been previously described[1,11,14,24,25]. Mice were bred in the animal facilities of the University of Basel, Genentech Inc., Heinrich-Heine-University Duesseldorf or the University of Osaka. Generation of mice with *Gbp5* KO alleles by zinc finger nuclease (ZFN) technology: A ZFN pair was obtained from Sigma-Aldrich (SAGE Labs). The ZFN pair recognizes a sequence in mouse *Gbp5* exon 2 (cut site is underlined): 5′-TGCCATCACACAGCCAGTGGTGGTGGTAGCCATTGTGGGT-3′. ZFN mRNA and a donor plasmid harbouring a 10-bp deletion in *Gbp5* exon 2 was co-microinjected into C57BL/6N zygotes using established procedures. One male founder carrying the 10-bp deletion was obtained by homologous recombination (10-bp deletion is underlined): 5′-TGCCATCACACAGCCAGTGGTGGTGGTAGCCATTGTGGGT-3. This founder was bred with C57BL/6N females to generate heterozygous progeny for subsequent intercrossing. Two founders (a male and a female) carrying identical 1-bp deletions were obtained by non-homologous end-joining (deleted bp is underlined): 5′-TGCCATCACACAGCCAGTGGTGGTGGTAGCCATTGTGGGT-3. These two founders were intercrossed to directly generate homozygous progeny. Both the 10-bp (designated KO line 1) and 1 bp (designated KO line 2) deletions lead to frameshifts and premature stop codons in *Gbp5* exon 2.

Animal infection. All animal experiments were approved (license 2239, Kantonales Veterinäramt Basel-Stadt) and performed according to local guidelines (Tierschutz-Verordnung, Basel-Stadt) and the Swiss animal protection law (Tierschutz-Gesetz). Female BALB/c mice (10–14 weeks old) were infected intravenously with mCherry-positive *Salmonella* (1,000 c.f.u.) and euthanized 4–5 days later. For antibody injections, mice ($n = 3$ per group) received on day 3 two intraperitoneal injections of 200 µl PBS containing 0.2 mg anti-IFN-γ monoclonal antibody (Clone XMG1.2, BioLegend) or 0.2 mg rat IgG1, κ isotype control antibody (clone RTK2071, BioLegend). No randomization or blinding was performed.

Cell culture and infections. BMDMs were differentiated in DMEM (Invitrogen) with 10% v/v FCS (Thermo Fisher Scientific), 10% MCSF (L929 cell supernatant), 10 mM HEPES (Invitrogen), and nonessential amino acids (Invitrogen). 1 day before infection, macrophages were seeded into 6-, 24-, or 96-well plates at a density of 1.25×10^6, 2.5×10^5, or 5×10^4 per well. If required macrophages were pre-stimulated with PAM3CSK4, LPS O111:B4 (InvivoGen), mIFN-β or mIFN-γ (eBioscience). For infections with *S. typhimurium*, *V. cholerae*, *E. cloacae*, *C. koseri* and *B. thailandensis*, bacteria were grown overnight in LB or TSB at 37 °C with aeration. The bacteria were diluted in fresh pre-warmed macrophage medium and added to the macrophages at an multiplicity of infection (m.o.i.) of 100:1 for measurements of caspase-11 and caspase-1 activity or 10:1 for all other assays. For assaying *Salmonella*-induced NLRC4 activation, *Salmonella* were subcultured for 4 h before infection to induce SPI-1 T3SS and flagellin expression. *S. flexneri* were cultured overnight in TSB medium and subcultured for 3 h before infection to induce T3SS expression. IFN-γ-primed BMDMs (to induce GBP expression) were infected with m.o.i. of 30:1 with *S. flexneri* for FACS analysis. When required, chemical reagents, Apocynin (Sigma Aldrich, 100µM), L-NG-nitroarginine methyl ester (L-NAME; Sigma Aldrich, 100 µM) and 3-methyladenine (Sigma Aldrich, 5 mM) were added 30 min before infection. The plates were centrifuged for 15 min at 500 *g* to ensure comparable adhesion of the bacteria to the cells and placed at 37 °C for 60 min. Next, 100 µg ml^{-1} gentamycin (Invitrogen) was added to kill extracellular bacteria. After a 60-min incubation, the cells were washed once with DMEM and given fresh macrophage medium containing 10 µg ml^{-1} gentamicin for the remainder of the infection. For infections with killed bacteria, *Salmonella* were grown as above. Shortly before the infection, bacteria were left untreated or incubated for 30 min at 95 °C, in 4% paraformaldehyde or in 70% ethanol. Following the treatment, bacteria were washed with PBS and prepared for infections as outlined above. The effectiveness of the killing procedures was verified by plating serial dilutions. Transfection with poly(dA:dT) or treatment with MSU, alum or nigericin was done as described previously[2] or as indicated.

siRNA knockdown. Gene knockdown was done using GenMute (SignaGen) and siRNA pools (siGenome, Dharmacon). Briefly, wild-type BMDMs were seeded into 24-, or 96-well plates at a density of 1.5×10^5 or 3×10^4 per well. siRNA complexes were prepared at 25 nM siRNA in 1× GenMute Buffer according to the manufacturer's instructions for forward knockdowns. siRNA complexes were mixed with BMDM medium and added onto the cells. BMDMs were infected with *S. typhimurium* at an m.o.i. of 100:1 after 56 h of knockdown and analysed for inflammasome activation as outlined below. siRNA pools included: *Casp11* (that is, *Casp4*) (M-042432-01), *Gbp1* (M-040198-01), *Gbp2* (M-040199-00), *Gbp3* (M-063076-01), *Gbp4* (M-047506-01), *Gbp5* (M-054703-01), *Gbp6* (M-041286-01), *Gbp7* (M-061204-01), *Gbp8* (M-059726-01), *Gbp9* (M-052281-01), *Gbp10* (M-073912-00), *Gbp11* (M-079932-00) and NT (non-targeting) pool 2 (D-001206-14). See Supplementary information for sequences.

LPS transfection. Macrophages were seeded as described above. Cells were pre-stimulated with 10 ug ml^{-1} of PAM3CSK4 for 4 h in Opti-MEM and transfected for 16 h with ultrapure LPS *E. coli* O111:B4, ultrapure LPS *E. coli* K12 or ultrapure LPS *Salmonella minnesota* (InvivoGen) in complex with FuGeneHD (Promega) as described previously[2].

Cytokine and LDH release measurement. IL-1β and tumour necrosis factor (TNF)-α was measured by ELISA (eBioscience). LDH was measured using LDH Cytotoxicity Detection Kit (Clontech). To normalize for spontaneous lysis, the percentage of LDH release was calculated as follows: (LDH infected − LDH uninfected)/(LDH total lysis − LDH uninfected)*100.

Western blotting. Western blotting was done as described before[4]. Antibodies used were rat anti-mouse caspase-1 antibody (1:1,000; 4B4; Genentech), rat anti-mouse caspase-11 (1:500; 17D9; Sigma), rabbit anti-IL-1α (1:1,000; ab109555; Abcam), rabbit anti-IL-18 (1:500; 5180R; Biovision), goat anti-mouse IL-1β antibody (1:500; AF-401-NA; R&D Systems) and rabbit anti-GBP2 and rabbit anti-GBP5 (1:1,000; 11854-1-AP/13220-1-AP; Proteintech). Cell lysates were probed with anti-β-actin antibody (Sigma) at 1:2,000.

Statistical analysis. Statistical data analysis was done using Prism 5.0a (GraphPad Software, Inc.). To evaluate the differences between two groups (cell death, cytokine release, FACS, CFU and immunofluorescence-based counts) the two-tailed *t*-test was used. In figures NS indicates 'not significant', *P* values are given in figure legends.

Immunofluorescence. Macrophages were seeded on glass coverslips and infected as described above. At the desired time points cells were washed 3× with PBS and fixed with 4% paraformaldehyde for 15 min at 37 °C. Following fixation coverslips were washed and the fixative was quenched with 0.1 M glycine for 10 min at room temperature. Coverslips were stained with primary antibodies at 4 °C for 16 h, washed 4× with PBS, incubated for 1 h with appropriate secondary antibodies at room temperature (1:500, AlexaFluor, Invitrogen), washed 4× with PBS and mounted on glass slides with Vectashield containing 4′,6-diamidino-2-phenylindole (DAPI) (Vector Labs). Antibodies used were rabbit anti-LC3 (1:1,000; NB600-1384, Novus), mouse anti-LC3 (1:100, 2G6, NanoTools), guinea-pig anti-p62 (1:100, GP62-C, Progen), goat anti-*Salmonella* (1:500, CSA-1 and CSA-1-FITC, KPL), mouse anti-galectin-8 (1:1,000, G5671, Sigma), goat anti-galectin-8 (1:100, AF1305, R&D), rabbit anti-Optineurin (1:100, ab23666, Abcam), rabbit anti-NDP52 (1:100, D01, Abnova), anti-PDI (1:100, ADI-SPA-890, Enzo Lifesciences), anti-Calnexin (1:100, ADI-SPA-860-D, Enzo Lifesciences), goat anti-GBP1-5 (1:100, sc-166960, Santa Cruz Biotech), rabbit anti-GBP2 and rabbit anti-GBP5 (1:100; 11854-1-AP/13220-1-AP; Proteintech). Coverslips were imaged on a Zeiss LSM700 or a Leica SP8 at ×63 magnification. Colocalization studies were performed as blinded experiments, with in general a minimum count of 100 bacteria per coverslip and performed in triplicate. Immunofluorescence based counts of live (mCherry$^+$/FITC$^+$) and dead (mCherry$^-$/FITC$^+$) bacteria were done as blinded experiment on *z* stacks taken from 15 random fields in three biological replicates, with a total of approximately 10,000 bacteria counted.

Immunohistochemistry. Cryosections were blocked in 1% blocking reagent (Invitrogen) and 2% mouse serum (Invitrogen) in TBST (0.05% Tween in 1× TBS pH 7.4), and stained with primary and secondary antibodies (goat anti-CSA1; 1:500; 01-91-99-MG; KPL and anti-GBP2; 1:100; 11854-1-AP; Proteintech). Secondary antibodies included Santa Cruz Biotech sc-362245 and Molecular Probes A21206, A21445 and A21469.

ROS assay. Measurement of oxygen-dependent respiratory burst of BMDMs was performed by chemiluminescence in the presence of 5-amino-2,3-dihydro-1,4-phtalazinedione (luminol, Sigma Aldrich, 66 µM) using a thermostatically (37 °C) controlled luminometer. Both oxygen and nitrogen species were detected ($O_2^{\bullet -}$, $ONOO^-$, $OH^\bullet$). Chemiluminescence generation was monitored every minute for 1 h after IFN-γ (100 U ml^{-1}) and/or *Salmonella* challenge and expressed as counts per minute.

NO assay. Nitrite production was measured by the Griess assay as previously described[26]. Briefly, in 96-well plates, BMDMs were infected as described above in presence or absence of IFN-γ or IL-1β for 16 h. Supernatants were mixed 1:1 with 2.5% phosphoric acid solution containing 1% sulfanilamide and 0.1% naphthylenediamine. After 30 min incubation at room temperature, the nitrite concentration was determined by measuring absorbance at 550 nm. Sodium nitrite (Sigma) was used as a standard to determine nitrite concentrations in the cell-free medium.

Digitonin assay. For flow-cytometry-based quantification of cytoplasmic and vacuolar bacteria, macrophages were infected with mCherry$^+$ *S. typhimurium* or mCherry$^+$ *S. flexneri* as described above. At the desired time point, cells were washed 3× with KHM buffer (110 mM potassium acetate, 20 mM HEPES, 2 mM $MgCl_2$,

RESEARCH LETTER

pH 7.3) and incubated for 1 min in KHM buffer with 150 μg ml^{-1} digitonin (Sigma). Cells were immediately washed 2× with KHM buffer and then stained for 12 min with anti-*Salmonella*-FITC (1:500, CSA-1, KPL) or anti-*Shigella* (1:100, BP1064, Acris) in KHM buffer with 2% BSA. Secondary antibodies used for *S. flexneri* staining were: anti-Rabbit-488 (1:500, Invitrogen). Cells were washed 3× with PBS and lysed in PBS with 0.1% Triton-X (Sigma) and analysed on a FACS-Canto-II. Controls were included in every assay and are described in (Extended Data Fig. 9).

Live/dead analysis by FACS. Infection of macrophages was performed using mCherry^{+} bacteria as described above. At 16 h post-infection cells were washed and lysed with PBS solution containing 0.1% Triton X-100 (Sigma Aldrich) to release intracellular bacteria. *Salmonella* were counterstained using an anti-*Salmonella* antibody (CSA-1, KPL) and analysed using a FACS Canto-II for fluorescence intensities in FL-1 and FL-2 channels. Data were analysed with FlowJo 10.0.6 software. The gate was set for the bacterial population based on the FSC/SSC and the anti-*Salmonella* staining (CSA-1-FITC, KPL). Controls included live mCherry-expressing and mCherry-negative *Salmonella* stained with anti-*Salmonella* antibodies (CSA-1, KPL).

24. Mariathasan, S. *et al.* Differential activation of the inflammasome by caspase-1 adaptors ASC and Ipaf. *Nature* **430,** 213–218 (2004).
25. Zhao, Z. *et al.* Autophagosome-independent essential function for the autophagy protein Atg5 in cellular immunity to intracellular pathogens. *Cell Host Microbe* **4,** 458–469 (2008).
26. Lima-Junior, D. S. *et al.* Inflammasome-derived IL-1β production induces nitric oxide-mediated resistance to *Leishmania*. *Nature Med.* **19,** 909–915 (2013).

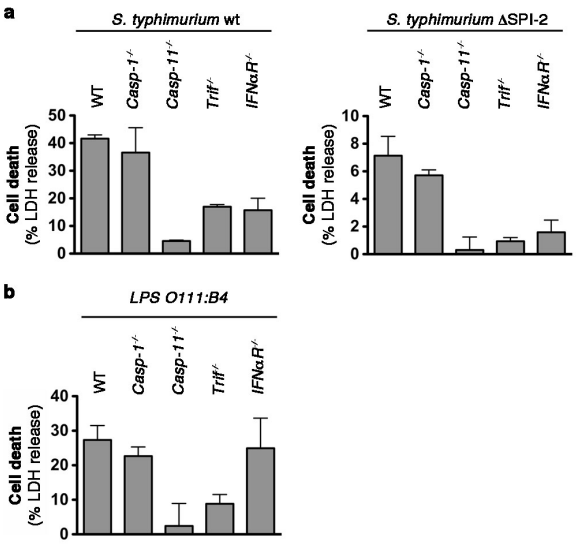

Extended Data Figure 1 | Type-I-interferon signalling is required to induce caspase-11-dependent cell death in response to bacterial infection, but not in response to LPS transfection. **a**, LDH release from unprimed BMDMs infected for 16 h with wild-type (WT) *S. typhimurium* or ΔSPI-2 *S. typhimurium* grown to stationary phase. **b**, LDH release from primed BMDMs transfected with LPS O111:B4. Graphs show the mean and s.d. of quadruplicate wells and are representative of three independent experiments.

RESEARCH LETTER

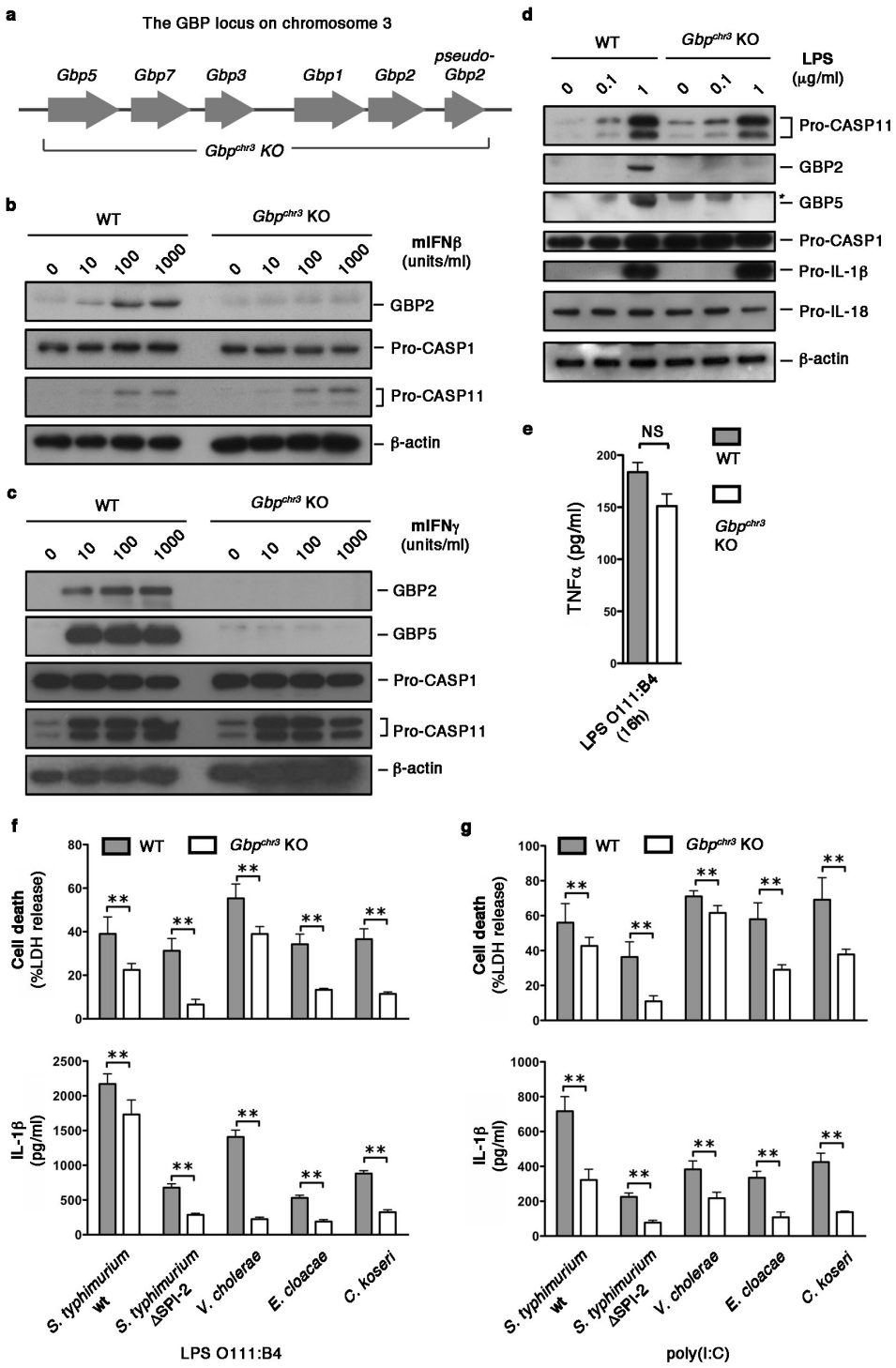

Extended Data Figure 2 | BMDMs from *Gbp*^{chr3} KO mice have normal responses to priming stimuli, but fail to activate the non-canonical inflammasome during bacterial infections. **a**, Schematic representation of the GBP locus on murine chromosome 3. The extent of the deletion in *Gbp*^{chr3} KO mice is indicated. **b**–**d**, Induction of pro-caspase-11, GBP2 and GBP5 expression in lysates of wild-type and *Gbp*^{chr3} KO BMDMs stimulated for 16 h with the indicated amounts of murine IFN-β, murine IFN-γ or LPS O111:B4. **e**, TNF-α release from BMDMs stimulated for 16 h with LPS O111:B4. **f**, **g**, LDH release and IL-1β secretion from wild-type and *Gbp*^{chr3} KO BMDMs infected for 16 h with wild-type (WT) *S. typhimurium*, ΔSPI-2 *S. typhimurium*, *V. cholerae*, *E. cloacae* or *C. koseri* grown to stationary phase. Cells were primed overnight with LPS (**f**) or poly(I:C) (**g**). *Indicates background band. Graphs show the mean and s.d. of quadruplicate wells and data are representative of two independent experiments. $^{**}P < 0.01$, NS, not significant (two-tailed *t*-test).

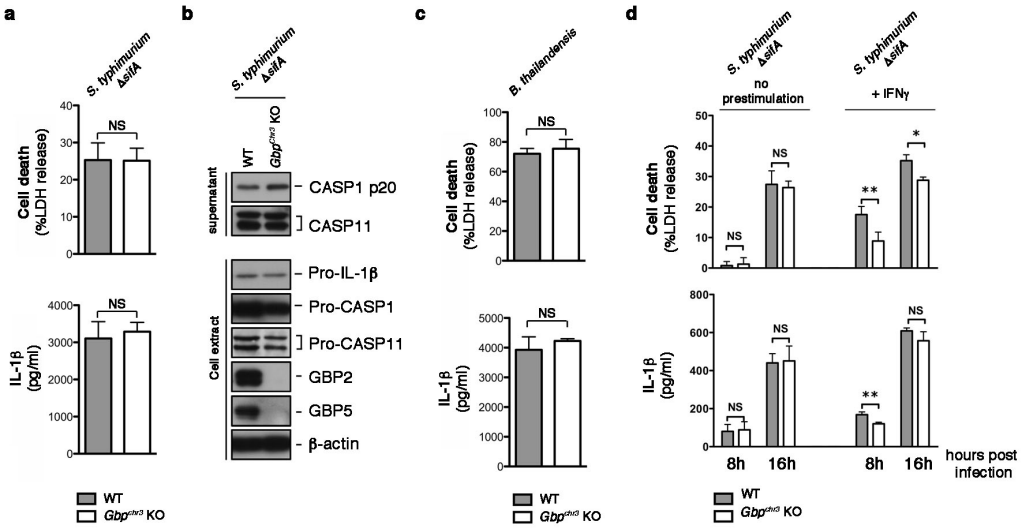

Extended Data Figure 3 | GBPs assist the detection of bacteria that escape into the cytosol only in primed macrophages. **a**–**c**, LDH release, IL-1β secretion and immunoblots for processed caspase-1 and caspase-11 released from unprimed BMDMs infected for 8–16 h with *ΔsifA S. typhimurium* or *B. thailandensis* grown to stationary phase. **d**, LDH release and IL-1β secretion from unprimed or IFN-γ-primed BMDMs infected for 16 h with *ΔsifA S. typhimurium* grown to stationary phase. Ext, extract; SN, supernatant. Graphs show the mean and s.d. of quadruplicate wells and data are representative of two independent experiments. $^{*}P < 0.05$; $^{**}P < 0.01$; NS, not significant (two-tailed *t*-test).

RESEARCH LETTER

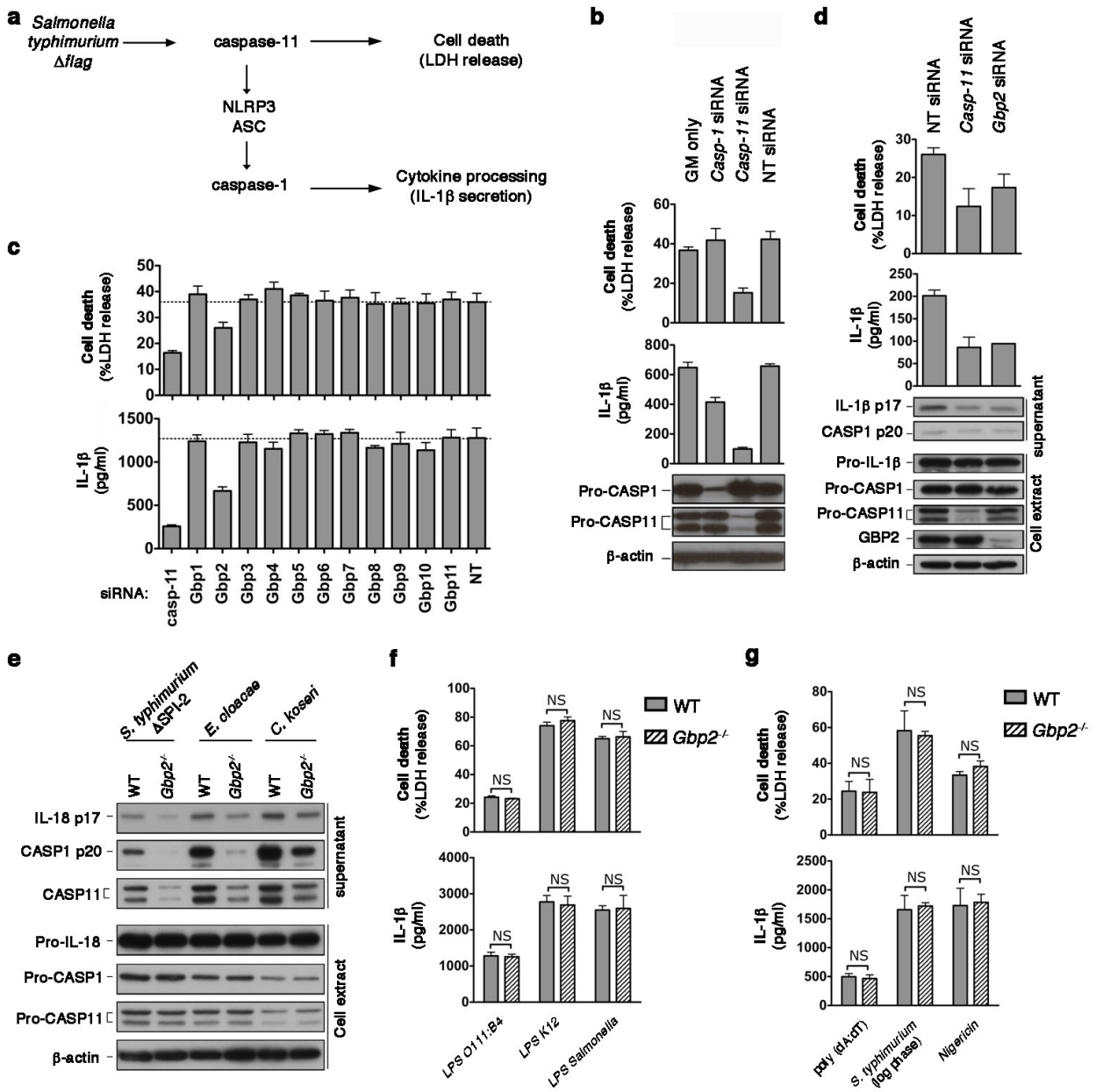

Extended Data Figure 4 | Murine GBP2 controls non-canonical inflammasome activation during *Salmonella* infection, but is dispensable for direct LPS sensing and canonical inflammasomes. **a**, Schematic drawing of the inflammasome pathways activated by flagellin-deficient *Salmonella*. **b**–**d**, LDH release, IL-1β secretion and immunoblots for processed caspase-1 and processed IL-1β released from unprimed BMDMs infected for 17 h with Δflag *S. typhimurium* grown to stationary phase. BMDMs were treated with the indicated siRNA for 56 h before infection. **e**, Immunoblots for processed caspase-1, IL-18 and caspase-11 released from unprimed BMDMs infected for 16 h with ΔSPI-2 *S. typhimurium*, *E. cloacae* or *C. koseri* grown to stationary phase. **f**, **g**, LDH release and IL-1β secretion from primed wild-type and *Gbp2*$^{-/-}$ BMDMs transfected with the indicated types of LPS for 16 h, treated with nigericin for 1 h, infected with SPI-1 T3SS expressing logarithmic phase wild-type *S. typhimurium* for 1 h, or transfected with poly(dA:dT) for 6 h. Cell were primed with PAM3CSK4 in **f** or LPS **g**. Graphs show the mean and s.d. of quadruplicate wells and data are representative of two (**e**) and three (**b**–**d**, **f**, **g**) independent experiments. NT, non-targeting siRNA; GM, GenMute transfection reagent; NS, not significant (two-tailed *t*-test).

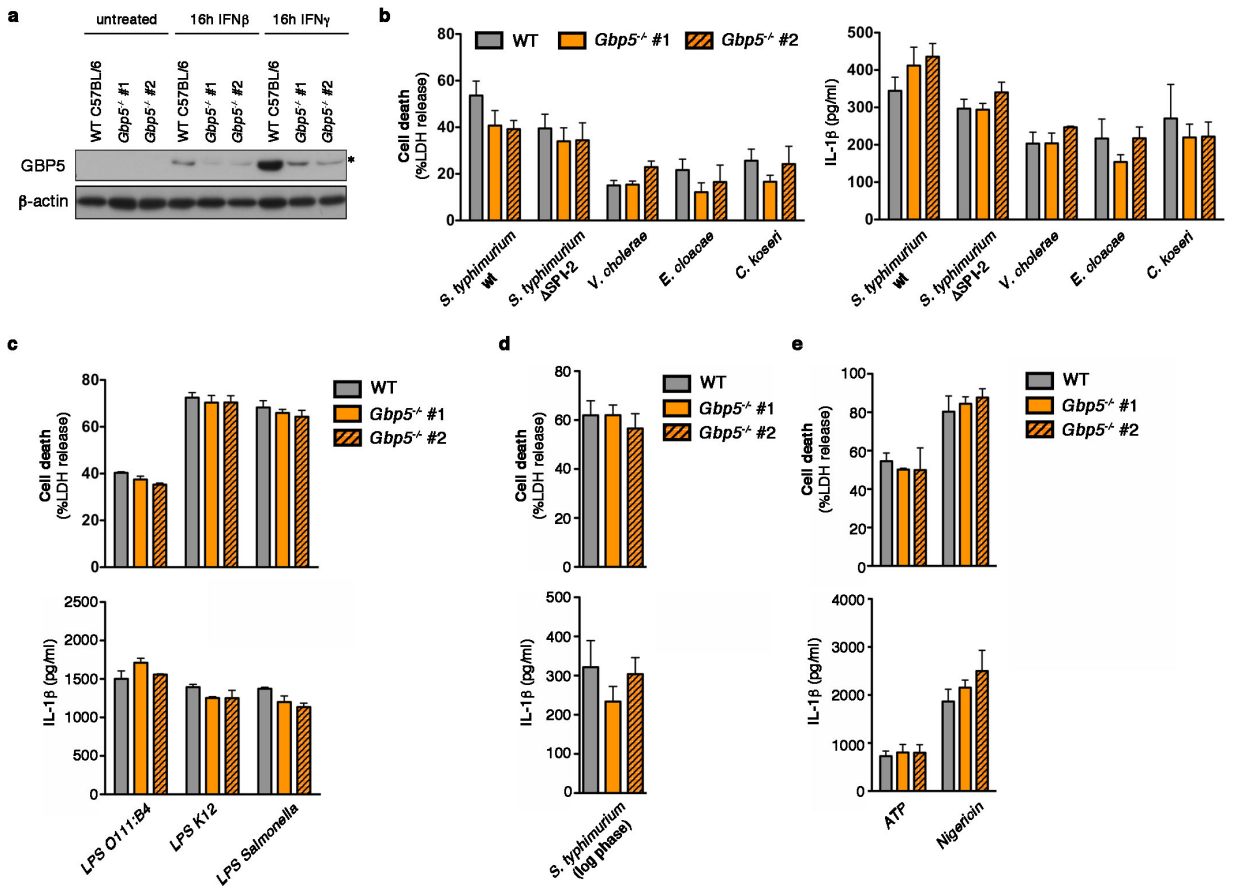

Extended Data Figure 5 | Normal activation of non-canonical and canonical inflammasomes in *Gbp5*$^{-/-}$ BMDMs. **a**, Expression of GBP5 in wild-type and two lines of *Gbp5*$^{-/-}$ BMDMs (1 and 2). *Indicates a cross-reactive band. **b**–**e**, LDH release and IL-1β secretion from BMDMs infected for 16 h with wild-type (WT) *S. typhimurium*, ΔSPI-2 *S. typhimurium*, *V. cholerae*, *E. cloacae* or *C. koseri* grown to stationary phase (**b**), transfected with the indicated LPS for 16 h (**c**) infected for 1 h with SPI-1 T3SS expressing logarithmic phase wild-type *S. typhimurium* (**d**), or treated with 5 mM ATP or 20 mM nigericin for 4 h (**e**). Cells were left unprimed (**b**) or primed with PAM3CSK4 in (**c**) or LPS (**d**, **e**). Graphs show the mean and s.d. of triplicate or quadruplicate wells and data are representative of three independent experiments.

RESEARCH LETTER

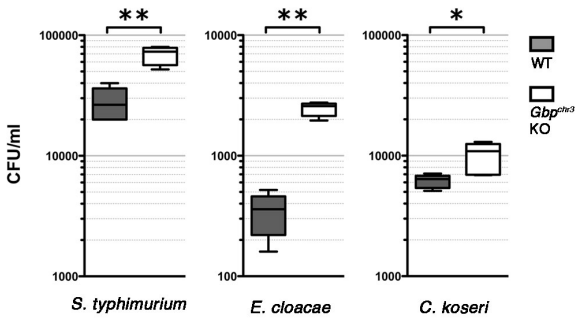

Extended Data Figure 6 | GBPs control bacterial replication. c.f.u.s at 16 h post-infection in wild-type and *Gbp*^{chr3} KO BMDMs infected with the indicated bacterial strains. Experiments are representative of two independent experiments.

LETTER RESEARCH

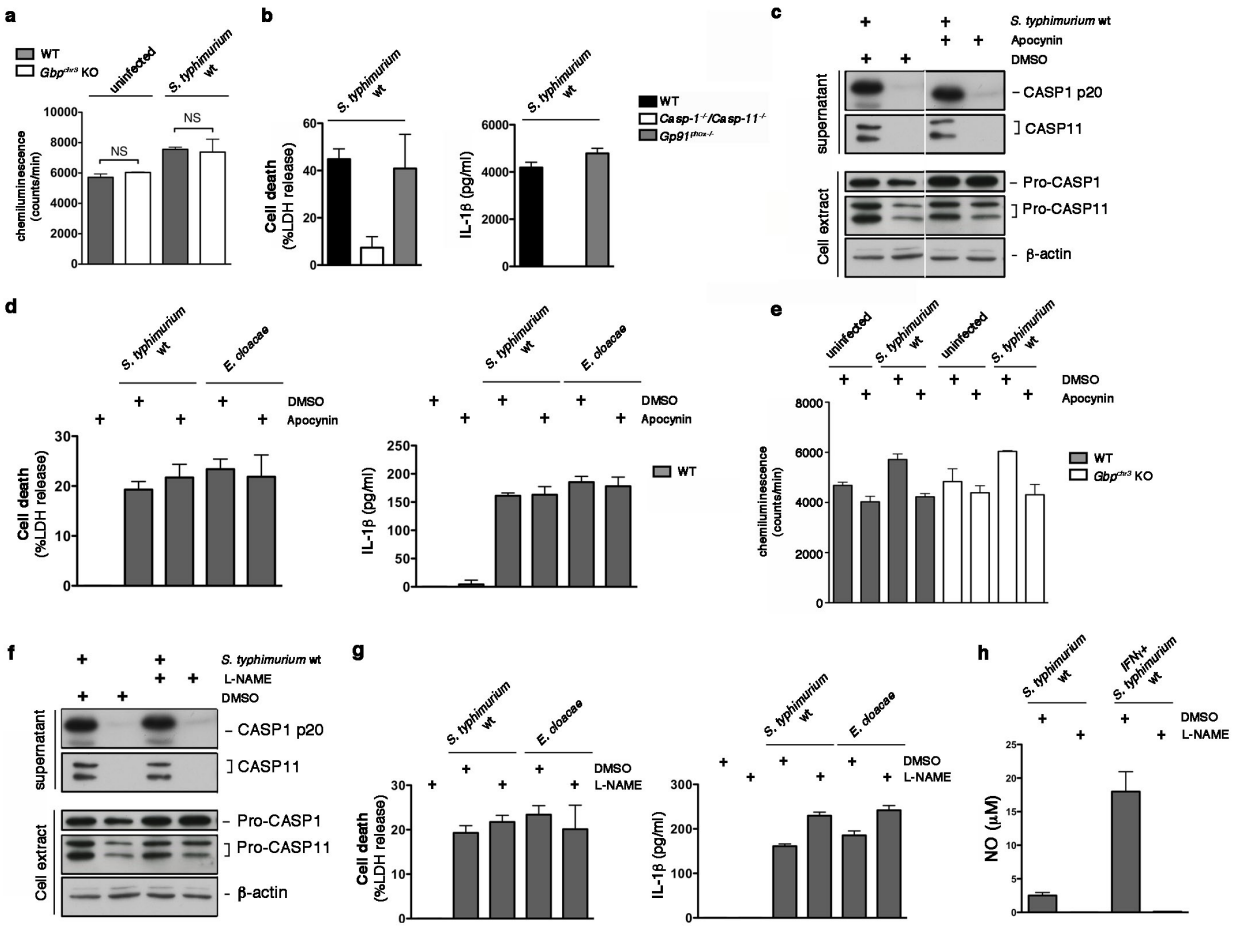

Extended Data Figure 7 | Inhibition of ROS and NO production does not affect non-canonical inflammasome activation. **a**, **b**, ROS levels, LDH release and IL-1β secretion in unprimed BMDMs left uninfected or infected for 16 h with wild-type *S. typhimurium* grown to stationary phase. **c**–**e**, LDH release, IL-1β secretion, ROS levels and immunoblots for processed caspase-1 and caspase-11 released from unprimed BMDMs infected for 16 h with wild-type (WT) *S. typhimurium* or *E. cloacae* grown to stationary phase in the presence of the ROS inhibitor (apocynin) or a vehicle control (DMSO). **f**, **g**, LDH release, IL-1β secretion and immunoblots for processed caspase-1 and caspase-11 released from unprimed BMDMs infected for 16 h with wild-type *S. typhimurium* or *E. cloacae* grown to stationary phase in the presence of the iNOS inhibitor (L-NAME) or a vehicle control (DMSO). **h**, NO release from unprimed or IFN-γ-primed BMDMs infected for 16 h with *S. typhimurium* in presence of the iNOS inhibitor (L-NAME) or a vehicle control (DMSO). Ext, extract; SN, supernatant. Graphs show the mean and s.d. of quadruplicate wells and data are representative of two (**a**–**c**, **e**–**g**) and three (**d**, **h**) independent experiments. NS, not significant (two-tailed *t*-test).

RESEARCH LETTER

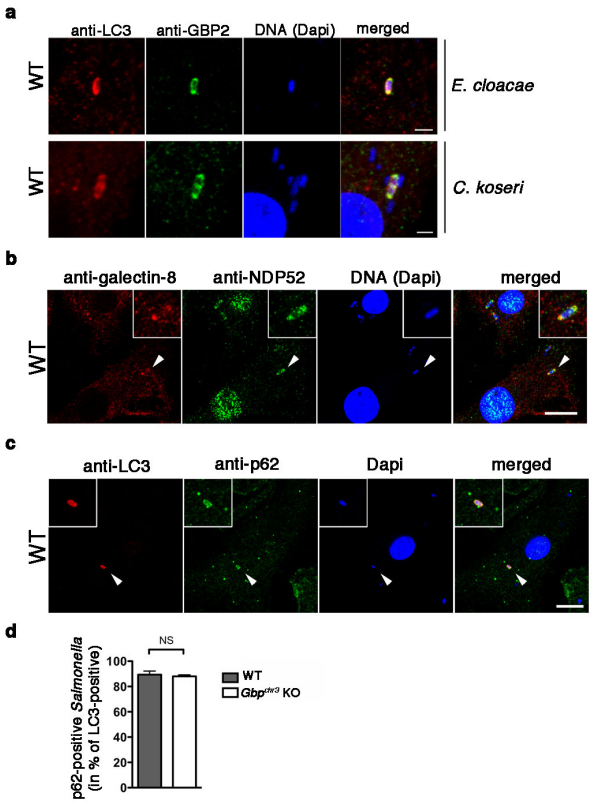

Extended Data Figure 8 | Colocalization of GBPs and autophagy proteins on intracellular bacteria. **a**, Colocalization of LC3 with GBPs in unprimed wild-type BMDMs infected with *E. cloacae* or *C. koseri* for 4 h and stained for LC3, GBP2 and DNA. **b**, Colocalization of galectin-8 and NDP52 in unprimed wild-type BMDMs infected with wild-type *S. typhimurium* for 4 h and stained for galectin-8, NDP52 and DNA. **c**, Colocalization of p62 and LC3 in unprimed wild-type BMDMs infected with wild-type *S. typhimurium* for 4 h and stained for LC3, p62 and DNA. **d**, Quantification of p62 and LC3 co-staining in wild-type and Gbp^{chr3} KO BMDMs at 4 h post-infection with *Salmonella*. Arrowheads indicate region shown in insets. Scale bars, 1 µm (**a**) and 10 µm (**b**, **c**). Graph shows the mean and s.d. of triplicate counts and images and graph are representative of at least two independent experiments. NS, not significant (two-tailed *t*-test).

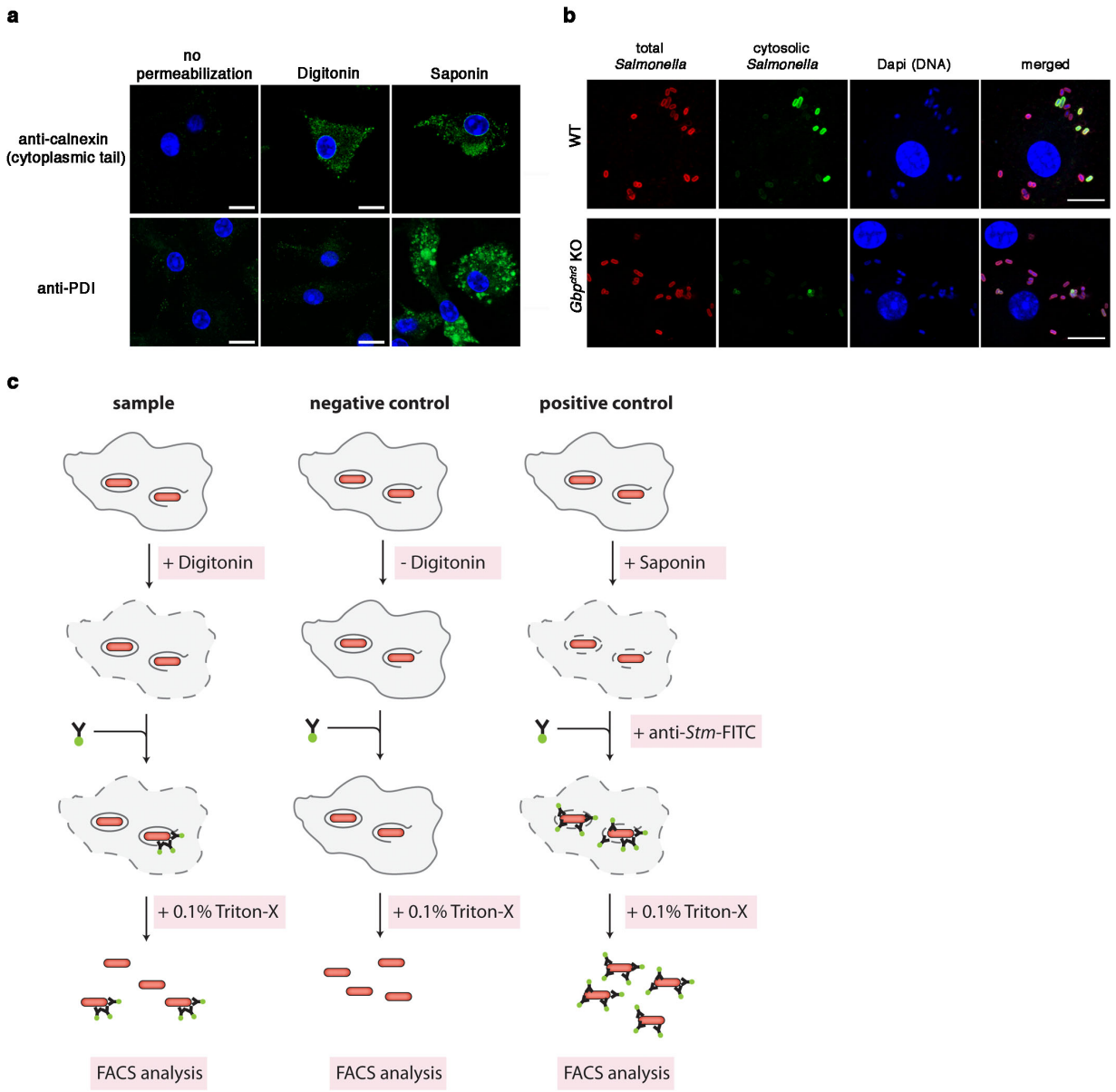

Extended Data Figure 9 | Digitonin-based quantification of cytoplasmic bacteria. **a**, Immunostaining for calnexin and PDI (protein disulphide isomerase) in wild-type BMDMs left untreated or permeabilized with digitonin or saponin. **b**, Differentially permeabilized macrophages stained for cytosolic and vacuolar *Salmonella* at 4 h post-infection. **c**, Schematic representation of FACS-based analysis of cytosolic and vacuolar bacterial populations of *Salmonella*. Scale bars, 10 µm.

RESEARCH LETTER

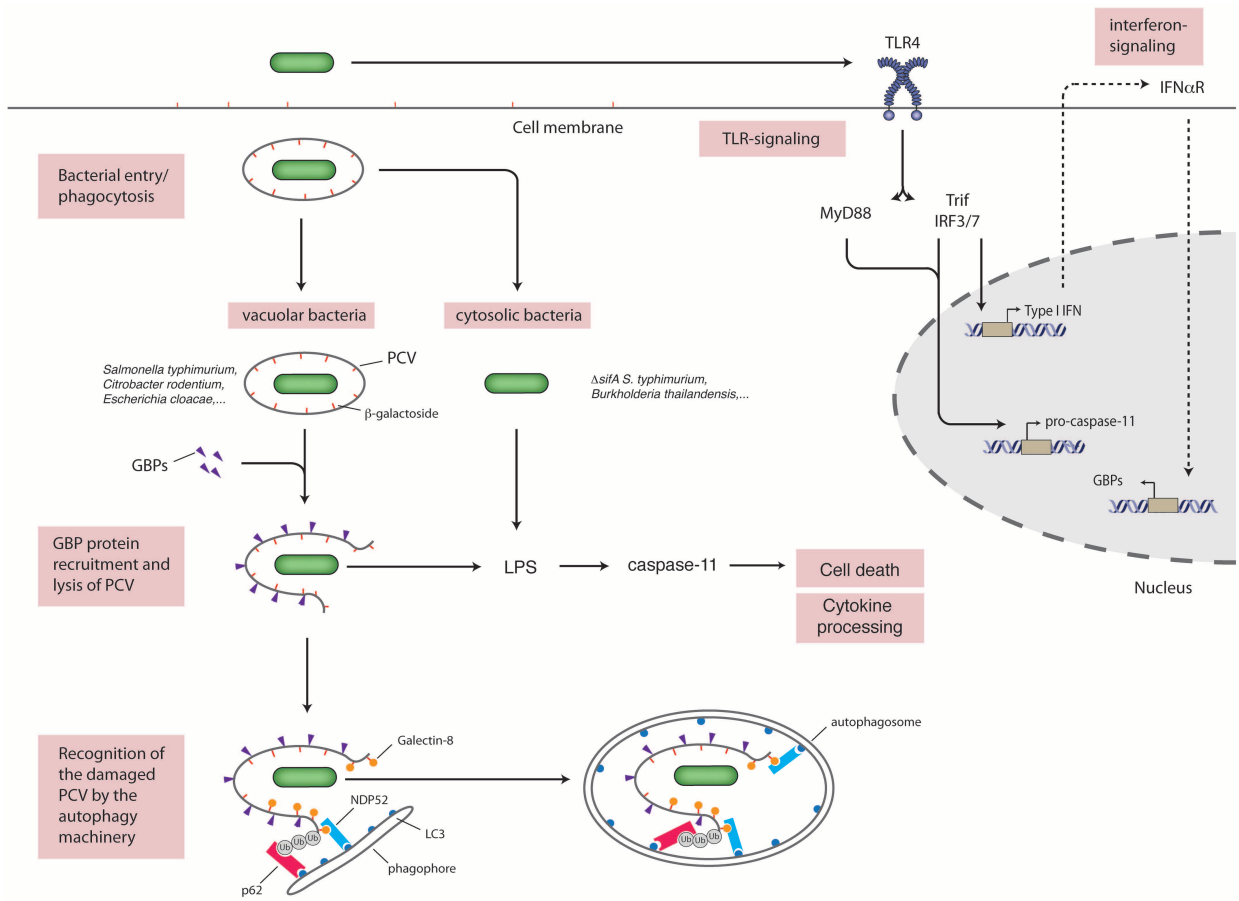

Extended Data Figure 10 | Model for the role of GBPs and autophagy in caspase-11 activation. The pathogen-containing vacuole of vacuolar bacterial pathogens is recognized by interferon-induced GBPs in an unknown manner. GBPs promote the lysis of the PCV either directly or indirectly, resulting in the release of the bacteria into the cytosol and activation of caspase-11 by bacterial LPS. β-galactosides of the lysed vacuole serve as danger signals upon exposure to the cytosol and are recognized by galectin-8 leading to the recruitment of the autophagy machinery. p62 participates in this process by recognizing ubiquitin-chains on the vacuole or the bacterium. Uptake of the bacterium and the lysed vacuole into autophagosomes reduces caspase-11 activation by removing the source of LPS from the cytosol.

SUPPLEMENTARY INFORMATION

doi:10.1038/nature13157

Dharmacon Pool Catalog Number	Dharmacon Duplex Catalog Number	Gene Symbol	Gene Accession	GINumber	Sequence
M-042432-01	D-042432-01	Casp4	NM_007609	157951737	GUGCAACAAUCAUUUGAAA
M-042432-01	D-042432-02	Casp4	NM_007609	157951737	GCUAAUGUCUCAUGGCACA
M-042432-01	D-042432-03	Casp4	NM_007609	157951737	GAUGUGCUACAGUAUGAUA
M-042432-01	D-042432-04	Casp4	NM_007609	157951737	CGAAAGGCUCUUAUCAUAU
M-040198-01	D-040198-01	GBP1	NM_010259	134031981	GCAACUACGUCAAGAGAUA
M-040198-01	D-040198-02	GBP1	NM_010259	134031981	GGAAAGACUUCUCAAGCAA
M-040198-01	D-040198-03	GBP1	NM_010259	134031981	GAUCAUGCACCAUACUUUA
M-040198-01	D-040198-04	GBP1	NM_010259	134031981	CAACUCAGCUAACUUUGUG
M-040199-00	D-040199-01	GBP2	NM_010260	6753949	UGAAGAAGCUGACUGAGAA
M-040199-00	D-040199-02	GBP2	NM_010260	6753949	GAAGUGCACUAUACUCUGA
M-040199-00	D-040199-03	GBP2	NM_010260	6753949	GGAGCUGUGUGGUGAAUUU
M-040199-00	D-040199-04	GBP2	NM_010260	6753949	GGAGCUAACUGAUCUUAUC
M-063076-01	D-063076-01	Gbp3	NM_018734	134053870	GAACGAAGCAGCAUCUAUU
M-063076-01	D-063076-02	Gbp3	NM_018734	134053870	GGACUUUGGUGCAGACCUA
M-063076-01	D-063076-03	Gbp3	NM_018734	134053870	GGCCAUUGUUGGUUUAUAU
M-063076-01	D-063076-04	Gbp3	NM_018734	134053870	CACAAGCGACAAACGUUUA
M-047506-01	D-047506-01	Gbp4	NM_008620	126157520	GGACAUAACAUCAAGGAAA
M-047506-01	D-047506-02	Gbp4	NM_008620	126157520	CCAAUUGGAUCCUACGUUU
M-047506-01	D-047506-03	Gbp4	NM_008620	126157520	GAUAUAAGACACAAGCUGA
M-047506-01	D-047506-04	Gbp4	NM_008620	126157520	GGAAUUGCGUCGAGAGAUC
M-054703-01	D-054703-01	GBP5	NM_153564	91064875	CGCAGGAGUUCUAUCAUAA
M-054703-01	D-054703-02	GBP5	NM_153564	91064875	UGACUGUGUUAUAAGCUAA
M-054703-01	D-054703-03	GBP5	NM_153564	91064875	ACUCAGAUCUUUGCACUAG
M-054703-01	D-054703-04	GBP5	NM_153564	91064875	GCGAGAGGCCAUAGAAAUC
M-041286-01	D-041286-02	Mpa2l	NM_194336	170650636	AAGAAACACUGAUCGAAUU
M-041286-01	D-041286-04	Mpa2l	NM_194336	170650636	GGGACAGAAUCACGGCUUU
M-041286-01	D-041286-05	Mpa2l	NM_194336	170650636	GGAAUUAAUAGGAGAGAAC
M-041286-01	D-041286-06	Mpa2l	NM_194336	170650636	GCACAAUCAAGUCAGGUUA
M-061204-01	D-061204-01	Gbp6	NM_001083312	134032013	AAGAAUAGCUCAUUGGGUG
M-061204-01	D-061204-02	Gbp6	NM_001083312	134032013	CGACCUACGUGGAUGCUAU
M-061204-01	D-061204-03	Gbp6	NM_001083312	134032013	GGACUAUACCGUACGGGAA
M-061204-01	D-061204-04	Gbp6	NM_001083312	134032013	GACGUGCCGUGUUUAGAGA
M-059726-01	D-059726-01	5830443L24RIK	NM_029509	115292436	CACCAAAUCCUGAUGGAAU
M-059726-01	D-059726-03	5830443L24RIK	NM_029509	115292436	GUGACAACCUAUGUAGAUG
M-059726-01	D-059726-17	5830443L24RIK	NM_029509	115292436	AUUAAUAGGUGAGGCGAAA
M-059726-01	D-059726-18	5830443L24RIK	NM_029509	115292436	ACGGAGAGAUACAGCAACU
M-052281-01	D-052281-01	BC057170	NM_172777	118129953	UAGAGAGACUGGAACAUAA
M-052281-01	D-052281-02	BC057170	NM_172777	118129953	GAGGAAGGAUUUACGAACA
M-052281-01	D-052281-03	BC057170	NM_172777	118129953	GAUCUUCGCCCUAAGUGUG
M-052281-01	D-052281-04	BC057170	NM_172777	118129953	AAACAUUGGUCCCAUUCUG
M-073912-00	D-073912-09	Gbp10	NM_001039646	116812913	CCAUAUGAGUAAAGACACA
M-073912-00	D-073912-10	Gbp10	NM_001039646	116812913	GGAAUUAAUAGGAGAGAAC
M-073912-00	D-073912-11	Gbp10	NM_001039646	116812913	GCUGAUCCCAGGUGACAAA
M-073912-00	D-073912-12	Gbp10	NM_001039646	116812913	AGAAACACUGAUCGAAUUA
M-079932-00	D-079932-13	EG634650	NM_001039647	88900482	UGUAAGAGACCUUGCUUUA
M-079932-00	D-079932-14	EG634650	NM_001039647	88900482	GGAAUUAAUAAGUGAGAAG
M-079932-00	D-079932-15	EG634650	NM_001039647	88900482	GAAGAGAGAUCUAUCGACU
M-079932-00	D-079932-16	EG634650	NM_001039647	88900482	GCUAUAAGAAGAAAGCUGA

Supplementary information 1: Sequences of siRNA duplexes

SUPPLEMENTARY INFORMATION

doi:10.1038/nature13157

Dharmacon Pool Catalog Number	Dharmacon Duplex Catalog Number	Gene Symbol	Gene Accession	GINumber	Sequence
M-042432-01	D-042432-01	Casp4	NM_007609	157951737	GUGCAACAAUCAUUUGAAA
M-042432-01	D-042432-02	Casp4	NM_007609	157951737	GCUAAUGUCUCAUGGCACA
M-042432-01	D-042432-03	Casp4	NM_007609	157951737	GAUGUGCUACAGUAUGAUA
M-042432-01	D-042432-04	Casp4	NM_007609	157951737	CGAAAGGCUCUUAUCAUAU
M-040198-01	D-040198-01	GBP1	NM_010259	134031981	GCAACUACGUCAAGAGAUA
M-040198-01	D-040198-02	GBP1	NM_010259	134031981	GGAAAGACUUCUCAAGCAA
M-040198-01	D-040198-03	GBP1	NM_010259	134031981	GAUCAUGCACCAUACUUUA
M-040198-01	D-040198-04	GBP1	NM_010259	134031981	CAACUCAGCUAACUUUGUG
M-040199-00	D-040199-01	GBP2	NM_010260	6753949	UGAAGAAGCUGACUGAGAA
M-040199-00	D-040199-02	GBP2	NM_010260	6753949	GAAGUGCACUAUACUCUGA
M-040199-00	D-040199-03	GBP2	NM_010260	6753949	GGAGCUGUGUGGUGAAUUU
M-040199-00	D-040199-04	GBP2	NM_010260	6753949	GGAGCUAACUGAUCUUAUC
M-063076-01	D-063076-01	Gbp3	NM_018734	134053870	GAACGAAGCAGCAUCUAUU
M-063076-01	D-063076-02	Gbp3	NM_018734	134053870	GGACUUUGGUGCAGACCUA
M-063076-01	D-063076-03	Gbp3	NM_018734	134053870	GGCCAUUGUUGGUUUAUAU
M-063076-01	D-063076-04	Gbp3	NM_018734	134053870	CACAAGCGACAAACGUUUA
M-047506-01	D-047506-01	Gbp4	NM_008620	126157520	GGACAUAACAUCAAGGAAA
M-047506-01	D-047506-02	Gbp4	NM_008620	126157520	CCAAUUGGAUCCUACGUUU
M-047506-01	D-047506-03	Gbp4	NM_008620	126157520	GAUAUAAGACACAAGCUGA
M-047506-01	D-047506-04	Gbp4	NM_008620	126157520	GGAAUUGCGUCGAGAGAUC
M-054703-01	D-054703-01	GBP5	NM_153564	91064875	CGCAGGAGUUCUAUCAUAA
M-054703-01	D-054703-02	GBP5	NM_153564	91064875	UGACUGUGUUAUAAGCUAA
M-054703-01	D-054703-03	GBP5	NM_153564	91064875	ACUCAGAUCUUUGCACUAG
M-054703-01	D-054703-04	GBP5	NM_153564	91064875	GCGAGAGGCCAUAGAAAUC
M-041286-01	D-041286-02	Mpa2l	NM_194336	170650636	AAGAAACACUGAUCGAAUU
M-041286-01	D-041286-04	Mpa2l	NM_194336	170650636	GGGACAGAAUCACGGCUUU
M-041286-01	D-041286-05	Mpa2l	NM_194336	170650636	GGAAUUAAUAGGAGAGAAC
M-041286-01	D-041286-06	Mpa2l	NM_194336	170650636	GCACAAUCAAGUCAGGUUA
M-061204-01	D-061204-01	Gbp6	NM_001083312	134032013	AAGAAUAGCUCAUUGGGUG
M-061204-01	D-061204-02	Gbp6	NM_001083312	134032013	CGACCUACGUGGAUGCUAU
M-061204-01	D-061204-03	Gbp6	NM_001083312	134032013	GGACUAUACCGUACGGGAA
M-061204-01	D-061204-04	Gbp6	NM_001083312	134032013	GACGUGCCGUGUUUAGAGA
M-059726-01	D-059726-01	5830443L24RIK	NM_029509	115292436	CACCAAAUCCUGAUGGAAU
M-059726-01	D-059726-03	5830443L24RIK	NM_029509	115292436	GUGACAACCUAUGUAGAUG
M-059726-01	D-059726-17	5830443L24RIK	NM_029509	115292436	AUUAAUAGGUGAGGCGAAA
M-059726-01	D-059726-18	5830443L24RIK	NM_029509	115292436	ACGGAGAGAUACAGCAACU
M-052281-01	D-052281-01	BC057170	NM_172777	118129953	UAGAGAGACUGGAACAUAA
M-052281-01	D-052281-02	BC057170	NM_172777	118129953	GAGGAAGGAUUUACGAACA
M-052281-01	D-052281-03	BC057170	NM_172777	118129953	GAUCUUCGCCCUAAGUGUG
M-052281-01	D-052281-04	BC057170	NM_172777	118129953	AAACAUUGGUCCCAUUCUG
M-073912-00	D-073912-09	Gbp10	NM_001039646	116812913	CCAUAUGAGUAAAGACACA
M-073912-00	D-073912-10	Gbp10	NM_001039646	116812913	GGAAUUAAUAGGAGAGAAC
M-073912-00	D-073912-11	Gbp10	NM_001039646	116812913	GCUGAUCCCAGGUGACAAA
M-073912-00	D-073912-12	Gbp10	NM_001039646	116812913	AGAAACACUGAUCGAAUUA
M-079932-00	D-079932-13	EG634650	NM_001039647	88900482	UGUAAGAGACCUUGCUUUA
M-079932-00	D-079932-14	EG634650	NM_001039647	88900482	GGAAUUAAUAAGUGAGAAG
M-079932-00	D-079932-15	EG634650	NM_001039647	88900482	GAAGAGAGAUCUAUCGACU
M-079932-00	D-079932-16	EG634650	NM_001039647	88900482	GCUAUAAGAAGAAAGCUGA

Supplementary information 1: Sequences of siRNA duplexes

2 Research article V

Guanylate-binding proteins promote activation of the AIM2 inflammasome during infection with *Francisella novicida*

E. Meunier*, P. Wallet*, **R. F. Dreier**, S. Costanzo, L. Anton, S. Rühl, S. Dussurgey, M. S. Dick, A. Kistner, M. Rigard, D. Degrandi, K. Pfeffer, M. Yamamoto, T. Henry and P. Broz.
* denotes equal contribution.

Nature Immunology
2015 May 16; 16(5):467-84. doi: 10.1038/ni.3119. [463]

Statement of contribution

I performed infections in mice and production of bone marrow-derived macrophages. Furthermore, I was involved in the discussion of the results and writing of the manuscript.

ARTICLES

nature immunology

Guanylate-binding proteins promote activation of the AIM2 inflammasome during infection with *Francisella novicida*

Etienne Meunier[1,6], Pierre Wallet[2,6], Roland F Dreier[1], Stéphanie Costanzo[2], Leonie Anton[1], Sebastian Rühl[1], Sébastien Dussurgey[3], Mathias S Dick[1], Anne Kistner[1], Mélanie Rigard[2], Daniel Degrandi[4], Klaus Pfeffer[4], Masahiro Yamamoto[5], Thomas Henry[2] & Petr Broz[1]

The AIM2 inflammasome detects double-stranded DNA in the cytosol and induces caspase-1-dependent pyroptosis as well as release of the inflammatory cytokines interleukin 1β (IL-1β) and IL-18. AIM2 is critical for host defense against DNA viruses and bacteria that replicate in the cytosol, such as *Francisella tularensis* subspecies *novicida* (*F. novicida*). The activation of AIM2 by *F. novicida* requires bacteriolysis, yet whether this process is accidental or is a host-driven immunological mechanism has remained unclear. By screening nearly 500 interferon-stimulated genes (ISGs) through the use of small interfering RNA (siRNA), we identified guanylate-binding proteins GBP2 and GBP5 as key activators of AIM2 during infection with *F. novicida*. We confirmed their prominent role *in vitro* and in a mouse model of tularemia. Mechanistically, these two GBPs targeted cytosolic *F. novicida* and promoted bacteriolysis. Thus, in addition to their role in host defense against vacuolar pathogens, GBPs also facilitate the presentation of ligands by directly attacking cytosolic bacteria.

The innate immune system detects invading pathogens through membrane-bound and cytosolic pattern-recognition receptors, which recognize microbe- and damage-associated molecular patterns and induce conserved signaling pathways. Nucleic acids and their derivatives are detected by RIG-I-like receptors, cGAS, DAI and RNA polymerases, which results in the induction of type I interferons via the signaling molecule STING and the kinase TBK1 (refs. 1–3). Cytosolic microbial and host DNA also induces inflammasome formation through AIM2, a member of the PYHIN family of receptors[4–7]. AIM2 binds double-stranded DNA through its HIN-200 domain[8] and recruits the inflammasome adaptor ASC. ASC rapidly oligomerizes to form a macromolecular inflammasome complex known as an 'ASC speck', which activates caspase-1. Active caspase-1 promotes the maturation and release of the pro-inflammatory cytokines interleukin 1β (IL-1β) and IL-18. In addition, it induces pyroptosis, a lytic form of cell death that restricts pathogen replication. The AIM2 inflammasome mediates the recognition of DNA viruses as well as that of various Gram-negative and Gram-positive cytosolic bacteria, such as *Listeria monocytogenes*, *Legionella pneumophila*, *Mycobacterium* species and *Francisella tularensis* subspecies *novicida* (*F. novicida*)[8–14]. Notably, several studies have shown that activation of AIM2 by these bacteria requires bacteriolysis and the subsequent release of bacterial chromosomal DNA into the cytosol[10,12,15]. However, whether the bacteriolysis is accidental or is an active, host-directed mechanism has remained unclear.

The activation of AIM2 via the transfection of synthetic DNA or during infection with a DNA virus is independent of signaling via Toll-like receptors or interferons[9,13,16]. In contrast, the activation of AIM2 during infection with *F. novicida* requires the production of type I interferons, which are induced as a result of the recognition of an as-yet-undefined *F. novicida*–derived nucleic acid ligand in the cytosol[9,10,17–20]. Consistent with that, the activation of AIM2 inflammasomes in *F. novicida*–infected cells requires signaling through STING and the transcription factor IRF3 (refs. 9,10,17). It has been speculated that interferon signaling is necessary to increase cellular AIM2 for the detection of *F. novicida* DNA[9], yet interferon-mediated induction of AIM2 is contested, and even small amounts of transfected DNA efficiently trigger activation of AIM2 in an interferon-independent manner[9]. Therefore, it is likely that one or several interferon-inducible factor(s) is (are) required for efficient activation of AIM2 during bacterial infection.

Type I and type II interferons are potent cytokines that exert anti-microbial effects through the induction of a broad transcriptional program involving ~2,000 genes, the so-called 'interferon-stimulated genes' (ISGs), many of which remain uncharacterized.

[1]Focal Area Infection Biology, Biozentrum, University of Basel, Basel, Switzerland. [2]Centre International de Recherche en Infectiologie, Inserm U1111, CNRS UMR 5308, Université Claude Bernard Lyon-1, Ecole Normale Supérieure, Lyon, France. [3]Structure Fédérative de Recherche Biosciences, UMS344/US8, Inserm, CNRS, Université Claude Bernard Lyon-1, Ecole Normale Supérieure, Lyon, France. [4]Institute of Medical Microbiology and Hospital Hygiene, Heinrich-Heine-University Duesseldorf, Duesseldorf, Germany. [5]Department of Microbiology and Immunology, Osaka University, Osaka, Japan. [6]These authors contributed equally to this work. Correspondence should be addressed to T.H. (thomas.henry@inserm.fr) or P.B. (petr.broz@unibas.ch).

Received 11 November 2014; accepted 6 February 2015; published online 16 March 2015; doi:10.1038/ni.3119

Prominent among the products of these ISGs are several families of interferon-inducible GTPases, such as the 47-kilodalton immunity-related GTPases and the 65- to 73-kilodalton guanylate-binding proteins (GBPs)[21,22]. GBPs are conserved among vertebrates, with 11 GBPs in mice and 7 in humans, and exert anti-microbial effects on intracellular bacteria and protozoa[23]. GBP1 and GBP7 restrict *Mycobacterium bovis* bacillus Calmette-Guérin and *L. monocytogenes* by recruiting anti-microbial effectors to the pathogen-containing vacuole (PCV)[24]. Several GBPs are recruited onto the *Toxoplasma* parasitophorous vacuole[25], and most are also required for restricting the replication of *Toxoplasma gondii*[23,26–28]. In addition, GBPs encoded by genes on mouse chromosome 3 promote recognition of the vacuolar, Gram-negative bacterium *Salmonella typhimurium* by the innate immune system by destabilizing its PCV, which leads to egress of the bacteria into the cytosol and subsequent detection of its lipopolysaccharide (LPS) by the caspase-11 inflammasome[29]. In this study we found that GBPs encoded by genes on mouse chromosome 3 were a key factor for the activation of AIM2 during infection with *F. novicida*. In particular, GBP2 and GBP5 controlled the activation of AIM2 by targeting cytosolic *F. novicida* and inducing lysis of these bacteria by an as-yet-uncharacterized mechanism. We demonstrated that GBP-deficient mice were unable to control infection with *F. novicida in vivo*. Together our data reveal a function for GBPs during microbial infection, in that GBPs promoted bacteriolysis in the cytosol and the exposure of bacterial DNA to cytosolic sensors of the innate immune system.

RESULTS

AIM2 activation during *F. novicida* infection requires interferons

F. novicida is a facultative intracellular Gram-negative bacterium that avoids phagosomal degradation in phagocytes by escaping into the cytosol, a process that requires the *Francisella* pathogenicity island (FPI). After escaping from the phagosome, *F. novicida* replicates in the cytosol but also triggers AIM2-dependent activation of caspase-1 (refs. 10,13). Infection of mouse bone marrow–derived macrophages (BMDMs) with wild-type *F. novicida* resulted in cell death (pyroptosis; measured by the release of lactate dehydrogenase (LDH)) and the release of IL-1β dependent on AIM2, ASC and caspase-1, while a mutant lacking the FPI (ΔFPI) did not activate the inflammasome (**Fig. 1a**). STING is linked to the activation of AIM2 during infection with *F. novicida*[10,12]. Macrophages deficient in STING (via the 'goldenticket' (Gt) *N*-ethyl-*N*-nitrosourea–induced nonfunctional mutation of alleles encoding *Tmem173* (called '*Sting*$^{Gt/Gt}$' here)) had considerable attenuation of their ability to induce expression of type I interferons and activation of the AIM2 inflammasome upon infection with *F. novicida*[5] (**Fig. 1b** and **Supplementary Fig. 1a**). Consistent with a role for type I interferons in activation of the AIM2 inflammasome[17,19], macrophages from mice deficient in *Ifnar1*, which encodes the receptor for interferon-α (IFN-α) and IFN-β (IFNAR1), or *Stat1*, which encodes the transcription factor STAT1, displayed significantly less pyroptosis and release of IL-1β when infected with *F. novicida* than did their wild-type counterparts (**Fig. 1c**). To further confirm that activation of AIM2 during infection with *F. novicida* depended on signaling via type I interferons, we assessed whether exogenous interferons were able to restore inflammasome activation in STING-deficient BMDMs. As expected, IFN-β restored cell death and the release of cytokines in *Sting*$^{Gt/Gt}$ BMDMs (**Fig. 1d**). The addition of IFN-γ restored cell death and the release of cytokines in both *Sting*$^{Gt/Gt}$ BMDMs and *Ifnar1*$^{-/-}$ BMDMs (**Fig. 1d**), which indicated a requirement for a general interferon signature.

The induction of *Aim2* mRNA could explain the considerable dependence on type I interferons and signaling via STAT1 during infection with *F. novicida*[10]. However, activation of the AIM2 inflammasome by transfection of DNA or infection with DNA viruses is independent of interferon signaling[9,13,16]. In accordance with those reports, induction of cell death by transfection of the synthetic

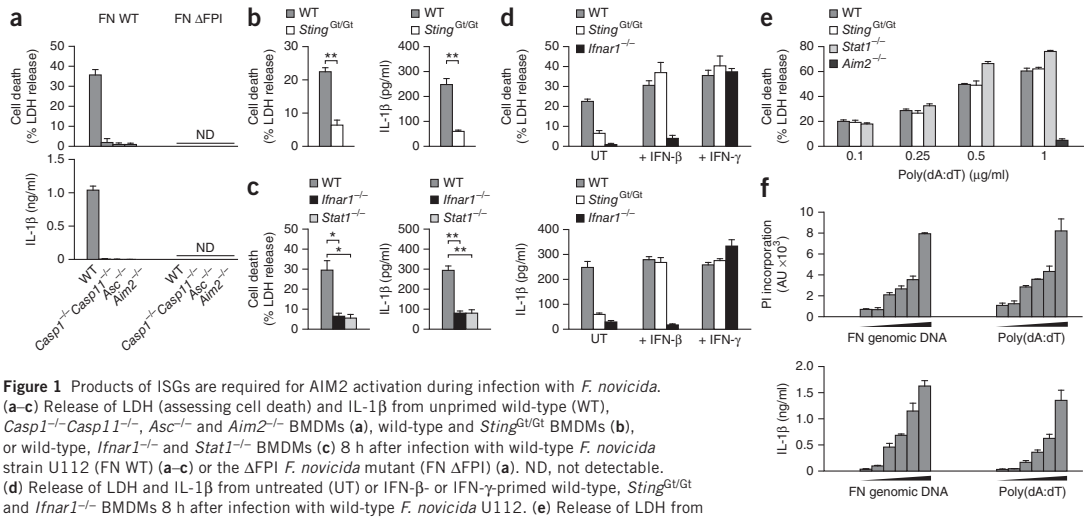

Figure 1 Products of ISGs are required for AIM2 activation during infection with *F. novicida*. (**a**–**c**) Release of LDH (assessing cell death) and IL-1β from unprimed wild-type (WT), *Casp1*$^{-/-}$*Casp11*$^{-/-}$, *Asc*$^{-/-}$ and *Aim2*$^{-/-}$ BMDMs (**a**), wild-type and *Sting*$^{Gt/Gt}$ BMDMs (**b**), or wild-type, *Ifnar1*$^{-/-}$ and *Stat1*$^{-/-}$ BMDMs (**c**) 8 h after infection with wild-type *F. novicida* strain U112 (FN WT) (**a**–**c**) or the ΔFPI *F. novicida* mutant (FN ΔFPI) (**a**). ND, not detectable. (**d**) Release of LDH and IL-1β from untreated (UT) or IFN-β- or IFN-γ-primed wild-type, *Sting*$^{Gt/Gt}$ and *Ifnar1*$^{-/-}$ BMDMs 8 h after infection with wild-type *F. novicida* U112. (**e**) Release of LDH from wild-type, *Sting*$^{Gt/Gt}$, *Stat1*$^{-/-}$ and *Aim2*$^{-/-}$ BMDMs transfected with increasing concentrations of poly(dA:dT) (horizontal axis). (**f**) Incorporation of propidium iodide (PI) (assessing cell death) and release of IL-1β by wild-type BMDMs primed with Pam_3CSK_4 and then transfected with increasing concentrations (wedges) of purified *F. novicida* (FN) genomic DNA or poly(dA:dT) (0, 20, 100, 250, 500 and 1000 ng/ml), assessed 1 h after transfection. $^*P < 0.01$ and $^{**}P < 0.001$ (two-tailed unpaired *t*-test). Data are representative of three (**a**,**c**,**e**) or two (**b**,**d**,**f**) independent experiments (mean and s.d. of quadruplicate wells).

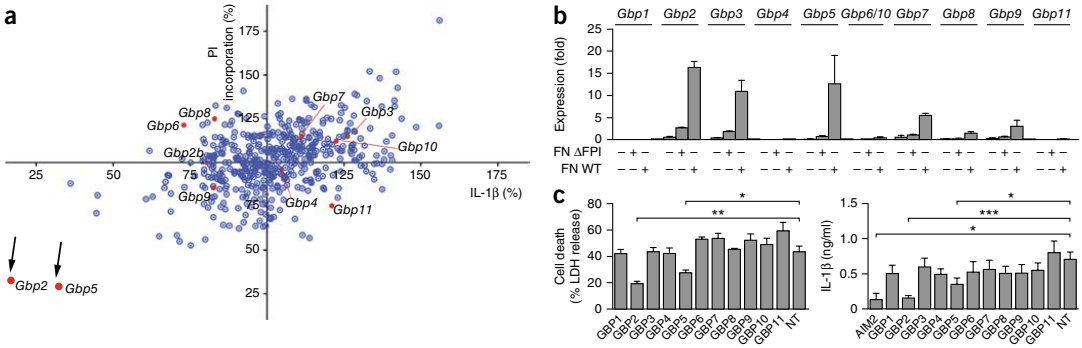

Figure 2 Screening by RNA-mediated interference identifies members of the GBP family as activators of AIM2. (**a**) Screening results for wild-type BMDMs treated with siRNA targeting various genes (red, genes encoding members of the GBP family; black arrows, *Gbp2* and *Gbp5*), presented as incorporation of propidium iodide and release of IL-1β, normalized to the average values obtained with all siRNA (set as 100%) and to the values obtained with *Aim2*-specific siRNA (set as 0%). (**b**) Expression of mRNA from various GBP-encoding genes (top) in wild-type BMDMs left uninfected (–) or infected (+) with wild-type *F. novicida* strain U112 or the ΔFPI mutant, assessed 8 h after infection. (**c**) Release of LDH and IL-1β from unprimed wild-type BMDMs pretreated with nontargeting control siRNA (NT) or with siRNA targeting genes encoding various GBPs (horizontal axis) 48 h before infection with wild-type *F. novicida* strain U112, assessed 8 h after infection. $^{*}P < 0.05$, $^{**}P < 0.01$ and $^{***}P < 0.001$ (two-tailed unpaired *t*-test). Data are representative of one experiment (**a**) or two (**b**) or three (**c**, LDH) independent experiments or are pooled from six independent experiments (**c**, IL-1β) (mean and s.d. of quadruplicate wells in **b**,**c**).

B-form double-stranded DNA poly(dA:dT) at a concentration of 1 μg/ml required AIM2 but was completely independent of STING and STAT1 (**Fig. 1e**). The transfection of large amounts of DNA might overload the system and render it independent of interferon signaling. To rule out this possibility, we 'titrated down' the amount of transfected DNA. The activation of AIM2 remained interferon independent even upon the transfection of small quantities of DNA (**Fig. 1e**). These results indicated that basal AIM2 was sufficient to initiate inflammasome activation[9,13]. Indeed, we observed only weak induction of *Aim2* mRNA following infection with *F. novicida* (**Supplementary Fig. 1b**).

Finally, we confirmed that *F. novicida* genomic DNA was as stimulatory as synthetic DNA by transfecting increasing amounts of each into macrophages that had been primed with the synthetic lipopeptide Pam_3CSK_4 to induce expression of pro-IL-1β. Both types of DNA triggered similar cell death and release of IL-1β (**Fig. 1f**), which excluded the possibility that *F. novicida* DNA had properties that allowed it to evade recognition by AIM2. Together these results indicated that one (or several) IFN-β- or IFN-γ-inducible gene(s) was (were) needed to activate AIM2 specifically during bacterial infection.

Identification of the GBP family by genetic screening

To identify ISGs encoding products involved in *F. novicida*–mediated activation of the AIM2 inflammasome, we screened BMDMs by RNA-mediated interference with small interfering RNA (siRNA). We selected 443 genes with at least twofold higher expression in *F. novicida*–infected wild-type macrophages than in *F. novicida*–infected *Ifnar1*$^{-/-}$ macrophages[17] and selected 40 additional genes on the basis of published reports[9,10,17,18] (data not shown and **Supplementary Table 1**). At 48 h after transfection of siRNA specific for those genes, we infected macrophages with *F. novicida* and monitored inflammasome activation by measuring the release of IL-1β and incorporation of propidium iodide (as a measure of cell death). Knockdown of most of the 483 genes did not substantially affect the release of IL-1β or cell death (**Fig. 2a**). In contrast, knockdown of *Gbp2* or *Gbp5* resulted in much less *F. novicida*–mediated release of IL-1β and macrophage death than that of cells treated with nontargeting siRNA, while knockdown of other GBP-encoding genes showed no comparable effect (**Fig. 2a**). *Gbp2* and *Gbp5* had the highest expression among the GBP-encoding genes in macrophages and were substantially and specifically induced upon infection with wild-type *F. novicida* in a STING- and IFNAR-dependent manner but independently of Toll-like receptor 2 and MyD88 (**Fig. 2b** and **Supplementary Fig. 1c–e**). We confirmed by RT-PCR the efficiency of siRNA-mediated knockdown of GBP-encoding genes expressed during infection with *F. novicida* (**Supplementary Fig. 2a**). We next confirmed the screening results by knocking down all 11 mouse GBP-encoding genes individually and measuring cell death and IL-1β release (**Fig. 2c**). Knockdown of *Gbp2* and *Gbp5* specifically decreased the *F. novicida*–mediated release of IL-1β and cell death, as assessed by two different techniques (**Fig. 2c** and **Supplementary Fig. 2b**). In conclusion, our screening approach identified GBP2 and GBP5 as two possible ISG products that controlled the activation of AIM2 during infection with *F. novicida*.

AIM2 activation requires GBP-encoding genes on chromosome 3

To confirm our screening data, we obtained macrophages from wild-type mice, mice deficient in both caspase-1 and caspase-11 (*Casp1*$^{-/-}$*Casp4*$^{-/-}$; called '*Casp1*$^{-/-}$*Casp11*$^{-/-}$' here) or mice that lack the locus on chromosome 3 encoding GBP1, GBP2, GBP3, GBP5 and GBP7 (called '*Gbp*^{chr3}' here)[23] and infected naive or primed macrophages with *F. novicida*. Consistent with defective activation of the AIM2 inflammasome, *Gbp*^{chr3}-deficient BMDMs displayed a significant reduction in cell death and cytokine release and had a diminished abundance of processed caspase-1 p20 compared with that of their wild-type counterparts, even though their expression of pro-caspase-1, ASC and AIM2 protein was similar to that of wild-type cells (**Fig. 3a,b** and **Supplementary Fig. 3a**). Measuring the incorporation of propidium iodide in real time following infection showed that *Gbp*^{chr3}-deficient BMDMs died with delayed kinetics compared with that of wild-type cells and similar to that of *Ifnar1*$^{-/-}$ BMDMs (**Supplementary Fig. 3b**). To determine if GBPs encoded by genes on

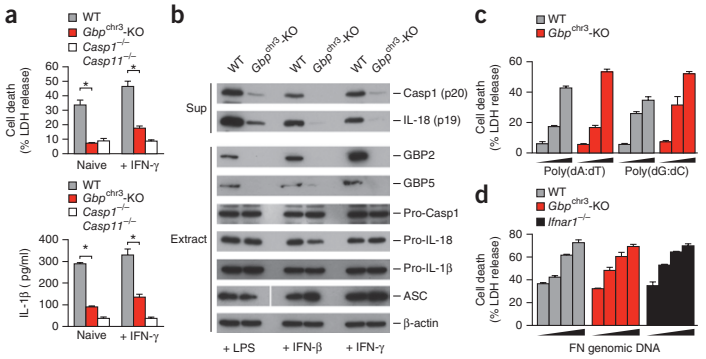

Figure 3 Macrophages from *Gbp*^{chr3}-deficient mice have deficient activation of AIM2 in response to *F. novicida*. (**a**) Release of LDH and IL-1β from naive or IFN-γ-primed wild-type, *Gbp*^{chr3}-deficient (*Gbp*^{chr3}-KO) and *Casp1*$^{-/-}$*Casp11*$^{-/-}$ BMDMs 8 h after infection with wild-type *F. novicida* strain U112. (**b**) Immunoblot analysis of cleaved caspase-1 (p20) and IL-18 (p19) in culture supernatants (Sup), and of GBP2, GBP5, pro-caspase-1 (Pro-Casp1), pro-IL-18, pro-IL-1β, ASC and β-actin (loading control) in extracts (Extract), of wild-type and *Gbp*^{chr3}-deficient BMDMs primed with LPS, IFN-β or IFN-γ (below blots) and then infected with wild-type *F. novicida* strain U112, assessed 8 h after infection. (**c**) Release of LDH from wild-type and *Gbp*^{chr3}-deficient BMDMs 8 h after transfection of increasing concentrations (wedges) of poly(dA:dT) or poly(dG:dC) (0.25, 0.5 or 1 μg/ml). (**d**) Release of LDH from wild-type, *Gbp*^{chr3}-KO and *Ifnar1*$^{-/-}$ BMDMs 8 h after transfection of increasing concentrations (wedges) of *F. novicida* genomic DNA (0.1, 0.25, 0.5 or 1 μg/ml). $^{*}P < 0.001$ (two-tailed unpaired *t*-test). Data are representative of six (**a**) three (**b**,**c**) or two (**d**) independent experiments (mean and s.d. of quadruplicate wells in **a**,**c**,**d**).

chromosome 3 were directly involved in the activation of AIM2, we engaged AIM2 by transfecting synthetic DNA into unprimed wild-type and *Gbp*^{chr3}-deficient macrophages. Cytosolic DNA triggered LDH release to a similar extent in both groups of cells, even when the amount of transfected DNA was 'titrated down' (**Fig. 3c**). Wild-type, *Gbp*^{chr3}-deficient and *Ifnar1*$^{-/-}$ cells also responded similarly to the transfection of purified *F. novicida* genomic DNA (**Fig. 3d**). Thus, GBPs were not required in the context of DNA transfection, which suggested that they functioned upstream of AIM2-mediated DNA detection.

GBP2 and GBP5 direct parallel pathways of AIM2 activation

Since our screening data suggested that mainly GBP2 and GBP5 were required for the activation of AIM2 (**Fig. 2a**), we infected BMDMs from wild-type, *Casp1*$^{-/-}$*Casp11*$^{-/-}$, *Gbp*^{chr3}-deficient, *Gbp2*$^{-/-}$ or *Gbp5*$^{-/-}$ mice with *F. novicida* and measured activation of the AIM2 inflammasome. *Gbp2*$^{-/-}$ BMDMs displayed less death and cytokine release than did wild-type BMDMs (**Fig. 4a**,**b**). Similarly, *Gbp5*$^{-/-}$ BMDMs also displayed attenuated inflammasome activation when infected with *F. novicida* relative to that of their wild-type counterparts (**Fig. 4a**,**b**). Deficiency in *Gbp2* or *Gbp5* did not affect cell death in response to DNA transfection, even when we used very small amounts of DNA (**Fig. 4c**). To determine if expression of GBP2 or GBP5 could restore activation of the AIM2 inflammasome in *Ifnar1*$^{-/-}$ cells, we retrovirally transduced macrophages with constructs expressing GBP2 or GBP5 or with an empty vector (control) and infected them with *F. novicida*. Such ectopic expression was not able to complement the deficiency in inflammasome activation (**Supplementary Fig. 4a–c**), which suggested that other products of ISGs might be required for the function of GBP2 and GBP5, in line with data showing that GBPs are active and correctly targeted only in the context of the interferon response[25].

Single deficiency in *Gbp2* or *Gbp5* did not reduce the activation of AIM2 during infection with *F. novicida* as much as *Gbp*^{chr3} deficiency did (**Fig. 4a**,**b**), which suggested that GBP2 and GBP5 promoted activation of AIM2 through independent pathways. To investigate whether GBP2 and GBP5 acted sequentially or in parallel, we knocked down *Gbp2* expression in wild-type, *Gbp2*$^{-/-}$ and *Gbp5*$^{-/-}$ BMDMs (control

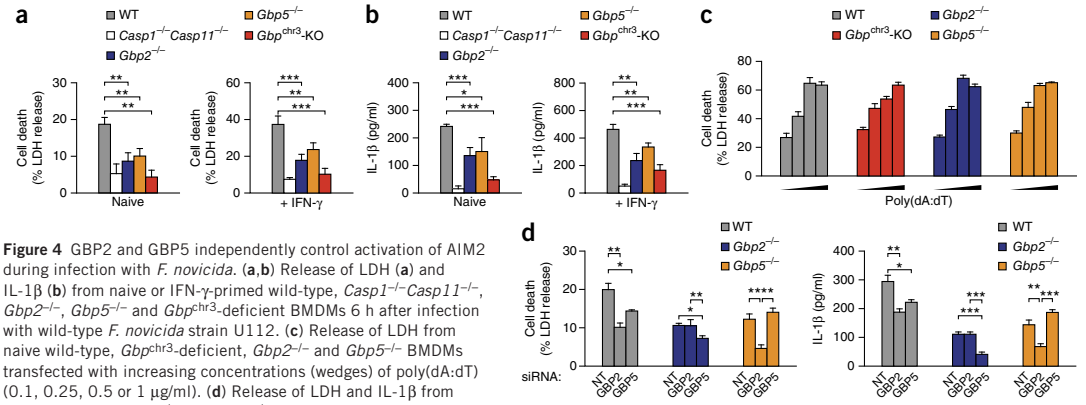

Figure 4 GBP2 and GBP5 independently control activation of AIM2 during infection with *F. novicida*. (**a**,**b**) Release of LDH (**a**) and IL-1β (**b**) from naive or IFN-γ-primed wild-type, *Casp1*$^{-/-}$*Casp11*$^{-/-}$, *Gbp2*$^{-/-}$, *Gbp5*$^{-/-}$ and *Gbp*^{chr3}-deficient BMDMs 6 h after infection with wild-type *F. novicida* strain U112. (**c**) Release of LDH from naive wild-type, *Gbp*^{chr3}-deficient, *Gbp2*$^{-/-}$ and *Gbp5*$^{-/-}$ BMDMs transfected with increasing concentrations (wedges) of poly(dA:dT) (0.1, 0.25, 0.5 or 1 μg/ml). (**d**) Release of LDH and IL-1β from naive wild-type, *Gbp2*$^{-/-}$ and *Gbp5*$^{-/-}$ BMDMs treated with nontargeting control siRNA or siRNA specific for the gene encoding GBP2 or GBP5 (horizontal axis), then, 22 h later, infected with wild-type *F. novicida* U112, assessed 8 h after infection. $^{*}P < 0.05$, $^{**}P < 0.01$ and $^{***}P < 0.001$ (two-tailed unpaired *t*-test). Data are representative of four (**a**,**b**), three (**c**) or two (**d**) independent experiments (mean and s.d. of quadruplicate wells).

of siRNA knockdown efficacy, **Supplementary Fig. 4d**) and measured inflammasome activation after infection with *F. novicida*. Knockdown of *Gbp2* reduced cell death and release of IL-1β in wild-type BMDMs but not in *Gbp2*-deficient BMDMs (**Fig. 4d**). Treatment with *Gbp2*-specific siRNA also significantly reduced inflammasome activation in *Gbp5*$^{-/-}$ BMDMs (**Fig. 4d**), which demonstrated that in *Gbp5*-deficient cells, GBP2 was still active and was able to promote activation of AIM2. Consistent with that, knockdown of *Gbp5* reduced activation of the inflammasome in both wild-type BMDMs and *Gbp2*$^{-/-}$ BMDMs (**Fig. 4d**). In conclusion, our data suggested that the interferon-inducible GTPases GBP2 and GBP5 controlled non-redundant, parallel pathways that promoted activation of AIM2 during infection with *F. novicida*.

Escape of *F. novicida* from phagosomes is GBP independent

Since cytosolic localization of *F. novicida* is required for the activation of AIM2 and since GBPs promote the destabilization of phagosomes and/or pathogen-containing vacuoles of protozoan parasites or bacteria[23,27,29], we speculated that GBPs might facilitate the escape of *F. novicida* from phagosomes. We used a phagosome-protection assay[29,30] based on selective permeabilization of the plasma membrane with digitonin to assay the escape of *F. novicida* from phagosomes. As reported before[30], we observed that 90–95% of wild-type *F. novicida* escaped from phagosomes within a few hours of infection, but this frequency was similar for wild-type BMDMs and *Gbp*^{chr3}-deficient BMDMs at various time points after infection (**Fig. 5a**). In contrast, ΔFPI *F. novicida* remained in the phagosome (data not shown).

F. novicida is naturally resistant to β-lactam antibiotics and secrete the β-lactamase FTN_1072. Taking advantage of this, we developed an alternative assay to detect cytosolic bacteria based on cleavage of the FRET (Förster resonance energy transfer) reporter probe CCF4 by FTN_1072, which leads to a loss of FRET activity[31,32] (**Supplementary Fig. 5**). We preloaded wild-type, *Gbp2*$^{-/-}$ and *Gbp*^{chr3}-deficient BMDMs with CCF4-AM, the membrane-permeable form of the reporter, and subsequently infected the cells with wild-type *F. novicida*, an FTN_1072-deficient strain (the β-lactamase mutant Δbla) or the ΔFPI mutant. We observed no difference among wild-type, *Gbp2*$^{-/-}$ or *Gbp*^{chr3}-deficient BMDMs in terms of FRET activity after infection with wild-type *F. novicida* (**Fig. 5b** and **Supplementary Fig. 5**). The ΔFPI and Δbla mutant strains did not produce any significant FRET signals, similar to the signaling of uninfected macrophages (**Supplementary Fig. 5**). Thus, we concluded that GBPs did not control the activation of AIM2 by promoting the escape of *F. novicida* from phagosomes but that they were active after *F. novicida* reached the cytosol. This was consistent with our data showing that in unprimed cells, *F. novicida*–induced expression of GBP-encoding mRNA was dependent on the FPI and on the escape from phagosomes (**Fig. 2b**) and that cytosolic recognition was required for interferon induction (**Supplementary Fig. 1a**).

GBPs promote cytosolic lysis of *F. novicida*

To identify the mechanism by which GBPs controlled the activation of AIM2 during infection with *F. novicida*, we investigated the subcellular localization of GBPs in infected cells. GBPs are known to co-localize with vacuolar pathogens such as *S. typhimurium*, *M. bovis* bacillus Calmette-Guérin and *T. gondii*, consistent with the ability of GBPs to recruit anti-microbial effector mechanisms to the pathogen and to destabilize PCVs[24,27,29]. We observed that both GBP2 and GBP5 were targeted to intracellular *F. novicida* (**Fig. 6a**). Closer examination of GBP-positive *F. novicida* revealed that GBPs localized to different spots close to or onto the surface of the bacterium (data not shown). However, it was unclear if GBPs targeted the bacterium directly or

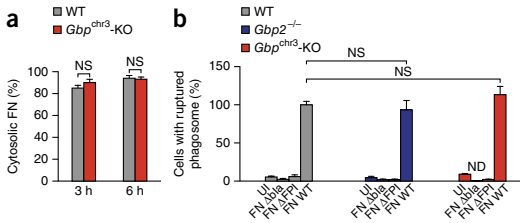

Figure 5 The escape of *F. novicida* from phagosomes is GBP independent. (**a**) Frequency of cytosolic *F. novicida* (FN) among total bacteria at 3 h and 6 h after infection of wild-type and *Gbp*^{chr3}-deficient BMDMs with wild-type *F. novicida* strain U112, assessed by phagosome-protection assay. (**b**) Quantification of cells with ruptured phagosomes at 16 h after infection of wild-type, *Gbp2*$^{-/-}$ and *Gbp*^{chr3}-deficient BMDMs with wild-type *F. novicida* U112, the β-lactamase-deficient mutant Δbla or the ΔFPI mutant or in uninfected cells (UI), assessed with the β-lactamase-cleavable FRET probe CCF4 and presented relative to that of wild-type cells infected with wild-type *F. novicida*. NS, not significant (two-tailed unpaired *t*-test). Data are pooled from four independent experiments with 300 bacteria counted in each (**a**; mean and s.d.) or three independent experiments with 1.5×10^5 cells counted three times in each (**b**; mean and s.d.).

targeted remnants of the host membrane (i.e., lysed phagosomes) or another closely associated membrane compartment.

Since the irregular shape of GBP-positive bacteria suggested that they were lysed, we next determined if wild-type and *Gbp*^{chr3}-deficient cells differed in the abundance of lysed intracellular *F. novicida*. Viable and lysed intracellular bacteria can be quantified on the basis of propidium iodide staining, since intact bacteria remain protected from the influx of propidium iodide[33] (**Fig. 6b**). We tested the assay by quantifying lysed bacteria in wild-type BMDMs infected with wild-type *F. novicida* or an *F. novicida* mutant in which the gene encoding the outer membrane protein FopA is deleted (Δ*fopA*) and thus it has lower membrane stability that results in increased intracellular lysis and hyperactivation of the AIM2 inflammasome[15]. We detected significantly larger amounts of propidium iodide–positive Δ*fopA F. novicida* than wild-type *F. novicida* (**Fig. 6c**), which confirmed the validity of our assay. We next compared the frequency of lysed bacteria in wild-type and *Gbp*^{chr3}-deficient macrophages. The *Gbp*^{chr3}-deficient BMDMs had a significantly lower frequency of lysed bacteria (positive for staining with antibodies to *F. novicida* and propidium iodide) (23% on average) than the wild-type BMDMs had (40% on average) (**Fig. 6c**).

The macromolecular inflammasome complex known as the 'ASC speck' assembles on genomic DNA released from lysed cytosolic *F. novicida*[10]. Immunofluorescence analysis revealed mostly irregularly shaped *F. novicida* in the vicinity of ASC specks (**Fig. 6d**). These bacteria released DNA and were often also positive for GBP staining (**Fig. 6d** and **Supplementary Fig. 6**). Consistent with that, the number of ASC speck-containing cells was significantly lower in GBP-deficient (*Gbp2*$^{-/-}$, *Gbp5*$^{-/-}$ or *Gbp*^{chr3}-deficient) BMDMs than in wild-type BMDMs (**Fig. 6e**). In conclusion, these findings indicated that GBPs associated with cytosolic *F. novicida* and, by an as-yet-undefined mechanism, induced lysis of the bacterium, which resulted in DNA release and detection by the cytosolic DNA sensor AIM2, followed by oligomerization of ASC.

GBPs control *F. novicida* replication

Inflammasome-induced cell death (pyroptosis) restricts intracellular bacteria by removing their replicative niche and reexposing

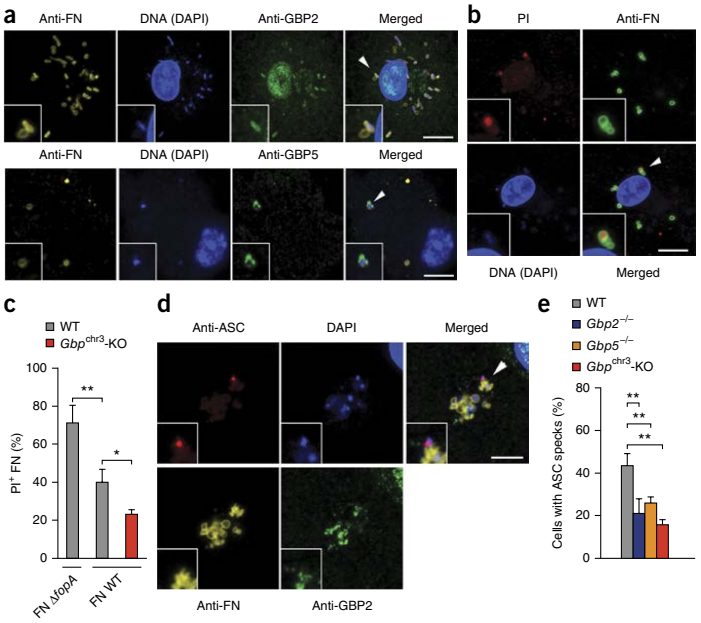

Figure 6 GBPs promote the activation of AIM2 by inducing bacteriolysis. (**a**) Immunostaining with antibody to *F. novicida* (anti-FN), antibody to GBP2 (anti-GBP2) and anti-GBP5, and staining with the DNA-binding dye DAPI, in IFN-γ-primed wild-type BMDMs 8 h after infection with wild-type *F. novicida*. (**b**) Microscopy of lysed (propidium iodide–positive) *F. novicida* in IFN-γ-primed wild-type BMDMs 8 h after infection with wild-type *F. novicida*. (**c**) Quantification of lysed (propidium iodide–positive) *F. novicida* (PI+ FN) in IFN-γ-primed wild-type and *Gbp*^{chr3}-deficient BMDMs 8 h after infection with wild-type *F. novicida* (FN WT) or the Δ*fopA* mutant (FN Δ*fopA*). (**d**) Immunostaining of ASC, GBP2 and *F. novicida* in IFN-γ-primed wild-type BMDMs 8 h after infection with wild-type *F. novicida*. (**e**) Quantification of ASC speck formation in IFN-γ-primed wild-type, *Gbp2*$^{-/-}$, *Gbp5*$^{-/-}$ and *Gbp*^{chr3}-deficient BMDMs 8 h after infection with wild-type *F. novicida*. Outlined areas (**a**,**b**,**d**) contain 2× enlargment of areas marked by arrowheads. Scale bars (**a**,**b**,**d**), 10 μm. $^{*}P < 0.05$ and $^{**}P < 0.01$ (two-tailed unpaired *t*-test). Data are representative of three independent experiments (**a**,**b**,**d**) or are pooled from three independent experiments with 300 bacteria (**c**) or cells (**e**) counted in each (mean and s.d.).

them to extracellular immunological mechanisms[34]. Cell-autonomous immunity, on the other hand, relies on cell-intrinsic mechanisms to restrict bacterial growth without the need for killing the host cell[21]. To determine whether GBPs restricted *F. novicida* growth through cell-autonomous mechanisms or inflammasome-dependent mechanisms, we infected wild-type, *Aim2*$^{-/-}$, *Gbp*^{chr3}-deficient and *Ifnar1*$^{-/-}$ BMDMs with wild-type *F. novicida* expressing green fluorescent protein (GFP) and used flow cytometry to quantify infected cells (more than two bacteria per cell, our specific fluorescence-detection threshold) among the live cell population. We observed a significantly higher percentage of live infected *Aim2*$^{-/-}$, *Gbp*^{chr3}-deficient and *Ifnar1*$^{-/-}$ BMDMs than live infected wild-type BMDMs (**Fig. 7a**). This suggested that deficiency in *Ifnar1* or *Gbp*^{chr3}, similar to deficiency in *Aim2*, resulted in a reduction in inflammasome-mediated killing of host cells upon infection.

Cell-autonomous growth restriction is an interferon-induced mechanism that is at least partially independent of inflammasome-mediated cell death[35,36]. Therefore, we next determined if *Gbp*^{chr3}-deficient BMDMs and *Ifnar1*-deficient BMDMs also had a defect in restricting intracellular bacterial replication. We infected macrophages with GFP+ *F. novicida* and quantified bacteria (per cell) by both automated microscopy in flow and microscopy at various

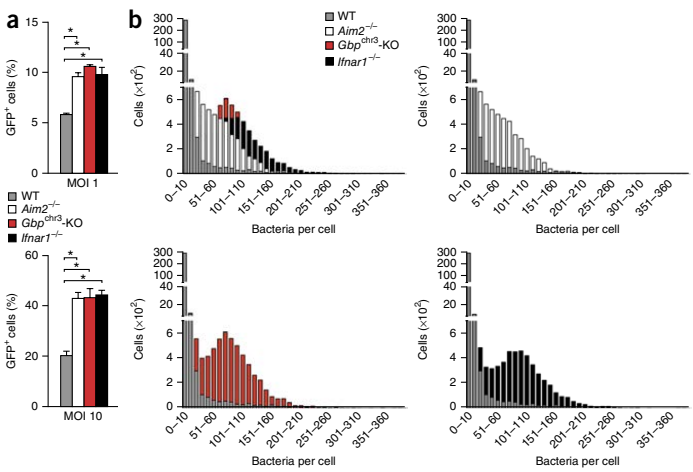

Figure 7 GBPs restrict the intracellular replication of *F. novicida*. (**a**) Flow cytometry–based quantification of infected (GFP+) cells among live wild-type, *Aim2*$^{-/-}$, *Gbp*^{chr3}-deficient and *Ifnar1*$^{-/-}$ BMDMs 12 h after infection with GFP-expressing wild-type *F. novicida* at a multiplicity of infection (MOI) of 1 (top) or 10 (bottom). $^{*}P < 0.001$ (two-tailed unpaired *t*-test). (**b**) Quantification of bacterial loads in single cells among wild-type, *Aim2*$^{-/-}$, *Gbp*^{chr3}-deficient and *Ifnar1*$^{-/-}$ BMDMs 12 h after infection with GFP-expressing wild-type *F. novicida* at a multiplicity of infection of 10, assessed by high-resolution microscopy in flow and presented as a comparison of all four genotypes (top left) or a comparison of wild-type cells with each other genotype, with bacteria-per-cell values grouped by increments of 10 (horizontal axes). $P < 0.0001$, wild-type versus *Aim2*$^{-/-}$, wild-type versus *Gbp*^{chr3}-deficient, and wild-type versus *Ifnar1*$^{-/-}$ (Kolmogorov-Smirnov test with Bonferroni correction). Data are representative of three independent experiments (**a**; mean and s.d. of triplicate wells) or are pooled from three independent experiments (**b**).

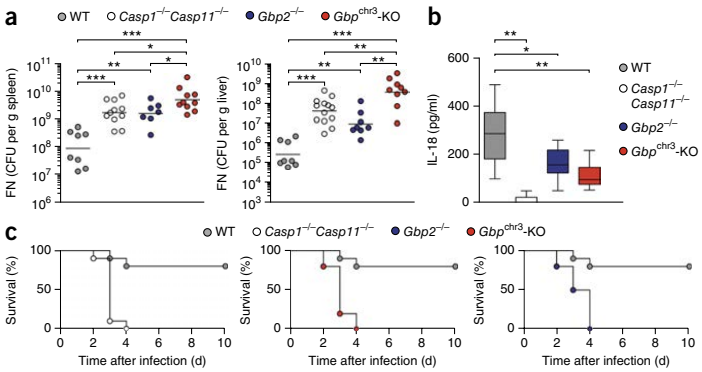

Figure 8 GBPs control host defense against *F. novicida in vivo*. (**a**) Bacterial burden (as colony-forming units (CFU) of *F. novicida* (FN) per gram tissue) in the liver and spleen at day 2 after subcutaneous infection of wild-type, *Casp1*$^{-/-}$*Casp11*$^{-/-}$, *Gbp2*$^{-/-}$ and *Gbp*^{chr3}-deficient mice with 5×10^3 wild-type *F. novicida*. Each symbol represents an individual mouse ($n = 8$ (wild-type), 10 (*Casp1*$^{-/-}$*Casp11*$^{-/-}$), 7 (*Gbp2*$^{-/-}$) and 10 (*Gbp*^{chr3}-deficient) (spleen), or $n = 8$ (wild-type), 13 (*Casp1*$^{-/-}$*Casp11*$^{-/-}$), 8 (*Gbp2*$^{-/-}$) and 9 (*Gbp*^{chr3}-deficient) (liver)); small horizontal lines indicate the mean. $^*P < 0.05$, $^{**}P < 0.01$ and $^{***}P < 0.001$ (Mann-Whitney test). (**b**) IL-18 in serum obtained from wild-type mice ($n = 12$), *Casp1*$^{-/-}$*Casp11*$^{-/-}$ mice ($n = 11$), *Gbp2*$^{-/-}$ mice ($n = 12$) and *Gbp*^{chr3}-deficient mice ($n = 14$) 16 h after subcutaneous infection with 1.5×10^5 wild-type *F. novicida*. $^*P < 0.01$ and $^{**}P < 0.001$ (Mann-Whitney test). (**c**) Survival of wild-type, *Casp1*$^{-/-}$*Casp11*$^{-/-}$, *Gbp2*$^{-/-}$ and *Gbp*^{chr3}-deficient mice ($n = 10$ per genotype) after subcutaneous infection with 5×10^3 wild-type *F. novicida*. $P < 0.0001$, wild-type versus *Casp1*$^{-/-}$*Casp11*$^{-/-}$ or wild-type versus *Gbp*^{chr3}-deficient, and $P = 0.0005$, wild-type versus *Gbp2*$^{-/-}$ (log-rank (Mantel-Cox) test). Data are representative of two independent experiments (**a**,**c**) or are pooled from two individual experiments (**b**; with 10th–90th percentiles).

time points after infection. Wild-type macrophages efficiently controlled intracellular replication, but *Aim2*$^{-/-}$ BMDMs contained large numbers of intracellular *F. novicida* (30 or more per cell) (**Fig. 7b** and **Supplementary Fig. 7a**,**b**), consistent with a loss of inflammasome-mediated killing of host cells. Bacterial loads were even higher in *Gbp*^{chr3}-deficient or *Ifnar1*-deficient BMDMs, with many cells containing up to 100 bacteria (**Fig. 7b** and **Supplementary Fig. 7a**,**b**). The production of reactive oxygen species and nitric oxide is a potent cell-intrinsic anti-microbial mechanism that can also be activated in an interferon-dependent manner. GBP7 has been shown to recruit subunits of the NADPH oxidase to intracellular *L. monocytogenes* and *M. bovis* bacillus Calmette-Guérin[24], and inducible nitric oxide synthase can restrict bacterial growth in a cell-intrinsic manner[21]. However, deficiency in these mechanisms achieved through the use of BMDMs deficient in both inducible nitric oxide synthase and Nox2 did not significantly alter bacteriolysis and inflammasome activation after infection with *F. novicida* ($P = 0.3081$, $P = 0.2786$ and $P = 0.0529$; **Supplementary Fig. 8a**,**b**). Overall, these data indicated that GBPs encoded by the locus on chromosome 3 participated in growth restriction in two ways: directly, by promoting the lysis of intracellular bacteria by an as-yet-unknown mechanism; and indirectly, by promoting the inflammasome-mediated killing of host cells, thereby removing the intracellular replicative niche of *F. novicida*.

GBPs control *F. novicida* replication *in vivo*

AIM2, ASC and caspase-1 control the replication of *F. novicida in vivo* in mice[9,10,37]. Since GBPs are required for inflammasome activation *in vitro*, we investigated whether these proteins also have a physiological role in host defense. We infected age- and sex-matched wild-type, *Casp1*$^{-/-}$*Casp11*$^{-/-}$, *Gbp2*$^{-/-}$ and *Gbp*^{chr3}-deficient mice subcutaneously with 5×10^3 colony-forming units of wild-type *F. novicida* strain U112 and measured the bacterial burden in the liver and spleen at 2 d after infection. As published before[37], *Casp1*$^{-/-}$*Casp11*$^{-/-}$ mice displayed a significantly higher bacterial burden in the liver and spleen than that of wild-type mice (**Fig. 8a**). Similarly, *Gbp2*$^{-/-}$ and *Gbp*^{chr3}-deficient mice showed higher bacterial counts than wild-type mice, similar to or even higher than those of *Casp1*$^{-/-}$*Casp11*$^{-/-}$ mice (**Fig. 8a**). Consistent with diminished inflammasome activation *in vivo*, we detected a significantly lower serum concentration of IL-18 in *Casp1*$^{-/-}$*Casp11*$^{-/-}$, *Gbp2*$^{-/-}$ and *Gbp*^{chr3}-deficient mice than in wild-type mice (**Fig. 8b**). To further assess the effects of GBP deficiency *in vivo*, we analyzed survival. Within 4 d of infection, all *Casp1*$^{-/-}$*Casp11*$^{-/-}$, *Gbp2*$^{-/-}$ and *Gbp*^{chr3}-deficient mice died, while most wild-type mice survived until the end of the experiment (day 10) (**Fig. 8c**). These results confirmed the relevance of our *in vitro* data and demonstrated that GBPs encoded by the locus on chromosome 3 were important for inflammasome activation and host defense against *F. novicida in vivo*.

DISCUSSION

Since the activation of AIM2 during infection with the cytosolic pathogen *F. novicida* required interferon signaling, we investigated the role of the products of ISGs in this process. Our results showed that the interferon-inducible GTPases GBP2 and GBP5 promoted *F. novicida*–mediated activation of the AIM2 inflammasome but were dispensable for the activation of AIM2 upon transfection of DNA. Members of the GBP family take part in interferon-induced cell-autonomous immunity and are known to induce disruption of the PCVs of vacuolar bacteria and parasites[23,27,29]. However, the cytosolic localization of *F. novicida* was similar in wild-type and *Gbp*^{chr3}-deficient cells, which indicated that GBPs must have been involved later during infection, after the bacteria had entered the cytosol. This was consistent with results showing that the escape from phagosomes is an interferon-independent process[36] and that cytosolic localization of *F. novicida* is a prerequisite for interferon induction[17]. Since the activation of AIM2 during infection with *F. novicida* or *L. monocytogenes* is known to require cytosolic bacteriolysis[12,15], we investigated whether GBPs controlled the bacteriolysis and replication of *F. novicida* in the cytosol. Significantly fewer lysed and more overall *F. novicida* were present in cells deficient in GBP-encoding genes or *Ifnar1* than in wild-type cells, which indicated that GBPs were required for interferon-mediated cell-autonomous immunity to the pathogen. Furthermore, our results demonstrated that in addition to their known function in destabilizing PCVs, GBPs can also promote the lysis of cytosolic bacteria.

GBPs are also critical for the cytosolic recognition of LPS and for activation of the caspase-11 inflammasome pathway. In this context, they act by promoting the release of vacuolar *S. typhimurium* into the cytosol or by promoting activation of caspase-11 during infection with *L. pneumophila*[29,38]. At present, no model fully explains how GBPs restrict pathogen growth during infection with microbes or protozoa

and at the same time control inflammasome signaling. It is, however, conceivable that the membrane-destabilizing activity of GBPs in combination with their bacteriolytic activity could not only result in the entry of bacteria into the cytosol but also release microbe-associated molecular patterns (for example, LPS and DNA) directly. Such a model might explain their effect on both the caspase-11 pathway[38] and the AIM2 pathway in response to cytosolic bacteria. Thus, bacteriolysis would also release *F. novicida* LPS into the cytosol. However, since *F. novicida* LPS is tetra-acylated, it does not trigger caspase-11 activation[39]. Conversely, we would expect GBPs to lyse cytosolic *Salmonella* or *Legionella*, which would result in activation of AIM2. But in this case, activation of AIM2 is most probably masked by a high degree of caspase-11-dependent cell death and cytokine release.

GBP-mediated bacteriolysis might also be expected to release DNA and amplify the production of type I interferons via STING. Notably, what triggers initial STING signaling and the induction of GBP-encoding genes during infection with *F. novicida* is still undefined, but two possibilities exist. One is the direct activation of STING via a secreted bacterial cyclic nucleotide, analogous to infection with *L. monocytogenes*[40], and another is activation of the DNA sensor cGAS by *F. novicida* DNA and subsequent production of the cyclic dinucleotide cGAMP[41,42]. Lysis of *F. novicida* within the phagosome followed by translocation of its DNA into the cytosol could trigger interferon production[9]. Alternatively, low levels of *F. novicida* extracellular DNA could reach the cytosol by sticking to the surface of the infecting bacteria, as suggested for infection with *M. tuberculosis*[43]. Finally, small amounts of spontaneous bacteriolysis might occur in the host-cell cytosol. If DNA indeed triggers initial STING-mediated production of interferons, it remains to be shown why it is insufficient to trigger activation of AIM2. Additional experiments are needed to determine the relative DNA-binding affinities of cGAS and AIM2 and how their signaling hierarchy is controlled.

Our results have revealed an underappreciated, close connection between cell-autonomous immunity and recognition by the innate immune system. The attack of GBPs on PCVs or pathogens liberates microbe-associated molecular patterns and thus ensures subsequent immunological recognition of the pathogen, which explains the role of interferon signaling in the detection of bacterial DNA by AIM2 or LPS from vacuolar bacteria by the caspase-11 pathway[9,10,13,44,45]. Additional questions remain, such as how GBP targeting is regulated and how GBPs act mechanistically. Ectopic expression of GBP2 or GBP5 did not 'rescue' the inflammasome deficiency of *Ifnar1*$^{-/-}$ cells, which suggests that other products of ISGs are necessary for proper targeting and activity of GBPs[24,25]. Indeed, members of the IRGM family, a subclass of the immunity-related GTPases, can act as guanine-dissociation inhibitors and control the targeting of both immunity-related GTPases and GBPs to pathogen-containing vacuoles, yet the molecular mechanism of this is still unclear[46–49]. Additional biochemical studies are needed to define the mechanism of GBP targeting and action during bacterial infection and how this promotes the exposure of bacterial ligands to cytosolic recognition pathways.

METHODS

Methods and any associated references are available in the online version of the paper.

Note: Any Supplementary Information and Source Data files are available in the online version of the paper.

ACKNOWLEDGMENTS
We thank N. Gekara (Umea University) for *Sting*$^{Gt/Gt}$ mice; M. Roth and S. Hofer for support with mouse experiments; D. Monack (Stanford University) for chicken antibody to *F. novicida*; N. Kayagaki (Genentech) and V. Dixit (Genentech) for *Gbp5*$^{-/-}$ and *Aim2*$^{-/-}$ mice, rat antibody to ASC and rat antibody to caspase-1; L. Gallagher and C. Manoil (University of Washington) for plasmid pFFlp; O. Allatif for statistical analysis; the Imaging and FACS Core Facilities of the Biozentrum, University of Basel, for technical assistance; and the Plateau de Biologie Expérimentale de la Souris and the flow cytometry platform of SFR Biosciences Gerland-Lyon Sud. Supported by Swiss National Science Foundation (PP00P3_139120/1 to P.B.), the University of Basel (ID2153162 to P.B.), the European Research Council (311542 to T.H.) and the Déléguation Générale de l'Armement (M.R.).

AUTHOR CONTRIBUTIONS
E.M., P.W., T.H. and P.B. conceived of the research; E.M., P.W., R.F.D., S.C., L.A., S.R., S.D., M.S.D., A.K., M.R., T.H. and P.B. performed experiments; D.D., K.P. and M.Y. provided reagents; and T.H. and P.B. wrote the manuscript.

COMPETING FINANCIAL INTERESTS
The authors declare no competing financial interests.

1. Paludan, S.R. & Bowie, A.G. Immune sensing of DNA. *Immunity* **38**, 870–880 (2013).
2. Ishikawa, H., Ma, Z. & Barber, G.N. STING regulates intracellular DNA-mediated, type I interferon-dependent innate immunity. *Nature* **461**, 788–792 (2009).
3. Sauer, J.D. *et al.* The *N*-ethyl-*N*-nitrosourea-induced Goldenticket mouse mutant reveals an essential function of Sting in the in vivo interferon response to *Listeria monocytogenes* and cyclic dinucleotides. *Infect. Immun.* **79**, 688–694 (2011).
4. Hornung, V. *et al.* AIM2 recognizes cytosolic dsDNA and forms a caspase-1-activating inflammasome with ASC. *Nature* **458**, 514–518 (2009).
5. Fernandes-Alnemri, T., Yu, J.W., Datta, P., Wu, J. & Alnemri, E.S. AIM2 activates the inflammasome and cell death in response to cytoplasmic DNA. *Nature* **458**, 509–513 (2009).
6. Roberts, T.L. *et al.* HIN-200 proteins regulate caspase activation in response to foreign cytoplasmic DNA. *Science* **323**, 1057–1060 (2009).
7. Bürckstümmer, T. *et al.* An orthogonal proteomic-genomic screen identifies AIM2 as a cytoplasmic DNA sensor for the inflammasome. *Nat. Immunol.* **10**, 266–272 (2009).
8. Ge, J., Gong, Y.N., Xu, Y. & Shao, F. Preventing bacterial DNA release and absent in melanoma 2 inflammasome activation by a Legionella effector functioning in membrane trafficking. *Proc. Natl. Acad. Sci. USA* **109**, 6193–6198 (2012).
9. Fernandes-Alnemri, T. *et al.* The AIM2 inflammasome is critical for innate immunity to *Francisella tularensis*. *Nat. Immunol.* **11**, 385–393 (2010).
10. Jones, J.W. *et al.* Absent in melanoma 2 is required for innate immune recognition of *Francisella tularensis*. *Proc. Natl. Acad. Sci. USA* **107**, 9771–9776 (2010).
11. Kim, S. *et al.* *Listeria monocytogenes* is sensed by the NLRP3 and AIM2 inflammasome. *Eur. J. Immunol.* **40**, 1545–1551 (2010).
12. Sauer, J.D. *et al.* *Listeria monocytogenes* triggers AIM2-mediated pyroptosis upon infrequent bacteriolysis in the macrophage cytosol. *Cell Host Microbe* **7**, 412–419 (2010).
13. Rathinam, V.A. *et al.* The AIM2 inflammasome is essential for host defense against cytosolic bacteria and DNA viruses. *Nat. Immunol.* **11**, 395–402 (2010).
14. Briken, V., Ahlbrand, S.E. & Shah, S. *Mycobacterium tuberculosis* and the host cell inflammasome: a complex relationship. *Front. Cell. Infect. Microbiol.* **3**, 62 (2013).
15. Peng, K., Broz, P., Jones, J., Joubert, L.M. & Monack, D. Elevated AIM2-mediated pyroptosis triggered by hypercytotoxic Francisella mutant strains is attributed to increased intracellular bacteriolysis. *Cell. Microbiol.* **13**, 1586–1600 (2011).
16. Muruve, D.A. *et al.* The inflammasome recognizes cytosolic microbial and host DNA and triggers an innate immune response. *Nature* **452**, 103–107 (2008).
17. Henry, T., Brotcke, A., Weiss, D.S., Thompson, L.J. & Monack, D.M. Type I interferon signaling is required for activation of the inflammasome during Francisella infection. *J. Exp. Med.* **204**, 987–994 (2007).
18. Cole, L.E. *et al.* Macrophage proinflammatory response to *Francisella tularensis* live vaccine strain requires coordination of multiple signaling pathways. *J. Immunol.* **180**, 6885–6891 (2008).
19. Cole, L.E. *et al.* Toll-like receptor 2-mediated signaling requirements for *Francisella tularensis* live vaccine strain infection of murine macrophages. *Infect. Immun.* **75**, 4127–4137 (2007).
20. Jones, J.W., Broz, P. & Monack, D.M. Innate immune recognition of *Francisella tularensis*: activation of type-I interferons and the inflammasome. *Front Microbiol* **2**, 16 (2011).
21. Kim, B.H., Shenoy, A.R., Kumar, P., Bradfield, C.J. & MacMicking, J.D. IFN-inducible GTPases in host cell defense. *Cell Host Microbe* **12**, 432–444 (2012).
22. Howard, J.C., Hunn, J.P. & Steinfeldt, T. The IRG protein-based resistance mechanism in mice and its relation to virulence in *Toxoplasma gondii*. *Curr. Opin. Microbiol.* **14**, 414–421 (2011).
23. Yamamoto, M. *et al.* A cluster of interferon-γ-inducible p65 GTPases plays a critical role in host defense against *Toxoplasma gondii*. *Immunity* **37**, 302–313 (2012).

24. Kim, B.H. *et al.* A family of IFN-gamma-inducible 65-kD GTPases protects against bacterial infection. *Science* **332**, 717–721 (2011).
25. Degrandi, D. *et al.* Extensive characterization of IFN-induced GTPases mGBP1 to mGBP10 involved in host defense. *J. Immunol.* **179**, 7729–7740 (2007).
26. Kresse, A. *et al.* Analyses of murine GBP homology clusters based on in silico, in vitro and in vivo studies. *BMC Genomics* **9**, 158 (2008).
27. Degrandi, D. *et al.* Murine guanylate binding protein 2 (mGBP2) controls *Toxoplasma gondii* replication. *Proc. Natl. Acad. Sci. USA* **110**, 294–299 (2013).
28. Kravets, E. *et al.* The GTPase activity of murine guanylate-binding protein 2 (mGBP2) controls the intracellular localization and recruitment to the parasitophorous vacuole of *Toxoplasma gondii*. *J. Biol. Chem.* **287**, 27452–27466 (2012).
29. Meunier, E. *et al.* Caspase-11 activation requires lysis of pathogen-containing vacuoles by IFN-induced GTPases. *Nature* **509**, 366–370 (2014).
30. Checroun, C., Wehrly, T.D., Fischer, E.R., Hayes, S.F. & Celli, J. Autophagy-mediated reentry of *Francisella tularensis* into the endocytic compartment after cytoplasmic replication. *Proc. Natl. Acad. Sci. USA* **103**, 14578–14583 (2006).
31. Nothelfer, K., Dias Rodrigues, C., Bobard, A., Phalipon, A. & Enninga, J. Monitoring *Shigella flexneri* vacuolar escape by flow cytometry. *Virulence* **2**, 54–57 (2011).
32. Juruj, C. *et al.* Caspase-1 activity affects AIM2 speck formation/stability through a negative feedback loop. *Front. Cell. Infect. Microbiol.* **3**, 1–11 (2013).
33. Chong, A. *et al.* Cytosolic clearance of replication-deficient mutants reveals *Francisella tularensis* interactions with the autophagic pathway. *Autophagy* **8**, 1342–1356 (2012).
34. Miao, E.A. *et al.* Caspase-1-induced pyroptosis is an innate immune effector mechanism against intracellular bacteria. *Nat. Immunol.* **11**, 1136–1142 (2010).
35. Zhou, H. *et al.* Genome-wide RNAi screen in IFN-γ-treated human macrophages identifies genes mediating resistance to the intracellular pathogen *Francisella tularensis*. *PLoS ONE* **7**, e31752 (2012).
36. Edwards, J.A., Rockx-Brouwer, D., Nair, V. & Celli, J. Restricted cytosolic growth of *Francisella tularensis* subsp. tularensis by IFN-γ activation of macrophages. *Microbiology* **156**, 327–339 (2010).
37. Mariathasan, S., Weiss, D.S., Dixit, V.M. & Monack, D.M. Innate immunity against *Francisella tularensis* is dependent on the ASC/caspase-1 axis. *J. Exp. Med.* **202**, 1043–1049 (2005).
38. Pilla, D.M. *et al.* Guanylate binding proteins promote caspase-11-dependent pyroptosis in response to cytoplasmic LPS. *Proc. Natl. Acad. Sci. USA* **111**, 6046–6051 (2014).
39. Hagar, J.A., Powell, D.A., Aachoui, Y., Ernst, R.K. & Miao, E.A. Cytoplasmic LPS activates caspase-11: implications in TLR4-independent endotoxic shock. *Science* **341**, 1250–1253 (2013).
40. Woodward, J.J., Iavarone, A.T. & Portnoy, D.A. c-di-AMP secreted by intracellular *Listeria monocytogenes* activates a host type I interferon response. *Science* **328**, 1703–1705 (2010).
41. Sun, L., Wu, J., Du, F., Chen, X. & Chen, Z.J. Cyclic GMP-AMP synthase is a cytosolic DNA sensor that activates the type I interferon pathway. *Science* **339**, 786–791 (2013).
42. Li, X.D. *et al.* Pivotal roles of cGAS-cGAMP signaling in antiviral defense and immune adjuvant effects. *Science* **341**, 1390–1394 (2013).
43. Manzanillo, P.S., Shiloh, M.U., Portnoy, D.A. & Cox, J.S. *Mycobacterium tuberculosis* activates the DNA-dependent cytosolic surveillance pathway within macrophages. *Cell Host Microbe* **11**, 469–480 (2012).
44. Broz, P. *et al.* Caspase-11 increases susceptibility to Salmonella infection in the absence of caspase-1. *Nature* **490**, 288–291 (2012).
45. Rathinam, V.A. *et al.* TRIF licenses caspase-11-dependent NLRP3 inflammasome activation by gram-negative bacteria. *Cell* **150**, 606–619 (2012).
46. Martens, S. *et al.* Disruption of *Toxoplasma gondii* parasitophorous vacuoles by the mouse p47-resistance GTPases. *PLoS Pathog.* **1**, e24 (2005).
47. Howard, J.C., Hunn, J.P. & Steinfeldt, T. The IRG protein-based resistance mechanism in mice and its relation to virulence in *Toxoplasma gondii*. *Curr. Opin. Microbiol.* **14**, 414–421 (2011).
48. Bekpen, C. *et al.* The interferon-inducible p47 (IRG) GTPases in vertebrates: loss of the cell autonomous resistance mechanism in the human lineage. *Genome Biol.* **6**, R92 (2005).
49. Haldar, A.K. *et al.* IRG and GBP host resistance factors target aberrant, "non-self" vacuoles characterized by the missing of "self" IRGM proteins. *PLoS Pathog.* **9**, e1003414 (2013).

ONLINE METHODS

Bacterial strains and plasmids. *F. novicida* strain U112 and isogenic ΔFPI mutants have been published[10]. Where applicable, strains were transformed with the plasmid pKK219-GFP (**Supplementary Table 2**). The β-lactamase mutant Δ*bla* was generated by PCR-mediated homologous recombination with a kanamycin selection cassette through use of the following primers (upper case indicates *F. novicida* sequence; lower case indicates the kanamycin-resistance casette sequence): ForUpstream, GTCGAGTACGCT AATATAAAAATTCTAAAAA; RevUpstream, gcttatcgataccgtcgacctcGGGA TTAATGATAAAGTTGTAACTAATATACGC; ForDownstream, gatatcgat cctgcagctatgcCACTTATAAATAAGCGGTACGCCAC; and RevDownstream, AAGACGGTGATGTACCATTTGTCTATAG. The kanamycin-resistance casette was removed by transformation of the mutant obtained with the thermosensitive plasmid pFFlp (provided by L. Gallagher and C. Manoil) encoding the recombinase Flp. Following loss of the plasmid, genomic deletion was verified by sequencing.

Mice. *Gbp*^{chr3}-deficient, *Gbp2*$^{-/-}$, *Gbp5*$^{-/-}$, *Nos2*$^{-/-}$*Cybb*$^{-/-}$, *Casp1*$^{-/-}$*Casp11*$^{-/-}$ ('caspase-1-knockout'), *Asc*$^{-/-}$, *Aim2*$^{-/-}$, *Stat1*$^{-/-}$, *Ifnar1*$^{-/-}$, *Sting*$^{Gt/Gt}$, *Tlr2*$^{-/-}$ and *Myd88*$^{-/-}$ mice have been described[3,10,23,27,29,44]. Mice were bred in the animal facilities of the University of Basel or at the Plateau De Biologie Expérimentale De La Souris.

Animal infection. All animal experiments were approved (license 2535, Kantonales Veterinäramt Basel-Stadt and ENS_2012_061) and were performed according to local guidelines (Tierschutz-Verordnung, Basel-Stadt and CECCAPP, Lyon) and the Swiss animal protection law (Tierschutz-Gesetz). Age- and sex-matched mice (8–10 weeks of age) were infected subcutaneously with 5×10^3 or 1.5×10^5 colony-forming units of stationary-phase wild-type *F. novicida* strain U112 in 50 μl PBS. Mice were killed at the appropriate time point after infection. No randomization or 'blinding' of researchers to sample identity was used.

Cell culture and infection. BMDMs were differentiated in DMEM (Invitrogen) with 10% vol/vol FCS (Thermo Fisher Scientific), 10% MCSF (supernatants of L929 mouse fibroblasts), 10 mM HEPES (Invitrogen) and nonessential amino acids (Invitrogen). 1 d before infection, macrophages were seeded into 6-, 24- or 96-well plates at a density of 1.25×10^6, 2.5×10^5 or 5×10^4 cells per well. Where required, macrophages were pre-stimulated with Pam_3CSK_4 (tripalmitoyl cysteinyl seryl tetralysine), LPS (from *Escherichia coli* strain O111:B4 (InvivoGen)), mouse IFN-β or mouse IFN-γ (eBioscience). For infection with *F. novicida*, bacteria were grown overnight at 37 °C with aeration in brain-heart–infusion medium or tryptic soy broth. The bacteria were added to the macrophages at a multiplicity of infection of 100 or the appropriate value. The plates were centrifuged for 15 min at 500*g* to ensure similar adhesion of the bacteria to the cells and were incubated for 120 min at 37 °C. Next, cells were washed and fresh medium with 10 μg/ml gentamycin (Invitrogen) was added to kill extracellular bacteria, then plates were incubated for the desired length of time. Transfection with poly(dA:dT) or poly(dG:dC) was done as described[29] or as indicated in the figures and legends (**Figs. 1** and **3**).

siRNA-mediated knockdown. Genes were knocked down with GenMute (SignaGen Laboratories) and siRNA pools (siGenome; Dharmacon). Wild-type BMDMs were seeded into 24- or 96-well plates at a density of 1.5×10^5 or 3×10^4 cells per well. siRNA complexes were prepared at a concentration of 25 nM siRNA in GenMute Buffer according to the manufacturer's instructions for forward knockdown (SignaGen laboratories). siRNA complexes were mixed with BMDM medium (described above) and were added onto the cells. After 22–48 h of gene knockdown, BMDMs were infected with *F. novicida* at a multiplicity of infection of 100:1 and were analyzed for inflammasome activation as outlined below. siRNA pools targeted the following genes (numbers in parentheses indicate Dharmacon reference): *Aim2* (M-044968-01), *Casp11* (that is, *Casp4*) (M-042432-01), Gbp1 (M-040198-01), Gbp2 (M-040199-00), Gbp3 (M-063076-01), Gbp4 (M-047506-01), Gbp5 (M-054703-01), Gbp6 (M-041286-01), Gbp7 (M- 061204-01), Gbp8 (M-059726-01), Gbp9 (M-052281-01), Gbp10 (M-073912-00), Gbp11 (M-079932-00) and NT (non-targeting) pool 2 (D-001206-14).

siRNA screening. Knockdown of the 483 selected genes was performed as described above in the 36 central wells of 96-well plates; this included the nontargeting control siRNA and siRNA specific for *Asc* and *Aim2* on each plate. Macrophages were infected with *F. novicida* at a multiplicity of infection of 100:1 and, following a wash at 1 h after infection, cells were incubated with medium supplemented with propidium iodide at 5 μg/ml. At 6 h after infection, the fluorescence of propidium iodide was determined on a plate reader (Tecan) and supernatants were collected for analysis of the release of IL-1β by enzyme-linked immunosorbent assay (DuoSet; R&D Systems). The fluorescence of propidium iodide and concentration of IL-1β in cells transfected with each siRNA were normalized to the average value of the full plate set, set as 100, and to the value obtained with *Aim2*-specific siRNA, set as 0, with the following calculation (for gene 'X'): normalized value obtained with X-specific siRNA = (value obtained with X-specific $siRNA_x$ – value obtained with *Aim2*-specific siRNA) / (average value obtained with siRNA – value obtained with *Aim2*-specific siRNA). All the siRNA presenting variation of more than 50% in either one of the two parameters have been retested two or three times. Average normalized values are presented in the display items.

Ectopic expression of GBP2 and GBP5. Mouse *Gbp2* and *Gbp5* were cloned into the lentiviral plasmid TRIP iziE-SSFV-GFP with the following primers and restriction enzymes (upper case indicates gene sequence; lower case indicates restriction site (underlined) and four bases flanking in the 5′ direction): For_mGBP2_AvrII, attacctaggGACATGGCCTCAGAGATCCACATG; Rev_mGBP2_EcoRV, aatagataTCAGAGTATAGTGCACTTCCCAGACG; For_mGBP5_AvrII, aaatcctagGACATGGCCCCAGAGATTCACATG; and Rev_mGBP5_HpaI, atttgttaacTTAGCTTATAACACAGTCATGATGATGT CTAC. The production of lentiviruses in 293T human embryonic kidney cells and the transduction of primary BMDMs were performed by standard methods. IFNAR1-deficient macrophages were transduced after 8 d of differentiation by spin-inoculation (1,500*g* for 2 h at room temperature). Transduced macrophages were infected 48 h later. Transduction frequency was determined by flow cytometry based on GFP expression. Specific ectopic expression was checked by quantitative RT-PCR.

Cytokine and LDH release measurement. IL-1β, IL-18 and tumor-necrosis factor were measured by enzyme-linked immunosorbent assay (eBioscience). LDH was measured with an LDH Cytotoxicity Detection Kit (Clontech). To normalize for spontaneous lysis, the percentage of LDH release was calculated as follows: (LDH infected – LDH uninfected) / (LDH total lysis – LDH uninfected) × 100.

Immunoblot analysis. Immunoblot analysis was done as described[29]. Antibodies used were rat anti–mouse caspase-1 (1:1,000 dilution; 4B4; Genentech), rabbit anti-IL-1α (1:1,000 dilution; ab109555; Abcam), rabbit anti-IL-18 (1:500 dilution; 5180R; Biovision), goat anti–mouse IL-1β (1:500 dilution; AF-401-NA; R&D Systems), rabbit anti-GBP2 (1:1,000 dilution; 11854-1-AP; Proteintech) and rabbit anti-GBP5 (1:1,000 dilution; 13220-1-AP; Proteintech). Cell lysates were probed with monoclonal anti-β-actin (1:2,000 dilution; AC-15; A1978; Sigma). Secondary antibodies were as follows (all conjugated to horseradish peroxidase and all at a dilution of 1:3,000): goat anti-rat (NA935V; GE Healthcare), goat anti-rabbit (G21234; Invitrogen), rabbit anti-goat (811620; Invitrogen) and rabbit anti-mouse (816720; Invitrogen).

Real-time PCR. Primers used for mRNA quantification are in **Supplementary Table 3**. Experiments were performed with an iCycler (Bio-Rad) and SYBR green (Applied Biosystems) with standard protocols.

Statistical analysis. Prism 5.0a software (GraphPad Software) was used for statistical analysis of data. For evaluation of the differences between two groups (cell death, cytokine release, flow cytometry, colony-forming units and immunofluorescence-based counts), a two-tailed *t*-test was used. The Kolmogorov-Smirnov test was used for comparison of the cell distribution as determined by ImageStream microscopy in flow. *P* values were adjusted for multiple comparisons with the Bonferroni correction approach. Animal experiments were evaluated with the Mann-Whitney or log-rank Cox-Mantel test.

Immunofluorescence. Macrophages were seeded on glass coverslips and were infected as described above. At the desired time points, cells were washed three times with PBS and were fixed for 15 min at 37 °C with 4% paraformaldehyde. Following fixation, coverslips were washed, and the fixative was quenched for 10 min at room temperature with 0.1 M glycine. Coverslips were stained for 16 h at 4 °C with primary antibodies (identified below), then were washed with PBS and then incubated for 1 h at room temperature with the appropriate Alexa Fluor–conjugated secondary antibodies (identified below) (1:500 dilution; Invitrogen), then were washed with PBS and mounted on glass slides with Vectashield containing DAPI (6-diamidino-2-phenylindole; Vector Labs). Antibodies used were chicken anti–*F. novicida* (1:1,000 dilution; a gift from D. Monack), rat anti-ASC (1:1,000 dilution; Genentech), rabbit anti-GBP2 (1:100 dilution; 11854-1-AP; Proteintech) and rabbit anti-GBP5 (1:100 dilution; 13220-1-AP; Proteintech). Secondary antibodies used were as folllows (all at a dilution of 1:500 and all from Life Technologies): goat anti-rat coupled to Alexa Fluor 488 (A11006), Alexa Fluor 568 (A11077) or Alexa Fluor 633 (A21094); goat anti-rabbit coupled to Alexa Fluor 488 (A11008) or Alexa Fluor 568 (A10042); and goat anti-chicken coupled to Alexa Fluor 488 (A11032), Alexa Fluor 568 (A11047) or Alexa Fluor 633 (A21103). Coverslips were imaged on a Zeiss LSM700 or a Leica SP8 at a magnification of ×63 and vacuolar versus cytosolic bacteria, total intracellular bacteria or ASC specks were quantified as described in the figure legends.

Phagosome protection assay. For quantification of cytoplasmic and vacuolar bacteria, macrophages were infected with GFP$^+$ *F. novicida* as described above. At the desired time point, cells were washed with KHM buffer (110 mM potassium acetate, 20 mM HEPES and 2 mM MgCl2, pH 7.3), followed by incubation for 1 min in KHM buffer with 50 μg/ml digitonin (Sigma). Cells were immediately washed three times with KHM buffer and then were stained for 12 min with Texas Red–coupled chicken antibody to *F. novicida* (identified above) in KHM buffer with 2% BSA. Cells were washed with PBS, then were fixed and analyzed by microscopy. Controls were included in every assay as described[29].

Intracellular viability measurement. For measurement of the intracellular lysis of *F. novicida*, we adapted a published propidium iodide–staining method[33]. Infected BMDMs were incubated for 12 min at 37 °C with Alexa Fluor 488–conjugated mouse antibody to *F. novicida* (identified above) and 2.6 μM propidium iodide (Sigma) in KHM buffer (described above) for labeling of accessible cytosolic bacteria and compromised bacteria, respectively, in permeabilized cells. Cells were fixed and imaged as described above.

CCF4 measurements. Quantification of escape from vacuoles with the β-lactamase–CCF4 assay was performed following manufacturer's instructions (Life Technologies). Macrophages seeded onto non-treated plates were infected for 1 h as described above, washed and then incubated for 1 h at room temperature in CCF4 in the presence of 2.5 mM probenicid (Sigma). Live (propidium iodide–negative) cells were used for quantification of cells containing cytosolic *F. novicida*, with excitation at 405 nm and detection at 450 nm (cleaved CCF4) or 510 nm (intact CCF4).

Flow cytometry. For assessment of bacterial replication by flow cytometry, macrophages seeded onto untreated plates were infected as described above with GFP-expressing *F. novicida* strains. At 8 h after infection, cells were lifted with trypsin and were immediately analyzed by flow cytometry on a FACSCanto II cytometer (BD Biosciences). Dead cells were excluded on the basis of staining with propidium iodide.

ImageStream flow cytometry. Macrophages infected with GFP-expressing bacteria were fixed in 4% PFA and were analyzed on an ImageStream X Mark II (Amnis; EMD-Millipore) with Inspire software, with the extended depth-of-field function activated to increase the accuracy of spot counts. Images of single cells were analyzed with Ideas software (Amnis; EMD-Millipore) with the following steps (each step being confirmed by visualization of at least 20 single cells). Doublets and debris were excluded by morphological parameters (aspect ratio and area in the brightfield channel). Defocused images were eliminated by the Gradient RMS function of the brightfield function. For spot counts and definition of the mean fluorescence of single bacterium, the specific GFP fluorescence signal was defined by application of a mask combining an intensity threshold and a spot to cell background ratio (peak) function. Automatic spot counts were performed with the mask described above. Cells containing a single spot (either a single bacterium or a tight cluster of several bacteria) were gated. The area of the specific signal was analyzed in single cells on the gated population. For the exclusion of bacterial clusters and quantification of the fluorescence of single bacterium, the mean fluorescence intensity was calculated on the GFP$^+$ signal covering an area of $1 \pm 0.5\ \mu m^2$ in 1,599 cells.

Bacteria in single cells were quantified by the automatic spot count function or their numbers were calculated based on the fluorescence of single bacterium. The quantification was identical for cells containing fewer than seven bacteria ($R^2 > 0.99$). For higher intracellular burden, the spot-count function largely underestimated the number of bacteria per cell due to the difficulty to discriminate bacterial cluster. We thus relied on the specific fluorescence of the bacteria within the cells as defined by the mask described above and the calculated fluorescence value of single intracellular bacterium to quantify bacteria per cell. The mask was applied to at least 10,000 images of single cells per sample to extract the specific fluorescence of the intracellular bacteria in single cells.

doi:10.1038/ni.3119

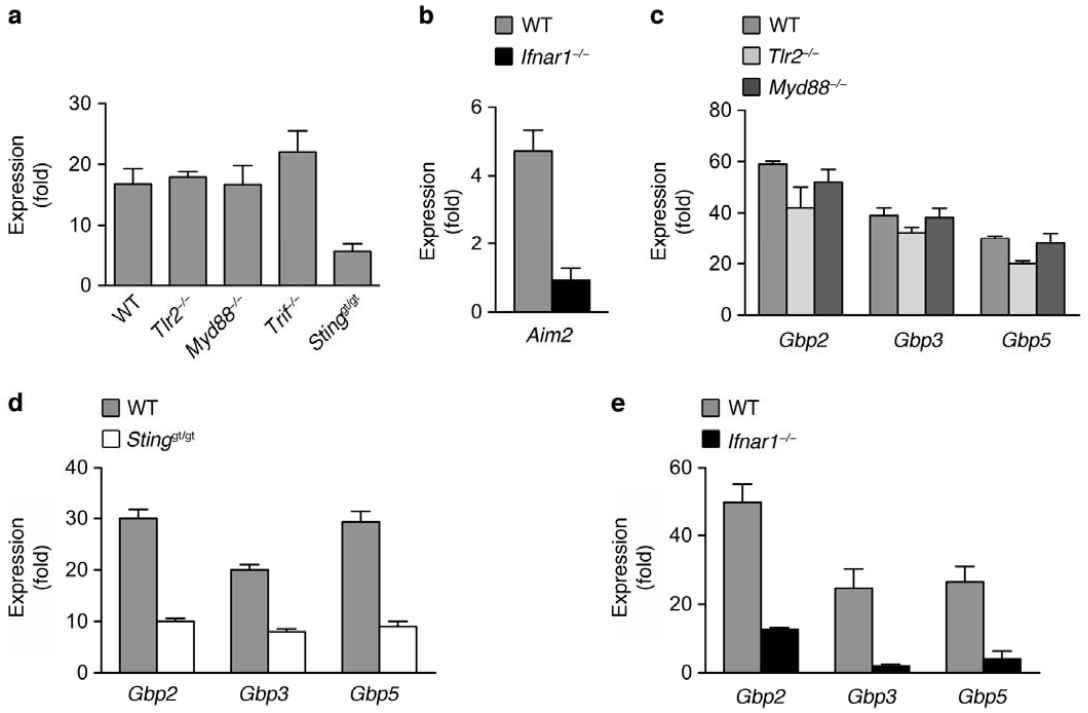

Supplementary Figure 1

Induction of *Ifnb, Aim2* or *Gbp* mRNA in dependence of STING and IFNAR signaling.

(**a**) Induction of *Ifnb* expression from unprimed wild-type (WT), *Tlr2*$^{-/-}$, *Myd88*$^{-/-}$, *Trif*$^{-/-}$ and *Sting*$^{gt/gt}$ bone-marrow derived macrophages (BMDMs) following infection with wild-type *F. novicida* U112 for 6 h. (**b**–**e**) Induction of *Gbp2, Gbp3*, *Gbp5* or *Aim2* expression from unprimed wild-type, *Tlr2*$^{-/-}$, *Myd88*$^{-/-}$, *Ifnar1*$^{-/-}$ and *Sting*$^{gt/gt}$ BMDMs following infection with wild-type *F. novicida* U112 for 6 h. Graphs show mean and s.d. of quadruplicate assays and data are representative of two (**b-d**) or three (**a**) independent experiments.

Nature Immunology: doi:10.1038/ni.3119

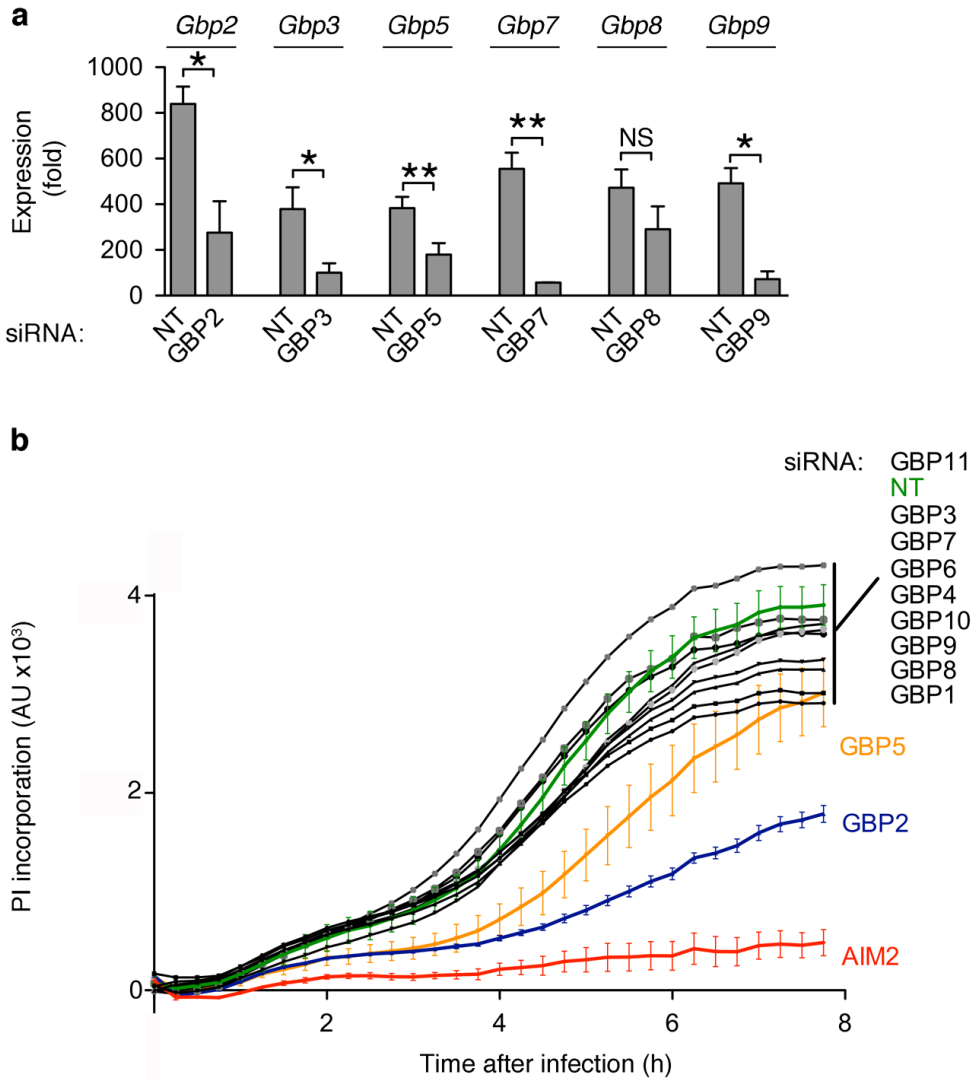

Supplementary Figure 2

***Gbp* knockdown efficiency and real-time cell death after knock-down of *Gbps*.**

(**a**) Induction of the expression of individual *Gbps* from LPS/IFNγ-primed wild-type BMDMs treated with Non-Targeting (NT) or the indicated gene-specific siRNA for 22 h. Graph shows mean and s.d. of quadruplicate wells. *Gbp1*, *4, 6/10, 11* were not tested due to their low expression (see **Fig. 2b**). (**b**) Cell death as measured by propidium iodide (PI) influx in real-time in unprimed wild-type BMDMs infected with wild-type *F. novicida* U112. BMDMs were treated with Non-Targeting (NT) or indicated gene-specific siRNA for 48 h before infection. Graphs show mean and s.d. of triplicate assays and data are representative of three• independent experiments. *, $p<0.05$; **, $p<0.01$; NS, not significant (two-tailed unpaired t-test).

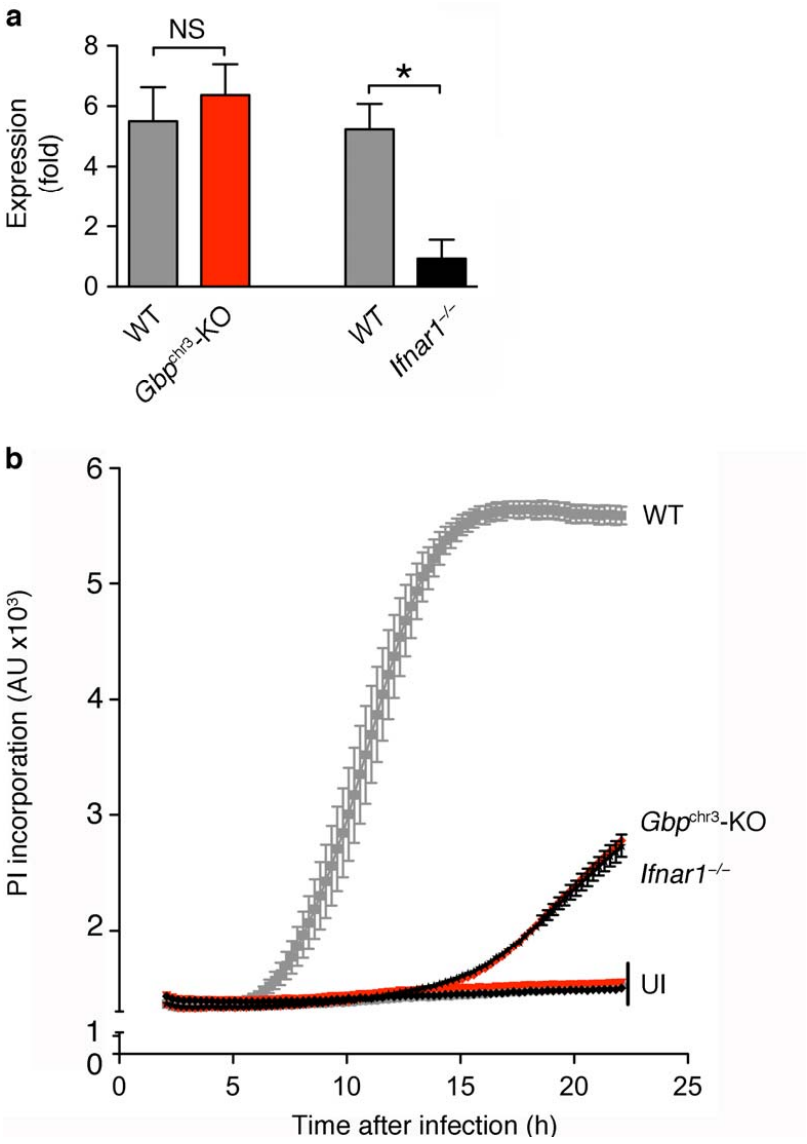

Supplementary Figure 3

***Aim2* induction and real-time cell death assay in *Gbp*-deficient and *Ifnar1*-deficient cells**.

(**a**) Induction of *Aim2* expression from unprimed wild-type, *Gbp*^{chr3}-deleted and *Ifnar1*$^{-/-}$ BMDMs infected with wild-type *F. novicida* U112 for 6 h. *, p<0.01; NS, not significant (two-tailed unpaired t-test). (**b**) Cell death as measured by propidium iodide influx in real-time in unprimed wild-type, *Gbp*^{chr3}-deleted and *Ifnar1*$^{-/-}$ BMDMs left uninfected (UI) or infected with wild-type *F. novicida* U112. Graphs show mean and s.d. of triplicate assays and data are representative of two (**a**) and three (**b**) independent experiments.

Nature Immunology: doi:10.1038/ni.3119

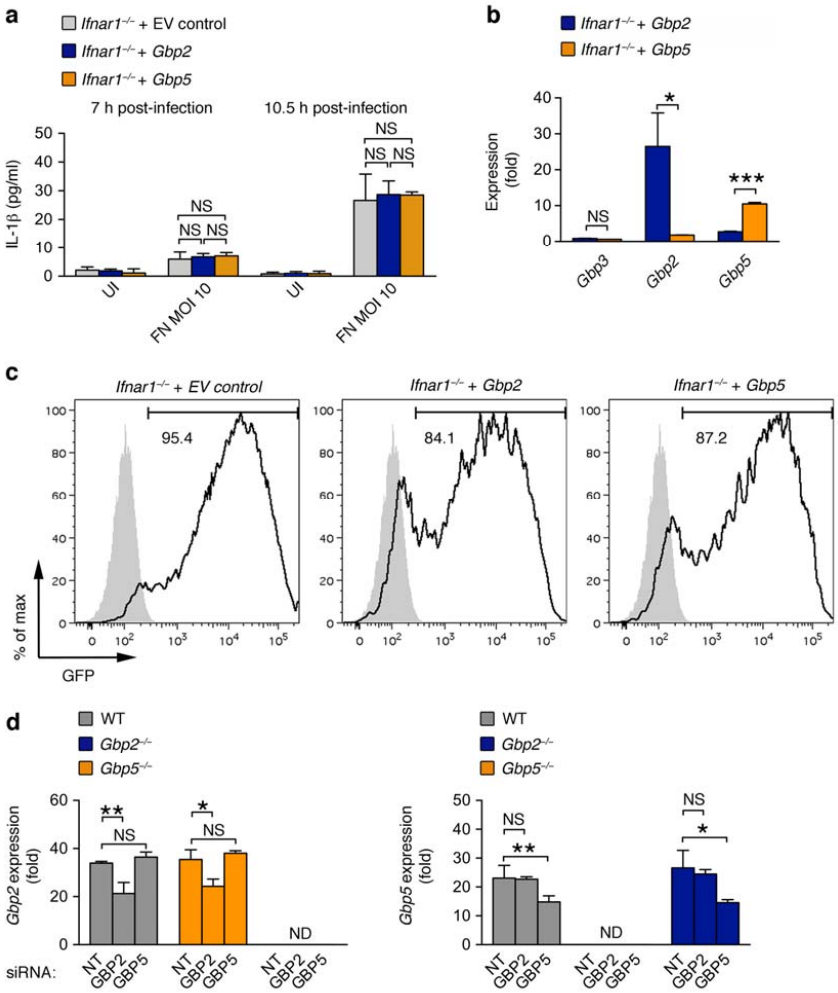

Supplementary Figure 4

Ectopic expression of GBPs in *Ifnar1*$^{-/-}$ cells and efficiency of *Gbp2* and *Gbp5* knockdown.

(**a**–**c**) Ectopic expression of GBP2 or GBP5 do not complement type-I-IFN receptor deficiency. *Ifnar1*$^{-/-}$ macrophages were transduced with lentivirus encoding either GFP only (EV = empty vector) and GFP-GBP2 and GFP-GBP5. 48 h post transduction, macrophages were infected with *F. novicida* at the indicated MOI. IL-1β concentration in the supernatant was determined at 7 h and 10.5 h post infection (**a**). Specific ectopic expression was verified by quantifying the *Gbp3* (control), *Gbp2* and *Gbp5* transcript levels. Results are expressed as fold induction relative to the transcript level in *Ifnar1*$^{-/-}$ macrophages transduced with empty vector control (**b**). Graphs show mean and s.d. of triplicate assays. The percentage of transduced cells was determined by flow cytometry based on GFP expression (**c**). (**d**) RT-PCR for *Gbp2* and *Gbp5* expression from unprimed wild-type, *Gbp2*$^{-/-}$ and *Gbp5*$^{-/-}$ BMDMs treated with Non-Targeting or the indicated gene-specific siRNA for 22 h and infected for 8 h with wild-type *F. novicida* U112. Graphs show mean and s.d. of quadruplicate assays and data are representative of independent two experiments. *, $p<0.05$; **, $p<0.01$; NS, not significant (two-tailed unpaired t-test). ND, not detected.

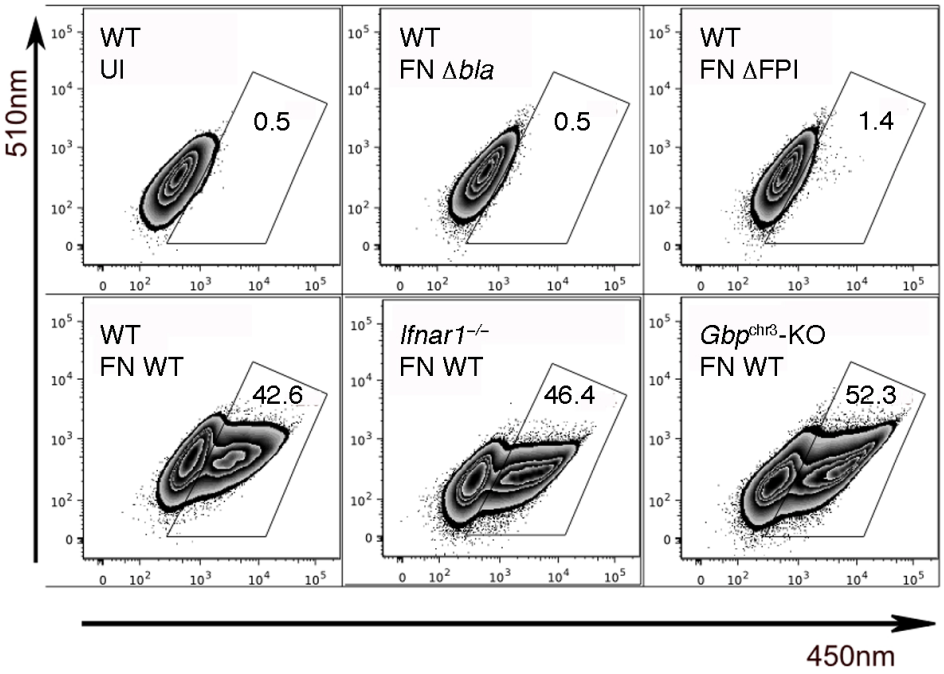

Supplementary Figure 5

Phagosomal rupture assay using the CCF4/β-lactamase system.

Wild-type, *Ifnar1*$^{-/-}$ and *Gbp*^{chr3}-deleted BMDMs were primed for 16 h with IFN-β (500 units/ml), infected for 1 h with wild-type *F. novicida* (FN) U112, a β-lactamase-deficient mutant (Δbla) or a ΔFPI mutant and loaded with CCF4-AM for 1 h before analysis by flow cytometry. Phagosomal rupture is associated with β-lactamase (encoded by FTN_1072) release into the cytosol and cleavage of the CCF4 substrate (maximum emission at 520 nm) into a product which emits with a maximum of fluorescence at 447 nm. FACS plots show pooled data from three independent samples and representative of three independent experiments. Live cells (propidium iodide negative) are shown.

Nature Immunology: doi:10.1038/ni.3119

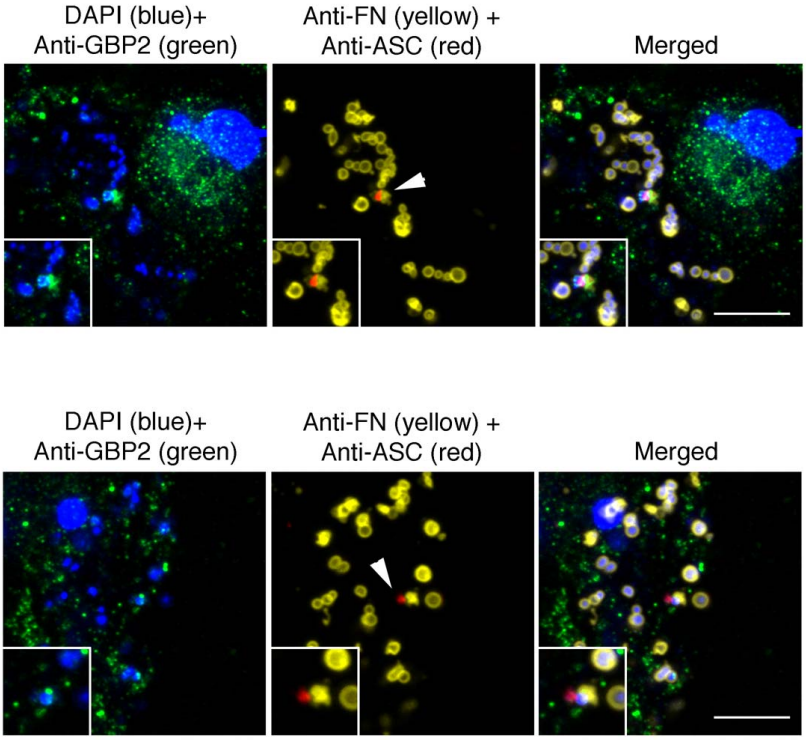

Supplementary Figure 6

GBPs co-localize with irregularly shaped bacteria next to ASC specks.

Wild-type BMDMs infected with wild-type *F. novicida* for 8 h, stained for DNA (DAPI), GBP2, *F. novicida* and ASC. Scale bars: 10 μm. Data are representative of three• independent experiments.

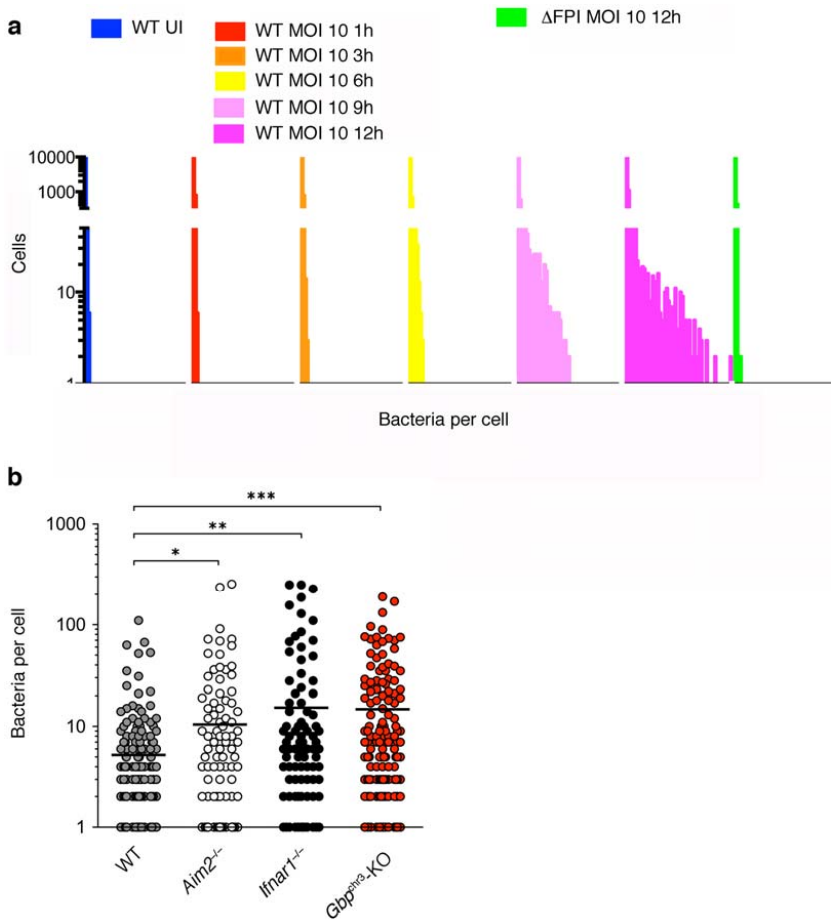

Supplementary Figure 7

Analysis of bacterial replication in infected macrophages.

(**a**) Quantification of bacterial loads in single cells by high-resolution microscopy in flow over time. Wild-type BMDMs were left uninfected or infected with GFP^{+}-wild-type *F. novicida* or a ΔFPI mutant at an MOI of 10 for 0-12 h, fixed and analyzed by ImageStream^{TM} microscopy in flow. Each bar corresponds to the number of cells with the indicated numbers of bacteria per cell grouped by increments of 5... Wild-type UI vs. wild-type MOI 10 3h p>0.9999, wild-type UI vs. wild-type MOI 10 6h p>0.9999, wild-type UI vs. wild-type MOI 10 9h p<0.0001, wild-type UI vs. wild-type MOI 10 12h p<0.0001, wild-type MOI 10 12h vs. ΔFPI MOI 10 12h p<0.0001 Kolmogorov-Smirnov test with Bonferroni correction). (**b**) Quantification of bacterial loads as determined by microscopy. Wild-type, *Aim2*$^{-/-}$, *Gbp*^{chr3}-deleted and *Ifnar1*$^{-/-}$ BMDMs were infected with GFP^{+}-wild-type *F. novicida* at an MOI of 10 for 16 h, fixed and analyzed by confocal microscopy. Graph show pooled data from 2 independent experiments (n>1000 bacteria counted). *, p<0.05; **, p<0.01; ***, p<0.001 (two-tailed unpaired t-test).

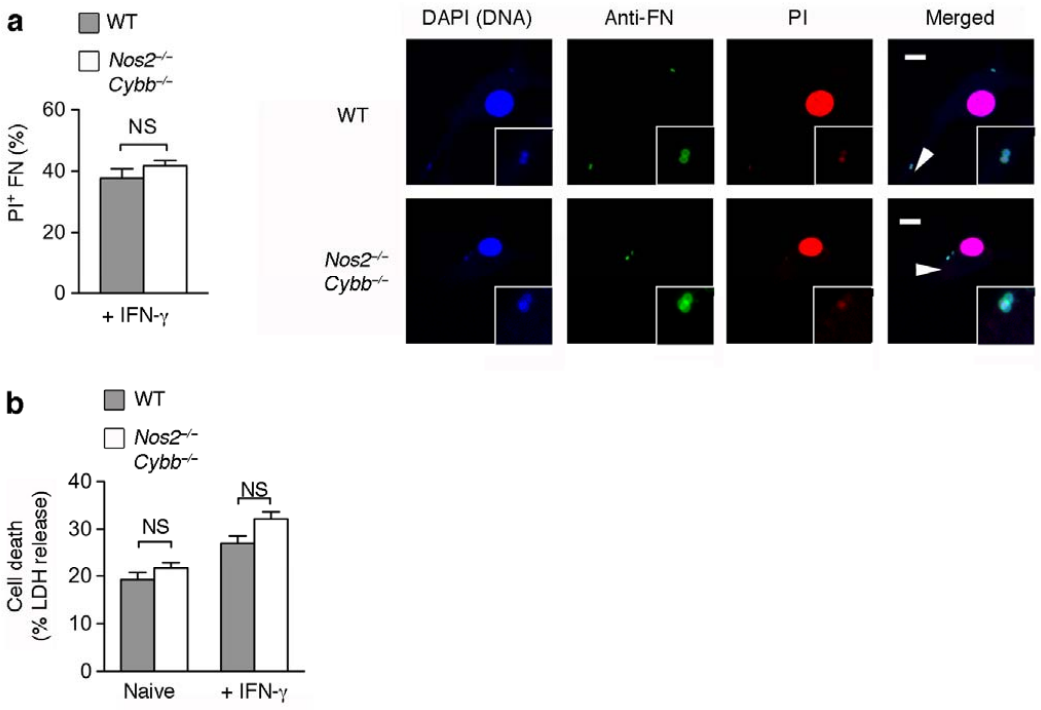

Supplementary Figure 8

Bacteriolysis and cell death during *F. novicida* infection are independent of ROS or NO production.

(**a**) Quantification of lysed (propidium iodide^{+} *F. novicida*) in IFN-γ-primed wild-type and *Nos2*$^{-/-}$/*Cybb*$^{-/-}$BMDMs infected for 8 h with wild-type *F. novicida*. Imaging of lysed (propidium iodide$^{+)}$ *F. novicida* in IFN-γ-primed wild-type and *Nos2*$^{-/-}$/*Cybb*$^{-/-}$BMDMs infected for 8 h with wild-type *F. novicida*. Arrowheads indicate region in insets. Scale bars 10 μm. (**b**) LDH release from naïve or IFN-γ-primed wild-type and *Nos2*$^{-/-}$/*Cybb*$^{-/-}$ BMDMs infected for 8 h with wild-type *F. novicida* U112. Graphs show mean and s.d. of quadruplicate wells and data are representative of three• independent experiments. NS, not significant (two-tailed unpaired t-test).

Supplementary Table 2 Bacterial strains and plasmid used in this study.

Name	Parental strain	Characteristic
wild-type *F. novicida* U112	–	–
ΔFPI	wild-type *F. novicida* U112	ΔFTN_1309-1325::Kan
Δbla	wild-type *F. novicida* U112	ΔFTN_1072
ΔfopA	wild-type *F. novicida* U112	fopA::T20
pKK219-GFP	–	GFP expressing plasmid

Supplementary Table 3 | Primers used for qRT-PCR. Target gene, sequence and size of amplicon are indicated.

Target gene	Forward primer	Reverse primer	Amplicon (bp)
mGBP1	aataagctggctggaaagca	tgtgtgagactgcacagtgg	60
mGBP2	accagctgcactatgtgacg	tcagaagtgacgggttttcc	172
mGBP3	gtctggagaacgcagtgaca	gtgctccatgaagacagcaa	182
mGBP4	gagcagctcatcaaagacca	ttcctcacggaaagtcttttg	72
mGBP5	ccagagtaaagcggaacaag	gtgcaactcttgccttctcc	158
mGBP6/10	tggagcagctgcattatgtc	gcattctgggtttgtcacct	228
mGBP7	aacagcatgagcaccatcaa	gaagtggactttgccctgat	89
mGBP8	tgctatgacccaaccacaaa	ccttggtctgagactgcaca	227
mGBP9	tgtgcagtctcagaccaagg	aagcacacttagggcgaaga	154
mGBP11	agcaactgagaaggaagctga	caaggagagccttttgttcct	99
mβ-actin	gtggatcagcaagcaggagt	agggtgtaaaacgcagctca	96

Nature Immunology: doi:10.1038/ni.3119

3 Dharmacon siRNA library

Pool Catalog Number	Duplex Catalog Number	Gene Symbol	GENE ID	Gene Accession	GI Number	Sequence
L-058899-00	J-058899-05	Tgm2	21817	NM_009373	31543859	GCAACGACUUCGACGUGUU
L-058899-00	J-058899-06	Tgm2	21817	NM_009373	31543859	CCGAUGAUGUGUACCUAGA
L-058899-00	J-058899-07	Tgm2	21817	NM_009373	31543859	GAACAGCAUCCCACUUCGA
L-058899-00	J-058899-08	Tgm2	21817	NM_009373	31543859	CGACGGGAAUAUGUCCUUA
L-047145-01	J-047145-09	Lrrfip1	16978	NM_008515	6678721	CCAUAAGGAGCGAACGAGA
L-047145-01	J-047145-10	Lrrfip1	16978	NM_008515	6678721	CUGACGAAGACGAGCGCUU
L-047145-01	J-047145-11	Lrrfip1	16978	NM_008515	6678721	GCGAUGGUCUAGACGUAAA
L-047145-01	J-047145-12	Lrrfip1	16978	NM_008515	6678721	CGGAGAAACACGUCGGCUU
L-046134-01	J-046134-09	Hcls1	15163	NM_008225	6680186	GGGCAUGAUGUAUCGGUUU
L-046134-01	J-046134-10	Hcls1	15163	NM_008225	6680186	CCAAGGAGAGGGAAGCGAU
L-046134-01	J-046134-11	Hcls1	15163	NM_008225	6680186	UGGAAGAGCCAGUGUACGA
L-046134-01	J-046134-12	Hcls1	15163	NM_008225	6680186	GUAAAGAUGAGCCGAGAAG
L-060939-01	J-060939-09	Snx5	69178	NM_024225	31560123	CUUACUGAAACAACGGAUU
L-060939-01	J-060939-10	Snx5	69178	NM_024225	31560123	AGUGUUAGACGGAAGAAUA
L-060939-01	J-060939-11	Snx5	69178	NM_024225	31560123	AUUUCAGAGCCCAGAGUUU
L-060939-01	J-060939-12	Snx5	69178	NM_024225	31560123	CGAGAGAAGAUGCAGAAAC
L-041172-00	J-041172-05	Ptpn6	15170	NM_013545	7305132	GGUAAAGAAUCUACACCAA
L-041172-00	J-041172-06	Ptpn6	15170	NM_013545	7305132	AUACAAACUGCGAACAUUA
L-041172-00	J-041172-07	Ptpn6	15170	NM_013545	7305132	AUAUCAAGGUUAUGUGUGA
L-041172-00	J-041172-08	Ptpn6	15170	NM_013545	7305132	AGAUAUGGCACUACCAGUA
L-040984-01	J-040984-09	Coro1c	23790	NM_011779	31542412	CGAACUAGCUCGCGUUUCU
L-040984-01	J-040984-10	Coro1c	23790	NM_011779	31542412	CCGUUGAAUUAAUUACGUA
L-040984-01	J-040984-11	Coro1c	23790	NM_011779	31542412	GUAUAAACACUCACGAGAA
L-040984-01	J-040984-12	Coro1c	23790	NM_011779	31542412	GGUUGAGAGAGGCGGGAGU
L-040963-01	J-040963-09	Ifit3	15959	NM_010501	6754287	GAACUGAGACGAUUAACGA
L-040963-01	J-040963-10	Ifit3	15959	NM_010501	6754287	GGAAGAAAUGAACGAGCAA
L-040963-01	J-040963-11	Ifit3	15959	NM_010501	6754287	ACUCAGAUCUCAUCGAUUU
L-040963-01	J-040963-12	Ifit3	15959	NM_010501	6754287	GGAAGGAUGGACACGCCUA
L-047321-01	J-047321-09	Arpc1b	11867	NM_023142	12963526	GCACGGACCGCAAUGCCUA
L-047321-01	J-047321-10	Arpc1b	11867	NM_023142	12963526	GCACUGUAUGCCUGGUAGA
L-047321-01	J-047321-11	Arpc1b	11867	NM_023142	12963526	GCUUCAAAAUGUGGGCUAA
L-047321-01	J-047321-12	Arpc1b	11867	NM_023142	12963526	GGGAACUGCCUAUUUAACA
L-050915-01	J-050915-09	Swap70	20947	NM_009302	40789274	AGUUGGAGUUGGAGCGGAA
L-050915-01	J-050915-10	Swap70	20947	NM_009302	40789274	AGACAACAGAGGCGGAGAA
L-050915-01	J-050915-11	Swap70	20947	NM_009302	40789274	GAAAGGUCACAAACGGAAA
L-050915-01	J-050915-12	Swap70	20947	NM_009302	40789274	GCAGUAUGAGGGAGUUAAA
L-063252-02	J-063252-09	Sec23b	27054	NM_001252545	357527457	UGUAAAGACCUCUCGGGAA
L-063252-02	J-063252-10	Sec23b	27054	NM_001252545	357527457	GUGAAAGGGCCAUGCGUGU
L-063252-02	J-063252-12	Sec23b	27054	NM_001252545	357527457	CGUUGUUGAUAGCGUCCUA
L-063252-02	J-063252-19	Sec23b	27054	NM_001252545	357527457	AGAAAGAUAACGCACGAUU
L-064059-01	J-064059-09	Rnh1	107702	NM_145135	31981747	CCUCCAAAGCUUCGCUACA
L-064059-01	J-064059-10	Rnh1	107702	NM_145135	31981747	CCAUGAACCUGGUGUCCGU
L-064059-01	J-064059-11	Rnh1	107702	NM_145135	31981747	GAGCUUUGGUUGGGAGACU
L-064059-01	J-064059-12	Rnh1	107702	NM_145135	31981747	CAAUAAGCACUGUGGUCUU
L-064380-01	J-064380-09	Adsl	11564	NM_009634	31982252	GUCCGAAAGCUGCGGGCAU
L-064380-01	J-064380-10	Adsl	11564	NM_009634	31982252	CAGAUUGGCUCCAGUGCGA
L-064380-01	J-064380-11	Adsl	11564	NM_009634	31982252	GGACAGACGUACACACGGA
L-064380-01	J-064380-12	Adsl	11564	NM_009634	31982252	GGUACAAGUUCCAGACGUG
L-043701-00	J-043701-05	Fyb	23880	NM_011815	33469118	CGAGAUCUAUGACGGAAUA
L-043701-00	J-043701-06	Fyb	23880	NM_011815	33469118	GUACGACGGUGAAAUUCGA
L-043701-00	J-043701-07	Fyb	23880	NM_011815	33469118	GGAGGGAGCCCAAGAUUUG
L-043701-00	J-043701-08	Fyb	23880	NM_011815	33469118	GGGCAAAUAUGGUUAUGUC
L-054838-01	J-054838-09	Gart	14450	NM_010256	93102414	GCACAAGACCAUAAGCGAU

Pool Catalog Number	Duplex Catalog Number	Gene Symbol	GENE ID	Gene Accession	GI Number	Sequence
L-054838-01	J-054838-10	Gart	14450	NM_010256	93102414	AGAUGUAGAUGCCGGACAA
L-054838-01	J-054838-11	Gart	14450	NM_010256	93102414	CCGCUUUGGUGAUCCGGAA
L-054838-01	J-054838-12	Gart	14450	NM_010256	93102414	ACUCGUAGUUGUCGGACCA
L-047667-01	J-047667-09	Wdr1	22388	NM_011715	6755994	UGGAUGACACAGUGCGGUA
L-047667-01	J-047667-10	Wdr1	22388	NM_011715	6755994	CUACAGUGGACAAGGCGUU
L-047667-01	J-047667-11	Wdr1	22388	NM_011715	6755994	CAACAGGGAGUGAUGAUAA
L-047667-01	J-047667-12	Wdr1	22388	NM_011715	6755994	GGAGCAUCUUCUAAAGUAU
L-065589-01	J-065589-09	Samhd1	56045	NM_018851	46909601	UCACUAAGUUGACGGAUAA
L-065589-01	J-065589-10	Samhd1	56045	NM_018851	46909601	CAGAUCAGUGAGCGAGAUA
L-065589-01	J-065589-11	Samhd1	56045	NM_018851	46909601	GGAAUGGCAUCGACGUAGA
L-065589-01	J-065589-12	Samhd1	56045	NM_018851	46909601	GAUUACAAGGAUCGAGACA
L-048239-01	J-048239-09	Cmpk2	22169	NM_020557	31340573	GAAAUGACGUACCAGCGUA
L-048239-01	J-048239-10	Cmpk2	22169	NM_020557	31340573	CCAAUAAUGUGUUUCGUCA
L-048239-01	J-048239-11	Cmpk2	22169	NM_020557	31340573	CUGAAUAGGAAGUCGUAGU
L-048239-01	J-048239-12	Cmpk2	22169	NM_020557	31340573	CGUGGAUUCUGGAACGAGA
L-047866-01	J-047866-09	Drg2	13495	NM_021354	10946677	GGAGAUCGCUCGAACGCAG
L-047866-01	J-047866-10	Drg2	13495	NM_021354	10946677	CGAGGUACUCUUCCGAGAA
L-047866-01	J-047866-11	Drg2	13495	NM_021354	10946677	UGGAACACACAAACGGGAA
L-047866-01	J-047866-12	Drg2	13495	NM_021354	10946677	CUAUGGAGCAUGAGGACGU
L-048873-01	J-048873-09	Hspa14	50497	NM_015765	82880661	GGGCCGAUGUGGUUGCAAA
L-048873-01	J-048873-10	Hspa14	50497	NM_015765	82880661	GUGAACAGGUGGUUGGACU
L-048873-01	J-048873-11	Hspa14	50497	NM_015765	82880661	GCACAGUAGUGAAAGUGAA
L-048873-01	J-048873-12	Hspa14	50497	NM_015765	82880661	CAAAGUAGAAUAAGACAUG
L-167568-00	J-167568-05	Rnf213	672511	XM_001477846	407263730	CGGAGGAGCUGUACCGAAA
L-167568-00	J-167568-06	Rnf213	672511	XM_001477846	407263730	CAAGAUCGCUAGUGGAUAA
L-167568-00	J-167568-07	Rnf213	672511	XM_001477846	407263730	GCGUUUAACCCACGGGAUA
L-167568-00	J-167568-08	Rnf213	672511	XM_001477846	407263730	UCACAAAACUGUCGAGAAU
L-051439-01	J-051439-09	Pycard	66824	NM_023258	31581581	CGAGAAGGCUAUGGGCGCA
L-051439-01	J-051439-10	Pycard	66824	NM_023258	31581581	GAAACAAACCAGUCCGUAG
L-051439-01	J-051439-11	Pycard	66824	NM_023258	31581581	GCUACUAUCUGGAGUCGUA
L-051439-01	J-051439-12	Pycard	66824	NM_023258	31581581	GAGCAGAGCUGAGGUAUCU
L-053455-00	J-053455-05	Nlrp3	216799	NM_145827	48675839	GGUGAAAUGUACUUAAAUC
L-053455-00	J-053455-06	Nlrp3	216799	NM_145827	48675839	GGAUGGGUUUGCUGGGAUA
L-053455-00	J-053455-07	Nlrp3	216799	NM_145827	48675839	ACACACCUCUAUCUACGAA
L-053455-00	J-053455-08	Nlrp3	216799	NM_145827	48675839	GAAGUGGACUGCGAGAGAU